Kingdom of Saudi Arabia
Ministry of Education
Jazan University

JAZAN UNIVERSITY

JOURNAL OF
JAZAN UNIVERSITY
For
Applied Sciences

A Refereed Scientific Periodical

ISSN:1658-6913

Vol. 11 No 1 June 2023(Thul Qi'dah 1444 H)

Publication Rules

The University of Jazan provides an opportunity for scholars to publish their scholarly work on research. The editorial board will consider manuscripts from all fields of knowledge. Manuscripts submitted in either Arabic or English, and if the due accepted for publication, may not be published elsewhere, without permission of the Editor-in-Chief. The journal issues one volume per year. The types of manuscript classification used by the Editorial Board run as follows:

1. **Article:**
   An author's original work contributing new knowledge to the field in which research was conducted.
2. **Review Article:**
   A critical synthesis of the current literature in a particular filed, or a synthesis of the literature in a particular field during an explicit period of time.
3. **Brief Article:**
   A short article (note) with the characteristics of an article.
4. Book Reviews
5. **Forum:**
   Letters to the editor, comments, responses, preliminary results or findings, and miscellany

General Instructions

1. Submission of manuscripts:

Original manuscripts should be typewritten (one side only), using an A4 size paper, double spaced along with 3 copies. All pages are to be numbered consecutively, including tables and graphs. Tables, other illustrations, and references should be presented on separate sheets with their proper text position indicated.

2. Abstracts:

Manuscripts for articles, review articles, and brief articles require both Arabic and English abstracts, using no more than 200 words, in single column (13cm wide), for each version.

3. Tables and other illustrations:

Tables, charts, figures, and plates should fit the journal's page size (12.5 com x 18cm). All inner drawings must be presented on high quality. Tracing paper is necessary, using black Indian ink as well. Photographs may be submitted, but on glossy print paper in either black or color.

4. Abbreviations and Units:

A4 sizes and quantities should be expressed according to international standards. Standardized abbreviation should only be used. The names of periodicals should be abbreviated in accordance with the words of scientific periodicals.

5. Title Page:

Should contain the title, name of the authors, name and address of the institution, where the work was carried out. The title should be brief and use strong keywords. Scientific names of organism should be clearly stated and should be typed italic.

6. Text:

The organization of the manuscript should be as follows: Introduction, materials, results, discussion, and references. Results and discussions can be combined in one section. Acknowledgement (if needed) should be brief and added before the reference sections.

1. References:

Citation of the references (within the text) should be indicated by author. Date, style, and references should be listed in an alphabetical order and conform to the following examples: Periodical citations in the text are to be enclosed in one line brackets, e.g.(6).

Periodical references are to be presented in the following

form:

References number in line brackets ( ), author's name followed by a given name and/or initials, the title of an article or periodical (italicized), volume number, year of publication (in parentheses) and pages e.g.

Basahy, A.Y. (1992). Protein and Amino Acid contents in seeds of some soybean cultivate (Glycin Max 1) Arab Gulf J. Sci. Res. 11(2), 221-228.

Book Citation:

Book references should include the following:

Reference number ( ), author's surname followed by a given name and/or title of the book (italicized), place of publication, publisher, and year of publication.

Example:

Lehman. H.C. (1953). Age and Achievement. Princeton: Princeton University Press.

2. Content Notes:

Content notes are to be presented on separate sheets. They will be printed below a solid line separating the content notes from the text.

9. The manuscripts and forum items submitted to the journal for publication contain the author's conclusions and opinions, and if published they do no bear a conclusion or opinion of the Editorial Board.

10. Authors will be provided with 20 reprints free of charge, along with two issues of the journal. Additional copies could be purchased, if ordered when the proofs are returned. Price will be shown on the order form.

11. It is the responsibility of the researcher to make sure that the manuscript is free of linguistic, grammatical and typo errors.

12. The editors' board has the right to set priorities of publishing the research.

13. The journal is not obligated to repeat the research it reaches, whether it was approved for publication or not.

14. All the received research is subject to primary examination by the editorial board in order to determine their eligibility for arbitration. The editorial board is entitled to excusing itself from accepting the research without giving reasons.

15. The journal is published twice a year.

IN THE NAME OF ALLAH, THE MOST GRACIOUS,
THE MOST MERCIFUL

Kingdom of Saudi Arabia
Ministry of Education
Jazan University

JOURNAL OF
JAZAN UNIVERSITY
For
Applied Sciences

A Refereed Scientific Periodical

Vol. 11 No 1 June 2023(Thul Qi'dah 1444 H)

ISSN:1658-6913

Journal Jazan University

for applied sciences

Correspondence

All correspondence should be directed to:
Editor-in-chief of Jazan University Journal of Applied Sciences, Jazan - University City
Administrative Tower - PO Box 114 - Zip Code 4514, Kingdom of Saudi Arabia
jas@jazanu.edu.sa

فهرس المحتويات

الموضوع

صفحة

Blockchain-based Non-Fungible Tokens for IoT Security

Faisal Alshanketi
Department of Computer Science, Jazan University Saudi Arabia

Abstract

IoT devices are being used in various domains and their numbers are increasing drastically. IoT devices are becoming part of our daily life and they are infiltrating our day-to-day work. Although the applications of these IoT sensing devices are providing a lot of valuable solutions but their security is still a big concern due to the limited hardware resources. Blockchain technology is being proposed in various domains for providing security and immutability to the system and data and it is also being applied in case of providing security to IoT devices. There are many variations and applications of blockchain technology. Non-fungible tokens (NFTs) are one of the prominent and rising applications. Non-fungible tokens (NFTs) are cryptographically unique tokens that are linked to digital (and sometimes physical) content, providing proof of ownership. In this paper, we will investigate the applications of NFTs for providing security to IoT infrastructure and propose a solution.

Keywords: IoT devices, Blockchain technology, Non-fungible tokens, Physical Unclonable Functions

I. INTRODUCTION

A. Internet of Things (IoT)

The main goal of the IoT is to enhance our way of life by interacting, gathering, sharing data and information in many domains and applications to do regular jobs and duties. Using terminology ”smart” with other words like ”smart house,” ”smart city,” and ”smart transportation” are related to the Internet of Things. IoT has become popular, and many application areas use that technology for personal and business purposes. People may use personal devices and social domain apps to connect with their surroundings IoT devices while maintaining and creating social ties. Smart cities use IoT in the transportation sector, where intelligent automobiles, smart roads, and innovative traffic lights provide safe and convenient transit. In the businesses and industries domain, inter-and intra-organizational operations use IoT technology in their applications like finance, banking, marketing, and other areas to enable various service and utility monitoring sectors, which encompasses agricultural, breeding, energy management, recycling activities, and so on, is the last application domain [4].

Recently, Radio Frequency Identification (RFID) and Wireless Sensor Networks (WSN) technologies have accelerated IoT development due to the rapid growth of IoT applications. Every device can be tagged or labeled with RFID tags to serve as the basis of IoT identification. The WSN transforms every ”thing,” such as people, devices, and other objects, into a wirelessly identified item capable of transferring data across the physical, cyber, and digital worlds [1]. IoT architecture is composed of layers defined by their functionality and the devices they employ. Different experts differ on the number of levels in IoT. However, several [5]–[7] believe the IoT primarily functions on three layers: perception, communication, and actions. Each layer of IoT has its own set of security challenges. Figure 1 depicts IoT’s fundamental three-layer architectural framework regarding each layer’s devices and technologies.

B. Security Issue of IoT

Each layer of IoT is vulnerable to threats, either active or passive, and from inside or outside networks. Active attacks disable IoT networks, while passive attacks monitor them without interfering. Devices, resources, and networks linked to IoT.

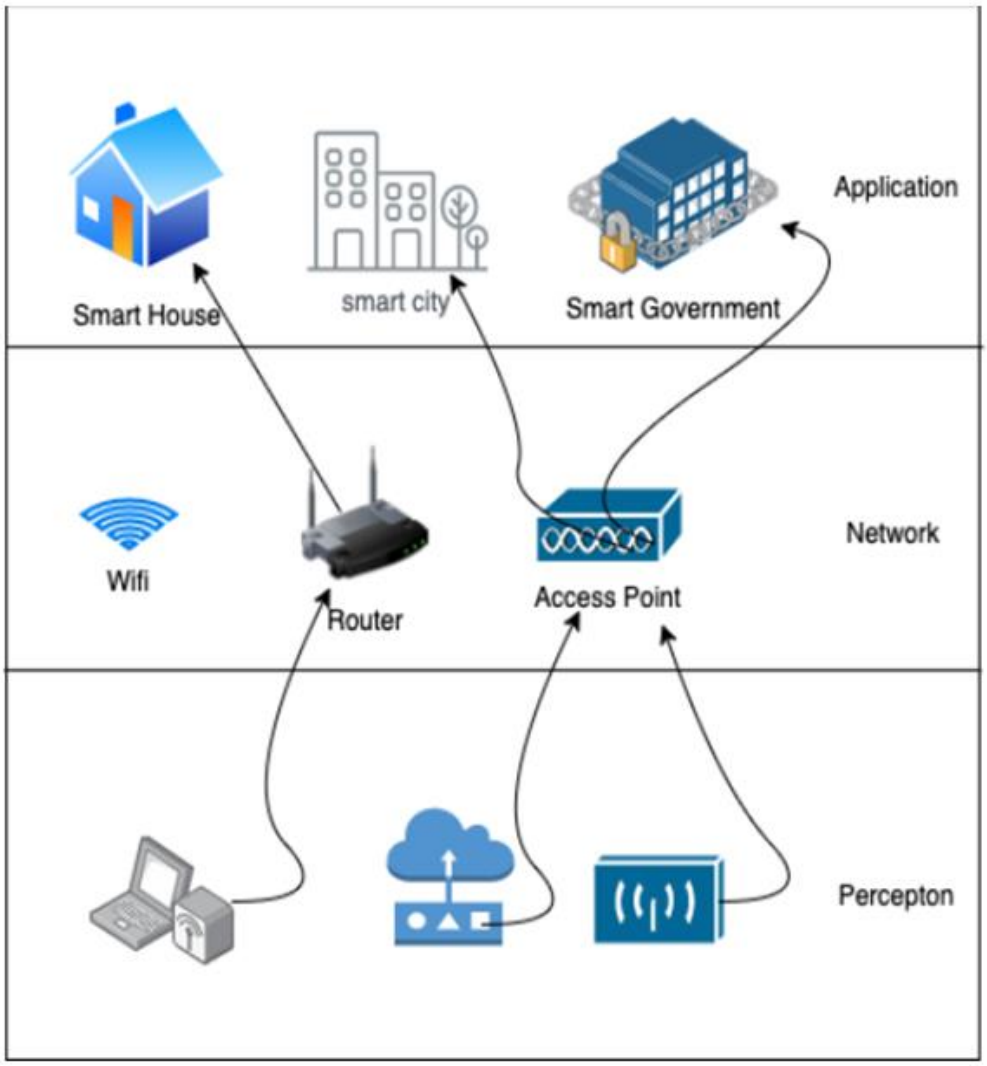

Fig. 1. Three-layer IoT architecture

Each layer of IoT is vulnerable to threats, either active or passive, and from inside or outside networks. Active attacks disable IoT networks, while passive attacks monitor them without interfering. Devices, resources, and networks linked to IoT can be hacked with Denial-of-Service (DoS) attacks, shutting them down for authorized users [1]. The sections below analyze different attacks for each layer of IoT.

1) Perception Layer

The perception layer of IoT has three security vulnerabilities as follows:

a) Wireless signal frequency. The IoT uses wireless technology to send signals between sensor nodes, which might be affected by disruptive waves.

b) Because IoT nodes frequently operate in outdoor areas, attackers can physically attack IoT sensors

and devices, tampering with their hardware components.

c) The network topology is constantly changing as IoT nodes are relocated. Because IoT sensors and RFIDs have limited storage, power, and processing capabilities, they are vulnerable to several risks and assaults. Access control and authentication (to verify the sender's genuine identity) can solve the preceding security vulnerabilities at the perception layer [1], [8].

The perception layer is subject to the Replay Attack, which violates the layer's secrecy by impersonating, changing, or replaying one of the IoT devices' identity information. In a Timing Attack, the attacker determines the encryption key, calculating the required encryption time. Another danger to confidentiality is when an intruder takes control of a node and grabs all data and information. An attacker may transmit malicious data to the network, jeopardizing the data's integrity at this layer. Lowering the system's energy and keeping the nodes from resting may result in a DoS attack [9]. Access control and authentication (to verify the sender's genuine identity) can solve the preceding security vulnerabilities at the perception layer [8].

2) **Network Layer**

DoS attacks violate the IoT network layer as the previous layer. The hacker can use different attacks such as passive monitoring, traffic analysis, and eavesdropping to breach network security as confidentiality and privacy. The most common attacks with a high chance of occurrence are the remote access protocols and information sharing of devices. The network layer has high-security issues to Man-in-the-Middle (MIM) attack [1], which eavesdropping can monitor. If the intruder intercepts the keying mechanism of the IoT nodes, the secure data exchange channel through the network layer will be compromised. IoT must be confident enough through a suitable key exchange mechanism to avoid identity theft and prevent any intruder from eavesdropping.

In terms of communication, IoT is not restricted from machines to humans. The machine-to-machine communication used by IoT nodes has a compatibility issue. Because network components are heterogeneous, it is not easy to employ present network protocols to safeguard effectively. Attackers can also leverage interconnectedness to get additional helpful information related to users and use it for illegal operations [5].

Protecting the network is essential in the IoT, but safeguarding the network's object is also critical. Both network and IoT objects are equally necessary to protect the entire environment. Checking the state of the network must be an integral part of the objects to deal with various attacks by having suitable protocols and software to achieve high protection security mechanisms [10].

3) **Application Layer**

Various difficulties are linked to application security since the IoT lacks global regulations and does not have standards that regulate connectivity and development. Because various apps use different authentication methods, ensuring con fidentiality, integrity, availability, and authenticity is complicated. Many linked devices exchanging data will pressure data-analysis tools, possibly impacting service availability [4].

When creating IoT apps, keep in mind

how different people will interact with them, the amount of information they will divulge, and who will maintain them. . Users must be able to manage what data they share and know-how, how, and when it will be utilized [4].

*C. **Blockchain***

A blockchain is a network of people who aim to use a decentralized, linked, and cryptographically secure information architecture (ledger) of linked blocks that any member can trace. In a blockchain, each block has transactions that contain information about, who participated in the transaction, the data integrity of the league, and how the partnership is linked to the preceding one. The role (via consensus protocol, ownership, permission, etc.) of adding a new partnership through a secure process by applying a consensus algorithm where the majority of miners (typically more than 50%) vote to connect the block. It is exceedingly expensive for hackers to break or change any block because of the robust mechanism (via consensual agreement) of linking a new partnership and sharing a new copy of the blockchain between participants (nodes) [3].

It is interesting to combine IoT and blockchain technologies to perform various transactions in bright areas, including IoT devices [5], [6], [11]. While it is not viable for IoT devices to act as hubs or miners due to their insufficient memory and computing resources, it is feasible for them to connect to their cryptocurrency accounts linked with their symmetric encryption to engage in and sign transactions. The rest of the blockchain participants will be able to trace the connected devices and their information/actions, boosting their security. The well-known blockchain consideration requires security, decentralization, and scalability all at the same time, manifests itself when a large number of blocks and objects (whether they be IoT devices or not) must be managed [11].

Table 1: Fungible Token Vs Non-Fungible Token.

Technologies	**Standard**	**Examples**	**Properties**	**Content**
Fungible token	ERC-20	Bitcoin, currency, gold	Interchangeable, Non-unique, and divisible	Stores content
Non-fungible token	ERC-721	Artwork and Ticket	Non-Interchangeable, unique, indivisible nature, and distinction	Stores data

Smart contracts are a mechanism for participants in the new generation of blockchain technology to establish agreements. Typical agreements call for a fungible token representing a coin with characteristics (i.e., its owner) and functionalities (such as the method for changing the owner). The same fungible token is split into smaller parts and identical (like coins with different values). In contrast, Non-fungible token (NFT) has recently been utilized to demonstrate distinct assets (such as collectibles, certificates of any type, access rights of any kind, artifacts, and so on). An NFT is distinct from other tokens of the same type because it is one-of-a-kind, indivisible, and unique as shown in table I. The ERC-721 standard, in particular, explains how to create non-fungible tickets on the Ethereum network [12]. The following are standard ERC-721: NFT has three attributes: the token identifier (TkId), the

NFT owner's blockchain account (BCA), and the owner's authorized BCA to transfer the token to another buyer. TkId is a unique digital identifier that allows an NFT to be recorded and tracked on the blockchain. On the other hand, the TkId should not be linked to a physical attribute. In reality, when the ERC-721 NFT is established, it generates it automatically [12].

D. Fungible token (FT) and Non-fungible token (NFT)

The distinction between FT and NFT is an ancient one in economics. In the Middle Ages, English monks employed tokens known as "Abbot's money" to pay for services rendered by foreigners [13]. Understanding the notion of fungibility in economics may aid the understanding of FT and NFT tokens. The main distinction is that crypto tokens use a coding script to represent their fungibility. Tokens or assets that are fungible are divisible and non-unique. Currencies, such as the US dollar, are fungible in the following ways: In New York City, a dollar bill is worth the same as a dollar bill in any city in the United States. An FT can also be a cryptocurrency, such as Bitcoin (BTC), in which 1 BTC is equivalent to 1 BTC regardless of the country of its issuance [13]. Another example of a fungible token is a cryptocurrency, such as Bitcoin, in which one Bitcoin is valued regardless of where it is produced. On the other side, Non-fungible tokens are unique and cannot be divided. They should be recognized as a category of property or ownership title for a unique and non- duplicatable object. A train ticket, for instance, is non-fungible because it contains unique data that cannot be duplicated. Because they are one-of-a-kind, a home, a boat, or a vehicle are non-fungible physical assets [13].

Non-fungible tokens, like photographs or intellectual property, represent a single unique and indivisible entity – physical or intangible. Blockchain technology is the foundation for proving digital intangibles ownership property. The critical distinction between fungible and nonfungible assets is the content they contain. FT, such as Bitcoin, holds value, while NFT, such as a monograph title or a piece of art, stores data [13].

ERC (Ethereum Request for Comments) was developed by the Ethereum community, which has two standards, namely ERC-20 standard for FTs and ERC-721 standard for NFTs. An essential feature of an ERC-721 NFT is its owner, uniquely recognized by its blockchain account address. The first FT, ERC-20, was created on the Ethereum network. They establish the guidelines that enable developers to create a variety of apps. NTF, on the other side, had existed since 2012, when the notion of colored coins was introduced to the Bitcoin community for the first time. The ERC-721 standard on the Ethereum blockchain explicitly explains how to produce NFTs due to their uniqueness, indivisible nature, and distinction from other tokens of the same sort [3].

1) Physical Unclonable Functions (PUFs): PUFs were first described as a cryptographic primitive in 2001 and maybe thought of as the physical counterpart of a one-way operation [15]. Even if the same manufacturing process is repeated, a silicon PUF is a solid object encapsulated in a spatial form that is easy to make but difficult to clone, replicate, or anticipate [14]. The authentication mechanism of PUFs is based on challenge-response pairs rather than a private key associated with the device identity. Due to the complicated interaction between the stimulus and the machine's physical microstructure, which is unpredictable and unclonable in nature, an electrical stimulus, referred to as the challenge, is applied to the physical structure to react as the response unexpectedly. PUFs have a low hardware overhead, making them ideal for the Internet of Things. PUFs have

previously been used on devices, including device identification and authentication, software platform linking, secure key management, and secure contactless connection. The usage of PUFs for device identification is shown in Figure 2 since they may be considered the device's biometric template [14].

PUF protocol is used by Chatterjee et al. [16] to secure communication between IoT objects connected in the same domain server, where several challenge-response pairs (CRPs) for each node have securely stored in the server. The proposed scheme consists of a PUF based vital agreement and a secure communication mechanism. The proposed approach comprises a protocol for crucial deals based on PUFs and a protocol for secure communication. The PUF generates each device's public key in the key agreement protocol.

According to Brussel et al. [14], PUF protocol is vulnerable to impersonation, replay, and MIM attacks. Additionally, they provided a more efficient PUF-based methodology for the critical agreement step. Furthermore, they demonstrate more efficient alternatives in the literature for the secure communication session than the suggested one. Similar to [14], many challenges and replies are kept at the server's setup session and utilized during the critical agreement session to generate a public key that is certified by the authentication server.

PUFs are classified as either strong or weak. The difference is made owing to the maximum number of possible responses. A strong PUF can produce many CRPs, while a weak PUF can generate just one or two [14].

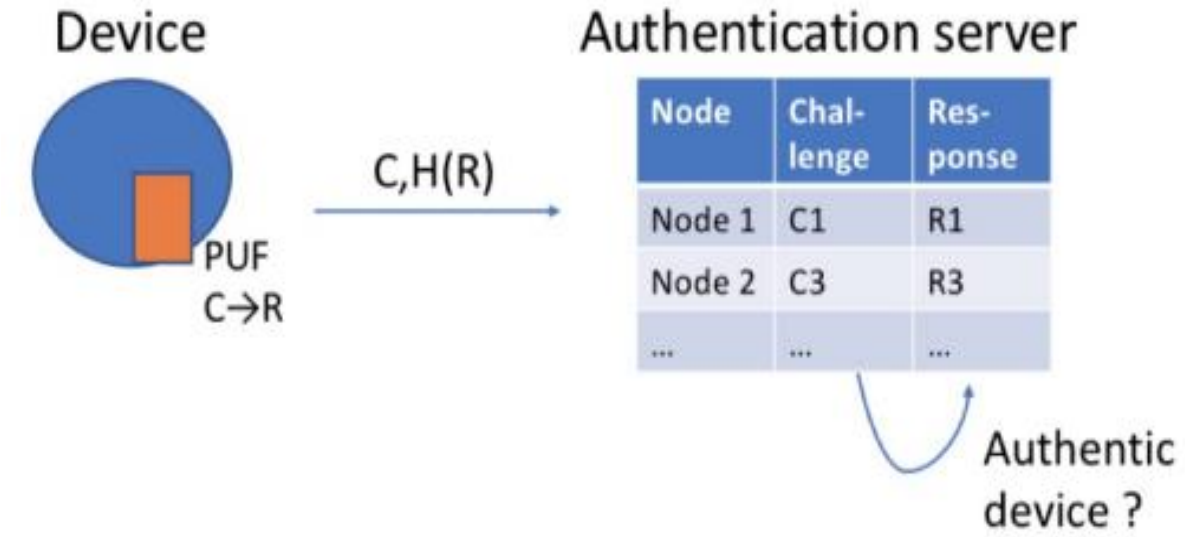

Fig. 2. Example of Physical Unclonable Functions (PUFs) usage for device identification (C = Challenge, R = Response).

II. APPLICATIONS OF NON-FUNGIBLE TOKENS (NFTS) FOR IOT SECURITY

IoT nodes are clustered into IoT systems (such as smart supply chain models, smart shelters, and so on), and each arrangement is connected to a nearby blockchain-enabled fog module. A smart contract for distributed validation and authorization of IoT devices is built on the base of a blockchain-based fog module. If blockchain-enabled fog nodes register and authenticate IoT devices, they can connect with one another in this idea. The device id, device public address, and IoT device identity are all incorporated in the certifications tokens. Therefore, the unique identification of the IoT devices is essential

for providing security to the IoT devices handled using NFT. Following are the attributes that are necessary for NFT to be used for IoT security:

1) Authenticity: The standardized NFT makes each token independently distinct and genuine, and the token metadata may be recorded in a blockchain, making them immutable and credible, thanks to the use of blockchain and smart contracts. There is no efficient way to reproduce or duplicate a token once it is stored on the blockchain, which helps to prevent fraud and protect intellectual property. Furthermore, due to the openness of blockchain, each NFT's legitimacy can be verified and proven. As a result, when NFT and blockchain are combined, forgery and deception may be successfully combated in a number of industrial applications, including art and collectibles.

2) Ownership: Uniqueness and ownership are at the heart of NFT, and a token is necessary to verify ownership of an item. Because of the smart contracts and associated rights, an NFT can only be traded and transferred by the asset's owner (rather than the issuer's owner). Without the owner's consent, even the issuer of an NFT cannot copy or transmit the NFT. On a blockchain, an NFT token can monitor ownership and, as a result, authenticity, proving possession irrefutably. For instance, the ERC-721 specification defines the bare minimum of interfaces, which contain proof of ownership, safety, and ownership is passed to the entity's owner.

3) Transferability: NFTs must be decentralized, and no centralized authority can regulate how these tokens are exchanged between blockchain systems. A single NFT generally belongs to just one proprietor at a time, and its specific data format makes it simple to verify ownership and transfer the token between owners [14]. Special information can be stored in them by the creator's owner to identify ownership, allowing NFTs to be transferred. Moreover, millions of people now have simple access to NFT tokens, which they may trade for other cryptocurrencies, owing to the blockchain.

III. DISCUSSION

Apart from available attributes in the NFT, various possible attacks on NFT need to be addressed to make it secure for IoT applications. Such risks include spoofing, tampering, repudiation, data exposure, DoS, and privilege escalation, to name a few. These attacks need to be handled for better security of the NFT and, consequently, the IoT devices. Table 2 below provides a list of attack types on NFT and related security issues that will come with these attacks along with possible solutions for each attack. These solutions can be effective in countering the security threats on the NFT and make it secure and reliable.

Table 2: Type of possible attacks on NFT and list of solutions.

Attack Type	**Security Issues**	**Solution**
Privilege Escalation	• If a smart contract is badly designed, FTs may lose their features.	• Systematic verification of smart contracts is required.
Spoofing	• An attacker could take advantage of authentication flaws. • A user's private key could be stolen by an attacker.	• The smart contract is subjected to validation. • Using the cold wallet to prevent private key leakage.
Tampering	• Data held outside the blockchain can be tampered with.	• While exchanging NFTs, provide both original and hash data to the NFT purchaser.
Information disclosure	• An adversary can easily connect a specific FT purchaser using the hash and transactions.	• Protecting the user's privacy by using privacy-preserving smart contracts.
Repudiation	• The hash value could be linked to the address of an intruder.	• Partially to use a multi-signature contract.
DoS	• If the assets are kept outside of the blockchain, the FT data may become inaccessible.	• Using a weak consensus method and a hybrid blockchain architecture.

IV. CONCLUSION

This paper discusses how blockchain and NFT can be used for providing security to resource-constrained IoT devices. It starts with the review of the technicalities of IoT networks and analyses the security issue with the IoT networks at each layer. Further, this paper reviews the blockchain technology and tokenization concepts in the form of fungible and non-fungible tokens (NFT). Finally, it discusses the role of NFT for IoT security and its desired attributes. This paper concludes that NFT can be effectively used for device authentication which is a prerequisite for the authentication and security of IoT devices. Still, there are various possible attacks on the NFT that need to be addressed while using them for IoT security. The related security issues to these attacks and possible solutions to these attacks have been given in this study for making the NFT applications secure.

ACKNOWLEDGMENT

The author would like to express the most significant appreciation to the Deanship of Scientific Research (DSR), Jazan University, Jazan, for this publication's financial support.

REFERENCES

[1]. Abomhara, M. & Køien, G. Security and privacy in the Internet of Things: Current status and open issues. *2014 International Conference On Privacy And Security In Mobile Systems (PRISMS)*. pp. 1-8 (2014)

[2]. Arcenegui, J., Arjona, R., Roman, R. & Baturone, I. Secure Combination of IoT and Blockchain by Physically Binding IoT Devices to Smart Non-Fungible ´ Tokens Using PUFs. *Sensors*. 21, 3119 (2021)

[3]. Arcenegui, J., Arjona, R. & Baturone, I. Secure management of IoT devices based on blockchain non-fungible tokens and physical unclonable functions. *International Conference On Applied Cryptography And Network Security*. pp. 24-40 (2020)

[4]. Mahmoud, R., Yousuf, T., Aloul, F. & Zualkernan, I. Internet of things (IoT) security: Current status, challenges and prospective measures. *2015 10th International Conference For Internet Technology And Secured Transactions (ICITST)*. pp. 336-341 (2015)

[5]. Zhao, K. & Ge, L. A survey on the internet of things security. *2013 Ninth International Conference On Computational Intelligence And Security*. pp. 663-667 (2013)

[6]. Atzori, L., Iera, A., Morabito, G. & Nitti, M. The social internet of things (siot)–when social networks meet the internet of things: Concept, architecture and network characterization. *Computer Networks*. 56, 3594-3608 (2012)

[7]. Leo, M., Battisti, F., Carli, M. & Neri, A. A federated architecture approach for Internet of Things security. *2014 Euro Med Telco Conference (EMTC)*. pp. 1-5 (2014)

[8]. Wen, Q., Dong, X. & Zhang, R. Application of dynamic variable cipher security certificate in internet of things. *2012 IEEE 2nd International Conference On Cloud Computing And Intelligence Systems*. 3 pp. 1062-1066 (2012)

[9]. Farooq, M., Waseem, M., Mazhar, S., Khairi, A. & Kamal, T. A review on internet of things (IoT). *International Journal Of Computer Applications*. 113, 1-7 (2015)

[10]. Roman, R., Najera, P. & Lopez, J. Securing the internet of things. *Computer*. 44, 51-58 (2011)

[11]. Network Raiden. https://raiden.network/. Accessed: 19 Aug 2020

[12]. ERC-721. http://www.erc721.org. Accessed: 19 Aug 2020

[13]. Cointelegraph. https://cointelegraph.com/. Accessed: 19 Aug 2020

[14]. Braeken, A. PUF based authentication protocol for IoT. *Symmetry*. 10, 352 (2018)

[15]. Pappu, R. Physical One-Way Functions. Massachusetts Ave. *Massachusetts Institute Of Technology*. (2001)

[16]. Chatterjee, U., Chakraborty, R. & Mukhopadhyay, D. A PUF-based secure communication protocol for IoT. *ACM Transactions On Embedded Computing Systems (TECS)*. 16, 1-25 (2017)

الرموز الغير قابلة للاستبدال المستندة الى سلاسل الامداد الأمان انترنت الاشياء

فيصل الشنقيطي

قسم علوم الحاسب، جامعة جازان، المملكة العربية السعودية

الملخص

تُستخدم أجهزة إنترنت الأشياء في مجالات مختلفة وتتزايد أعدادها بشكل كبير. أصبحت أجهزة إنترنت الأشياء جزءًا من حياتنا اليومية وهي تتسلل إلى عملنا اليومي. على الرغم من أن تطبيقات أجهزة استشعار إنترنت الأشياء هذه توفر الكثير من الحلول القيمة ، إلا أن أمانها لا يزال مصدر قلق كبير بسبب موارد الأجهزة المحدودة. يتم اقتراح تقنية تقنية البلوكشين في مجالات مختلفة لتوفير الأمن والثبات للنظام والبيانات ويتم تطبيقها أيضًا في حالة توفير الأمان لأجهزة إنترنت الأشياء. هناك العديد من الاختلافات والتطبيقات لتكنولوجيا البلوكشين. الرموز غير قابلة للاستبدال (ان اف تي) هي واحدة من التطبيقات البارزة والمتنامية. الرموز المميزة غير القابلة للاستبدال هي رموز فريدة مشفرة مرتبطة بالمحتوى الرقمي (وأحيانًا المادي) ، مما يوفر دليلًا على الملكية. في هذه الورقة ، سنبحث في تطبيقات (ان اف تي) توفير الأمن للبنية التحتية لإنترنت الأشياء ونقترح حلًا.

Design, synthesis and characterization of new triazolopyrimidine and triazolopyridine derivatives containing a sulfonamide moiety

Ibrahim Ali Radini

Chemistry Department, Faculty of Science, Jazan University, Kingdom of Saudi Arabia.

Abstract

A new series of fused [1,2,3] triazolo[4,5-d]pyrimidine derivatives containing sulfonamide moiety was synthesized. Click reaction of azide **2** with malononitrile in the presence of catalytic amount of piperidine gave the corresponding o-aminonitrile 1,2,3-triazole derivative **3**. Treatment of compound **3** with various reagents (formic acid, acetic acid, formamide, carbon disulfide) afforded the corresponding [1,2,3] triazolo[4,5-d]pyrimidine derivatives. While the Click reaction of azide **2** with malononitrile dimer furnished the corresponding 1,2,3-triazolopyridine derivative **9**. Reaction of **3** with dimethylformamide-dimethylacetal (DMF-DMA) or triethylorthoformat gave the corresponding bis-enamine derivative which stirred with hydrazine hydrate at room temperature giving triazolopyrimidine derivative **12**. Treatment of **3** with ethylene diamine in the presence of carbon disulfide as a catalyst afforded imidazolinyl derivative which was subjected to cyclization reaction with carbon disulfide to afford imidazo[1,2-c][1,2,3]triazolo[4,5-e]pyrimidine derivative (**15**).

Keywords: Azide, Triazole, Sulfonamide, Pyrimidine, triazolopyrimidine.

1. INTRODUCTION

Pyrimidine nucleus is one of the most privileged building blocks in drug discovery. Pyrimidines, are widely found as the core structure in a large variety of compounds of highly biological and pharmaceutical activity exhibiting anticancer,(Yousif et al., 2017) antiviral,(El-Sayed et al., 2009) anti-inflammatory(Falcao et al., 2006) and antibacterial activities.(Fathalla et al., 2009) Fused pyrimidines are found in various natural products (e.g., purines), agrochemicals, and veterinary products(Roth and Cheng 1982, Brown 1984, Petrie et al., 1985) and continue to attract much interest due to the wide variety of interesting biological activities observed for these compounds, such as anticancer,(ABD EL-AAL EL-GABY et al., 1999) antiviral,(Nasr and Gineinah 2002) antitumor,(Baraldi et al., 2002) anti-inflammatory,(Sondhi et al., 2001) antifungal,(Mangalagiu et al., 2001) antihistaminic,(Shishoo et al., 2001) and analgesic(Bruno et al., 2002) activities.

Triazoles are known to exhibit broad spectrum of applications in biochemical and medicinal chemistry(Singh et al., 2018) and known as antimicrobial,(Rajasekaran et al., 2006, Wang et al., 2010, Gupta and Jain 2015) anti-inflammatory,(Paprocka et al., 2015) anti-convulsant,(Rajasekaran et al., 2006) antimalarial,(Jarrahpour et al., 2018) antiviral,(Kharb et al., 2011, He et al., 2014) anti-proliferative,(Bollu et al., 2015, Fu et al., 2017) as carbonic anhydrase inhibitors,(Vats et al., 2018) and anticancer agent.(Yan et al., 2010, Ma et al., 2012, Abd-Rabou et al., 2018) In addition, 1, 2, 3-triazolo[4, 5-d]pyrimidine derivatives (comprising of triazole and pyrimidine moieties) are an important class of heterocyclic compounds with renown biological activities which attract the attention of medicinal community in their exploration as anti-inflammatory,(Lazrak et al., 2002, Lazrak et al., 2004) anticancer,(Song and Deng 2018) antimicrobial,(Basu and Rose 1963, Wu et al., 2018) diuretics,(Kumar et al., 2008) analgesics(El-wassimy et al., 1992, Singh et al., 2018) and antioxidant.(Mavrova et al., 2014)

Moreover, sulfa drugs, also called sulfonamides, are extensively used for the treatment of several diseases including antibacterial,(Hansch et al., 1989) antifungal,(Stokes et al., 2012) anti-inflammatory,(Li et al., 1995) antiprotozoal,(Chibale et al., 2001) antihypertensive agent bosentan,(Kanda et al., 2001) nonpeptidic vasopressin receptor antagonists,(Natarajan et al., 2004) and translation initiation inhibitors.(Serradeil-

Le 2001) Sulfonamides are also effective for the treatment of urinary, intestine, and ophthalmic infections, scalds, ulcerative colitis(Kołaczek et al., 2014) and obesity.(Hu et al., 2001) Recently, sulfonamides are performed as an anticancer agent(Ma et al., 2015) and in Alzheimer's disease.(Kołaczek et al., 2014) Based on all previous commentaries of the importance in pharmaceutical and biological field of pyrimidine, 1,2,3-triazole and sulfonamide derivatives and in continuation of our ongoing interest in the synthesis of biologically active heterocycles, (Khidre and Radini 2019, Khidre and Radini 2021) it was thought interest hybrid pyrimidine, triazole and sulfonamide moieties in a single molecular frame work to synthesize some new heterocyclic compounds with potential biological activity.

2. Experimental

Melting points were obtained on a digital Gallenkamp MFB-595 melting point apparatus. ^{1}H NMR (500 MHz) and ^{13}C NMR (125 MHz) spectra were performed on BRUKER ultra-shield Avance III spectrometer using (TMS) as an internal stander and DMSO-d_6 as solvents. Chemical shifts were expressed as δ ppm. The IR spectra were performed on Shimadzu FTIR-440 spectrophotometer (KBr pellet). The electron impact (EI) mass spectra were performed on a Shimadzu GCMS-QP 1000 EX mass spectrometer at 70 eV. The Elemental analyses were performed on a PERKIN-ELMER 2400 C, H Elemental Analyzer were done at the Microanalytical Center, Cairo University, Cairo, Egypt.

4-(5-amino-4-cyano-1H-1,2,3-triazol-1-yl)benzenesulfonamide (**3**).

A mixture of Azide compound **2** (10 g, 0.05 mol) and malononitrile (3.3 g, 0.05 mol) in absolute ethanol (100 ml) containing piperidine (1 ml) was refluxed on water bath for 2 h. The precipitated solid was filtered off and crystallized from acetic acid to give **3**. Yield 11.6 g (87 %); m.p.:>300^{o}C (El-Gazzar et al., 2018), m.p. 100-101 ^{o}C]. IR (KBr, *v*, cm^{-1}): 3335, 3258 (NH_2), 2243 (CN), 1600 (C=C aromatic),1340, 1153 (SO_2). ^{1}H-NMR (500 MHz, *δ*, ppm, DMSO-d6): 8.02 (d, 2H, *J* = 8.5 Hz, Ar–H), 7.80 (d, 2H, *J* = 8.5 Hz, Ar–H), 7.51-7.32 (br, 4H, $SO_2\underline{NH_2}$, $\underline{NH_2}$, D_2O exch.); ^{13}C-NMR (125 MHz, *δ*, ppm, DMSO-d_6): 148.1, 144.9, 136.5, 127.4 (2C), 125.3 (2C), 113.4, 101.6; MS, *m/z* (%): 264 [M+] (10), 210 (52), 198 (35), 197 (45), 169 (33), 130 (89), 129 (100). Anal. Calcd for $C_9H_8N_6O_2S$: C, 40.91; H, 3.05; N, 31.80 Found C, 41.10; H, 3.10; N, 31.92.

4-(7-oxo-6,7-dihydro-3H-[1,2,3]triazolo[4,5-d]pyrimidin-3-yl)benzenesulfonamide (**4**).

A suspension of **3** (2.64 g, 0.01 mol) in formic acid (85%; 20 ml) was heated at reflux temperature for 10 h. The obtained solid product was filtered off and recrystallized from DMF to yield **4** as a grey powder. Yield 2.0 g (64.5 %), m.p ٢٣٨-٢٤٠°C, IR (KBr, *v*, cm^{-1}): 3447 (NH), 3344, 3336 (NH_2), 1661 (CO), 1590 (C=C aromatic),1317, 1160 (SO_2). ^{1}H-NMR (500 MHz, *δ*, ppm, DMSO- d_6): 9.0 (s, 1H, CONH, D_2O exch.), 7.97 (s, 1H, $H_{pyrimidine}$), 7.73 (d, 2H, *J* = 8.5 Hz, Ar–H), 7.68 (d, 2H, *J* = 8.5 Hz, Ar–H), 7.16 (s, 2H, SO_2NH_2, D_2O exch.); ^{13}C-NMR (125 MHz, *δ*, ppm, DMSO- d_6): 164.3 (CO), 162.6, 148.6, 144.2, 135.2, 127.5 (2C), 125.9, 115.7 (2C); MS, *m/z* (%): 292 [M+] (15), 282 (100), 210 (17), 201 (38). Anal. Calcd for $C_{10}H_8N_6O_3S$: C, 41.10; H, 2.76; N, 28.75 Found C, 41.10; H, 3.0; N, 28.90.

4-(5-methyl-7-oxo-6,7-dihydro-3H-[1,2,3]triazolo[4,5-d]pyrimidin-3-yl)benzenesulfonamide (**5**).

A suspension of **3** (2.64 g, 0.01 mol) in acetic acid (20 ml) was heated at reflux temperature for 10 h. The obtained solid product was filtered off and recrystallized from DMF to yield **5** as a white powder. Yield 2.0 g (64.5 %), m.p ٢٤٠-٢٤٢°C, IR (KBr, *v*, cm^{-1}): 3252 (NH), 3212, 3189 (NH_2), 1712 (CO), 1595 (C=C aromatic),1205, 1163 (SO_2). ^{1}H-NMR (500 MHz, *δ*, ppm, DMSO- d_6): 10.0 (s, 1H, CONH, D_2O exch.), 7.87 (d, 2H, *J* = 8.5 Hz, Ar–H), 7.81 (d, 2H, *J* = 8.5 Hz, Ar–H), 7.56 (s, 2H, SO_2NH_2, D_2O exch.), 1.90 (s, 3H, CH_3); ^{13}C-NMR (125 MHz, *δ*, ppm, DMSO- d_6): 172.1 (CO), 168.5, 145.9, 130.0, 129.4 (2C), 115.6 (2C), 113.8, 108.1, 22.9; MS, *m/z* (%): 306 [M+] (2), 279 (12), 237 (20), 215 (100). Anal. Calcd for $C_{11}H_{10}N_6O_3S$: C, 43.13; H, 3.29; N, 27.44 Found C, 43.40; H, 3.1; N, 27.60.

4-(5,7-dithioxo-4,5,6,7-tetrahydro-3H-[1,2,3]triazolo[4,5-d]pyrimidin-3-yl)benzenesulfonamide (**7**).

To a solution of **3** (2.64 g, 0.01 mol) in 10% alcoholic KOH (10 ml), carbon disulfide (10 ml) was added dropwise. The reaction mixture was refluxed for 3 h, cooled, poured onto cold water and neutralized with 1M HCl. The solid product was filtered off, washed with water, dried and recrystallized from DMF to afford **7** as a yellow powder. Yield 2.5 g (73.5 %), m.p ١٨٥-١٨٧°C; IR (KBr, *v*, cm^{-1}): 3421 (NH), 3331 (NH), 3289, 3211 (NH_2), 1629 (C=C aromatic),1312, 1161 (SO_2). ^{1}H-NMR (500 MHz, *δ*, ppm, DMSO- d_6): 15.07 (s, 1H, NH, D_2O exch.), 8.54 (s, 1H, NH, D_2O exch.), 7.76 (d, 2H, *J* = 8.5 Hz, Ar–H), 7.66 (d, 2H, *J* = 8.5 Hz, Ar–H), 7.22 (s, 2H, SO_2NH_2, D_2O exch.); ^{13}C-NMR (125 MHz, *δ*, ppm, DMSO- d_6): 163.4, 149.1, 144.1, 144.0, 135.4, 135.1, 127.3, 127.1, 115.9, 115.5; MS, *m/z* (%): 340 [M+] (2), 240 (10), 239 (100), 223

(34), 156 (89). Anal. Calcd for $C_{10}H_8N_6O_2S_3$: C, 35.29; H, 2.37; N, 24.69 Found C, 35.40; H, 2.52; N, 25.0.

4-(7-amino-3H-[1,2,3]triazolo[4,5-d]pyrimidin-3-yl)benzenesulfonamide (**8**).

A solution of **3** (2.64 g, 0.01 mol) in formamide (10 ml) in DMF (10 ml) was refluxed for 3 hours. The solution was cooled to room temperature and diluted with 100 ml ice-cooled water and the obtained precipitate was filtered off and recrystallized from ethanol to give **8** as a brown powder. Yield 2.4 g (82.5%), m.p 147-148 °C; IR (KBr, *v*, cm^{-1}): 3447, 3387 (NH_2), 3344, 3222 (NH_2), 1590 (C=C aromatic),1317, 1160 (SO_2). ^{1}H-NMR (500 MHz, *δ*, ppm, DMSO- d_6): 8.21 (s, 1H, $H_{pyrimidine}$), 7.82 (d, 2H, *J* = 8.5 Hz, Ar–H), 7.75 (d, 2H, *J* = 8.5 Hz, Ar–H), 7.0 (s, 2H, $SO_2\underline{NH_2}$, D_2O exch.), 6.70 (s, 2H, NH_2, D_2O exch.).

4-(5,7-diamino-6-cyano-3H-[1,2,3]triazolo[4,5-b]pyridin-3-yl)benzenesulfonamide (**9**).

Method 1: A mixture of Azide compound **2** (9.9 g, 0.05 mol) and malononitrile dimer (6.6 g, 0.05 mol) in absolute ethanol (100 ml) containing piperidine (1 ml) was refluxed on water bath for 2 h. The obtained solid product was filtered off and recrystallized from acetic acid to give **9** as brown powder. Yield 15.0 g (90.1 %).

Method 2: A mixture of **3** (2.64 g, 0.01 mol) and malononitrile (0.66 g, 0.01 mol) in DMF (30 ml) containing triethyl amine (0.5 ml) was refluxed for 6 h. The obtained solid product was filtered off and recrystallized from acetic acid to give **9** as brown powder. Yield 1.8 g (54 %), m.p >300°C; IR (KBr, *v*, cm^{-1}): 3525, 3431 (NH_2), 3387, 3366 (NH_2), 3250, 3202 (NH_2), 2207 (CN), 1602 (C=C aromatic),1381, 1161 (SO_2). ^{1}H-NMR (500 MHz, *δ*, ppm, DMSO- d_6): 8.35 (d, 2H, *J* = 8.5 Hz, Ar–H), 8.0 (d, 2H, *J* = 8.5 Hz, Ar–H), 7.50 (s, 4H, $2NH_2$, D_2O exch.), 7.01 (s, 2H, NH_2, D_2O exch.); ^{13}C-NMR (125 MHz, *δ*, ppm, DMSO- d_6): 162.4, 151.3, 147.6, 142.8, 138.7, 127.1 (2C), 125.0, 123.0 (2C), 116.1 (CN), 70.2; MS, *m/z* (%): 330 [M+] (9). Anal. Calcd for $C_{12}H_{10}N_8O_2S$: C, 43.63; H, 3.05; N, 33.92 Found C, 43.80; H, 3.2; N, 34.1.

(E)-N'-(4-cyano-1-(4-(N-((E)-(dimethylamino)methylene)sulfamoyl)phenyl)-1H-1,2,3-triazol-5-yl)-N,N-dimethylformimidamide (**10**).

To a well-stirred solution of **3** (2.64 g, 0.01 mol) in dioxane, excess dimethylformamide dimethylacetal (DMF-DMA) was added gradually. Stirring was continued for 2 h at room temperature. The mixture was refluxed for 3 h and cooled to room temperature. The solid product was filtered off and recrystallized from dioxane to give **10** as white crystals. Yield 3.7 g (99 %), m.p ٢٢٠-٢٢٢°C; IR (KBr, *v*, cm^{-1}): 2226 (CN), 1631 (N=C), 1584 (C=C

aromatic),1335, 1153 (SO_2). ^{1}H-NMR (500 MHz, δ, ppm, DMSO- d_6): 8.34 (s, 1H, N=CH), 8.26 (s, 1H, N=CH), 7.98 (d, 2H, J = 8.5 Hz, Ar–H), 7.96 (d, 2H, J = 8.5 Hz, Ar–H), 3.16 (s, 3H, CH_3), 3.15 (s, 3H, CH_3), 3.0 (s, 3H, CH_3), 2.92 (s, 3H, CH_3); ^{13}C-NMR (125 MHz, δ, ppm, DMSO- d_6): 160.0, 157.6, 151.7, 142.8, 137.5, 127.1 (2C), 123.6 (2C), 114.1 (CN), 106.0, 41.0, 40.5, 35.2, 34.5; MS, *m/z* (%): 374 [M+] (24), 346 (18), 211 (100), 210 (86). Anal. Calcd for $C_{15}H_{18}N_8O_2S$: C, 48.12; H, 4.85; N, 29.93 Found C, 48.40; H, 5.1; N, 30.2.

4-(6-amino-7-imino-6,7-dihydro-3H-[1,2,3]triazolo[4,5-d]pyrimidin-3-yl)benzenesulfonamide (**12**).

Method 1: To a well-stirred solution of **10** (3.74 g, 0.01 mol) in ethanol (30 ml), hydrazine hydrate (5 ml) was added gradually. Stirring was continued for 6 h at room temperature. The solid product was filtered off and recrystallized from dioxane to give **12** as brown crystals. Yield 1.9 g (62 %),

Method 2: To a well-stirred solution of **13** (3.76 g, 0.01 mol) in ethanol (30 ml), hydrazine hydrate (5 ml) was added gradually. Stirring was continued for 6 h at room temperature. The solid product was filtered off and recrystallized from dioxane to give **12** as brown crystals. Yield 1.3 g (42 %).

m.p 178-181°C; IR (KBr, v, cm^{-1}): 3451 (NH), 3339, 3298 (NH_2), 3201, 3156 (NH_2),1651 (C=N), 1599 (C=C aromatic), 1321, 1151 (SO_2). ^{1}H-NMR (500 MHz, δ, ppm, DMSO- d_6): 8.36 (s, 1H, C=NH, D_2O exch.), 7.84 (s, 1H, $H_{pyrimidine}$), 7.55 (d, 2H, J = 8.5 Hz, Ar–H), 7.04 (s, 2H, NH_2, D_2O exch.), 6.66 (d, 2H, J = 8.5 Hz, Ar–H), 5.71 (s, 2H, SO_2NH_2, D_2O exch.); ^{13}C-NMR (125 MHz, δ, ppm, DMSO- d_6): 145.8, 140.0, 134.9, 133.4, 127.3, 126.6 (2C), 122.2, 115.0 (2C); MS, *m/z* (%): 306 [M+] (4), 172 (100). Anal. Calcd for $C_{10}H_{10}N_8O_2S$: C, 39.21; H, 3.29; N, 36.58 Found C, 38.8; H, 3.11; N, 36.80.

ethyl (E)-N-(4-cyano-1-(4-(N-((E)-ethoxymethylene)sulfamoyl)phenyl)-1H-1,2,3-triazol-5-yl)formimidate (**13**).

To a mixture of triethylorthoformate (1.48 g, 0.01 mol) and acetic anhydride (20 ml), compound **3** (2.64 g, 0.01 mol) was added and the reaction mixture was refluxed for 5h. The solvent was removed under reduced pressure. Gummy product was purified through column chromatography by eluting with 50% of a mixture of petroleum ether 40–60 and ethyl acetate to afford **13** Yield 1.7 g (45 %); m.p 87-89°C, IR (v, cm^{-1}): 2231 (CN), 1630 (N=C), 1592 (C=C aromatic),1321, 1161 (SO_2). ^{1}H-NMR (500 MHz, δ, ppm, DMSO- d_6): 8.42 (s, 1H, N=CH), 8.26 (s, 1H, N=CH), 8.12 (d, 2H, J = 8.5 Hz, Ar–H), 7.96 (d, 2H, J = 8.5 Hz, Ar–H), 4.16 (q, 4H, J = 6.5 Hz, $2CH_2$), 1.15 (t, 6H, J = 6.5 Hz, $2CH_3$).

General procedures for the reaction of 10 with primary amines.

A mixture of compound **10** (3.74 g, 0.01 mol) and primary amines, (ammonia, hydrazine hydrate and ethanol amine), (0.01 mol) in DMF (20 mL) was heated under reflux for 2 h. The reaction mixture was cooled, poured onto cold water, the brown precipitate formed was filtered off and dried. to afford **3** as brown powder.

4-(5-amino-4-(4,5-dihydro-1H-imidazol-2-yl)-1H-1,2,3-triazol-1-yl)benzenesulfonamide (**14**).

A mixture of **3** (2.64 g, 0.01 mol) in ethylenediamine (7 ml) and carbon disulfide (1 ml) was heated on a water bath for 8 h. After cooling the reaction mixture was diluted with an ice-water. The precipitate formed was filtered off, washed with H_2O, and recrystallized from ethanol to give **14** as brown crystals. Yield 2.6 g (85 %); m.p 272-275°C [lit.[51] m.p 278-280°C].

4-(5-thioxo-4,5,7,8-tetrahydro-3H-imidazo[1,2-c][1,2,3]triazolo[4,5-e]pyrimidin-3-yl)benzenesulfonamide (**15**).

A mixture of **14** (3.07 g, 0.01mol) and (7 ml) and carbon disulfide in pyridine (20 ml) was heated on a water bath for 8 h. After cooling the reaction mixture was diluted with an ice-water and neutralized with dil. HCl. The precipitate formed was filtered off, washed with H_2O, and recrystallized from ethanol to give **15** as brown crystals. Yield 2.6 g (85 %); m.p > 300°C; IR (KBr, ν, cm^{-1}) : 3425 (NH), 338, 3238 (NH_2), 1317, 1230 (SO_2). ^{1}H-NMR (500 MHz, δ, ppm, DMSO- d_6): 9.87 (s, 1H, NH, D_2O exch.), 7.98 (d, 2H, J = 8.5 Hz, Ar–H), 7.93 (d, 2H, J = 8.5 Hz, Ar–H), 7.23 (s, 2H, $SO_2\underline{NH_2}$, D_2O exch.), 3.48 (s, 4H, $H_{imidazole}$); MS, m/z (%): 349 [M+] (2), 187 (27), 171 (18), 170 (28).

3. RESULTS AND DISCUSSION

4-azido benzenesulfonamide **2** was prepared according to literature procedure through the diazotization of the sulfonamide **1** followed by treatment with sodium azide. (Batra et al., 2015) (Batra et al., 2015) (Batra et al., 2015) (Batra et al., 2015) (Batra et al., 2015) (Batra et al., 2015) (Batra et al., 2015) (Batra et al., 2015). Click reaction of azide **2** with malononitrile in absolute ethanol in the presence of catalytic amount of piperidine at reflux temperature afforded 4-(5-amino-4-cyano-1H-1,2,3-triazol-1-yl)benzenesulfonamide (**3**), in a good yield (El-Gazzar et al., 2018). Reported melting point of compound **3** in literature is 100-101 ^oC, but our melting point was fixed above 300 ^oC. This discrepancy in melting point encourage us to perform the spectral data of compound **3**. The structure of **3** was confirmed by appearance the new two absorption bands related to NH_2 and CN

functions at 3335, 3258 and 2243 cm^{-1} respectively in IR spectrum. The ^1H NMR spectrum of **3** revealed that two NH_2 groups as broad band exchangeable with D_2O at δ 7.51-7.32 ppm for SO_2NH_2 and NH_2, while the aromatic protons appears as two doublet signals at δ 8.02 and 7.80 ppm with coupling constant J = 8.5 Hz.

Reaction of **3** with formic acid at reflux temperature yielded 4-(7-oxo-6,7-dihydro-3H-[1,2,3]triazolo[4,5-d]pyrimidin-3-yl)benzenesulfonamide (**4**). the structure of **4** was substantiated by spectral and elemental analyses (cf. Experimental). IR spectrum of **4** manifested disappearance of NH_2 and CN bands and appearance of new carbonyl at 1661 cm^{-1}. ^1H-NMR spectrum of **4** exhibited two singlet signals at δ 9.00 and 7.97 ppm assigned to NH and pyrimidine =CH respectively, while ^{13}C-NMR showed band at 164.3 attributed to carbonyl group (C=O). Finaly, mass spectrum data was in agreement with the proposed structure.

Similarly, refluxing of **3** with acetic acid afforded 4-(5-methyl-7-oxo-6,7-dihydro-3H-[1,2,3]triazolo[4,5-d]pyrimidin-3-yl)benzenesulfonamide (**5**). The structures of triazolopyrimidine derivative **5** was established and confirmed for the reaction product on the basis of its elemental and spectral analyses (cf. Experimental). In ^1H-NMR spectrum of **5**, the presence of singlet signals at 10.00 and 1.90 ppm for NH and CH_3 protons respectively confirm the structure. ^{13}C NMR showed a signal at 172.1 ppm for carbonyl function and an aliphatic signal for CH_3 at 22.9 ppm.

Synthesis of compound 4-(5,7-dithioxo-4,5,6,7-tetrahydro-3H-[1,2,3]triazolo[4,5-d]pyrimidin-3-yl)benzenesulfonamide (**7**) was achieved by heating compound **3** with carbon disulfide in 10% alcoholic KOH via the Dimroth's rearrangement. ^1H NMR spectrum of **7** revealed two NH groups as singlet peaks at about δ 15.07 ppm and δ 8.54 ppm. ^{13}C NMR exhibited two C=S groups at 163.4 and 149.1 ppm (Allouche et al., 2011). The preparation of 4-(7-amino-3H-[1,2,3]triazolo[4,5-d]pyrimidin-3-yl)benzenesulfonamide (**8**) was accomplished by refluxing the starting material **3** with formamide. The structures of **8** was confirmed for the reaction product on the basis of its spectral analyses (see Scheme 1). ^1H-NMR spectrum of **8** exhibited two singlet signals at δ 6.70 and 8.21 ppm assigned to NH_2 and pyrimidine =CH respectively.

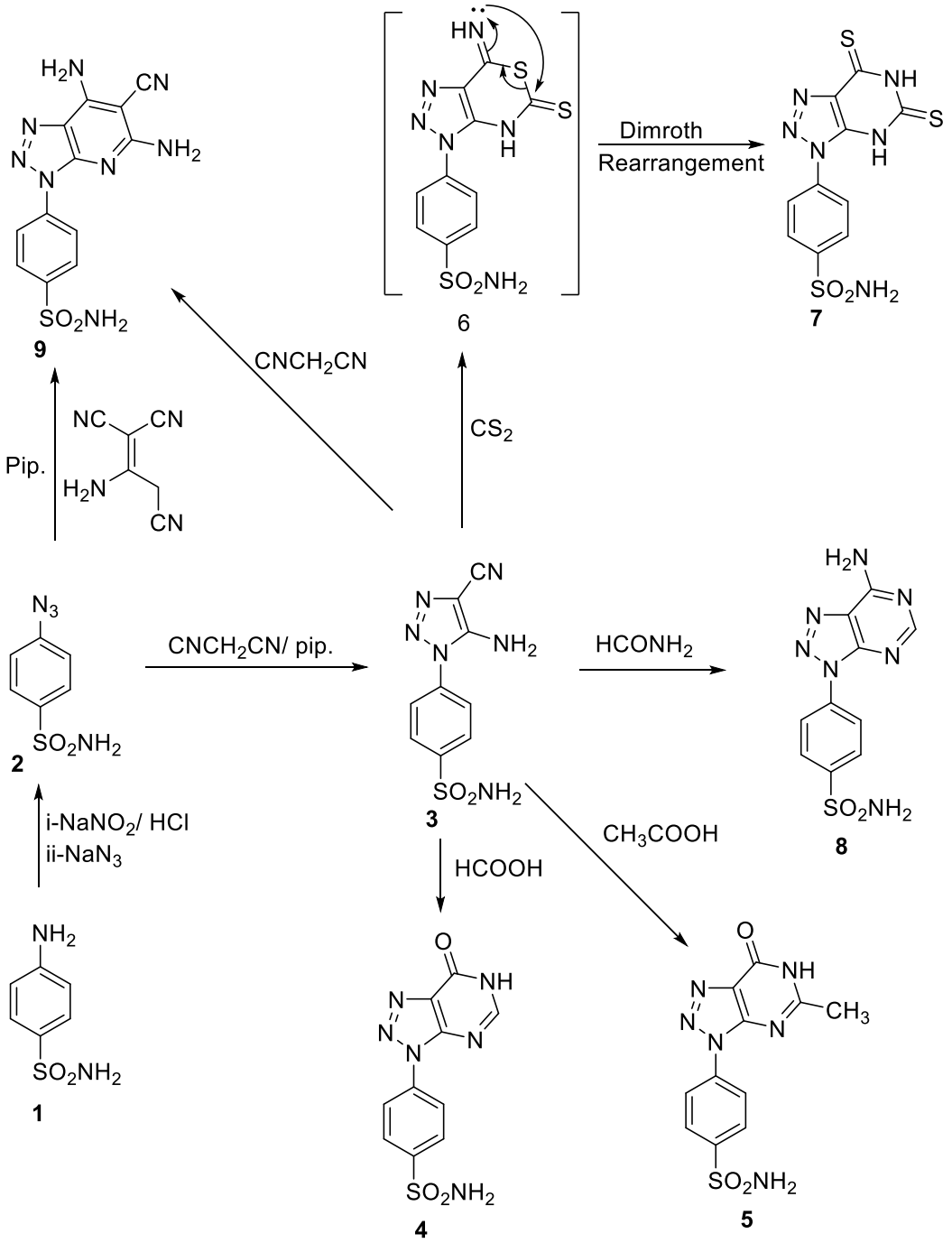

Scheme 1. Synthesis of triazolopyrimidine.

On the other hand, Click reaction of azide **2** with malononitrile dimer in absolute ethanol in the presence of piperidine as a catalyst afforded the corresponding 1,2,3-triazolo[4,5-b]pyridine derivative (**9**) through cascade cyclization (El-Gazzar et al., 2018). The pyridine ring closure product **9** was formed by intramolecular nucleophilic attacks on the cyano moiety (see Scheme 2) (El-Gazzar et al., 2018). Further elucidation of compound

9 was acquired through its preparation by the reaction of **3** with malononitrile in the presence of catalytic amount of triethyl amine at reflux temperature (see Scheme 1).

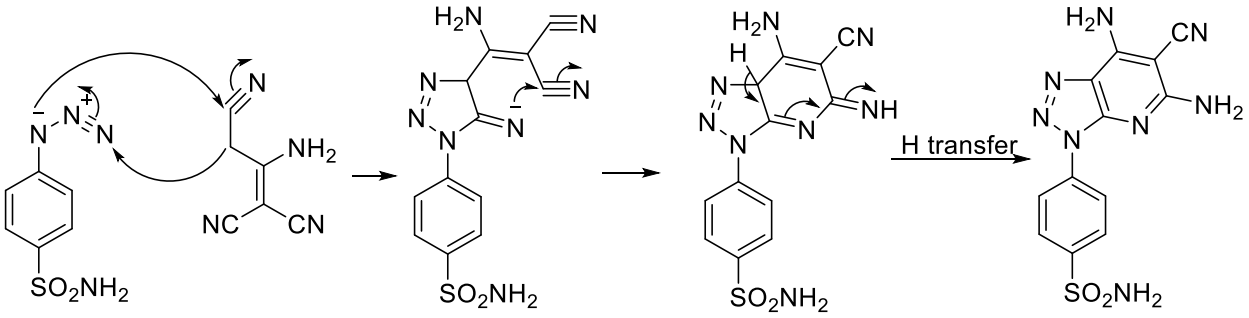

Scheme 2. Mechanism of synthesis of triazolopyridine.

Another strategy to obtain triazolopyrimidine derivatives is treatment of amino group in position 5 with dimethylformamide-dimethylacetal (DMF-DMA) or triethylorthoformat followed by treatment with primary amine to furnish fused triazolopyrimidines. Thus, compound **3** was reacted with excess dimethylformamide-dimethylacetal (DMF-DMA) in dioxane at reflux temperature to afford (E)-N'-(4-cyano-1-(4-(N-((E)-(dimethylamino)methylene)sulfamoyl)phenyl)-1H-1,2,3-triazol-5-yl)-N,N-dimethylformimidamide (**10**) in good yield. The structure of **10** was elucidated by spectral analyses. The ^{1}H NMR spectrum of **10** showed the presence of two singlet signals of two N=CH at about δ 8.34 and 8.26 ppm, and four singlet signals for four CH_3 at 3.16, 3.15, 3.0 and 2.96 ppm, while the signals of NH_2 groups were disappeared. ^{13}CNMR of **10** revealed four aliphatic signals for four CH_3 at 41.0, 40.5, 35.2 and 34.5 ppm. In addition, mass spectrum data was in agreement with the proposed structure. All attempts to prepare a mono-enamine derivative with amino group at position 5 through treatment of **3** with DMF-DMA were failed and we obtained compound **10** as a sole product.

Refluxing of **10** with various primary amines such as ammonia, hydrazine hydrate and ethanolamine afforded **3** as sole product without any detection of the compound **11** through cleavage of the N,N-dimethylformimidamide residue. On the other hand, stirring of compound **10** with hydrazine hydrate at room temperature afforded 4-(6-amino-7-imino-6,7-dihydro-3H-[1,2,3]triazolo[4,5-d]pyrimidin-3-yl)benzenesulfonamide (**12**). The structure of **12** was elucidated through spectral analyses. IR spectrum of **12** showed new bands at 3451 and 3339, 3298 cm^{-1} for NH and NH_2 function. ^{1}H-NMR spectrum of **12** showed downfield signals at δ 8.36, 7.04

and 5.71 ppm which exchangeable with D_2O assigned to =NH, SO_2NH_2 and NH_2 respectively, and singlet signal at 7.84 ppm for pyrimidine =CH. Moreover, ^{13}CNMR spectrum of **12** showed disappearance of all aliphatic carbon indicating the cleavage of the N,N-dimethylformimidamide residue.

Further elucidation of compound **12** was achieved through treatment of compound **3** with triethylorthoformate in acetic anhydride to afford ethyl (E)-N-(4-cyano-1-(4-(N-((E)-ethoxymethylene)sulfamoyl)phenyl)-1H-1,2,3-triazol-5-yl)formimidate (**13**) followed by treatment with hydrazine hydrate to give **12**. ^{1}H-NMR spectrum of **13** exhibited two singlet signals at δ 8.42 and 8.261 ppm assigned to two N=CH moieties and two signals at 4.16 (quartet with coupling constant *J* = 8.5 Hz) and 1.15 (triplet with coupling constant *J* = 8.5 Hz) for two $–OCH_2CH_3$ moieties.

Finally, the nitrile function of starting material **3** could be easily converted into the corresponding imidazolinyl group through the reaction with ethylenediamine in the presence of carbon disulfide as a catalyst to furnish compound **14**. Compound **14** could be ring closed into the fused tricyclic imidazotriazolopyrimidine *via* the reaction of **14** with carbon disulfide affording the thione derivative **15** (see Scheme 3).

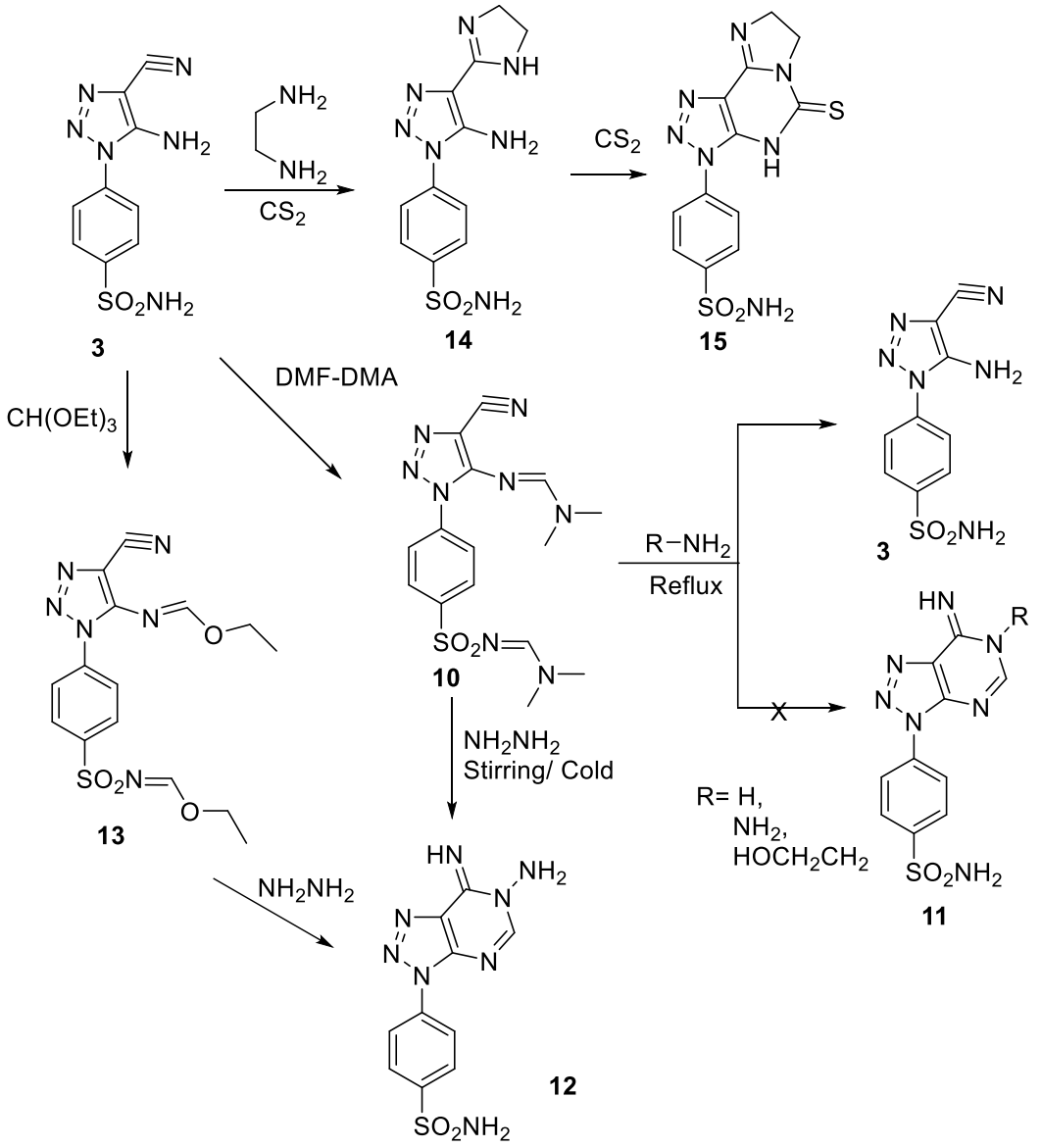

Scheme 3. Synthesis of aminoimino and Imidazo triazolopyrimidine.

4. CONCLUSIONS

We prepared new series of fused triazolopyrimidine and triazolopyridine derivatives containing sulfonamide moiety starting with *o*-aminonitrile 1,2,3-triazole derivative **3** which obtained through Click reaction of azide **2** with malononitrile. Direct treatment of compound **3** with various reagents (formic acid, acetic acid, formamide, carbon disulfide) afforded the corresponding triazolopyrimidine derivatives. While, the reaction of **3** with DMF-DMA or triethylorthoformat followed by stirring with hydrazine hydrate at room temperature gave the corresponding triazolopyrimidine derivative **12**. Imidazo[1,2-c][1,2,3]triazolo[4,5-e]pyrimidine derivative **15** obtained via reaction of **3** with ethylene diamine in the presence of carbon disulfide. Finally, the Click reaction of azide **2** with malononitrile

dimer furnished the corresponding 1,2,3-triazolopyridine derivative **9**.

5. REFERENCES

Abd-Rabou, A. A., B. F. Abdel-Wahab and M. S. Bekheit (2018) Synthesis, molecular docking, and evaluation of novel bivalent pyrazolinyl-1, 2, 3-triazoles as potential VEGFR TK inhibitors and anti-cancer agents. Chem. Pap. 72, 2225-2237.

ABD EL-AAL EL-GABY, M., S. Abdel-Hamide, M. Ghorab, et al. (1999) Synthesis and anticancer activity in vitro of some new pyrimidines. Acta Pharm. 49, 149-158.

Allouche, F., F. Chabchoub, M. Salem, et al. (2011) Synthesis of New Pyrazolopyrimidinedithiones and Pyrazolopyrimidinephosphines from Aminocyanopyrazoles. Synth. Commun. 41, 1500-1507. https://doi.org/10.1080/00397911.2010.486516

Baraldi, P. G., M. G. Pavani, C. Nuñez Mdel, et al. (2002) Antimicrobial and antitumor activity of N-heteroimmine-1,2,3-dithiazoles and their transformation in triazolo-, imidazo-, and pyrazolopirimidines. Bioorg. Med. Chem. . 10, 449-456. https://doi.org/10.1016/s0968-0896(01)00294-2

Basu, N. K. and F. L. Rose (1963) 1081. S-triazolopyridazines: synthesis as potential therapeutic agents. J. Chem. Soc. 5660-5664. https://doi.org/10.1039/JR9630005660

Batra, N., B. Roy, S. Mazumder, et al. (2015) Synthesis and antibacterial evaluation of novel sulfonamide based [1, 2, 3]-triazoles. Ind. J. Chem. . 54B, 650– 655.

Bollu, R., J. D. Palem, R. Bantu, et al. (2015) Rational design, synthesis and anti-proliferative evaluation of novel 1, 4-benzoxazine-[1, 2, 3] triazole hybrids. Eur. J. Med. Chem. 89, 138-146.

Brown, D. J., 1984. Pyrimidines and Their Benzo Derivatives

Comprehensive Heterocyclic Chemistry. A. R. Katritzky and C. W. Rees. Oxford, Pergamon Press. 3: 443.

Bruno, O., C. Brullo, S. Schenone, et al. (2002) Progress in 5H [1] benzopyrano [4, 3-d] pyrimidin-5-amine series: 2-methoxy derivatives effective as antiplatelet agents with analgesic activity. Farmaco 57, 753-758.

Chibale, K., H. Haupt, H. Kendrick, et al. (2001) Antiprotozoal and cytotoxicity evaluation of sulfonamide and urea analogues of quinacrine. Bioorg. Med. Chem. Lett. 11, 2655-2657.

El-Gazzar, M. G., N. H. Nafie, A. Nocentini, et al. (2018) Carbonic anhydrase inhibition with a series of novel benzenesulfonamide-triazole conjugates. Journal of Enzyme Inhibition and Medicinal Chemistry. 33, 1565-1574. https://doi.org/10.1080/14756366.2018.1513927

El-Sayed, W. A., A. A. Abdel-Rahman and M. M. Ramiz (2009) Anti-Hepatitis B virus activity of new N4-β-D-glycoside pyrazolo [3, 4-d] pyrimidine derivatives. Z. Naturforschung 64, 323-328.

El-wassimy, M. T. M., M. Abdel-rahman, A. B. A. G. Ghattas, et al. (1992) SYNTHESIS AND REACTIONS OF N-CHLOROMETHYL-1,2,4-TRIAZOLES WITH SULFUR AND OXYGEN NUCLEOPHILES. Phosphorus, Sulfur, and Silicon and the Related Elements. 70, 99-108. https://doi.org/10.1080/10426509208049156

Falcao, E. P. d. S., S. J. de Melo, R. M. Srivastava, et al. (2006) Synthesis and antiinflammatory activity of 4-amino-2-aryl-5-cyano-6-{3-and 4-(N-phthalimidophenyl)} pyrimidines. Eur. J. Med. Chem. 41, 276-282.

Fathalla, O., I. Zeid, M. Haiba, et al. (2009) Synthesis, antibacterial and anticancer evaluation of some pyrimidine derivatives. World J. Chem. . 4, 127-132.

Fu, D.-J., Y.-C. Liu, J.-J. Yang, et al. (2017) Design and synthesis of sulfonamide-1, 2, 3-triazole derivatives bearing a dithiocarbamate moiety as antiproliferative agents. J. Chem. Res. . 41, 523-525.

Gupta, D. and D. Jain (2015) Synthesis, antifungal and antibacterial activity of novel 1, 2, 4-triazole derivatives. J. Adv. Pharm. Technol. Res. . 6, 141.

Hansch, C., P. G. Sammes and J. B. Taylor, 1989. Comprehensive medicinal chemistry: the rational design, mechanistic study & therapeutic applications of chemical compounds, Pergamon Pr.

He, Y.-W., C.-Z. Dong, J.-Y. Zhao, et al. (2014) 1, 2, 3-Triazole-containing derivatives of rupestonic acid: click-chemical synthesis and antiviral activities against influenza viruses. Eur. J. Med. Chem. 76, 245-255.

Hu, B., J. Ellingboe, S. Han, et al. (2001) Novel (4-piperidin-1-yl)-phenyl sulfonamides as potent and selective human β3 agonists. Bioorg. Med. Chem. 9, 2045-2059.

Jarrahpour, A., M. Aye, J. A. Rad, et al. (2018) Design, synthesis, activity evaluation and QSAR studies of novel antimalarial 1, 2, 3-triazolo-β-lactam derivatives. J. Iran. Chem. Soc. . 15, 1311-1326.

Kanda, Y., Y. Kawanishi, K. Oda, et al. (2001) Synthesis and structure–activity relationships of potent and orally active sulfonamide ETB selective antagonists. Bioorg. Med. Chem. Lett. 9, 897-907.

Kharb, R., M. Shahar Yar and P. Chander Sharma (2011) Recent advances and future perspectives of triazole analogs as promising antiviral agents. Mini. Rev. Med. Chem. 11, 84-96.

Khidre, R. E. and I. A. M. Radini (2019) Synthesis and Antimicrobial Activity of Novel Heterocycles Utilizing 3-(1,4-Dioxo-3,4-dihydrophthalazin-2(1H)-yl)-3-oxopropanenitrile as Precursors. J. Heterocycl. Chem. 56, 850-858. https://doi.org/https://doi.org/10.1002/jhet.3463

Khidre, R. E. and I. A. M. Radini (2021) Design, synthesis and docking studies of novel thiazole derivatives incorporating pyridine moiety and assessment as antimicrobial agents. Scientific Reports. 11, 7846. https://doi.org/10.1038/s41598-021-86424-7

Kołaczek, A., I. Fusiarz, J. Ławecka, et al. (2014) Biological activity and synthesis of sulfonamide derivatives: a brief review. CHEMIK 68, 620-628.

Kumar, H., S. A. Javed, S. A. Khan, et al. (2008) 1,3,4-Oxadiazole/thiadiazole and 1,2,4-triazole derivatives of biphenyl-4-yloxy acetic acid: Synthesis and preliminary evaluation of biological properties. Eur. J. Med. Chem. 43, 2688-2698. https://doi.org/https://doi.org/10.1016/j.ejmech.2008.01.039

Lazrak, F., N. Ahabchane, A. Keita, et al. (2002) Synthesis and crystal structure of 3-methoxycarbonyl-5-methyl-1-p-tolyl-1, 2, 4-triazolo [3, 4-c]-1, 2, 4-triazole. Indian J. Chem. B Org. . 41, 821-825.

Lazrak, F., E. Essassi, Y. K. Rodi, et al. (2004) Synthesis of new condensing systems containing 1,2,4-triazole, 1,3-thiazine, 1,3-thiazepine and 1,3,5,7-dithiadiazocine Phosphorus, Sulfur, and Silicon 179, 1799-1808.

Li, J. J., G. D. Anderson, E. G. Burton, et al. (1995) 1, 2-Diarylcyclopentenes as selective cyclooxygenase-2 inhibitors and orally active anti-inflammatory agents. J. Med. Chem. . 38, 4570-4578.

Ma, L.-Y., B. Wang, L.-P. Pang, et al. (2015) Design and synthesis of novel 1, 2, 3-triazole–pyrimidine–urea hybrids as potential anticancer agents. Bioorg. Med. Chem. 25, 1124-1128.

Ma, T., A. D. Fuld, J. R. Rigas, et al. (2012) A phase I trial and in vitro studies combining ABT-751 with carboplatin in previously treated non-small cell lung cancer patients. Chemotherapy 58, 321-329.

Mangalagiu, G., M. Ungureanu, G. Grosu, et al., 2001. New pyrrolo-pyrimidine derivatives with antifungal or antibacterial properties in vitro. Annales pharmaceutiques françaises.

Mavrova, A. T., D. Wesselinova, J. A. Tsenov, et al. (2014) Synthesis and antiproliferative activity of some new thieno[2,3-d]pyrimidin-4(3H)-ones containing 1,2,4-triazole and 1,3,4-thiadiazole moiety. Eur. J. Med. Chem. 86, 676-683. https://doi.org/https://doi.org/10.1016/j.ejmech.2014.09.032

Nasr, M. N. and M. M. Gineinah (2002) Pyrido [2, 3-d]pyrimidines and Pyrimido[5′ , 4′ :5, 6]pyrido[2, 3-d]pyrimidines as New Antiviral Agents: Synthesis and Biological Activity. Arch. Pharm. 335, 289-295. https://doi.org/10.1002/1521-4184(200208)335:6<289::Aid-ardp289>3.0.Co;2-z

Natarajan, A., Y. Guo, F. Harbinski, et al. (2004) Novel arylsulfoanilide−oxindole hybrid as an anticancer agent that inhibits translation initiation. J. Med. Chem. . 47, 4979-4982.

Paprocka, R., M. Wiese, A. Eljaszewicz, et al. (2015) Synthesis and anti-inflammatory activity of new 1, 2, 4-triazole derivatives. Bioorg. Med. Chem. Lett. 25, 2664-2667.

Petrie, C. R., H. B. Cottam, P. A. McKernan, et al. (1985) Synthesis and biological activity of 6-azacadeguomycin and certain 3,4,6-trisubstituted pyrazolo[3,4-d]pyrimidine ribonucleosides. J. Med. Chem. 28, 1010-1016. https://doi.org/10.1021/jm00146a007

Rajasekaran, A., S. Murugesan and K. AnandaRajagopal (2006) Antibacterial, antifungal and anticonvulsant evaluation of novel newly synthesized 1-[2-(1H-tetrazol-5-yl)ethyl]-1H-benzo[d][1,2,3]triazoles. Arch. Pharm. Res. 29, 535-540. https://doi.org/10.1007/BF02969261

Roth, B. and C. C. Cheng, 1982. 6 Recent Progress in the Medicinal Chemistry of 2,4-Diaminopyrimidines. Progress in Medicinal Chemistry. G. P. Ellis and G. B. West, Elsevier. 19: 269-331.

Serradeil-Le, G. C. (2001) An Overview of SR121463, a Selective Non-Peptide Vasopressin V2 Receptor Antagonist. Cardiovasc. Drug. Rev. . 19, 201-214. https://doi.org/10.1111/j.1527-3466.2001.tb00065.x

Shishoo, C. J., V. S. Shirsath, I. S. Rathod, et al. (2001) Design, synthesis and antihistaminic (H1)activity of some condensed 2-(substituted)arylaminoethylpyrimidin-4(3H)-ones. Arzneimittelforschung. 51, 221-231. https://doi.org/10.1055/s-0031-1300028

Singh, R., S. Kashaw, V. Mishra, et al. (2018) Design and synthesis of new bioactive 1, 2, 4-Triazoles, potential antitubercular and antimicrobial agents. Indian J. Pharm. Sci. 80, 36-45.

Sondhi, S. M., M. Johar, S. Rajvanshi, et al. (2001) Anticancer, anti-inflammatory and analgesic activity evaluation of heterocyclic compounds synthesized by the reaction of 4-isothiocyanato-4-methylpentan-2-one with substituted o-phenylenediamines, o-diaminopyridine and (un)substituted o-diaminopyrimidines. Aust. J. Chem. 54, 69-74. https://doi.org/10.1071/ch00141

Song, M.-X. and X.-Q. Deng (2018) Recent developments on triazole nucleus in anticonvulsant compounds: a review. J. Enzyme Inhib. Med. Chem. 33, 453-478. https://doi.org/10.1080/14756366.2017.1423068

Stokes, S. S., R. Albert, E. T. Buurman, et al. (2012) Inhibitors of the acetyltransferase domain of N-acetylglucosamine-1-phosphate-uridylyltransferase/glucosamine-1-phosphate-acetyltransferase (GlmU). Part 2: optimization of physical properties leading to antibacterial aryl sulfonamides. Bioorg. Med. Chem. Lett. . 22, 7019-7023.

Vats, L., V. Sharma, A. Angeli, et al. (2018) Synthesis of novel 4-functionalized 1, 5-diaryl-1, 2, 3-triazoles containing benzenesulfonamide moiety as carbonic anhydrase I, II, IV and IX inhibitors. Eur. J. Med. Chem. 150, 678-686.

Wang, X.-L., K. Wan and C.-H. Zhou (2010) Synthesis of novel sulfanilamide-derived 1, 2, 3-triazoles and their evaluation for antibacterial and antifungal activities. Eur. J. Med. Chem. 45, 4631-4639.

Wu, G., Y. Gao, D. Kang, et al. (2018) Design, synthesis and biological evaluation of tacrine-1,2,3-triazole derivatives as potent cholinesterase inhibitors. Med. Chem. Comm. 9, 149-159. https://doi.org/10.1039/C7MD00457E

Yan, S.-J., Y.-J. Liu, Y.-L. Chen, et al. (2010) An efficient one-pot synthesis of heterocycle-fused 1, 2, 3-triazole derivatives as anti-cancer agents. Bioorg. Med. Chem. Lett. 20, 5225-5228.

Yousif, M. N., W. A. El-Sayed, H.-A. S. Abbas, et al. (2017) Anticancer activity of new substituted pyrimidines, their thioglycosides and thiazolopyrimidine derivatives. J. Appl. Pharm. Sci. . 7, 21-32.

تصميم وتشييد وتوصيف مشتقات تريازولوبيريميدين وتريازولوبيريدين الجديدة المحتوية على جزء من سلفوناميد

إبراهيم علي رديني

قسم الكيمياء- كلية العلوم- جامعة جازان - المملكة العربية السعودية

الملخص

تم تشييد سلسلة جديدة من مشتقات [١،٢،٣] تريازولو[٤،٥-d] بيريميدين المحتوية على جزء السلفوناميد وذلك بتفاعل الآزيد (٢) مع مالونونيتريل في وجود كمية من البيبيريدين كمادة حفازة ليعطي المشتق المقابل (٣). عند تفاعل المركب (٣) بكواشف مختلفة (حمض الفورميك ، حمض الأسيتيك ، فورماميد ، ثاني كبريتيد الكربون) أعطى مشتقات بيريميدين المقابلة [١،٢،٣] تريازولو [٤،٥-d]، في حين أن تفاعل الآزيد (٢) مع ثنائي مالونونيتريل أعطى المشتق المقابل ١،٢،٣-تريازولوبيريدين (٩). بينما أعطى تفاعل المركب (٣) مع ثلاثي إيثيل أورثوفورمات أو مع ثنائي ميثيل فورماميد - ثنائي ميثيل أسيتال (DMF-DMA) مشتق ثنائي إنامين المقابل الذي تم تفاعله مع الهيدرازين هيدرات عند درجة حرارة الغرفة مما أعطى مشتق تريازولوبيريميدين (١٢). وبتفاعل المركب (٣) مع إيثيلين ديامين في وجود ثاني كبريتيد الكربون كمحفز تم الحصول على مشتق إيميدازولينيل والذي تفاعل مع ثاني كبريتيد الكربون وأعطى مشتق إيميدازو [١،٢-c] [١،٢،٣] تريازولو [٤،٥-e] بيريميدين (١٥).

كلمات مفتاحية: الآزيد. ترايازول. سلفوناميد. بيريميدين. ترايازولو بيريميدين.

Stability and Convergence Analysis of a Finite Difference Technique for Solving a Class of Convection-Diffusion Equation with Non-Linear Source Term

Reem Edwan

Department of Mathematics, Taibah University, Al Madinah Al Munawara, Kingdom of Saudi Arabia

Abstract

Particles and physical quantities are transferred inside a physical system by diffusion and convection processes, this physical process can be modeled by convection-diffusion equations with and without source term. In this paper, a new approach of the finite difference method (FDM) is implemented for solving a class of convection-diffusion equations (CDEs) with non-linear source term. This technique converts the issue to the implicit scheme by using the fractional Grünwald-Letnikov formula. Our numerical example shows that the comparison between the approximated solution and the exact solution that reveals the reliability and capability of the proposed method.

Keywords: Finite difference method, Convection-diffusion equations, Riemann-Liouville fractional derivative.

1. Introduction

Many phenomena such as earthquakes and non-Markov Processes can be represented by diffusion and convection processes. By these processes the physical quantities are transferred and can be modeled this phenomenon by convection-diffusion equations (Chandrasekhar, 1943)(Shongsheng & Jianing, 1998).

Various methods have been introduced for finding a reliable approximate technique for solving a class of diffusion equations. (Salkuyeh, 2006) applied the finite difference method for solving the convection-diffusion equation. (Saadatmandi et al., 2012) improved the sinc–legendre collocation method for solving fractional CDEs. In 2015 (Izadkhah & Saberi- Nadjafi, 2015) used the Lagrange polynomials and Gegenbauer polynomials for solving a class of convection-diffusion equations. Moreover, (Wang, 2015) introduced a finite difference method for finding an implicit scheme that solves the time fractional CDEs with variable coefficients.

In 2016 (Sayevand & Arjang, 2016) used a finite volume element method for solving the sub-diffusion equation. Jia and Wang (Jia & Wang, 2016) applied a volume-penalization approximation for solving a class of fractional diffusion equations. While (Zhao et al., 2016) used spatial quasi-Wilson nonconforming to convert a time-fractional diffusion equation to an unconditionally stable scheme. In 2017 (Abolhasani et al., 2017) improved the variational iteration method by an auxiliary parameter for solving a class of fractional CDE in large domains. In 2018 (Zhang et al., 2018) a discrete form based on the finite difference method was proposed for solving time-fractional CDEs.

This paper aims to improve a finite difference method (FDM) in finding approximate solutions for a class of fractional Convection-diffusion equation (FCDE) in the following form:

$$\frac{\partial\phi(x,t)}{\partial t}+\epsilon\frac{\partial}{\partial x}J_a^{\alpha}\phi(x,t)-v\frac{\partial^2\phi(x,t)}{\partial x^2}=f(x,t), t>0\ , 0\le\alpha<1, \quad (1)$$

subject to the initial condition

$$\phi(x,0)=g(x),\ a\le x\le b, \quad (2)$$

where α is the order of space fractional integral, $\phi(x,t)$ is concentration, $f(x)$ is nonlinear source term, ϵ and v are positive parameters, and J_a^{α} is the Riemann-Liouville integral with respect to x.

In this approach, the finite difference scheme can be implemented when tackling FCDE with nonlinear source term and can deal with unlimited kinds of the initial condition. Also, it can handle fractional integral without difficulty by using the fractional Grünwald-Letnikov formula. Moreover, it is easy to increase the nodes in the regular grid to get higher-order accuracy.

This paper is organized as follows: Some preliminary about the fractional derivatives and integrals are presented in section 2. In Section 3 a new formulation of FDM for solving the initial value problems (IVPs) (1) and (2) is introduced. The Section 4 is devoted to theoretical analysis. A numerical example is given in Section 5 to show the validity of the method. Finally, in Section 6 some conclusions are given.

2. Preliminaries

In this section, we introduce some preliminary definitions and theorems related to the Riemann-Liouville fractional integral and the Grünwald-Letnikov formula.

2.1. Definition 1. (see (Podlubny, 1998)) The fractional integral of order $\alpha>0$ in Riemann-Liouville sense $J_a^{\alpha}\phi(x)$ is defined as:

$J_a^{\alpha}\phi(x)=\frac{1}{\Gamma(\alpha)}\int_a^x(x-t)^{\alpha-1}\phi(t)dt$, provided that $\phi\in L_1[a,b]$,

where $\Gamma(\alpha)=\int_0^{\infty}s^{\alpha-1}e^{-s}ds,\ \alpha>0,\Gamma(\alpha+1)=\alpha\Gamma(\alpha),\Gamma(\alpha)\Gamma(1-\alpha)=\frac{\pi}{sin\pi\alpha}$, and $\phi\in L_1[a,b],\phi:[a,b]\to\mathbb{C}$, ϕ is measurable on [a, b] and $\int\ |\phi(x)|\ dx\ <\ \infty$.

2.2. Definition 2. (see (Podlubny, 1998)) Let $\phi\in C^{\lceil\alpha\rceil}[a,b],\alpha>0$. Then the fractional derivative of order α in Grünwald-Letnikov sense $\widetilde{\mathcal{D}}_a^{\alpha}\phi(x)$ is defined as:

$$\widetilde{\mathcal{D}}_a^{\alpha}\phi(x)=\lim_{h\to0}\frac{1}{h^{\alpha}}\sum_{k=0}^{\left[\frac{x-a}{h}\right]}(-1)^k\binom{\alpha}{k}\phi(x-kh),\ a<x\le b, h=\frac{x-a}{N},$$

where $C^{\lceil\alpha\rceil}[a,b]$ the set of functions with continuous $\lceil\alpha\rceil^{th}$derivative on $[a,b]$, $\lceil\alpha\rceil$ the least integer that is greater than or equal to α, $\left[\frac{x-a}{h}\right]$ the greatest integer function of $\frac{x-a}{h}$, and $\binom{\alpha}{k}=\frac{\Gamma(\alpha+1)}{\Gamma(k+1)\Gamma(\alpha-k+1)}$.

2.3. Theorem 1. *Let $\alpha>0$, and $\phi\in C[a,b]$. Then,*

$J_a^{\alpha}\phi(x)=\lim_{h\to0}h^{\alpha}\sum_{k=0}^{\left[\frac{x-a}{h}\right]}w_k^{\alpha}\phi(x-kh),\ h=\frac{x-a}{N}\ , a<x\le b,$ *where* $w_0^{\alpha}=1,\ w_1^{\alpha}=\alpha$ *and* $w_k^{\alpha}=\left(1-\frac{(1-\alpha)}{k}\right)w_{k-1}^{\alpha}, k=2,3,\ldots.$

Proof of theorem 1. see (Arqub et al., 2020).

3. Finite difference formulation

A new formulation of FDM is introduced for solving a class of FCDE given in equation (1) subject to the initial condition (2). First, we discretize the finite domain $I = [a, b]$ such that the nodes $x_i = a + ih, h = \frac{b-a}{N}, i = 0,1, \dots, N$, and we define a temporal partition $t_n = n\tau$ where τ is the time step and $n = 0, 1, 2, \dots$.

Using the central difference formula for evaluating the first and second derivative in equation (2) at $x = x_i$, and the standard Grünwald-Letnikov formula for approximate the Riemann-Liouville integral $J_a^\alpha \phi(x,t)$ at $x = x_{i+1}$ and $x = x_{i-1}$ we get

$$\left.\frac{\partial \phi(x,t)}{\partial x}\right|_{x=x_i} = \frac{\phi(x_{i+1},t)-\phi(x_{i-1},t)}{2h} + \mathcal{O}(h^2), \tag{3}$$

$$\left.\frac{\partial^2 \phi(x,t)}{\partial x^2}\right|_{x=x_i} = \frac{\phi(x_{i-1},t)-2\phi(x_i,t)+\phi(x_{i+1},t)}{h^2} + \mathcal{O}(h^2), \tag{4}$$

$$J_a^\alpha \phi(x,t) = h^\alpha \sum_{j=0}^{N} w_j^\alpha \phi(x - jh, t) + o(1), \tag{5}$$

then the equation (2) at (x_i, t_{n+1}) becomes

$$\left.\frac{d\phi(x_i,t)}{dt}\right|_{t=t_{n+1}} = -\frac{\epsilon}{2h}\left[[h^\alpha \sum_{j=0}^{i+1} w_j^\alpha \phi(x_{i-j+1}, t_{n+1}) + o(1) - h^\alpha \sum_{j=0}^{i-1} w_j^\alpha \phi(x_{i-j-1}, t_{n+1}) + o(1)] + \mathcal{O}(h^2)\right] + v\left[\frac{\phi(x_{i-1},t_{n+1})-2\phi(x_i,t_{n+1})+\phi(x_{i+1},t_{n+1})}{h^2} + \mathcal{O}(h^2)\right] + f(x_i, t_{n+1}). \tag{6}$$

Now, utilizing the backward difference to approximate for the time derivative in (6)

$$\left.\frac{d\phi(x_i,t)}{dt}\right|_{t=t_{n+1}} = \frac{\phi(x_i,t_{n+1})-\phi(x_i,t_n)}{\tau} + \mathcal{O}(\tau). \tag{7}$$

Letting $\phi_i^n \approx \phi(x_i, t_n)$ denote the numerical solution, we have

$$\frac{\phi_i^{n+1}-\phi_i^n}{\tau} + \mathcal{O}(\tau) = -\frac{\epsilon}{2h}\left[h^\alpha \sum_{j=0}^{i+1} w_j^\alpha \phi_{i-j+1}^{n+1} + o(1) - h^\alpha \sum_{j=0}^{i-1} w_j^\alpha \phi_{i-j-1}^{n+1} + o(1)\right] + \mathcal{O}(h^2) + v\left[\frac{\phi_{i-1}^{n+1}-2\phi_i^{n+1}+\phi_{i+1}^{n+1}}{h^2} + \mathcal{O}(h^2)\right] + f_i^{n+1}. \tag{8}$$

This equation shows that the given numerical scheme (8) is consistent, with first order accuracy in time and second order accuracy in space.

Rewriting equation (8) as:

$$\frac{\phi_i^{n+1}-\phi_i^n}{\tau} + \sum_{j=0}^{N} a_{ij}\phi_j^{n+1} = f_i^{n+1}, \tag{9}$$

where $$a_{ij} = \begin{cases} \frac{\epsilon h^{\alpha-1}[w^{\alpha}_{i-j+1} - w^{\alpha}_{i-j-1}]}{2} & ,j < i-1 \\ \frac{\epsilon h^{\alpha-1}[w^{\alpha}_{2} - w^{\alpha}_{0}]}{2} - \frac{v}{h^2} & ,j = i-1 \\ \frac{\epsilon h^{\alpha-1} w^{\alpha}_{1}}{2} + \frac{2v}{h^2} & ,j = i \\ \frac{\epsilon h^{\alpha-1} w^{\alpha}_{0}}{2} - \frac{v}{h^2} & ,j = i+1 \\ 0 & ,j > i+1 \end{cases}. \quad (10)$$

By denoting the numerical solution vector $\phi^n = [\phi_0^n, \phi_1^n, \dots, \phi_N^n]$ and source vector $f^{n+1} = [f(x_0, t_{n+1}), f(x_1, t_{n+1}), \dots, f(x_N, t_{n+1})]$, then the vector equation is given by

$$(I + \tau C)\phi^{n+1} = \phi^n + \tau f^{n+1}, \quad (11)$$

where the matrix C has elements $c_{ij} = a_{ij}$.

4. Numerical Analysis

The study of the numerical analysis of FDM has been made by a lot of researchers in various fields, we refer to (Lax & Richtmyer, 1956)(Qiu & Sloan, 1999)(Allen III & Isaacson, 2011). In this approach, proving convergence directly from the definition is quite difficult, but the consistency and stability are typically more accessible to prove, hence convergence is usually shown via the Lax equivalence theorem (Palencia & Sanz-Serna, 1984)(Strikwerda, 2004).

The Lax equivalence theorem in the analysis of finite difference methods for the numerical solution of partial differential equations guarantees the convergence for this method, that is a consistent finite difference method for IVP is convergent if and only if it is stable (Thomas, 2013)(Tekriwal et al., 2021).

In this section, we can rewrite the scheme (11) as:

$$\phi^{n+1} = S(\phi^n + \tau f^{n+1}), \quad (12)$$

where $S = (I + \tau C)^{-1}$ is the iteration matrix.

Theorem 2. *Given* $0 \le \alpha < 1$, *and* $v > \frac{\epsilon h^{\alpha+1}}{2}$, *then coefficients* c_{ij} *satisfy*

$$|c_{ii}| > \sum_{\substack{j=0 \\ j \neq i}}^{N} |c_{ij}| \quad ,i = 1,2, \dots, N.$$

Proof of theorem 2. For a given i, consider the sum

$$\sum_{\substack{j=0 \\ j \neq i}}^{N} |c_{ij}| \sum_{j=0}^{i-2} \left| \frac{\epsilon h^{\alpha-1}[w^{\alpha}_{i-j+1} - w^{\alpha}_{i-j-1}]}{2} \right| + \left| \frac{\epsilon h^{\alpha-1}[w^{\alpha}_{2} - w^{\alpha}_{0}]}{2} - \frac{v}{h^2} \right| + \left| \frac{\epsilon h^{\alpha-1} w^{\alpha}_{0}}{2} - \frac{v}{h^2} \right|.$$

Replacing the finite sum with infinite sum, the weight function w_k^{α} guarantee the telescoping sum have the form: see((Arqub et al., 2020))

$$(w_1^{\alpha} - w_3^{\alpha}) + (w_2^{\alpha} - w_4^{\alpha}) + (w_3^{\alpha} - w_5^{\alpha}) + (w_4^{\alpha} - w_6^{\alpha}).$$

So, we have:

$$\sum_{\substack{j=0 \\ j\neq i}}^{N}|c_{ij}| < \frac{\epsilon h^{\alpha-1}[w_1^{\alpha}+w_2^{\alpha}]}{2}+\left(\frac{v}{h^2}-\frac{\epsilon h^{\alpha-1}[w_2^{\alpha}-w_0^{\alpha}]}{2}\right)+(\frac{v}{h^2}-\frac{\epsilon h^{\alpha-1}w_0^{\alpha}}{2})$$

$$= \frac{\epsilon h^{\alpha-1}w_1^{\alpha}}{2}+\frac{2v}{h^2} \qquad = |c_{ii}|.$$ Which complete the proof. □

Corollary 1. *The matrix S in (12) is convergent, and hence the numerical scheme (12) is conditionally stable.*

Proof of corollary 1. The given matrix C has positive diagonal elements and theorem 2 shows that this matrix is strictly diagonally dominant. Hence so too is $I+\tau C$, so, the matrix $S=(I+\tau C)^{-1}$ exists and the spectral radius $\rho(S)$ satisfies

$$\rho(S)=\rho(I+\tau C)^{-1}=\left(1+\tau\rho(C)\right)^{-1}<1. \square$$

The given numerical scheme (8) is consistent, with first-order accuracy in time and second-order accuracy in space. Moreover, the numerical scheme (12) is stable, so that by the Lax equivalence theorem of numerical methods for IVP, the given numerical scheme is convergent.

5. Numerical Examples

In this section, we introduced a numerical problem with nonlinear source term. The calculations are performed by Mathematica Software 11.0.

Example 5.1: Considering the FCDE

$$\frac{\partial\phi(x,t)}{\partial t}+\frac{\partial}{\partial x}J_a^{\alpha}\phi(x,t)-2\frac{\partial^2\phi(x,t)}{\partial x^2}=f(x,t), 0\leq\alpha<1,\ x\in[1,2], t\geq 0, \qquad (13)$$

subject to the initial condition

$$\phi(x,0) = -sin(\pi x),$$
$$f(x,t) = cox(\pi x),$$

where the exact solution for $\alpha = 0$ is given by

$$\phi(x,t) = -sin(\pi x)\ exp(-(\pi^2\ t)).$$

Next, we solve the Example 5.1 using the proposed finite deference method given in section 3, with the time step $\tau = 0.01$ and $h = 0.015625$. The behavior of the solutions $\phi(x,t)$ at time $t = 0.5$, with varying $\alpha, x \in [1,2]$ are shown in Figure 1. In Table 1 we present the numerical results of $\phi(x,t)$ at $t = 0.5$, with varying $\alpha, x \in [1,1.25]$. Noting that when the value of $\alpha \to 0$, the FCDE converge to the classical convection-diffusion equation (Podlubny, 1998). And the numerical results presented in Figure 1 and Table 1 show that the approximated solution when $\alpha \to 0$ converge to the exact solution for $\alpha = 0$ which agreed with the theory.

The Table 2 shows a numerical result of $\phi(x,t)$ for $\alpha = 0$ with $t = 0.5$ and $x \in$

[1,1.25]. We observe that, the approximate solution of $\phi(x,t)$ at $\alpha = 0$ is very closed to the exact solutions.

In Table 3, we present a numerical result of $\phi(x,t)$ for $\alpha = 0.25$ with $t = 0.5$, $t = 1.0$, and $x \in [1,1.25]$. And we note that the values of numerical results along $x \in [1,1.25]$ at $t = 1$ are positive comparing with negative values at $t = 0.5$, even if they have the same value of α. Moreover, along $x \in [1,1.25]$ the numerical results are decreasing if $t = 0.5$ or $t = 1.0$.

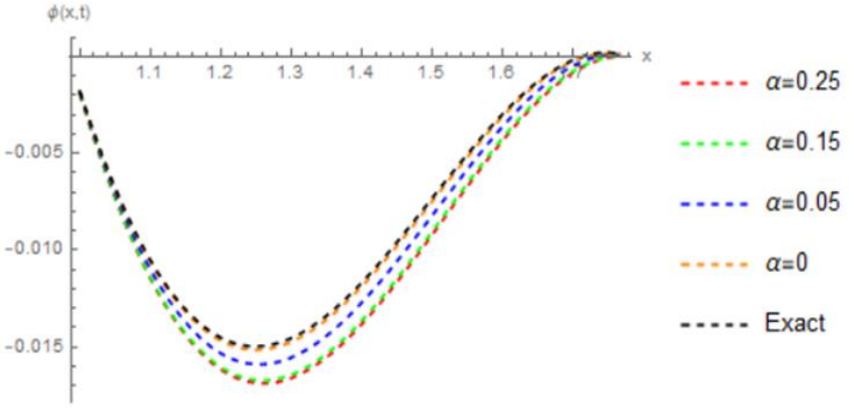

Figure 1. Behavior of solution $\phi(x,t)$of Example 5.1 for with varying α, at t = 0.5.

Table1. The numerical results of $\phi(x,t)$ of Example 5.1 at t = 0.5, with varying α.

x	$\alpha = 0.25$	$\alpha = 0.15$	$\alpha = 0.05$	$\alpha = 0$	
				Approximate	Exact
1.	-19.3861×10^{-4}	-19.2899×10^{-4}	-18.7328×10^{-4}	-18.2127×10^{-4}	-18.0875×10^{-4}
1.015625	-37.5515×10^{-4}	-37.3592×10^{-4}	-36.2449×10^{-4}	-35.2049×10^{-4}	-34.9543×10^{-4}
1.03125	-54.4978×10^{-4}	-54.2093×10^{-4}	-52.5379×10^{-4}	-50.9778×10^{-4}	-50.6020×10^{-4}
1.046875	-70.2257×10^{-4}	-69.8410×10^{-4}	-67.61422×10^{-4}	-65.5359×10^{-4}	-65.0353×10^{-4}
1.0625	-84.7377×10^{-4}	-84.2570×10^{-4}	-81.4786×10^{-4}	-78.8866×10^{-4}	-78.2624×10^{-4}
1.078125	-98.0384×10^{-4}	-97.4619×10^{-4}	-94.1386×10^{-4}	-91.0401×10^{-4}	-90.2941×10^{-4}
1.09375	-110.1351×10^{-4}	-109.4635×10^{-4}	-105.6046×10^{-4}	-102.0095×10^{-4}	-101.1442×10^{-4}
1.109375	-121.0379×10^{-4}	-120.2721×10^{-4}	-115.8897×10^{-4}	-111.8108×10^{-4}	-110.8295×10^{-4}
1.125	-130.7597×10^{-4}	-129.9010×10^{-4}	-125.0100×10^{-4}	-120.4629×10^{-4}	-119.3694×10^{-4}
1.140625	-139.3164×10^{-4}	-138.3667×10^{-4}	-132.9845×10^{-4}	-127.9872×10^{-4}	-126.7861×10^{-4}
1.15625	-146.7271×10^{-4}	-145.6884×10^{-4}	-139.8352×10^{-4}	-134.4080×10^{-4}	-133.1044×10^{-4}
1.171875	-153.0135×10^{-4}	-151.8885×10^{-4}	-145.5867×10^{-4}	-139.7524×10^{-4}	-138.3518×10^{-4}
1.1875	-158.2006×10^{-4}	-156.9922×10^{-4}	-150.2665×10^{-4}	-144.0497×10^{-4}	-142.5584×10^{-4}
1.203125	-162.3159×10^{-4}	-161.0277×10^{-4}	-153.9049×10^{-4}	-147.3322×10^{-4}	-145.7566×10^{-4}
1.21875	-165.3901×10^{-4}	-164.0260×10^{-4}	-156.5346×10^{-4}	-149.6342×10^{-4}	-147.9814×10^{-4}
1.234375	-167.4565×10^{-4}	-166.0207×10^{-4}	-158.1912×10^{-4}	-150.9927×10^{-4}	-149.2699×10^{-4}
1.25	-168.5512×10^{-4}	-167.0484×10^{-4}	-158.9125×10^{-4}	-151.4467×10^{-4}	-149.6615×10^{-4}

Table2. Exact, approximate, and absolute error results of $\phi(x,t)$ of Example 5.1 at $t = 0.5$, $\alpha = 0$.

x	Approximate	Exact	Absolute error
1.	-18.2127×10^{-4}	-18.0875×10^{-4}	1.2526×10^{-5}
1.015625	-35.2049×10^{-4}	-34.9543×10^{-4}	2.5053×10^{-5}
1.03125	-50.9778×10^{-4}	-50.6020×10^{-4}	3.7580×10^{-5}
1.046875	-65.5359×10^{-4}	-65.0353×10^{-4}	5.0058×10^{-5}
1.0625	-78.8866×10^{-4}	-78.2624×10^{-4}	6.2422×10^{-5}
1.078125	-91.0401×10^{-4}	-90.2941×10^{-4}	7.4602×10^{-5}
1.09375	-102.0095×10^{-4}	-101.1442×10^{-4}	8.6529×10^{-5}
1.109375	-111.8108×10^{-4}	-110.8295×10^{-4}	9.8133×10^{-5}
1.125	-120.4629×10^{-4}	-119.3694×10^{-4}	10.9347×10^{-5}
1.140625	-127.9872×10^{-4}	-126.7861×10^{-4}	12.0110×10^{-5}
1.15625	-134.4080×10^{-4}	-133.1044×10^{-4}	13.0364×10^{-5}
1.171875	-139.7524×10^{-4}	-138.3518×10^{-4}	14.0053×10^{-5}
1.1875	-144.0497×10^{-4}	-142.5584×10^{-4}	14.9131×10^{-5}
1.203125	-147.3322×10^{-4}	-145.7566×10^{-4}	15.7552×10^{-5}
1.21875	-149.6342×10^{-4}	-147.9814×10^{-4}	16.5279×10^{-5}
1.234375	-150.9927×10^{-4}	-149.2699×10^{-4}	17.2278×10^{-5}
1.25	-151.4467×10^{-4}	-149.6615×10^{-4}	17.8522×10^{-5}

Table3. The numerical results of $\phi(x,t)$ of Example 5.1 at α = 0.25, with varying time t.

x	$t = 0.5$	$t = 1$
1.	-19.3861×10^{-4}	1.38027×10^{-3}
1.015625	-37.5515×10^{-4}	2.8825×10^{-3}
1.03125	-54.4978×10^{-4}	4.50643×10^{-3}
1.046875	-70.2257×10^{-4}	8.11578×10^{-3}
1.0625	-84.7377×10^{-4}	1.0098×10^{-2}
1.078125	-98.0384×10^{-4}	1.21969×10^{-2}
1.09375	-110.1351×10^{-4}	1.44092×10^{-2}
1.109375	-121.0379×10^{-4}	1.67324×10^{-2}
1.125	-130.7597×10^{-4}	1.91636×10^{-2}
1.140625	-139.3164×10^{-4}	2.16993×10^{-2}
1.15625	-146.7271×10^{-4}	2.46993×10^{-2}
1.171875	-153.0135×10^{-4}	2.7069×10^{-2}
1.1875	-158.2006×10^{-4}	2.98947×10^{-2}
1.203125	-162.3159×10^{-4}	3.28081×10^{-2}
1.21875	-165.3901×10^{-4}	3.58044×10^{-2}
1.234375	-167.4565×10^{-4}	3.88784×10^{-2}
1.25	-168.5512×10^{-4}	4.20244×10^{-2}

6. Conclusions

In this paper, a finite-difference technique has been successfully applied to approximate the solution of a class of convection-diffusion equations with non-linear source terms. The method has been used the difference formula for approximating the first and second derivative, and the fractional Grünwald-Letnikov formula for approximate the Riemann-Liouville integral $J_a^{\alpha}\phi(x,t)$ and yield an implicit scheme that is consistent and stable. The numerical example has been indicated that the FDM is effective, precise, and good to get results.

Acknowledgment. the author expresses they're thanks to unknown referees for reading and helpful comments.

Conflicts of Interest. "The author declares no conflict of interest.

References.

Abolhasani, M., Abbasbandy, S., & Allahviranloo, T. (2017). A new variational iteration method for a class of fractional convection-diffusion equations in large domains. *Mathematics*, *5*(2), 26.

Allen III, M. B., & Isaacson, E. L. (2011). *Numerical analysis for applied science* (Vol. 35). John wiley & sons.

Arqub, O. A., Edwan, R., Al-Smadi, M., & Momani, S. (2020). Solving space-fractional Cauchy problem by modified finite-difference discretization scheme. *Alexandria Engineering Journal*.

Chandrasekhar, S. (1943). Stochastic problems in physics and astronomy. *Reviews of Modern Physics*, *15*(1), 1.

Izadkhah, M. M., & Saberi- Nadjafi, J. (2015). Gegenbauer spectral method for time-fractional convection–diffusion equations with variable coefficients. *Mathematical Methods in the Applied Sciences*, *38*(15), 3183–3194.

Jia, J., & Wang, H. (2016). A fast finite volume method for conservative space-fractional diffusion equations in convex domains. *Journal of Computational Physics*, *310*, 63–84.

Lax, P. D., & Richtmyer, R. D. (1956). Survey of the stability of linear finite difference equations. *Communications on Pure and Applied Mathematics*, *9*(2), 267–293.

Palencia, C., & Sanz-Serna, J. M. (1984). An extension of the Lax-Richtmyer theory. *Numerische Mathematik*, *44*(2), 279–283.

Podlubny, I. (1998). *Fractional differential equations: an introduction to fractional derivatives, fractional differential equations, to methods of their solution and some of their applications*. Elsevier.

Qiu, Y., & Sloan, D. M. (1999). Analysis of difference approximations to a singularly perturbed two-point boundary value problem on an adaptively generated grid. *Journal of Computational and Applied Mathematics*, *101*(1–2), 1–25.

Saadatmandi, A., Dehghan, M., & Azizi, M.-R. (2012). The Sinc–Legendre collocation method for a class of fractional convection–diffusion equations with variable coefficients. *Communications in Nonlinear Science and Numerical Simulation*, *17*(11), 4125–4136.

Salkuyeh, D. K. (2006). On the finite difference approximation to the convection–diffusion equation. *Applied Mathematics and Computation*, *179*(1), 79–86.

Sayevand, K., & Arjang, F. (2016). Finite volume element method and its stability analysis for analyzing the behavior of sub-diffusion problems. *Applied Mathematics and Computation*, *290*, 224–239.

Shongsheng, D., & Jianing, P. (1998). Application of convection-diffusion equation to the analyses of contamination between batches in multi-products pipeline transport. *Applied Mathematics and Mechanics*, *19*(8), 757–764.

Strikwerda, J. C. (2004). *Finite difference schemes and partial differential equations*. SIAM.

Tekriwal, M., Duraisamy, K., & Jeannin, J.-B. (2021). A formal proof of the Lax equivalence theorem for finite difference schemes. *NASA Formal Methods Symposium*, 322–339.

Thomas, J. W. (2013). *Numerical partial differential equations: finite difference methods* (Vol. 22). Springer Science & Business Media.

Wang, Y.-M. (2015). A compact finite difference method for a class of time fractional convection-diffusion-wave equations with variable coefficients. *Numerical Algorithms*, *70*(3), 625–651.

Zhang, J., Zhang, X., & Yang, B. (2018). An approximation scheme for the time fractional convection–diffusion equation. *Applied Mathematics and Computation*, *335*, 305–312.

Zhao, Y., Zhang, Y., Shi, D., Liu, F., & Turner, I. (2016). Superconvergence analysis of nonconforming finite element method for two-dimensional time fractional diffusion equations. *Applied Mathematics Letters*, *59*, 38–47.

تحليل الاستقرار والتقارب لتقنية الفروق المحدودة لحل فئة من معادلة انتشار الحمل الحراري بشرط مصدرغير خطي

ريم العدوان

قسم الرياضيات- جامعة طيبة- المدينة المنورة- المملكة العربية السعودية

الملخص

يتم نقل الجسيمات والكميات الفيزيائية داخل نظام فيزيائي عن طريق عمليات الانتشار والحمل الحراري، ويمكن نمذجة هذه العملية الفيزيائية من خلال معادلات الحمل الحراري مع وبدون شرط المصدر. في هذا البحث ، تم تنفيذ نهج جديد لطريقة الفروق المحدودة FDM لحل فئة من معادلات CDEs ذات الاستخدام الحراري بشرط مصدر غير خطي. تقوم هذه التقنية بتحويل المشكلة إلى المخطط الضمني باستخدام صيغة Grünwald-Letnikov الكسرية. يوضح مثالنا العددي أن المقارنة بين الحل التقريبي والحل الدقيق تكشف عن موثوقية وقدرة الطريقة المقترحة.

الكلمات المفتاحية: طريقة الفروق المحدودة ، معادلات الحمل الحراري ، مشتق ريمان، ليوفيل الجزئي.

Evaluation of efficacy of two bacterial insecticides as natural larvicidal agents against *Culex pipiens*

Tariq Saeed Alghamdi

Biology Department, Faculty of Science, Albaha University, Al-Baha, Saudi Arabia

Abstract

Mosquitoes are transporters of eminent pathogens such as malaria, dengue, etc. These diseases result noteworthy morbidity and mortalities of humans and livestock all over the globe. Culex pipiens is one of the main and common mosquito species in Saudi Arabia. it is accountable for transmission other diseases such as Lymphatic filariasis and West Nile virus. The conventional approach to control Cx. pipiens is usage of insecticides which played an operative part in dropping off the mosquito population. However, this control method is being escorted with certain public distresses and mosquito confrontation to insecticides. The investigation aims to estimate larvicidal action of two bacterial biocontrol agents, Vectobac (Bacillus thuringiensis) and Tracer (Saccharopolyspora spinosa) against the larvae of Cx. Pipiens. The present research investigated the lethal effects of these bacterial insecticides against the larvae under laboratory conditions. The concentrations used for Vectobac were 0.02 to 0.2 ppm. While, the concentrations used for Tracer compound were 0.02 to 0.5 ppm. The outcomes demonstrated that death frequency of larvae extended from 15% to 98% for Vectobac and 33% to 99% for Tracer respectively after 24 h of treatment. According to LC50 value, it is evident that Tracer possess strong larvicidal efficiency as compared to Vectobac compound by about 1.46 fold. The obtained results suggest that the studied bioinsecticides could possibility act as a suitable candidate to control the major vectors of filarial parasite which are frequently predominant in Saudi Arabia as well as they are safer for living community and environment.

Keywords*:* Insecticides, *Culex pipiens*, *Lymphatic filariasis*, *B. thuringiensis, S. spinosa*, Larvicidal.

1. Introduction

Globally the vector-borne infections are main cause of community health complications as well as their occurrence has increased significantly, especially in poor countries. Mosquitoes (Diptera: Culicidae) are well recognized vectors of several human and animal pathogens (Samy et al., 2016) as well as being a nuisance insect. For example, the dengue and malaria are communicated to human beings via *Aedes* spp. and *Anopheles* spps. Annually, they cause approximately more than one million

deaths (Holt et al., 2002) and severely affect the socioeconomic development of infected countries (Ghramh et al., 2018). *Culex pipiens* L. is unique type of mosquitoes, distributed widely particularly in temperate regions (Weitzel et al., 2001). *Culex pipiens* is major vector of filariasis, known as elephantiasis and arboviruses for instance; West Nile fever and Rift Valley fever viruses (Zayed et al., 2006). Furthermore, the *Cx. pipiens* has been known for its high adaptability and laying eggs in a variety of sites such as ground pools, drains, dishes and clean water in which they reproduce and develop their own species successfully (Rockett , 1987, Vinogradova, 2000,Becker et al., 2012). The traditional method to control and reduce mosquitoes breeding is to apply chemical insecticides Pyrethroids and Organophosphate groups (Peter et al.,2005). Although these types of pesticides demonstrated the success in control programs, but they also produce harmful effects to humans and the environment and they are expensive (Mitra et al, 2001, Jayaraj et al., 2016, Wilson and Tisdell,2001). In addition, the regular use of these chemical compounds could lead resistance to insects (Smith et al. 2019). On the other hand, the use of microbial insecticides amplified during past decades because they are considered pathogenic to insects and eco-friendly method (Chandler et al., 2008, Thomas and Read, 2007). Federici (1995) stated that the bacteria are the major pathogen groups that can be used against vectors due to their effectiveness in killing mosquito larvae as well as their ability to produce in large quantities using inexpensive culture media through fermentation process. A lot of microbes that are pathogenic to insect larvae are now ideal choice to chemicals owing to their superior specificity and lesser amount of resistance development (Chandler et al., 2008, Thomas and Read, 2007). In this regard the two principal microorganisms are *Bacillus thuringiensis* (*Bt*) and *Saccharopolyspora spinosa*, which belongs to Gram-positive sporulating soil bacteria and are capable of synthesizing cytoplasmic crystalline toxins having specific larvicidal activity (Schnepf et al., 1998, Aarthi & Murugan, 2010). At present the larvicidal characteristics of *Bt* toxin inclusions are being exploited commercially as harmless protein-based bioinsecticides in agriculture and forestry pest administration, also in management of disease-carrying vectors (Schnepf et al., 1998; Federici , 2005). *Bt* cells synthesize extremely specific larvicidal proteins in ample amount (Schnepf et al., 1998) and when the larvae feed on it, a toxic effect occurs by making small holes in the wall of the larva's stomach, which eventually leads to the decomposition of its cells and then the death of the larva (Goldberg and Margalit, 1977; Fast, 1985). The current investigation was intended to assess effect of larvicidal properties of two selected bacterial bioinsecticides Vectobac, *B. thuringiensis and* Tracer, *Saccharopolyspora spinosa* against the *Culex pipiens* which is most predominant mosquito species in Saudi Arabia and is accountable for spread of various sicknesses to humans.

2. Material and Methods

2.1 Mosquito rearing

Cx. pipiens mosquito was reared as per Mahyoub et al. (2016) procedure with slight amendments. The culture

temperature and relative humidity was retained 27 ± 1 °C and 70 ± 5% in the laboratory of Research Unit of Dengue Fever and Vector Control, King Abdualaziz University, Saudi Arabia. The adults were nourished on animal blood for three days with a gap of two hours. These generations were raised to acquire ample amount of larvae for investigational purposes.

2.2 Bacterial strain and Stock solution Preparation.

The bacterial bioinsecticides Vectobac 12AS, derived from *B. thuringiensis subsp. Israelensis* and Tracer 480SC, derived from *Saccharopolyspora spinosa* were evaluated as toxic agents against larvae of *Culex pippins*. They were obtained from the Research Unit of Dengue Fever and Vector Control, King Abdualaziz University

In order to prepare the standard stock solution of selected bacterial insecticide (Vectobac 12AS and Tracer 480SC). One gram was taken from each of them and dispensed in 100 ml of distilled water separately and properly mixed to get bacterial uniform solution having concentration of 10000 ppm. Various working concentrations have been developed from the stock solution using the previous methods described elsewhere (Mizerakis et al). The WHO procedure was applied to assess the sensitivity of mosquito larvae to the bacterial insecticides.

2.3 Evaluation of larvicidal toxicity

In order to determine the toxic effect on the tested larvae, 20 primary developing fourth-stage larvae has been placed into a 400 ml glass containers having 100 ml tap water. Treatments started by exposing larvae to various concentrations of each selected bacterial insecticide (Vectobac): 0.02, 0.04, 0.06, 0.08, 0.2 ppm and (Tracer 480SC): 0.02, 0.03, 0.05, 0.1, 0.5 ppm and control groups were adjusted under controlled laboratory conditions. Five replicates have been utilized for every concentration of the selected bacterial insecticide and larvae death was documented at 24 h post-treated. The treated larvae and control were supplied with meals during the experimental assessment to avoid starvation cases.

2.4 Analysis of data

The laboratory toxicity of the studied bacterial for biological assessment tests against mosquitoes was analyzed using LdP-Line software (by Ehab Bakr). Percentages of larval mortality, plot toxicity lines, LC_{50} (lethal concentration required to kill 50% of larvae), Slop value and chi-square (Chi) were calculated according to the method of Finney (1971). The composed data was statistically evaluated by means of one-way ANOVA and mean values were equated by LSD test at $P \leq 0.05$ using SPSS software package version 23.

3. Results and Discussion

In current times, the finest available control mechanisms for these ailments are established on vector control that is chiefly accompanied by means of synthetic insecticides (Ibarra et al. 2003). Also, mosquitoes have established resistance to generally utilized chemical insecticides for instance; global DDT and Organophosphate (Smith et al,2019, Muhammad et al, 2021). Therefore, the usage of entomopathogenic bacteria such as *Bacillus thuringiensis* and *Bacillus*

sphaericus as biolarvicides, is feasible substitute for bugs Management.

In the present study the bacterial pathogens have been used against insects of public health relevance, primarily mosquitoes. The obtained results indicated that under laboratory environment, the bacterial insecticides, Vectobac, *B. thuringiensis* and Tracer, *Saccharopolyspora spinosa* were lethal to fourth-stage larvae of *Cx. pipiens*. The outcomes indicated that effective concentration was between 0.02-0.2 ppm with corresponding larval death percentage ranged from 15% to 98 and amongst 0.02 – 0.5 ppm with corresponding larval death ranging from 33% to 99% at 24 h of exposure to Vectobac and Tracer compounds respectively (Table 1 and 2).

Table 1: Susceptibility level of *Culex pipiens* larvae to bioinsecticides, Vectobac after continuous exposure for 48 h.

Bioinsecticide	**Treatment conditions**	**Conc.(ppm)**	**Mortality (%)Mean *± SD**	**LC_{50} (ppm) (LCL-UCL)**	**Chi****	**Slope**
Vectobac (*B. thuringiensis*)	Lab	0.02 0.04 0.06 0.08 0.2	15± 0.15e 45± 0.17d 65± 0.5c 80±0.57b 98±0.5a	0.0438 (0.0395 – 0.0483)	0.153	3.089

Five replicates, 20 larvae each; control mortalities ranged from (0.0 – 4.0%)
*Means followed by different letter(s) are significantly different from each other (P < 0.05) by LSD test.
**Chi (when chi-square tabulated larger than at 0.05 level of significance indicates the homogeneity of results)

Table 2: Susceptibility level of *Culex pipiens* larvae to bioinsecticides, Tracer following continuous exposure for 48 h.

Bioinsecticide	**Treatment conditions**	**Conc.(ppm)**	**Mortality (%)Mean *± SD**	**LC_{50} (ppm) (LCL-UCL)**	**Chi****	**Slope**
Tracer (*S. spinosa*)	lab	0.02 0.03 0.05 0.1 0.5	33 ± 0.12e 53 ± 0.5d 66 ± 1.14c 88 ± 0.5b 99 ±0.7a	0.0301 (0.0253 – 0.0349)	1.505	2.097

Five replicates, 20 larvae each; control mortalities ranged from (0.0 – 4.0%)
*Means followed by different letter(s) are significantly different from each other (P < 0.05) by LSD test.
**Chi (when chi-square tabulated larger than at 0.05 level of significance indicates the homogeneity of results)

The generated results determine the vulnerability of *Cx. Pipiens* to bacterial insecticide tested under controlled lab atmosphere. The LC50 values was observed at 0.04 ppm for Vectobac and at 0.03 ppm for Tracer. This indicated that the Tracer was more effective against larvae of *Cx. Pipiens* than Vectobac by approximately 1.46 times (Table 3).

Table 3: The lethal concentration required to kill 50% of larvae (IC50) for the selected bioinsecticides, Vectobac and Tracer compounds.

No.	Line name	LC_{50}	Lower limit	Upper limit	RR
2	Vectobac (*B. thuringiensis*)	0.044	0.039	0.048	1.467
1	Tracer (*S. spinosa*)	0.03	0.025	0.035	

Resistance Ratio (RR) Compared with Tracer

Additionally, the testers of treated larvae displayed homogeneousness to diverse quantities of studied insecticide as displayed in Fig.1. The outcome of current research was consistent with preceding indications on bacterial pathogens against mosquito vectors (Mahesh Kumar et al. 2013). It was found that spraying of *Bti* on the breeding site of *Aedes triseriatus* resulted in high mortality rates and effective concentrations were between 1-10 ppm (DeMaio et al., 1981). Mittal (2003) reported that the aqueous suspension of *Bti* (Vectobac 12 AS) was operative towards *An. culicifacies* and *An. stephensi* under laboratory and field settings (Mittal 2003). Interestingly, the Spinosad compound, derived from Saccharopolyspora spinosa has been found to eradicate the counts of immature aquatic stages of *Ae. aegypti* and *Ae. albopictus* in cemetery as well as in water reservoirs (Alsobhi et al. 2016).

Likewise, in another research investigation it has been reported that B. *sphaericus* is extremely lethal against *An. Stephensi* with LC_{50} values of 44.29 ppm for first-stage larvae and 95.55 ppm for pupae (Mahesh Kumar et al. 2013). Additionally, it also has been reported that the *B. sphaericus* is toxic to first- to fourth larvae stages and pupae *An. stephensi* with LC_{50} values ranged between 0.051% (first-stage) and 0.073% (pupae)(Mahesh Kumar et al. 2013). Similarly, earlier workers have observed the larvicidal, fecundity and endurance efficacy of *B. sphaericus* on the malarial vector *An. stephensi* (Kamal and Khater 2013). Furthermore, it has also been described that amalgamation of *B. thuringiensis kurstaki* and botanical insecticides resulted in two-fold reduction in gut enzyme action of larvae of rice leaf folder (Dua et al. 2009) . This might confirm the important role of natural components in insect control and their ability to cause harm to insects. In current research, the toxic impact of selected strains of bacteria (*Bacillus thuringiensis* and *Saccharopolyspora spinose*) against *Cx. pipiens* which led to larvae death is attributed probably to their lethal effect on insect stomach or might their impact on physiological function of insect such as nerve system. These observations are correspondent to Poopathi and Abidha study who found that a disruption and separation in the epithelial cells midgut of mosquito larvae eventually caused death (Poopathi and Abidha, 2010). Panneerselvam et al (2013) testified that poisonousness of bacterial insecticide against *Ae. aegypti* is attributed to the excitation of insect nervous system which resulted in contraction of involuntary muscle and paralysis. This clearly indicates that these biopesticides are promising biological agents and safe options to control mosquitoes and other pest.

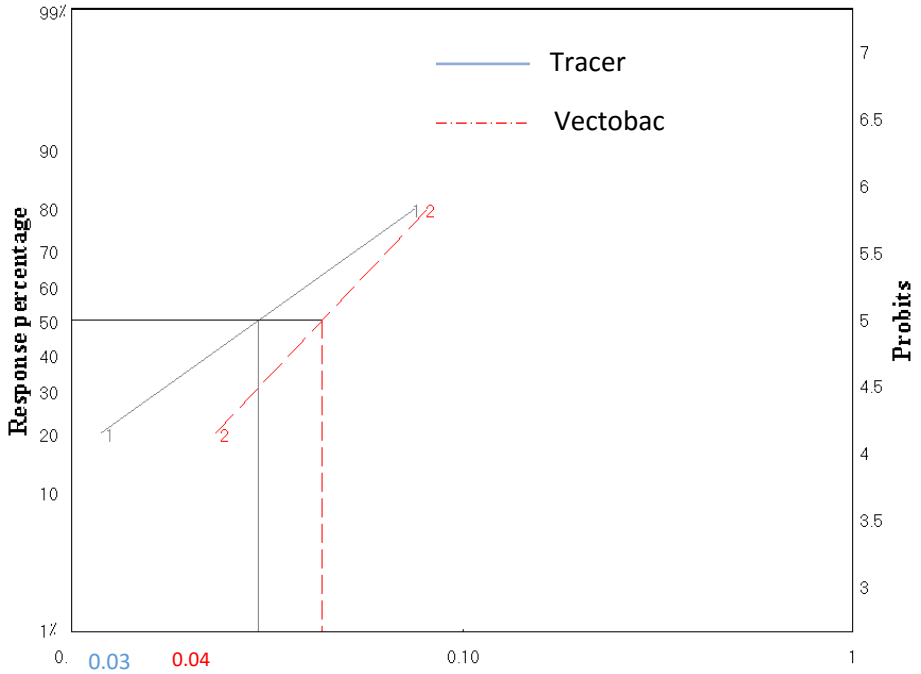

Fig. 1. The relationship between concentrations of selected bioinsecticides and mortality percentage of 4th instar larvae of *Culex pipiens* after 24 h of treatment.

4. Conclusion

The bacterial bioinsecticides Vectobac (*B. thuringiensis*) and Tracer (*S. spinosa*) were used to check their insecticidal effect on the larvae of *Cx. pipiens.* It is obvious from present results that both the studied bioinsecticides had lethal effect on the tested larvae, but Tracer was more efficient than the Vectobac compound. To conclude, this finding that the studied biolarvicidal might be utilized to control various larvae of mosquitoes which are prevalent in the Saudi Arabia, thus help in reducing dangerous diseases. They are impending future candidates which can be some safe replacements to the commonly used chemical pesticides as well as to being an ecological friendly process.

References:

Alsobhi A.S., Al-Ghamdi K., Mahyoub J.A., Khatter N.A., Saggu S., Rehman H., Panneerselvam

C., Murugan K., Higuchi A., Nicoletti M. (2016). Slow release formulations of Bacillus thuringiensis israelensis (AM 65-52) and spinosyns: Effectiveness against the West Nile vector *Culex pipiens* in Saudi Arabia. *Asian Pacific Journal of Tropical Disease*, 6(7):533- 538.

Angsuthanasombat C. (2010). Structural basis of pore formation by mosquito-larvicidal proteins

from Bacillus thuringiensis. The Open Toxinology Journal , 3(1).

Aarthi N., and Murugan, K. (2010). Larvicidal and repellent activity of Vetiveria zizanioides L,

Ocimum basilicum Linn and the microbial pesticide spinosad against malarial vector, Anopheles stephensi Liston(Insecta:Diptera: Culicidae). *Journal of Biopesticides*, 3(1), 199.

Becker N., Jöst A., and Weitzel T. (2012). The *Culex pipiens* complex in Europe. *Journal of the American Mosquito Control Association*, 28(4s), 53-67.

Chandler D, Davidson G, Grant WP, Greaves J, Tatchell GM. (2008). Microbial biopesticides for integrated crop management: an assessment of environmental and regulatory sustainability. *Trends Food Sci Technol* , 19: 275-83

DeMaio J.D., Beier J.C. and Durso S.L. (1981). Larvicidal activity of *Bacillus thuringiensis var. israelensis* against *Aedes triseriatus* in treehole and tire habitats. *Mosq. News*, 41(4): 765- 769.

Dua V.K, Pandey A.C., Raghavendra K, Gupta A., Sharma T., Dash A.P. (2009). Larvicidal activity of neem oil (Azadirachta indica) formulation against mosquitoes. *Malaria Journal*, 8(1):1-6

Fast, P.G. (1981). The crystal toxin of *Bacillus thuringiensis* . In: Burgess, H .D. (ed.) Microbial control of pest and plant diseases 1970-1980. *Academic Press London* , pp. 223-248.

Finney D.J. (1972). Probit analysis: a statistical treatment of sigmoid response curve. University Press, Cambridge.

Federici B. A. (1995). The future of microbial insecticides as vector control agents. *Journal of the American Mosquito Control Association-Mosquito News*,11(2), 260268.

Federici B. A. (2005). Insecticidal bacteria: an overwhelming success for invertebrate pathology. *Journal of Invertebrate Pathology*, 89(1), 30-38.

Ghramh H. A., Al-Ghamdi K. M., Mahyoub, J. A., and Ibrahim, E. H. (2018).

Chrysanthemu extract and extract prepared silver nanoparticles as biocides to control *Aedes aegypti* (L.), the vector of dengue fever. *Journal of Asia-Pacific Entomology*, 21(1), 205-210..

Goldberg L.J. and Margalit J. (1977). A bacterial demonstrating rapid larvicidal activity against *Anopheles sergenti*, *Uranotaenia unguiculata, Culex inivittatus*, *Aedes agypti* and *Culex pipiens*. *Mosq. News*, 37: 355-358.

Holt R. A., Subramanian G. M., Halpern A., Sutton G. G., Charlab R., Nusskern, D. R., ... and

Hoffman, S. L. (2002). The genome sequence of the malaria mosquito *Anopheles gambiae*. *science*, 298(5591), 129-149

Ibarra J.E., del Rincón M.C., Ordúz S, Noriega D., Benintende G., Monnerat R., Regis L., de

Oliveira C.M., Lanz H., Rodriguez M.H. (2003). Diversity of *Bacillus thuringiensis* strains

from Latin America with insecticidal activity against different mosquito species. *Applied and*

Environmental Microbiology,69(9):5269-5274

Jayaraj, R., Megha, P., and Sreedev, P. (2016). Organochlorine pesticides, their toxic effects on

living organisms and their fate in the environment. *Interdisciplinary toxicology*, 9(3-4), 90.

Kamal H.A., Khater E.I. (2013). Potency and persistence of the bacterial mosquitocide *Bacillus*

sphaericus against culicine mosquitoes under field conditions. *Journal of the Egyptian Society of Parasitology* ,43(1):115-124

Mahesh Kumar P., Kovendan K., Murugan K. (2013). Integration of botanical and bacterial insecticide against *Aedes aegypti* and *Anopheles stephensi*. *Parasitology research* ,112(2):761-771.

Mittal P. (2003). Biolarvicides in vector control: challenges and prospects. *Journal of vector borne diseases*,40(1/2):20

Mitra A., Chatterjee, C., and Mandal, F. B. (2011). Synthetic chemical pesticides and their effects on birds. *Res J Environ Toxicol*, 5(2), 81-96.

Muhammad A., Ibrahim S. S., Mukhtar M. M., Irving, H., Abajue, M. C., Edith, N. M., ... and Wondji, C. S. (2021). High pyrethroid/DDT resistance in major malaria vector Anopheles coluzzii from Niger-Delta of Nigeria is probably driven by metabolic resistance mechanisms. *Plos one*, 16(3), e0247944.

Panneerselvam C., Murugan K., Kovendan K., Kumar P.M., Subramaniam J. (2013).

Mosquito larvicidal and pupicidal activity of Euphorbia hirta Linn.(Family: Euphorbiaceae) and *Bacillus sphaericus* against *Anopheles stephensi* Liston.(Diptera: Culicidae). *Asian Pacific journal of tropical medicine*, 6(2):102-109.

Peter R. J., Van den Bossche P., Penzhorn, B. L., and Sharp, B. (2005). Tick, fly, and mosquito

control lessons from the past, solutions for the future. *Veterinary parasitology*, 132(3-4), 205-215.

Poopathi S. and Abidha S., Mosquitocidal bacterial toxins (*Bacillus sphaericus* and *Bacillus thuringiensis* serovar israelensis): Mode of action, cytopathological effects and mechanism of resistance. *J Physiol Pathophysiol*, 1(3), 22-38 (2010).

Rockett, C. L. (1987). Bacteria as ovipositional attractants for *Culex pipiens* (Diptera:Culicidae).*The Great Lakes Entomologist*, 20(3), 10.

Samy A. M., Elaagip A. H., Kenawy M. A., Ayres C. F., Peterson A. T., and Soliman D. E.

(2016). Climate change influences on the global potential distribution of the mosquito *Culex*

quinquefasciatus, vector of West Nile virus and lymphatic filariasis. *PloS one*, 11(10), e0163863.

Schnepf E., Crickmore N., Van Rie J.(1998). *Bacillus thuringiensis* and its pesticidal crystal proteins. *Microbiol Mol Biol Rev*, 62: 775-806.

Smith L. B., Sears C., Sun H., Mertz R. W., Kasai S., and Scott J. G. (2019). CYP-mediated resistance and cross-resistance to pyrethroids and organophosphates in *Aedes aegypti* in the presence and absence of kdr. *Pesticide biochemistry and physiology*, 160, 119-126.

Thomas MB, Read AF. (2007). Can fungal biopesticides control malaria? *Nature Rev Microbiol* , 5: 377-83.

Vinogradova E.B. (2000). Culex pipiens pipiens mosquitoes: taxonomy, distri-bution, ecology,physiology, genetics, applied importance and control. *Pen-soft Publishers*, p. 253.

Weitzel T., Braun K., Collado A., Jöst A., Becker N. (2011). Distribution and frequency of *Culex pipiens* and *Culex torrentium* (Culicidae) in Europe and diagnostic allozyme markers. *Eur Mosq Bull*, 29:22-37.

WilsonC.,and Tisdell C.(2001). Why farmers continue to use pesticides despite environmental,health and sustainability costs. *Ecological economics*, 39(3),449-462.

Zayed A. B. B., Szumlas D. E., Hanafi H. A., Fryauff D. J., Mostafa A. A., Allam K. M., and Brogdon, W. G. (2006). Use of bioassay and microplate assay to detect and measure insecticide resistance in field populations of *Culex pipiens* from filariasis endemic areas of Egypt. *Journal of the American Mosquito Control Association*, 22(3), 473-482.

تقييم فعالية اثنين من المبيدات البكتيرية كمبيدات طبيعية ضد يرقات بعوض الكيولكس بيبينز(*Culex pipiens*)

الدكتور طارق سعيد الغامدي

جامعة الباحة – كلية العلوم – قسم الأحياء

الملخص

يعد البعوض ناقلا للعديد من المسببات المرضية الشائعة مثل تلك التي تسبب مرض الملاريا وحمى الضنك وغيرها من الامراض والتي تؤدي الى معدلات كبيرة من الوفيات للعديد من البشر والحيوان على حد سواء في جميع انحاء العالم . بعوض الكيولكس بيبنز (*Culex pipiens*) هو احد أنواع الأكثر شيوعا وتواجدا في المملكة العربية السعودية. حيث يعتبر هذا النوع الناقل الرئيس لمرض داء الفيلاريا اللمفي او ما يعرف بداء الفيل وكذلك مرض فيروس حمى غرب النيل. ان استخدام المبيدات التقليدية أظهرت دورا فعالا في تقليل كثافة وانتشار مجتمعات هذا النوع من البعوض الا ان ذلك صاحبه العديد من الاضرار الصحية على السكان بالإضافة الى اكساب البعوض نوع من المقاومة ضد هذه المبيدات . يهدف هذا البحث إلى تقييم التأثير الضار لاثنين من المبيدات الحيوية البكتيرية Vectobac *(Bacillus thuringiensis)* و Tracer *(Saccharopolyspora spinosa)* ضد يرقات بعوض الكيولكس بيبينز (*Culex pipiens*) تحت الظروف المعملية المثالية. التركيزات المستخدمة للمركب البكتيري Vectobac كانت تتراوح من ٠,٠٢ الى ٠,٢ جزء في المليون بينما في المركب الآخر *Tracer* كانت تتراوح ما بين ٠,٠٢ الى ٠,٥ جزء في المليون. أظهرت النتائج ان مشاهدات موت اليرقات وفقا لهذه التراكيز (من اقل الى اعلى تركيز) كانت ما بين ١٥ الى ٩٨ % لمركب Vectobac بينما كانت تتراوح من ٣٣ الى ٩٩% لمركب Tracer وذلك بعد ٢٤ ساعة من المعالجة. ووفقا لقيمة LC50 فانه يتضح بان مركب Tracer يمتلك كفاءة اقوى في قتل اليرقات بـ ١,٤٦ مرة مقارنة بمركب Vectobac . وبشكل عام فان هذه النتائج المتحصل عليها تشير إلى أن المبيدات الحيوية البكتيرية المستخدمة في هذا الدراسة يمكن أن تنتخب كمركبات مناسبة للسيطرة على النواقل الرئيسية لطفيل الفيلاري السائد في المملكة العربية السعودية بالإضافة إلى كونها أكثر أمانًا للمجتمع الحيوي والبيئة.

الكلمات المفتاحية:المبيدات الحشرية، بعوض الكيولكس بيبنز (*Culex pipiens*)، داء الفيلاريا اللمفي، بكتيريا *B. thuringiensis*، بكتيريا *S. spinosa* ، مبيد يرقي

IoT and Machine Learning based Green AI Sustainability Model for Predicting Electronic Waste

Fathe Jeribi

College of Computer Science and Information Technology, Jazan University, Saudi Arabia

Abstract

Environmental sustainability is a major concern of any firm or a government in the current technological era. Green computing is an initiative to reduce the environmental impact of technology through less energy spending, minimize electronic waste and to promote sustainability. Artificial Intelligence (AI) research is at the forefront of addressing various environmental issues related to product design, product maintenance, energy utilization and many more. In an effort to add value to this green AI initiative, a Machine Learning (ML)- based Electronic Waste (e-Waste) prediction model is proposed. Data from an organization's electronic device is obtained using an Internet of Things (IoT) enabled mechanism. Linear Regression (LR) is introduced in the model to estimate the dynamic condition of the equipment, time of maintenance, and disposal of the equipment. The various metrics such as Pearson r Correlation Coefficient (r-CC), Relative Absolute Error (RAE) and Mean Absolute Error (MAE) are used to evaluate the performance of the estimators. The prediction model is evaluated using real-time data obtained from IoT enabled university campus. On evaluation, the proposed model showcased better performance in prediction.

Keywords: IoT, Machine Learning, Linear Regression, Green AI, e-Waste, Sustainability

1. INTRODUCTION:

Old gadgets are being replaced and abandoned as innovation improves. An electric and electronic device that is discarded by consumers is referred to as "e-Waste." E-Waste is rapidly increasing in the current technological world and is now one of the world's most important challenges to environmental sustainability.

The National Oceanic and Atmospheric Administration (NOAA) of USA has issued a warning that atmospheric CO_2 levels have risen substantially [1], and the earth's temperature has risen at a pace of 0.14° F (0.08° C) every decade since 1880 [2]. It is important to take into account the environmental damage produced by electrical devices. Nobody can deny that every technology has a carbon footprint, which means that we humans are contributing to global warming. A startling fact is that it takes ten tonnes of CO2 to produce one tonne of laptop. When looking at a device's overall CO2 emissions, the majority of it occurs during manufacturing, that is, before the product comes to the consumer's hand [3]. Reduced carbon production techniques, optimal product use through recycling, and safe e-Waste disposal are thus essential factors to consider for a beneficial impact on the environment. Furthermore, keeping a close eye on electronic products is essential for getting the most out of them and disposing of them safely. Hence, it is vital to predict potential scenarios in

Neural Network (NN) to estimate e-Waste week by week for each village. Various information-driven approaches include regular machine learning computations as well as the existing developed model and its modification. This work used advanced techniques to handle various situations by estimating the e-Waste, but was lacking in optimizing the lifespan of the products. TV Balakrishnan et al. [7] proposed a big data analytics method for e-Waste disposal by designing a five-step process without providing technical information about e-Waste processing, which they claim is effective. In their comprehensive review, Agarwal, S. et al. [8] show the breadth of AI in the management of e-Waste. To obtain the data, they used the data retrieval and synchronization method. Furthermore, they presented computational techniques for e-Waste segregation, and the techniques provided an efficient strategy in solving recurring problems related to e-Waste in an intelligent way, implying that artificial intelligence's impact and scope are high in the near future as well as now.

The following uncertainties remain after reviewing the findings of the bench marking literatures related to AI-based e-Waste management:

- In the literatures, the sources of product data are ambiguous [6][7].
- Prediction models fail to handle key aspects of e-Waste management, such as maintenance and recycling [4][5][6].
- The evaluation measures by which the ML-based e-Waste prediction frameworks [5][6][7] justify their advance for proper maintenance of the electronic products and to extend their life time. Machine Learning has made real-time forecasting easy, and it's much easier when combined with IoT capabilities. Although a wide range of ML-based forecasting models for sustainability were brought out by the researchers, only a few were found to be used for e-Waste prediction.

Sujinna Karnasuta et al. [4] proposed a statistical model for predicting the e-Waste generation in a university campus with an objective of making the green campus with 0% carbon emission. The experiments handled various issues including electrical equipments, batteries etc. The research fails to address electronic devices and their optimum use in the campus in order to avoid recurrent buying rather than maintenance and recycling. AV Shreyas Madhav et al. [5] were developed a mobile robot that uses transfer learning to identify typical electronic debris and can be attached to conventional municipal garbage trucks. With its arm-based lift and storage mechanism, the robot goes around, locates e-Waste, and executes segregation of the recognized material. The e-Waste is identified and separated using a deep learning-based image identification method. Despite this, the study fails to find electronic products that could be put to better use by extending their lifespan. Haomiao Li et al. [6] offers an e-Waste management framework based on machine learning with the goal of developing a predictive model by combining Gradient Boosting Regression Tree (GBRT) and deep learning-based

An energy consumption predictive analytics model was presented in [9] for a IoT enabled smart home. The forecasting model adopted Linear Regression (LR) and Support Vector Machine (SVM) algorithms, which are used to predict whole-house energy usage and demand. The performances of the two ML algorithms in the forecasting model are studied. It is claimed that IoT enabled system is reliable in observing the data from the nodes. The eccentric factor observed is that the work has not given importance to the forecasting model's performance.

An IoT-connected deep learning framework for electricity price predictions was introduced in [10]. With existing energy pricing datasets, a Long Short-Term Memory (LSTM)-based technique is employed for real-time power price prediction. Using deep neural networks, the strategy overcomes the limitations of classic machine learning models in dealing with certain nonlinear issues. Through decision-level fusion in IoT, it facilitates local asynchronous processing of multisensory data, decreasing bandwidth requirements and offering flawless outcomes in prediction. It is noted that the adopted deep learning framework is claimed to be effective in forecasting in comparison with linear regression.

A university-based waste management project employing IoT and ML is suggested in [11] as part of a Green AI effort. It was proposed to predict trash accumulation by integrating a low-cost digital circuit and long range radio third-generation (LoRa) technology framework's superiority were not reported.

Consequently, in an attempt to overcome the above limitations, this paper presents a comprehensive literature review on ML-based prediction frameworks and subsequently provides a methodology for a ML-based e-Waste prediction framework coupled with IoT. Summarily, the major contributions of this paper are stated as follows:

- A complete analysis on IoT enabled ML-based prediction frameworks especially for addressing sustainability issues.
- Assess the performances of the machine learning algorithms in the selected frameworks.
- Design and propose a ML-based sustainability model for e-Waste prediction and management.

The following is how the rest of this article is organized: The review of related studies is summarized in Section 2. The proposed work is put on in Section 3 by elaborating on the methodology. The experimental results are presented in Section 4, followed by discussion. The paper comes to an end in Section 5 with a conclusion.

2. RELATED WORKS

The essence of various literatures relevant to IoT and ML-based prediction and forecasting models are discussed in this section. Diverse micro level techniques used in the frameworks are also observed. The benefits and shortcomings of such works will also be explored.

studies. Green AI-based energy usage prediction models for optimization are state-of-the-art with ML capabilities and IoT technologies. The prediction framework reported in [16] is one of

these and uses highly appropriate ML and DL algorithms for prediction in an IoT enabled smart farm with the objective of predicting optimum energy usage to take appropriate measures. With a similar objective, [17] proposed a ML based energy saving model, in which they used Wireless Sensor Network (WSN) for getting data and employed Simulated Annealing (SA) method for optimization.

Energy optimization is the key to achieving environmental sustainability. AI and IoT technologies are at the forefront of this mission, with their various prediction models for energy distribution, energy consumption, and energy optimization. Many frameworks have been put forth in recent days [18] [19] [20] [21] in an effort to achieve the above mission through various ML algorithms as well as IoT-based edge and cloud computing capabilities. The properties of energy prediction frameworks are quite similar to those of waste prediction frameworks, and they remain relevant in the methodologies used, such as ML and DL-based prediction algorithms, as well as in gathering real-time data from IoT sensors or edge nodes.

While browsing through the literatures, it is evident that the data processing method in the cloud-based edge computing environment surfaces as a

into the system. Using LR, the system may optimize waste collection by taking the shortest path possible. It is stated that the technology saves time

by determining the ideal path for waste handling.

IoT sensor enabled energy optimization system is facilitated in [12] using ant colony optimization algorithm. The performances were studied and reached 10% energy saving upon real-time adoption of the system. With the help of IoT and ML, an automated waste management system was introduced. There they used microcontrollers and sensors to detect the waste in the city. According to [13], the ML-based image processing technique for classifying waste material is quite interesting and useful.

Various Green AI models have been presented in order to address various sustainability challenges, and some methods are designed to improve on existing frameworks. For example, as reported in [14], Deep Learning (DL) based sustainability model was materialised for segregating degradable and non-degradable wastes. It collects data using IoT and Wireless 4.0. IoT allows for remote control of real-time data, whilst Bluetooth allows for short-range data monitoring via a mobile application. In [15], another interesting simulation model for sustainability that is IoT connected and DL-based for optimizing power energy use is presented. It is stated that the DL technique achieves a high degree of reliability with a low error rate and produces better results than previous

cloud-enabled IoT is depicted in Figure

similar pattern. Whatever the application, data processing is accomplished through a three-layered cloud architecture. The tiered architecture of data processing with

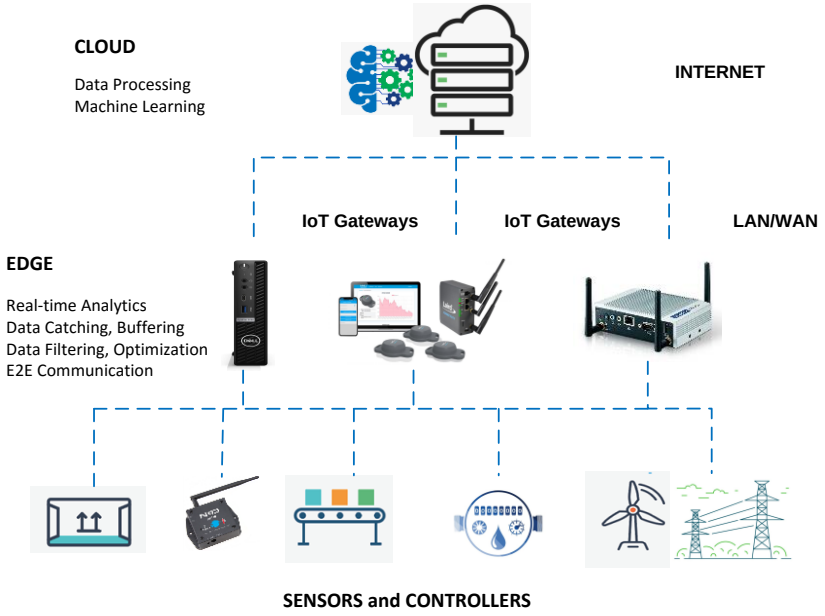

Figure 1: Tiered Architecture of Internet of Things (IoT) for Green AI

with Unique Identifiers (UIDs) and the ability to send data over a network without the need for human intervention. Organizations in a range of industries are increasingly utilizing IoT to work more efficiently, understand better customers in order to provide better customer service, improve decision-making, and raise the value of the business. IoT and Cloud Computing complement one another, and are frequently labelled together while addressing technical services and collaborating to give a better overall IoT solution. Cloud computing in IoT is used to preserve IoT data as part of a collaborative effort. The cloud is a centralized server that contains

3. METHODOLOGY

This section consists of four parts: the first part elaborates on the topology of the edge data collection in the IoT environment; the second subsection provides the proposed prediction model using Linear Regression (LR) followed by the dataset description in the third part; and the fourth part presents the performance metrics of the ML algorithm.

3.1 Internet of Things (IoT) Framework

The internet of things, or IoT, is a network of interconnected computing devices, mechanical and digital machinery, items, animals, or people

devices send device information to the edge server, such as the device's age, operational condition, and maintenance history. Through a router, the data from each campus is subsequently sent to the central cloud. The central cloud

uses machine learning to forecast the device's real-time life span, periodic maintenance, and recycling. The connection between the central cloud and edge clouds is done over a wired network in both directions. The edge cloud, as well as each sensor, is sent across the wireless network. This approach improves the transmission speed while simultaneously lowering the cost of gathering various sensor data [10].

computer resources that may be accessed at any time.

Figure 2 illustrates a tree-like topology of an edge that collects data and uploads it to the cloud. This topology consists primarily of a decision center, a central cloud, and an edge cloud, the latter of which is connected to many wired and wireless, electric and electronic devices, through which data is collected. Data from user electronic and electrical appliances are among the edge data sources.

Figure 2 shows the collecting of edge data by two campuses. They collect data from network nodes and sensors, such as electrical appliances and user terminals. Wireless transmission

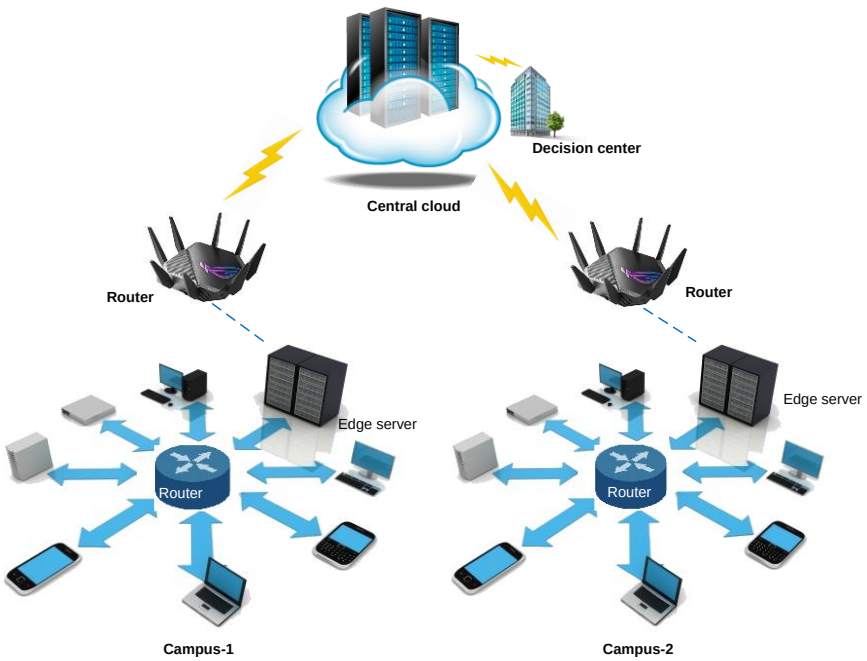

Figure 2: Edge Data Collection Topology

prediction problems and are implemented on diversified platforms. On the basis of the meta-analysis carried out in section 2, the LR model

3.2 The Proposed Machine Learning Model

There are wide ranges of ML algorithms that are being used for

approach can be utilized, which entails minimizing the squared differences between the target and projected outcomes [22]. To do so, the Residual Sum of Squares (RSS) is calculated as follows:

$$RSS = \sum_{i=1}^{n}(y_i - \hat{y_i})^2 \quad (3)$$

The gradient decent method, utilizing the least square approach, might then be used to reduce this error. Minimization is achieved in this way through an iterative approach in the machine learning algorithm.

3.2.2 The Proposed Framework

The process flow of the linear regression-based prediction framework for the e-Waste prediction model is depicted in Figure 3. Data preprocessing is carried out as the first step to clean and remove outliers, complete the data by filling in the gaps with average values, and normalize the data. Here min-max normalization is applied to guarantee the uniform scales of the different features. Outlier analysis aids in the understanding of the dataset. In the next step, normalized data is being prepared for analysis in the form of training (100 each for CPUs and Monitors and 50 sets for Network routers) and test sets (20% of the training sets). The training epochs are carried out with a training dataset and are then validated with new datasets. In the final phase, the test set is used to forecast the outcome by feeding the test data into the trained linear regression model.

is chosen by considering the nature of the prediction problem and the limited number of features. LR is an ideal method for forecasting problems with less number of features and moderated amount of data values [23].

3.2.1 Linear Regression (LR)

A single predictor variable is produced during preprocessing in the proposed forecasting model by considering numerous characteristics connected to the devices and products, and so a simple linear regression model is recommended for this purpose. This regression model includes a predictor variable, which is stated by using a

simple linear equation, which facilitates in the prediction of the output variable. The goal behind the regression, however, is to estimate the parameters of the model commonly stated as from a data sample for the sake of generality [22].

$$\hat{\boldsymbol{y}} = \boldsymbol{\beta_0} + \boldsymbol{\beta_1 x_1} + \ldots\ldots + \boldsymbol{\beta_n x_n} + \boldsymbol{\epsilon} \quad \textbf{(1)}$$

where $\hat{y}$ is the output variable, $x_1, x_2 \ldots x_n$ are the predictor variables (device characteristics in this problem) and $\beta_1, \beta_2, \ldots \beta_n$ are the learning coefficients (parameters) in the model. ε is the iteration error which lies between 0 and input variance (σ^2), which is written as:

$$\varepsilon \sim N(0, \sigma^2) \quad (2)$$

In order to acquire the best prediction, it's important to calculate learning coefficients (β). For estimating this coefficients, the ordinary least squares

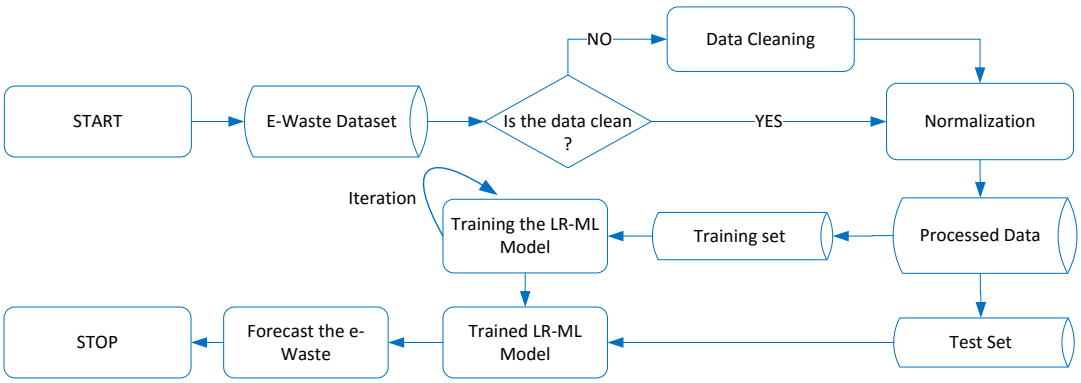

Figure 3: Process Flow of LR-ML Model for e-Waste Prediction

The learning rate of the algorithm has an impact on how quickly it learns. The number of epochs is the number of times the gradient descent algorithm iterates until the cost is minimized. In a nutshell, the following procedures were followed:

a) Determine the predictor and outcome variables
b) Select the appropriate hyperparameters
c) State the activation function
d) Train the model with training dataset
e) Test the model's performance using test dataset
f) Use the model for predictions

Based on the above factors, a predictor variable is created (value between 1 - 100) which is named “E-score”. Higher value indicated more durable and lower value indicates about to recycle. E-score of every CPU is updated in the frequent intervals based on the factors which are related to the CPU. The corresponding output variable is the anticipated lifespan of the CPUs (in months) which is termed “E-life”. The scatter plot showing the data points of ‘E-Score versus E-life’ of 100 CPUs, 100 display monitors and 50 network routers in the campus since the past 3 years is shown in Figure 4 before preprocessing.

3.3 Dataset

The dataset for the implementation of the proposed framework is obtained from the university campus. Because CPU, display monitors, and network routers are in such high demand on campus, they are factored into the forecasting model. In the same way other electrical and electronic devices dataset can be created and used in the framework.

The dataset is created by considering various factors related to the CPU including, data of purchase, configuration (RAM capacity, processor speed), number of failures and number of maintenance attempts.

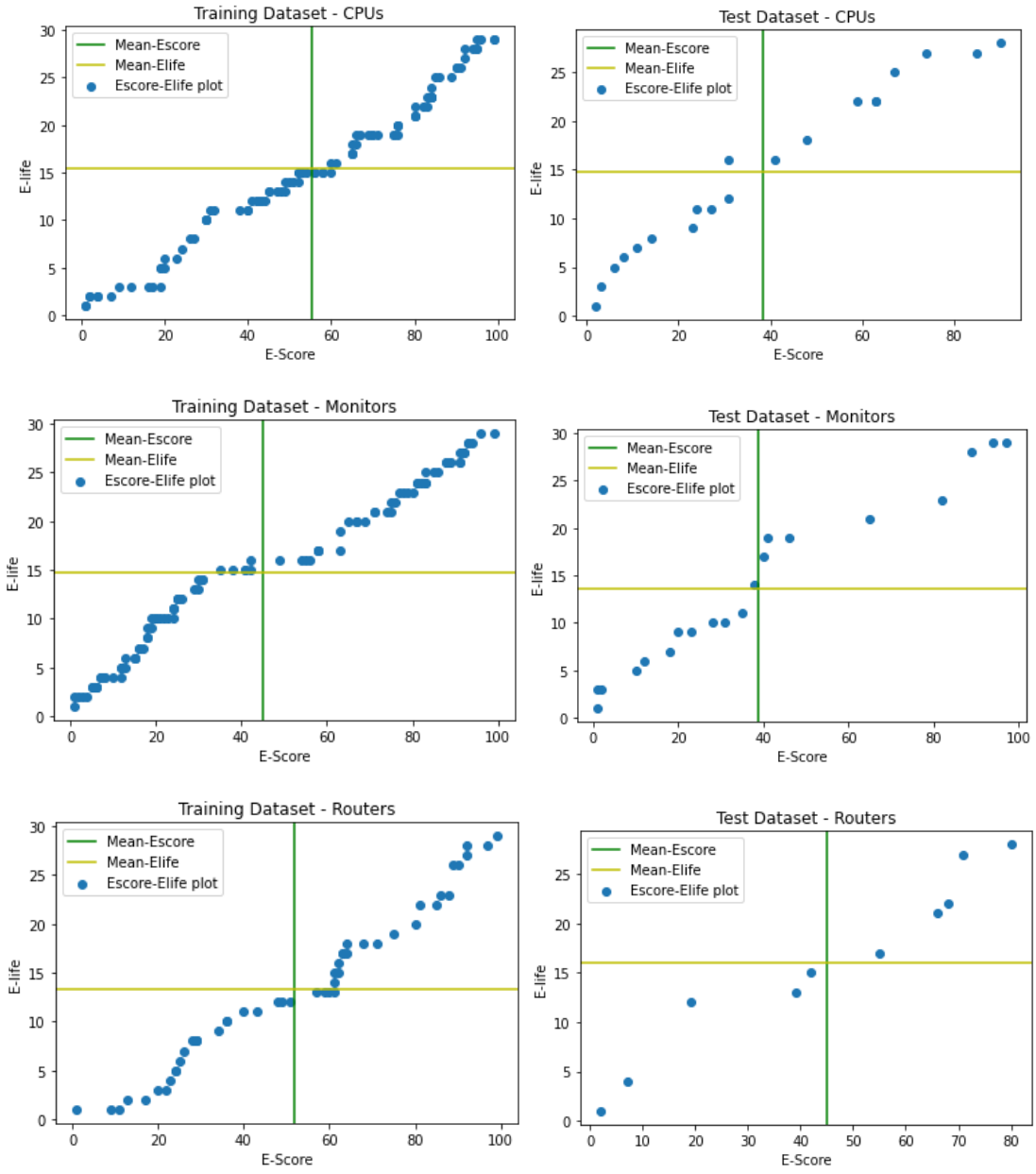

Figure 4: Scatter Plots Showing the Data Points of Training and Test Datasets

3.4.1 Pearson r Correlation Coefficient (r-CC)

A statistical technique called correlation is used to assess and describe the strength and direction of a relationship between two variables. The strength of a relationship between two variables is determined by the degree to which they are related, whereas the direction of a relationship is determined by how one variable changes its value when the value of the other variable changes. It is a measure

3.4 Performance Metrics

Reach out to the evaluation parameters once the LR model has been trained to see how it performs with the new data. Correlation Coefficient (CC), Relative Absolute Error (RAE), and Mean Absolute Error (MAE) are the most significant measures to measure prediction performance of a regression problem [24]. Hence, the three significant measures such as CC, RAE, and MAE, are used to evaluate this prediction model.

value of "E-life." RAE is thus calculated as follows:

$$RAE = \frac{\sum_{i=1}^{n} |P_i - A_i|}{\sum_{i=1}^{n} |\bar{A} - A_i|} \times 100 \quad (5)$$

Where P_i is the value predicted by the model during the test phase for the data sample i, A_i is the target value for the sample i during the training phase and $\bar{A}$ is the mean of the target values during the training phase.

3.4.3 Mean Absolute Error (MAE)

The MAE is a measurement of the difference between a model's actual output (testing phase output) and the desired output (training phase output) for the same equipment. It is calculated as follows:

$$MAE = \frac{1}{n}\sum_{i=1}^{n} |P_i - A_i| \quad (6)$$

During the testing process, this measure is used to confirm that the model is error-free. This measure's values ranging from 0 to infinity. With a value of 0, the model remains error-free.

4. RESULTS AND DISCUSSION

By employing the IoT enabled mechanism as discussed in section 3, the data related to the devices on the campus is sensed and obtained through the cloud server [25]. The device features are further subjected to preprocessing to create the datasets as explained in section 3.3. After preprocessing the data obtained in the central cloud, the datasets of the campus's CPUs, display monitors, and network routers are prepared as training sets and test sets. The results of the proposed forecasting model using linear regression are obtained for

to investigate the relationship between the two variables as they change over time.

Pearson's r correlation is a commonly used statistic for determining the degree of relation between linearly related variables. When looking at this dataset, the Pearson's *r* correlation, for example, can be used to determine the degree to which "E-score" and "E-life" are associated while taking into account historical data. The Pearson's r correlation is calculated using the following formula:

$$r = \frac{N\sum xy - \sum x \sum y}{\sqrt{[N\sum x^2 - (\sum x)^2][N\sum y^2 - (\sum y)^2]}} \quad (4)$$

where N is the input size, (x_i, y_i) are the input paired instances. The Pearson correlation coefficient *r* is a number that varies from -1 to 1, with 1 indicating that the relationship between x and y can be explained using a linear equation. For instance, the Pearson correlation for the training data set (for the CPUs) of this problem is estimated at 0.941, indicating that the predictor and outcome variables are strongly correlated. The correlation factor of the proposed predictor model, along with other metrics, is discussed in the following section for a completely new data set.

3.4.2 Relative Absolute Error (RAE)

The Relative Absolute Error (RAE) is the ratio of a model's cumulative absolute error (test phase) to a predictor's cumulative absolute error (training phase). In this case, the predictor's cumulative absolute error is derived by summing up the difference of each predictor value and the mean

these devices. Tables 1 to 3 exhibit the correlation coefficient, RAE, and MAE of this proposed LR prediction model for the three devices: CPU, display monitor, and network router, respectively.

Table 1 Testing Phase Performance of the LR Model with CPU Dataset

Dataset (20 samples each)	**r-CC**	**RAE (%)**	**MAE**
Set1	0.901	45.6	0.73
Set2	0.881	44.3	0.84
Set3	0.872	44.8	0.67
Set4	0.886	43.6	0.74
Set5	0.913	44.8	0.81
Average	0.891	44.6	0.758

Table 2 Testing Phase Performance of the LR Model with Monitor Dataset

Dataset (20 samples each)	**r-CC**	**RAE (%)**	**MAE**
Set1	0.877	44.1	0.99
Set2	0.796	45.1	0.75
Set3	0.851	44.3	0.80
Set4	0.837	43.8	0.77
Set5	0.891	44.2	0.98
Average	0.850	44.3	0.858

Table 3 Testing Phase Performance of the LR Model with Router Dataset

Dataset (20 samples each)	r-CC	RAE (%)	MAE
Set1	0.603	42.8	0.74
Set2	0.794	43.9	0.79
Set3	0.763	45.0	0.86
Set4	0.866	43.5	0.93
Set5	0.695	42.5	0.95
Average	0.7442	43.54	0.854

The Pearson Correlation Coefficient (abbreviated as r-CC) for all three devices reached above 0.74, which means the predictor values and the outcome values obtained from the model are strongly correlated. Among the three products, r-CC for the CPUs is close to 0.9. The RAE percentage is in the middle, which shows that the ratio between the testing phase total absolute error and the training phase total absolute error is almost similar with a slight margin. This will also indicate the model's best performance in future datasets. The MAE of all the devices is very low (i.e., 1), indicating that the prediction model is error-free and compatible with the dataset. The overall performance of the LR prediction model is shown in table 4.

Table 4 Overall Performance of Proposed LR Prediction Model

Device	r-CC	RAE (%)	MAE
CPUs	0.891	44.6	0.758
Monitors	0.850	44.3	0.858
Routers	0.744	43.5	0.854

For the reason that the analogous works of e-Waste prediction for sustainability are scarce, and even the few chosen works employed different estimates for the forecast, the suggested study may be deemed unique.

5. CONCLUSION

Sustainability is the hot topic these days, and e-Waste is a key source of concern among environmentalists. In order to address this issue, computer scientists from all over the world are proposing green AI initiatives. One of the most promising e-Waste prediction models utilizing IoT and ML is presented here, and it adds feathers to the green AI efforts, especially in large firms. The prime objective of the proposed work was to design and evolve a forecasting model for e-Waste prediction and to apply appropriate

recycling measures for the optimum utilization of the equipment. A Linear Regression (LR) based ML algorithm was used to train the model with preprocessed data samples. Though the model uses preprocessed data obtained from a university campus for training and testing in the prediction experiments, the framework is designed to use the data in real-time through IoT sensors and cloud infrastructures. The various performance measures are used to validate the prediction performance of the LR model. While looking at the correlation coefficients and the error measures of the model's test results, it clearly shows that the forecasting framework is working well for the e-Waste prediction. This will help to extending the life of the equipment, facilitating the recycling and reducing the need for further procurement. In this way, this work contributes to environmental sustainability. The work could be further improved by adopting appropriate ML models or kernel functions in order to address nonlinear

issues that may appear in the dataset while using real-time IoT sensor data.

ABBREVIATIONS:

AI – Artificial Intelligence

DL – Deep Learning

e-Waste – Electronic Waste

GBRT - Gradient Boosting Regression Tree

IoT – Internet of Things

LR – Linear Regression

MAE – Mean Absolute Error

ML – Machine Learning

NN - Neural Network

NOAA - National Oceanic and Atmospheric Administration

RAE - Relative Absolute Error

r-CC - Pearson r Correlation Coefficient

SA – Simulated Annealing

SVM – Support Vector Machine

WSN - Wireless Sensor Network

REFERENCES

[1] ESRL's Global Monitoring Laboratory (GML) of the National Oceanic and Atmospheric Administration (NOAA). https://gml.noaa.gov/ccgg/trends/

[2] Bernhard, Germar H., Richard L. McKenzie., Kathleen, Lantz., Scott, Stierle. (2022). Updated analysis of data from Palmer Station, Antarctica (64° S), and San Diego, California (32° N), confirms large effect of the Antarctic ozone hole on UV radiation. Photochemical & Photobiological Sciences.

https://doi.org/10.1007/s43630-022-00178-3

[3] Geneva Environment Network. 14 October 2021. https://www.genevaenvironmentnetwork.org/resources/updates/international-e-Waste-day-2021/

[4] SujinnaKarnasuta., Panya, Lao-Anantana. (2021). Forecasting of Generation of Electronic Waste on Green Community with Statistical Assessment of Numerical Models. Turkish Journal of Computer and Mathematics Education. 12(11).

[5] Ke, Xie., Yiwang, Luo., Wenjing. Li., Zhipeng, Chen., Nan, Zhang., Cai,

Liu. (2022). Deep Learning with Multisource Data Fusion in Electricity Internet of Things for Electricity Price Forecast. Wireless Communications and Mobile Computing. https://doi.org/10.1155/2022/3622559

[6] Tran Anh Khoa, Cao Hoang Phuc, Pham Duc Lam, Le Mai Bao Nhu, Nguyen Minh Trong, Nguyen Thi

Hoang Phuong, Nguyen Van Dung, Nguyen Tan-Y, Hoang Nam Nguyen, and Dang Ngoc Minh Duc. (2020). Waste Management System Using IoT-Based Machine Learning in University. Wireless Communications and Mobile Computing. https://doi.org/10.1155/2020/6138637

[7] Chen, Dr., Lai, Kong-Long. (2020). Machine Learning based Energy Management at Internet of Things Network Nodes. Journal of Trends in Computer Science and Smart Technology. 2. 127-133. https://doi.org/10.36548/jtcsst.2020.3.001

[8] Rijwan, Khan., Santosh, Kumar., Akhilesh, Kumar, Srivastava., Niharik,a Dhingra., Mahima, Gupta., Neha, Bhati., Pallavi, Kumari. (2021). Machine Learning and IoT-Based Waste Management Model

Computational Intelligence and Neuroscience. https://doi.org/10.1155/2021/5942574

[9] Md. Wahidur, Rahman., Rahabul, Islam., Arafat, Hasan., Nasima, Islam, Bithi., Md. Mahmodul, Hasan., Mohammad, Motiur, Rahman. (2020).

[10] Shreyas, Madhav, AV., Rajaraman, R., Harini S, Kiliroor, CC. (2021). Application of artificial intelligence to enhance collection of E-waste: A potential solution for household WEEE collection and segregation in India. Waste Manag Res. https://doi.org/10.1177/0734242X211052846

[11] Haomiao, Li., Zian. Jin., Sujatha, Krishnamoorthy. (2021). E-Waste Management Using Machine Learning. 2021 6th International Conference on Big Data and Computing. Association for Computing Machinery, New York, NY, USA, 30–35. https://doi.org/10.1145/3469968.3469973

[12] TV, Balakrishnan., R, Kalaiarasi. (2021). E-Waste Prediction and Disposal Model using Analytics, International Research Journal of Engineering and Technology, 8(5).

[8] V, Agarwal., S, Goyal., S, Goel. (2020). Artificial Intelligence in Waste Electronic and Electrical Equipment Treatment: Opportunities and Challenges. International Conference on Intelligent Engineering and Management (ICIEM). 2020. pp. 526

529, https://doi.org/10.1109/ICIEM48762.2020.9160065

[13] Sofiene, Haboubi., Oussama, Bben, Salem. (2022). Predictive Analytics for Energy Consumption in Smart Homes with Fog and Cloud Computing Using Support Vector Regression. International Journal on Information Technologies and Security. 14(1), pp. 49-60.

Big Data and Machine Learning-Based Smart Home System for Energy

Saving. Energies. 13, 1097. https://doi.org/10.3390/en13051097

[14] Mamoona, Humayun., Mohammed, Saleh, Alsaqer., Nz.

Jhanjhi. (2022). Energy Optimization for Smart Cities Using IoT. Applied Artificial Intelligence. https://doi.org/10.1080/08839514.2022.2037255

[15] Alenazi. MM., Yosuf, BA., Mohamed, SH. (2021). Energy-Efficient Distributed Machine Learning in Cloud Fog Networks. In: 2021 IEEE 7th World Forum on Internet of Things (WF-IoT). 14 Jun - 31 Jul 2021, New Orleans, Louisiana, USA/Virtual. IEEE, pp. 935-941. https://doi.org/10.1109/WF-IoT51360.2021.9595351

[16] Schulz, E., Speekenbrink, M., Krause, A. (2018). A Tutorial on Gaussian Process Regression: Modelling, Exploring, and Exploiting Functions. J. Math. Psychol. 85, 1–16.

[17] Fox, John. Applied Regression Analysis and Generalized Linear Models. 2015. Sage Publications.

[18] Cebekhulu, Eric, Adeiza J. Onumanyi, and Sherrin J. Isaac. 2022. Performance Analysis of Machine Learning Algorithms for Energy Demand–Supply Prediction in Smart Grids. Sustainability. 14(5), 2546. https://doi.org/10.3390/su14052546

[19] Van den Abeele F, Hoebeke J, Moerman I, Demeester P. (2015). Integration of Heterogeneous Devices and Communication Models via the Cloud in the Constrained Internet of Things. International Journal of Distributed Sensor Networks. https://doi.org/10.1155/2015/683425

Intelligent waste management system using deep learning with IoT. Journal

of King Saud University - Computer and Information Sciences. https://doi.org/10.1016/j.jksuci.2020.08.016

[20] S. Abbas et al., (2020). Modeling, Simulation and Optimization of Power Plant Energy Sustainability for IoT Enabled Smart Cities Empowered with Deep Extreme Learning Machine. IEEE Access. vol. 8, pp. 39982-39997. https://doi.org/10.1109/ACCESS.2020.2976452

[21] Venkatesan, S., Lim, J., Ko, H., Cho, Y. (2022). A Machine Learning Based Model for Energy Usage Peak Prediction in Smart Farms. Electronics. 11(218). https://doi.org/10.3390/electronics11020218

[22] J. Kang., J. Kim., M. Kim., M. Sohn. (2020). Machine Learning-Based Energy-Saving Framework for Environmental States-Adaptive Wireless Sensor Network. IEEE Access. vol. 8, pp. 69359-69367. https://10.1109/ACCESS.2020.2986507

[23] Dimpal, Tomar., Pradeep, Tomar., Arpit, Bhardwaj., G. R. Sinha. (2022). Deep Learning Neural Network Prediction System Enhanced with Best Window Size in Sliding Window Algorithm for Predicting Domestic Power Consumption in a Residential Building. Computational Intelligence and Neuroscience. https://doi.org/10.1155/2022/7216959

[24] Machorro-Cano, I., Alor-Hernández, G., Paredes-Valverde, M.A., Rodríguez-Mazahua, L., Sánchez-Cervantes, J.L., Olmedo-Aguirre, J.O. (2020). HEMS-IoT: A

نموذج إستدامة الذكاء الإصطناعي Green القائم على إنترنت الأشياء وتعلم الآلة لتنبؤ Electronic Waste

فتحي جريبي

كلية علوم الحاسب وتقنية المعلومات، جامعة جازان، جازان، المملكة العربية السعودية

الملخص

تعتبر الاستدامة البيئية مصدر قلق كبير لأي شركة أو حكومة في العصر التكنولوجي الحالي. الحوسبة الخضراء هي مبادرة لتقليل التأثير البيئي للتكنولوجيا من خلال إنفاق أقل للطاقة وتقليل electronic waste وتعزيز الاستدامة. تحتل أبحاث الذكاء الاصطناعي (AI) الصدارة في معالجة مختلف القضايا البيئية المتعلقة بتصميم المنتج وصيانة المنتج واستخدام الطاقة وغيرها الكثير. في محاولة لإضافة قيمة إلى مبادرة الذكاء الاصطناعي الخضراء، تم اقتراح نموذج للتنبؤ ب (electronic waste) يعتمد على تعلم الآله. يتم الحصول على البيانات من الجهاز الإلكتروني للمنظمة باستخدام آلية تمكين إنترنت الأشياء (IoT). تم إدخال Linear Regression (LR) في النموذج لتقدير الحالة الديناميكية للمعدات ووقت الصيانة والتخلص من الأجهزة. يتم استخدام المقاييس المختلفة مثل Pearson r correlation coefficient (r-CC) و relative absolute error (RAE) و mean absolute error (MAE) لتقييم أداء estimators. يتم تقييم نموذج التنبؤ باستخدام بيانات الوقت الفعلي التي تم الحصول عليها من الحرم الجامعي الذي يدعم إنترنت الأشياء. في التقييم ، أظهر النموذج المقترح أداءً أفضل في التنبؤ.

الكلمات المفتاحية: إنترنت الأشياء، تعلم الآله، Linear Regression، الذكاء الإصطناعي Green، e-Waste، الإستدامة.

Mathematical model for Molecular Communication among GnRH Neurons in Human Brain

Zico Mutum[1*]

[1]Department of Mathematics, Faculty of Science, Jazan University, Saudi Arabia;

Abstract

GnRH neurons are brain cells which are localized within the hypothalamus. It secretes Gonadotropin releasing hormones (GnRH). It regulates the secretion of gonadotropins, viz, follicle stimulating hormone (FSH) and luteinizing hormone (LH) both in males and females. In this paper, we use mathematical model to understand the complex dynamic behaviour of GnRH signaling to the pituitary and its effect of GnRH frequency on gonadotropin secretion. Our model predicts the occurrence of oscillation and steady state of the signals released by the neurons. It also shows a phase transition behaviour with both synchronized and desynchronized phases of the GnRH signaling which act as a synchronizing agent.

Keywords: Mathematical model; Cell signaling; Synchronization; Autocrine signaling; Neurons.

1. Introduction

GnRH (Gonadotropin releasing hormone) neuron cells are present in the hypothalamic region of brain [1]. The GnRH neuron play an important role in releasing reproduction hormones by producing GnRH, which stimulates the biosynthesis and secretion of FHS (follicle stimulating hormone) and LH (luteinizing hormone). The sharp oscillating pulse of GnRH produced by GnRH neurons in the hypothalamus is considered an intrinsic property of the neurons that helps in controlling important, functions in mammals, for instance the reproduction functions [2-4]. These pulses released from the GnRH neurons effect the targeted cells and depend on the dynamic behaviour of the pulses. Various studies reported that GnRH is a core regulator of gonadotropins through follicle stimulating hormone (FSH) and luteinizing hormone (LH) [5]. Study suggests that many factors are associated with the activation of GnRH neurons, which leads to an increase in the concentration level of GnRH [6-8]. Furthermore, this increased concentration level of GnRH enhanced the concentration of both FSH and LH [9,10]. Moreover, GnRH is believed to be responsible for the onset of puberty and the regulation of hormone release from the pituitary [11]. This pulsating phenomenon of GnRH is done through its own release via three G-protein types, and it is essential for the reproduction system in mammals because the absence of this signal leads to various reproductive diseases such as sterility, endometriosis, etc. [12].

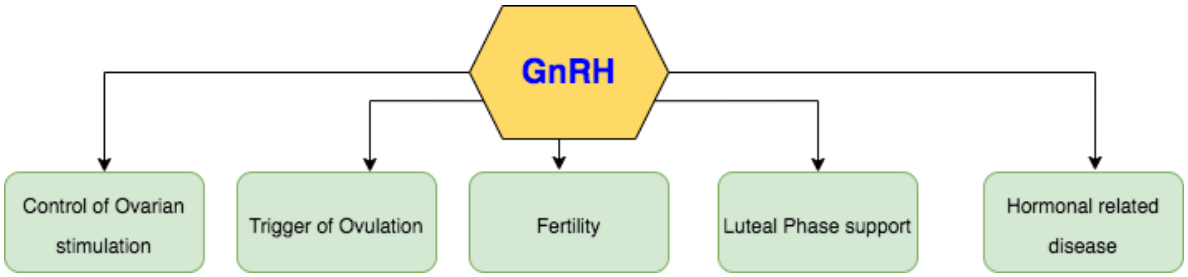

Figure 1: Important role of GnRH (Gonadotropin releasing hormone) neuron cells.

Figure 1 shows the role of GnRH at various levels in ovarian stimulation, fertility preservation, and hormonal related diseases. One of the most studied axes is the secretion of testosterone in males. Besides, testosterone, luteinizing hormone (LH) and GnRH are also secreted in the pituitary gland and hypothalamus (by hypothalamic neurons in a pulse manner). This secretion is in the part of brain, hence LH and GnRH are closely related to the neural behaviour and dynamics and known as pulsatile. These hormones facilitate gonadal function and therefore also affect fertility which is shown in Figure 2. At the gonads level, the FSH and LH are continuous to produce germ cell and hormone secretion.

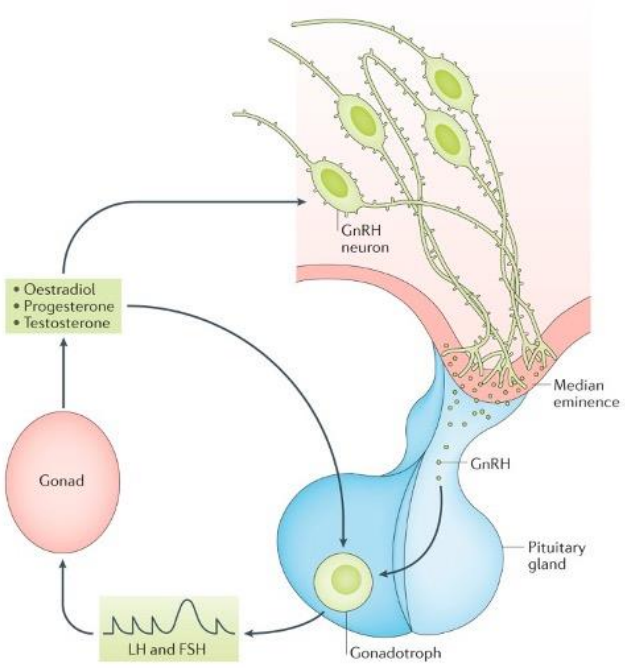

Figure 2: Control structure of puberty and fertility by GnRH [25].

The sparsely distributed GnRH secreting neurons in the pulse generators are small in number, so the GnRH molecules secreted into the extracellular medium may act as diffusing molecules among the neurons to maintain synchronization of neurons [10,13]. Therefore, GnRH has both the roles of a feedback regulator as well as a synchronizing agent. However, still how the cells coupled via GnRH molecules is not fully investigated and understood. Mathematical models are used to understand the complex dynamic behaviour of these cell coupling. In [29], mathematical modelling is used to understand the mechanism of controlling the dynamic of GnRH signaling

by gonadal steroids across the ovarian cycle by changing KNDy neurons' signaling properties.

Recent studies suggest that the rate of activation of GnRH neurons stabilizes the concentration level of gonadotropins. Moreover, various experimental as well as theoretical approaches have proposed that GnRH can diffuse within the cells and participate in autocrine signaling to produce gonadotropins. It is clear that the gonadotropin synthesis and secretion are effected by the high and low frequencies of GnRH. The high frequency signaling of GnRH increases secretion of LH while suppressing FSH secretion and causing disturbance in the reproduction cycle. These dynamic behaviours of the frequency could be relevance in fertility related conditions. Mathematical modelling is able to explain the difference between LH and FSH secretion patterns in responds to the dynamics of signaling of GnRH [30]. Motivated by the recent research findings, we use mathematical modelling to understand the GnRH secretion neurones in the form of signals and provide oscillation among the neurons that would facilitates the LH and FSH secretion pattern. Our model predicts the period of occurrence of the oscillation of the signals shared by the neurons for their communication.

In this paper, Section 2 provides some mathematical models to understand the dynamic behaviour of gonadotropin releasing hormone neuron signaling and pulsatile. Section 3 provides a model of the neuron with autocrine signaling mechanism and a method to analyze the coupling of the cells via GnRH signaling molecules. Furthermore, the numerical results and discussions are explained in Section 4. And finally, section 5 states the conclusion of our study

2. Mathematical Models for GnRH

Mathematical modelling is an essential tool in modern bioscience and its applications, enabling quantitative analysis and integration of data and formulation of complex biological systems. It is important to provide an overview of the mathematical modelling work in the context of GnRH research. Mathematical models help to understand the system of GnRH. In this section, we highlight some of the most popular research areas where mathematical modelling has been particularly adopted to understand the dynamic behaviour of GnRH.

2.1 Modeling for GnRH pulse

In [26], the authors used a system of four-dimensional differential equations to represent the coupling between the GnRH neuron network and other interneuron networks. The mathematical representation was used for the GnRH secretion pattern as follows;

$$\epsilon\alpha\frac{dx}{dt} = -y + f(x), \tag{1}$$

$$\epsilon\frac{dy}{dt} = ax + by + c + dX, \tag{2}$$

$$\epsilon\varphi\beta\frac{dx}{dt} = -Y + F(X), \tag{3}$$

$$\frac{dY}{dt} = b_0 Y + b_1 Y + b_2, \tag{4}$$

$$z(t) = \chi\{y(t) > y_s\}, \tag{5}$$

where the parameters $\boldsymbol{a, b, c, d, b_0, b_1, b_2, \alpha, \epsilon, \varphi, \beta > 0}$. The variable $\boldsymbol{x, X}$ represent the neuron signal activities and the variable $\boldsymbol{y, Y}$ denote the ionic and secretory dynamics. The function $\boldsymbol{z(t) = \chi\{y(t) > y_s\}}$ represents the GnRH signal. They have predicted that the bifurcation may be possible with the change the value of $\boldsymbol{X}$. The values of the parameters $(\boldsymbol{a, b})$ were chosen in such a way that there was one single stationary point with varied in $\boldsymbol{X}$. Bifurcation and stability analysis were done considering the three-dimensional system Eq (1)-(3). The model equations were able to show the complex behaviour of the frequency of GnRH pulses.

The function $\boldsymbol{\gamma(t) = \sum_{n=0}^{\infty} \lambda_n \delta\,(\,t - t_n)}$ where $\boldsymbol{\delta(t)}$ is the Dirac delta-function. These functions are usually a model for spiking neurons of the brain. The values of the parameters are chosen so as to clearly illustrate the dynamic behaviour of the biological system. Parameter bifurcations of the five mathematical models were studied and explained the effectiveness of the male reproduction axis. Experimental data were used for the model validation with two pulses of GnRH.

The authors in [27] used a system of differential equations that are used to model the pulses of GnRH. They have studied the parameter bifurcation, particularly in the change of pulse period mode of gonadotropin releasing hormone. Simulations of the model equations were validated with the experimental data. The model equations are given as follows;

$$\frac{dR}{dt} = \boldsymbol{\gamma(t) + b_1 R}, \tag{6}$$

$$\frac{dL}{dt} = \boldsymbol{g_1 R - b_2 L}, \tag{7}$$

$$\frac{dT}{dt} = \boldsymbol{g_2 L - b_3 T}. \tag{8}$$

Where $\boldsymbol{R(t)}$, $\boldsymbol{L(t)}$ and $\boldsymbol{T(t)}$ are the serum concentration of GnRH, LH, and testosterone, respectively. The terms $\boldsymbol{b_1 R}$, $\boldsymbol{b_2 L}$, $\boldsymbol{b_3 T}$ represents the clearing rates of the hormones and $\boldsymbol{g_1 R}$, $\boldsymbol{g_2 L}$, $\boldsymbol{\gamma(t)}$ denotes the rates of their secretion, and $\boldsymbol{b_i}$, $\boldsymbol{g_i}$ are positive numbers. The above system of equations (6)- (8) can be written as

$$\frac{dx}{dt} = \boldsymbol{Ax + B\gamma(t)}\ ,\ \boldsymbol{y = Cx}. \tag{9}$$

where $\boldsymbol{A} = \begin{pmatrix} -b_1 & 0 & 0 \\ g_1 & -b_2 & 0 \\ 0 & g_2 & -b_3 \end{pmatrix}$, $\boldsymbol{B} = \begin{pmatrix} 1 \\ 0 \\ 0 \end{pmatrix}$, $\boldsymbol{C^T} = \begin{pmatrix} 0 \\ 0 \\ 1 \end{pmatrix}$. (10)

2.2 Modeling for GnRH signaling

Mathematical models and theoretical approaches are mainly used to understand the dynamics of pulsatile signaling. The pulsatile secretion of GnRH stimulates FSH and LH production. The signaling pathway of GnRH, FHS, and LH associates with many reproduction disorders. In [28], the authors proposed a partial differential equation model to understand the role of parameters in the signaling pathway of GnRH such as the velocity of the medium flow or fraction collection time.

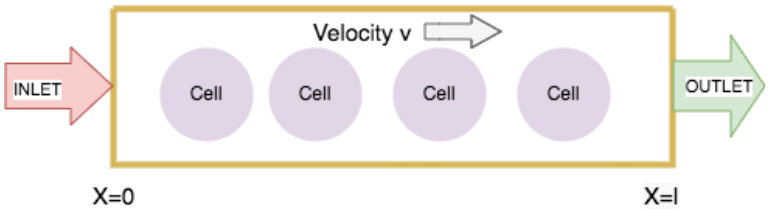

Figure 3: Diagram for GnRH signaling through pituitary cells in the cell chamber.

The above Figure 3 shows the GnRH signaling in the cells (immobilized cells) inside the cell chamber with the constant velocity flow rate. GnRH enters the cell chamber along with the new medium through the inlet, where its concentration in the entering chamber is under controlled. The cell culture medium enters the chamber through the inlet with a velocity v and exit the chamber through outlet. It was considered that the length of the cell chamber is l.

The system of partial differential equations governing the model is given as follows;

$$F_t\,(x,t) + vF_x\,(x,t) = -k_1\big(R(x,t) - A(x,t)\big)F(x,t) + k_2A(x,t), \tag{11}$$

$$A_t\,(x,t) = k_1\big(R(x,t) - A(x,t)\big)F(x,t) - k_2A(x,t), \tag{12}$$

$$R_t\,(x,t) = a_0 - b_0R(x,t) - c_0A(x,t), \tag{13}$$

$$\boldsymbol{K_t\,(x,t) = b_1A(x,t) - a_1K(x,t)P(x,t)}, \tag{14}$$

$$\boldsymbol{P_t\,(x,t) = b_2K(x,t) - a_2P(x,t)}, \tag{15}$$

$$\boldsymbol{L_t\,(x,t) = -v\,L_x(x,t) + bs + b_3K(x,t)}, \tag{16}$$

where $\boldsymbol{x \in [0,l]}$ and $\boldsymbol{t \geq 0}$ with the following conditions;

$$\boldsymbol{F(x,0) = A(x,0) = K(x,0) = P(x,0) = L(x,0) = 0\,, R(x,0) = R_{in}}\,, \tag{17}$$

$$\boldsymbol{L(0,t) = 0, F(0,t) = f(t)}, \tag{18}$$

and $\boldsymbol{R_{in}}$ is the total receptor concentration. The definition of the parameters is shown in the following Table 1.

Table 1: Definitions of the parameters in the model.

Parameter	**Definitions**	**Parameter**	**Definitions**
$F(x,t)$	Free GnRH	k_1, k_2	binding rate of GnRH
$A(x,t)$	Receptor	a_0, b_0, c_0	rate for synthesis, internalization and desensitization respectively
$R(x,t)$	Total receptor concentration	a_1,	Kinase deactivate rate
$K(x,t)$	Active kinase	b_2, a_2	Active and deactivate rate of phosphatase
$P(x,t)$	Active phosphatase	bs, b_3	LH secretion rate
$L(x,t)$	LH secretion		

The mathematical model is able to couple the intercellular signaling with the flow of substances in the cell chamber. It suggested that there was a requirement of two feedback loops (fast and slow acting) to explain the real data.

3. Material and Methods

The single cell model developed in [13] was based on the experimental data of *Krsmanovic* [14] and was optimized and simplified by Li and Khadra [3] which is schematized in Figure 4. The binding of GnRH to its receptors on the neurons produces three proteins G_s, G_q and G_i. In this simple model, S, Q, I, and G denote dimensionless concentration of α_s, α_q and α_i which are subunits of α and GnRH neurons. The α_s, α_q and α_i promote secretion of intracellular messengers cAMP , Ca2+, and IP3 [6,15]. The complete model of six variables was simplified based on the idea that two of the six variables are much faster than the other variables and using quasi-steady state approximations. The dimensionless equation with four variables in the simplified GSQI model are given as follows;

$$\frac{dG}{dt} = \lambda[\nu + \eta F(S,Q,I) - G], \tag{19}$$

$$\frac{dS}{dt} = \phi\left[\frac{G^4}{\sigma^4 + G^4} - S\right], \tag{20}$$

$$\frac{dQ}{dt} = \Psi\left[\frac{G^4}{\rho^4 + G^4} - Q\right], \tag{21}$$

$$\frac{dI}{dt} = \varepsilon\left[\frac{G^2}{k^2 + G^2} - I\right]. \tag{22}$$

Where, the function

$$[F(S,Q,I) = [C_\infty(Q)a_\infty(S,I)]^3, C_\infty(Q) = \frac{j_{in} + (\mu + Q\delta)c_0}{\mu + 1 + Q\delta} \tag{23}$$

and $a_\infty(S,I) = l + \theta S\frac{\omega}{\omega + I}$.

The parameters λ, ϕ, ψ and ε are dimensionless characterizing the respective time scale of G, S, Q and I [3], whereas σ, ρ, and k are constants related to inhibition of S, Q and I respectively. The dimensionless rate of Ca2+ influx from the extracellular medium through the voltage gated Ca2+ channel is represented by j_{in}. Single cell model is equivalent to a population model of identical neurons [13]. One can consider a population of neurons (heterogeneous) in a common pool of extracellular GnRH as shown in Figure 4. GnRH in the extracellular medium plays the role of feedback regulator and synchronizing agent [13]. The system of differential equations in i^{th} neuron is given as follows;

$$\frac{dG_i}{dt} = \frac{1}{N}\sum_{j=1}^{N}\lambda_j\left[\nu_j + \eta_j F_j(S_j, Q_j, F_j) - G\right], \tag{24}$$

$$\frac{dS_i}{dt} = \phi_i\left[\frac{G^4}{\sigma_i{}^4 + G^4} - S_i\right], \tag{25}$$

$$\frac{dQ_i}{dt} = \Psi_i\left[\frac{G^4}{\rho_i{}^4 + G^4} - Q_i\right], \tag{26}$$

$$\frac{dI_i}{dt} = \varepsilon_i \left[\frac{G^2}{k_i^2 + G^2} - I_i\right], \quad (27)$$

where, $\boldsymbol{i = 1, 2, \ldots N}$.The equation (24) indicates the averaging of all contributions from $\boldsymbol{N}$ cells, which is similar to the mean field coupling. G is taken to be common to all cells. The neurons interact with each other by secreting G in the pool and responding to the G in the pool.

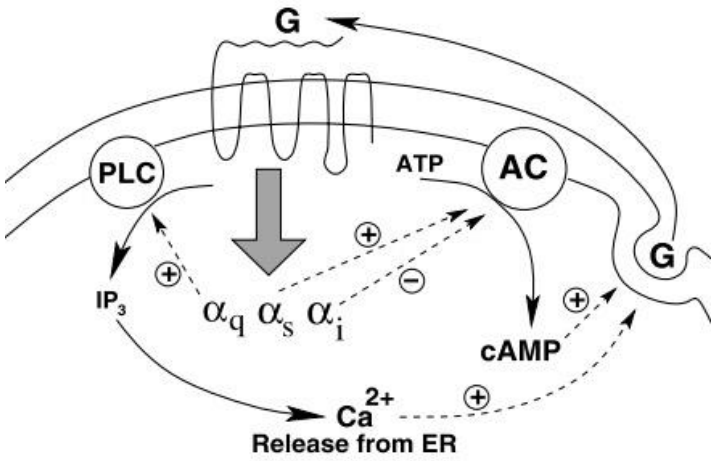

Figure 4. The schematic diagram of the molecular mechanism of autocrine signaling in the model [3].

The extracellular signal G is shared by the neurons to communicate each other and processing information. For instance, a variable, say G_i in our case is common to N identical oscillators, then this situation can be an effective by means of *mean-field* coupling, the coupling happens for each oscillator with one another through $\frac{1}{N}\sum_{i=1}^{N} G_i$. This coupling provides a *mean–field* where the oscillators communicate and synchronization happens for the other variables[16,17]. To measure the synchronization process of the time evolution of two independent and identical systems is possible [18] by using Hilbert transform [19]. The instantaneous phase for an arbitrary signal $\eta(t)$ is given as follows;

$$\tilde{\eta}(t) = \frac{1}{\pi} CP \int_{-\infty}^{+\infty} \frac{\eta(t)}{t-\tau} d\tau \quad (28)$$

where, CP represents the Cauchy principal value. We use the equation $A(t)e^{i\phi(t)} = \eta(t) + i\tilde{\eta}(t)$ to obtain the instantaneous phase $\phi(t)$ and amplitude $A(t)$ of a given arbitrary signal. For instance, we can defined the instantaneous phases for any given pair of signals $[(i,j); j = 1,2,\ldots.,N, i \neq j]$ as ϕ_i and ϕ_j. The phase synchronization of the signals can be written as $\Delta\phi_{ij} = m\phi_i - n\phi_j$, where which m and n are constants (integers). With different initial conditions the dynamic behaviour of the coupled oscillators show phase synchrony [19-23], however, for the uncoupled oscillators the dynamic behaviour is not correlated. We can measure the rate of synchronization of two coupled oscillators by plotting the two variables that show oscillators along the two-dimensional Cartesian plane (*Pecora-caroll type*) [24]. When the oscillators are uncoupled, then the points in the plane are scattered away from the diagonal and if it is coupled, the points are concentrated towards the diagonal. From the dynamic behaviour of the concentration of the points towards the diagonal, we can predict the rate the synchrony. The values of the parameters we have taken in the simulation are given in the following Table 2.

Table 2: Values of the parameters [13] used in the model equations.

Parameter	Value	Parameter	Value
l	0.067	λ	0.706
j_{in}	9.227×10^{-6}	η	3.292
m	0.012	$\sigma = \phi = \psi$	1
$c_0 = \delta$	0.588	ρ	61.765
θ	216.67	ε	0.0125
k	1	ω	0.01125

Table 2 shows the values of the dimensionless parameters and the three parameters $\boldsymbol{\sigma}$, $\boldsymbol{\phi}$, and $\boldsymbol{\psi}$ are equal to 1. We use MATLAB software to simulate our model equations using the values of the parameters from the above table.

4. Numerical Results and Discussions

We have simulated the system of differential equations (5)-(8) using MATLAB software for ten cells using the parameters illustrated in Figure 5. The upper panel represents the dynamic of I as a function of time (minutes) showing the following behaviour; (i) uncoupled dynamics in time interval (0-500) minutes (no mean field coupling is switched on), (ii) synchronized behavior at k = 464 and in the time interval (50-500) minutes (when mean field coupling is switched on) and (iii) mean field coupling is still switch on but simulated for different values of $k = 1 - 100$ after time 500 minutes. The dynamics in time < 500 minutes of different cells with different peaks which are smaller as the value of k increases but synchronous at foot. To see the synchronized and desynchronized behaviour in another way, we show the phase plots of the pairs of cells for variable I for all three regions in the lower panel. For uncoupled cells, $\Delta\phi$ fluctuates randomly in time < 200 minutes, whereas it becomes constant for the synchronized regime, i.e., in (200 < time < 500) minutes. Furthermore, since $\Delta\phi$ fluctuates but not randomly in (500 < time < 700) minutes, the dynamics are weakly synchronized. Based on the above system of equations 19-22, we have the following MATLAB code to be defined as a function.

```
function gsqi=gsqifunctions(~,ggt,phi,sai,nu,eta,eps,rho,sigma,theta,del,l,lamdah,j,c,m,w,k)
        G=ggt(1);
        S=ggt(2);
        Q=ggt(3);
        I=ggt(4);
Gdot=lamdah*(nu+eta*((((j+c*m+c*del*Q)/(m+1+Q*del))^3)*(l+(theta*S*w)/(w+I))^3)-G);
        Sdot=phi*(G^4/(sigma^4+G^4)- S);
        Qdot=sai*(G^4/(rho^4+G^2)- Q);
        Idot=eps*(G^2/(k^2 +G^2)- I);
        gsqi=[Gdot;Sdot;Qdot;Idot];
```

```
end
```

The above function is called and solved our model equations by using MATLAB ode45 as follows;

```
[t,soln]=ode45(@(t,y)gsqifunctions(t,y,phi,sai,nu,eta,eps,rho,sigma,theta
,l,del,lamdah,j,c,m,w,k),tspan,y);
```

To see the synchronization of a group of neurons coupled via GnRH, we take $N = 100$ neurons and the coupling is switched on at $t = 150$ minutes as shown in the following figures.

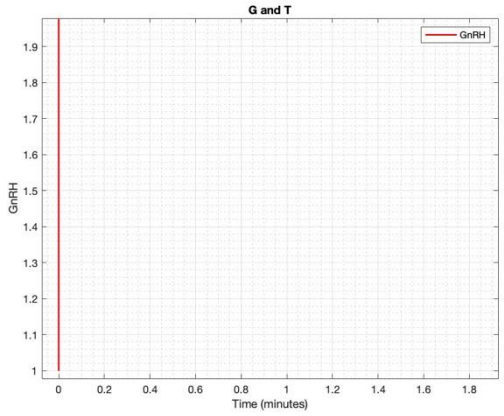

(a)

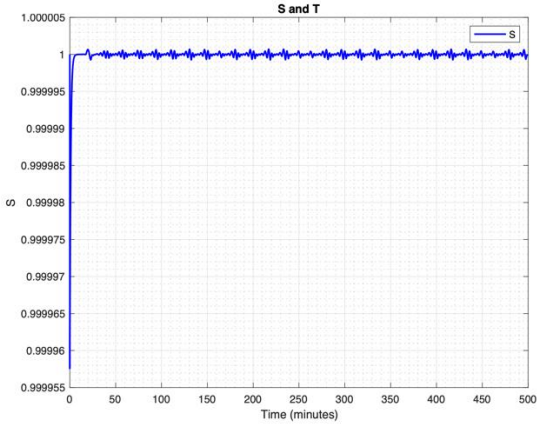

(b)

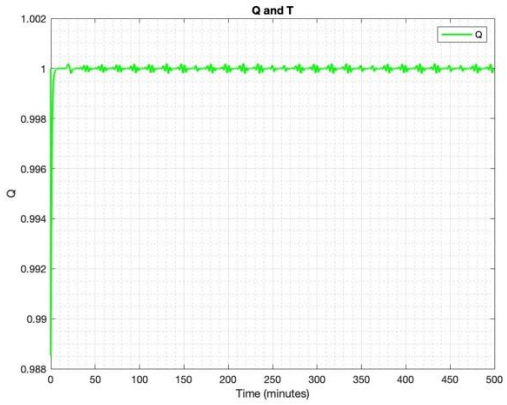

(c)

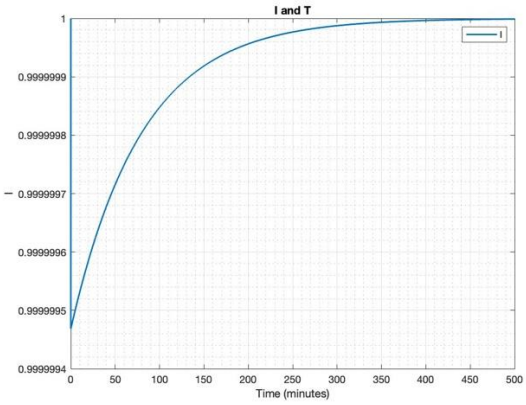

(d)

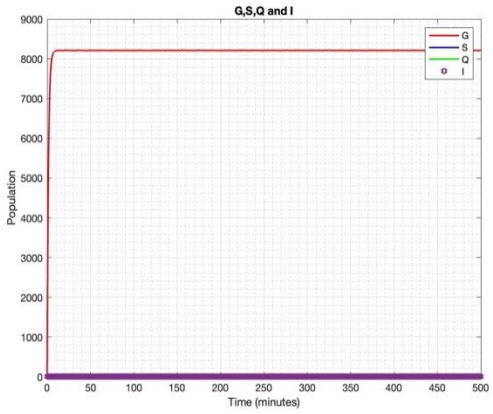

(e)

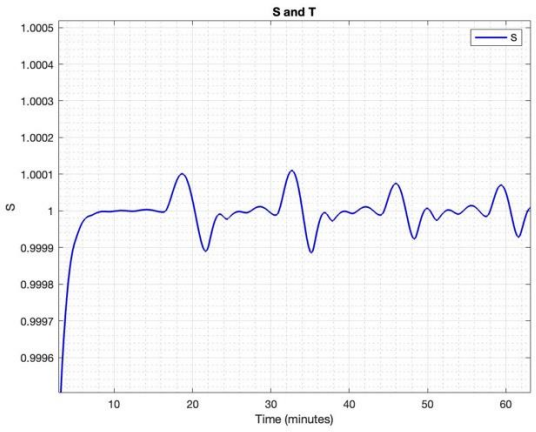

(f)

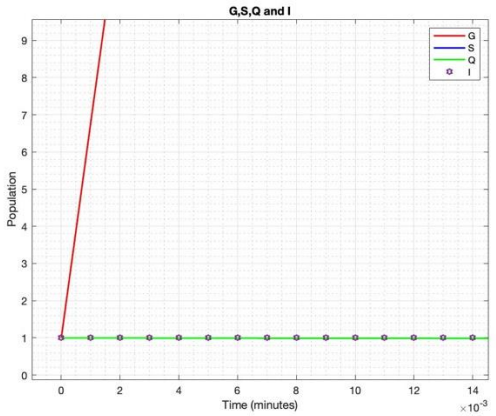

(g)

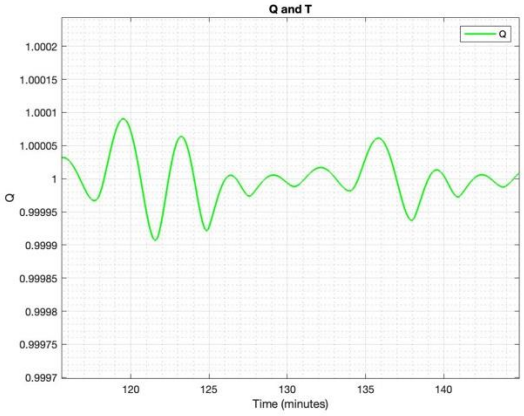

(h)

Figure 5. Plots of G, S, Q and I concentration variables, $(j = 1,2, \ldots ,10)$of 10 cells with common GnRH (G) at k = 500 showing desynchronized and synchronized regimes; (a) GnRH with respect to time t (minutes), (b) α_s promote secretion with respect to time t (minutes) (c) α_q promote secretion with respect to time t (d) α_i promote secretion with respect to time t, (e) G, S, Q, I with respect to time t (f) oscillation happened in the S equation,
(g) synchronization of G, S, Q, I equations, (h) oscillation happens in the G equation.

The simulations of the system of equations (19-23) representing the generated GnRH pulses are done using MATLAB software. It is clear that all neurones share a common extracellular pool of G and are continuously stirred so that the secretion of GnRH by neurons is diluted. The above Figure 5(a) shows the simulation of G and the variation is much faster than the other variables. The simulation of equation (25) representing the concentration of α_s for the pulse generation in GnRH is shown in Figure 5(b). In this case we can see the oscillation occurs after time $t > 20$ minutes. Figure 5(f) shows the simulation of neural oscillation. We can also see the oscillation of the equation (26) happens at time $t > 100$ minutes, and shown in figures 5(c),(h). From the simulation of equation (27), we can see from figure 5(d) that the concentration of α_i gives the higher amplitude in the pulse of G, however, there is no occurrence of oscillation. Figure 5(e),(g) shows the simulation of GSQI model and synchronization occurs for SQI in a heterogeneous population of GnRH neurons in brain.

5. Conclusions

Mathematical modelling plays an important role to help us understand the complex dynamic behaviour between hormones and an approach to deal with applications in endocrinology. We use GSQI model to study the dynamic signaling mechanism of GnRH neurons that effects LH and FSH secretion. Our mathematical model predicted that the cells could be able to send signals to other cells of the same type, but also they could send signals to themselves. The cell coupling is achieved by the mean field coupling mechanism. GnRH neurons diffuse in coupled cells which lead to cellular signaling in brain. GnRH neurons can diffuse not only to the cell itself but also can diffuse to other cells. Therefore, synchronization of the cells is achieved via this signaling molecule. Mathematical modelling approaches have limitations such as incapability of providing a proof of a fact that requires experimental evidence. The simulations using the mathematical model equations may not show similar responds results with the wet-lab data. However, our

results suggest that GnRH neurons act as a strong synchronizing agent. We conclude that our study will also be useful to understand the dynamic behaviour of gonadotropins. Our future research directions would focus on extension of our model using fractional-order derivatives.

Acknowledgments: I would like to thank all the reviewers for their valuable comments towards improving this manuscript.

References

1. S. Constantin, "Progress and Challenges in the Search for the Mechanisms of Pulsatile Gonadotropin-Releasing Hormone Secretion," *Frontiers in endocrinology*, 2017; Vol.8, No.180, 2017.
2. A. Kaprara, I.T. Huhtaniemi, "The hypothalamus-pituitary-gonad axis: Tales of mice and men," *Metabolism,* Vol. 86: pp.3-17, 2018.
3. Y.X. Li, A. Khadra, "Robust synchrony and rhythmogenesis in endocrine neurons via autocrine regulations in vitro and in vivo," *Bull. Math. Biol*, Vol. 70, pp. 2103-2125, 2008.
4. A. Khadra, "Synchrony due to parametric averaging in neurons coupled by a shared signal," *Physica D. Nonlinear Pheomena*, Vol. 7, No.238, pp.771- 781, 2009.
5. G.A. Stamatiades, U.B Kaiser, "Gonadotropin regulation by pulsatile GnRH: Signaling and gene expression," *Molecular and cellular endocrinology*, Vol. 7, No. 463, pp.131-141, 2018.
6. J.D Spergel, "Modulation of Gonadotropin-Releasing Hormone Neuron Activity and Secretion in Mice by Non-peptide Neurotransmitters, Gasotransmitters, and Gliotransmitters.," *Frontiers in Endocrinology*, Vol. 10, 329, 2019.
7. S.Y.J Han, G. Kane, et al., "Characterization of GnRH pulse generator activity in male mice using GCaMP fiber photometry," *Endocrinology*, Vol.160, pp.557-160, 2019.
8. C. Fergani, S. Leon, et al., "NKB signaling in the posterodorsal medial amygdala stimulates gonadotropin release in a kisspeptin-independent manner in female mice," *Elife*, e40476, 2018.
9. L.Z. Krsmanovic, N.Mores, et al., "An agonist-induced switch in G protein coupling of the gonadotropin-releasing hormone receptor regulates pulsatile neuropeptide secretion," *Proc. Natl. Acad. Sci*, Vol. 100, pp. 2969-2974, 2003.
10. M.M Naugle and A.C Gore, "GnRH Neurons of Young and Aged Female Rhesus Monkeys Co-Express GPER but Are Unaffected by Long-Term Hormone Replacement," *Neuroendocrinology*, Vol.100, pp.334-346, 2014.
11. M. Voliotis M, X.F Li, et al., "Tsaneva-Atanasova K. The Origin of GnRH Pulse Generation: An Integrative Mathematical-Experimental Approach," *J Neurosci*., Vol.39, No. 49, pp. 9738-9748, 2020.
12. A.E Herbison, "Control of puberty onset and fertility by gonadotropin-releasing hormone neurons," *Nat Rev Endocrinol.*, Vol.8, pp.452-466, 2016.
13. A. Khadra A, Y.X Li, "A model for the pulsatile secretion of gonadotropin-releasing hormone from synchronized hypothalamic neurons," *Biophys*, Vol.91, pp.74-83, 2006.
14. P.R Protachevicz, M. Hansen, et al., "Emergence of neuronal synchronisation in coupled areas," *Frontiers Computational Neuroscience*, 15:663408, 2021.
15. L.Z Krsmanovic, N. Mores, et al., "An agonist-induced switch in G protein coupling of the gonadotropin-releasing hormone receptor regulates pulsatile neuropeptide secretion," *Proc. Natl. Acad. Science*, Vol.100, pp.2969-2974, 2003.
16. A.V Roland, S.M Moenter, "Glucosensing by GnRH neurons: inhibition by androgens and involvement of AMP-activated protein kinase," *Mol Endocrinol*, Vol. 25, pp.847-858, 2011.
17. D. Gonze and A. Goldbeter, "Circadian rhythms and molecular noise," *Chaos: An interdisciplinary Journal of Nonlinear Science*, 026110, 2006.
18. M.G Rosenblum and A.S Pikovsky, "Controlling Synchronization in an Ensemble of Globally Coupled Oscillators Phys," *Physical Review Letters*, Vol.92, 114102, 2004.
19. H. Sakaguchi and Y. Kuramoto, "A Soluble Active Rotater Model Showing Phase Transitions via Mutual Entertainment," *Progress of Theoretical Physics*, Vol.76,576, 1986.
20. M.G Rosenblum, A.S Pikovsky and J. Kurths, "Phase Synchronization of Chaotic

Oscillators," *Physical Review Letters*, Vol.76, 1804, 1996.

21. A. Pikovsky, M. Rosenblum, J. Kurths, "Synchronization: A Universal Concept in Nonlinear Science", Cambridge University Press, Cambridge, 2001.
22. S. Aviyente, E.M Bernat, W.S Evans, S.R Sponheim, "A phase synchrony measure for quantifying dynamic functional integration in the brain", *Hum Brain Mapp*, Vol. 32, pp.80-93, 2011.
23. B. Umberto, Z. Enrique, "A Stochastic Approach to the Synchronization of Coupled Oscillators", *Frontiers in Energy Research*, Vol.8, No.115, 2020.
24. L.M Pecora, T.L Caroll, "Synchronization in chaotic systems", *Phys. Rev. Lett*. Vol. 64, pp. 821-824,1996.
25. A. E Herbison, "Control of puberty onset and fertility by gonadotropin-releasing hormone neurons," *Nature Reviews Endocinology*, Vol.12, pp.452- 466, 2016.
26. F. Clement and J.P Francoise, "Mathematical modeling of the GnRH pulse and surge generator", *SIAM Journal on Applied Dynamical System*, Vol.6, No.2, 2005.
27. A. Churilov, A. Medvedev and A. Shepeljavyi, "Bifurcations in a mathematical model of non-basal testosterone production," *IFAC Proceedings Volumes*, Vol. 41, No. 2, pp. 10319-10324, 2008.
28. N.E Temamogullari, H.F Nijhout and M.C Reed, "Mathematical modeling of perifusion cell culture experiments on GnRH signaling", *Mathematical Biosciences*, Vol. 276, pp. 121-132, 2016.
29. M.Voliotis, X.F. Li, et al., "Modulation of pulsatile GnRH dynamics acress the ovarian cycle via changes in the network excitability and basal activity of the arcuate kisspeptin network", *eLife*, Vol. 10, e71252, 2021.
30. M.Voliotis, Z. Plain, "Mathematical models in GnRH research", *Journal of Neuroendocrinology*, e13085, 2021.

النموج الرياضي للتواصل الجزيئي بين الخلايا العصبية GnRH في الدماغ البشري

د زيكوميتي ميوتيوم
قسم الرياضيات-كلية العلوم- جامعة جازان

الملخص

خلايا GnRH من الخلايا العصبية التي تقع في منطقة الهيبوثلامس (تحت االمهاد). هذه الخلايا مسئولة عن إفراز هرمون الجونادوتروبين GnRH المحفز للغدد التناسلية. يتم هذا التحفيز عن طريق تنظيم إفراز هرمون هرمون (FSH) والهرمون اللوتيني (LH) في الذكور والإناث. في هذه الورقة العلمية سنستعين بالنمذجة الرياضية لفهم السلوك الديناميكي العقدي لتلك الاشارات التي ترسلها الخلايا العصبية وتأثيرها على إفرازات الغدد التناسلية المتكررة. في هذا البحث سيتمكن نموذجنا الرياضي من التنبؤ بحدوث التذبذب والحالة المستقرة للإشارات الصادرة عن الخلايا العصبية. بالإضافة إلى ذلك سندرس العوامل المؤثرة والسلوك الناتج عن التزامن وعدم التزامن في المراحل المختلفة لبث إشارات من الخلايا GnRH.

الكلمات المفتاحية: نموذج رياضي، إشارات الخلية، التزامن، إشارات الأوتوكرين ، الخلايا العصبية.

Fourth Type Derivations of I^{st} Class Filiform Leibniz-Algebras for $(m+1)$ Dimensions

Al-Hossain Ahmad Al-Nashri
Department of Mathematics - Al- Qunfudha University College- Umm Al-Qura University

Abstract

The derivations of algebras of the fourth type from filiform Leibniz-algebras of the I^{st} class with derivations of dimensions $(m+1)$ are described in this article. In contrast to previous works on algebras of the first, second, and third types of filiform Leibniz -algebras of the first derivations class of dimension $(m+1)$, we show that the Basis $(Der(\mathcal{L}_m))$ (that is the set of all derivations of the algebra $\mathcal{L}_m$) that cannot be established from the description of the deductions.

Keywords: Filiform Leibniz-algebra, Leibniz-algebra, gradation, natural gradation, derivation.

1. Introduction

For a long time, numerous researchers have been investigating Leibniz's-algebra theory (cf. [7], ...,[12]). Any algebra with associativity can give Lie algebra and Leibniz-algebra. This can be considered as an interesting idea that was defined by JL Loday. This is first type of filamentous Leibniz-algebras. We have investigated the low dimensionality of algebra, just to get the basis of the space $Der(\mathcal{L}_m(\partial))$. Contrary to the previous work on the first, second and third types of algebras of the first-order filamentous Leibniz-algebra of the dimensionality derivation $(m+1)$, we have not found the basis for the derivation of this algebra, as well as the relationship between the algebra and its derivations. It is derived by studying this algebra table from the 4^{th} dimension to the m^{th} dimension.

2. Preliminary Results

This section is comprises with some definitions and results based on them that is required throughout this paper.

Definition 2.1. [10] $\mathcal{L}$ is called a Leibniz-algebra say over a field K if following Leibniz identity is satisfies by a bilinear operation say $[\cdot,\cdot]$ as given below: by:

$\big[a,[b,c]\big]=\big[[a,b],c\big]-\big[[a,c],b\big]$, for any $a,b,c\in\mathcal{L}$.

We have considered all algebras here over the complex field $\mathbb{C}$. We suppose $\mathcal{L}$ to be a Leibniz-algebra. Further assume $\mathcal{L}^1=\mathcal{L},\ \mathcal{L}^{k+1}=[\mathcal{L}^k,\mathcal{L}],\ K\geq 1$.

Definition 2.2. [1] We say $\mathcal{L}$ nilpotent if $\exists\, s\in N$ such that $0=\mathcal{L}^s\subset\cdots\subset\mathcal{L}^2\subset\mathcal{L}^1$.

Definition 2.3. [2] $\mathcal{L}$ is called filiform with the condition that $dim\mathcal{L}^j=m-j$, where $m=dim\mathcal{L}$ and $2\leq j\leq m$.

Definition 2.4. [14] A k-linear transformation ∂ of an algebra $\mathcal{L}$ is a derivation of $\mathcal{L}$ if

$\partial([a,b]) = [\partial(a),b] + [a,\partial(b)]$ for all $a,b \in \mathcal{L}$

$Der(\mathcal{L})$ indicates derivational set of $\mathcal{L}$: With the word Leibniz we always mean that it is collection of ($m+1$)-dimensional filiform form for Leibniz-algebra.

We consider that the below given theorem [11] that breaks set of all fixed dimensions filiform Liebniz-algebras in 3 disjoint subsets. In general we suppose the concern results regarding $FLeib_{m+1}$ only.

Theorem 2.1. A filiform $(m+1)$-dimensional Leibniz-algebra $\mathcal{L}$ over set of complex numbers returns a basis $\xi_0, \xi_1, \dots, \xi_m$ that is called adapted, whose table of multiplication with $\mathcal{L}$ can be shown as given below, where those products that are not defined are considered as zero:

$$FLeib_{m+1} = \begin{cases} [\xi_o, \xi_0] = \xi_2, \\ [\xi_i, \xi_0] = \xi_{i+1}, \quad \mathbf{1 \le i \le m-1}, \\ [\xi_0, \xi_1] = \sigma_3\xi_3 + \sigma_4\xi_4 + \cdots + \sigma_{m-1}\xi_{m-1} + \sigma_m\xi_m \\ [\xi_j, \xi_1] = \sigma_3\xi_{j+2} + \sigma_4\xi_{j+3} + \cdots + \sigma_{m+1-j}\xi_m, \quad \mathbf{1 \le j \le m-2} \end{cases}$$

for $\sigma_3, \sigma_4, \dots, \sigma_m,\ \sigma \in \mathbb{C}$.

Lemma 2.1. [14] Consider ∂ is in $Der(\mathcal{L}_m)$. Then $\partial = \partial_0 + \partial_1 + \partial_2 + \cdots + \partial_{m-1}$ where $\partial_k \in End(\mathcal{L}_m)$ and $\partial_k(\mathcal{L}_\iota) \subseteq \mathcal{L}_{\iota+k}$ for $1 \le l \le n$.

Proof. We suppose that $\mathfrak{S}_\iota$ stands for natural filtration of $\mathcal{L}_m$. From [[14], Corollary 1] the main filtration is coinciding with the natural filtration of $\mathcal{L}_m$. Hence

$\mathfrak{S}_k = \bigoplus_{\iota \ge K} \mathcal{L}_m$ and $\partial(\mathfrak{S}_\iota) \subseteq \mathfrak{S}_\iota$ (for more details see Corollary 3 in [14]). Therefore we obtain $\partial \in F_0Z^1(\mathcal{L}_m, \mathcal{L}_m)$ implies $\partial_k \in End(\mathcal{L}_m)$ text color white and $\partial_k(\mathcal{L}_\iota) \subseteq \mathcal{L}_{\iota+k}$ Hence, it is proved.

3. The Algebra $\mathcal{L}_m(\partial)$ of the Class I^{st} Filiform Leibniz-Algebras

Let us consider the given system

$$\mathcal{L}_m(\partial) = \begin{cases} [\xi_o, \xi_0] = \xi_2, \\ [\xi_i, \xi_0] = \xi_{i+1}, \quad \mathbf{1 \le i \le m-1}, \\ [\xi_0, \xi_1] = 2\xi_m \\ [\xi_j, \xi_1] = \xi_m \\ 0 \qquad Otherwise \end{cases}$$

Algebra in low dimension with the derivations of this kind can be presented as in the table below:

Table 1: Dimension derivation of Leibniz-algebra of low dimension

dimensions	Equation ($dim\ Der$)	$dim\ Der$	No. of equations
4	$\partial_1(\xi_0) = \xi_2,$ $\partial_1(\xi_i) = \xi_{i+1},\ 1 \le i \le 2$ $\partial_2(\xi_0) = \xi_3, \partial_3(\xi_1) = \xi_3,$	3	5
5	$\partial_1(\xi_0) = \xi_2,$ $\partial_1(\xi_i) = \xi_{i+1},\ 1 \le i \le 3$ $\partial_2(\xi_0) = \xi_3, \partial_2(\xi_i) = \xi_{i+2},\ 1 \le i \le 2$ $\partial_3(\xi_0) = \xi_4, \partial_4(\xi_1) = \xi_4,$	4	9
6	$\partial_1(\xi_0) = \xi_2,$ $\partial_1(\xi_i) = \xi_{i+1},\ 1 \le i \le 4$ $\partial_2(\xi_0) = \xi_3, \partial_2(\xi_i) = \xi_{i+2},\ 1 \le i \le 3$ $\partial_3(\xi_0) = \xi_4, \partial_3(\xi_i) = \xi_{i+3},\ 1 \le i \le 2$ $\partial_4(\xi_0) = \xi_5, \partial_5(\xi_1) = \xi_5,$	5	14
7	$\partial_1(\xi_0) = \xi_2,$ $\partial_1(\xi_i) = \xi_{i+1},\ 1 \le i \le 5$ $\partial_2(\xi_0) = \xi_3, \partial_2(\xi_i) = \xi_{i+2},\ 1 \le i \le 4$ $\partial_3(\xi_0) = \xi_4, \partial_3(\xi_i) = \xi_{i+3},\ 1 \le i \le 3$ $\partial_4(\xi_0) = \xi_5, \partial_4(\xi_i) = \xi_{i+4},\ 1 \le i \le 2$ $\partial_5(\xi_0) = \xi_6, \partial_6(\xi_1) = \xi_6,$	6	20
8	$\partial_1(\xi_0) = \xi_2,$ $\partial_1(\xi_i) = \xi_{i+1},\ 1 \le i \le 6$ $\partial_2(\xi_0) = \xi_3, \partial_2(\xi_i) = \xi_{i+2},\ 1 \le i \le 5$ $\partial_3(\xi_0) = \xi_4, \partial_3(\xi_i) = \xi_{i+3},\ 1 \le i \le 4$ $\partial_4(\xi_0) = \xi_5, \partial_4(\xi_i) = \xi_{i+4},\ 1 \le i \le 3$ $\partial_5(\xi_0) = \xi_6, \partial_5(\xi_i) = \xi_{i+5},\ 1 \le i \le 2$ $\partial_6(\xi_0) = \xi_7, \partial_7(\xi_1) = \xi_7,$	7	27

9	$\partial_1(\xi_0)=\xi_2,$ $\partial_1(\xi_i)=\xi_{i+1},\ 1\le i\le 7$ $\partial_2(\xi_0)=\xi_3, \partial_2(\xi_i)=\xi_{i+2},\ 1\le i\le 6$ $\partial_3(\xi_0)=\xi_4, \partial_3(\xi_i)=\xi_{i+3},\ 1\le i\le 5$ $\partial_4(\xi_0)=\xi_5, \partial_4(\xi_i)=\xi_{i+4},\ 1\le i\le 4$ $\partial_5(\xi_0)=\xi_6, \partial_5(\xi_i)=\xi_{i+5},\ 1\le i\le 3$ $\partial_6(\xi_0)=\xi_7, \partial_6(\xi_i)=\xi_{i+6},\ 1\le i\le 2$ $\partial_7(\xi_0)=\xi_8, \partial_8(\xi_1)=\xi_8,$	8	35
⋮	⋮	⋮	⋮
m	$\partial_1(\xi_0)=\xi_2,$ $\partial_1(\xi_i)=\xi_{i+1},\ 1\le i\le m-2$ $\partial_2(\xi_0)=\xi_3, \partial_2(\xi_i)=\xi_{i+2},\ 1\le i\le m-3$ $\partial_3(\xi_0)=\xi_4, \partial_3(\xi_i)=\xi_{i+3},\ 1\le i\le m-4$ $\partial_4(\xi_0)=\xi_5, \partial_4(\xi_i)=\xi_{i+4},\ 1\le i\le m-5$ ⋮ $\partial_{m-3}(\xi_0)=\xi_{m-2}, \partial_{m-3}(\xi_i)=\xi_{i+(m-3)},$ $1\le i\le 2$ $\partial_{m-2}(\xi_0)=\xi_{m-1}, \partial_{m-1}(\xi_1)=\xi_{m-1},$	$m-1$	$(m-1)$ $+\sum_{i=1}^{m-1}(m-i)$

Remark 3.1. From the table above, we give the conjecture as in the following fundamental points:

- We get some basis for space $Der(\mathcal{L}_m(\partial))$ that is given as following proposition:
- We can calculate $dimDer$ with applying the formula: $dimDer(\mathcal{L}_m)=m,\ dim(\mathcal{L}_m)=m+1$, for $m\ge 3$. As a result, we see that number of

equations that can be found for any dimension obtained from derivations can be given by the following rule: No. of equations (NE)

$$NE=(m-1)+\sum_{i=1}^{m-1}(m-i)$$

- Consider $\partial\in Der(\mathcal{L}_m(\partial))$. From Lemma 2:1, we get that

$$\partial=\partial_0+\partial_1+\partial_2+\partial_3+\partial_4+\cdots+\partial_{m-2}+\partial_{m-1}$$

where $\partial_0\in Der(\mathcal{L}_m(\partial))$ is defined in the proof of Lemma 3.1, $\partial_k\in Der(\mathcal{L}_m(\partial)), 1\le k\le (m-2)$ is defined in Lemma 3.2 and $\partial_{m-1}\in Der(\mathcal{L}_m(\partial))$is defined in the proof of Lemma 3.3.

Lemma 3.1. Suppose T_1 is given as

$$T_1 = \lambda_0\xi_2 + \lambda_1\xi_2 + \sum_{i=1}^{m} \lambda_i\xi_i$$

Then

$$T_1(\xi_i) = \begin{cases} \xi_2, & i = 0 \\ \xi_{i+1}, & 1 \leq i \leq m-1 \end{cases}$$

Proof. Consider $\partial_0 \in Der\big(\mathcal{L}_m(\partial)\big)$ which is defined by

$$\partial_0(\xi_i) = \begin{cases} \sigma_0\xi_2, & i = 0, \\ \gamma_i\xi_{i+1}, & 1 \leq i \leq m-1 \end{cases} \qquad (1)$$

where σ_0 and γ_i, $1 \leq i \leq m-1$ are scalars.

We consider the following as set of derivations

$$\partial_0\big([\xi_i, \xi_j]\big) = \big[\partial_0(\xi_i), \xi_j\big] + \big[\xi_i, \partial_0(\xi_j)\big]$$

Let us consider the following cases, and in every situation, we continously consider algebra $\mathcal{L}_m(\partial)$ and (1):

- First case: taking $i = 0,\ j = 0$, we get

$$\partial_0([\xi_0, \xi_0]) = [\partial_0(\xi_0), \xi_0] + [\xi_0, \partial_0(\xi_0)]$$

thus,

$$\partial_0(\xi_2) = [\sigma_0\xi_2, \xi_0] + [\xi_0, \sigma_0\xi_2]$$

thenwe obtain

$$\gamma_2\xi_3 = \sigma_0\xi_3$$

then

$$\sigma_0 = \gamma_2 \qquad (2)$$

- Second case: if $i = 1,\ j = 0,$ then

$$\partial_0([\xi_1, \xi_0]) = [\partial_0(\xi_1), \xi_0] + [\xi_1, \partial_0(\xi_0)]$$

and so, we obtain

$$\partial_0(\xi_2) = [\gamma_1\xi_2, \xi_0] + [\xi_1, \sigma_0\xi_2]$$

which implies

$$\gamma_1\xi_3 = \gamma_2\xi_3$$

and hence

$$\gamma_1 = \gamma_2 \qquad (3)$$

- Third case: taking $2 \leq i \leq m-1,\ j = 0$. We get,

$$\partial_0\left(\left[\sum_{i=2}^{m-1} \xi_i, \xi_0\right]\right) = \left[\partial_0\left(\sum_{i=2}^{m-1} \xi_i\right), \xi_0\right] + \left[\sum_{i=2}^{m-1} \xi_i, \partial_0(\xi_0)\right]$$

so that,

$$\partial_0\left(\sum_{i=2}^{m-1} \xi_{i+1}\right) = \left[\sum_{i=2}^{m-1} \gamma_i \xi_{i+1}, \xi_0\right] + \left[\sum_{i=2}^{m-1} \xi_i, \sigma_0 \xi_1\right]$$

which implies

$$\sum_{i=2}^{m-1} \gamma_{i+1} \xi_{i+2} = \sum_{i=2}^{m-1} \gamma_i \xi_{i+2}$$

and so,

$$\gamma_{i+1} = \gamma_i, \quad 2 \leq i \leq m-1 \tag{4}$$

From (2), (3), and (4) we get

$$\sigma_0 = \gamma_1 = \gamma_2 = \gamma_3 = \gamma_4 = \cdots = \gamma_m. \tag{5}$$

Thus

$$\partial_0\left(\sum_{i=0}^{m} \lambda_i \xi_i\right) = \partial_0(\lambda_0 \xi_0) + \sum_{i=1}^{m} \partial_0(\lambda_i \xi_i)$$

$$= \lambda_0(\sigma_1 \xi_2) + \lambda_1(\gamma_1 \xi_2) + \sum_{i=1}^{m+1} \lambda_i(\gamma_i \xi_{i+1}) \qquad by\ (1)$$

$$= \sigma_0\left[\lambda_0 \xi_2 + \sum_{i=1}^{m+1} \lambda_i \xi_{i+1}\right] \qquad by(5)$$

$$= \sigma_1 T_1$$

Hence we get

$T_1(\xi_0) = \xi_2$ and $T_1(\xi_i) = \xi_{i+1}$, $1 \leq i \leq m-1$ (6)

Lemma 3.2. Let $\partial_k \in Der\big(\mathcal{L}_m(\partial)\big),\quad 1 \leq k \leq m-2$ such that ∂_k is given by

$$\partial_k(\xi_i) = \begin{cases} \tau_0\xi_{k+1}, & i = 0 \\ \tau_i\xi_{k+i}, & 1 \le i \le m-k \end{cases} \qquad (7)$$

where τ_0 and τ_i, $1 \le i \le m-k$ are scalars.

Then $\partial_k(\xi_0) = \xi_{k+1}$ and $\partial_k(\xi_i) = \xi_{k+i}, \quad 1 \le i \le m-k$

Proof. Suppose the collection of derivations

$$\partial_k([\xi_i, \xi_j]) = [\partial_k(\xi_i), \xi_j] + [\xi_i, \partial_k(\xi_j)]$$

Considering the same approach, we compute all cases as following and using repeatedly $\mathcal{L}_m(\partial)$ and (7).

- First case: if $i = 0, j = 0,$ then

$$\partial_k([\xi_0, \xi_0]) = [\partial_k(\xi_0), \xi_0] + [\xi_0, \partial_k(\xi_0)]$$

Then

$$\partial_k(\xi_2) = [\tau_0\xi_{k+1}, \xi_0] + [\xi_0, \tau_0\xi_{k+1}]$$

which implies

$$\tau_2\xi_{k+2} = \tau_0\xi_{k+2}$$

to obtain

$$\tau_2 = \tau_0 \qquad (8)$$

- Second case: if $i = 0, j = 1$ then

$$\partial_k([\xi_0, \xi_1]) = [\partial_k(\xi_0), \xi_1] + [\xi_0, \partial_k(\xi_1)]$$

so that,

$$\partial_k(2\xi_m) = [\tau_0\xi_{k+1}, \xi_1] + [\xi_0, \tau_1\xi_{k+1}]$$

If $\tau_0, \tau_1 \neq 0$. Then, we get

$\partial_k(\xi_m) = 0$ as will as $[\tau_0\xi_{k+1}, \xi_1]$ and $[\xi_0, \tau_1\xi_{k+1}]$

- Third case: if $1 \le i \le m-k, j = 0,$ then

$$\partial_k\left(\left[\sum_{i=1}^{m-k}\xi_i, \xi_0\right]\right) = \left[\partial_k\left(\sum_{i=1}^{m-k}\xi_i\right), \xi_0\right] + \left[\sum_{i=1}^{m-k}\xi_i, \partial_k(\xi_0)\right]$$

which implies

$$\partial_k\left(\sum_{i=1}^{m-k}\xi_{i+1}\right) = \left[\sum_{i=1}^{m-k}\tau_i\xi_{k+i}, \xi_0\right] + \left[\sum_{i=1}^{m-k}\xi_i, \tau_0\xi_{k+i}\right]$$

Thus

$$\sum_{i=1}^{m-k} \tau_{i+1}\xi_{k+i+1} = \sum_{i=1}^{m-k} \tau_i \xi_{k+i+1}$$

and so we obtain

$$\tau_{i+1} = \tau_i, \quad 1 \leq i \leq m-1 \tag{9}$$

From (8) and (9)

$$\tau_0 = \tau_1 = \tau_2 = \tau_3 = \tau_4 = \cdots = \tau_{m-1} \tag{10}$$

and hence

$$\partial_k\left(\sum_{i=0}^{m} \lambda_i \xi_i\right) = \partial_k(\lambda_0\xi_0) + \sum_{i=1}^{m} \partial_k(\lambda_i\xi_i)$$

$$= \lambda_0(\tau_0\xi_{k+1}) + \sum_{i=1}^{m} \lambda_i(\tau_i\xi_{k+i}) \qquad by\ (7)$$

$$= \tau_0\left(\lambda_0\xi_{k+1} + \sum_{i=1}^{m-k} \lambda_i\xi_{k+i}\right) \qquad by\ (10)$$

Thus

$\partial_k(\xi_0) = \xi_{k+1}$ and $\partial_k(\xi_i) = \xi_{k+i}, \quad 1 \leq i \leq m-k$ (11)

Lemma 3.3. We consider $T_2 = \lambda_1\xi_m$, Then we get $T_2(\xi_1) = \xi_m$

Proof. Let $\partial_{m-1} \in Der(\mathcal{L}_m(\partial))$ and ∂_{m-1} is de_ned by

$$\partial_{m-1}(\xi_i) = \begin{cases} \eta_1\xi_m, & i = 1 \\ 0 & Otherwise \end{cases} \tag{12}$$

for scalar η_1. Then considering

$$\partial_{m-1}([\xi_i, \xi_j]) = [\partial_{m-1}(\xi_i), \xi_j] + [\xi_i, \partial_{m-1}(\xi_j)]$$

as family of derivation.

Next, suppose case where $i = 1,\ j = 0,$

$$\partial_{m-1}([\xi_1, \xi_0]) = [\partial_{m-1}(\xi_1), \xi_0] + [\xi_1, \partial_{m-1}(\xi_0)]$$

by $\mathcal{L}_m(\partial)$ and (12), thus

$$\partial_{m-1}(\xi_2) = [\eta_1\xi_m, \xi_0] + [\xi_0, 0]$$

If $\eta_1 \neq 0$

$$0 = 0 + 0.$$

Thus

$$\partial_{m-1}\left(\sum_{i=0}^{m} \lambda_i\xi_i\right) = \partial_{m-1}(\lambda_1\xi_1) + \sum_{i=2}^{m} \partial_{m-1}(\lambda_i\xi_i)$$

$$= \lambda_1(\eta_1\xi_m) \qquad by(12)$$

$$= \eta_1(\lambda_1\xi_m)$$

$$= \eta_1 T_2.$$

also we get that

$$T_2(\xi_1) = \xi_m. \qquad (13)$$

Lemma 3.4. The mappings T_1, T_2 and ∂_k for $1 \leq k \leq (m-2)$ are LD.

Proof. The mapping T_1, T_2 and ∂_k for $1 \leq k \leq (m-2)$ are LD, i.e. linearly dependent with the condition $\sigma_1, \sigma_2, \tau_k, k = 1, \dots, m-2$ scalars number not all zero.

$$\sigma_1 T_1(\xi_i) + \sigma_2 T_2(\xi_i) + \sum_{k=1}^{m-2} \tau_k \partial_k(\xi_i) = 0$$

for all $\xi_\iota \in \mathcal{L}_m(\partial), \iota = 0,1,2,3, \dots, m-1$

Taking $0 \leq \iota \leq m-1$ we get

$$\sum_{\iota=0}^{m-1} \left[\sigma_1 T_1(\xi_\iota) + \sigma_2 T_2(\xi_\iota) + \sum_{k=1}^{m-2} \tau_k \partial_k(\xi_\iota)\right]$$

$$= \sum_{\iota=0}^{m-1} [\sigma_1 T_1(\xi_\iota) + \sigma_2 T_2(\xi_\iota) + \tau_1\partial_1(\xi_\iota) + \tau_2\partial_2(\xi_\iota) + \cdots + \tau_{m-3}\partial_{m-3}(\xi_\iota) + \tau_{m-2}\partial_{m-2}(\xi_\iota)]$$

$$= \sigma_1 T_1(\xi_0) + \sigma_2 T_2(\xi_0) + \tau_1 \partial_1(\xi_0) + \tau_2 \partial_2(\xi_0) + \cdots + \tau_{m-3}\partial_{m-3}(\xi_0) + \tau_{m-2}\partial_{m-2}(\xi_0) + \sigma_1 T_1(\xi_1)$$
$$+ \sigma_2 T_2(\xi_1) + \tau_1 \partial_1(\xi_1) + \tau_2 \partial_2(\xi_1) + \cdots + \tau_{m-3}\partial_{m-3}(\xi_1) + \tau_{m-2}\partial_{m-2}(\xi_1)$$
$$+ \sigma_1 T_1(\xi_2) + \sigma_2 T_2(\xi_2) + \tau_1 \partial_1(\xi_2) + \tau_2 \partial_2(\xi_2) + \cdots + \tau_{m-3}\partial_{m-3}(\xi_2)$$
$$+ \tau_{m-2}\partial_{m-2}(\xi_2) + \sigma_1 T_1(\xi_3) + \sigma_2 T_2(\xi_3) + \tau_1 \partial_1(\xi_3) + \tau_2 \partial_2(\xi_3) + \cdots$$
$$+ \tau_{m-3}\partial_{m-3}(\xi_3) + \tau_{m-2}\partial_{m-2}(\xi_3) + \sigma_1 T_1(\xi_4) + \sigma_2 T_2(\xi_4) + \tau_1 \partial_1(\xi_4) + \tau_2 \partial_2(\xi_4)$$
$$+ \cdots + \tau_{m-3}\partial_{m-3}(\xi_4) + \tau_{m-2}\partial_{m-2}(\xi_4) + \cdots + \cdots + \sigma_1 T_1(\xi_{m-2}) + \sigma_2 T_2(\xi_{m-2})$$
$$+ \tau_1 \partial_1(\xi_{m-2}) + \tau_2 \partial_2(\xi_{m-2}) + \cdots + \tau_{m-3}\partial_{m-3}(\xi_{m-2}) + \tau_{m-2}\partial_{m-2}(\xi_{m-2})$$
$$+ \sigma_1 T_1(\xi_{m-1}) + \sigma_2 T_2(\xi_{m-1}) + \tau_1 \partial_1(\xi_{m-1}) + \tau_2 \partial_2(\xi_{m-1}) + \cdots + \tau_{m-3}\partial_{m-3}(\xi_{m-1})$$
$$+ \tau_{m-2}\partial_{m-2}(\xi_{m-1}) = 0$$

This gives us

$$(\sigma_1\xi_2 + \tau_1\xi_2 + \tau_2\xi_3 + \tau_3\xi_4 + \tau_4\xi_5 + \cdots + \tau_{m-3}\xi_{m-2} + \tau_{m-2}\xi_{m-1}) + (\sigma_1\xi_2 + \tau_1\xi_2 + \tau_2\xi_3 +$$
$$\tau_3\xi_4 + \tau_4\xi_5 + \cdots + \tau_{m-3}\xi_{m-2} + \tau_{m-2}\xi_{m-1} + \sigma_2\xi_m) + (\sigma_1\xi_2 + \tau_1\xi_3 + \tau_2\xi_4 + \tau_3\xi_5 + \tau_4\xi_6 + \cdots +$$
$$\tau_{m-3}\xi_{m-1}) + (\sigma_1\xi_3 + \tau_1\xi_4 + \tau_2\xi_5 + \tau_3\xi_6 + \tau_4\xi_7 + \cdots + \tau_{m-4}\xi_{m-1}) + (\sigma_1\xi_5 + \tau_1\xi_6 + \tau_2\xi_7 +$$
$$\tau_3\xi_8 + \tau_4\xi_9 + \cdots + \tau_{m-5}\xi_{m-1}) + \cdots + \cdots + (\sigma_1\xi_{m-2} + \tau_1\xi_{m-2} + \tau_2\xi_{m-1}) + (\sigma_1\xi_{m-1} +$$
$$\tau_1\xi_{m-1}) = 0$$

Thus, we have

$$2(\sigma_1 + \tau_1)\xi_2 + (2\tau_2 + \tau_1 + \sigma_1)\xi_3 + (2\tau_3 + \tau_2 + \tau_1 + \sigma_1)\xi_4 + (2\tau_4 + \tau_3 + \tau_2 + \tau_1 + \sigma_1)\xi_5$$
$$+ (2\tau_5 + \tau_4 + \tau_3 + \tau_2 + \tau_1 + \sigma_1)\xi_6 + (2\tau_6 + \tau_5 + \tau_4 + \tau_3 + \tau_2 + \tau_1 + \sigma_1)\xi_7$$
$$+ (2\tau_7 + \tau_6 + \tau_5 + \tau_4 + \tau_3 + \tau_2 + \tau_1 + \sigma_1)\xi_8 + \cdots$$
$$+ (2\tau_{m-3} + \tau_{m-4} + \tau_{m-5} + \tau_{m-6} + \cdots + \tau_3 + \tau_2 + \tau_1 + \sigma_1)\xi_{m-2}$$
$$+ (2\tau_{m-2} + \tau_{m-3} + \tau_{m-4} + \tau_{m-5} + \cdots + \tau_3 + \tau_2 + \tau_1 + \sigma_1)\xi_{m-1}$$
$$+ (\tau_{m-2} + \tau_{m-3} + \tau_{m-4} + \tau_{m-5} + \cdots + \tau_3 + \tau_2 + \tau_1 + \sigma_1 + \sigma_2)\xi_m = 0$$

Now we have the following results:

- $2(\sigma_1 + \tau_1) = 0$
- $\sigma_1 + \tau_1 + \tau_{P-1} + \sum_{j=2}^{P-1} \tau_j = 0$, for $3 \le p \le m-1$
- $\sigma_1 + \tau_1 + \sigma_2 + \sum_{j=2}^{m-2} \tau_j = 0$,

Which implies

$\sigma_1 + \tau_1 = 0$ (15)

$\tau_{P-1} + \sum_{j=2}^{P-1} \tau_j = 0,$ for $3 \leq p \leq m-1$ (16)

$\sigma_2 + \sum_{j=2}^{n-2} \tau_j = 0,$ (17)

The previous system of algebraic equation has nontrivial solution $\sigma_1 = 2, \tau_1 = -2$ and $\sigma_2 = \tau_2 = \tau_3 = \tau_4 = \tau_5 = \cdots = \tau_{m-2} = 0$ which verify the system,

moreover σ_1 and τ_1 are not zero. Hence, the family of vectors are linearly dependent.

4. Conclusion

We find that the algebra $\mathcal{L}_m(\partial)$ is nilpotent. Moreover characteristic ($\mathcal{L}_m(\partial)$) is also nilpotent and this algebra is suitable for working with basis derivations more and Four dimension. Number of derivations of $\mathcal{L}_m(\partial)$ on any dimension is given by the rule:

$$dimDer\big(\mathcal{L}_m(\partial)\big) = m - 1.$$

Number of equations (NE) can be calculated based on the result:

$$NE = (m-1) + \sum_{i=1}^{m-1} (m-i)$$

For further study one can see and go through Second class and more Filiform Leibniz-algebras.

References

[1] Albeverio, S.; Ayupov, Sh. A.; Omirov, B. A., On nilpotent and simple Leibniz algebras, Comm. in Algebra Vol. 33(2005), 159-172.

[2] Albeverio, S., Omirov, B. A., Rakhimov, I. S., (2006), Classification of 4-dimensional nilpotent complex Leibniz algebras, Extracta Math., 3(2006), 197-210.

[3] AL-hossain, A. A.; Khiyar, A. A., Derivations of some Filiform Leibniz algebras. Pure and Applied mathematics Journal.Vol. 3,No.6,(2014), 121-125.

[4] Alnashri. A. A., Derivations of one type of algebra of First class Filiform Leibniz algebras of Dimension Derivation (n+1), International Journal of Advanced Scientific and Technical Research,Vol. 1,No.5,(2015), 41-55.13

[5] Alnashri. A. A., Derivations of Second type of algebra of first class Filiform Leibniz

algebras of Dimension Derivation (n+1), International Journal of Advanced Scientific and Technical Research,Vol. 3,No.5,(2015), 29-43.

[6] Ayupov, Sh. A.; Omirov, B. A., On Leibniz algebra, Algebra and Operator Theory. Proceeding of the Colloquium in Tashkent (1997), Kluwer (1998), Doi 10.1007/978-94-011-5072-9-1 Springer, p 1-13.

[7] Ayupov, Sh. A.; Omirov, B. A., On 3-dimensional Leibniz algebra, Uzbek Math. J. (1999), 9-14.

[8] Dixmier. J. and Lister. W. G. , Derivations of nilpotent Lie algebras, Proc. Amer. Math. Soc. 8(1957), 155-158.

[9] Jacobson. N. , A note on automorphisms and derivations of Lie algebras, Proc. Amer. Math. Soc. 6(1955), 281{283.

[10] Loday.J. -L. , Une version non commutative des algebras de Lie: les algebras de Leibniz, L'Ens. Math., 39 (1993), 269-293.

[11] M.Goze AND Khakimdjanov,Nilpotent Lie algebras, printed in the Netherlands,(1996),336 p.

[12] Rakhimov.I. S and AL-nashri. A. A.. , On Derivations of Some Classes
of Filiform Leibniz Algebras, Generalized Lie Theory and Applications, 6(2012), 1-12.

[13] Rakhimov.I. S and AL-nashri. A. A.. , Derivations of low-dimensional Leibniz Algebras. Charscteistically Nilpotent Leibniz Algebras, LA PLAMBERT, (2012), 196 p.

[14] Omirov.B. A. , On the Derivations of Filiform Leibniz Algebras, Mathematical Notes, 5(2005), 677-685.

اشتقاقات النوع الرابع من الفئة الأولى لجبرات فيلي فورم-ليبنيز الجبرة في البعد (m+١)

الحسين أحمد الناشري

قسم الرياضيات - الكلية الجامعية بالقنفذة - جامعة أم القرى - المملكة العربية السعودية

الملخص

في هذه الورقة تم وصف اشتقاقات الجبرة في شكلها الرابع من التصنيف الأول من فيلي فورم ليبنز الجبرة في البعد (m+1). وعلى عكس الأعمال السابقة للأنواع الأولى والثانية والثالثة من جبرات فيلي فورم-ليبنيز الجبرة من فئة المشتقة الأولى من البعد (م+١)، فإننا نوضح هنا أن الأساس ($Der(\mathcal{L}_m)$) (مجموعة جميع اشتقاقات الجبر $\mathcal{L}_m$)، والتي لا يمكن إثباتها عن طريق وصف الاستقطاعات.

الكلمات المفتاحية: جبر ليبنيز الخطي ، جبر ليبنيز، التتدرج ، التدرج الطبيعي ، الاشتقاق.

Basket Study 1: Monitoring of Lead Concentration and Potential Health Risks in Some Types Of Fruits and Vegetables Collected from Production and Market Sites in Jazan Region.

Tawfiq. H. Al faifi[1] and Ahmed. S. Mabrouk[1]

[1] Biology Department, Faculty of Science, Jazan University, Saudi Arabia.

Abstract

The current study was carried out to provide and investigated content of lead (Pb) as heavy metal in 14 types of collected fresh fruits and vegetables from Gizan-Sabya roads and markets, Jazan, Saudi Arabia were measured using Inductively Coupled Plasma-Atomic Emission Spectroscopy ICP-AES. The results of this study showed that the average concentrations detected ranged from 0.465 to 6.385 parts per million (ppm). The highest mean levels of lead (6.385, 3.51, 2.365, 1.625 and1.045 ppm) were detected in *Pithecellobium dulce, Hibiscus esculentus, Psidium guajava, Solanum lycopersicum and Cucumis sativus* respectively. The daily human intakes of Pb ascribed to a diet of fruits and vegetables in this region have also been estimated. Current results of Pb values within the study samples are similar to those reported by some researchers in previous studies and the range of values presented for this element in other analyses measured using Inductively Coupled Plasma-Atomic Emission Spectroscopy were wide range between (0.465-1.04ppm) except *Cucumis sativus, Solanum lycopersicum, Psidium guajava, Hibiscus esculentus and Pithecellobium dulce* respectively which had a relatively high lead content ranged between (1.045-6.385ppm), So this need to more studies. This study agrees with previous studies that high-traffic city and roads areas have substantially more lead in the air than rural areas and those plants are capable of absorbing extra lead; some plants, naturally absorb far more lead than others. Current study also shows that ought to be attainable are grown and collected away from polluted areas to ensure a safe food production system.

Keywords: lead toxicity, Jizan Region, Health hazards, food chain contamination

1. Introduction

Fresh fruits and vegetables are important because they contain vitamins, minerals, and other components that promote healthier eating and the prevention of various diseases (Shaheen et al 2016). Nonetheless, these plants may contain both essential and toxic metal concentrations. The concentration of heavy metals in plants may be influenced by the nature of the soil, environmental pollution, and harvesting time (Scott et al 1996).

Lead (Pb) is a non-disintegrative heavy metal that is highly noxious. It has an atomic number of 82, a molecular weight of 207.2, a density of 11.34 g/cm3, and a melting point

of 621.43°F. It is easily shaped and molded, and it can be mixed with other metals to form alloys. Also lead can exist in organic and inorganic forms. Inorganic lead (Pb) is found primarily in soil, dust, old paint, and other user products, whereas organic lead (Tetra-ethyl Pb) is found primarily in leaded gasoline. Both of these forms of Pb are toxic, but organic Pb-complexes are much more toxic to biological systems than inorganic Pb. Industrial and manufacturing processes generate a significant amount of heavy metals (Ahmed et al., 2020; Tang et al., 2020a; Sharma et al., 2021a; Yong et al., 2021; Kiciska and Wikar, 2021). Heavy metals like Pb(II) and Ni(II) are released from these manufacturing units and spread along their channels, resulting in their long-term persistence in the environment via bioaccumulation (Hossain et al., 2021; Kulkarni et al., 2018). Chemical contamination of foods, according to Rusin et al (2021), poses a significant risk to consumers. Consumption of heavy metal-contaminated products such as cadmium and lead is one source of this risk. According to Wang et al. (2005), lead is the second most toxic metal after arsenic (As). Food quality and safety are possibly the most important public health issues. Food on the market should be free of all chemical contaminants that endanger consumer health, and its safety is the responsibility not only of food producers, but also of state governments and agencies that systematically monitor and control food quality World Health Organization (WHO 2010).The effect of heavy metal contamination of fruit and vegetables cannot be underestimated as these foods us are important components of human diet. Fruits and vegetables consider and important sources with minerals, vitamins, and fibers also have beneficial antioxidant effects. However, the intake of heavy metal contaminated fruit and vegetables may pose a risk to human health; hence food contamination with heavy metal is one of the most important manifestations of food quality assurance (Khan et al 2008). Heavy metals, in general, are not biodegradable, have long biological half-lives, and have the potential for accumulation in different body organs, leading to unwanted side effects (Sathawara et al 2004 and Järup 2003).Plants take up heavy metals by absorbing them from airborne deposits on the parts of the plants exposed to the air from the polluted environments as well as from contaminated soils through root systems. Also, the heavy metal contamination of fruit and vegetables may occur due to their irrigation with contaminated water Demirezen and Aksoy (2006) have investigated the concentrations of some heavy metals in different vegetables grown in various regions in Turkey. The levels of heavy metals such as (lead, copper, cadmium and zinc) have been examined in selected fruit and vegetables sold in local Egyptian markets (Radwan and. Salama 2006).

Fytianos et al (2001) studied heavy metals contents in vegetables grown in an industrial area of Northern Greece, and Sobukola et al (2010) investigated from selected markets in Lagos, Nigeria, concentrations of some heavy metals in fruits and leafy vegetables.

The analytical process, which included repeated tests of the samples against globally certified plant standard reference material (SRM) from the National Institute

of Standards and Technology, yielded results that were within 1% of the certified values. Knowledge of the contamination of fruit and vegetables with heavy metals from the Jizan Region areas of Saudi Arabia has not yet been established; therefore, the present study was undertaken with the aim as first time to investigate the concentration of lead which found in some selected fruit and vegetables from this region. Allowable Limit of Heavy metals Safe values for lead in fruit and vegetables recommended by the WHO/FAO are 0.3 ppm Husain et al (1995).

2. Material and Methods

The analytical procedure, repeated analyses of the samples against internationally certified plant standard reference material (SRM) of the National Institute of Standard and Technology were used, and the results were found to lie within ±1% of the certified values.

2.1. Sample Collection. As in (**Table 1)** a total of 14 samples of fruits and vegetable belong to 11 plant families produce were purchased from several local suppliers and markets in Gizan-Sabya road, Jazan, Saudi Arabia during April 2022. Samples were randomly chosen from the streets and markets where farmers export their local farm products to sell. One kilogram of each fruits and vegetables listed here was bought. To mimic the reality, we picked the good looking fruits and vegetables as if they are for consumption.

2.2. Sample preparing and analyzing. After collecting them and bring them to the lab, they washed with distilled water to avoid any additional contamination added from the air or surfaces upon transportation and dried them in an oven on 80^{o} C. Then, we measured the weight of each over a weak until a stable weigh had been observed.

We randomly picked two of each fruit and vegetable to prepare for analysis. The edible parts were taken then. A core from outside the fruit into the center of the fruit or the vegetable was taken in case it is consumed with the peel, or only the inside parts of which in case the fruit peel should be removed. The parts that were taken were grinded to have them as powder. Sample Preparation and Treatment. Subsamples (each of 100g) were taken at random from the composite sample (1 kg) and were processed for analysis by the dry-ashing method. All samples were first oven dried at 105◦C for 24 H. The dried samples were then powdered manually in a grinder and were subjected to analysis for their content from lead (Pb).

Powdered samples (14 g each), with three replicates taken for each food sample, were accurately weighed and placed in a silica crucible, and few drops of concentrated nitric acid were added to the solid as an aid to ashing. The dry-ashing process was carried out in a muffle furnace by stepwise increase of the temperature up to 550◦C and the samples left to ash at this temperature for 6 hours.

Then, one to two grams of the powder was digested in hydrochloric acid (7.5 ml conc) and nitric acid (2.5 ml conc.) as ratio 3:1 respectively. Then the sample were filtered (Whatman, Ashless, Diameter 125 mm), and additional HCL (5 ml) and reagent water (20 ml) were added to the samples for washing the filters according

(**US EPA 3050B, Acid Digestion of Sediments, Sludge, and Soils 1996**). Then, digested samples were sent to analyzing using Inductively Coupled Plasma-Atomic Emission Spectroscopy ICP-AES in the Center for Environmental Research and Studies, collage of science, Jazan University.

After being dried out in desiccators, the ash was washed with 3 N Hydrochloric acid (HCl). Whatman No. 1 filter paper was used to filter the ash suspension into a 50 mL volumetric flask, and the standards were made from the separate 1000 mg/L standards (Merck) supplied in 0.1 N HNO3. These standard stock solutions were used to create several working standards. Quality Control. The dependability of the results was ensured by using the proper quality assurance methods and safety measures. To prevent cross contamination, samples were handled carefully.

Glassware was adequately cleaned, and analytical-grade reagents were employed. The entire investigation was conducted with deionized water. The instrument readings were adjusted using reagent blank determinations.

For validation of the daily fruit and vegetable consumption was obtained through a formal survey conducted in the study area.

Table 1. The study samples of fresh fruits and vegetables.

No	Family name	scientific name	English name	Arabic Name
1	Solanaceae	*Solanum lycopersicum*	Tomatoes	طماطم
2		*Capsicum annuum*	Green pepper	فلفل أخضر
3		*Solanum melongena*	Eggplant	باذنجان
4	Cucurbitaceae	*Cucumis sativus*	Cucumber	خيار
5		*Citrullus lanatus*	Watermelon	بطيخ
6	Rhamnaceae	*Ziziphus spina-christi*	Nabq	نبق
7	Musaceae	*Musa balbisana*	Banana	موز
8	Caricaceae	*Carica papaya*	Anbroud (*papaya*)	عنبرود(باباظ)
9	Moraceae	*Ficus carica*	Fig	تين
10	Anacardiaceae	*Mangifera indica*	Mango	مانجو
11	Apiaceae	*Daucus carota*	Carrots	جزر
12	Malvaceae	*Hibiscus esculentus*	Okra	بامية
13	Fabaceae	*Pithecellobium dulce*	Indian almond	لوز هندي
14	Myrtaceae	*Psidium guajava*	Guava	جوافة

3. Results and Discussion

The present study reports on the content of Pb determined in selected fruit and vegetables collected from production and market sites in the gizan region area of Saudi Arabia. The observed concentrations of Pb in the fruit and vegetables were compared with the recommended limit as established by the **FAO/WHO (1999)** to assess the levels of food contamination. Our results of Pb values in fruit samples are similar to those reported by some researchers and the range of values presented for this element in other analyses was very wide.

The mean concentrations and range of lead found in fresh fruit and vegetables sampled from the local markets in gizan region, Saudi Arabia, are summarized in Table 2 and Figures 1.

Fig. 1: **Mean concentration of Lead in selected fruits and vegetables per ppm.**

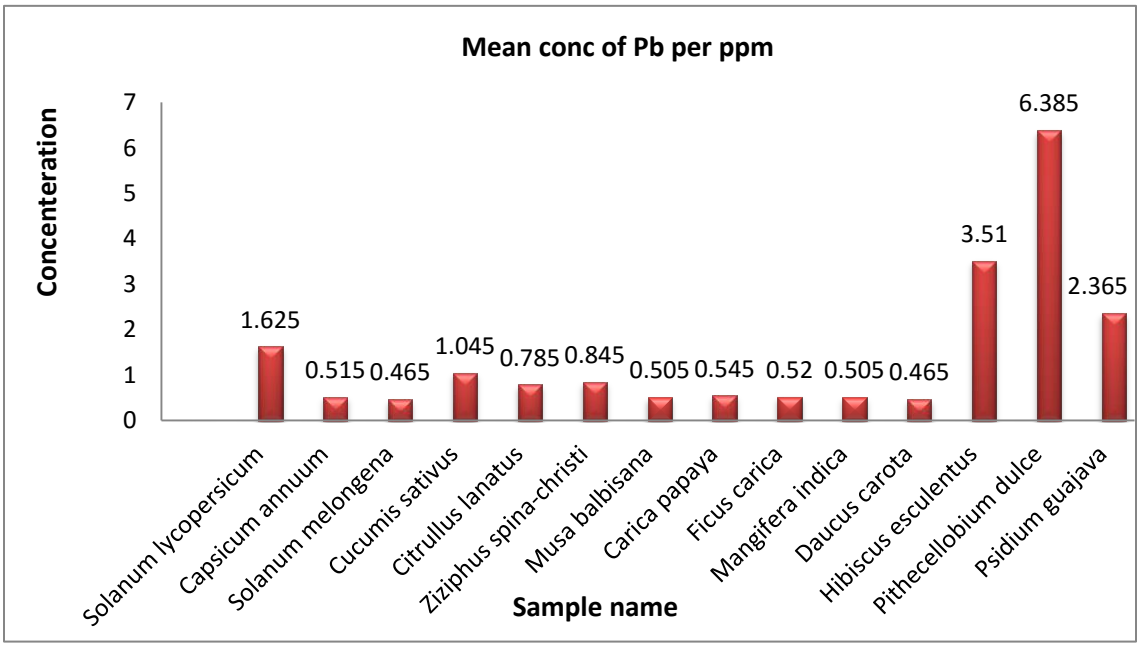

Table 2. The mean values of Pb concentrations in the study samples of fruits and vegetables per (ppm).

No	Family name	Scientific name	Mean conc **of Pb** per **ppm**	**Standard Deviation(SD)**
1	Solanaceae	*Solanum lycopersicum*	±1.625	0.007
2		*Capsicum annuum*	±0.515	0.007
3		*Solanum melongena*	±0.465	0.021
4	Cucurbitaceae	*Cucumis sativus*	±1.045	0.035
5		*Citrullus lanatus*	±0.785	0.049
6	Rhamnaceae	*Ziziphus spina-christi*	±0.845	0.049
7	Musaceae	*Musa balbisana*	±0.505	0.021
8	Caricaceae	*Carica papaya*	±0.545	0.021
9	Moraceae	*Ficus carica*	±0.52	0.014
10	Anacardiaceae	*Mangifera indica*	±0.505	0.007
11	Apiaceae	*Daucus carota*	±0.465	0.021
12	Malvaceae	*Hibiscus esculentus*	±3.51	0.028
13	Fabaceae	*Pithecellobium dulce*	±6.385	0.035
14	Myrtaceae	*Psidium guajava*	±2.365	0.021

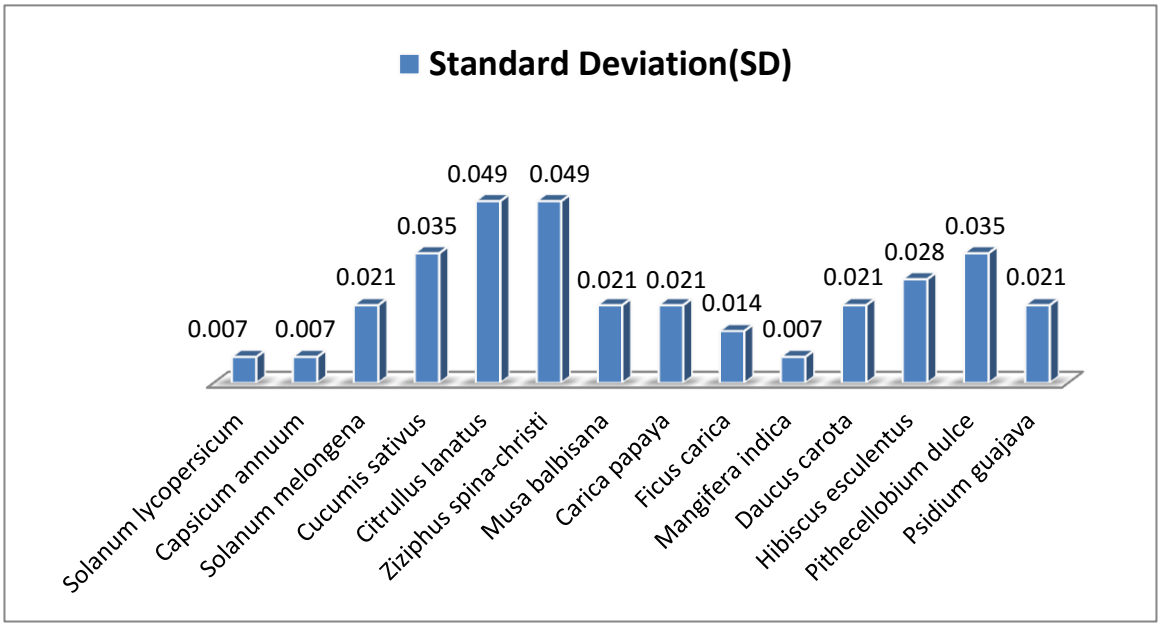

Fig. ٢: Standard Deviation (SD) in selected samples of fruits and vegetables.

The heavy metal concentrations determined were based on sample dry weight. The results showed that the levels of Pb in all commodities ranged between 0.465 ppm in Eggplant (*Solanum melongena*) and carrot (*Daucus carota*), this is the lowest and normal values of lead concentration in this samples, while values were 0.505 ppm in Banana (*Musa balbisana*) and Mango (*Mangifera indica*); also in Green pepper (*Capsicum annuum*) was 0.515 ppm, while in Fig (*Ficus carica),* papaya *(Carica papaya),* Watermelon *(Citrullus lanatus)* and Nabq *(Ziziphus spina-christi*) were (0.52, 0.545, 0.785 and 0.845ppm) respectively.

Within the selected fruit and vegetables, the highest concentrations of Pb were noticed in Indian almond *(Pithecellobium dulce)* followed by Okra *(Hibiscus esculentus),* Guava *(Psidium guajava),* Tomatoes *(Solanum lycopersicum),* and Cucumber *(Cucumis sativus)* were (6.385, 3.51, 2.365, 1.625 and 1.045ppm) respectively in decreasing concentrations. The higher levels of heavy metal contamination detected in various fruits and vegetables may be directly linked to the pollutants in farm soil, irrigation water, and pesticides or they may instead be caused by traffic pollution on the highways, as was the case in this study.

Standard Deviation

The standard deviation describes the dispersion of these samples and observations about the sample mean and the typical measure of the variability among experimental measurements **(Brown 1982, Curran-Everett and Benos 2007; and R Development Core 2008)**. the variability using a standard deviation for All 14 selected samples of fruits and vegetables observations are distributed in normal range of possible values between (0.007and 0.049), and Because it reflects the dispersion of

individual sample observations about the samples mean, a standard deviation characterizes the variability of those observations and of individual sample because it reflects the theoretical dispersion of samples mean (Table 1 and Fig 2).

Comparison of lead content in fruits and vegetables in some other parts of the world was revealed that the levels are generally comparable in Saudi Arabia and elsewhere. On the other hand, the concentration of Pb in apples was significantly lower than that detected in India, Egypt, Jordan and Turkey (Mohamed (2000), Massadeh et al. (2018) and Saracoglu et al 2009). In contrast, the concentration of Pb in potatoes was found to be higher than that found in the USA, for example (Pennington et al 1995). Also Standard Deviation (SD) showed This study demonstrates that lead concentrations in the air are significantly higher in high-traffic urban and rural areas than in rural areas, and that those plants are capable of absorbing additional lead (Pb). Some plants, however, naturally absorb much more lead than the others. This study also shows that should be attainable are grown and collected away from polluted areas. Within the safe limits prescribed by the World Health Organisation (WHO 2010). This is a significant finding since eating fruits and vegetables directly affects human health. Because fleshy fruits are frequently the primary source of food for people around the world, bio-monitoring of trace elements in them must continue.

4. Conclusion

In conclusion, industries have been growing rapidly in all over the world and exert a serious problem to the environment. Exposure to the elevated levels of heavy metals associated with health risks in the food in high traffic city and road markets in Jazan region had not been testified extensively previously. Therefore, the focus of this study was to determine the lead concentration as heavy metals. The concentration of the investigated result shows that confirms and investigated content of lead (Pb) in 14 types of collected fruits and vegetables from Gizan-Sabya road markets, Jazan, Saudi Arabia were measured using Inductively Coupled Plasma-Atomic Emission Spectroscopy.

Current results of Pb values within the study samples are similar to those reported by some researchers in previous studies and the range of values presented for this element in other analyses measured using Inductively Coupled Plasma-Atomic Emission Spectroscopy were wide range between (0.465-1.04ppm) except five samples of this study first sample is Cucumber (*Cucumis*

sativus), followed by Tomatoes *(Solanum lycopersicum),* Guava *(Psidium guajava), Okra (Hibiscus esculentus), and Indian almond (Pithecellobium dulce)* respectively which had a relatively high lead content ranged between (1.045-6.385ppm), So this need to more studies. This study agrees with previous studies that high-traffic city and roads areas have substantially more lead in the air than rural areas and those plants are capable of absorbing extra lead; some plants, naturally absorb far more lead than others. Current study also shows that should be attainable are grown and collected away from polluted areas to ensure a safe food production system Within the safe limits prescribed by the (**FAO/WHO 2010**) at (0.473 mg/kg) consumed daily, the contribution of heavy metal intake for an average human. This is an important result to human health which directly affected by ingestion of fruits and vegetables; the biomonitoring of trace elements in fleshy fruits needs to be continued because these are the main sources of food for humans in many parts of the world to ensure a safe food production system.

5. Acknowledgements:

The authors would like to thank Prof. Dr. Zarraq AL-Faifi, Head of Center for Environmental Research and Studies, Faculty of Science, Jazan University for his cooperation and all staff members in the center for helping and cooperation in analyzing the samples for this study.

6. REFERENCES

Ahmed. M. S. Yesmin M., Jeba F., SirajulHoquec M., Jamee A. R. and AbdusSalam. Risk assessment and evaluation of heavy metals concentrations in blood samples of plastic industry workers in Dhaka, Bangladesh Toxicol Rep (2020).

Brown GW.Standard deviation, standard error. Which “standard” shouldwe use? Am J Dis Child136: 937–941, (1982).

Curran-Everett D, Benos DJ.Guidelines for reporting statistics in journals published by the American Physiological Society: the sequel.AdvPhysiol Educ31: 295–298, (2007).

Demirezen D. and Aksoy A. Heavy metal levels in vegetables in Turkey are within safe limits for Cu, Zn, Ni and exceeded for Cd and Pb. *Journal of Food Quality*, vol. 29, no. 3, pp. 252– 265, (2006).

FAO/WHO Expert Committee on Food Additives, “Summary and conclusions,” in Proceedings of the 53rd Meeting Joint FAO/WHO *Expert Committee on Food Additives*, Rome, Italy, June (1999).

Fytianos K., Katsianis G., Triantafyllou P., and Zachariadis G., “Accumulation of heavy metals in vegetables grown in an industrial area in relation to soil,” *Bulletin of Environmental Contamination and Toxicology*, vol. 67, no. 3, pp. 423–430,(2001).

Hossain. M. M., Chowdhurya A.M., Hasan J., Harun-ArRashid M., Acter T., Khan M. N., Mahatabuddin S. and NizamUddin. Heavy metal pollution in the soil-vegetable system of Tannery Estate. *Environ. Nanotechnol. Monit. Mana*g. (2021).

Husain A., Baroon Z., Al-khalafawi M., Al-Ati T., and Sawaya W., “Toxic metals in imported fruits and vegetables marketed in Kuwait,” *Environment International*, vol. 21, no. 6, pp. 803–805, (1995).

Ja¨rup L. Hazards of heavy metal contamination, *British Medical Bulletin*, vol. 68, pp. 167–182, (2003).

Khan. S., Cao Q., Zheng. Y. M., Huang. Y. Z., and Zhu Y. G., “Health risks of heavy metals in contaminated soils and food crops irrigated with wastewater in Beijing, China,” *Environmental Pollution*, vol. 152, no. 3, pp. 686–692, (2008).

Kicińska . A. and J. Wikar. Ecological risk associated with agricultural production in soils contaminated by the activities of the metal ore mining and processing industry example from southern Poland. *Soil Tillage Res*. (2021).

Kulkarni. V. V. Animes Golder A., Ghosh P. K. Critical analysis and valorization potential of battery industry sludge: speciation, risk assessment and metal recovery. *J. Clean. Prod*. (2018).

Massadeh A. M., Allah, A. and Al-Massaedh T., T. Determination of heavy metals in canned fruits and vegetables sold in Jordan market. Environ. *Sci. Pollut. Res*. 25, 1914–1920. https://doi.org/10.1007/s11356-017-0611-0 (2018).

Mohamed A. E., “Trace element levels in some kinds of dates” *Food Chemistry*, vol. 70, no. 1, pp. 9–12, (2000).

Pennington J., Schoen S., Salmon G., Young B., Johnson R., and Marts R. W., “Composition of core foods of the U.S. Food Supply, 1982–1991. III. Copper, manganese, selenium, and iodine, ”*Journal of Food Composition and Analysis*, vol. 8, no. 2, pp. 171–217, (1995).

R Development Core Team.R: a Language and Environment for Statistical Computing. Vienna, Austria: R Foundation for Statistical Computing, (2008); http://www.R-project.org.

Radwan. M. A. and Salama. A. K., "Market basket survey for some heavy metals in Egyptian fruits and vegetables," *Food and Chemical Toxicology*, vol. 44, no. 8, pp. 1273–1278, (2006).

Rusin. M. , Domagalska. J., Rogala. D., Razzaghi. M. & Szymala. I. Concentration of cadmium and lead in vegetables and fruits. *Naturepotifolio scientific reports*. 11:11913 https://doi.org/10.1038/s41598-021-91554-z(2021).

Saracoglu S., Tuzen M., and Soylak M., "Evaluation of trace element contents of dried apricot samples from Turkey," *Journal of Hazardous Materials*, vol. 167, no. 1–3, pp. 647–652, (2009).

Sathawara N. G., Parikh D. J., and Agarwal Y. K., "Essential heavy metals in environmental samples from Western India," *Bulletin of Environmental Contamination and Toxicology*, vol. 73, no. 4, pp. 756–761, (2004).

Scott D, Keoghan JM, Allan BE (1996) Native and low input grasses—a New Zealand high country perspective. *NZ J Agric Res* 39:499–512.

Shaheen N, Irfan NM, Khan IN, Islam S, Islam MS, Ahmed MK (2016) Presence of heavy metals in fruits and vegetables: health risk implications in Bangladesh. *Chemosphere* 152:431–438.

Sharma B. et al. Lead bioaccumulation mediated by Bacillus cereus BPS-9 from an industrial waste contaminated site encoding heavy metal resistant genes and their transporters. *J. Hazard Mater*. (2021).

Sobukola O. P., Adeniran O. M., Odedairo A. A., and Kajihausa O. E., "Heavy metal levels of some fruits and leafy vegetables from selected markets in Lagos, Nigeria," *African Journal of Food Science*, vol. 4, no. 2, pp. 389–393, (2010).

Tang, L., Hamid, Y., Zehra, A., Shohag, M.J., He, Z.L., Liu, D , Feng, Y. and Yang, X.E., Foliar application of zinc and selenium alleviates cadmium and lead toxicity of water spinach bioavailability/cytotoxicity study with human cell lines *Environ. Int*. 145:106122. (2020).

US EPA (1996) Method 3050B: Acid Digestion of Sediments, Sludges, and Soils, Revision 2, Washington DC.

Wang. X., Saro. T., Xing. B, and Tao. S., *Science of The Total Environment*, vol. 330, no. 1–3, p. 28, (2005).

Yong. Y. et al. Co-treatment of electroplating sludge, copper slag, and spent cathode carbon for recovering and solidifying heavy metals. *J. Hazard Mater*. (2021).

World Health Organisation (WHO). Action Is Needed on Chemicals of Major Public Health Concern. *Public Health Environ*. (2010), 1–4. Available online: https://www.who.int/ipcs/assessment/public_health/chemicals_phc/en/ (accessed on: 27.November 2019).

دراسة السلة الغذائية ١: رصد تركيز الرصاص والمخاطر الصحية المحتملة في بعض أنواع الفواكه والخضروات المجمعة من مواقع الإنتاج والأسواق في منطقة جازان

توفيق هادي الفيفي وأحمد سعيد مبروك
قسم الأحياء ، كلية العلوم ، جامعة جازان ، المملكة العربية السعودية

الملخص

في هذه الدراسة ، تم فحص محتوى الرصاص (Pb) كمعدن ثقيل في ١٤ نوعًا من الفواكه والخضروات الطازجة المجمعة من طرق وأسواق جيزان- صبيا ، جازان ، المملكة العربية السعودية ، تم قياسها باستخدام التحليل الطيفي للانبعاثات الذرية بالبلازما الحثي ICP-AES. أظهرت نتائج هذه الدراسة أن متوسط التركيزات المكتشفة تراوحت بين ٠,٤٦٥ إلى ٦,٣٨٥ جزء في المليون. تم رصد أعلى مستويات للرصاص (٦,٣٨٥ ، ٣,٥١ ، ٢,٣٦٥ ، ١,٦٢٥ و ١,٠٤٥ جزء في المليون) في اللوز الهندي *Pithecellobium dulce* و البامية*Hibiscus esculentus* و الجوافه *Psidium guajava* و *الطماطم Solanum lycopersicum* و *الخيار Cucumis sativus* على التوالي. كما تم تقدير مآخذ الإنسان اليومية من الرصاص المنسوبة إلى نظام غذائي من الفواكه والخضروات في هذه المنطقة. نتائجنا لقيم الرصاص في العينات مماثلة لتلك التي أبلغ عنها بعض الباحثين وكان نطاق القيم المقدمة لهذا العنصر في تحليلات أخرى واسعًا جدًا باستثناء اللوز الهندي *Pithecellobium dulce* و البامية*Hibiscus esculentus* و الجوافه *Psidium guajava* و *الطماطم Solanum lycopersicum* و *الخيار Cucumis sativus* على التوالي والتي كانت تحتوي على نسبة عالية نسبيًا من الرصاص ، لذلك يحتاج هذا إلى مزيد من الدراسات في الفترة المقبلة ، في حين أن جميع النباتات الأخرى في هذه الدراسة تحتوي على أقل من ٠,٩ جزء في المليون. تؤكد هذه الدراسة أن المدن والطرق ذات الإزدحام الشديد بها نسبة الرصاص في الهواء أكثر بكثير من المناطق الريفية وأن تلك النباتات قادرة على امتصاص الرصاص الإضافي ؛ بعض النباتات تمتص الرصاص بشكل طبيعي أكثر من غيرها. تظهر هذه الدراسة أيضًا أنه ينبغي تحقيق الزراعة وجمعها بعيدًا عن المناطق الملوثة لضمان نظام إنتاج غذائي آمن.

الكلمات المفتاحية: سمية الرصاص ، منطقة جازان ، المخاطر الصحية ، تلوث السلسلة الغذائية

Microvesicles: Clinical Importance and Methods of Detection

Abdullah A. Mobarki*

*Department of Medical Laboratory Technology, Faculty of Applied Medical Sciences, Jazan University, Kingdom of Saudi Arabia

Abstract

Microvesicles (MVs) are small membrane vesicles, which are released from almost all cell types. MVs are heterogenous in size (10nm-1000nm) and are found in blood, saliva, semen, urine, tissue, and all the other body fluids. The majority of MVs in the circulation of healthy individuals are derived from platelets and account for up to 90%. Other cell-derived MVs are elevated in many physiological and pathological conditions. This current review highlights the role of MVs in hemostasis, thrombosis, and inflammation including COVID-19 infection and methods of MVs detection, characterization, and enumeration. Elevated MVs have been described in COVID-19 infection, which have been associated with the incidence of prothrombotic tendency and driven inflammatory responses. Thus, better understanding of MVs and their role in prothrombotic tendency and driven inflammatory responses will lead to better management of the disease outcomes.

Keywords: Microvesicles, phospholipids**,** COVID-19, detection methods, flow cytometry **.**

Introduction

Microvesicles (MVs) are small membrane, submicron, heterogeneous vesicles, which were earlier described in 1967 as platelet dust (Wolf, 1967). In 1971, MVs were characterized to be released from reticulocytes during the RBCs' maturation process (Schrier et al., 1971). MVs are also heterogenous in size (10nm-1000nm) and contents and are found in blood, saliva, semen, urine, tissue, and all the other body fluids (Berckmans et al., 2011; Foster et al., 2016; Franz et al., 2013; Viñuela-Berni et al., 2015). Also, the MVs are released from almost all cell types including platelets microvesicles (PMVs) (Nomura et al., 2002), megakaryocytes microvesicles (MMVs), endothelial cells microvesicles (EMVs) (Garcia et al., 2005; Preston et al., 2003), leukocytes (LMVs) (Nomura et al., 2002), erythrocytes microvesicles (RMVs), stem cells microvesicles (SMVs), vascular smooth muscle cells microvesicles (VMVs), mast cells microvesicles (MsMVs) and even *in vitro* from culture cell lines (Gieseler et al., 2018; Krawczenko et al., 2020). The contents and antigenic features of MVs are similar to the cells they originated from (Emerson & Cone, 1981; Jimenez et al., 2003). Subpopulations of MVs can be generated from blood cells with a different signature from their parent cells with

different and distinct features under certain stimuli, which suggest a distinct role and function of MVs (Shai et al., 2012).

The majority of MVs in the circulation of healthy individuals are derived from platelets and account for up to 90% of MVs in circulation (Jimenez et al., 2003). MVs have a short half-life of a few hours (Rank et al., 2011). The levels of MVs can be elevated in various physiological states (including exercise (Shill et al., 2018) and pregnancy (Aharon & Brenner, 2011; VanWijk et al., 2002)) and pathological conditions (Jimenez et al., 2003; Mallat et al., 2000; Pankoui Mfonkeu et al., 2010; van der Zee et al., 2006) (including anemia (H. Hamali et al., 2015), viral infection (H. A. Hamali et al., 2020; Zahran et al., 2021), bacterial infection (Nieuwland et al., 2000), renal disease (Burton et al., 2013), thrombosis (Bidot et al., 2008), cancer (Hisada & Mackman, 2021), diabetes, and pre-eclampsia (VanWijk et al., 2002)). The main function of MVs has been attributed to hemostasis and coagulation due to their procoagulant nature. MVs richly express negatively charged phospholipids (PLs) on their outer surface mainly phosphatidylserine (PS), which are found to support thrombin both *in vivo* and *in vitro* (Berckmans et al., 2001; Morel et al., 2006), but their exact function is not fully understood. Beyond hemostasis, their role has been also suggested in supporting coagulation, thrombosis, inflammation, angiogenesis, vascular injury and dysfunction, cell-to-cell communication, signal transduction, cell differentiation and survival, organ development and remodeling, tissue homeostasis, drug resistance, apoptosis and waste removal (Abid Hussein et al., 2007; Baj-Krzyworzeka et al., 2002; Brill et al., 2005; Jaiswal et al., 2017; Morel et al., 2006; Qu et al., 2020). In addition, MVs involvement has been suggested in blood transfusion reactions, adverse effects, and its complications (Belizaire et al., 2012; Jy et al., 2011; Said & Doctor, 2017). MVs have been shown to be cargo harboring RNA, protein, bioactive mediators, and other metabolites of their parent cells to modify other cells (Rozmyslowicz et al., 2003; Sims et al., 1988). The current review will be mainly focused on MVs' generation, clinical applications and recent advances in methods of MVs detection. Other extracellular vesicles such as apoptotic bodies and exosomes are excluded from this review.

Microvesicles generation

Microvesicles are released from activated cells mainly platelets, cells undergoing apoptosis, upon shear stress, and even after cell injury. The mechanism of MVs formation is known as the flip-flop mechanism and budding (blebbing) of the cell membrane. The flip-flop is responsible for the localization and translocation of membrane amino-phospholipids (PLs) across the cell membrane, which is controlled by specific channels (flippase, floppase and scramblase). In all resting cells, the PLs are asymmetrically distributed across the cell membrane keeping the inner leaflet of the cell membrane rich in negatively charged PLs including phosphatidylserine (PS) and phosphatidylethanolamine (PE), and the outer leaflet of the cell membrane rich in neutral PLs mainly phosphatidylcholine (PC) and sphingomyelin. This is mediated by an active ATP-dependent "flippase" channel moving rapidly PS and PE inward across the cell membrane, whereas the outward, slow, movement of all PLs mainly neutral PLs is controlled by the other ATP-dependent "floppase" channel. The Scramblase, which is inactive in resting cells, controls the bi-directional movement of all PLs (Zwaal et al., 2005).

In the activated platelet or the cell undergoing apoptosis, the Scramblase is switched on and becomes activated leading to externalization of negatively charged PLs mainly PS. And, with ATP-depletion, there is reduction in the flippase and floppase channels leading to disruption of PLs across cell membrane further leading to the exposure of the negatively charged PLs, mainly PS. Simultaneously, the cytoskeleton is broken down due to calpin activation and the signaling pathways in platelet activation, while apoptosis is driven by caspases, however, eventually in both the processes activation or apoptosis leads to the destruction of cytoskeleton structure. This local disruption of the cell membrane composition and structure leads to the budding "blebbing" and then shedding of MVs into the extracellular environment (Bevers et al., 1982; Lhermusier et al., 2011; VanWijk et al., 2003).

Structure and Composition of Microvesicles

The structure and composition of MVs rely on their cell of origin, mechanism of generation, as well as type of stimuli. Platelet-, endothelial- and RBC- derived MVs have been shown to express negatively charged PLs mainly PS and PE, and express antigen features, and surface markers of their parent cells. For example, PMVs express P-selectin, Glycoprotein (GP) Ib, and GP IIb-IIIa (Table 1: summarizes the common markers of MVs from different cells). In, addition, MVs contain other components such as protein, DNA, miRNA, mRNA, Histones, tissue factor, functional cytoadherence, cytoskeleton and nucleosome components, chaperones, and many bioactive lipids materials (Italiano et al., 2010; VanWijk et al., 2003)

Clinical Importance of Microvesicles

The interest in the clinical importance of MVs is a topic of research for many years due to MVs' heterogenicity and diverse roles especially in the field of hemostasis and thrombosis. Although the levels of MVs elevated in many diseases, such as in Scott syndrome, a rare bleeding disorder, the ability of platelets' to expose PS and MVs formation is impaired (Lhermusier et al., 2011). Elevated levels of MVs are a risk factor for prothrombotic tendency and thromboembolic complications. The clinical importance and significance of MVs were extended to cardiovascular disorder, renal disorder, and other pathological conditions. It was proposed that MVs could be an early biomarker in the diagnosis, progression, and severity of many diseases and reflect and predict complications. The new key role of MVs is pointed out by many researchers in almost all fields of medicine and clinical practices including drug delivery, vascular integrity, cell-to-cell communication, waste removal, and angiogenesis, this is solely due to their diversity and heterogenicity (Abid Hussein et al., 2007; Baj-Krzyworzeka et al., 2002; Brill et al., 2005; Jaiswal et al., 2017; Morel et al., 2006; Qu et al., 2020). Therefore, a better understanding of MVs' roles and involvement in physiological and pathological conditions could open the door for early diagnosis of disease onsets, new therapeutic strategies, and preventative measures of diseases.

Circulatory Microvesicles in Health and Disease

Circulatory MVs in healthy individuals are mainly derived from platelet (up to 90%) and low levels from other cell types. Elevated levels of circulatory MVs have been reported after exercise (Shill et al., 2018; Sossdorf et al., 2011), pregnancy (Aharon & Brenner, 2011; VanWijk et al., 2002), and food consumption (diet) (Spectre et al., 2019). Untrained and trained healthy individuals have shown elevated levels of MVs derived from platelets, endothelial cells, and monocytes after 45 minutes of moderate exercise, which dropped to baseline levels after 2 hours only in trained individuals but stayed high in untrained individuals, suggesting the relative slower

clearance from the circulation (Sossdorf et al., 2011). The increase in MVs levels may have a role in hemostatic potential between individuals (Sossdorf et al., 2011).

Microvesicles in Haemostasis and Coagulation

MVs are procoagulant in nature as they express the negatively charged PLs mainly PS on their outer surface. The procoagulant surface is similar to the surface of activated platelets, in its action of supporting the assembly of coagulation factors in healthy individuals (Berckmans et al., 2001). Furthermore, MVs are more procoagulant by 50-100-fold than activated platelets (Sinauridze et al., 2007). Masking PS on the surface of MVs had been shown to reduce the procoagulant activity and the catalytic efficiency of coagulation complexes by up to 1000-fold (del Conde et al., 2005). The procoagulant activity of MVs increased in the presence of tissue factor (TF) and PS on the surface MVs enhance TF. TF is the principal initiator of the coagulation cascade, TF-bearing MVs can initiate coagulation (Wolberg et al., 1999). As mentioned previously, MVs express other antigenic features from their parent cells and can bind to other cells, EMVs have been shown to induce TF procoagulant activity when interacting with monocytes *in vitro* (del Conde et al., 2005). TF-bearing MVs derived from platelets, monocytes, and other cells have been described. Apart from TF, MVs mainly PMVs also express other hemostatic molecules such as but not limited to von-Willebrand factor, glycoprotein IIb/IIIa, and glycoprotein Ib (Morel et al., 2006). The anticoagulant properties of MVs through tissue factor pathway inhibitor and thrombomodulin pathway and fibrinolytic pathways have been proposed, but need further studies and understanding (Morel et al., 2006).

Microvesicles in Thrombosis

The role of MVs in thrombosis has been a primary interest of scientists since their discovery. MVs express adhesion molecules such as P-selectin, which has been shown to bind leukocytes in thrombus formation at the site of vascular injury (del Conde et al., 2005). Furthermore, P-selectin showed to attract TF-bearing MVs to the growing thrombus. The role of TF-bearing MVs was observed to induce fibrin formation through the activation of coagulation (Wagner, 2005). An extended understanding of the role of MVs has been observed in atherothrombosis.

Microvesicles in Inflammation and Development of Atherothrombosis

MVs play a role in driving not only inflammation but also affect endothelium causing endothelium distribution and also participate in vascular remodeling (Mesri & Altieri, 1998; Morel et al., 2006). This is mainly due to the chemokines, and chemoattractants carried by MVs, which all are the bases in driving atherothrombosis (Mesri & Altieri, 1998; Morel et al., 2006). Elevated levels of MVs including PMVs, EMVs, RMVs, and LMVs have been observed in inflammatory conditions such as sepsis, multiple organ dysfunction syndrome, vasculitis, viral infection, and hemodialysis, with the ability to support thrombin generation (Burton et al., 2013; Daniel et al., 2006; H. A. Hamali et al., 2020, 2022; Joop et al., 2001). In addition, TF-bearing MVs are elevated and associated with thrombus formation in vasculitis (Kambas et al., 2014). MVs have been shown to induce TF, IL-6, and monocyte chemoattractant protein release from endothelial cells *in vitro*. MVs modulate inflammation, by recruiting cells including leukocytes and promoting cellular adhesiveness (Mesri & Altieri, 1998; Nomura et al., 2001). In addition, P-selectin

plays a key role in the recruitment of leukocyte to the site of infection and augment the inflammatory response (Panicker et al., 2017; Wagner, 2005). P-selectin can be expressed by endothelium cells, platelets and also by MVs, which also contribute to the atherosclerotic lesions (Burger & Wagner, 2003). Furthermore, MVs have shown the ability to manipulate endothelial cells to induce cyclooxygenase - 2 expression, prostacyclin (Barry et al., 1997), cytokines, and interleukins up-regulations and production (Mesri & Altieri, 1998; Nomura et al., 2001). In addition, MVs cause up-regulation of cytokines and adhesive receptors in endothelial cells and monocytes (Mause et al., 2005). Moreover, monocytes' adhesion and infiltration to plaques and development of atherosclerotic lesions are driven by MVs, as they deliver RANTES to damaged endothelium (Mause et al., 2005), eventually leading to platelet activation and proliferation and mitogenesis of vascular smooth muscle cells (Weber et al., 2000). MVs have been shown to affect the nitric oxide signaling pathway and lead to endothelial dysfunction, which impairs the effect of endothelium-dependent-relaxation in rats with acute MI (Boulanger et al., 2001).

Plaques are a suitable environment for elevated MVs levels due to the accumulation of many cells including activated leukocytes, damaged endothelial, and erythrocytes. Apoptosis occurs within plaque leading to an increase in the release of MVs, especially procoagulant MVs, which are mainly derived from leukocytes. MVs within plaque are more procoagulant than circulatory MVs and harbor TF. Activated leukocytes and damaged endothelial inflammation markers, with the involvement of erythrocytes, have been proposed for intraplaque hemorrhage, which is a sign of vulnerability. Furthermore, MVs contain bioactive mediators which could induce the recruitment and adhesion of inflammatory cells including leukocytes and endothelial damage (Angelillo-Scherrer, 2012; Chironi et al., 2006; Leroyer et al., 2007).

Microvesicles in COVID-19

Endothelial dysfunction and damage are the known complications in the pathogenesis of viral infection including COVID-19. Furthermore, vascular damage is a key sign in the alteration of hemostasis in viral infection and the development of coagulopathy in COVID-19 (Ackermann et al., 2020; Canzano et al., 2021). Elevated levels of MVs have been seen in many viral infections (H. A. Hamali et al., 2020) and respiratory disorders (Nieri et al., 2016; Tőkés-Füzesi et al., 2018) including COVID-19 (Campbell et al., 2021; Morel et al., 2021; Rosell et al., 2021; Zahran et al., 2021) compared to healthy controls, which indicates the occurrence of endothelial damage (Morel et al., 2021). Emerging data showed that MVs are involved in lung injuries and pulmonary thrombosis in COVID-19 (Morel et al., 2021). MVs are known to contribute to clot formation and elevated levels of MVs have been suggested to be associated with prothrombic tendency and subsequent thrombosis. They transfer active mediators, which can modulate inflammatory responses. This can be observed by the ability of MVs to induce endothelial cells to release several inflammatory modulators including TF, and interleukin-6 (IL-6), cytokines. Thus, attracts other circulatory cells to adhere to the damaged endothelium (Barry et al., 1997; Mause et al., 2005; Mesri & Altieri, 1998; Nomura et al., 2001). In addition, inflammatory response in viral infection has the ability to induce TF expression as free TF and in WBCs (monocytes and granulocytes). Subsequently, these cells release TF-bearing MVs (Nomura & Shimizu, 2015).

Another source of MVs and TF-bearing MVs is platelets. The involvement of platelets in viral infection has been described (Hottz et al., 2018). In COVID-19 and other viral infections, platelet activation and increased consumption is linked to thrombus formation and inflammatory responses and enhances their prothrombotic tendency and thrombosis in viral infection.

Endothelial markers such as MVs, proinflammatory cytokines such as IL-6, monocyte chemotactic protein 1 (MCP-1), and cyto-adhesion molecules such as intercellular adhesion molecule 1 (ICAM-1) and vascular cell adhesion molecule 1 (VCAM-1) were significantly elevated in a patient suffering with COVID-19 compared to match, which indicates the occurrence of endothelial damage (Morel et al., 2021). In lung injury, EMVs carry angiotensin-converting enzyme (Abbas et al., 2017; Takei et al., 2019) and have been suggested to be an early marker for lung diseases (Bakouboula et al., 2008; Gordon et al., 2011). New studies have linked angiotensin-converting enzymes to regulating endothelial cells (Abbas et al., 2017) and contribute to thrombosis in COVID-19 (Dalan & Boehm, 2021).

Coagulopathy is a characteristic abnormality of COVID-19 that involves elevated levels of D-dimer and fibrinogen, but less involvement of prothrombin time and platelet count, which is distinct from other bacterial-induced coagulopathy (Iba et al., 2020). D-Dimer is a biomarker associated with the severity and has been proposed to predict the outcome of COVID-19. Venous and arterial thrombosis are complications associated with COVID-19 (Iba et al., 2020). MVs and TF-bearing MVs are positively correlated with levels of D-dimer (Guervilly et al., 2021) and negatively correlated with platelet count (H. A. Hamali et al., 2022). The involvement of TF-bearing MVs is observed in patients with thrombosis events (Guervilly et al., 2021). In, addition fibrinolytic system is continuously activated in COVID-19.

Canzano *et al.* demonstrated the involvement of MVs, TF, and platelet-leukocytes aggregates in COVID-19 coagulopathy, which might contribute to pulmonary microthrombi (Canzano et al., 2021). The increase in MVs formation, TF expression, and platelet-leukocyte aggregates have been attenuated by the antiplatelet drugs and interleukin-16 blocker tocilizumab (Canzano et al., 2021).

In summary, MVs play a key role in driving prothrombotic tendency in COVID-19 infection by exerting an effect on endothelial cells and other blood types. The understanding of the behavior and mechanism of MVs in COVID-19 could change the strategy of treatment and prognosis.

Methods of Microvesicles Detection

There are several methods for detection, enumeration, and characterization MVs, and other extracellular vesicles (van der Pol et al., 2014). However, due to their size and heterogenicity, it is still a challenging goal to obtain an ideal single method that can accurately detect and enumerate MVs. The emerging techniques could open a new horizon for MVs' clinical importance (Ayers et al., 2014; Lal et al., 2009; Sokolova et al., 2011; van der Pol et al., 2014). The following methods including Flow cytometry, Electron microscope, Nanoparticles Tracking Analysis, Atomic Force microscopy (AFM) and Assays that rely on either PS or TF for MVs detections will be discussed in the following paragraphs (van der Pol et al., 2010). Other methods also exit to measure, characterize and enumerate MVs including Immunoblotting (Burton et al., 2013), resistive pulse sensing (van der Pol et al., 2014) but will be excluded from this review.

Flow Cytometry

Flow cytometry (FCM) is considered the most widely used technique for MVs detection, characterization, and enumeration. Flow cytometric analysis (FCA) is almost available in many research laboratories, which relies on the detection of the antigenic characteristics of MVs (Gelderman & Simak, 2008; Mesri & Altieri, 1998; Nielsen et al., 2014; Shantsila et al., 2014). It provides abundant information as it uses different laser colors by relaying on forward scatter for size detection and side scatter for granularity of MVs. Antigenic markers of MVs are targeted by the antibody of interest labeled with fluorescent dye. One of the heavily studied markers on MVs is Annexin-V to detect the negatively charged PLs specifically PS, which is considered a pan marker for procoagulant MVs (Gelderman & Simak, 2008; Shantsila et al., 2014). Other markers have been studied according to the research interest and cell-driven analysis of MVs (a summary of markers and antigenic features of Cell-derived is shown in Table1).

One of the advantages of FCM is the ability to study the subpopulation of MVs according to the antigenic markers. Although the FCM has the advantages of being widely used in research and clinical settings as it is a simple approach and provides plenty of information, it has a very detectable threshold, due to the size of MVs especially smaller MVs <500nm, FCM faced challenges in detecting these smaller MVs, which are challenging and difficult to investigate. Smaller MVs are beyond the threshold limit of FCM and lie in the background noise of the machine (Shantsila et al., 2014). The introduction of megamix calibration beads had increased the sensitivity toward MVs detection and characterization but still smaller MVs can be missed and are of great concern (Lacroix et al., 2010; Nielsen et al., 2014; Strasser et al., 2013). In addition, the new generation of FCM has overcome the MVs size obstacles (Nielsen et al., 2014). Although the analysis of MVs by FCM was the work for standardization of the subcommittee of the International Society of Thrombosis and Haemostasis (SSC-ISTH), still no consensus between centers. Overall, FCM is considered a great tool for providing size, complexity, and cellular information of MVs, but it is labor intensive and needs experience.

Electron Microscope

Electronic microscope (EM) mainly transmission electronic microscope (TEM) and scanning electronic microscope (SEM) are very useful techniques in the analysis of MVs. TEM and SEM identify the details of MVs in terms of size (down to 1 nm), morphology, antigenic features, and composition. TEM has the upper hand over SEM as TEM has higher resolution. The immunolabeling step in TEM gives the advantage of characterization of MVs and it has been used to detect MVs from chronic kidney patients (Burton et al., 2013).

However, the extensive pre-analytical steps of sample preparation including dehydration and fixation for MVs analysis on TEM are of great concern as these pre-analytical steps might affect the size and morphology of MVs (van der Pol et al., 2014).

Nanoparticles Tracking Analysis

The Nanoparticles Tracking Analysis (NTA) relays on the brownie motion law. It is very useful in providing absolute count and size disruption of MVs in real-time by tracking moving particles through a microscopic lens. NTA is considered a promising technology as compared to other new technologies because of its fast and reliable detection method with an accurate count of even smaller particles. Also, it uses a small sample volume and no fixation like TEM. The range of NTA detection can range between 30 to 1000 nm of MVs size. On the other hand, NTA lacks the ability to identify

the cell origin, antigenic, and biochemical features of MVs (Gardiner et al., 2013).

Atomic Force Microscopy

It is a very useful and sensitive method for the determination of the shape, size, and subset of MVs, which is considered a major breakthrough and overcomes the limitation of FCM in size detection (Yuana et al., 2010). It uses a fixation step of MVs on a mica platform with washing and drying involving extensive steps of sample analysis. Then it uses a scanning step to scan MVs and recorded the topography information. The disadvantage of the AFM is difficult to be used in clinical settings and the cost of running and maintenance (Nassir et al., 2021).

Assays that rely on either PS or TF for MVs detections

These assays which rely on the MVs expression either PS, TF, or both are called MVs bulk assays. The main principle is the ability for procoagulant activity and prothrombinase activity. The type of methods has the ability to detect the procoagulant activity of MVs but lack the ability to detect the size and count of MVs or even sometimes cell of origin. Enzyme-linked immunosorbent assay (ELISA) method either captures MVs either their procoagulant surface PS to be captured on immobilized annexin-V, as the 96-well plate is coated with Annexin-V (Burton et al., 2013; H. Hamali et al., 2015) or according to their cell of origin, which can be observed with platelet-derived MVs (PDMVs) (Nomura et al., 2003). Then the result is expressed as concertation of PS in nanomolar. ELISA quantified the concentration of MVs and it is an easy and reproducible method. The introduction of the ELISA analysis PDMVs in a larger cohort showed a similar outcome as to FCM (Nomura et al., 2009).

Procoagulant Microvesicles Activity

The activity of procoagulant microvesicles to support thrombin generation is another method. The thrombin generation assay has the ability to detect the procoagulant activity of MVs in the plasma (Bidot et al., 2008; Burton et al., 2013; Mooberry et al., 2016). The assay lasts for 1 hour and represents the results in 4 parameters known as lag time, peak thrombin, endogenous thrombin potential, and time to peak.

Conclusion

The huge interest in research to understand the behavior and phenotypic characteristics and enumeration of MVs in basic sciences and cell biology and the correlation into clinical research would further enhance their potential and impact role in health and disease conditions including COVID-19. It is worth mentioning that there is no ideal method for MVs analysis as each one has its own advantages and disadvantages over the other methods, and a combination of more than one method in the MVs could be used in the future without discrepancies in the outcomes.

Table1: Origin and antigenic features of MVs.

Cell of origin	CD Marker (antigen)	Disease	References
Procoagulant MVs	Annexin-V (negatively charged phospholipids [-ve PL]; pan marker for -ve PL) Lactadherin (phosphatidyl serine)	In health and disease	(Burton et al., 2013; Nielsen et al., 2014; Nomura & Shimizu, 2015; Tőkés-Füzesi et al., 2018)
Platelet	CD31 (PECAM-1), CD40L, CD41 (GPIIb/IIIa), CD42a (GPIX) , CD42b (GPIb), CD61 (GPIIIa), CD62P (P-selectin), CD63, PAC1 (GPIIb/IIIa)	Hypertension, rheumatoid arthritis, malaria infection, Peripheral artery disease, COVID-19, malignancy, COPD chronic kidney disease	(Burton et al., 2013; Garcia et al., 2005; Guervilly et al., 2021; Nomura et al., 2002; Pankoui Mfonkeu et al., 2010; Tőkés-Füzesi et al., 2018; van der Zee et al., 2006; Viñuela-Berni et al., 2015; Zahran et al., 2021)
Endothelial	CD31 (PECAM-1), CD51 (Vitronectin), CD54 (ICAM-1), CD62E (E-selectin), CD62P (P-selectin), CD105 (Endoglin), CD106 (VCAM-1), CD144 (VE-cadherin), CD146 (MelCAM-S-Endo 1)	Acute coronary syndrome, Heart transplantation, Hypertension, rheumatoid arthritis, Malaria infection, COVID-19, malignancy, COPD, chronic kidney disease,	(Abbas et al., 2017; Burton et al., 2013; Garcia et al., 2005; Guervilly et al., 2021; Lal et al., 2009; Mallat et al., 2000; Pankoui Mfonkeu et al., 2010; Preston et al., 2003; Tőkés-Füzesi et al., 2018; Viñuela-Berni et al., 2015; Zahran et al., 2021)
Leukocyte	CD45 (Pan marker for leukocytes), CD11a, CD13 (aminopeptidase N-monocytes and granulocytes), CD66e, CD66b, CD15	Acute coronary syndrome, Malaria infection, COPD	(Lal et al., 2009; Pankoui Mfonkeu et al., 2010; Tőkés-Füzesi et al., 2018)
Monocyte	CD66 (Endotoxin receptor), CD11a, CD 14 (LPS, Endotoxin receptor), CD16	Acute coronary syndrome, malaria infection, Hypertension, rheumatoid arthritis, COVID-19, COPD	(Guervilly et al., 2021; Lal et al., 2009; Nomura et al., 2002; Pankoui Mfonkeu et al., 2010; Tőkés-Füzesi et al., 2018; Viñuela-Berni et al., 2015)
Neutrophil	CD66b (CEACAM-1)	Rheumatoid arthritis	(Headland et al., 2015)
Lymphocyte B cell - T cell	CD8, CD19, CD20, CD3, CD25, CD20, CD4, CD56 (NCAM)	Preeclampsia, Acute coronary syndrome, COPD, rheumatoid arthritis, malaria infection	(Lal et al., 2009; Pankoui Mfonkeu et al., 2010; Tőkés-Füzesi et al., 2018; VanWijk et al., 2002; Viñuela-Berni et al., 2015)
Erythrocyte	CD235a (Glycophorin A)	Malaria infection, COVID-19, COPD	(Pankoui Mfonkeu et al., 2010; Tőkés-Füzesi et al., 2018; van der Pol et al., 2014)
Granulocytes	CD66, CD11b	Preeclampsia, COVID-19	(van der Pol et al., 2014; VanWijk et al., 2002)

* Chronic obstructive pulmonary disease (COPD)

References

Abbas, M., Jesel, L., Auger, C., Amoura, L., Messas, N., Manin, G., Rumig, C., León-González, A. J., Ribeiro, T. P., Silva, G. C., Abou-Merhi, R., Hamade, E., Hecker, M., Georg, Y., Chakfe, N., Ohlmann, P., Schini-Kerth, V. B., Toti, F., & Morel, O. (2017). Endothelial Microparticles from Acute Coronary Syndrome Patients Induce Premature Coronary Artery Endothelial Cell Aging and Thrombogenicity: Role of the Ang II/AT1 Receptor/NADPH Oxidase-Mediated Activation of MAPKs and PI3-Kinase Pathways. *Circulation*, *135*(3), 280–296. https://doi.org/10.1161/CIRCULATIONAHA.116.017513

Abid Hussein, M. N., Böing, A. N., Sturk, A., Hau, C. M., & Nieuwland, R. (2007). Inhibition of microparticle release triggers endothelial cell apoptosis and detachment. *Thrombosis and Haemostasis*, *98*(5), 1096–1107. https://doi.org/10.1160/TH05-04-0231

Ackermann, M., Verleden, S. E., Kuehnel, M., Haverich, A., Welte, T., Laenger, F., Vanstapel, A., Werlein, C., Stark, H., Tzankov, A., Li, W. W., Li, V. W., Mentzer, S. J., & Jonigk, D. (2020). Pulmonary Vascular Endothelialitis, Thrombosis, and Angiogenesis in Covid-19. *New England Journal of Medicine*, *383*(2), 120–128. https://doi.org/10.1056/NEJMoa2015432

Aharon, A., & Brenner, B. (2011). Microparticles and pregnancy complications. *Thrombosis Research*, *127 Suppl*, S67-71. https://doi.org/10.1016/S0049-3848(11)70019-6

Angelillo-Scherrer, A. (2012). Leukocyte-derived microparticles in vascular homeostasis. *Circulation Research*, *110*(2), 356–369. https://doi.org/10.1161/CIRCRESAHA.110.233403

Ayers, L., Harrison, P., Kohler, M., & Ferry, B. (2014). Procoagulant and platelet-derived microvesicle absolute counts determined by flow cytometry correlates with a measurement of their functional capacity. *Journal of Extracellular Vesicles*, *3*. https://doi.org/10.3402/jev.v3.25348

Baj-Krzyworzeka, M., Majka, M., Pratico, D., Ratajczak, J., Vilaire, G., Kijowski, J., Reca, R., Janowska-Wieczorek, A., & Ratajczak, M. Z. (2002). Platelet-derived microparticles stimulate proliferation, survival, adhesion, and chemotaxis of hematopoietic cells. *Experimental Hematology*, *30*(5), 450–459. https://doi.org/10.1016/s0301-472x(02)00791-9

Bakouboula, B., Morel, O., Faure, A., Zobairi, F., Jesel, L., Trinh, A., Zupan, M., Canuet, M., Grunebaum, L., Brunette, A., Desprez, D., Chabot, F., Weitzenblum, E., Freyssinet, J.-M., Chaouat, A., & Toti, F. (2008). Procoagulant membrane microparticles correlate with the severity of pulmonary arterial hypertension. *American Journal of Respiratory and Critical Care Medicine*, *177*(5), 536–543. https://doi.org/10.1164/rccm.200706-840OC

Barry, O. P., Pratico, D., Lawson, J. A., & FitzGerald, G. A. (1997). Transcellular activation of platelets and endothelial cells by bioactive lipids in platelet microparticles. *The Journal of Clinical Investigation*, *99*(9), 2118–2127. https://doi.org/10.1172/JCI119385

Belizaire, R. M., Prakash, P. S., Richter, J. R., Robinson, B. R., Edwards, M. J., Caldwell, C. C., Lentsch, A. B., & Pritts, T. A. (2012). Microparticles from stored red blood cells activate

neutrophils and cause lung injury after hemorrhage and resuscitation. *Journal of the American College of Surgeons*, *214*(4), 647–648. https://doi.org/10.1016/j.jamcollsurg.2011.12.032

Berckmans, R. J., Nieuwland, R., Böing, A. N., Romijn, F. P. H. T. M., Hack, C. E., & Sturk, A. (2001). Cell-derived microparticles circulate in healthy humans and support low grade thrombin generation. *Thrombosis and Haemostasis*, *85*(4), 639–646. https://doi.org/10.1055/s-0037-1615646

Berckmans, R. J., Sturk, A., Van Tienen, L. M., Schaap, M. C. L., & Nieuwland, R. (2011). Cell-derived vesicles exposing coagulant tissue factor in saliva. *Blood*, *117*(11), 3172–3180. https://doi.org/10.1182/blood-2010-06-290460

Bevers, E. M., Comfurius, P., van Rijn, J. L., Hemker, H. C., & Zwaal, R. F. (1982). Generation of prothrombin-converting activity and the exposure of phosphatidylserine at the outer surface of platelets. *European Journal of Biochemistry*, *122*(2), 429–436. https://doi.org/10.1111/j.1432-1033.1982.tb05898.x

Bidot, L., Jy, W., Bidot, C. J., Jimenez, J. J., Fontana, V., Horstman, L. L., & Ahn, Y. S. (2008). Microparticle-mediated thrombin generation assay: increased activity in patients with recurrent thrombosis. *Journal of Thrombosis and Haemostasis : JTH*, *6*(6), 913–919. https://doi.org/10.1111/j.1538-7836.2008.02963.x

Boulanger, C. M., Scoazec, A., Ebrahimian, T., Henry, P., Mathieu, E., Tedgui, A., & Mallat, Z. (2001). Circulating microparticles from patients with myocardial infarction cause endothelial dysfunction. *Circulation*, *104*(22), 2649–2652. https://doi.org/10.1161/hc4701.100516

Brill, A., Dashevsky, O., Rivo, J., Gozal, Y., & Varon, D. (2005). Platelet-derived microparticles induce angiogenesis and stimulate post-ischemic revascularization. *Cardiovascular Research*, *67*(1), 30–38. https://doi.org/10.1016/j.cardiores.2005.04.007

Burger, P. C., & Wagner, D. D. (2003). Platelet P-selectin facilitates atherosclerotic lesion development. *Blood*. https://doi.org/10.1182/blood-2002-07-2209

Burton, J. O., Hamali, H. A., Singh, R., Abbasian, N., Parsons, R., Patel, A. K., Goodall, A. H., & Brunskill, N. J. (2013). Elevated Levels of Procoagulant Plasma Microvesicles in Dialysis Patients. *PLoS ONE*, *8*(8), e72663. https://doi.org/10.1371/journal.pone.0072663

Campbell, R. A., Hisada, Y., Denorme, F., Grover, S. P., Bouck, E. G., Middleton, E. A., Wolberg, A. S., Rondina, M. T., & Mackman, N. (2021). Comparison of the coagulopathies associated with COVID-19 and sepsis. *Research and Practice in Thrombosis and Haemostasis*, *5*(4), e12525. https://doi.org/10.1002/rth2.12525

Canzano, P., Brambilla, M., Porro, B., Cosentino, N., Tortorici, E., Vicini, S., Poggio, P., Cascella, A., Pengo, M. F., Veglia, F., Fiorelli, S., Bonomi, A., Cavalca, V., Trabattoni, D., Andreini, D., Omodeo Salè, E., Parati, G., Tremoli, E., & Camera, M. (2021). Platelet and Endothelial Activation as Potential Mechanisms Behind the Thrombotic Complications of COVID-19 Patients. *JACC. Basic to Translational Science*, *6*(3), 202–218. https://doi.org/10.1016/j.jacbts.2020.12.009

Chironi, G., Simon, A., Hugel, B., Del Pino, M., Gariepy, J., Freyssinet, J.-M., & Tedgui, A. (2006). Circulating leukocyte-derived microparticles predict subclinical atherosclerosis burden in asymptomatic subjects. *Arteriosclerosis, Thrombosis, and Vascular Biology*, *26*(12), 2775–2780. https://doi.org/10.1161/01.ATV.0000249639.36915.04

Dalan, R., & Boehm, B. O. (2021). Thrombosis post COVID-19 vaccinations: Potential link to ACE pathways. In *Thrombosis research* (Vol. 206, pp. 137–138). https://doi.org/10.1016/j.thromres.2021.08.018

Daniel, L., Fakhouri, F., Joly, D., Mouthon, L., Nusbaum, P., Grunfeld, J.-P., Schifferli, J., Guillevin, L., Lesavre, P., & Halbwachs-Mecarelli, L. (2006). Increase of circulating neutrophil and platelet microparticles during acute vasculitis and hemodialysis. *Kidney International*, *69*(8), 1416–1423. https://doi.org/10.1038/sj.ki.5000306

del Conde, I., Nabi, F., Tonda, R., Thiagarajan, P., López, J. A., & Kleiman, N. S. (2005). Effect of P-selectin on phosphatidylserine exposure and surface-dependent thrombin generation on monocytes. *Arteriosclerosis, Thrombosis, and Vascular Biology*, *25*(5), 1065–1070. https://doi.org/10.1161/01.ATV.0000159094.17235.9b

Emerson, S. G., & Cone, R. E. (1981). I-Kk and H-2Kk antigens are shed as supramolecular particles in association with membrane lipids. *Journal of Immunology (Baltimore, Md. : 1950)*, *127*(2), 482–486.

Foster, B. P., Balassa, T., Benen, T. D., Dominovic, M., Elmadjian, G. K., Florova, V., Fransolet, M. D., Kestlerova, A., Kmiecik, G., Kostadinova, I. A., Kyvelidou, C., Meggyes, M., Mincheva, M. N., Moro, L., Pastuschek, J., Spoldi, V., Wandernoth, P., Weber, M., Toth, B., & Markert, U. R. (2016). Extracellular vesicles in blood, milk and body fluids of the female and male urogenital tract and with special regard to reproduction. *Critical Reviews in Clinical Laboratory Sciences*, *53*(6), 379–395. https://doi.org/10.1080/10408363.2016.1190682

Franz, C., Böing, A. N., Hau, C. M., Montag, M., Strowitzki, T., Nieuwland, R., & Toth, B. (2013). Procoagulant tissue factor-exposing vesicles in human seminal fluid. *Journal of Reproductive Immunology*, *98*(1–2), 45–51. https://doi.org/10.1016/j.jri.2013.02.002

Garcia, S., Chirinos, J., Jimenez, J., Del Carpio Muñoz, F., Canoniero, M., Jy, W., Jimenez, J., Horstman, L., & Ahn, Y. (2005). Phenotypic assessment of endothelial microparticles in patients with heart failure and after heart transplantation: switch from cell activation to apoptosis. *The Journal of Heart and Lung Transplantation : The Official Publication of the International Society for Heart Transplantation*, *24*(12), 2184–2189. https://doi.org/10.1016/j.healun.2005.07.006

Gardiner, C., Ferreira, Y. J., Dragovic, R. A., Redman, C. W. G., & Sargent, I. L. (2013). Extracellular vesicle sizing and enumeration by nanoparticle tracking analysis. *Journal of Extracellular Vesicles*, *2*. https://doi.org/10.3402/jev.v2i0.19671

Gelderman, M. P., & Simak, J. (2008). Flow Cytometric Analysis of Cell Membrane Microparticles. *Methods in Molecular Biology (Clifton, N.J.)*, *484*, 79–93.

https://doi.org/10.1007/978-1-59745-398-1_6

Gieseler, F., Plattfaut, C., Quecke, T., Freund, A., Ungefroren, H., & Ender, F. (2018). Heterogeneity of microvesicles from cancer cell lines under inflammatory stimulation with TNF-α. *Cell Biology International*. https://doi.org/10.1002/cbin.11040

Gordon, C., Gudi, K., Krause, A., Sackrowitz, R., Harvey, B.-G., Strulovici-Barel, Y., Mezey, J. G., & Crystal, R. G. (2011). Circulating endothelial microparticles as a measure of early lung destruction in cigarette smokers. *American Journal of Respiratory and Critical Care Medicine*, *184*(2), 224–232. https://doi.org/10.1164/rccm.201012-2061OC

Guervilly, C., Bonifay, A., Burtey, S., Sabatier, F., Cauchois, R., Abdili, E., Arnaud, L., Lano, G., Pietri, L., Robert, T., Velier, M., Papazian, L., Albanese, J., Kaplanski, G., Dignat-George, F., & Lacroix, R. (2021). Dissemination of extreme levels of extracellular vesicles: tissue factor activity in patients with severe COVID-19. *Blood Advances*, *5*(3), 628–634. https://doi.org/10.1182/bloodadvances.2020003308

Hamali, H. A., Mobarki, A. A., Akhter, M. S., Saboor, M., Madkhali, A. M., Halawani, A. J., Hakami, A. M., Eisa, Z. M., Dobie, G., & Hobani, Y. (2020). Elevated levels of procoagulant microvesicles in patients with dengue fever. *Future Virology*. https://doi.org/10.2217/fvl-2020-0202

Hamali, H. A., Saboor, M., Dobie, G., Madkhali, A. M., Akhter, M. S., Hakamy, A., Al-Mekhlafi, H. M., Jackson, D. E., Matari, Y. H., & Mobarki, A. A. (2022). Procoagulant Microvesicles in COVID-19 Patients: Possible Modulators of Inflammation and Prothrombotic Tendency. *Infection and Drug Resistance*, *15*, 2359–2368. https://doi.org/10.2147/IDR.S355395

Hamali, H., Elhussein, O., Jamil, A., Hussain, S., Alshraim, M., & Alshehri, A. (2015). Elevated levels of pro- coagulant microvesicles in children in- steady state sickle cell disease. *Journal of Applied Hematology*, *6*, 115–118.

Headland, S. E., Jones, H. R., Norling, L. V., Kim, A., Souza, P. R., Corsiero, E., Gil, C. D., Nerviani, A., Dell'accio, F., Pitzalis, C., Oliani, S. M., Jan, L. Y., & Perretti, M. (2015). Neutrophil-derived microvesicles enter cartilage and protect the joint in inflammatory arthritis. *Science Translational Medicine*. https://doi.org/10.1126/scitranslmed.aac5608

Hisada, Y., & Mackman, N. (2021). Tissue Factor and Extracellular Vesicles: Activation of Coagulation and Impact on Survival in Cancer. *Cancers*, *13*(15). https://doi.org/10.3390/cancers13153839

Hottz, E. D., Bozza, F. A., & Bozza, P. T. (2018). Platelets in Immune Response to Virus and Immunopathology of Viral Infections. *Frontiers in Medicine*, *5*, 121. https://doi.org/10.3389/fmed.2018.00121

Iba, T., Levy, J. H., Connors, J. M., Warkentin, T. E., Thachil, J., & Levi, M. (2020). The unique characteristics of COVID-19 coagulopathy. *Critical Care (London, England)*, *24*(1), 360. https://doi.org/10.1186/s13054-020-03077-0

Italiano, J. E., Mairuhu, A. T., & Flaumenhaft, R. (2010). Clinical relevance of microparticles from

platelets and megakaryocytes. *Current Opinion in Hematology*, *17*(6), 578–584. https://doi.org/10.1097/MOH.0b013e32833e77ee

Jaiswal, R., Johnson, M. S., Pokharel, D., Krishnan, S. R., & Bebawy, M. (2017). Microparticles shed from multidrug resistant breast cancer cells provide a parallel survival pathway through immune evasion. *BMC Cancer*, *17*(1), 104. https://doi.org/10.1186/s12885-017-3102-2

Jimenez, J. J., Jy, W., Mauro, L. M., Soderland, C., Horstman, L. L., & Ahn, Y. S. (2003). Endothelial cells release phenotypically and quantitatively distinct microparticles in activation and apoptosis. *Thrombosis Research*, *109*(4), 175–180. https://doi.org/10.1016/s0049-3848(03)00064-1

Joop, K., Berckmans, R. J., Nieuwland, R., Berkhout, J., Romijn, F. P., Hack, C. E., & Sturk, A. (2001). Microparticles from patients with multiple organ dysfunction syndrome and sepsis support coagulation through multiple mechanisms. *Thrombosis and Haemostasis*, *85*(5), 810–820.

Jy, W., Ricci, M., Shariatmadar, S., Gomez-Marin, O., Horstman, L. H., & Ahn, Y. S. (2011). Microparticles in stored red blood cells as potential mediators of transfusion complications. *Transfusion*, *51*(4), 886–893. https://doi.org/10.1111/j.1537-2995.2011.03099.x

Kambas, K., Chrysanthopoulou, A., Vassilopoulos, D., Apostolidou, E., Skendros, P., Girod, A., Arelaki, S., Froudarakis, M., Nakopoulou, L., Giatromanolaki, A., Sidiropoulos, P., Koffa, M., Boumpas, D. T., Ritis, K., & Mitroulis, I. (2014). Tissue factor expression in neutrophil extracellular traps and neutrophil derived microparticles in antineutrophil cytoplasmic antibody associated vasculitis may promote thromboinflammation and the thrombophilic state associated with the disease. *Annals of the Rheumatic Diseases*, *73*(10), 1854–1863. https://doi.org/10.1136/annrheumdis-2013-203430

Krawczenko, A., Bielawska-Pohl, A., Paprocka, M., Kraskiewicz, H., Szyposzynska, A., Wojdat, E., & Klimczak, A. (2020). Microvesicles from Human Immortalized Cell Lines of Endothelial Progenitor Cells and Mesenchymal Stem/Stromal Cells of Adipose Tissue Origin as Carriers of Bioactive Factors Facilitating Angiogenesis. *Stem Cells International*. https://doi.org/10.1155/2020/1289380

Lacroix, R., Robert, S., Poncelet, P., Kasthuri, R. S., Key, N. S., & Dignat-George, F. (2010). Standardization of platelet-derived microparticle enumeration by flow cytometry with calibrated beads: results of the International Society on Thrombosis and Haemostasis SSC Collaborative workshop. *Journal of Thrombosis and Haemostasis : JTH*, *8*(11), 2571–2574. https://doi.org/10.1111/j.1538-7836.2010.04047.x

Lal, S., Brown, A., Nguyen, L., Braet, F., Dyer, W., & Dos Remedios, C. (2009). Using antibody arrays to detect microparticles from acute coronary syndrome patients based on cluster of differentiation (CD) antigen expression. *Molecular & Cellular Proteomics : MCP*, *8*(4), 799–804. https://doi.org/10.1074/mcp.M800335-MCP200

Leroyer, A. S., Isobe, H., Lesèche, G., Castier, Y., Wassef, M., Mallat, Z., Binder, B. R., Tedgui, A., &

Boulanger, C. M. (2007). Cellular origins and thrombogenic activity of microparticles isolated from human atherosclerotic plaques. *Journal of the American College of Cardiology*, *49*(7), 772–777. https://doi.org/10.1016/j.jacc.2006.10.053

Lhermusier, T., Chap, H., & Payrastre, B. (2011). Platelet membrane phospholipid asymmetry: from the characterization of a scramblase activity to the identification of an essential protein mutated in Scott syndrome. *Journal of Thrombosis and Haemostasis*, *9*, 1883–1891.

Mallat, Z., Benamer, H., Hugel, B., Benessiano, J., Steg, P. G., Freyssinet, J. M., & Tedgui, A. (2000). Elevated levels of shed membrane microparticles with procoagulant potential in the peripheral circulating blood of patients with acute coronary syndromes. *Circulation*, *101*(8), 841–843. https://doi.org/10.1161/01.cir.101.8.841

Mause, S. F., von Hundelshausen, P., Zernecke, A., Koenen, R. R., & Weber, C. (2005). Platelet microparticles: a transcellular delivery system for RANTES promoting monocyte recruitment on endothelium. *Arteriosclerosis, Thrombosis, and Vascular Biology*, *25*(7), 1512–1518. https://doi.org/10.1161/01.ATV.0000170133.43608.37

Mesri, M., & Altieri, D. C. (1998). Endothelial cell activation by leukocyte microparticles. *Journal of Immunology (Baltimore, Md. : 1950)*, *161*(8), 4382–4387.

Mooberry, M. J., Bradford, R., Hobl, E. L., Lin, F. C., Jilma, B., & Key, N. S. (2016). Procoagulant microparticles promote coagulation in a factor XI-dependent manner in human endotoxemia. *Journal of Thrombosis and Haemostasis : JTH*, *14*(5), 1031–1042. https://doi.org/10.1111/jth.13285

Morel, O., Marchandot, B., Jesel, L., Sattler, L., Trimaille, A., Curtiaud, A., Ohana, M., Fafi-Kremer, S., Schini-Kerth, V., Grunebaum, L., & Freyssinet, J.-M. (2021). Microparticles in COVID-19 as a link between lung injury extension and thrombosis. *ERJ Open Research*, *7*(2), 00954–02020. https://doi.org/10.1183/23120541.00954-2020

Morel, O., Toti, F., Hugel, B., Bakouboula, B., Camoin-Jau, L., Dignat-George, F., & Freyssinet, J. M. (2006). Procoagulant microparticles: Disrupting the vascular homeostasis equation? *Arteriosclerosis, Thrombosis, and Vascular Biology*, *26*(12), 2594–2604. https://doi.org/10.1161/01.ATV.0000246775.14471.26

Nassir, C. M. N. C. M., Ghazali, M. M., Hashim, S., Idris, N. S., Yuen, L. S., Hui, W. J., Norman, H. H., Gau, C. H., Jayabalan, N., Na, Y., Feng, L., Ong, L. K., Abdul Hamid, H., Ahamed, H. N., & Mustapha, M. (2021). Diets and Cellular-Derived Microparticles: Weighing a Plausible Link With Cerebral Small Vessel Disease. *Frontiers in Cardiovascular Medicine*, *8*, 632131. https://doi.org/10.3389/fcvm.2021.632131

Nielsen, M. H., Beck-Nielsen, H., Andersen, M. N., & Handberg, A. (2014). A flow cytometric method for characterization of circulating cell-derived microparticles in plasma. *Journal of Extracellular Vesicles*, *3*(1), 20795. https://doi.org/10.3402/jev.v3.20795

Nieri, D., Neri, T., Petrini, S., Vagaggini, B., Paggiaro, P., & Celi, A. (2016). Cell-derived microparticles and the lung. *European Respiratory Review : An*

Official Journal of the European Respiratory Society, *25*(141), 266–277. https://doi.org/10.1183/16000617.0009-2016

Nieuwland, R., Berckmans, R. J., McGregor, S., Böing, A. N., Romijn, F. P., Westendorp, R. G., Hack, C. E., & Sturk, A. (2000). Cellular origin and procoagulant properties of microparticles in meningococcal sepsis. *Blood*, *95*(3), 930–935.

Nomura, S., Kanazawa, S., & Fukuhara, S. (2002). Effects of efonidipine on platelet and monocyte activation markers in hypertensive patients with and without type 2 diabetes mellitus. *Journal of Human Hypertension*, *16*(8), 539–547. https://doi.org/10.1038/sj.jhh.1001447

Nomura, S., & Shimizu, M. (2015). Clinical significance of procoagulant microparticles. *Journal of Intensive Care*, *3*(1), 2. https://doi.org/10.1186/s40560-014-0066-z

Nomura, S., Shouzu, A., Taomoto, K., Togane, Y., Goto, S., Ozaki, Y., Uchiyama, S., & Ikeda, Y. (2009). Assessment of an ELISA kit for platelet-derived microparticles by joint research at many institutes in Japan. *Journal of Atherosclerosis and Thrombosis*, *16*(6), 878–887. https://doi.org/10.5551/jat.2642

Nomura, S., Tandon, N. N., Nakamura, T., Cone, J., Fukuhara, S., & Kambayashi, J. (2001). High-shear-stress-induced activation of platelets and microparticles enhances expression of cell adhesion molecules in THP-1 and endothelial cells. *Atherosclerosis*, *158*(2), 277–287. https://doi.org/10.1016/s0021-9150(01)00433-6

Nomura, S., Uehata, S., Saito, S., Osumi, K., Ozeki, Y., & Kimura, Y. (2003). Enzyme immunoassay detection of platelet-derived microparticles and RANTES in acute coronary syndrome. *Thrombosis and Haemostasis*, *89*(3), 506–512.

Panicker, S. R., Mehta-D'souza, P., Zhang, N., Klopocki, A. G., Shao, B., & McEver, R. P. (2017). Circulating soluble P-selectin must dimerize to promote inflammation and coagulation in mice. *Blood*, *130*(2), 181–191. https://doi.org/10.1182/blood-2017-02-770479

Pankoui Mfonkeu, J. B., Gouado, I., Fotso Kuaté, H., Zambou, O., Amvam Zollo, P. H., Grau, G. E. R., & Combes, V. (2010). Elevated cell-specific microparticles are a biological marker for cerebral dysfunctions in human severe malaria. *PloS One*, *5*(10), e13415. https://doi.org/10.1371/journal.pone.0013415

Preston, R. A., Jy, W., Jimenez, J. J., Mauro, L. M., Horstman, L. L., Valle, M., Aime, G., & Ahn, Y. S. (2003). Effects of severe hypertension on endothelial and platelet microparticles. *Hypertension (Dallas, Tex.: 1979)*, *41*(2), 211–217. https://doi.org/10.1161/01.hyp.0000049760.15764.2d

Qu, M., Zou, X., Fang, F., Wang, S., Xu, L., Zeng, Q., Fan, Z., Chen, L., Yue, W., Xie, X., & Pei, X. (2020). Platelet-derived microparticles enhance megakaryocyte differentiation and platelet generation via miR-1915-3p. *Nature Communications*, *11*(1), 4964. https://doi.org/10.1038/s41467-020-18802-0

Rank, A., Nieuwland, R., Crispin, A., Grützner, S., Iberer, M., Toth, B., & Pihusch, R. (2011). Clearance of platelet microparticles in vivo. *Platelets*, *22*(2), 111–116.

https://doi.org/10.3109/09537104.2010.520373

Rosell, A., Havervall, S., von Meijenfeldt, F., Hisada, Y., Aguilera, K., Grover, S. P., Lisman, T., Mackman, N., & Thålin, C. (2021). Patients With COVID-19 Have Elevated Levels of Circulating Extracellular Vesicle Tissue Factor Activity That Is Associated With Severity and Mortality-Brief Report. *Arteriosclerosis, Thrombosis, and Vascular Biology*, *41*(2), 878–882. https://doi.org/10.1161/ATVBAHA.120.315547

Rozmyslowicz, T., Majka, M., Kijowski, J., Murphy, S. L., Conover, D. O., Poncz, M., Ratajczak, J., Gaulton, G. N., & Ratajczak, M. Z. (2003). Platelet- and megakaryocyte-derived microparticles transfer CXCR4 receptor to CXCR4-null cells and make them susceptible to infection by X4-HIV. *AIDS (London, England)*, *17*(1), 33–42. https://doi.org/10.1097/00002030-200301030-00006

Said, A. S., & Doctor, A. (2017). Influence of red blood cell-derived microparticles upon vasoregulation. *Blood Transfusion = Trasfusione Del Sangue*, *15*(6), 522–534. https://doi.org/10.2450/2017.0353-16

Schrier, S. L., Godin, D., Gould, R. G., Swyryd, B., Junga, I., & Seeger, M. (1971). Characterization of microvesicles produced by shearing of human erythrocyte membranes. *Biochimica et Biophysica Acta*, *233*(1), 26–36. https://doi.org/10.1016/0005-2736(71)90354-3

Shai, E., Rosa, I., Parguiña, A. F., Motahedeh, S., Varon, D., & García, Á. (2012). Comparative analysis of platelet-derived microparticles reveals differences in their amount and proteome depending on the platelet stimulus. *Journal of Proteomics*, *76*, 287–296. https://doi.org/https://doi.org/10.1016/j.jprot.2012.02.030

Shantsila, E., Montoro-García, S., Gallego, P., & Lip, G. Y. H. (2014). Circulating microparticles: challenges and perspectives of flow cytometric assessment. *Thrombosis and Haemostasis*, *111*(6), 1009–1014. https://doi.org/10.1160/TH13-11-0937

Shill, D. D., Lansford, K. A., Hempel, H. K., Call, J. A., Murrow, J. R., & Jenkins, N. T. (2018). Effect of exercise intensity on circulating microparticles in men and women. *Experimental Physiology*, *103*(5), 693–700. https://doi.org/10.1113/EP086644

Sims, P. J., Faioni, E. M., Wiedmer, T., & Shattil, S. J. (1988). Complement proteins C5b-9 cause release of membrane vesicles from the platelet surface that are enriched in the membrane receptor for coagulation factor Va and express prothrombinase activity. *The Journal of Biological Chemistry*, *263*(34), 18205–18212.

Sinauridze, E. I., Kireev, D. A., Popenko, N. Y., Pichugin, A. V., Panteleev, M. A., Krymskaya, O. V., & Ataullakhanov, F. I. (2007). Platelet microparticle membranes have 50- to 100-fold higher specific procoagulant activity than activated platelets. *Thrombosis and Haemostasis*. https://doi.org/10.1160/TH06-06-0313

Sokolova, V., Ludwig, A.-K., Hornung, S., Rotan, O., Horn, P. A., Epple, M., & Giebel, B. (2011). Characterisation of exosomes derived from human cells by nanoparticle tracking analysis and scanning electron microscopy. *Colloids and Surfaces. B, Biointerfaces*, *87*(1), 146–150. https://doi.org/10.1016/j.colsurfb.2011.05.013

Sossdorf, M., Otto, G. P., Claus, R. A., Gabriel, H. H. W., & Lösche, W. (2011). Cell-derived microparticles promote coagulation after moderate exercise. *Medicine and Science in Sports and Exercise*, *43*(7), 1169—1176. https://doi.org/10.1249/mss.0b013e3182068645

Spectre, G., Mobarrez, F., Stålesen, R., Östenson, C.-G., Varon, D., Wallen, H., & Hjemdahl, P. (2019). Meal intake increases circulating procoagulant microparticles in patients with type 1 and type 2 diabetes mellitus. *Platelets*, *30*(3), 348–355. https://doi.org/10.1080/09537104.2018.1445837

Strasser, E. F., Happ, S., Weiss, D. R., Pfeiffer, A., Zimmermann, R., & Eckstein, R. (2013). Microparticle detection in platelet products by three different methods. *Transfusion*, *53*(1), 156–166. https://doi.org/10.1111/j.1537-2995.2012.03720.x

Takei, Y., Yamada, M., Saito, K., Kameyama, Y., Sugiura, H., Makiguchi, T., Fujino, N., Koarai, A., Toyama, H., Saito, K., Ejima, Y., Kawazoe, Y., Kudo, D., Kushimoto, S., Yamauchi, M., & Ichinose, M. (2019). Increase in circulating ACE-positive endothelial microparticles during acute lung injury. *The European Respiratory Journal*, *54*(4). https://doi.org/10.1183/13993003.01188-2018

Tőkés-Füzesi, M., Ruzsics, I., Rideg, O., Kustán, P., Kovács, G. L., & Molnár, T. (2018). Role of microparticles derived from monocytes, endothelial cells and platelets in the exacerbation of COPD. *International Journal of Chronic Obstructive Pulmonary Disease*, *13*, 3749–3757. https://doi.org/10.2147/COPD.S175607

van der Pol, E., Coumans, F. A. W., Grootemaat, A. E., Gardiner, C., Sargent, I. L., Harrison, P., Sturk, A., van Leeuwen, T. G., & Nieuwland, R. (2014). Particle size distribution of exosomes and microvesicles determined by transmission electron microscopy, flow cytometry, nanoparticle tracking analysis, and resistive pulse sensing. *Journal of Thrombosis and Haemostasis : JTH*, *12*(7), 1182–1192. https://doi.org/10.1111/jth.12602

van der Pol, E., Hoekstra, A. G., Sturk, A., Otto, C., van Leeuwen, T. G., & Nieuwland, R. (2010). Optical and non-optical methods for detection and characterization of microparticles and exosomes. *Journal of Thrombosis and Haemostasis : JTH*, *8*(12), 2596–2607. https://doi.org/10.1111/j.1538-7836.2010.04074.x

van der Zee, P. M., Biró, E., Ko, Y., de Winter, R. J., Hack, C. E., Sturk, A., & Nieuwland, R. (2006). P-selectin- and CD63-exposing platelet microparticles reflect platelet activation in peripheral arterial disease and myocardial infarction. *Clinical Chemistry*, *52*(4), 657–664. https://doi.org/10.1373/clinchem.2005.057414

VanWijk, M. J., Nieuwland, R., Boer, K., van der Post, J. A. M., VanBavel, E., & Sturk, A. (2002). Microparticle subpopulations are increased in preeclampsia: possible involvement in vascular dysfunction? *American Journal of Obstetrics and Gynecology*, *187*(2), 450–456. https://doi.org/10.1067/mob.2002.124279

VanWijk, M. J., VanBavel, E., Sturk, A., & Nieuwland, R. (2003). Microparticles in cardiovascular diseases.

Cardiovascular Research, *59*(2), 277–287. https://doi.org/10.1016/s0008-6363(03)00367-5

Viñuela-Berni, V., Doníz-Padilla, L., Figueroa-Vega, N., Portillo-Salazar, H., Abud-Mendoza, C., Baranda, L., & González-Amaro, R. (2015). Proportions of several types of plasma and urine microparticles are increased in patients with rheumatoid arthritis with active disease. *Clinical and Experimental Immunology*, *180*(3), 442–451. https://doi.org/10.1111/cei.12598

Wagner, D. D. (2005). New links between inflammation and thrombosis. *Arteriosclerosis, Thrombosis, and Vascular Biology*, *25*(7), 1321–1324. https://doi.org/10.1161/01.ATV.0000166521.90532.44

Weber, A., Köppen, H. O., & Schrör, K. (2000). Platelet-derived microparticles stimulate coronary artery smooth muscle cell mitogenesis by a PDGF-independent mechanism. *Thrombosis Research*, *98*(5), 461–466. https://doi.org/10.1016/s0049-3848(00)00192-4

Wolberg, A. S., Monroe, D. M., Roberts, H. R., & Hoffman, M. R. (1999). Tissue factor de-encryption: ionophore treatment induces changes in tissue factor activity by phosphatidylserine-dependent and -independent mechanisms. *Blood Coagulation & Fibrinolysis : An International Journal in Haemostasis and Thrombosis*, *10*(4), 201–210.

Wolf, P. (1967). The nature and significance of platelet products in human plasma. *British Journal of Haematology*, *13*(3), 269–288. https://doi.org/10.1111/j.1365-2141.1967.tb08741.x

Yuana, Y., Oosterkamp, T. H., Bahatyrova, S., Ashcroft, B., Garcia Rodriguez, P., Bertina, R. M., & Osanto, S. (2010). Atomic force microscopy: a novel approach to the detection of nanosized blood microparticles. *Journal of Thrombosis and Haemostasis : JTH*, *8*(2), 315–323. https://doi.org/10.1111/j.1538-7836.2009.03654.x

Zahran, A. M., El-Badawy, O., Ali, W. A., Mahran, Z. G., Mahran, E. E. M. O., & Rayan, A. (2021). Circulating microparticles and activated platelets as novel prognostic biomarkers in COVID-19; relation to cancer. *PLoS ONE*, *16*(2 February), 1–17. https://doi.org/10.1371/journal.pone.0246806

Zwaal, R. F. A., Comfurius, P., & Bevers, E. M. (2005). Surface exposure of phosphatidylserine in pathological cells. In *Cellular and Molecular Life Sciences* (Vol. 62, Issue 9, pp. 971–988). https://doi.org/10.1007/s00018-005-4527-3

الحويصلات الدقيقة: الأهمية السريرية وطرق الكشف

عبدالله أحمد مباركي

قسم تقنية المختبرات الطبية، كلية العلوم الطبية التطبيقية، جامعة جازان، المملكة العربية السعودية

الملخص

الحويصلات الدقيقة هي عبارة عن حويصلات غشائية صغيرة يتم إطلاقها تقريباً من جميع أنواع الخلايا. وهي غير متجانسة في الحجم (١٠ نانومتر-١٠٠٠ نانومتر) وفي محتوياتها وتوجد في الدم، اللعاب، السائل المنوي، البول، الأنسجة وجميع سوائل الجسم الأخرى. غالبية الحويصلات الدقيقة في الدورة الدموية للأشخاص الأصحاء تكون مستمدة من الصفائح الدموية وتمثل ما يصل إلى ٩٠%. وترتفع الحويصلات الدقيقة المشتقة من الخلايا في العديد من الحالات الفسيولوجية والمرضية. تسلط هذه المقالة العلمية الضوء على الحويصلات الدقيقة ودورها في الإرقاء، تخثر الدم، الاتهابات بما في ذلك عدوى كوفيد-١٩ وكذلك طرق إكتشافها وتوصيفها وتعدادها. إرتفاع عدد الحويصلات الدقيقة في عدوى كوفيد-١٩ ارتبط بحدوث ميل الى حدوث تخثر الدم وردات فعل إلتهابية. لذلك الفهم الأفضل للحويصلات الدقيقة وطرق تحليلها سوف يؤدي إلى تحكم أفضل بتبعات هذا المرض.

الكمات المفتاحية: الحويصلات الدقيقة، الفوسوليبيدات، كوفيد-١٩، طرق البحث، التدفق الخلوي

Synthesis and cathodoluminescence characteristics of rare earth ions incorporated $BaMgAl_{10}O_{17}$ (BAM) phosphor

Yahya Alajlani

Physics DepartmentKingdom of Saudi Arabia, Jazan University

Abstract

In this study, wet combustion method was used to create $BaMgAl_{10}O_{17}$ (BAM) phosphors doped with 2% Ce^{3+} and Tb^{3+} ions. Cathodoluminescence (CL), Energy Dispersive Spectroscopy (EDS), Scanning Electron Microscopy (ESEM), and X-ray diffraction (XRD) have been employed to analyse the samples' crystal structure, elemental composition, and optical characteristics. At the excitation of the electron beam, CL spectra were collected. The $^5D_4 \rightarrow {}^7F_J$ transition caused typical green emission of Tb^{3+} at 542 nm. Emission peak of BAM:Ce phosphor is obtained at 520 nm assigned to the 4f↔5d transition of Ce ions. According to current research, BAM incorporated with Tb may function well in a variety of applications as a suitable material for green phosphors.

Keywords: $BaMgAl_{10}O_{17}$, cathodluminescence, rare earth and phosphor

1. Introduction

Recent years have seen a great deal of attention paid to inorganic phosphors for their applications in high-resolution devices, including field emission displays (FEDs), new plasma display panels (PDPs) and mercury free lamps, as well as biomedical applications [1-4]. In the industrial application of phosphors, the morphology (shaped, sized, and distributed sizes of the particles) is an essential parameter. To achieve this goal, different methods have been tested in order to improve morphology control [5]. An important factor in determining the efficacy of the device is the shape, size, shape distribution and morphology of the phosphor particles.

There are a variety of photonic applications that use phosphor, including light sources, displays, light emitting diodes (LED), detectors, and signal converters. Luminescence activator is embedded within a matrix of host composition and a matrix of luminescence activator. A non-centrosymmetric field from surround ligands has been commonly used to enhance the emission of Lanthanide ions from intra 4f-4f transitions [6]. There has been extensive use of Ce^{3+} in phosphors. Aside from reduced costs, phosphors incorporated with Ce^{3+} ions show a broad spectrum of excitations and emissions. The host matrix is extremely sensitive to the energetic position of Ce^{3+} ions in a 5d space. Due to this, they are capable of

tuning from red to UV luminescence [7-8]. Phosphors activated with Ce^{3+} ions also exhibit large absorption cross sections and strong f-d transitions in their spectra, which result in intense spectral bands. In most host lattices, this parity-allowed feature allows Ce^{3+} to emit with heavy intensity and a short decay time (30–60 ns) [9].

Synthesis efforts in the materials such as $B_2MgAl_{10}O_{17}$, $BaMg_2Al_{16}O_{27}$ to date have focused primarily on the development of alternative liquid solution techniques, including sol–gel, combustion, spray pyrolysis, microwave irradiation, etc. [10]. Recently, solid-state reactions have been used mainly in industry for mass production of $BaMgAl_{10}O_{17}$ phosphors [11]. In spite of these advantages, the method has a number of disadvantages, which include high annealing temperatures (about 1400–1500 °C), a long period of time, and low chemical stability. As for BAM, there are many studies in the literature on BAM samples doped with various rare earth elements: BAM:Mn^{2+} solution combustion [12], BAM:Eu^{2+} spray pyrolysis [13], BAM:Eu^{2+} sol-gel [14], BAM:Eu^{2+} precipitation [15], BAM:Eu^{2+} microwave-assisted combustion synthesis [16]. As can be seen from the literature examples above, although the host material and rare earth element additives are the same, different chemical production techniques lead to different results. However, there are studies with different rare earth elements in the literature: Gd doped BAM (combustion method) [17], Mn doped BAM (Solid state reaction) [18] and Mn and K doped BAM (Solid state reaction) [19]. Based on the literature survey, it is seen that rare earth element additions to BAM samples were investigated only by photoluminescence. To do our best knowledge, there have been no studies on electron beam excited BAM samples (cathodoluminescence).

In this work, the wet combustion method to produce the BAM phosphors doped with Ce and Tb were employed here. Crystal structure, morphology and CL characteristics at room temperature of Ce doped BAM samples have been investigated in detail.

2. Materials and Methods

2.1. Material synthesis

By using a gel combustion method, nanocrystalline $BaMgAl_{10}O_{17}$ materials were prepared with Tb and Ce doping. A starting material for this process was high purity Barium nitrate, Magnesium nitrate, Magnesium nitrate ($Mg(NO_3)_2.6H_2O$), Aluminum nitrate, and Tb_2O_3,, $Ce(NO_3)_3.6H_2O$, and NH_2CONH_2. Fuel/oxidant (f/o) ratios of all materials (1.00; 2.36; 5.00; 6.00; 7.00; and 8.00) were used for weighting. In a quartz beaker containing 20 ml distilled water, the nitrates are dissolved and stirred for an hour at 80 °C. Once the gel has been formed, in order to evaporate the excess water, the beaker is stirred and left at the same temperature without being covered. The ash put into the oven, which was preheated at 550°C is used to keep the gel-like solution for 20 minutes. The combustion reaction takes place

nanocrystalline $BaMgAl_{10}O_{17}$ host material in the form of fly ash once the water in the solution evaporates. The reaction mixture was naturally cooled down to RT after annealing at 1100 °C for 2 h i to enhance purity of crystalline BAM phosphors by removing organic residues.

2.2 Characterization

For room temperature XRD analysis, a Philips PW-1710/00 diffractometer using CuKα radiation (λ =1.5418 Å) over an angle range of 10°-60° with a step size of 0.001° was used. COD and PDF2 databases have been employed for data processing phase identification along with EVA and TOPAS software. The CL spectra were recorded using a Gatan Mono CL3 detector coupled to a FEI Company ESEM Inspect providing electrons at Low Vacuum for Energy Dispersive Spectroscopy (EDS) at 25 kV.

3. Results and discussions

3.1. X-ray diffraction analysis

An X-ray powder diffraction (XRD) experiment was conducted on powder samples of BaMgAl10O17 without doping and with Ce^{3+} and Tb^{3+} incorporated. The discrepancies found in previous studies should be highlighted before evaluating the XRD data obtained. Synthesis of BaMgAl10O17 phosphors was carried out by combustion reaction. Based on propellant chemistry, the combustion reaction stoichiometry is determined. Typically, elements such as H, Ba, Mg, Al in the host material are taking into consideration to be reducing elements, with valences of +1, +2, +2 (the ion's valence in the compound) and +3. When oxygen is added to combustion, it acts as an oxidant whose value is 2.. Utilizing total oxidation (o) and reduction (f), calculated are metal nitrates molar ratios and urea, as well as the values of each element that makes up the compounds (apart from nitrogen). [20]. It is believed by some researchers that the oxidizer-to-fuel ratio of 1: 1 is required for redox combustion to take place with the greatest combustion temperature and a combustion reaction to occur. [21]. Unfortunately, such XRD examination of BAM powder samples have resulted in data misinterpretation by some parties in some situations. First, numerous articles have presented differing fuel/oxidant (f/o) ratios such as 2.36:1, 7:1 [22-25]. As can be seen from Figure 1, the XRD diffraction peaks of pure, and Ce and Tb activated samples match with JCPDS card No 26-0163, indicating single-phase crystalline nature. Apparently, another phase of crystallization does not exist. Incorporating Tb^{3+} and Ce^{3+} ions does not result in significant structural changes due to the modest volume of dopant present.

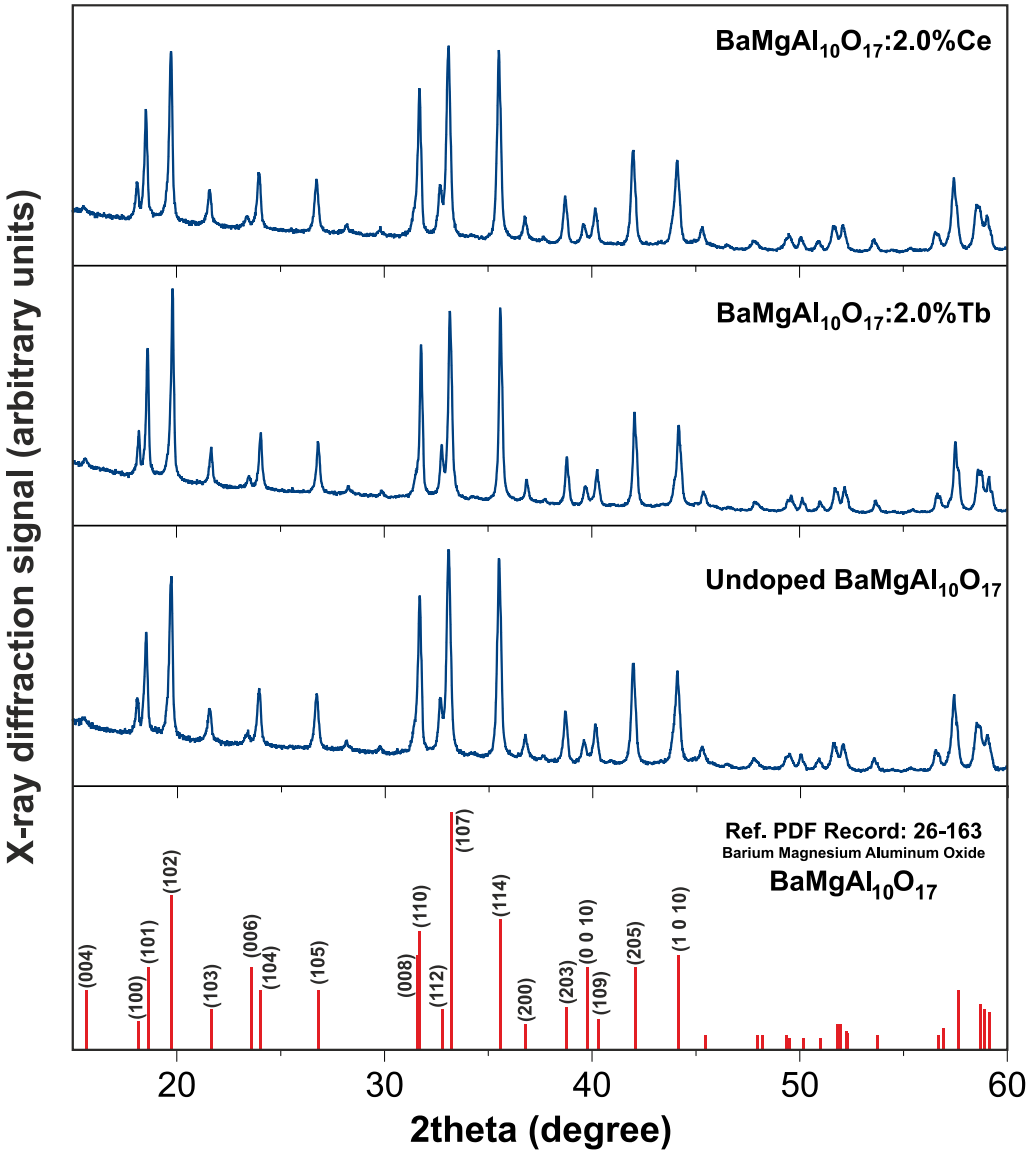

Figure 1 Measured XRD data of undoped BAM, BAM:Ce, and BAM:Tb samples

3.2 Morphological and elemental study

With Scanning Electron Microscopy and Energy Dispersive X-Ray Analysis, we study surface morphology and elemental compositions of undoped, Ce and Tb doped BAM. It is evident from Figure 2a that BAM bulk phosphor has an irregular stone structure, whereas Figures 2 b-c show a crystallite with sharp edges and grains, while the particles are made of strongly agglomerated crystallites and have a sharp, hard stone mass structural morphology.

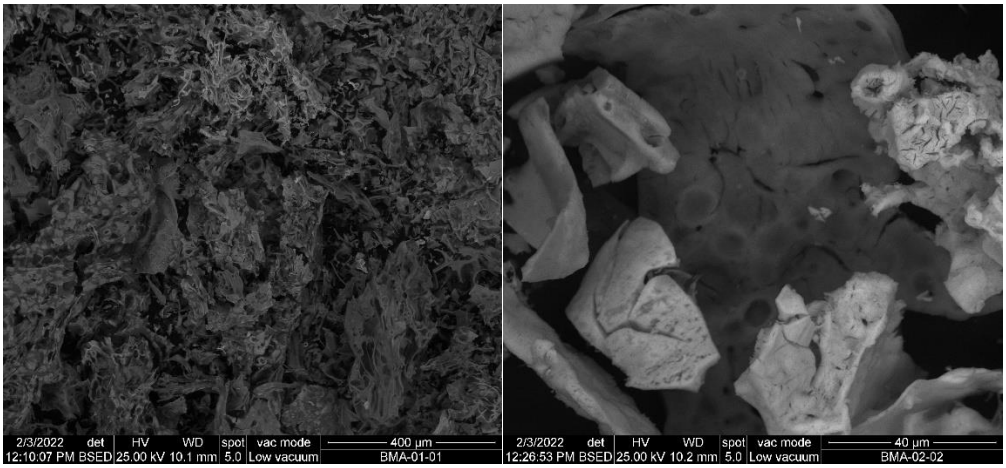

(a) (b)

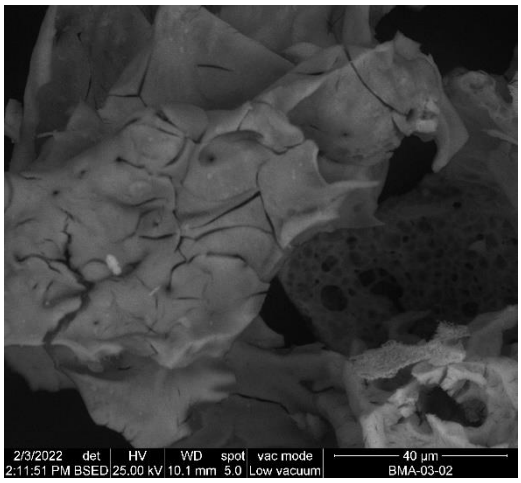

(c)

Figure 2 ESEM images of undoped, Ce and Tb doped BAM samples

EDS spectrums illustrating the elemental composition of undoped and Ce and Tb doped BAM are shown in Figure 3. All the necessary elements were present in the final BAM nanophosphors and contributed to chemical reactions. In Table 1, each element's weight and atom percentage are listed. This table illustrates the presence of all constituent elements of nanophosphors. A high level of agglomeration results in particles with foam-like morphologies [17].

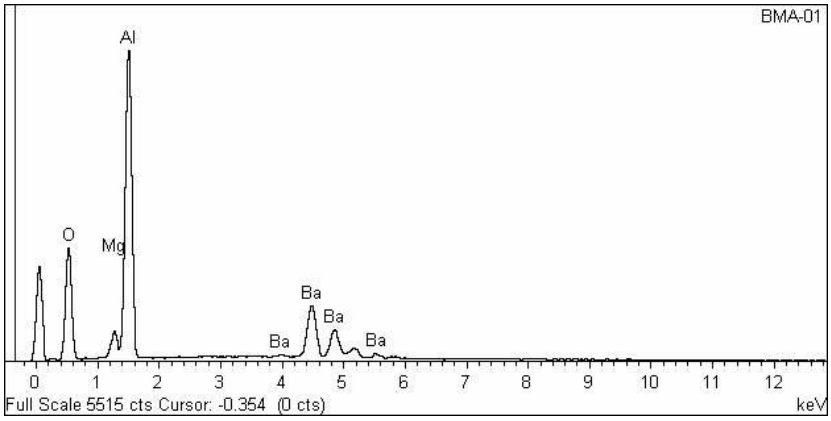

(a)

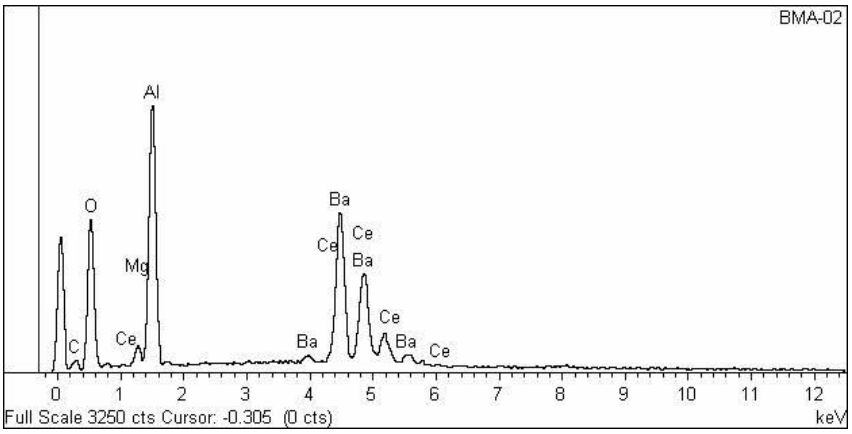

(b)

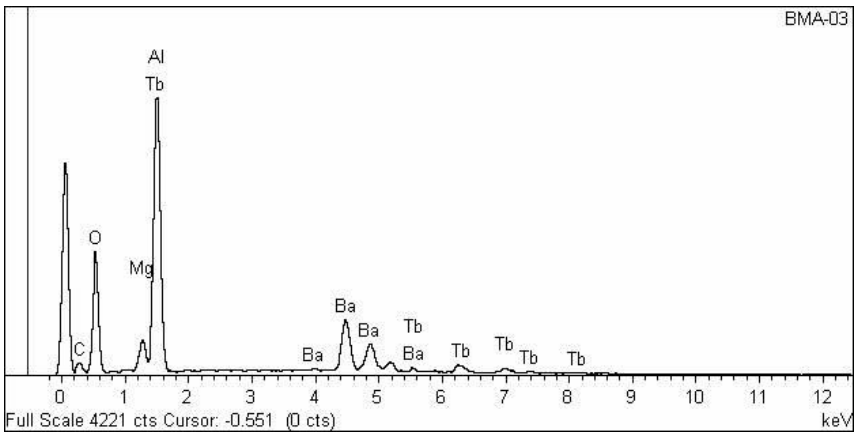

(c)

Figure 3 EDS spectrum of undoped, Ce and Tb doped BAM samples

Table 1 Elemental compositions of undoped, Ce and Tb doped BAM samples based on EDS data

Undoped BAM sample

Element	App Conc.	Intensity Corrn.	Weight%	Weight% Sigma	Atomic%
O K	83.06	1.0434	39.14	0.46	59.77
Mg K	3.99	0.5507	3.56	0.18	3.58
Al K	44.11	0.5963	36.37	0.37	32.93
Ba L	37.08	0.8715	20.92	0.36	3.72
Totals			100.00		

Ce doped BAM sample

Element	App Conc.	Intensity Corrn.	Weight%	Weight% Sigma	Atomic%
C K	5.42	0.4186	6.57	0.92	14.72
O K	63.60	1.0084	31.98	0.62	53.81
Mg K	1.82	0.4450	2.07	0.18	2.30
Al K	21.47	0.4971	21.90	0.40	21.84
Ba L	60.37	0.9045	33.84	0.58	6.63
Ce L	6.67	0.9280	3.64	0.46	0.70
Totals			100.00		

Tb doped BAM sample

Element	App Conc.	Intensity Corrn.	Weight%	Weight% Sigma	Atomic%
C K	9.80	0.3565	10.98	1.21	19.66
O K	86.63	0.8647	40.07	0.77	53.84
Mg K	4.36	0.5694	3.06	0.32	2.71
Al K	38.15	0.5845	26.09	0.50	20.78
Ba L	34.51	0.8684	15.89	0.41	2.49
Tb L	8.07	0.8266	3.90	0.31	0.53
Totals			100.00		

3.3 Cathodoluminescence (CL) analysis

Figure 4 shows CL spectrum of Ce incorporated BAM samples. Natural mineral borates contain a great deal of molecular water and hydroxyl group (OH), as seen in the formulas of many mineral contents present in nature. Note that hydroxyl group strongly attracts water molecules and hydrogen bonds are formed. During exfoliation, calcite crystals are chemisorbed with OH- and H+ because OH- fills the empty O sites at the Ca's octahedral sites [26]. Based on the microphysical explanation of the CL 380 nm broad band in BAM , several items are taken into account: (i) there is a small shoulder around 450 nm which occurs in many other compounds; (ii) materials such as BAM, which are nominally anhydrous are related to molecular water and OH group including Ba, Al, and O groups; (iii) By chemisorbing oxygen-deficient centers (ODCs), oxygen dangling bonds or nonbridging oxygen hole centers (NBOHC) and defects at grain boundaries and cracks, YAB surfaces capture oxygen deficiency defects. The grain boundary and cracks contain a large number of defects. There has been evidence that hydroxyl groups contribute to defect formation. The broad CL band of BAM located at 380 nm with a shoulder at 420 nm following synthesis and thermal quenching in environmental conditions. As a result of the chemisorption of hydroxyl precursors of potential oxygen-deficient centers (ODCs) and nonbridging oxygen hole centers (NBOHCs), BAM surfaces show hydrous precursors that are linked to the main structure, while cracks and grain boundaries tend to have the most defect.

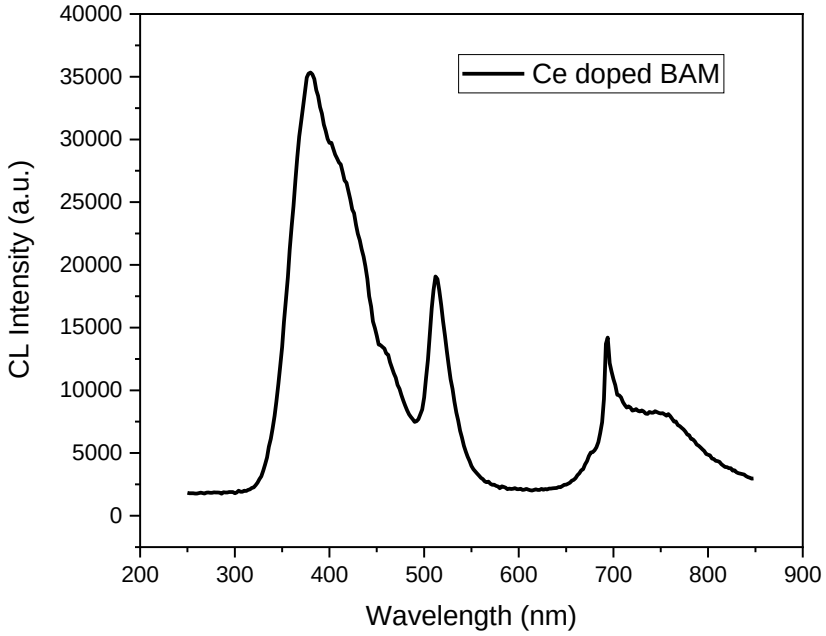

Figure 4 CL spectrum of Ce doped BAM sample under electron beam excitation

From the data in Figure 4, it is worth noting that the CL data displays a red sharp peak located at 694 nm along with a broad band. Although the cause of CL emission is still unclear and up for debate, the wide range of emission properties point to transitions of trivalent rare earth ions with permitted parity, transition metal ions, or defect centers. Precursors may also contain unintentional impurities (used Mg_2SiO_4 has Mn content of 5 mg/kg). Knowing the source of the emission due to imperfections in the visible region is important. The morphology of the host material, the varieties of defects present, and ultimately the luminescence spectra have all been attributed to various of synthesis techniques. Therefore, various defects are to hold responsible for the variations in visible emissions. For instance, in research published by Gong et al. (2007), they claimed that red emissions occurring in the range of 620–780 nm were caused by either oxygen interstitials or oxygen vacancies [27]. These outcomes undoubtedly support our conclusions.

As can be seen from the graph in Figure 4, emission peaks caused by the Ce contribution can be seen as well as the signals given by the host structure. When we look at the literature, there is almost no publication on Ce-doped BAM phosphor samples, more studies have focused on photoluminescence. More recently, S. Tigga et al (2016) demonstrated that the transition of Ce^{3+} ions from their excited 5d state to their 4f ground state caused Ce doped BAM to exhibit one broad peak centred at 440 nm [28]. Our results contradict the earlier research that was described aforementioned. Contrary to what was earlier seen, we detect a peak of Ce-activated BAM phosphor at 520 nm, ranging from the excited $5d_1$ to the two-spin-orbit split of $4f_1$ into $^2F_{7/2}$ and $^2F_{5/2}$. The crystalline environment has a significant impact on where the 5d level is located. However, this outcome is consistent with previous findings by J. Xu et al. (2019) and U.H. Kaynar et al (2020) [29-30]. It's possible that the Mg-induced Ce^{3+}-Ce^{4+} conversion is what's causing the variation in the emission band between experiments.

Figure 5 shows the CL emission characteristic of BAM samples activated with Tb ions excited by electron beams. Tb emission predominates in the CL signals. Figure 5 illustrates the spectrum, which included four primary emission peaks at wavelengths of 488 nm, 542 nm, 587 nm, and 624 nm, respectively, assigned to the $^5D_4 \rightarrow {}^7F_6$ (blue), $^5D_4 \rightarrow {}^7F_5$ (green), $^5D_4 \rightarrow {}^7F_4$ and $^5D_4 \rightarrow {}^7F_2$ transitions of Tb^{3+}. 5s and 5p shells that are filled effectively act as a barrier for the 4f electrons, preventing them from being significantly impacted by the surrounding chemistry. This shielding effect produces strong emission lines in the CL spectra. Additionally, it is suggested that many *f-f* transitions are spin prohibited, making them partly forbidden. Contrary to many transition metal ions that lack any outside orbitals of shielding, the majority of rare earth ions' energy level configurations are independent of the structure of the host matrix . [31]. The ground state is transformed into the 5d excited

state once Tb^{3+} ions absorb the excitation energy. Tb^{3+} ions then transition to the $^5D_4$ state. Two potential processes are possible that could populate the $^5D_4$ state: (a) a nonradiative multiphonon relaxation from the Tb^{3+} emissions at the 5d levels, and (b) a cross relaxation coming from transitions between Tb^{3+} ions at the $^5D_3$-$^5D_4$ and $^7F_6$-$^7F_0$ levels. The $^5D_4 \rightarrow {}^7F_5$ transition (green) at 542 nm is shown in Figure 5 to be dominant over the others. Under UV light stimulation, BAM phosphor doped with Tb^{3+} ions can produce green light and may be used with green-emitting display materials [32].

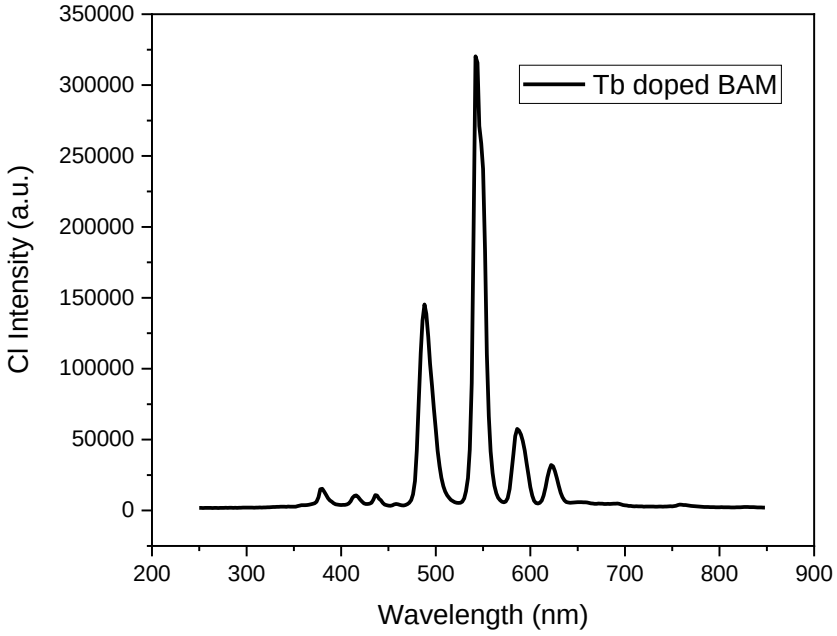

Figure 5 CL emission spectrum of Tb doped BAM phosphor under the electrom beam excitation.

4. Conclusions

In conclusion, wet combustion was used to create BAM phosphors that were doped with Ce and Tb ions, and XRD patterns were examined. According to XRD studies, Ce and Tb ions have been integrated into BAM and are mostly present as trivalent Ce and Tb. Potentially, the hydroxyl substance that BAM surfaces chemisorb may have a negligible impact on the effectiveness of the BAM luminescence. It has been determined which CL peaks correspond to the Ce^{3+} (4f–5d) transitions in the BAM:Ce phosphors. BAM phosphors incorporated with TB ions displayed good PL characteristics and a rich green hue with a peak at 542 nm as a consequence of the 4f-4f transition of Tb^{3+} ions.

References

[1]S. Zhang, Y. Hou, H. Fujii, T. Onishi, M. K okubu, M. Obata, H. Tanno, T. Kono, H. Uchii ke,Effect of nonstoichiometry on the

deterioration of Eu^{2+}-doped hexagonal aluminate phosphor for plasma display applications, J. Appl. Phys., 42 (2003) 477

[2]B. Howe, A.L. Diaz, Characterization of host-lattice emission and energy transfer in $BaMgAl_{10}O_{17}:Eu^{2+}$, J. Lumin., 109 (2004) 51-59

[3]L. Fu, Z. M. Liu, Y. Q. Liu, B. X. Han, J. Q. Wang, P. Hu, L. C. Cao, D.B. Zhu, Coating Carbon Nanotubes with Rare Earth Oxide Multiwalled Nanotubes, Adv. Mater., 16 (2004), 350-352

[4]F. Wang, W.B. Tan, Y. Zhang, X. Fan, M. Wang, Synthesis of polyethylenimine/$NaYF_4$ nanoparticiles with upconversion fluorescence, Nanotechnology, 17 (2006) 5786

[5] B.G. Wybourne, Spectroscopic Properties of Rare Earths, John Wiley & Sons. Inc., New York, 1965.

[6] B.G. Wybourne, in:B. Di Bartolo, O. Forte (Eds.), Advances in Spectroscopy for Lasers and Sensing, John Wiley & Sons. Inc., New York, 1965, pp. 403–433.

[7] Toquin R L, Cheetham A K, Red-emitting cerium-based phosphor materials for solid-state lighting applications, Original. Chem. Phys. Lett., 423 (2006) 352-356

[8 Li L, Liang H B, Tian Z F, Lin H H, Su Q, Zhanog G B, Luminescence of Ce^{3+} in different lattice sites of $La_2CaB_{10}O_{19}$. J. Phys. Chem. C, 112 (2008)13763.

[9] Lin H H, Liang H B, Han B, Zhong J P, Su Q, Dorenbos P, Birowosuto M D, Zhang G B, Fu Y B, Wu W Q. Luminescence and site occupancy of Ce^{3+} in $Ba_2Ca(BO_3)_2$. Phys. Rev. B, 2007, 76: 035117

[10] S. Ekambaram, K. Pati, Synthesis and properties of Eu activated blue phosphors, J. Alloys Compd., 248 (1997) 7-12

[11] S. Lee, H. Kim, S. Byeon, J. Park, D. Kim, Thermal-Shock-Assisted Solid-State Process for the Production of $BaMgAl_{10}O_{17}$:Eu Phosphor, Ind. Eng. Chem. Res., 44 (2005) 4300-4303

[12]M. Kumar, P. Rajbut, P.K. Singh, A.C. Yadav, S.L. Pradhan, V. Baranwal, U.B. Singh, S.N. Jha, F. Singh, Luminescence properties of $BaMgAl_{10}O_{17}:Mn^{2+}$ nanophosphors, J. Alloy. Comp., 799 (2019) 556-562

[13] Y. Zhou, J. Lin, Morphology control and luminescence properties of $BaMgAl_{10}O_{17}:Eu^{2+}$ phosphors prepared by spray pyrolysis. J. Solid State Chem., 178 (2005) 441-447

[14] C.H. Lu, C.T. Chen, B. Bhattachariee, Sol-gel preparation and luminescence properties of $BaMgAl_{10}O_{17}:Eu^{2+}$ phosphors, J. Rare Earths, 24 (2006)706-711

[15] Z. Wu, Y. Dong, J. Jiang, Synthesis of $BaMgAl_{10}O_{17}:Eu^{2+}$ particles with small grain size and regular morphology, J. Alloy. Comp., 467 (2009) 605-610.

[16]N. Pradal, A. Potdevin, G. Chadeyron, P. Bonville, B. Caillier, R. Mahiou,$BaMgAl_{10}O_{17}:Eu^{2+}$ blue phosphors for solid-state lighting, Opt. Mater., 64 (2017) 334-344

[17]

V. Singh, N. Singh, M.S. Pathak, S. Watanabe, T.K.G. Rao, N.A. Jadhav, Y.W. Kwon

PL and ESR study on UVB-emitting Gadolinium-doped $BaMgAl_{10}O_{17}$ hexagonal phase obtained by combustion synthesis, J. Electron. Mater., 47 (2018) 7365-7371

[18]
Y. Xu, L. Wang, B. Qu, D. Li, J. Lu, R. Zhou, The role of co-dopants on the luminescent properties of α-Al_2O_3:Mn^{4+} and $BaMgAl_{10}O_{17}$:Mn^{4+}, J. Am. Ceram. Soc., 102 (2019) 2737-2744
[19]
R.P. Cao, Y.J. Ye, Q.Y. Peng, S.L. Guo, Z.F. Hu, W. Hu, H. Ao, X.G. Yu, Luminescence Properties And Charge Compensation of $BaMgAl_{10}O_{17}$:Mn^{+4}, K^+ Red-Emitting Phosphor, 12 (2018)71-75.
[20] S. Ekambaram, K.C. Patil, M. Maaza, Synthesis of lamp phosphors: facile combustion approach, J. Alloy. Comp., 393 (2005), 81-92.
[21] S. Ekambaram, M. Maaza, Combustion synthesis and luminescent properties of Eu^{3+}-activated cheap red phosphors, J. Alloy. Comp., 395 (2005)132-134.
[22] Suninder Jeet, O.P. Pandey, Template free synthesis route to monophasic $BaMgAl_{10}O_{17}$:Eu^{2+} with high luminescence efficiency, J. Alloy. Comp., 750 (2018) 85-91.
[23] Manh Son Nguyen, Van Tuyen Ho, Nguyen Thuy Trang Pham, The synthesis of $BaMgAl_{10}O_{17}$:Eu^{2+} nanopowder by a combustion method and its luminescent properties, Adv. Nat. Sci. Nanosci. Nanotechnol., 2 (2011) 045005-045008
[24] Z. Chang-Wei, D. Yan-Hua, Z. Na, Z. Jian-Yong, F. Yong-Zheng, Z. Cheng, Eu^{2+}, Mn^{2+}, Sr^{2+} tri-doped $BaMgAl_{10}O_{17}$ phosphor: solution combustion synthesis and photoluminescence properties, J. Inorg. Chem., 32 (2016) 2075-2081
[25]Z. Chena, Y.W. Yan, J.M. Liu, Yi Yin, Hongmin Wen, Gaohua Liao, Chunlan Wu, Jiang qian Zao, Dehui Liu, Hongmin Tian, Chenshu Zhang, Shuidi Li, Microstructure and luminescence of surface-coated nano-$BaMgAl_{10}O_{17}$:Eu^{2+} blue phosphor, J. Alloy. Comp., 478 (2009) 679-683.
[26] SI Kuriyavar, R.Vetrivel, S.G. Hegde, A.V. Ramaswamy, D. Chakrabarty and S. Mahapatra Insights into the formation of hydroxyl ions in calcium carbonate: temperature dependent FTIR and molecular modelling studies. Journal of Materials Chemistry. 10, 2000, 1835–1840.
[27]
Y. Gong, T. Andelman, G.F. Neumark, S. O'Brien, I.L. Kuskovsky, Origin of defect-related green emission from ZnO nanoparticles: effect of surface modification, Nanoscale Res. Lett., 2 (2007) 297-302.[28]
S. Tigga, N. Brahme, D.P. Bisen, Investigations on luminescence behaviour of Ce-activated $BaMgAl_{10}O_{17}$ phosphorLuminescence, 31 (2016)1306-1312.
[29]J. Xu, A. Thorseth, C. Xu, A. Krasnoshchoka, M. Rosendal, C.D. Hansen, B. Du, Y. Gong, O.B. Jensen, Investigations of laser-induced luminescence saturation in a single-crystal YAG:Ce phosphor: towards unique architecture, high saturation threshold, and high-brighness laser-driven white lighting, J. Lumin., 212 (2019) 279-285
[30] U.H. Kaynar, S. Cam Kaynar, M. Ayvacikli, Y. Karabulut, G.O. Souadi, N. Can, Influence of laser excitation power on temperature-dependent luminescence behaviour of Ce- and Tb-incorporated

[32]R. Naik, S.C. Prashantha, H. Nagabhushana, H.P. Nagaswarupa, K.S. Anantharaju, S.C.Sharma, B.M. Nagabhushana, H.B. Premkumar, K.M. Girish,$Mg_2SiO_4:Tb^{3+}$ nanophosphor: auto ignition route and near UV excited photoluminescence properties for WLEDs, J. Alloy. Comp., 617 (2014) 69-75.

$BaMgAl_{10}O_{17}$ phosphors, Radiation Physics and Chemistry, 168, 2020, 108617.

[31] Y. Zhang, J. Hao, Metal ion doped luminescence thin films for opto electronic applications, J. Mater. Chem. C, 1 (2013) 5607-5618.

تحضير وخصائص التلألأ المهبطي للمعادن الأرضية النادرة والمدمجة مع فوسفور الومينات الباريوم والماغنسيوم $BaMgAl_{10}O_{17}$(BAM)

الملخص

في الدراسة الحالية، تم استخدام طريقة الحرق الرطب لتحضير ألومينات الباريوم والمغنسيوم والمطعم بنسبة ٢ % من أيونات السيريوم والتربيوم .تم توصيف التركيب البلورى والنسب التركيبية للعناصر وكذلك الخواص البصرية للمادة المحضرة باستخدام تقنيات مشتت الطاقة الطيفي والمجهر الإلكتروني وحيود الأشعة السينية. كما تم قياس التلألأ المهبطي عن طريق تقنية الإثارة بالحزمة الإلكترونية. دلت النتائج على حصول الانتقال الإلكترونى من $^5D_4$ الى ^7F_J داخل أيونات التربيوم الثلاثي نتيجة لانبعاث الطيف الأخضر عند طول موجي ٥٤٢ نانومتر. كما تم الحصول علي الطيف ألأخضر الفسفوري للعينة المحضرة عند طول موجي ٥٢٠ نانومتروالذي يعزي إلي الانتقال الإكتروني بين المدارين 4f و 5d لأيونات السيريوم. طبقاً للنتائج التي تم الحصول عليها في هذا البحث فإن عملية تطعيم مادة أليومينات الباريوم والماغنسيوم بأيونات التربيوم والسيريوم من الممكن أن يؤدي إلي الحصول علي مادة لها العديد من التطبيقات كأحد المواد ذات الوهج الفوسفوري المستمر.

In Vitro Assessment of Antioxidant, Anti-Inflammatory and Cytotoxicity Activities of *Cylindropuntia rosea* Methanol Extract

Abdullah A. A. Alghamdi

Department of Biology, Faculty of Science, Al-Baha University, Saudi Arabia

Abstract

The present work focuses on investigating the effect of the methanol extract of the aerial parts of *Cylindropuntia rosea* on cytotoxicity, anti-inflammatory and antioxidant activities. The methanol extract showed the scavenging of DPPH, H_2O_2 and ferric ion reducing antioxidant power with IC_{50} = 200.47 µg/mL, 243.28 µg/mL and 397.3 µg/mL, respectively; whereas it inhibited inflammatory markers, COX-1 enzyme with IC_{50} = 12.52µg/mL and protein denaturation with IC_{50} = 9.64 µg/mL significantly, compared to standard drugs Indomethacin and Diclofenac. The cytotoxicity results demonstrated that the extract showed potent toxicity on MCF-7, A2780, HepG2, TK10, HT29, HCT-116 and PC3 cancer cells with IC_{50} in the range of 5.16- 49.21 µg/mL, compared to Doxorubicin. Furthermore, the extract was found to be more sensitive to MCF-7 cells and it inhibited colony proliferation as observed in the clonogenicity experimentation. To support the biological activity results, HPLC was performed, which showed the presence of bioactive constituents like gallic acid, cinnamic acid, ellagic acid, caffeic acid, syringic acid and salicylic acid. In conclusion, the methanol extract of the aerial parts of *C. rosea* exhibited cytotoxic, anti-inflammatory, and antioxidant properties; therefore, it could be utilized for the isolation of potent molecules for the synthesis of novel drugs.

Keywords: *Cylindropuntia rosea*, cytotoxicity, anti-inflammatory, antioxidant

INTRODUCTION

Reactive oxygen species (ROS) occur in balance with the biological system in aerobic cells. However, disruption of this balance due to excess of ROS cause oxidative stress.[1] It is widely accepted that oxidative stress is a major factor in the development of many diseases, such as cancer, chronic inflammation, diabetes and atherosclerosis.[2 ,3] As ROS facilitate tumor development and progression, they are considered as potential carcinogens.[4] Besides this, ROS modulates inflammatory cytokines, such as interlukins, NF-kB, COX, TNF-α and iNOS; therefore, they play a central role in the development of inflammatory disorders.[5] Since oxidants are responsible for the progression of inflammatory diseases and cancer, treatments involving antioxidant from natural sources are efficacious due to lesser side effects and ease of availability.

Natural products from plants or plant extracts have been historically used in traditional medicine due to the presence of pharmacologically active phytoconstituents, such as flavonoids, phenolics, tannins, and terpenoids. *Cylindropuntia rosea (C. rosea*) [synonyms: *Cactus subquadriflorus*,

Cylindropuntia pallida (Rose), *Grusonia rosea* (DC.), *Opuntia rosea* DC, *Cylindropuntia rosea* var. atrorosea, and *Opuntia pallida*] is a species of the Cactaceae family, commonly named as Hudson pear. *C. rosea* is a native Mexican cactus with dense spines. The plant was recognized to naturalize in Peru and invade Zimbabwe, South Africa, Namibia, Australia and France.[6] In Mexico, this species is distributed in three states: Tlaxcala, Puebla, and Hidalgo,[7] forming dense stands.[8] It is also known to grow in Spain, Australia and South Africa as an ornamental plant, as well as used in Namibia and Botswana as a barrier plant. In Asia, this species was first reported in Baljurashi province, which is geographically located in Al Baha region, in the southern portion of Saudi Arabia between 19/20 latitude and 41/42 longitude, and at an altitude of 2,034 meter above sea level.[9-10] Humans, vehicle tires, and animals are all capable of spreading this plant easily,[11] allowing it to invade the grazing area in the Al Baha region, and may cause the injury or death of the livestock. [9] The plant flowers are consumed by rural community in the form of different types of traditional dishes and consumed as fodder by animals.[12] Recently, the flowers of *C. rosea* has been shown to exhibit potent antioxidant property and different compounds belonging to flavonoids, anthocyanins, and phenolic acids have been observed in flower ethanolic extracts. [13] The information on this plant is scanty and needs exploration of its biological activities and phytoconstituents. This study investigated the antioxidant, anti-inflammatory and anticancer activities of the aerial parts of *C. rosea*. Hitherto there has been no report on the assessment of aforementioned biological activities of this plant, and this is the first report from Al Baha region of Saudi Arabia.

METHODS

Chemicals

Bovine serum albumin (BSA), Folin reagent, sodium Diclofenac, dimethyl sulfoxide (DMSO) and trypan blue dye were purchased from Sigma-Aldrich (St. Louis, MO, USA). 0.25% Trypsin-EDTA, HEPES buffer solution, DMEM, gentamycin, L-glutamine and Fetal Bovine serum were obtained from Lonza (Belgium).

Extraction

C. rosea aerial parts were collected from Baljurashi province, Al Baha, Saudi Arabia, and identified by Dr. Haider Abd Algadir, taxonomist, Department of Biology, AlBaha University, Saudi Arabia. The collected plant was cut into small slices (1-2 mm), shade dried, and then powdered using a mechanical grinder. The dried materials were macerated in methanol (80% V/V) at room temperature for seven days, and then filtered. The obtained crude extract was then allowed to a complete dryness. The crude extract was finally kept at 4 ^{o}C until needed.

Phytochemical analysis

The determination of total phenolic content(TPC)was determined using Folin-Ciocalteu colorimetry assay,[14] while the total flavonoid content (TFC) was measured by Nurcholis*et al* [15] method, the total tannins content (TTC) was determined by Rebaya et al,[16] and the total alkaloids (TAC) was determined using the method of Ates*et al*.[17]

Antioxidant activity

The antioxidant activity of the extract was performed at the Regional Centre for Mycology and Biotechnology (RCMB) at Al-Azhar University by 2,2-diphenyl-1-picrylhydrazyl radical

scavenging (DPPH),[18] hydrogen peroxide scavenging (H_2O_2),[19] ferric reducing antioxidant power (FRAP)[20], and total antioxidant capacity (TAC)[21] assays.

Anti-inflammatory activity

Two methods were employed, an albumin denaturation assay was carried out according to Williams *et al*[22] with Diclofenac sodium as a reference drug and COX-1 inhibition assay was performed using a COX-1 inhibitor screening assay kit (Catalog number k548, Biovision, USA) as instructed by the manufacturer.

Anticancer activity

Cytotoxicity and selectivity index

The anticancer activity was evaluated on seven cancer cell lines (breast MCF-7, ovarian A2780, liver HepG2, kidney TK10, colon HT29, colon HCT-116 and prostate PC3) and one normal fibroblast cells (lung MRC-5), which were obtained from the American Type Culture Collection (ATCC). At 37 °C, 100% relative humidity and 5% CO_2, cancer cells were sub-cultured in RPMI-1640 media (10% FBS), while the MRC5 normal fibroblasts were grown in Eagles minimum essential medium (EMEM) and 10% FBS. It was performed according to the previously published method by Almalki *et al*[23] using Doxorubicin as a positive reference drug. GraphPad Prism (San Diego, CA, USA) was used to determine the extract concentrations causing 50% inhibition (IC_{50}) compared to control cell growth (100%); while by dividing IC_{50} of the extract against MRC-5 cells/IC_{50} against each of the other cells, the selectivity index (SI) for the extract was calculated.

Clonogenic survival assay

According to a previous report,[24] the clonogenic survival assay was used to determine the ability of individual cancer cells to form colonies. A low density (5×10^2) of MCF7 cells was seeded in duplicate in 6-well plates with 2 mL media, and then the cells were allowed to attach by incubating the plates overnight at 37 °C. This was followed by treating the cells with vehicle control and the ME (5, 10 and 20µg/mL). 72h later, the old medium of each concentration was replaced with 2 fresh medium. 14 days later, colonies of 50 cells or more were considered. After washing the cells twice with cold phosphate buffered saline (PBS), the cells were then fixed at room temperature for 5 min. This was followed by staining the cells with 0.5% *v/v* methylene blue in methanol: H_2O (1:1 *v/v*) for 15 min. After washing the colonies, the plates were left to dry, before starting to count the colonies.

HPLC analysis

HPLC-(Agilent 1100) was performed using the method described by Lin *et al*.[25] The instrument composed of a two LC- pumps, a UV/Vis detector and C18 column (125 mm × 4.60 mm, 5 µm particle size). Chromatograms were obtained and analyzed using the Agilent ChemStation. Phenol acids were separated by employing a mobile phase of two solvents, 0.1% methanol: phosphoric acid (50: 50 *v/v*, isocratic mode). The flow rate was adjusted to 1.0 mL/min; the detector was set at 280 nm with the mobile phase.

RESULTS

Phytochemical Analysis

The total flavonoid (TFC), total phenolic (TPC), total tannin (TTC) and total alkaloid contents (TAC) of the methanolic extract (ME) of *C.rosea* are shown in Table 1. It was observed that TPC was 59.41 ± 3.17 mg/gm, while TFC, TTC and TAC were 8.23 ± 0.75,

3.19 ± 0.33 and 4.74 ± 0.52 mg/gm, respectively. The ME was found to be rich in polyphenols than flavonoids, tannins and alkaloids. This was further supported by the HPLC analysis which showed the presence of important polyphenols in ME.

Table 1. Phytochemical analysis of methanol extract of *C. rosea*

Extract	TPC (mg/gm)	TFC (mg/gm)	TTC	TAC
Methanolic	59.41 ± 3.17	8.23 ± 0.75	3.19 ± 0.33	4.74 ± 0.52

TPC was expressed as mg gallic acid equivalents (GAE)/g extract; TFC as mg quercetin equivalents (QE) /g extract; TTC in mg tannic acid equivalent/g dry weight; TAC in mg caffeine equivalent/g dry weight; the analysis was performed in triplicate ± SD.

Polyphenolic profile by HPLC

The ME of *C. rosea* was analyzed by HPLC, which showed the presence of important polyphenols (Figure 1). The major compounds were caffeic acid (10.55 µg/mg) at retention time of 8 mins followed by ellagic acid (7.59 µg/mg) at RT 12.9 min, syringic acid (5.22 µg/mg) at RT 5.1 mins, whereas salicylic acid was found to be in lowest concentration (0.88 µg/mg) at RT 12 min. Other phytoconstituents, such as cinnamic acid and gallic acid, were identified as minor compounds. This result supported the highest concentration of TPC than TFC, TTC and TAC (Table 2, Figure 1).

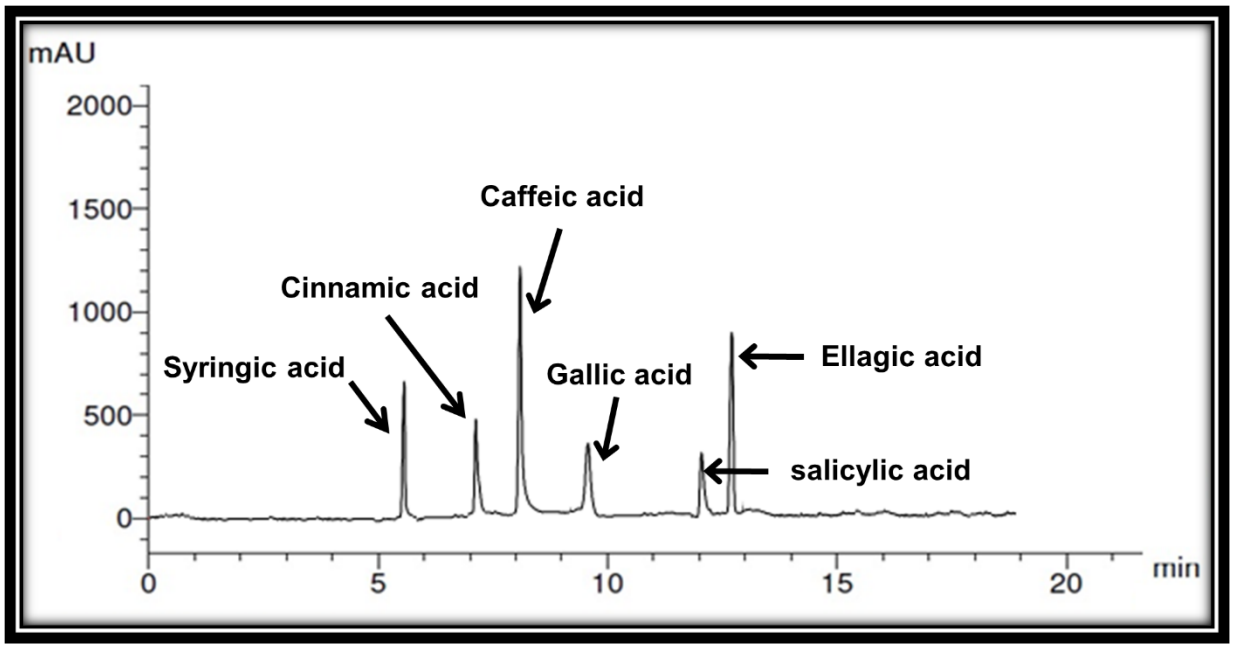

Figure 1. HPLC chromatogram of methanol extract of *C. rosea*

Table 2. Chemical compounds from *C.rosea* methanolic extract

S. No	Compound name	Molecular formula	RT	Conc. (µg/mg)
2	Syringic acid	$C_9H_{10}O_5$	5.1	5.22
3	Cinnamic acid	$C_9H_8O_2$	7.0	2.14
4	Caffeic acid	$C_9H_8O_9$	8.0	10.55
5	Gallic acid	$C_7H_6O_5$	9.7	1.46
6	Salicylic acid	$C_7H_6O_3$	12.0	0.88
7	Ellagic acid	$C_{14}H_6O_8$	12.9	7.59

Antioxidant activity

Phenolics rich extracts are known for hampering oxidative stress. Therefore, the ME of *C. rosea* is evaluated for antioxidant activity by 2,2-diphenyl-1-picrylhydrazyl radical scavenging activity (DPPH), hydrogen peroxide scavenging activity (H_2O_2), ferric reducing antioxidant power (FRAP), and total antioxidant capacity (TAC). The results are presented in Table 3 and Figure 2.

Table 3. Antioxidant activity of the methanol extract of *C. rosea*

Sample	IC_{50} (µg/mL)			TAC (mgGAE/g)
	DPPH (µg/ mL)	H_2O_2 (µg/ mL)	FRAP (µg/ mL)	
C. rosea extract	200.47 ± 5.19	243.28 ± 5.86	397.3 ± 11.78	37.29 ± 3.95
Ascorbic acid	9.73 ± 0.71	12.52 ± 0.84	26.67 ± 1.23	69.84 ± 3.98

Results are mean ± statistical deviation (SD)of three different experiments.

The ME dose dependently scavenges DPPH radical with an IC_{50} of 200.47 µg/mL, H_2O_2 radical with an IC_{50} 243.28 µg/mL and FRAP with an IC_{50} of 397.3 µg/mL compared to ascorbic acid, which scavenges DPPH, H_2O_2 and FRAP with IC_{50} of 9.73, 12.52 and 26.67 µg/mL, respectively. The total antioxidant capacity (TAC) exhibited by the extract was found to be 37.29 mg GAE/g, while ascorbic acid showed 69.84 mg GAE/g.

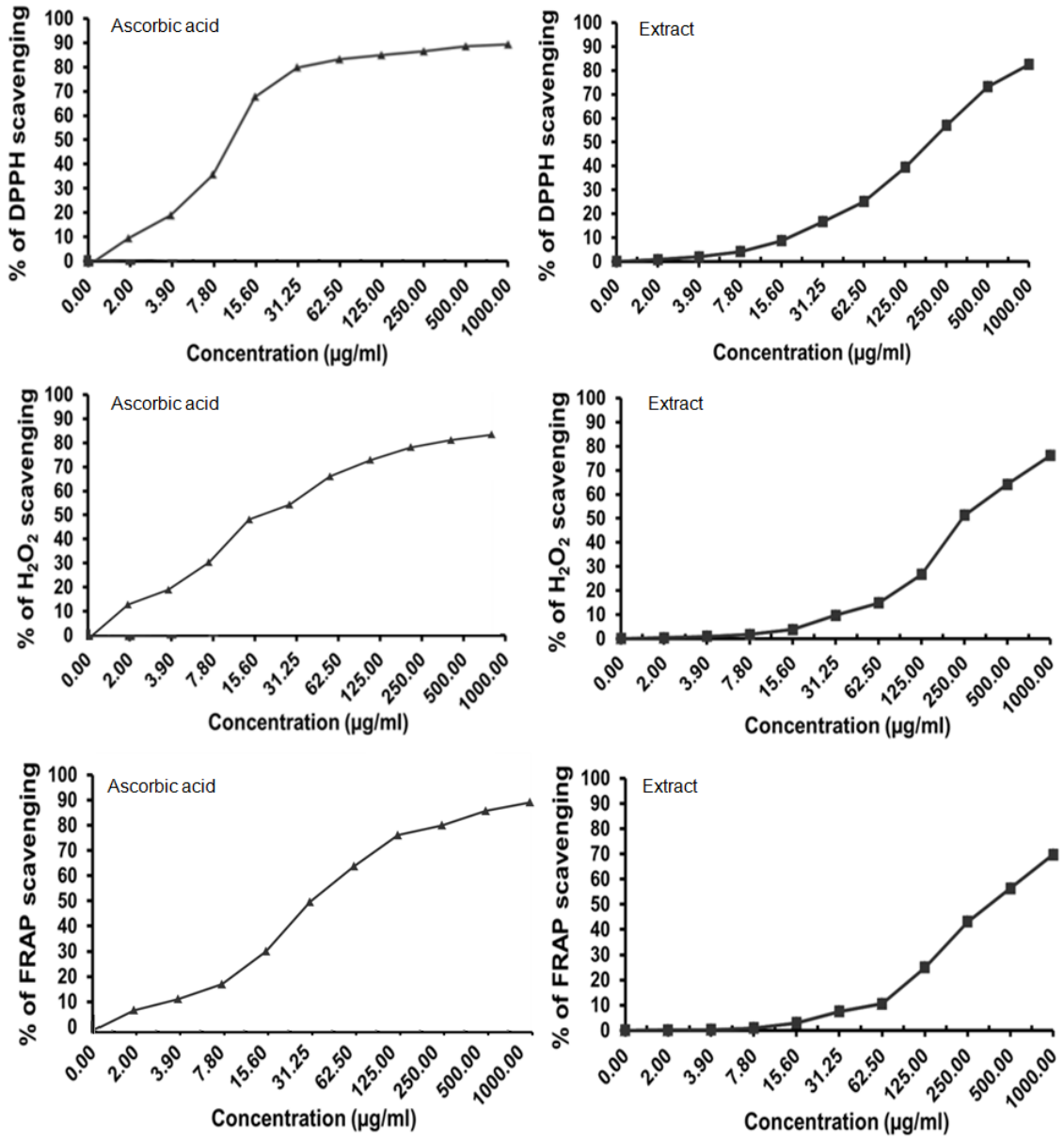

Figure 2. Dose response curve of % DPPH of ME of *C. rosea*, compared to ascorbic acid as a reference antioxidant. Results are mean of three separate experiments.

Cytotoxic activity

Oxidative stress is implicated in the development and progression of cancer; hence, the ME was screened for anticancer activity. The anticancer activity was performed on seven cancer cell lines (breast MCF-7, ovarian A2780, liver HepG2, kidney TK10, colon HT29, colon HCT-116 and prostate PC3) and one normal fibroblast cells (lung MRC-5), which were obtained from the ATCC and assessed by 3-(4,5-dimethylthiazol-2-yl)-2,5-diphenyltetrazolium bromide (MTT assay).[22] MTT assay is a colorimetric method in which the living (viable) cells by NADPH-dependent oxidoreductase enzymes reduce yellow tetrazolium salt to purple formazan. The ME of *C. rosea* exhibited variable cytotoxicity, ranging from IC_{50} 5.16-49.21 µg/mL, whereas normal cells treated with the ME showed an IC_{50} value of53.61 µg/mL (Table 4). The ME of *C. rosea* caused strong cytotoxicity against five cancer cell

lines (IC_{50} <20 µg/mL), breast cancer cells displayed promising sensitivity to the ME followed by PC3, HCT-116, HepG2 and TK10 cell lines. It has been established by U.S. National Cancer Institute that the crude extracts is categorized into three groups according to their degree of cytotoxicity,[26] active (IC_{50} < 20 µg/mL), moderately active (IC_{50} 20–100 µg/mL) and inactive (IC_{50} > 100 µg/mL). According to these criteria, the ME of *C. rosea* was active towards MCF-7, PC3, HCT-116, HepG2 and TK10 cell lines, while moderately active against HT29 and A2780 cancer cells. Furthermore, the ME of *C. rosea* showed selectivity towards six of the cancer cells compared to MRC5 normal cells, with selectivity index in the range of 2.33-10.39. A2780 cells were the least sensitive to ME, while MCF-7 displayed the highest sensitivity to the ME. This result revealed that the ME of *C. rosea* has cytotoxic activity, which might be helpful in preventing the cancer progression.

Table 4. Cytotoxicity of the methanol extract of *C. rosea* on cancer cell lines

Cell lines	Origin of cancerous cells	IC_{50} (µg/mL)		Selectivity index[b]
		Extract	Doxorubicin[a]	
Cancerous cells				
breast	MCF7	5.16±0.67	0.01 ± 0.06	10.39
colon	HT29	22.98±3.36	0.38 ± 0.03	2.33
colon	HCT116	13.96±3.19	0.47 ± 0.05	3.84
ovary	A2780	49.21±4.53	0.02 ± 0.01	1.08
liver	HepG2	18.29±2.21	1.16 ± 0.09	2.93
kidney	TK10	18.05±1.85	0.71 ±0.04	2.97
prostate	PC3	12.42±1.52	0.60 ± 0.07	4.32
Normal cells				
Lung	MRC-5	53.61±4.46	0.74± 0.06	-

Results are mean ± statistical deviation (SD) of three different experiments.
[a] Doxorubicin-positive control; [b] selectivity index = IC_{50} value against the normal MRC5 cells divided by the IC_{50} value against the corresponding cancer cell line.

Clonogenicity study of the extract

The clonogenicity of ME of *C. rosea* was tested using MCF7 cells, as it was the most sensitive cell line. MCF-7 cells treated with the ME of *C. rosea* showed significant inhibition of proliferation and decreased colony formation ability of cells dose dependently, compared to the control cells. As shown in Figure 3, the ME reduced colony formation significantly at 20 µM ($^{**}p< 0.010$) compared to untreated cells (control). These results showed that the ME of *C. rosea* has the ability to inhibit colony formation.

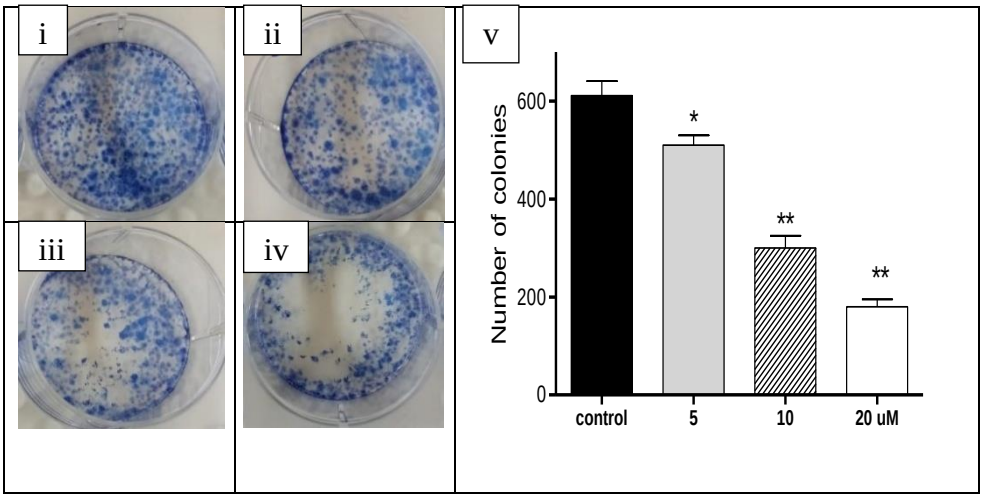

Figure 3. Clonogenicity of MCF7 cells following 72 h treatment in 6 well plate with: (i) Vehicle control, (ii) extract (5 µg/mL), (iii) (10µg/mL), and (iv) (20µg/mL). (v): the chart shows the treatments (x-axis) compare with the number of MCF7 colonies (y-axis). Three experimental repeats were performed. One-way ANOVA with the Tukey's post-hoc multiple comparison test was used to assess statistical differences compared to untreated control cells**.** $p < 0.100$ (*), $p < 0.010$ (**), $p < 0.001$ (***).

Anti-inflammatory activity

Reactive oxygen species is associated with the development of inflammatory diseases *via* modulation of cytokines, such as interlukins (ILs), inducible nitric oxide synthase (iNOS), tumor necrosis factor alpha (TNF-α), therefore the ME of *C. rosea* has been evaluated for anti-inflammatory activity by COX-1 and albumin denaturation inhibitory activities (Table 5).

Table 5. Anti-inflammatory activity of the methanol extract of *C. rosea*

COX-1 Inhibition IC_{50} (µg/mL)	
Extract	12.52 ± 0.84
Indomethacin	0.85 ± 0.03
Albumin denaturation inhibition IC_{50} (µg/mL)	
Extract	9.64 ± 0.68
Diclofenac	4.66 ± 0.39

Results are mean ± statistical deviation (SD) of three different experiments.

Two isoforms of cyclooxygenase enzymes (COX-1 and COX-2) that are responsible for prostaglandin synthesis from the precursor, arachidonic acid.[27] The

COX assay is a mechanistic assay that detects inhibitors of inflammation. The ME of *C. rosea* inhibited COX-1 enzyme to a degree similar to Indomethacin in a concentration dependent manner. It inhibited COX-1 enzyme significantly with IC_{50} 12.52 µg/mL, compared to the standard drug, Indomethacin, which displayed COX-1 inhibition with IC_{50} 0.85 µg/mL, indicating that the ME has shown great potential as COX-1 inhibitor. Albumin denaturation is a marker for inflammatory diseases in which protein upon the effect of external stress undergo denaturation.[28] The ME of *C. rosea* was effective in albumin denaturation inhibition in a concentration dependent manner with IC_{50} 9.64 µg/mL when compared to the control group, while the standard drug Diclofenac showed the similar effect. The ability of the ME to inhibit albumin denaturation further lends evidence for its anti-inflammatory activity. Therefore, the inhibition of COX-1 and albumin denaturation suggested that the ME possess an anti-inflammatory activity (Figure 4).

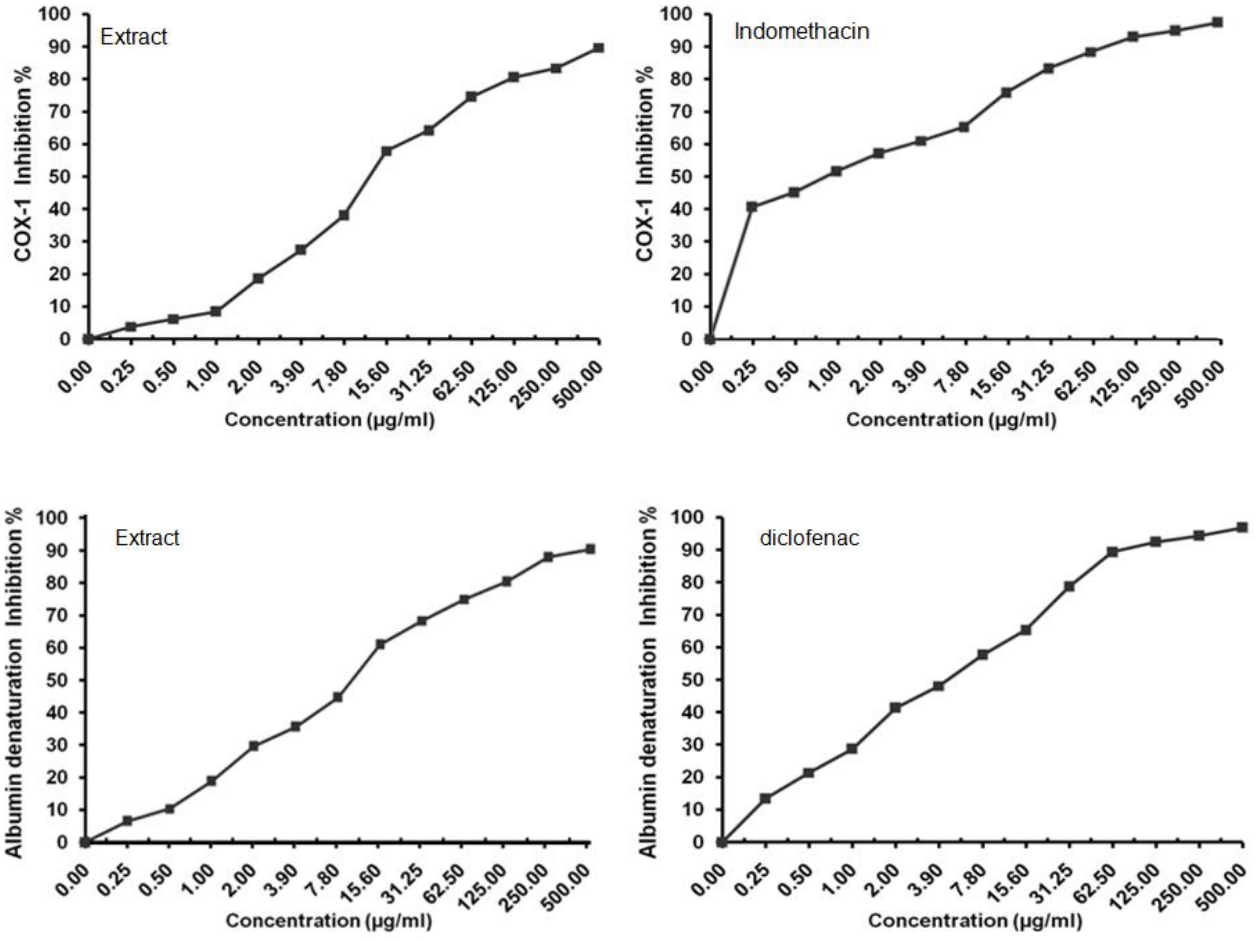

Figure 4. Dose response curve of %COX and % albumin denaturation inhibition of methanol extract of *C. rosea*, compared to standard drugs, indomethacin and Diclofenac. Results are mean of three separate experiments.

DISCUSSION

Oxidative stress resulting from the free radical formation is the major cause of the development of inflammation and cancer.[3, 29] Antioxidant, especially from natural sources, protects the body from the deleterious effects of free

radicals, and inhibits the oxidation of biomolecules and cell damage.[30] Plants are the sources of secondary metabolites like phenolics, tannins, flavonoids, etc[31], which possess diverse molecular structures and pharmacological effects. The presence of these metabolites in the extracts makes them efficacious against various diseases like cancer, diabetes, inflammation, atherosclerosis, etc.

In this study, the ME of *C. rosea* exhibited promising antioxidant property. It scavenged DPPH, hydrogen peroxide and FRAP significantly compared to ascorbic acid as a reference antioxidant. The antioxidant potential of the extract is attributed to the presence of phenolics, such as syringic acid, gallic acid, caffeic acid and ellagic acid. Several mechanisms have been proposed for these phenolic compounds for their antioxidant properties. Khan *et al* reported that caffeic acid exerts antioxidant activity by scavenging of peroxy and *o*-quinone radicals.[32] Syringic acid hampers oxidative stress markers like malondialdehyde, nitric oxide and oxidation of NADPH oxidase enzyme.[33] It has been reported that cinnamic acid is known for scavenging ROS by reducing the oxidation of lipoprotein, thus acting as a strong free radical scavenger.[34] Ellagic acid, a polyphenol, is a strong antioxidant due to the presence of four hydroxyl groups that can scavenge free radicals very efficiently. Its antioxidant activity is due to the enhancement of antioxidant enzymes like catalase (CAT), superoxide dismutase (SOD), reducing the level of oxidative stress markers and scavenging of hydrogen peroxide.[35] Another polyphenol, gallic acid, provides strong protection against both acute and chronic oxidative stress.[36] These reports indicate the ME of *C. rosea* might have the ability to stimulate the antioxidant defence system due to the presence of these polyphenols.

Inflammation is a protective response against foreign pathogens by the host.[37] ROS has been reported to be involved in intracellular signalling transduction inflammatory responses and its overproduction leads to chronic inflammation.[5] Plants with anti-inflammatory potential have long been used in traditional medicine as a source of biologically active agents to treat inflammatory disorders.[38] For instance, *Zingiber officinale*, *Curcuma longa*, *Salix alba*, *Urtica dioica*, *Arnica montana* , *Rosmarinus officinals* and *Matricaria chamomilla* are potential anti-inflammatory plants without side effects, unlike the synthetic anti-inflammatory agents[39]. For example, *Andrographis paniculata* extract has been reported to cure many inflammatory diseases *via* inhibiting proinflammatory cytokines, including IL-1β and TNF-α, due to the presence of andrographolide, a diterpene lactone.[40]*Polygonum amplexicaule* extract has been used to cure rheumatoid, fractures, muscle injury, arthritis and pain.[41] Among the active compounds found in the extracts are steroids, terpenoids, flavonoids, phenolics, and alkaloids, which contribute to the effectiveness of the treatment for inflammatory diseases.[42] Many anti-inflammatory compounds, such as curcumin that suppress NF-κB,[43] resveratrol inhibits iNOS and COX-2 expression,[44-45] boswellic acid inhibits NF-κB activation causing downregulation of TNF-α [46] have been isolated from plant extracts. In this study, the ME exhibited promising inhibition on COX-1enzyme and protein denaturation. The anti-inflammatory effect of the ME could be attributed to the presence of cinnamic acid, syringic acid, gallic acid, caffeic acid and ellagic acid, which act through various mechanisms. Ellagic acid causes anti-inflammatory effect by inhibiting TNF-α, modulating

proinflammatory cytokines expression, reduction in COX-2 levels by suppressing the protein synthesis of NF-kB.[47] Caffeic acid suppresses cascade enzymes like IRAK1, IRAK4, TAK1, MKK4/7, interleukins and TNF-α.[48] Syringic acid regulates various inflammatory genes, downregulates lipogenic genes, such as PPAR-γ expression, and represses the inflammatory cells and markers *via* inhibition of TNF-α.[34] It has been demonstrated that Gallic acid is a reported antiinflammatory agent, which inhibits IL-1β, TNF-α, NO, prostaglandin and MAPK pathways involved in inflammation.[49] Therefore, the promising anti-inflammatory effect exerted by the ME of *C. rosea* is attributed to these compounds.

Globally, cancer remains the major cause of mortality despite the advancements in the treatment. The limitations of the present treatments draw the attention of researchers towards plant-based anticancer drugs due to their lower toxicity and cost.[50] Plant extracts have the ability to act as therapeutic agents in the treatment of cancer triggered by oxidative stress due to polyphenols presence that inhibit cell proliferation by elevating the level of antioxidant enzymes and antiapoptotic proteins. Therefore, they play an outstanding role in chemoprevention and cancer treatment.[51] The present study showed that the ME of *C. rosea* exhibited promising toxicity on MCF-7, HT-29, HCT-116, HepG2, TK10 and PC-3 with IC_{50} between 5.16 – 22.98 µg/mL. Furthermore, the ME of *C. rosea* has the ability to inhibit colony formation in MCF-7 cells, suggesting that it may be useful in inhibiting tumor growth and cancer progression. It is reported that gallic acid induces BIK-BAK/BAK mediated apoptosis, caspase-9 and -3, and increases the expression level of apoptosis regulator Bcl-2 in SMMC-7721 cells,[52] caffeic acid inhibits mitogen-activated protein kinase (MAPK) pathways and caspases,[48] syringic acid exhibits antiproliferative effects *via* NF-kB-DNA binding, cell cycle arrests and apoptosis.[53] Cinnamic acid causes anticancer activity by the inhibition of DNA synthesis and histone deacetylase, production of interleukins 8, and suppression of NF-kB activation.[54] Cancer cell growth can be inhibited by ellagic acid through the regulation of metalloproteinases, Vascular endothelial growth factor (VEGF) expression, downregulating Bcl-2, and induction of apoptosis,[55] whereas, in cancer cells, salicylic acid induces activation of apoptosis and endoplasmic reticulum stress.[56] The underlying anticancer mechanism of gallic acid, cinnamic acid, ellagic acid, syringic acid, salicylic acid and caffeic acid present in the ME might be responsible for the significant anticancer activity exerted by the extract.

CONCLUSION

In the present work, the ME of *C. rosea* scavenges DPPH and $H_2O_2$with IC_{50} = 200.47 µg/mL and 243.28 µg/mL, respectively. Additionally, it inhibited inflammatory markers, COX-1 with IC_{50} = 12.52µg/mL and protein denaturation with IC_{50} = 9.64 µg/mL significantly, compared to the standard drugs Indomethacin and Diclofenac. The ME of *C. rosea* showed potent toxicity on MCF-7, A2780, HepG2, TK10, HT29, HCT-116 and PC3 cancer cells with IC_{50} in the range of 5.16–49.21 µg/mL, compared to Doxorubicin, as well as colony proliferation in MCF-7 cells. HPLC chromatogram showed the presence of gallic acid, cinnamic acid, ellagic acid, caffeic acid, syringic acid and salicylic acid. Further investigation is under process on the isolation and identification of bioactive compounds from the ME of *C. rosea*, which could

provide potential lead candidates as anti-inflammatory and anticancer agents in drug development. In conclusion, the ME of the aerial parts of *C. rosea* possesses cytotoxic, anti-inflammatory, and antioxidant properties.

Conflicts of Interest: The author declares no conflict of interest

References:

1. Klein JA, Ackerman SL. Oxidative stress, cell cycle, and neurodegeneration. J. Clin. Investig. 2003;111(6):785-93.
2. Waris G, Ahsan H. Reactive oxygen species: role in the development of cancer and various chronic conditions. J.Carcinogen. 2006;5:14.
3. Behrend L, Henderson G, Zwacka R. Reactive oxygen species in oncogenic transformation. Biochem.Soc. Trans. 2003;31(6):1441-4.
4. Aggarwal V, Tuli HS, Varol A, Thakral F, Yerer MB, Sak K, et al. Role of reactive oxygen species in cancer progression: molecular mechanisms and recent advancements. Biomolecules. 2019;9(11):735.
5. Mittal M, Siddiqui MR, Tran K, Reddy SP, Malik AB. Reactive oxygen species in inflammation and tissue injury. Antioxid.Redox Signal. 2014;20(7):1126-67.
6. Novoa A, Kaplan H, Kumschick S, Wilson JR, Richardson DM. Soft touch or heavy hand? Legislative approaches for preventing invasions: Insights from cacti in South Africa. Invasive Plant Science and Management. 2015;8(3):307-16.
7. Forster PI. The Cactus Family. JSTOR; 2001.

Acknowledgments: The authors are thankful to Al Baha University for the necessary facilities required for this work

8. Walters M, Figueiredo E, Zimmermann H, Mashope B. Naturalised and invasive succulents of southern Africa. 2011.
9. Al-Robai SA, Howladar SM, Mohamed HA, Ahmed AA. Cylindropuntia rosea (DC.) Backeb,(Cactaceae): a new generic alien record in the flora of Saudi Arabia. J. AsiaPac. Biodivers. 2018;11(2):320-3.
10. Al Zandi A, Al-Sagheer NA, wali Al-Khulaidi A. The Contribution of Land Uses in Determining the Vegetation Structure and Species Composition in High Altitude Areas of Al Baha Southwest Saudi Arabia. Environ. Sci. 2020;8(1):12-20.
11. Deltoro V, Ballester G, Oltra JE, Pérez-Botella J, Pérez-Rovira P, Gómez-Serrano MA, et al. The practicalities of eradicating an extremely invasive cactus: Hudson pear Cylindropuntia rosea in the Valencia region (East Spain). Aliens: The Invasive Species Bulletin. 2013;33:23-7.
12. Pérez Escandón BE. Lista de las plantas útiles del estado de Hidalgo: UAEH; 2003.
13. Pensamiento-Niño CA, Campos-Montiel RG, Añorve-Morga J, Ramírez-Moreno E, Ascacio-Valdés JA, Hernández-Fuentes A. Nutritional Characterization of the Functional and Antioxidant Activity of Cactus Flowers from Hidalgo, Mexico.

Applied Sciences. 2021;11(13):5965.
14. Baek SH, Cao L, Jeong SJ, Kim HR, Nam TJ, Lee SG. The Comparison of Total Phenolics, Total Antioxidant, and Anti-Tyrosinase Activities of Korean Sargassum Species. Journal of Food Quality 2021, Vol.2021, 1-7. https://doi.org/10.1155/2021/6640789
15. Nurcholis W, Putri DNS, Husnawati H, Aisyah SI, Priosoeryanto BP. Total flavonoid content and antioxidant activity of ethanol and ethyl acetate extracts from accession of Amomum compactum fruits. Annals of Agricultural Science 2021, Vol.66, 58-62. https://doi.org/10.1016/j.aoas.2021.04.001
16. Rebaya A, Belghith SI, Baghdikian B, Leddet VM, Mabrouki F, Olivier E, Cherif JK, Ayadi MT. Total phenolic, total flavonoid, Tannin content and antioxidant Capacity of Halimium halimfolium (Cistaceae). J Appl. Pharma. Sci. 2014; 5: 052-057.
17. Ates MT, Yildirim AB, Turker AU. Enhancement of alkaloid content (galanthamine and lycorine) and antioxidant activities (enzymatic and non-enzymatic) unders salt stress in summer snowflake (Leucojum aestivum L.) South African Journal of Botany 2021, Vol.140, 182-188. https://doi.org/10.1016/j.sajb.2021.04.016
18. Lahare RB, Yadav HS, Bisen YK, Dashahre AK. Estimation of Total Phenol, Flavonoid, Tannin and Alkaloid Content in Different Extracts of Catharanthus roseus from Durg District, Chhattisgarh, India. Scholar Bulletin 2021, Vol.7, 1-6. DOI: 10.36348/sb.2021.v07i01.001
19. Al-Amiery AA, Al-Majedy YK, Kadhum AA, Mohamad AB. Hydrogen Peroxide Scavenging Activity of Novel Coumarins Synthesized Using Different Approaches. PLoS One. 2015;10:e0132175.
20. El Jemli M, Kamal R, Marmouzi I, Zerrouki A, Cherrah Y, Alaoui K. Radical-Scavenging Activity and Ferric Reducing Ability of *Juniperus thurifera* (L.), *J. oxycedrus* (L.), *J. phoenicea* (L.) and *Tetraclinis articulata* (L.). Adv Pharmacol. Pharma. Sci. 2016; 2016: 1-6
21. Prieto P, Pineda M, Aguilar M. Spectrophotometric quantitation of antioxidant capacity through the formation of a phosphomolybdenum complex: specific application to the determination of vitamin E. Analy. Biochem. 1999;269(2):337-41.
22. Williams L, O'connar A, Latore L, Dennis O, Ringer S, Whittaker J, et al. The in vitro anti-denaturation effects induced by natural products and non-steroidal compounds in heat treated (immunogenic) bovine serum albumin is proposed as a screening assay for the detection of anti-inflammatory compounds, without the use of animals, in the early stages of the drug discovery process. West Ind. Med. J. 2008;57(4).
23 Almalki ASA, Nazreen S, Elbehairi SEI, Asad M, Shati AA, Alfaifi MY, Alhadhrami A, Elhenawy AA, Alorabi AQ, Asiri AM, Alam MM. Design,

synthesis, anticancer activity and molecular docking studies of new benzimidazole derivatives bearing 1,3,4-oxadiazole moieties as thymidylate synthase inhibitors. New J. Chem. 2022;46: 14967.

24. Abdalla AN, Qattan A, Malki WH, Shahid I, Hossain MA, Ahmed M. Significance of targeting VEGFR-2 and cyclin D1 in luminal-A breast cancer. Molecules. 2020;25(20):4606.
25. Lin Y-L, Juan I-M, Chen Y-L, Liang Y-C, Lin J-K. Composition of polyphenols in fresh tea leaves and associations of their oxygen-radical-absorbing capacity with antiproliferative actions in fibroblast cells. J. Agri. Food Chem. 1996;44(6):1387-94.
26. Skehan P, Storeng R, Scudiero D, Monks A, McMahon J, Vistica D, et al. New colorimetric cytotoxicity assay for anticancer-drug screening. JNCI: Journal of the National Cancer Institute. 1990;82(13):1107-12.
27. Attiq A, Jalil J, Husain K, Ahmad W. Raging the war against the inflammation with natural products. Front. Pharmacol. 2018;9: 976.
28. Dharmadeva S, Galgamuwa LS, Prasadinie C, Kumarasinghe N. *In vitro* anti-inflammatory activity of Ficus racemosa L. bark using albumin denaturation method. Ayu. 2018;39(4):239.
29. Saxena S, Jha S. ROS at the intersection of inflammation and immunity in cancer. In: Chakraborti, S., Ray, B.K., Roychowdhury, S. (eds) Handbook of Oxidative Stress in Cancer: Mechanistic Aspects. Springer, 2021;1-18.
30. Quero J, Mármol I, Cerrada E, Rodríguez-Yoldi MJ. Insight into the potential application of polyphenol-rich dietary intervention in degenerative disease management. Food Func.2020;11(4):2805-25.
31. Twaij BM, Hasan MN. Bioactive Secondary Metabolites from Plant Sources: Types, Synthesis, and Their Therapeutic Uses. *Int. J Plant Biol*. 2022; 13(1):4-14.
32. Pontiki E, Hadjipavlou-Litina D, Litinas K, Geromichalos G. Novel cinnamic acid derivatives as antioxidant and anticancer agents: Design, synthesis and modeling studies. Molecules. 2014;19(7):9655-74.
33. Khan FA, Maalik A, Murtaza G. Inhibitory mechanism against oxidative stress of caffeic acid. J.Food Drug Analys. 2016;24(4):695-702.
34. Srinivasulu C, Ramgopal M, Ramanjaneyulu G, Anuradha C, Kumar CS. Syringic acid (SA)–a review of its occurrence, biosynthesis, pharmacological and industrial importance. Biomed. Pharmacother. 2018;108:547-57.
35. Polce SA, Burke C, França LM, Kramer B, Paes AMdA, Carrillo-Sepulveda MA. Ellagic acid alleviates hepatic oxidative stress and insulin resistance in diabetic female rats. Nutrients. 2018;10(5):531.
36. Dludla PV, Nkambule BB, Jack B, Mkandla Z, Mutize T, Silvestri S, et al. Inflammation and oxidative stress in an obese state and the protective effects of gallic acid. Nutrients. 2018;11(1):23.
37. Chandra S, Chatterjee P, Dey P, Bhattacharya S. Evaluation of in vitro anti-inflammatory activity

of coffee against the denaturation of protein. Asian Pac. J. Trop. Biomed. 2012;2(1):S178-S80.

38. C Recio M, Andujar I, L Rios J. Anti-inflammatory agents from plants: progress and potential. Curr.Med.Chem. 2012;19(14):2088-103.
39. Nunes CdR, Barreto Arantes M, Menezes de Faria Pereira S, Leandro da Cruz L, de Souza Passos M, Pereira de Moraes L, Vieira IJC, Barros de Oliveira D. Plants as Sources of Anti-Inflammatory Agents. *Molecules*. 2020; 25(16):3726.
40. Denzler KL, Waters R, Jacobs BL, Rochon Y, Langland JO. Regulation of inflammatory gene expression in PBMCs by immunostimulatory botanicals. PloS one. 2010;5(9):e12561.
41. Xiang M-X, Xu Z, Su H-W, Hu J, Yan Y-J. Emodin-8-O-β-D-glucoside from Polygonum Amplexicaule D. Don var. Sinense Forb. promotes proliferation and differentiation of osteoblastic MC3T3-E1 Cells. Molecules. 2011;16(1):728-37.
42. Scalbert A, Manach C, Morand C, Rémésy C, Jiménez L. Dietary polyphenols and the prevention of diseases. Crit.Rev.Food Sci. Nutri. 2005;45(4):287-306.
43. Yu Y, Shen Q, Lai Y, Park SY, Ou X, Lin D, Jin M, Zhang W. Anti-inflammatory effects of curcumin in microglial cells. Front. Pharmacol. 2018; 9: 386.
44. Meng T, Xiao D, Muhammed A, Deng J, Chen L, He J. Anti-Inflammatory Action and Mechanisms of Resveratrol. Molecules 2021; 26: 229.
45. Sánchez-Fidalgo S, Cárdeno A, Villegas I, Talero E, de la Lastra CA. Dietary supplementation of resveratrol attenuates chronic colonic inflammation in mice. Eur. J. Pharmcol. 2010;633(1-3):78-84.
46. Ammon HPT. Modulation of the immune system by boswellia serrata extracts and boswellic acids. Phytomed. 2010; 17: 862-867.
47. Sharifi-Rad J, Quispe C, Castillo CMS, Caroca R, Lazo-Vélez MA, Antonyak H, et al. Ellagic Acid: A Review on Its Natural Sources, Chemical Stability, and Therapeutic Potential. Oxid. Med. Cell. Long. 2022;2022.
48. Wang W, Sun W, Jin L. Caffeic acid alleviates inflammatory response in rheumatoid arthritis fibroblast-like synoviocytes by inhibiting phosphorylation of IκB kinase α/β and IκBα. Int. Immunopharmacol. 2017;48:61-6.
49. BenSaad LA, Kim KH, Quah CC, Kim WR, Shahimi M. Anti-inflammatory potential of ellagic acid, gallic acid and punicalagin A&B isolated from Punica granatum. BMC Comp. Alter. Med. 2017;17(1):1-10.
50. Alam MM, Malebari AM, Syed N, Neamatallah T, Almalki AS, Elhenawy AA, et al. Design, synthesis and molecular docking studies of thymol based 1, 2, 3-triazole hybrids as thymidylate synthase inhibitors and apoptosis inducers against breast cancer cells. Bioorg. Med. Chem. 2021;38:116136.
51. Petty AJ, Yang Y. Tumor-associated macrophages: implications in cancer immunotherapy. Immunotherapy. 2017;9(3):289–302.

52. Sun G, Zhang S, Xie Y, Zhang Z, Zhao W. Gallic acid as a selective anticancer agent that induces apoptosis in SMMC-7721 human hepatocellular carcinoma cells. Oncology Lett. 2016;11(1):150-8.
53. Orabi KY, Abaza MS, El Sayed KA, Elnagar AY, Al-Attiyah R, Guleri RP. Selective growth inhibition of human malignant melanoma cells by syringic acid-derived proteasome inhibitors. Cancer cell international. 2013;13(1):1-16.
54. Hunke M, Martinez W, Kashyap A, Bokoskie T, Pattabiraman M, Chandra S. Antineoplastic actions of cinnamic acids and their dimers in breast cancer cells: A comparative study. Anticancer Res. 2018;38(8):4469-74.
55. Mohammadinejad A, Mohajeri T, Aleyaghoob G, Heidarian F, Oskuee RK. Ellagic acid as a potent anticancer drug. A comprehensive review on in vitro, in vivo, in silico and drug delivery studies. Biotech. Appl. Biochem. 2021 (online issue),https://doi.org/10.1002/bab.2288
56. Ausina P, Branco JR, Demaria TM, Esteves AM, Leandro JGB, Ochioni AC, et al. Acetylsalicylic acid and salicylic acid present anticancer properties against melanoma by promoting nitric oxide-dependent endoplasmic reticulum stress and apoptosis. Sci. Rep. 2020;10(1):1-15.

التقييم المعملي لأنشطة مضادات الأكسدة ومضادات الإلتهاب والسمية الخلوية لمستخلص الميثانول لنبتة سيليندروبونتيا روزيا

عبدالله عسير أحمد الغامدي

بيولوجيا الخلية- جامعة الباحة

ملخص

يركز العمل البحثي الحالي على دراسة تأثير المستخلص الميثانولي للأجزاء الهوائية من نبات *Cylindropuntia rosea* على أنشطة السمية الخلوية ومضادات الالتهاب ومضادات الأكسدة. وأظهر المستخلص الميثانولي قوة اكبر لإزالة أيون DPPH و H_2O_2 وقوة مضادات الأكسدة لأيون الحديديك وكانت قيمة IC_{50} = 200.47 ميكروغرام / مل و 243.28ميكروغرام / مل و ٣٩٧,٣ ميكروغرام / مل على التوالي. بينما قام بتثبيط مؤشرات الالتهاب لإنزيم COX-1 وكانت قيمة IC_{50} = 12.52 ميكروغرام / مل وتكسير البروتين كانت عند IC_{50} = 9.64 ميكروغرام / مل بشكل ملحوظ مقارنة بالعقاقير القياسية المستخدمة إندوميثاسين وديكلوفيناك. وأثبتت نتائج السمية الخلوية أن المستخلص أظهر سمية عالية للخلايا السرطانية MCF-7 و A2780 و HepG2 و TK10 و HT29و HCT-116 و PC3 وكانت قيمة IC_{50} في نطاق 5.16–49.21 ميكروغرام / مل مقارنة بالدوكسوروبيسين المستخدم. وعلاوة على ذلك، وجد أن المستخلص أكثر حساسية مع خلايا MCF-7 ومنع تكاثر المستعمرات الخلوية كما لوحظ في تجارب الاستنساخ الخلوية. ولدعم نتائج النشاط البيولوجي تم عمل تحليل HPLCوالذي أظهر وجود مكونات نشطة بيولوجيًا مثل حمض الجاليك وحمض السينامياك وحمض الإيلاجيك وحمض الكافيين وحمض السرينجيك وحمض الساليسيليك. وختاماً، أظهر مستخلص الميثانول للأجزاء الهوائية من نبات *C. rosea* خصائص سمية للخلايا ومضاد للإلتهاب وخصائص مضادة للأكسدة، لذلك يمكن استخدامه لعزل جزيئات فعّالة لتحضير أدوية جديدة.

كلمات مفتاحية: نبات سيليندرو بونتيا ، السمية الخلوية ، مضاد الإلتهاب ، مضاد الأكسدة

Evaluation of the root canal morphology of mandibular incisors in a Saudi Arabian subpopulation using cone-beam computed tomography

Ahmad Hassan Jabali[1] , Hemant Ramesh Chourasia[1] , Mohammed Y. Tarrosh[1],

Nezar Boreak[1] , Hashim Bajawi[1] , Abdulaziz Hassan Mohammed Al-Shehri[2]
Mazen Yahya Abuhawi[2]
Department of Restorative Dental Sciences College of Dentistry, Jazan University, Saudi Arabia[1]

General Dentist, Ministry of Health, Saudi Arabia[2]

ABSTRACT

Aim: To determine the root canal morphology of permanent mandibular central and lateral incisors in a Saudi Arabian subpopulation using cone-beam computed tomography (CBCT).
Materials and methods: CBCT images of 100 patients with 400 permanent mandibular incisors, aged 15–50 years, and fulfilling inclusion criteria were examined. The number of roots, root canals, and canal configurations according to Vertucci's classification was investigated. The Chi-square test was used to test the association between variables. The reliability of the inter- and intra-examiners was tested using the Kappa test.

Results: Most mandibular central and lateral incisors had a single canal. The overall prevalence of two canals in mandibular incisors was 37%. According to sex, the prevalence of two canals amongst males was 62.8%, whereas, in females, it was 37.2%. ($p<0.05$) The most common root canal configuration of mandibular incisors was Type I, followed by Type III.
Conclusions: Two canals are not infrequent in the mandibular incisor teeth of Saudi Arabian subpopulations, which must be considered while performing root canal treatment.

Keywords: CBCT, cone-beam computed tomography, mandibular incisors, root canal morphology, Saudi Arabian population

Introduction

The main procedures involved in successful endodontic therapy are (a) the discovery of root canals, leading to a complete debridement of the pulpal tissues, (b) thorough chemo-mechanical cleaning and sculpting, and (c) Three-dimensional (3D) root canal obturation (Slowey,1974). Untreated areas inside the tooth could develop from a failure to identify, thoroughly clean, precisely shape, or obturate all root canals (Vertucci,2005; Cantatore,2006). To increase the likelihood that endodontic treatment will succeed, every clinician should be adequately acquainted with the potential variations of the root canal system.

As per various researchers, all teeth have anatomical variations with varying incidences (Kulid,1990; Gulabivala,2001). Mandibular incisors commonly have a single root and a single canal (Vertucci,1984; Rahimi,2013). The most common anatomical abnormalities of mandibular incisors include the second root canal, lateral root canals, and apical deltas, which can complicate their endodontic treatment (Weine, 1969). The existence of an untreated isthmus or an undiagnosed lingual root canal is the most frequent cause of failure in endodontic treatment of permanent mandibular incisors (Ch,2004).

Race, gender, and population all affect the likelihood of having two root canals in a

mandibular incisor. Systematic review and meta-analysis on the variations in root canal morphology of permanent incisors among the Asian population reported a single canal in most mandibular anterior teeth. Still, variations, especially in mandibular lateral incisors, were common. International variations in root canal morphology have been observed by various researchers (Usha,2021). Mukhaimer and Jarbawi (2013), Nogueira (2017) and Bhat et al. (2017) discovered that 29.3%, 18% and 49% of mandibular incisors have two root canals in Palestinian, northern Brazilian and a North Indian subpopulation, respectively. Few researchers have studied the mandibular incisors' root canal morphology in Saudi Arabia. In the first study, Al-Fouzan et al. (2012) examined the likelihood of a second root canal in mandibular incisor teeth using canal staining and clearing procedures. They discovered a second root canal in one-third of the teeth they had examined. Two canals were found in 28.6% of the teeth analyzed using CBCT by Mashyakhy (2019) Ghabbani et al. (2020) in the Al-Madinah Al-Munawarah district, reported that only 50.3% of the investigated teeth have a single root canal.

The root canal anatomy of mandibular incisors has been studied using polyester resin impressions, radiographs in the mesiodistal and buccolingual directions, clear tooth specimens, and, more recently, cone-beam computed tomography (CBCT). The three-dimensional details of root morphology and its variations can be very clearly seen on CBCT (Kajan,2018; Ordinola-Zapata,2017). However, there are few reports on the root canal morphology of Saudi Arabian mandibular incisors using CBCT. Hence the present study was conducted to determine the root canal morphology in mandibular incisors among a Saudi subpopulation of the Jazan region of Saudi Arabia using CBCT.

Materials and Methods

A cross-sectional study was conducted to determine the root canal morphology of permanent mandibular central and lateral incisors in a Saudi Arabian subpopulation using cone-beam computed tomography (CBCT).

Four hundred CBCT images of mandibular incisors were collected from 100 subjects, from November 2017 to April 2018 including 53 males and 47 females aged 15–50 years who had undergone CBCT scanning for diagnostic purposes.

Ethical approval for the study was obtained from the Institutional Ethical Committee of Jazan University, Jazan, Saudi Arabia.

Inclusion criteria

1. Both male and female patients,
2. aged 15 years and above,
3. presence of all mandibular incisors with fully formed apices
4. No prior treatment, or pathologies in the lower incisors

Exclusion Criteria

1. a history of orthodontic treatment,
2. patients with missing mandibular anterior teeth;
3. blurred CBCT images.
4. Mandibular incisors with calcifications, root resorption, developmental anomalies

CBCT images were taken using the Pax-Flex3D imaging system (Morita, Osaka, Japan) operated at 50-90kVp and 2-10mA, with a field of view (FOV) of 50×50mm, an exposure time of 15-24 seconds, and a voxel size of 120µm. To standardise the measures, CBCT scans were positioned so that the axial view of the bilateral mandibular condyles was at the same level on both sides. In the coronal view, the mental foramina on both sides were parallel to the horizontal axis. The Frankfort plane served as the true horizontal axis in the sagittal view. The authors assessed the CBCT images. All tests were re-performed twice, one week apart, to minimise errors in identifying the root canal morphology. The Kappa test

was used to compare the differences between the two readings for examiner variances. The teeth under examination were categorised using the Vertucci system (Vertucci,1984).

Statistical Analysis

Statistical Package for the Social Sciences (SPSS) software was used to examine the data gathered statistically. $P<0.05$ was used to define the statistical significance level. The Chi-square test was used to test the association between variables. The reliability of the inter- and intra-examiners was tested using the Kappa test.

Results

The mean age of the included subjects was 28 years. The reliability of the inter- and intra-examiners showed excellent results of Kappa test with a value of 0.88 and 0.91, respectively. All mandibular incisors had one root. The majority of mandibular central incisors and lateral incisors had one canal. The prevalence of second canals was; left central incisors-38%, left lateral incisors-36%, right central incisor-35%, and right lateral incisors-39%. (Table 1)

Table 1. Prevalence of the number of root canals of Mandibular Incisor Teeth

No. of Canal	Left Central (31)	Left Lateral (32)	Right Central (41)	Right Lateral (42)	Total
1	62 (62.0%)	64 (64.0%)	65 (65.0%)	61 (61.0%)	252 (63.0%)
2	38 (38.0%)	36 (36.0%)	35 (35.0%)	39 (39.0%)	148 (37.0%)
	100 (100.0%)	100 (100.0%)	100 (100.0%)	100 (100.0%)	400 (100.0%)

The prevalence of two canals amongst males was 62.8%, whereas, in females, it was 37.2%. Men were more likely to get two canals in mandibular incisors than women in Saudi Arabian subpopulation ($\chi2=9.127$, p-value=0.003). (Table 2) Type I Vertucci classification was most prevalent (62.5%), followed by Type III (36.8%), type V (0.5%), and Type II (0.3%). (Table3)

Table 2. Cross-tabulation of Number of Canals versus Sex

	Sex			
No. of Canal	Female	Male	Total	Chi-Square (p-value)
1	133 (52.8%)	119 (47.2%)	252 (100.0%)	$\chi2=9.127$ df (1)
2	55 (37.2%)	93 (62.8%)	148 (100.0%)	p-value=0.003
Total	188 (47.0%)	212 (53.0%)	400 (100.0%)	Significant

Table 3. Distribution of Root Canal Types of Mandibular Incisor Teeth					
Vertucci's Classification	**Left Central (31)**	**Left Lateral (32)**	**Right Central (41)**	**Right Lateral (42)**	**Total**
Type I	61 (61.0%)	64 (64.0%)	64 (64.0%)	61 (61.0%)	250 (62.5%)
Type II	0 (0.0%)	0 (0.0%)	1 (1.0%)	0 (0.0%)	1 (0.3%)
Type III	38 (38.0%)	36	34 (34.0%)	39 (39.0%)	147 (36.8%)
Type V	1 (1.0%)	0	1 (1.0%)	0 (0.0%)	2 (0.5%)
Total	100 (100.0%)	100 (100.0%)	100 (100.0%)	100 (100.0%)	400 (100.0%)

There was a statistically significant association between the Vertucci classification and sex ($\chi 2$=11.940, p-value=0.008). Type I was slightly more common in females, whereas Type III was almost twice as common in males. (Table 4) (Figure1)

Table 4. Cross-tabulation of Root Canal Type versus Sex				
	Sex			
Vertucci's Classification	**Female**	**Male**	**Total**	**Chi-Square (p-value)**
Type I	133 (53.2%)	117 (46.8%)	250 (100.0%)	$\chi 2$=11.940, df (3)
Type II	0 (0.0%)	1 (100.0%)	1 (100.0%)	p-value=0.008
Type III	55 (37.4%)	92 (62.6%)	147 (100.0%)	Significant
Type V	0 (0.0%)	2 (100.0%)	2 (100.0%)	
Total	188 (47.0%)	212 (53.0%)	400 (100.0%)	

Figure 1

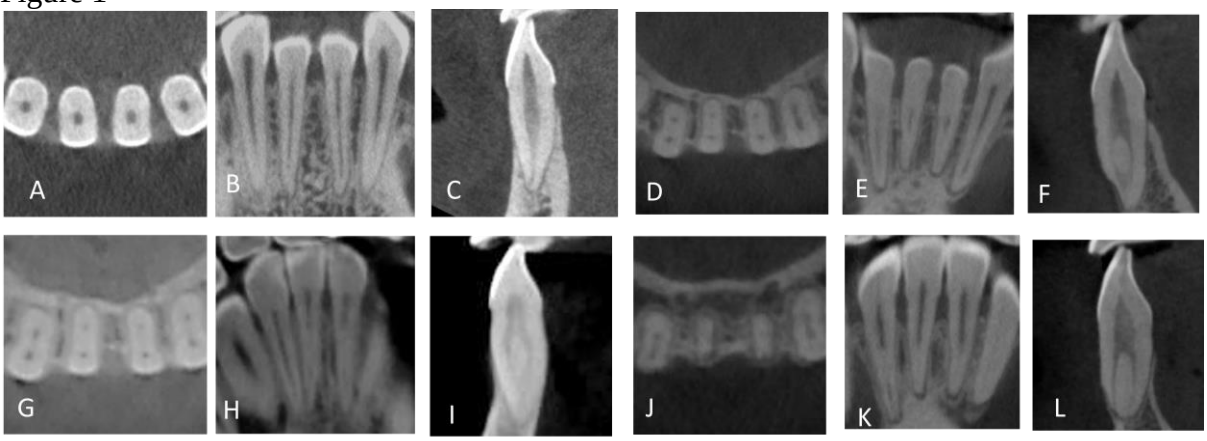

Figure 1. The axial, coronal and sagittal planes of CBCT images showing Type I (A-C), Type II (D-F), Type III (G-I) and Type V (J-L) canal pattern of mandibular incisors.

Discussion

The present study was conducted to determine the root canal morphology in mandibular incisors among a Saudi subpopulation of the Jazan region of Saudi Arabia using CBCT.

The anatomical structures can be examined in 3D with CBCT. It was discovered that CBCT is equally accurate at identifying the number of root canals as the clearing and staining methods (Kajan,2018). Moreover, it outperforms the clearing

method in determining the Type I Vertucci classification (Ordinola-Zapata,2017). CBCT is a simple, useful, non-invasive, and trustworthy method for assessing root canal morphology (Kajan,2018; Ordinola-Zapata,2017).

We evaluated 400 CBCT and found that almost one-third of the mandibular incisors in the study population had two canals. Type I, followed by type III Vertucci classification, was the most common configuration observed in the present study.

The various studies conducted in Saudi Arabia, the prevalence of two canals in mandibular incisors varies from 26% to 41%. Almohaimede et al.(2022) examined CBCT images of lower central and lateral incisors of Saudi patients in Riyadh and reported that 41% of these had two canals. Type I, followed by Type III was the most common canal configuration observed (Almohaimede,2022). Mashyakhy (2019) examined mandibular incisors of Saudi Arabian population using CBCT and found that 26.3% and 30.8 % of lower central and lateral incisors had two root canals, respectively. Alkahtany et al. (2020) reported a lower percentage (22.31%) of two canals in a Saudi subpopulation using CBCT. Al-Fouzan et al.(2012) and Mohamed et al.(2021) reported similar results, with approximately 30% of both lower central and lateral incisors having two canals. This finding was lower than the results found in our study. Using CBCT, Ghabbani et al (2020) examined 1624 mandibular incisors in the Al-Madinah region of Saudi Arabia. Similar to our findings, all incisors revealed one root; however, lower prevalence of two root canals were observed than in our samples (25.02% and 29.42% of central and lateral incisors, respectively). The contrasts in the observations may be due to differences in the methodology, sample size, and geographic areas.

Additionally, researchers have discovered that different populations had varying incidences of single-root canals in the central and lateral incisors of the mandible. The prevalence of two root canals varies from 5% in China, 12% in Malaysia, 24% in Germany, 30% in Portugal, 34% in Poland, 35% in Iran, and 45% in Italy (Martins,2018; Pan,2019; Baxter,2020; Sroczyk-Jaszczyńska,2020; Mirhosseini,2019; Valenti-Obino,2019).

We investigated the association of gender with the prevalence of two root canals and found that men were more likely to get two canals in mandibular incisors than women in Saudi Arabian subpopulation. Similar results were reported by Alkahtany et al. (2020) however, Mohamed et al. (2021) discovered that women were significantly more likely than males to have two root canals in another Saudi community. Almohaimede et al. (2022) and Mashyakhy (2019) in Saudi and Geduk et al (2015). in Turkey reported contrasting results with no association of two root canal prevalence to gender. Studies on various populations show conflicting results about the relationship between gender and the frequency of root canals. An Indian study revealed that females had a significantly higher prevalence of two root canals than males (Verma,2017). Conversely, men were more likely than women to have multiple canals in Caucasian and Chinese populations (Martins,2017; Lin,2014). These discrepancies might be explained by various sample sizes and various ethnic backgrounds.

It is not unusual for mandibular incisors to have several canals. Therefore, thorough radiographic interpretation, extending access preparation, and using dental microscopy to improve visibility can all aid physicians in locating and negotiating additional canals.

There are certain limitations of our study. Age also affects root canal morphology as increasing age may lead to calcifications of canals that cause the disappearance of root canals. However, the association of age was not tested in the present study. Also, this study is limited to one specific geographic area. Therefore, it is

recommended that a larger sample size representative of all the geographical several regions of Saudi Arabia should be examined.

Conclusion

It can be concluded that the prevalence of two canals in mandibular incisors varies from 35 -39%. Males showed significantly higher prevalence of two canals than females. Type I followed by Type III is the most common root canal configuration of mandibular incisors within a Saudi Arabian subpopulation.

References

1. Al-Fouzan, K. S., AlManee, A., Jan, J., & Al-Rejaie, M. (2012). Incidence of two canals in extracted mandibular incisors teeth of Saudi Arabian samples. *Saudi Endodontic Journal*, *2*(2), 65.
2. Alkahtany, M., Almadhi, K., & Madwas, A. (2020). Root canal morphology of mandibular anterior teeth using cone beam computerized tomography in Saudi Sub-population. *International Journal of Dentistry and Oral*, *6*, 1-6.
3. Almohaimede, A., Alqahtani, A., Alhatlani, N., Alsaloom, N., & Alqahtani, S. (2022). Analysis of Root Canal Anatomy of Mandibular Permanent Incisors in Saudi Subpopulation: A Cone-Beam Computed Tomography (CBCT) Study. *Scientifica*, *2022*.
4. Baxter, S., Jablonski, M., & Hülsmann, M. (2020). Cone-beam-computed-tomography of the symmetry of root canal anatomy in mandibular incisors. *Journal of oral science*, *62*(2), 180–183. https://doi.org/10.2334/josnusd.19-0113
5. Bhat, S. P., Sheth, R., Kumar, P., & Khilosiya, A. (2017). Root canal morphology and assessment of incidence, type, and position of isthmus in permanent mandibular central incisor in North Indian population: An in vitro study. *Endodontology*, *29*(2), 107.
6. Cantatore, G., Berutti, E., & Castellucci, A. (2006). Missed anatomy: frequency and clinical impact. *Endodontic Topics*, *15*(1), 3-31.
7. Ch, U., Ramachandran, S., Indira, R., & Shankar, P. (2004). Canal and isthmus morphology in mandibular incisors-An in vitro study. *Endodontology*, *16*(1), 7-11.
8. Geduk, G., Deniz, Y., Zengin, A. Z., & Eroglu, E. (2015). Cone-beam computed tomography study of root canal morphology of permanent mandibular incisors in a Turkish sub-population. *Journal of Oral and Maxillofacial Radiology*, *3*(1), 7.
9. Ghabbani, H. M., Marghalani, A. A., & Alabiri, H. R. (2020). Assessment of root canal morphology of mandibular incisors using cone-beam computed tomography among residents of Al-Madinah Al-Munawara Region, Saudi Arabia. *European Journal of General Dentistry*, *9*(01), 40-44.
10. Gulabivala, K., Aung, T. H., Alavi, A., & Ng, Y. L. (2001). Root and canal morphology of Burmese mandibular molars. *International endodontic journal*, *34*(5), 359-370.
11. Kajan, Z. D., Taramsari, M., Fard, N. K., & Kanani, M. (2018). Accuracy of cone-beam computed tomography in comparison with standard method in evaluating root canal morphology: an in vitro study. *Iranian Endodontic Journal*, *13*(2), 181.
12. Kulid, J. C., & Peters, D. D. (1990). Incidence and configuration of canal systems in the mesiobuccal root of maxillary first and second molars. *Journal of endodontics*, *16*(7), 311-317.

13. Lin, Z., Hu, Q., Wang, T., Ge, J., Liu, S., Zhu, M., & Wen, S. (2014). Use of CBCT to investigate the root canal morphology of mandibular incisors. *Surgical and Radiologic Anatomy*, *36*(9), 877-882.
14. Martins, J. N., Gu, Y., Marques, D., Francisco, H., & Caramês, J. (2018). Differences on the root and root canal morphologies between Asian and white ethnic groups analyzed by cone-beam computed tomography. *Journal of Endodontics*, *44*(7), 1096-1104.
15. Martins, J. N., Marques, D., Mata, A., & Caramês, J. (2017). Root and root canal morphology of the permanent dentition in a Caucasian population: a cone-beam computed tomography study. *International Endodontic Journal*, *50*(11), 1013-1026.
16. Mashyakhy, M. (2019). Anatomical analysis of permanent mandibular incisors in a Saudi Arabian population: An in Vivo cone-beam computed tomography study. *Nigerian journal of clinical practice*, *22*(11), 1611-1611.
17. Mirhosseini, F., Tabrizizadeh, M., Nateghi, N., Shafiei Rad, E., Derafshi, A., Ahmadi, B., & Daneshvar, M. (2019). Evaluation of Root Canal Anatomy in Mandibular Incisors Using CBCT Imaging Technique in an Iranian Population. *Journal of dentistry (Shiraz, Iran)*, *20*(1), 24–29. https://doi.org/10.30476/DENTJODS.2019.44559
18. Mohamed, A. N., Alhirabi, A. A., Elsantawy, A. H., & Aldakheel, F. S. (2021). Evaluation of root canal configuration of mandibular incisors among a Saudi subpopulation of Qassim region using cone-beam computed tomography: A retrospective study. *Saudi Endodontic Journal*, *11*(1), 49.
19. Mukhaimer, R., & Jarbawi, M. (2013). Radiographic study of the root canal system of mandibular incisors in Palestinian population. *Open J Stomatol*, *3*, 452.
20. Nogueira, B. M. L., Nogueira, B. C. L., Fagundes, N. C. F., Menezes, T. O. D. A., Lima, R. R., & Brandão, J. M. D. S. (2017). Root and canal morphology of permanent mandibular incisors. *Int J Odontostomat*, *11*(1), 95-100.
21. Ordinola-Zapata, R., Bramante, C. M., Versiani, M. A., Moldauer, B. I., Topham, G., Gutmann, J. L., ... & Abella, F. (2017). Comparative accuracy of the Clearing Technique, CBCT and Micro-CT methods in studying the mesial root canal configuration of mandibular first molars. *International endodontic journal*, *50*(1), 90-96.
22. Pan, J. Y. Y., Parolia, A., Chuah, S. R., Bhatia, S., Mutalik, S., & Pau, A. (2019). Root canal morphology of permanent teeth in a Malaysian subpopulation using cone-beam computed tomography. *BMC Oral Health*, *19*(1), 1-15.
23. Rahimi, S., Milani, A. S., Shahi, S., Sergiz, Y., Nezafati, S., & Lotfi, M. (2013). Prevalence of two root canals in human mandibular anterior teeth in an Iranian population. *Indian Journal of dental research*, *24*(2), 234.
24. Slowey, R. R. (1974). Radiographic aids in the detection of extra root canals. *Oral Surgery, Oral Medicine, Oral Pathology*, *37*(5), 762-772.
25. Sroczyk-Jaszczyńska, M., Kołecki, J., Lipski, M., Puciło, M., Wilk, G., Falkowski, A., Kot, K., & Nowicka, A. (2020). A study of the symmetry of roots and root canal morphology in mandibular anterior

teeth using cone-beam computed tomographic imaging in a Polish population. *Folia morphologica*, *79*(4), 835–844. https://doi.org/10.5603/FM.a2019.0128

26. Usha, G., Muddappa, S. C., Venkitachalam, R., Rajan, R. R., & Ravi, A. B. (2021). Variations in root canal morphology of permanent incisors and canines among Asian population: A systematic review and meta-analysis. *Journal of Oral Biosciences*, *63*(4), 337-350.
27. Valenti-Obino, F., Di Nardo, D., Quero, L., Miccoli, G., Gambarini, G., Testarelli, L., & Galli, M. (2019). Symmetry of root and root canal morphology of mandibular incisors: A cone-beam computed tomography study in vivo. *Journal of Clinical and Experimental Dentistry*, *11*(6), e527.
28. Verma, G. R., Bhadage, C., Bhoosreddy, A. R., Vedpathak, P. R., Mehrotra, G. P., Nerkar, A. C., ... & Chaubey, S. (2017). Cone beam computed tomography study of root canal morphology of permanent mandibular incisors in Indian subpopulation. *Polish Journal of Radiology*, *82*, 371-375.
29. Vertucci, F. J. (1984). Root canal anatomy of the human permanent teeth. *Oral surgery, oral medicine, oral pathology*, *58*(5), 589-599.
30. Vertucci, F. J. (2005). Root canal morphology and its relationship to endodontic procedures. *Endodontic topics*, *10*(1), 3-29.
31. Weine, F. S., Healey, H. J., Gerstein, H., & Evanson, L. (1969). Canal configuration in the mesiobuccal root of the maxillary first molar and its endodontic significance. *Oral surgery, oral medicine, and oral pathology*, *28*(3), 419–425. https://doi.org/10.1016/0030-4220(69)90237-0

تقييم شكل قناة الجذر للقواطع السفلية في مجموعة فرعية من سكان المملكة العربية السعودية باستخدام التصوير الاشعاعي المخروطي المحوسب CBCT

احمد حسن جبلي وهيمنت رامش شوراسيا ومحمد يحيى طروش وهاشم أحمد بجوي ونزار محمد بريك

قسم اصلاح الأسنان، جامعة جازان

عبدالعزيز حسن الشهري و مازن يحيى أبو حاوي

وزارة الصحة

الملخص

الهدف: تحديد شكل قناة الجذر للقواطع السفلية الدائمة في مجموعة سكانية فرعية في المملكة العربية السعودية باستخدام تصوير المقطعي المحوسب ذو الحزمة المخروطية

المواد والطرق

تم فحص أشعة مقطعية لـ ١٠٠ مريض لديهم ٤٠٠ قاطع سفلي دائم ، تتراوح أعمارهم بين ١٥-٥٠ سنة ، المستوفين للمعايير اللازمة لاجراء الدراسة.

لاختبار الارتباط بين عدد الجذور وقنوات الجذر وتكوينات القناة .Chi-square تم استخدام اختبار .لاختبار الموثوقية بين الفاحصين و عند الفاحصين أنفسهمKappa كما تم استخدام اختبار

النتائج:

معظم القواطع السفلية المركزية (الثنايا) والجانبية (الرباعية) تحتوي على قناة واحدة. كان معدل التواجد الإجمالي لقناتين في القواطع السفلية ٣٧%

وبحسب الجنس بلغت نسبة تواجد قناتين بين الذكور ٦٢,٨٪ 37.2 (p <0.05٪ بينما بلغت بين الإناث كان أكثر تكوين لقناة الجذر شيوعًا لقواطع الفك السفلي هو النوع الأول ، يليه النوع الثالث لتصنيف Vertucci

الاستنتاجات:

هناك قناتان بنسبة عالية في الأسنان القواطع السفلية للمجموعة السكانية الفرعية في المملكة العربية السعودية التي عمل الدراسة عليها، وبالتالي يجب أخذها في الاعتبار أثناء إجراء علاج عصب الأسنان.

الكلمات المفتاحية: التصوير المقطعي المحوسب ذو الحزمة المخروطية ، القواطع السفلية ، مورفولوجيا قناة الجذر ، سكان المملكة العربية السعودية .

Myricetin and Dihydromyricetin Mechanisms Associated with Autophagy Signaling in Several Experimental Disease Models

Rayan A. Ahmed, PhD[1*]

[1]Jazan University, College of Pharmacy, Department of Pharmacology and Toxicology, Kingdom of Saudi Arabia

Abstract

Natural substances have long been influential allies in fighting numerous diseases. Consumable vegetables, fruits, and herbs are abundant sources of flavonoids. Flavonoids are natural polyphenolic compounds that contain myricetin (MYR) and dihydromyricetin (DMY). These two compounds are recommended as dietary supplements for good health. MYR and DMY have numerous therapeutic benefits against viruses, bacteria, inflammation, cancer, and diabetes. However, little is known about their roles in autophagy and cellular death. Nowadays, searching for other therapeutic applications of MYR and DMY has received considerable attention. Autophagy is an early and reversible process that is one of the body's defense mechanisms to induce cell death or protection. It is reported in research articles that MYR and DMY were able to regulate several signaling pathways, including autophagy. For example, MYR and DMY managed several types of cancer, diabetic nephropathy, diabetic cardiomyopathy, alcoholic liver disease, and aging through autophagy-associated signaling transduction. Therefore, MYR and DMY combine favorable opportunities for further research associated with autophagy, trying to explore their roles in other pathological conditions. This review demonstrated the physicochemical and pharmacological characteristics of MYR and DMY and their potential molecular mechanisms of action, emphasizing autophagy in several disease models. This work will provide a solid base to start new projects exploring other potential molecular mechanisms of MYR and DMY, which are associated with autophagy.

Keywords: flavonoids, myricetin, dihydromyricetin, autophagy

1. Introduction

Natural products, an example of flavonoids, are novel, safe, and efficient medicinal agents(Kumar & Pandey, 2013). According to their chemical structure, flavonoids can be classified into numerous subgroups, six of which are regularly present in food, including (catechins, flavonoids, flavanones, flavonols, isoflavones, and anthocyanins). Flavonols differ from other subclasses by containing ketone and 3'-hydroxyl groups on their C ring structure(Kumar & Pandey, 2013). The most prevalent substances among the flavanols subclass are quercetin and kaempferol(Guven et al., 2019). Among all classes and subclasses of flavonoids, the focus of this review will be mainly on myricetin (MYR) and dihydromyricetin (DMY). The goal of this review article is to set the stage for future research by compiling data on the functions of MYR and DMY in autophagy in serveral disease models.

2. Myricetin

Myricetin (MYR) is a natural agent but can also be chemically synthesized. It is well known for its nutraceutical benefits(Taheri et al., 2020). Myricetin can be extracted from a broad spectrum of fruits, vegetables, and plants, such as berries, coffee, tea, red wine, beans, onions, grapes, and broccoli(Semwal et al., 2016). About two centuries ago, and for the first time, MYR was discovered in Myricaceae(Agraharam et al., 2022; Taheri et al., 2020). Additionally, myricetin is mainly produced by members of the families such as Anacardiaceae, Polygonaceae, Pinaceae, and Primulaceae(Imran et al., 2021). It is documented that the daily consumption of myricetin is less than 1.1 milligrams for men and 1 milligram for women(Lin et al., 2006).

Myricetin is a polyphenolic molecule (3, 3, 4, 5, 5, 7-hexahydroxy flavone). It exhibits structural similarities to other phenolic compounds such as morin, quercetin, fisetin, and kaempferol. Myricetin structure contains heterocyclic pyran ring "C" connects the two aromatic rings "A & B"(figure 1)(Panche et al., 2016). Six hydroxyl groups exist on these rings, which form (glycoside linkage) as (myricetin-3-O-(3″-acetyl)-L arabinosid)(Semwal et al., 2016). The hydroxyl groups participate in an oxidation-redox reaction(Sadžak et al., 2020).

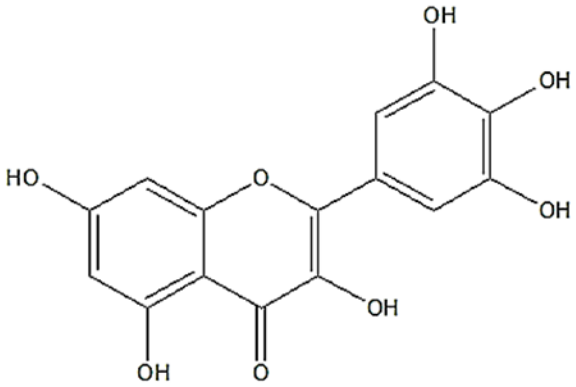

Figure 1. Myricetin (MYR) structure shows several (OH) functional groups on A, B, and C rings

Regarding the physicochemical properties of MYR, summarized in (table 1), ($C_{15}H_{10}O_8$) is the molecular formula of MYR. Myricetin has a molecular mass of 318.23 g/mol. It is extracted as a pale-yellow color and a solid form (crystal).

Table 1. Myricetin (MYR) physicochemical properties.

Myricetin (MYR)	
Molecular Formula	$C_{15}H_{10}O_8$
Synonyms	Cannabiscetin, Myricetol
Molecular Mass	(318.23) gram/mole
Color/Form	Solid crystalline, yellow powder
Boiling Point	747.63°C
Melting Point	357°C
Solubility	-Dissolves in alcohol (easily) (Barely) dissolves in boiling water -Insolvable in chloroform and acetic acid
Chemical Safety	Irritant

Myricetin is absorbed via the digestive system and primarily subjected to a hepatic metabolism forming 3, 5 dihydroxyphenylacetic acid as a metabolite. Then it is eliminated through the kidney.

Having more phenolic hydroxyl groups than other flavonoids, such as quercetin, kaempferol, catechin, and rutin, MYR is more effective in terms of antioxidant capacity. Generally speaking, MYR induces fewer pharmacological effects than dihydromyricetin (DMY). On the other hand, myricetin exhibits a broad spectrum of functions, such as its effects against Alzheimer's and Parkinson's as a degeneration disorder of the nervous system. In addition, it has been claimed in many research papers that MYR induces anti-proliferative anti-apoptotic, and anti-aging effects(Panche et al., 2016; Semwal et al., 2016; Song et al., 2021). Furthermore, myricetin plays preventive and treatment roles in various diseases such as osteoporosis, alcohol-induced fatty acid biogenesis, neurodegenerative disorders, and skin cancer. The therapeutic activities of myricetin are attributed to its potent antioxidant, iron-chelating, and scavenging free radicals characteristics(Abdolmaleki et al., 2017; Ahmad et al., 2022). Adding to the previous pharmacological effects, MYR can also produce antimicrobial activity. Furthermore, it has been recently documented that MYR plays a role in bone remodeling, fatty liver disease (non-alcohol induced), diabetic eye conditions, stomach injuries, wound

healing, cellular autophagy, and epigenetic modulations.

At the cellular level, MYR inhibits the oncoprotein Akt/PKB (protein kinase B) and MEK, besides Janus kinase and STAT transcription factor signaling. Myricetin (natural or synthetic) forms are potent telomerase inhibitors and could suppress p65 and telomerase reverse transcriptase (TERT) expression in breast cancer. Besides, it induced caspase 3 activity, which is an apoptotic protein.

Myricetin is known to be acceptable for human ingestion and has an excellent safety profile(Wu et al., 2017). Several experimental models have extensively studied MYR. However, only some researchers have raised questions about MYR's potential adverse effects. Moreover, MYR did not cause adverse effects or fatalities in mice (1000 milligrams per kilogram orally). In addition, administration of MYR at levels greater than 100 mg/kg (LD50 value) had no harmful effects on zebrafish. However, it might be cytotoxic at a high dose (450 μM)(Canada et al., 1989; Semwal et al., 2016).

To brighten the future of MYR, hard work and extensive research should be conducted on the following three points:

A. Researchers should try to induce synergistic effects by combining three flavonoids (kaempferol, MYR, and quercetin).
B. Researchers should try to explore the mechanisms of action extensively and find its exact cellular targets.
C. Researchers should try to enhance the pharmacokinetic parameters and the therapeutic applications of flavonoids by generating new formulations, such as encapsulating the drug inside the liposomes or making structural alterations.

3. Dihydromyricetin

Dihydromyricetin (DMY), often referred to as Aampelopsin(Li et al., 2017), is a naturally occurring flavonoid obtained from the Ampelopsis Michx and Ampelopsis Grossedentata plants, which are cultivated extensively in the Southern parts of China and consumed by Yao Chinese people(Li et al., 2017). In 1940, Kotake and Kubota extracted DMY for the first time from Ampelopsis Meliaefolia and Ampelopsis Drossedentata, which was later revealed to have a substantial amount of DMY(Yousheng et al., 2001). Moreover, it has been documented that the DMY content in the specific plant was intensely larger than the amount of MYR (1.5–3.0, 20–30% w/w), respectively.

Dihydromyricetin is also a polyphenolic compound with minor differences compared to MYR (figure 2). As DMY's (2, 3-double bond) is hydrogenated during oxidation, the MYR is formed (Wu et al., 2017).

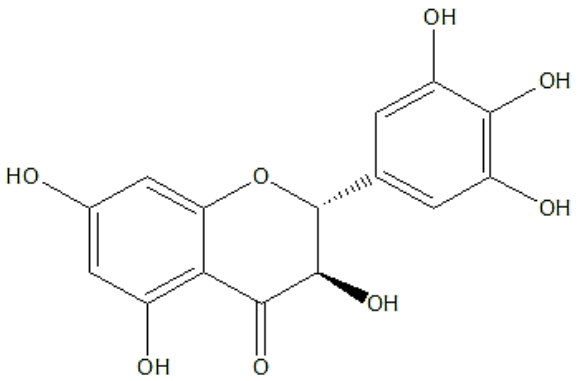

Figure 2. The structure of dihydromyricetin (DMY) shows several (OH) functional groups on A, B, and C rings.

The physical and chemical characteristics of DMY are illustrated in (table 2). Dihydromyricetin's molecular mass is around 320.25 g/mol, and its chemical formula is $C_{15}H_{12}O_8$. It is extracted as a white color and in a solid form. This substance has recently gained considerable attention because mounting evidence reveals its potent inhibition of numerous pathological conditions. However, the potential therapeutic applications are limited by a few factors, such as the weak bioavailability of polyphenolic substances due to their poor stability, structure, transmembrane capacity, low solubility, and fast metabolism. Numerous studies have revealed that polyphenols have a low oral bioavailability(J. Zhang et al., 2018). The instability of (DMY) is one factor associated with low bioavailability, mainly due to multi-(OH) functional groups in its structure. Regarding solubility, (DMY) is insoluble in water and more soluble and bioavailable as temperature rises, from (.2) milligram per milliliter at room temperature to (.9) milligram per milliliter at body temperature(Ruan et al., 2005). Dihydromyricetin is also soluble in DMSO and ethanol.

Table 2. Dihydromyricetin (DMY) physicochemical properties.

Dihydromyricetin (DMY)	
Molecular Formula	$C_{15}H_{12}O_8$
Synonyms	Ampeloptin
Molecular Mass	(320.25) gram/mole
Color/Form	Solid, white powder
Boiling Point	780.7±60.0°C
Melting Point	239-241°C
Solubility	-Water insoluble -Soluble in ethanol and DMSO
Chemical Safety	Safe

According to pharmacological effects, DMY has diverse effects such as antioxidant, anti-hypertensive, anticancer, and antimicrobial (bacteria, viruses) besides its roles in inflammation, free radical scavenging, anorexiant, antifatigue activities, anti-photo-aging, antiallergic, antiacne properties(Liu et al., 2017; J. Zhang et al., 2018), antiatherosclerosis, cardioprotective, dermo-protective, hepatoprotective, neuroprotective, and enhanced mesenchymal stem cells viability. It also plays a part in managing obesity, alcohol disorders, osteoporosis, and asthma with no effect on normal cells. Dihydromyricetin also prevents weight gain development and hyperlipidemia. Furthermore, DMY is utilized in managing and preventing nephritis, hepatitis, halitosis, and polyorexia with minimal toxic effects(Li et al., 2017).

In terms of cell signal transduction, numerous research revealed that DMY has a role in controlling inflammation and preventing apoptosis besides its anti-oxidative role. Dihydromyricetin induces its therapeutic effects via regulating several genes, transcription factors, and proteins, including (ABCA1, PPARγ, NF-κβ, MAPK, AMPK, Akt, Nrf2) which contribute to oxidative stress, cell death, and inflammatory pathways.

Despite flavonoids' huge spectrum of biological functions, one essential concern must be considered, which is the safety profile. Because flavonoids are typically found in healthy diets and utilized as traditional medicine, research into their potentially harmful impacts has got more attention. Therefore, dihydromyricetin's toxicological effects have been examined in various studies. For example, safety testing was conducted on Ampelopsis Grossedentata extract (tea) containing substantial quantities of DMY. This extract of Ampelopsis Grossedentata was claimed to be harmless and enhanced mice's immune reaction, as evidenced by the results of the 90-day feeding test, genetic toxicity test, and acute toxicity test(Zhao et al., 2009; Zheng, 2003). However, the overall flavone content of Ampelopsis Grossedentata is hazardous over the long term., The long-term and continuous dosing of DMY had no detrimental effects on the evolution and pathology, hematology, and biochemistry indices. Therefore, it has been concluded that Ampelopsis Grossedentata's total flavone (DMY) is toxicologically harmless. However, when scientists tested the DMY 's acute toxicity, they found that DMY was very weakly detrimental, with oral gavage rats demonstrating the highest tolerance rate at 5.0 g/kg(Min-chen, 2008).

The obstacles restricting DMY pharmacological effects and clinical uses have been tried to overcome by utilizing various delivery strategies. Scientists have investigated different formulations to enhance DMY bioavailability and solubility (aqueous and lipid phase-based formulations). Examples of tested formulations based on solid dispersion and aimed to raise lipid solubility include cyclodextrin inclusion complexes, phospholipid complexes, nanocapsule, microemulsion, co-crystallization, and chemical or enzymatic acylation. However, to increase the aqueous

solubility of DMY, nanoparticulate systems and cyclodextrin inclusion complex have been examined(Ruan et al., 2005; Vasconcelos et al.,2007).

According to this collective information, the scientists must study three significant points to see DMY in the clinic.

A. Researchers should try to explore the DMY mechanisms of action extensively and find its exact cellular targets.
B. Researchers should try to develop efficient delivery systems for DMY.
C. Researchers should try to enhance the pharmacokinetic characteristics of the molecule, like absorption, distribution, metabolism, and excretion (ADME).

4. Autophagy

The word autophagy is Greek in origin. It is divided into two parts: "auto," which stands for oneself, and "phagy," which stands for to eat. Autophagy is a highly conserved process(Chen et al., 2019) that contributes to cell death and cytoprotection, an apparent paradox. Autophagy plays an adaptive role in protecting organisms from infections, cancer, neurodegeneration, heart diseases, and aging(Levine & Kroemer, 2008). In eukaryotic cells and during the catabolic process of macroautophagy, also known as autophagy, lysosomes degrade and recycle the cytoplasmic components(Feng et al., 2014; Mizushima, 2007). According to Diaz-Villanueva et al., autophagy is recognized to be crucial not only for removing macromolecules, misfolded proteins, and damaged organelles but also has an essential role in survival, differentiation, development, and cellular homeostasis(Díaz-Villanueva et al., 2015; Feng et al., 2014; Levine & Kroemer, 2008). However, excessive autophagy causes (type II) programmed cell death because it severely degrades the mitochondria and other survival components, eventually leading to apoptosis(Doherty & Baehrecke, 2018). Moreover, autophagy is classified into three forms: (macro, micro, and chaperone-driven), distinguished by differences in their physiology and lysosomal-cargo delivery mechanisms(Levine & Kroemer,2008).

Numerous stressful conditions, including hypoxia, endoplasmic reticulum (ER) stress, and hunger, can trigger autophagy. The phagophore, an isolated dual-membrane sequestering vesicle that cells create during the autophagic process, is carried to the lysosome after evolving into the autophagosome. Then the autophagosome degrades the cell's internal cargo(Abada & Elazar, 2014). In more detail, the phagophore is formed and then expanded. Once the phagophore's edges have entirely fused, the creation of the autophagosome, a dual-membrane compartment that contains the component of the cytoplasm, forms. After that, the autolysosome is generated by merging the autophagosome with the lysosome (figure 3)(Levine & Kroemer, 2008). Moreover, the lysosome (transversal proteins) (LAMP-2/CLN3), along with the several lysosomal cathepsins (cysteine proteases), are necessary to properly fuse with the autophagosomes in mammals and the destruction of autophagosomal contents, respectively(Levine & Kroemer, 2008).

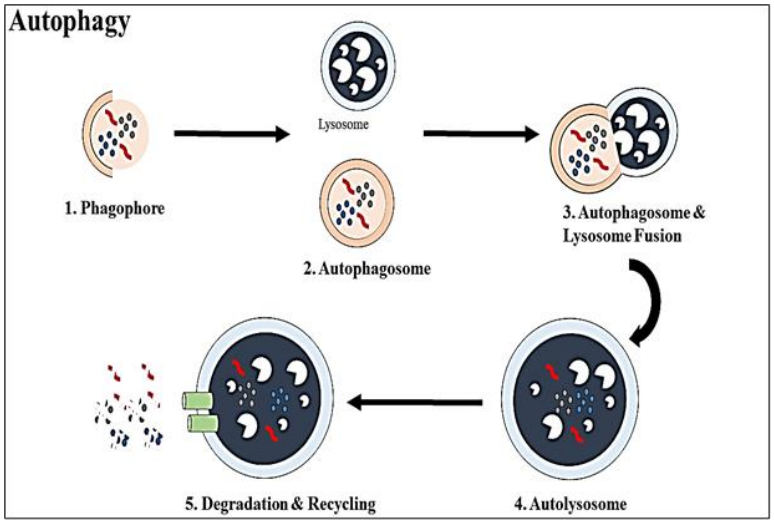

Figure 3. Five steps make up the autophagic process. **(1)** Vesicle nucleation (development of the isolated sheath/phagophore). **(2)** Vesicle extension and finishing (progress & closure). **(3)** Merging of the (autophagosome/lysosome) and degradation of autophagosome internal sheath. **(4)** Formation of the autolysosome. **(5)** Content's breakdown inside the autolysosome.

A set of proteins encoded by the autophagy-related genes (Atgs) can regulate how autophagy does its role(Pietrocola et al., 2012). Atg proteins' function is regulated by numerous cell signaling pathways such as p38-MAPK, Bax, STAT3, AMPK-LKB1, receptor tyrosine kinases induced-PI3K-AKT-mTOR(Jiménez-Mora et al., 2021; Levine & Kroemer, 2008; Xu et al., 2020; Ye et al., 2011). Specifically, mTOR enables the creation of proteins and cell growth by phosphorylating critical substrates, including S6 Kinase and 4E-BP1 (eukaryotic initiation factor 4E binding protein 1)(Kim & Guan, 2015; Laplante & Sabatini, 2012). Furthermore, mTOR regulates autophagy's initial and final phases by two distinct pathways. First,

by blocking the ULK1 complex and autophagosome biosynthesis, mTOR can prevent autophagy's initiation and progressing stage(Kim & Guan, 2015; Xu et al., 2014). Second, it is understood that lysosomal activity is inhibited by mTOR, in part, through phosphorylating TFEB, a transcription factor EB(Martina et al., 2012). However, abnormalities in autophagy have been connected to numerous sicknesses, such as cancer, inflammatory bowel disease, and

neurodegenerative diseases(Zhi & Zhong, 2015; Ziegler et al., 2022). The execution of autophagy in yeast depends on over 20 genes referred to as Atg genes(Mizushima & Klionsky, 2007). These genes produce proteins, many of which have a specific role and are known to be conserved throughout evolution (table 3).

Table 3. Atgs roles in the execution of autophagy.

Atg & Vps Protein Kinases	Classification & Function
Atg (6, 14) - Vps (15, 34)	Lipid kinase signaling complex (vesicle nucleation)
Atg (1, 13, 17)	(Serine/threonine) protein kinase complex.
Atg (8, 12)	Ubiquitin-like conjugation pathways (vesicle extension)
Atg (2, 9, 18)	Breakdown of developed autophagosomes
Atg (22)	Vacuolar permeases (outflow of amino acids from developed autophagosomes)

Moreover, autophagy can be targeted by several (inhibitors and activators) as shown in (figure 4)(Criollo et al., 2007; Maiuri et al., 2007; Rubinsztein et al., 2007). All these pharmaceuticals, though, are not autophagy pathway-specific. Even though some autophagy agents (chloroquine-lithium-rapamycin) are used in clinical practice and could be beneficial in managing illnesses related to autophagy dysregulation, silencing autophagy-related genes (Atg) by genetic techniques such as siRNA knockout could provide accurate knowledge of autophagy roles in health and disease.

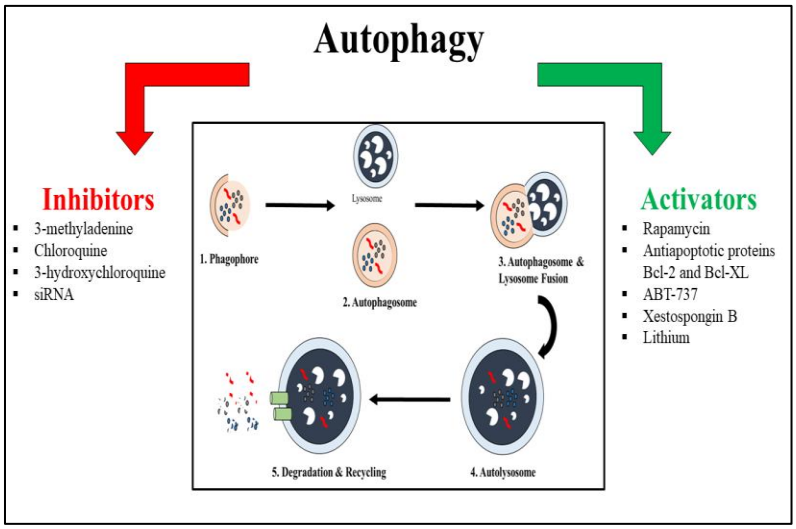

Figure 4. Several negative regulators (inhibit autophagy) and positive regulators (activate autophagy) are depicted on the left and right sides correspondingly.

Search strategies

First, we searched for the most recent literature on (PubMed and Google scholar) using these keywords (flavonoids, myricetin, dihydromyricetin, and autophagy). Then abstracts were retrieved and collected for further reading. Next, articles were sorted into separate folders to start writing the background information about the three major subtopics. After that, papers focusing on the mechanisms of myricetin and dihydromyricetin associated with autophagy in various disease models have been used to generate tables (4 & 5). In addition, other information such as doses, duration, and diseases used in those studies are included in the same tables. These two tables provide collective information for those interested in further investigating the role of myricetin (MYR) and dihydromyricetin (DMY) associated with autophagy in several disease models.

5. Myricetin and dihydromyricetin regulation of autophagy in several disease models

Tables 4 and 5 demonstrate preclinical studies of myricetin (MYR) and dihydromyricetin (DMY) associated with autophagy, respectively. These two tables list details information about MYR and DMY, starting with the preclinical study models (cell lines or animals) used, doses and length of treatment, changes in cell morphology, mechanisms of action, signaling pathways involved, and diseases managed

Table 4: Molecular mechanisms of myricetin (MYR) targeting autophagy signaling in several disease models.

Compound	Model Cell line/Animal	Dose & Duration	Role in Autophagy	Target Pathway and Mechanism of Action	Disease	References
Myricetin	-Cell line: Hep3B and HepG2 Human Hepatocyte Cancer Cells	-25, 50 μM -24 hr	Activation	-Inhibition of MARCH 1. -Regulation STAT3 and p38 MAPK signaling.	Hepatocellular carcinoma	(Yang et al., 2021)
Myricetin	-Cell line: HT-29, HCT116, SW480 and SW620 (Cancer Cells isolated from human colon and rectum)	-(50 μM or 100 μM) -48 hr	Activation	-Inhibition of (PI3K, Akt, mTOR) signaling. -Detection (LC3 I/II) (autophagy regulator: Beclin 1). -Detection number of autophagosomes.	Colorectal cancer	(Zhu et al., 2020)
Myricetin	-Cell line: HepG2 Human Hepatocyte Cancer Cells	-20, 50 uM -24 hr -10, 20, 50, 100 uM -24 hr -0, 50, 100 uM -24 hr	Activation	-Detection number of autophagosomes. -Inhibition of mTOR phosphorylation and its downstream signaling. -Detection of LC3 I/LC3 II. -Detection of crucial autophagic proteins. -Alter LC3 I from its soluble form to LC3-II, lipidated and linked with autophagosomes.	Hepatocellular carcinoma	(Cao et al., 2018)

Table 5: Molecular mechanisms of dihydromyricetin (DMY) targeting autophagy signaling in several disease models.

Compound	Model Cell line/Animal	Dose & Duration	Role in Autophagy	Target Pathway and Mechanism of Action	Disease	References
Dihydromyricetin	-Diabetic Nephropathy (DN) rat model	-100 mg/kg -10 weeks	Activation	-Reducing RIF. -Decrease levels of Col IV, α-SMA, and p62. -Increase (LC3 II/I, Beclin 1).	Diabetic Nephropathy (DN)	(Guo et al., 2020)
Dihydromyricetin	-Cell line: NRK-52E: Renal Tubular Epithelial Cells -Cell line: (HEK293): Human Embryonic Kidney	-1 μM -24 h and 48 hr	Activation	-Reducing fibrosis. -Decrease (Col IV, α-SMA, and p62). -Increase (LC3 II/I, Beclin 1). -Inhibition (Micro-RNA: miR-155-5p). -Inhibition (PI3K/AKT/mTOR pathway). -Activation of phosphatase (PTEN).	Diabetic Nephropathy (DN)	(Guo et al., 2020)
Dihydromyricetin	-Cell line: (A431): Cutaneous Squamous Cell Carcinoma	-25, 50, 100 μM -24 hr	Activation	-Increasing autophagic flux. -Increase (LC3II). -Decrease (P62/SQSTM1). -Dephosphorylation (Serine 142, which activates TFEB). -Nuclear translocation of TFEB is activated. -Enhancing TFEB reporter activity associated with expression of Atg genes & subsequent induction of the (Atg 5, MAP1LC3B, UVRAG, ATP6V0D1, LAMP1, and CTSB) mRNA of autophagic cell death. -Reducing lncRNA MALAT1 level, which is high level, reversed	Cutaneous Squamous Cell Carcinoma	(Tan et al., 2019)

				the activity of DMY on TFEB-dependent autophagy. -Excessive autophagy-associated cell death is induced, driven by the MALAT1-TFEB signaling.		
Dihydromyricetin	-Mice: C57BL/6	-at 75 and 150 milligrams per kilogram oral dosage every day for six weeks	Activation	-Activate (Keap-1/Nrf2, reactive oxygen species (ROS)-NF-kβ, MALAT1-TFEB) signaling (+ feedback effect).	Alcoholic Liver Disease (ALD	(Guo et al., 2020)
Dihydromyricetin	-Cell line: HepG2: Human Hepatocyte Cancer Cells	-5, 10, 25, 50 μM -6, 12, 24, 48 hr	Activation	-Inhibit growth. -Detection of autophagolysosome containing degraded cellular content. -mTOR role in regulating protein-kinases (ERK1/2), AMPK & (class III) PKB: (PI3K/PDK 1/Akt) signaling. -Diffusion of LC3 largely to punctate structures. -Detection of lysosomal-rich acidic compartments by (LysoTracker Red staining).	Hepatocellular Carcinoma	(Xia et al., 2014)
Dihydromyricetin	-Cell line: (SK-MEL-28): Human Melanoma Cells	-25-, 50, 100 μM -24 hr	Activation	-Increase NF-*κ*B phosphorylation induced by ROS.	Melanoma	(Zhou et al., 2017)
Dihydromyricetin	-Mice: STZ-induced diabetic C57BL/6 mice	-100 milligrams per kilogram per day -14 weeks	Activation	-Decrease (p62 and caspase 3,9). -Increase (Beclin 1, Atg 7, Bcl 2, LC3 II/I proportion).	Diabetic Cardiomyopathy	(Wu et al., 2017)
Dihydromyrice	-Cell line:	-5, 10, 25, 50	Activati	-Raising the activity of AMPK &	Suppressing	(Xia et al.,

tin	HepG2: Human Hepatocyte Cancer Cells	µM -6, 12, 24, 48 hr	on	lowering the concentrations of phosphorylated (ERK1/2 & Akt), as mTOR is suppressed. -Increasing the mRNA of Atg genes (Atg 5, Atg 12) & (LC3, BECN1).	apoptosis in hepatic cells	2014)
Dihydromyricetin	-Cell line: Cal27: Head and Neck Squamous Cell Carcinoma (HNSCC)	-12.5, 25, 50 µM -6, 12, 24 h	Activation	-Generating ROS to cause STAT3 to become phosphorylated and activated, which induces autophagy. -Increase autophagic markers (Beclin1, LC3, p62).	Squamous Cell Carcinoma isolated from (Head & Neck) of a human (HNSCC)	(Fan et al., 2016)
Dihydromyricetin	-Rats: Del rat with D-gal-induced brain aging revealing miR34a expression	-100, 200 milligrams per kilogram oral dosage every day for six weeks	Activation	-Increase levels of sirtuins (SIRT1). -Reduced mTOR signaling by miR-34a downregulation. -Reduce (miR-34a, p53/p21 signaling), both triggered by D-galactose (D-gal). -Inducing the phosphorylation of mTOR serine (2448) amino acid.	Aging	(Kou et al., 2016)

Concluding remarks

Autophagy is a highly preserved mechanism involved in cell hemostasis (survival and death). However, autophagy contributes to the initiation and development of certain disorders, including infections, tumor formation, neurodegeneration, aging, and several cardiac conditions. Additionally, the flavonoids myricetin (MYR) and dihydromyricetin (DMY) have many therapeutic benefits associated with regulating several cellular pathways, including autophagy. This paper compiles information about MYR and DMY roles in autophagy to establish a framework for future research. Pharmacologically speaking, flavonoids (MYR and DMY) are fascinating molecules that play protective functions in several diseases. However, additional mechanistic and toxicological investigations on myricetin (MYR) and dihydromyricetin (DMY) are required to expedite preclinical or experimental research toward commercially available formulas.

A list of abbreviations & symbols

(ALD)	Alcoholic liver disease
(α-SMA)	Alpha-smooth muscle actin
(ABCA1)	ATP-binding cassette (ABC) transporters
(ATP6V0D1)	ATPase H+Transporting V0 Subunit D1
(Bax)	Apoptosis regulator
(Atg)	Autophagy-related genes
(CTSB)	Cathepsin B
(Col IV)	Collagen IV
(p21)	Cyclin-dependent kinase inhibitor 1
(C57BL/6)	C57 black 6 mice
(DN)	Diabetic nephropathy
(DMY)	Dihydromyricetin
(DMSO)	Dimethyl sulfoxide
(ER)	Endoplasmic reticulum
(OH)	Hydroxyl function group
(JAK)	Janus kinase
(lncRNA)	Long non-coding RNA
(LKB1)	Liver kinase B1
(LAMP2)	Lysosome-associated membrane protein 2
(CLN3)	Lysosomal/endosomal transmembrane protein, battenin
(mTOR)	Mammalian target of rapamycin
(MARCH1)	Membrane-associated ring finger
(MALAT1)	Metastasis-associated lung adenocarcinoma transcript
(miR)	miRNA proinflammatory & oncogene
(MYR)	Myricetin
(PTEN)	Phosphatase and tensin homolog
(PI3K)	Phosphoinositide 3-kinases
(PE)	Phosphorylated with ethanolamine
(RIF)	Renal interstitial fibrosis
(p62/SQSTM1)	Sequestosome 1
(siRNA)	Small-interfering RNA
(STZ)	Streptozocin
(S6K)	S6 kinase

(TERT)	Telomerase reverse transcriptase
(p65)	Transcription factor, a subunit of NF-κB
(TFEB)	Transcription factor EB
(g/mol)	gram/mole
(hr)	Hour
(LD50)	Lethal dose 50
(mg)	Milligram
(mg/kg)	Milligram per kilogram
(μM)	Micromolar
(ml)	Milliliter
(w/w)	Weight by weight

Funding
There are no grants of any type supporting this publication.

Declaration of interest
None.

Ethical approval
This paper did not require ethical approval because it is a review paper.

References

Abada, A., & Elazar, Z., (2014). "Getting ready for building: signaling and autophagosome biogenesis." In *EMBO Rep.*, 15(8). Available at: https://doi.org/10.15252/embr.201439076

Abdolmaleki, F., et al., (2017). "The Effect of Myricetin Flavonoid on the Expression of Fyn Gene in Melanoma Cells (A375)". In *BHS, Bioinformatics*.

Agraharam, G., et al., (2022). "Myricetin: a Multifunctional Flavonol in Biomedicine." In *Curr. Pharmacol. Rep*. (Vol. 8, Issue 1). 48–61. https://doi.org/10.1007/s40495-021-00269-2

Ahmad, B., et al., (2022). "Myricetin (3,3′,4′,5,5′,7 hexahydroxyflavone) prevents ethanol-induced biochemical and inflammatory damage in the liver of Wistar rats". In *Hum Exp Toxicol*, 41. https://doi.org/10.1177/09603271211066843

Canada, T., et al., (1989). "The toxicity of flavonoids to guinea pig enterocytes." In *Toxicol. Appl. Pharmacol*., 99(2). https://doi.org/10.1016/0041-008X(89)90018-5

Cao, J., et al., (2018). "Myricetin Induces Protective Autophagy by Inhibiting the Phosphorylation of mTOR in HepG2 Cells". In *Anat. Rec*, 301(5). 786–795. https://doi.org/10.1002/ar.23754

Chen, R., et al., (2019). "Autophagy promotes aortic adventitial fibrosis via the IL-6/Jak1 signaling pathway in Takayasu's arteritis". In *J. Autoimmun*., 99. Available at: https://doi.org/10.1080/10408398.2016.1196334

Chua, S., et al., (2011). "Flavonoids and phenolic acids from Labisia pumila (Kacip Fatimah)." In *Food Chem.*, 127(3). Available at: https://doi.org/10.1016/j.foodchem.2011.01.122

Criollo, A., et al., (2007). "Regulation of autophagy by the inositol trisphosphate receptor." In *Cell Death Differ*, 14(5). https://doi.org/10.1038/sj.cdd.4402099

Díaz-Villanueva, F., et al., (2015). "Protein folding and mechanisms of proteostasis." In *Int. J. Mol. Sci.* (Vol. 16, Issue 8). Available at: https://doi.org/10.3390/ijms160817193

Doherty, J. & Baehrecke, H. (2018). "Life, death and autophagy." In *Nat. Cell Biol* (Vol. 20, Issue 10). Available at: https://doi.org/10.1038/s41556-018-0201-5

Fan, F., et al., (2016). "Dihydromyricetin promotes autophagy and apoptosis through ROS-STAT3 signaling in head and neck squamous cell carcinoma". In *Oncotarget*, 7(37). https://doi.org/10.18632/oncotarget.10836

Feng, Y., et al., (2014). "The machinery of macroautophagy." In *Cell Res.*, (Vol. 24, Issue 1). https://doi.org/10.1038/cr.2013.168

Guo, L., et al., (2020). "Dihydromyricetin promotes autophagy and attenuates renal interstitial fibrosis by regulating miR-155-5p/PTEN signaling in diabetic nephropathy". In *BJBMS*, 20(3). 372–380. https://doi.org/10.17305/bjbms.2019.4410

Guven, H., et al., (2019). "Flavonoids in Our Foods: A Short Review." In *JBACHS*. https://doi.org/10.30621/jbachs.2019.555

Imran, M., et al., (2021). "Myricetin: A comprehensive review on its biological potentials." In *Food Sci. Nutr.* (Vol. 9, Issue 10). https://doi.org/10.1002/fsn3.2513

Jiménez-Mora, E., et al., (2021). "V600e BRAF inhibition induces cytoprotective autophagy through AMPK in thyroid cancer cells". In *Int. J. Mol. Sci.*, 22(11), 6033. https://doi.org/10.3390/ijms22116033

Kim, C., & Guan, L., (2015). "MTOR: A pharmacologic target for autophagy regulation." In *J. Clin. Investig.* (Vol. 125, Issue 1). https://doi.org/10.1172/JCI73939

Kou, X., et al., (2016). "Ampelopsin attenuates brain aging of D-gal-induced rats through miR-34a-mediated SIRT1/mTOR signal pathway". In *Oncotarget*, 7(46). https://doi.org/10.18632/oncotarget.12811 Kumar, S., & Pandey, K., (2013). "Chemistry and biological activities of flavonoids: An overview." In *Sci. World J.*, (Vol. 2013).

Laplante, M., & Sabatini, M., (2012). "MTOR signaling in growth control and disease." In *Cell*, (Vol. 149, Issue 2). https://doi.org/10.1016/j.cell.2012.03.017

Levine, B., & Kroemer, G., (2008). "Autophagy in the Pathogenesis of Disease." In *Cell*, (Vol. 132, Issue 1). https://doi.org/10.1016/j.cell.2007.12.018

Li, H., et al., (2017). "The Versatile Effects of Dihydromyricetin in Health." In *Evid.-based Complement. Altern. Med.*, (Vol. 2017). https://doi.org/10.1155/2017/1053617

Lin, J., et al., (2006). "Flavonoid intake and colorectal cancer risk in men and women." In *Am. J. Epidemiol.*, 164(7). https://doi.org/10.1093/aje/kwj296

Liu, D., et al., (2019). "Dihydromyricetin: A review on identification and quantification methods, biological activities, chemical stability, metabolism, and approaches to enhance its bioavailability." In *Trends Food Sci. Technol.*, (Vol. 91). https://doi.org/10.1016/j.tifs.2019.07.038

Liu, L., et al., (2017). "Determination of dihydromyricetin in rat plasma by LC-MS/MS and its application to a pharmacokinetic study." In *Pharm. Biol.*, 55(1). https://doi.org/10.1080/13880209.2016.1266669

Maiuri, C., et al., (2007). "Functional and physical interaction between Bcl-XL and a BH3-like domain in Beclin-1". In *EMBO J.*, 26(10). https://doi.org/10.1038/sj.emboj.7601689

Martina, A., et al., (2012). "MTORC1 functions as a transcriptional regulator of autophagy by preventing nuclear transport of TFEB". In *Autophagy*, 8(6). https://doi.org/10.4161/auto.19653

Min-chen, W., (2008). "Study on Biological Efficacy of Dihydromyricetin." In *Food Sci.* 622-625.

Mizushima, N., (2007). "Autophagy: Process and function." In *Genes Dev.*, (Vol. 21, Issue 22). 2861–2873. https://doi.org/10.1101/gad.1599207.eralize

Mizushima, N., & Klionsky, J., (2007). "Protein turnover via autophagy: Implications for metabolism." In *Annu. Rev. Nutr.*, (Vol. 27). https://doi.org/10.1146/annurev.nutr.27.061406.093749

Panche, N., et al., (2016). "Flavonoids: An overview." In *J. Nutr. Sci.*, (Vol. 5). https://doi.org/10.1017/jns.2016.41

Pietrocola, F., et al., (2012). "Pro-autophagic polyphenols reduce the acetylation of cytoplasmic proteins." *Cell Cyc.*, 11(20). https://doi.org/10.4161/cc.22027

Qiu, P., et al., (2017). "Dihydromyricetin modulates p62 and autophagy crosstalk with the Keap-1/Nrf2 pathway to alleviate ethanol-induced hepatic injury". In *Toxicol. Lett.*, 274. https://doi.org/10.1016/j.toxlet.2017.04.009

Ruan, P., et al., (2005). "Improving the solubility of ampelopsin by solid dispersions and inclusion complexes." In *J. Pharm. Biomed. Anal*,38(3). https://doi.org/10.1016/j.jpba.2005.01.030

Rubinsztein, C., et al., (2007). "Potential therapeutic applications of autophagy." In *Nat. Rev. Drug Discov*, (Vol. 6, Issue 4). https://doi.org/10.1038/nrd2272

Sadžak, A., et al., (2020). "The structural integrity of the model lipid membrane during induced lipid peroxidation: The role of flavonols in the inhibition of lipid peroxidation." In *Antioxid.*, 9(5). https://doi.org/10.3390/antiox9050430

Semwal, K., et al., (2016). "Myricetin: A dietary molecule with diverse biological activities." In *Nutrients*, (Vol. 8, Issue 2). https://doi.org/10.3390/nu8020090

Song, X., et al., (2021). "Myricetin: A review of the most recent research." In *Biomedicine and Pharmacotherapy*, (Vol. 134).

Taheri, Y., et al., (2020). "Myricetin bioactive effects: Moving from preclinical evidence to potential clinical applications." In *BMC complement. med. ther.*, (Vol. 20, Issue 1). https://doi.org/10.1186/s12906-020-03033-z

Tan, M., et al., (2019). "Dihydromyricetin induced lncRNA MALAT1-TFEB-dependent autophagic cell death in cutaneous squamous cell carcinoma". In *J. Cancer*, 10(18). 4245–4255. https://doi.org/10.7150/jca.32807

Vasconcelos, T., et al., (2007). "Solid dispersions as strategy to improve oral bioavailability of poor water-soluble drugs." In *Drug Discov*, (Vol. 12, Issues 23–24). 1068–1075. https://doi.org/10.1016/j.drudis.2007.09.005

Wu, B., et al., (2017). "Dihydromyricetin Protects against Diabetic Cardiomyopathy in Streptozotocin-Induced Diabetic Mice." In *Biomed Res.* Int., 2017. https://doi.org/10.1155/2017/3764370

Xia, J., et al., (2014). "Dihydromyricetin induces autophagy in HepG2 cells involved in inhibition of mTOR and regulating its upstream pathways". In *Food Chem. Toxicol*, 66.

Xu, K., et al., (2014). "MTOR signaling in tumorigenesis". In *Acta Rev Cancer*, (Vol. 1846, Issue 2). https://doi.org/10.1016/j.bbcan.2014.10.007

Xu, Z., et al., (2020). "Targeting PI3K/AKT/mTOR-mediated autophagy for tumor therapy". In *Appl. Microbiol. Biotechnol.* (Vol. 104, Issue 2).

Yang, W., et al., (2021). "Myricetin Induces Autophagy and Cell Cycle Arrest of HCC by Inhibiting MARCH1-Regulated Stat3 and p38 MAPK Signaling Pathways". In *Front. pharmacol*, 12. https://doi.org/10.3389/fphar.2021.709526

Ye, C., et al., (2011). "TNFα-induced necroptosis and autophagy via supression of the p38-NF-κB survival pathway in L929 cells". In *J.* Pharmacol. Sci., 117(3). https://doi.org/10.1254/jphs.11105FP

Yousheng, Z., et al., (2001). "Basic constituent of Ampelopsis grossedentata". *Nat. Prod. Res. Dev.*, 13(5). 46-48.

Zhang, J., et al., (2018). "Recent update on the pharmacological effects and mechanisms of dihydromyricetin." In *Front. pharmacol*, 9. https://doi.org/10.3389/fphar.2018.01204

Zhao, L., et al., (2009). "Antioxidant and cytotoxic activity of dihydromyricetin from: Ampelopsis Grossedentata leaves." In *Agro Food ind. Hi-Tech*, 20(3).

Zheng, Z., (2003). "The Rat Chronic Toxicity Test of Total Flavone of Ampelopsis grossedentata from Guangxi". In *Lishizhen Medicine and Materia Medica Res.* 193-195.

Zhi, X., & Zhong, Q. (2015). "Autophagy in cancer." In *F1000 Prime Rep.*, 7. https://doi.org/10.1038/cddis.2013.422

Zhou, Z., et al., (2017). "Dihydromyricetin induces apoptosis and cytoprotective autophagy through ROS-NF-κB signalling in human melanoma" cells. In *Free Radic. Res.,* 51(5). 517–528. https://doi.org/10.1080/10715762.2017.1328552

Zhu, L., et al., (2020). "Myricetin induces apoptosis and autophagy by inhibiting PI3K/Akt/mTOR signalling in human colon cancer cells". In *BMC complement. med. ther.*,20(1). 209. https://doi.org/10.1186/s12906-020-02965-w

Ziegler, V., et al., (2022). "The intricate interplay between cell cycle regulators and autophagy in cancer." In *Cancers*, (Vol. 14, Issue 1). 153. https://doi.org/10.3390/cancers14010153

آليات عمل عقار الميريسيتين والميريسيتين ثنائي الهيدروجين المترتبط بمسار الإلتهام الذاتي في الخلية لعدة نماذج مخبرية مرضية

ريان عبد الباسط أحمد[1]*

[1]جامعة جازان، كلية الصيدلة، قسم علوم الأدوية والسموم ، جيزان، المملكة العربية السعودية

الملخص

تعتبر المواد الطبيعية حليفًا فعالًا في مكافحة العديد من الأمراض فعلى سبيل المثال تحتوي الفواكه والخضروات والأعشاب المستهلكة من قبل الإنسان على العديد من المركبات تسمى "فلافونويد". تحتوي هذه الفلافونويد على مركبات طبيعية بوليفينولية تعرف بالميريستين MYR والميريسيتين ثنائي الهيدروجين DMY والتي يوصى باستخدامها كمكملات غذائية للحصول على صحة جيدة. من المعروف أن لهذه المواد تأثيرات علاجية عديدة كمضادات للأكسدة، مضادات للسرطان، مضادات للعدوى البكتيرية والفيروسية، مضادات لارتفاع نسبة سكر الدم. إلا أنه لازال هناك الكثير من الغموض حول دورهما في عملية الالتهام الذاتي والموت الخلوي. نتيجةً لذلك، يجري البحث حاليًا على اكتشاف تطبيقات علاجية أخرى للMYR وDMY. الالتهام الذاتي هو عملية مبكرة وقابلة للعكس وهي إحدى آليات الدفاع لجسم الانسان ضد موت الخلايا المبرمج. فيما يتعلق بالمسارات الخلوية وطرق نقلها، تم نشر العديد من الأبحاث الطبية والتي تؤكد دور MYR و DMY التنظيمي للعديد منها، متضمنةً الالتهام الذاتي. فعلى سبيل المثال تم إثبات دور ال MYR وDMY في التحكم بأنواع عدة من السرطانات، أمراض الكلى والقلب الناشئة عن ارتفاع سكر الدم، الأمراض الكبدية الناشئة عن استخدام المشروبات الكحولية والشيخوخة وذلك عن طريق الاتصالات الخلوية الناتجة عن الالتهام الذاتي. تشكل هذه المركبات الطبيعية فرصًا مواتية لمزيد من البحث المتعلق بالالتهام الذاتي والأمراض المتعلقة به في محاولة لاكتشاف طرق أخرى لعمل هذه المركبات. شملت هذه المراجعة على معلومات محددة عن الخصائص الفيزيائية والكيميائية والدوائية لل MYR وDMY، إضافة إلى آليات عملهما المحتملة على المستوى الجزيئي الخلوي، مع التركيز على دورهما في عملية الالتهام الذاتي وذلك على عدة نماذج مخبرية مرضية. يعول على هذا العمل أن يكون مرجعًا متكاملًا لبدء مشاريع جديدة تهدف إلى استكشاف الآليات الجزيئية المحتملة لـ MYR وDMY والمرتبطة بالالتهام الذاتي.

الكلمات المفتاحية: فلافونويد، الميريسيتين، الميريسيتين ثنائي الهيدروجين، الإلتهام الذاتي.

Assessment of marginal integrity and load bearing capacity of class II restorations with direct biomineralizing restoratives

Thilla Sekar Vinothkumar
Department of Restorative Dental Sciences, Division of Operative Dentistry,
College of Dentistry, Jazan University

Abstract

Aim: This invitro study investigated the marginal integrity and load bearing capacity of conservative class II restorations using three different biomineralizing restoratives.

Materials: Forty extracted permanent maxillary premolars were subjected to conservative class II mesio-occlusal tooth preparation and received restorations with three different biomineralizing restoratives; Surefill One (SO), Activa (ACT), Cention N (CN) and a control; Tetric N-Ceram (TC). After thermomechanical ageing equivalent to 1 year, the samples were evaluated for marginal integrity under scanning electron microscope (SEM) and fracture resistance on a Universal Testing Machine. Fracture patterns were categorised as favourable or unfavourable type based on the extent of the fracture.

Results: CN showed the maximum percentage of intact margins (92.11 ± 4.13) and the difference from SO and TC was statistically significant ($P < 0.05$). SO possessed the maximum load bearing capacity of all the groups (593.73 ± 66.75) and the difference from ACT and CN was statistically significant ($P < 0.05$). Favourable fracture patterns were predominant in the SO group.

Conclusion: Restoring the class II cavity with CN and SO seems to be promising while ACT did not exhibit superior outcomes for all aspects of evaluation.

Keywords: bulk-fill, dual cure, fracture strength, marginal adaptation, smart materials

1. Introduction

Recent developments in the field of esthetic dentistry have led to extensive use of tooth-coloured direct restorations in both anterior and posterior teeth (Moraes et al., 2022). The most common causes for failure of posterior restorations are secondary caries and fracture (Opdam et al., 2014). In addition to fracture, deflection of weakened cusp due to shrinkage stresses leads to marginal opening and microleakage (Couegnat et al., 2006). They eventually result in demineralization of the cavity walls thereby indirectly leading to secondary caries (Diercke et al., 2009).

Bioactive materials are those materials and material combinations that releases ions for specific biomineralization that induces intentionally desired mineral attachment to the dentin in the clinical environment (Vallittu et al., 2018). The concept of producing “bioactive smart dental materials” has incorporated additional functionalities to restorative materials to improve their long-term marginal stability. A restorative material that could reseal the restorative margins with apatite like crystals would prevent secondary caries and ultimately protect the pulp (Jefferies et al., 2015).

Potential fluoride-releasing bioactive restoratives other than GIC include resin-modified glass ionomers, compomers, giomers, and enhanced RMGICs (Awad et al., 2020). One of the methods to overcome the shrinkage stress is to employ incremental filling technique during restorations (Bicalho

et al., 2014). However, this technique increases the chairside time and has the chance of incorporating voids when compared to bulk fill technique (Chesterman et al., 2017; de Assis et al., 2016). In the last decade, the manufacturers claimed the following bulk-fill restorative materials to possess bioactive properties; Activa BioACTIVE-RESTORATIVE (Pulpdent Corp., Watertown, MA, USA, launched in 2013), Cention N (Ivoclar-Vivadent AG, Schaan, Liechtenstein, launched in 2016) (François et al., 2021). Activa (ACT) is a self-adhesive restorative material with patented rubberized resin which stimulates hydroxyapatite formation and natural remineralization at the tooth material interphase by releasing fluoride, calcium and phosphate ions (Benetti et al., 2019; van Dijken et al., 2019). Cention N (CN) is an alkasite restorative with alkaline fillers which releases, fluoride, hydroxyl, and calcium ions to neutralize the acid attack (Firouzmandi et al., 2021). A recent one in the list is Surefil One (SO) (Dentsply DeTrey GmbH, Konstanz, Germany, launched in 2019) which claims to possess self-adhesive properties and release fluoride ion (François et al., 2021).

Benetti et al (2019) reported poor marginal adaptation of ACT to enamel and dentin when compared to universal composite. Firouzmandi et al (Firouzmandi et al., 2021) reported that the fracture strength of conservative class II restorations in premolars using CN is like that of conventional microhybrid composite, but the marginal adaptation of CN was significantly higher. Poor marginal adaptation can lead to loss of restoration as a result of microleakage and carious lesions (Mjör, 1997). An ideal restorative material should seal the margins, reinforce the remaining tooth structure after tooth preparation and resist fracture against the static and dynamic occlusal forces (Garoushi et al., 2006). Therefore, good marginal integrity and adequate load bearing capacity are essential properties for biomineralizing restoratives. However, the above-mentioned properties have not been compared so far for the three bioactive restoratives (ACT, CN and SO) in the literature.

Therefore, the purpose of the study is to assess the marginal integrity and load bearing capacity of class II restorations restored with three different direct bulk-fill biomineralizing restoratives in comparison with the non-biomineralizing bulk-fill restorative. The null hypothesis tested was that there is no difference in marginal integrity, load bearing capacity of class II restorations using bioactive composites.

2. Materials and Methods

The methodology has been approved by the Standing committee for Scientific Research - Jazan University (HAPO-10-Z-001; Ref. no. REC-44/02/289) prior to the conduct of research.

Sample size: The sample size for this in vitro study was calculated based on pilot study involving 20 teeth (n = 5 per group) for a power of 95%, alpha error at 5% with an effect size of 0.75. The final sample size calculated was 9 teeth per group. A sample failure allowance of 10% was added and the value was rounded to 10 teeth per group.

*Teeth Specimen***:** Forty freshly extracted non carious human single rooted maxillary premolars for orthodontic reasons with completely formed apices were selected based on similar dimensions absence of fracture lines or cracks. Teeth that were free from defect or discoloration were selected for the study after visual confirmation at x20 magnification under stereomicroscope (Leica Micro-system Imaging Solutions, Cambridge, UK). The teeth were immersed in 1% thymol for a week at 4°C and then immersed in saline until use. A Digital calliper (Absolute Caliper, Mitutoyo Kawasaki,

Japan) was used to measure the buccopalatal dimension of each and the average value of all the selected teeth was 9.2 ± 0.6 mm. Teeth with deviation by more than 20% from average dimension were replaced with suitable ones. All teeth were mounted individually in acrylic resin exposing 2mm of root below cementoenamel junction (CEJ). Standardized class II mesioocclusal cavities with occlusal convergence were prepared in all teeth with pear shaped diamond (012 Hi-Di 238, medium grit; Dentsply, Weybridge, UK); pulpal depth was 3 mm deep, proximal box was 4 mm deep with gingival seat at least 1mm above the CEJ), axial wall depth and buccolingual width of the cavity was 2 mm. They were randomly divided (n=10) into three experimental groups (Table 1): Group SO – Surefill One (Dentsply DeTrey GmbH), Group ACT – Activa BioACTIVE-RESTORATIVE (Pulpdent), Group CN - Cention N (Ivoclar Vivadent AG), and a control group – Tetric N-Ceram (TC) Bulk Fill restorative (Ivoclar Vivadent AG) which is a non-bioactive bulkfill nanocomposite. Tofflemire matrix was applied for all teeth and restored with the respective materials according to the manufacturer's instructions.

Group SO – SO capsule was activated and mixed with a capsule mixer for 10 sec at 4200-5000 rpm. The material is bulk filled into the cavity using the extruder, sculpt, carved and light cured for 20 sec using the LED light curing unit (Bluephase 20i; Ivovaclar Vivadent AG) with an output of 1200 mW/cm^2. Everything gets cured within 6 min of activation and polished with Soflex discs (3M ESPE, St. Paul, MN, USA).

Group ACT – The cavities were etched with 37% phosphoric acid gel for 10 sec, rinsed and blot dried. The cavities were bulk filled with ACT material extruded from the syringe through the spiral tips, carved and sculpt. They were allowed to self-cure for 3 min and then light cured for 20 sec. Finishing and polishing was done as mentioned for group SO.

Group CN – Two measuring spoons of powder and 2 drops of resin of CN were mixed on a mixing pad until a smooth consistency was achieved. Initial mixing was done with half of the powder to wet the liquid completely and then small quantities of remaining powder was incorporated. The mixing procedure was completed within 60 seconds. The material was bulk filled in the cavity and left for 10 minutes from the start of mixing. After carving and sculpting, the restorations were polished using Soflex discs (3M ESPE).

Group TC (control) – The cavities were bulk filled with TC by employing total etch technique using phosphoric acid gel (N-Etch; Ivoclar Vivadent AG) and single component bonding agent (Tetric® N-Bond; Ivoclar Vivadent AG). The occlusal surface was carved, sculpt and light cured for 20 sec. Finishing and polishing was done as above.

Thermomechanical ageing: All samples were subjected to thermomechanical ageing. The restored teeth were mounted on a specialized mold that is customised for a chewing simulator (CS-4.2, SD Mechatronik GmbH, Feldkirchen-Westerham, Germany). Conical stainless-steel antagonists of 2 mm tip diameter were customised to exert the force during chewing simulation. All samples were subjected to 250,000 cycles of 5 kg (49 N) of force. The antagonist is a cone-shaped stainless steel with the contact area of 3mm. Samples were also subjected to 500 thermal cycles alternating between 5℃ and 55℃, with a dwell time of 30 seconds (corresponding to 1 year period).

Marginal Integrity: Proximal surface of restorations were recorded were sputter coated (MED 020, Bal-Tec; Balzers, Liechtenstein) with platinum and viewed under scanning electron

microscope (Jeol IT800 SHL FE-SEM, Tokyo, Japan). The proximal margins in the restorations were observed under 400X magnification for the minimum gap width of 20 µm by a technician under blinded conditions. The length of the intact margins without gap was measured and recorded as a percentage of the entire margin length using Adobe Photoshop CS6 software (Adobe Systems; Mountain View, CA, USA) (Frankenberger et al., 2020).

Load bearing capacity: Forty restorations were wrapped on the root portion with aluminium foil and mounted separately in acrylic resin up to 2mm below cementoenamel junction (CEJ). For periodontal simulation, the aluminium foil was replaced with the light body poly-vinyl siloxane impression material (Elite HD+, Zhermack, Polesine, Italy) by injecting into the space created by the foil. All teeth were mounted in a universal testing machine (Instron Electropuls E3000 UTM, UK) and subjected to a compressive axial load applied to the slopes of the cusps with a round ended steel of 8 mm diameter at a crosshead speed of 0.5 mm/min. The load required to fracture the specimens was expressed in Newtons (N) (Firouzmandi et al., 2021).

Fracture type: The failure pattern of each specimen was categorized as favourable when the failure was 2 mm above the cementoenamel junction and unfavourable when the catastrophic fracture occurred 2 mm below the cementoenamel junction. The type of fracture was confirmed by two trained operators under stereomicroscope (Leica Micro-system Imaging Solutions) at 20x magnification (de Assis et al., 2016).

Statistical analysis: The data were statistically analyzed using SPSS software version 18 (SPSS Inc., Chicago, IL, USA). Shapiro-Wilk's test revealed the normal distribution pattern of data. One-way ANOVA was used to assess the difference in marginal integrity and load bearing capacity among the groups; Tukey's HSD post hoc test was performed for inter-group comparisons; type of fracture was expressed in percentage. The level of significance was considered as $P < 0.05$.

3. Results

The SEM micrograph illustrating the examination of tooth restoration interphase is shown in Figure 1A & 1B. Figure 2A shows the highest percentage of intact margins in CN restorations and least with SO restorations (One-way ANOVA; $P < 0.01$). The mean difference in percentage (Table 2) between CN and SO as well as TC was statistically significant ($P < 0.01$). There was no difference in percentage between ACT and CN ($P > 0.05$).

Figure 2B shows highest values of maximum load at fracture of teeth with SO restorations and least with CN restorations (One-way ANOVA; $P < 0.01$). The mean difference in load (Table 3) between SO and ACT as well as CN was statistically significant ($P < 0.001$). There was no difference in loads of SO versus TC and ACT versus CN ($P > 0.05$). Favourable fractures were relatively more in SO when compared with ACT and CN. The control group did not display any favourable fractures (Table 4).

4. Discussion

The primary focus of this *in vitro* study was to only provide clinical recommendations on the use of biomineralizing materials in class II cavities based on their mechanical properties and not to compare their biomineralizing properties. The null hypothesis was rejected, because the type of the restorative material influenced both the marginal integrity and load bearing capacity.

The bulk-fill composites can be conveniently classified as (a) high viscous or low viscous and (b) light or

dual or self-cured (Chesterman et al., 2017). Although low viscous flowable bulk-fill composites are advantageous in self-levelling ability during application and reduced polymerisation shrinkage stresses, they need to be capped with a final layer of conventional resin composite to meet the mechanical requirements (Chesterman et al., 2017). All the materials used in this experiment were uniformly high viscous without capping material. Hence, the results of load bearing capacity truly reflect the mechanical property of bulk-fill material *per se*. TC was selected as a control group due to its bulk-fill nature and it does not release any ions for mineralisation of dentin. Moreover, the total-etch technique with Tetric® N-Bond (Ivoclar Vivadent AG) followed for the TC group has been recommended by the manufacturer to possess superior marginal adaptation for comparison (Ivoclar Vivadent AG, 2014). Different factors affecting the marginal integrity of a restoration such as cavity depth (Firouzmandi et al., 2021), viscosity of the material (Chesterman et al., 2017), and tooth structure at the cavosurface margin (enamel/dentin) (Benetti et al., 2019) were standardised to rule out the confounding variables.

The mechanical properties of bulk-fill material are primarily affected by the depth of cure (Chesterman et al., 2017). Two of the methods adopted by the manufacturers to increase the depth of cure are by altering the filler content and size (Chesterman et al., 2017). Large filler particle size and relatively less filler composition facilitates more light absorption by minimising scattering which is readily utilised for activating the photoinitiators (Ilie et al., 2013). Type of photoinitator is yet another factor responsible for increasing the depth of cure. Ivocerin is a patented highly reactive photoinitiator that polymerises bulk increments when compared to camphoroquinone (Kowalska et al., 2021). Therefore, the depth of the class II tooth preparation was uniformly standardised to a maximum depth of 4 mm in order to meet the manufacturer's recommendations of all the experimental products. To exclude the effect of shade on light penetration and depth of cure (Chesterman et al., 2017), all the groups were restored with same shade (A1) of material except CN which is a self-cure material with no shade options.

In this study, the marginal integrity of CN was significantly high ($P < 0.05$) compared to that of other groups except ACT. This could be attributed to the unique isofiller present in CN. Isofiller is made of cured dimethacrylates, glass filler and ytterbium fluoride which is a special patented component partially functionalised by silanes. It reduces the polymerisation shrinkage stresses and relieves the shrinkage forces (Ivoclar Vivadent AG, 2016). Although TC possesses isofillers (Ivoclar Vivadent AG, 2014) and the adhesive was used for bonding, the percentage of its intact margins were low. It could be because of the difference in curing modes; light cured composites possess more internal stresses and high polymerisation rate affecting the marginal adaptation (Kuijs et al., 2003). Moreover, the volumetric shrinkage of the material is low due to the unique organic/inorganic ratio as well as the monomer composition (Ivoclar Vivadent AG, 2016). The liquid monomer (PEG 400 DMA) in the liquid enhances the wettability of CN to tooth structure (Ivoclar Vivadent AG, 2016). The results are in complete agreement with the previous study reported by Firouzmandi *et al* (2021); who observed superior marginal adaptation of CN in both conservative and extensive class II mesioocclusodistal (MOD) cavities of maxillary premolars when compared to conventional resin composite. The microleakage in class V cavities of

premolars were also found to be minimum when compared to GIC and Composites (Sujith et al., 2020). However, the results of SO and ACT disagreed with another study which showed that the marginal integrity of SO was superior than that of ACT (Frankenberger et al., 2020).

The load bearing capacity of SO group was significantly higher ($P < 0.05$) than that of the other groups except TC. These results could be corroborated with the previous study by Frankenberger *et al* (2020) who conducted similar experiments on Class II MOD cavities of maxillary premolars and found SO to possess high load bearing capacity. The bonding of SO was efficient and durable than CN when assessed on flat dentin samples and class I cavities (Yao et al., 2020). There is no difference in load bearing capacity between ACT and CN. However, the high value of ACT is clinically significant. The results of fracture resistance assessed on endodontically treated premolars closely resemble the present study in relation to ACT and CN (Alsamolly et al., 2021).

As far as fracture type is concerned, a relatively greater incidence of favourable fracture was observed in SO group than that of the other groups. This clearly confirms the reinforcing ability of SO with superior mechanical properties thereby ensuring the restorability and tooth survival outcome. Moreover, Rathke *et al* (2022) reported that one out of 60 teeth restored with SO was fractured with an annual failure rate of 2%.

Strength and limitations

Thermomechanical ageing for a period of 1 year was performed to simulate the clinical situation of subjecting the restorations to repeated masticatory forces and temperature fluctuations. Restoratives of all the four groups were cured on different modes (light, dual and self) as per the manufacturer's instructions which could have influenced the performance of materials. Application of bonding agent on the cavity walls might have positive impact on the marginal integrity and fracture resistance of the restoration (Benetti et al., 2019). On the other hand, it could also interfere with the biomineralizing potential of the restoration (Benetti et al., 2019); hence it was not included in the restoration protocol.

5. Conclusion

The present laboratory investigation revealed significant information from the clinical perspective. Cention N displayed better marginal integrity along the proximal enamel margins of premolars. The load bearing capacity of class II cavities restored with Surefill One was more than the other materials. Further investigations should be conducted *in vivo* to verify the obtained results and gain more knowledge on the long-term performance of biomineralizing restoratives.

Acknowledgement

The author would like to thank Dr. S. Jayalakshmi for the technical consultation.

Reference

Alsamolly, W., Sadek, G., & El-Shehawy, T. (2021). Evaluation of Fracture Resistance of Endodontic Treated Premolars Restored with Alkasite Restorative Materials: An in Vitro Study. *Al-Azhar Assiut Dental Journal*, *4*(2), 117–127.

Awad, M. M., Almutairi, N., Alhalabi, F., Robaian, A., Vohra, F. A., Ozcan, M., Maawadh, A., & Alrahlah, A. (2020). Influence of Surface Conditioning on the Repair Strength of Bioactive Restorative Material. *Journal of Applied Biomaterials & Functional Materials*, *18*, 2280800020926615.

Benetti, A. R., Michou, S., Larsen, L., Peutzfeldt, A., Pallesen, U., & van Dijken, J. W. V. (2019). Adhesion and marginal adaptation

of a claimed bioactive, restorative material. *Biomaterial Investigations in Dentistry*, *6*(1), 90–98.

Bicalho, A. A., Pereira, R. D., Zanatta, R. F., Franco, S. D., Tantbirojn, D., Versluis, A., & Soares, C. J. (2014). Incremental filling technique and composite material-Part I: Cuspal deformation, bond strength, and physical properties. *Operative Dentistry*, *39*(2), E71-82.

Chesterman, J., Jowett, A., Gallacher, A., & Nixon, P. (2017). Bulk-fill resin-based composite restorative materials: A review. *British Dental Journal*, *222*(5), 337–344.

Couegnat, G., Fok, S. L., Cooper, J. E., & Qualtrough, A. J. E. (2006). Structural optimization of dental restorations using the principle of adaptive growth. *Dental Materials*, *22*(1), 3–12.

de Assis, F. S., Lima, S. N. L., Tonetto, M. R., Bhandi, S. H., Pinto, S. C. S., Malaquias, P., Loguercio, A. D., & Bandéca, M. C. (2016). Evaluation of Bond Strength, Marginal Integrity, and Fracture Strength of Bulk- vs Incrementally-filled Restorations. *The Journal of Adhesive Dentistry*, *18*(4), 317–323.

Diercke, K., Lussi, A., Kersten, T., & Seemann, R. (2009). Isolated development of inner (wall) caries like lesions in a bacterial-based in vitro model. *Clinical Oral Investigations*, *13*(4), 439–444.

Firouzmandi, M., Alavi, A. A., Jafarpour, D., & Sadatsharifee, S. (2021). Fracture Strength and Marginal Adaptation of Conservative and Extended MOD Cavities Restored with Cention N. *International Journal of Dentistry*, 5599042.

François, P., Remadi, A., Le Goff, S., Abdel-Gawad, S., Attal, J.-P., & Dursun, E. (2021). Flexural properties and dentin adhesion in recently developed self-adhesive bulk-fill materials. *Journal of Oral Science*, *63*(2), 139–144.

Frankenberger, R., Dudek, M.-C., Winter, J., Braun, A., Krämer, N., von Stein-Lausnitz, M., & Roggendorf, M. J. (2020). Amalgam Alternatives Critically Evaluated: Effect of Long-term Thermomechanical Loading on Marginal Quality, Wear, and Fracture Behavior. *The Journal of Adhesive Dentistry*, *22*(1), 107–116.

Garoushi, S., Lassila, L. V. J., Tezvergil, A., & Vallittu, P. K. (2006). Load bearing capacity of fibre-reinforced and particulate filler composite resin combination. *Journal of Dentistry*, *34*(3), 179–184.

Ilie, N., Bucuta, S., & Draenert, M. (2013). Bulk-fill resin-based composites: an in vitro assessment of their mechanical performance. *Operative Dentistry*, *38*(6), 618–625.

Ivoclar Vivadent AG. (2014). *Scientific documentation Tetric® N-Ceram Bulk Fill*. Retrieved October 23, 2022, from https://downloadcenter.ivoclar.com/#search-text=tetric%20n-ceram&details=17649.

Ivoclar Vivadent AG. (2016). *Scientific documentation Cention N*. Retrieved September 13, 2022, from https://downloadcenter.ivoclar.com/#search-text=cention&details=23015.

Jefferies, S. R., Fuller, A. E., & Boston, D. W. (2015). Preliminary Evidence That Bioactive Cements Occlude Artificial Marginal Gaps. *Journal of Esthetic and Restorative Dentistry*, *27*(3), 155–166.

Kowalska, A., Sokolowski, J., Gozdek, T., Krasowski, M., Kopacz, K., & Bociong, K. (2021). The

Influence of Various Photoinitiators on the Properties of Commercial Dental Composites. *Polymers*, *13*(22), 3972.

Kuijs, R. H., Fennis, W. M. M., Kreulen, C. M., Barink, M., & Verdonschot, N. (2003). Does layering minimize shrinkage stresses in composite restorations? *Journal of Dental Research*, *82*(12), 967–971.

Mjör, I. A. (1997). The reasons for replacement and the age of failed restorations in general dental practice. *Acta Odontologica Scandinavica*, *55*(1), 58–63.

Moraes, R. R., Cenci, M. S., Moura, J. R., Demarco, F. F., Loomans, B., & Opdam, N. (2022). Clinical performance of resin composite restorations. *Current Oral Health Reports*, *9*(2), 22–31.

Opdam, N. J. M., van de Sande, F. H., Bronkhorst, E., Cenci, M. S., Bottenberg, P., Pallesen, U., Gaengler, P., Lindberg, A., Huysmans, M. C. D. N. J. M., & van Dijken, J. W. (2014). Longevity of posterior composite restorations: a systematic review and meta-analysis. *Journal of Dental Research*, *93*(10), 943–949.

Rathke, A., Pfefferkorn, F., McGuire, M. K., Heard, R. H., & Seemann, R. (2022). One-year clinical results of restorations using a novel self-adhesive resin-based bulk-fill restorative. *Scientific Reports*, *12*(1), 3934.

Sujith, R., Yadav, T. G., Pitalia, D., Babaji, P., Apoorva, K., & Sharma, A. (2020). Comparative Evaluation of Mechanical and Microleakage Properties of Cention-N, Composite, and Glass Ionomer Cement Restorative Materials. *The Journal of Contemporary Dental Practice*, *21*(6), 691–695.

Vallittu, P. K., Boccaccini, A. R., Hupa, L., & Watts, D. C. (2018). Bioactive dental materials-Do they exist and what does bioactivity mean? *Dental Materials*, *34*(5), 693–694.

van Dijken, J. W. V, Pallesen, U., & Benetti, A. (2019). A randomized controlled evaluation of posterior resin restorations of an altered resin modified glass-ionomer cement with claimed bioactivity. *Dental Materials*, *35*(2), 335–343.

Yao, C., Ahmed, M. H., Zhang, F., Mercelis, B., Van Landuyt, K. L., Huang, C., & Van Meerbeek, B. (2020). Structural/Chemical Characterization and Bond Strength of a New Self-Adhesive Bulk-fill Restorative. *The Journal of Adhesive Dentistry*, *22*(1), 85–97.

Table 1: Manufacturer, form of supply, composition and curing mode of the bulk-fill materials used

Materials	Manufacturer	Form of supply	Shade (Type)	Composition	Mode of cure	Lot #
Surefill One	Dentsply DeTrey GmbH, Konstanz, Germany	Capsule	A1 (Self-adhesive composite hybrid)	Aluminium-phosphor-strontium-sodium-fluoro-silicate glass, water, highly dispersed silicon dioxide, acrylic acid, polycarboxylic acid, ytterbium fluoride, bifunctional acrylate, self-cure initiator, 4-ter-Butyl-N, N-dimethylaniline, iron oxide pigments, barium sulfate pigment, manganese pigment, camphorquinone, stabilizer	Light cure	2011001057
Activa	Pulpdent Corp., Watertown, MA, USA	Dual syringe (base and catalyst)	A1 (Self-adhesive ionic restorative resins)	Base: silanated bioactive glass and calcium, silanated silica, sodium fluoride Catalyst: diurethane modified by the insertion of a hydrogenated polybutadiene and other methacrylate monomers, modified polyacrylic acid	Dual cure	211119
Cention N	Ivoclar-Vivadent AG, Schaan, Liechtenstein	Powder and liquid	U (Non-adhesive powder-liquid filling material)	Powder: barium glass, ytterbium trifluoride, iso filler, calcium barium aluminium fluorosilicate glass, calcium fluoro silicate glass (alkaline filler), initiators, and pigments Liquid: UDMA, tricyclodecandimethanol dimethacrylate, tetramethyl-xylylene diurethane dimethacrylate, polyethylene glycol 400 dimethacrylate, Ivocerin, hydroperoxide	Self-cure	Z02KZW
Tetric N-Ceram	Ivoclar-Vivadent AG, Schaan, Liechtenstein	Syringe	A1 (Nano-hybrid composite)	Bis-GMA, Bis-EMA, UDMA, Ivocerin, Barium aluminium silicate glass, isofiller, ytterbium trifluoride, silicon dioxide, mixed oxide, prepolymers	Light cure	Z03DLD

U, Universal; UDMA, Urethane dimethacrylate; Bis-GMA, bisphenol A-diglycidyl dimethacrylate; Bis-EMA, bisphenol A-ethoxylated diglycidyl dimethacrylate

Table 2: Mean and standard deviation of marginal integrity of the study groups

Groups	Intact margins Mean ± SD (%)	F value	P value*
SO	72.40 ± 8.19 [a]	27.838	0.001
ACT	88.77 ± 3.74 [b, c]		
CN	92.11 ± 4.13 [b]		
TC	83.60 ± 2.94 [c]		

* One-way ANOVA; P < 0.05)

Similar superscripts represent no difference (Tukey's HSD; P > 0.05)

Table 3: Mean and standard deviation of load bearing capacity of the study groups

Groups	Mean ± SD (Newtons)	F value	P value*
SO	593.73 ± 66.75 [a]	20.343	0.001
ACT	416.04 ± 76.06 [b]		
CN	393.44 ± 56.43 [b]		
TC	521.18 ± 45.12[a]		

* One-way ANOVA; P < 0.05)

Similar superscripts represent no difference (Tukey's HSD; P > 0.05)

Table 4: Fracture pattern distribution among the groups

Groups	Favourable n (%)	Unfavourable n (%)
SO	2 (20)	8 (80)
ACT	1 (10)	9 (90)
CN	1 (10)	9 (90)
TC	0 (0)	10 (100)

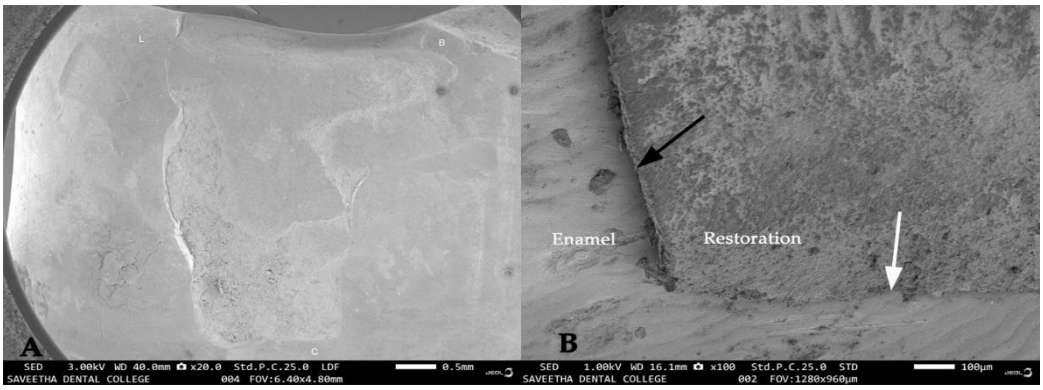

Figure 1. Scanning electron micrographs. **(A)** Representative image at 20X magnification showing the restoration. **(B)** Image at 100X magnification showing the tooth restoration junction; white arrow represents intact margin; black arrow represents the marginal gap.

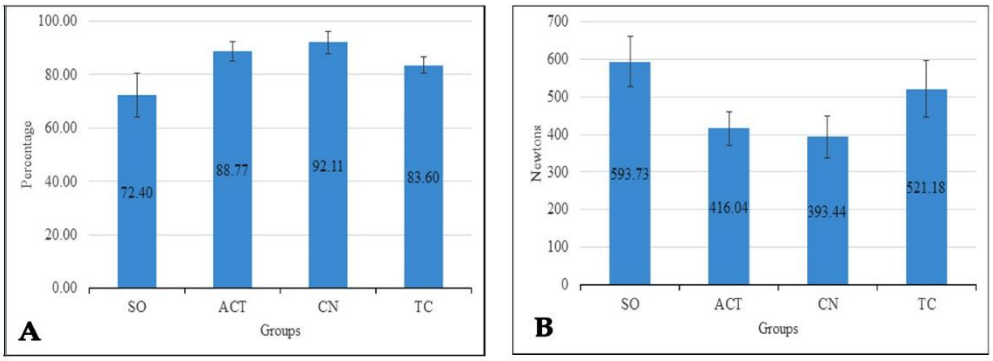

Figure 2. Bar chart comparing the four groups. **(A)** Mean percentage of intact proximal margins representing the marginal integrity. **(B)** Mean maximum load at fracture of teeth samples representing the load bearing capacity.

تقييم الكفاءة الجانبية وقدرة حشوات تجويف الأسنان من النوع الثاني على تحمل القوى باستخدام حشوات ذات تمعدن حيوي مباشر

فينوت كومار تيلا سيكار
قسم اصلاح الأسنان، كليه طب الأسنان، جامعة جازان

الملخص

الهدف: بحثت هذه الدراسة في الكفاءة الجانبية وقدرة حشوات تجويف الأسنان من النوع الثاني على تحمل القوى باستخدام ثلاثة مواد ترميمية معدنية حيوية مختلفة

المواد: خضع أربعون ضاحكًا علوياً لتحضير تحفظي من النوع الثاني وخضعت الأسنان لثلاثة حشوات ترميمية مختلفة من المعادن الحيوية ؛ Surefill One (SO)و Activa (ACT) و-Tetric N Cention N (CN) Ceram (TC)ومقارنتها بمادة أخرى مختلفة

بعد تقادم ميكانيكي حراري يعادل عام واحد ، تم تقييم عينات الحشوات للتأكد من كفائتها الجانبية تحت المجهر الإلكتروني (SEM) ومقاومة الكسر على جهاز اختبار عالمي. تم تصنيف أنماط الكسر كنوع موائم أو غير موائم بناءً على انتشار الكسر.

النتائج: أظهر CN الحد الأقصى لنسبة الجوانب السليمة (92.11 ± 4.13) وكان الاختلاف عن SO و TC ذا دلالة إحصائية (P <0.05). امتلكت عينة SO القدرة القصوى لتحمل القوى مقارنة بباقي العينات (593.73 ± 66.75) وكان الاختلاف عن ACT و CN ذو دلالة إحصائية
(P <0.05). كانت أنماط الكسر الموائمة هي المهيمنة في مجموعة SO

الخلاصة: تعويض تجويف الأسنان من النوع الثاني تبدو واعدة مع مواد CN و SO بينما لم تظهر مادة ACT نتائج متفوقة لجميع أنواع التقييم

الكلمات المفتاحية: التعبئة بالجملة، تصلب ثنائي، القدرة على التحمل، تكيف جانبي، مواد ذكية

Poly(vinylidene fluoride-co-hexafluoropropylene) with hydrophobic activated carbon and graphene oxide for improved oil/water separation

Ayman Yousef[1*]

[1]Chemical Engineering Department, Faculty of Engineering, Jazan University, Jazan, Saudi Arabia

Abstract

Due to the hazards that contaminated wastewater poses to both humans and the environment, oil–water separation has been an important topic of study in recent years. The oil–water separation performance of the membrane made from electrospun nanofibers (NFs) is very high. Electrospinning was used to prepare nanofiber membranes with a rough surface utilizing blend solutions of poly(vinylidene fluoride-co-hexafluoropropylene) (PVDF-HFP)-activated carbon (AC) and PVDF-HFP-graphene oxide (GO) as the raw material. According to the findings, GO@PVDF-HFP performs much better than both pristine PVDF-HFP and AC@PVDF-HFP when it comes to separating chloroform (CF) and dichloromethane (DCM) from water using the force of gravity. When GO@PVDF-HFP NFs are used in the separation of CF from water, the separation flux and efficiency have been found to reach 3038 L m^{-2} h^{-1} and 96%, respectively. When GO@PVDF-HFP NFs were used in the separation of DCM from water, the separation flux and efficiency were able to be increased to 2658.3 L m^{-2} h^{-1} and 84%, respectively. More notably, the obtained GO@PVDF-HFP NFs NFs membranes demonstrated outstanding separation performance of CF and DCM compared to pristine PVDF-HFP and AC@PVDF-HFP, which would provide them substantial benefits for the practical application of oil–water separation.

Keywords:PVDF-HFB; Graphene oxide; Activated carbon; membranes; Oil-Water separation.

1. Introduction

The widespread environmental pollution caused by oily wastewater discharge and frequent oil spills is a severe threat to ecosystems and human health on a global level [1, 2]. Therefore, it is environmentally and economically vital to recover oil and its fractions from contaminated waters. Oil and water may be separated using a variety of methods, such as centrifugation, air flotation, chemical flocculation, biological treatment, and gravity sedimentation. There are a number of problems with the conventional methods of separation now in use, including poor absorption rates, inadequate capacity, inadequate recycling, and simple secondary contamination [3, 4]. The features of the membrane separation technique over the classic oil-water separation method include a higher separation efficiency, an easier operating process, and better antifouling properties. These features make membrane separation the preferred approach for treating oily wastewater [5, 6]. Furthermore, membrane separation technology has emerged as a crucial method for treating wastewater, finding widespread usage because to its versatility and efficiency. The penetration rate of chemical species across the membrane is the most valuable attribute exploited [7]. Some examples of polymers used as membrane materials are poly(vinylidenefluoride-hexafluoropropylene) (PVDF-HFP), polysulfone (PSF), cellulose acetate (CA), cellulose triacetate (CTA), and polyvinylidene fluoride (PVDF) [8]. PVDF-HFP has excellent mechanical properties and strong thermal and chemical stability, making it a standout among the used polymers. Previous applications of PVDF-HFP membranes include oil/water separation, batteries, solar cells, and desalination of saltwater [9-11]. It is rare to find a polymer that is completely without drawbacks. Consequently, several adjustments have been made, including the inclusion of additional materials, to counteract the related drawbacks of those components and improve the membrane's performance. TiO_2 NPs [12], SiO_2 NPs [13], NaOH [14], Zeolite [15], multi-walled carbon nanotubes [16], ZrO_2 NPs [17], ZnO NPs [18], and Ag NPs [19] are only some of the inorganic materials that have been integrated into polymeric matrices to generate hybrid membranes. The membrane's permeability was increased and its surface characteristics were improved due to the incorporation of the inorganic particles [20]. The incorporation of inorganic NPs into PDF-HFB reduces the material's crystallization ability and increases its unique wettability, making it better suited for use in oil-water separation [21, 22]. Electrospun nanofiber membranes contribute significantly to the field of water purification because of their novel properties, such as their high surface area to volume ratio, huge porosity, outstanding mechanical properties, and high-water permeability [23]. Depending on the desired characteristics of nanofibers for water purification, such as thickness, porosity, and surface roughness, they were fabricated and used in a variety of applications. Many processes have taken use of electrospun nanofiber membranes, including microfiltration, ultrafiltration, nanofiltration, and reverse osmosis, and forward osmosis [9-11, 24, 25]. It is commonly acknowledged that AC and GO are the conventional absorbents materials that are the most effective in terms of both efficiency and cost when that comes to removing oils from water and recycling them[26, 27]. In addition,

they have the ability to make the surface extremely superhydrophobic[26]. In this study, PVDF-HFP electrospun nanofiber membranes were modified utilizing AC and GO for separation of petroleum fractions (chloroform and dichloromethane) from water. While the AC was purchased commercially, the GO were synthesized using Hummer's approach. After that, the inorganic particles were added to a mixture of PVDF-HFP solution and then electrospun used electrospinning machine. Once the membrane was formed, it was dried at 40 ° C in a vacuum.

2. Experimental

2.1. Materials

Poly(vinylidene fluoride-co-hexafluoropropene) ((PVDF-HFP), 98% assay, (MW) = 65,000 g/mol), graphene oxide was synthesized using graphite powder (~20 μm), hydrogen peroxide, and sulfuric acid (95–97%), chloroform (CF, 99.8%), and dichloromethane (DCM, 99.8%) were purchased from Aldrich Co., USA. Pharma-grade activated charcoal (acid wash, LOBACheme, 99.5%, Mumbai, India). Distilled water was used as a solvent. Distilled water, Dimethylformamide (DMF), and acetone were used as a solvent. All chemicals were utilized without any further modifications.

2.2. Graphene oxide preparation

Synthesis of GO from natural graphite powder using a modification of the Hummer's approach [28, 29]. Five grams of graphite that had been treated twice with 5% HCl were added to a frigid (0 °C) concentrated H_2SO_4 (130 mL) solution while stirring in an ice bath for two hours. Finally, the temperature was raised to 98 °C by diluting the mixture with DI water. **The mixture was left to cool to room temperature and then 50 mL of H_2O_2 (30 wt%) was added.** After the final slurry was filtered, the filter cake was washed many times with 10% aqueous HCl and dried at 50 °C.

2.3. Membrane preparation

To begin, 1.5 gm of PVDF- HFP was dissolved in a mixture of 4:1 DMF and acetone to produce a 15 wt% PVDF- HFP solution. In order to get a transparent sol-gel solution, the produced solution was agitated continuously for a whole night. The produced PVDF-HFP solution is combined with 30 mL of AC-based PVDF-HFP and GO-based PVDF-HFP at a weight of 5%wt. Electrospinning a lab-scale electrospinner (**Fig.1**), we successfully generated NF membranes from pure PVDF-HFP, 5%wt AC@PVDF-HFP, and 5%wt GO@PVDF-HFP. A capillary syringe made of plastic was used to feed the sol-gels. A copper wire was inserted into the syringe and connected to a high-voltage power source (positive electrode). The NF mats produced by electrospinning were collected by connecting the negative electrode to an aluminum-lined ground iron drum. The voltage was 18 kilovolts, applied between the syringe and the drum. Overnight, the collected electrospun NF mats were dried in a vacuum at 45 ° C.

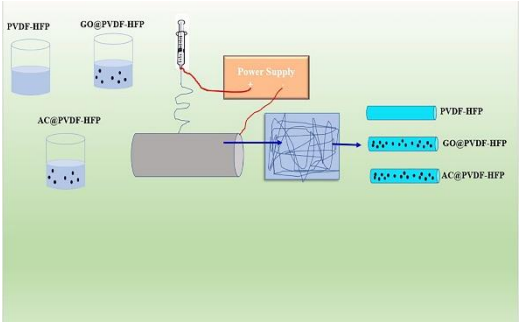

Fig.1: Schematic of membrane preparation.

2.4. Separation Cell

The oil-contaminated water is treated using a batch separation technique. A simplified representation of the arrangement is shown in **Fig. 2**. An open atmospheric vertical plastic perforated cylinder fitted inside a cone with a perforated surface. The prepared nanofibers membrane is placed between a perforated cone and a plastic cylinder serves as the primary cell in a typical setup, along with a pump, and a graduated cylinder work as a product tank. Water and oil (chloroform or dichloromethane) were combined in a volume ratio of 1:1 to produce the layered oil-water mixture. At a rate of 10 ml/min, the pump would mix the oil/water solution, where the petroleum portion would pass through the membrane to the graduated cylinder and the water would be collected on the plastic cylinder. The procedure was repeated until only water and the petroleum portion remained in the plastic cylinder and the graduated cylinder, respectively.

For the purpose of determining the oil flow, the following equation was used:

The flux (F) was calculated as follows:

$$F = m/At, \quad (1)$$

where m was the amount of separated oil (in litters), A was the effective surface area of the used NF membrane (m^2), and A was the separation duration time (h).

To determine the oil separation efficiency, the following equation was used:

$$\eta = M_1/M_0 \ X100\%. \quad (2)$$

The weight of the oil before and after separation, denoted as M_0 and M_1, respectively.

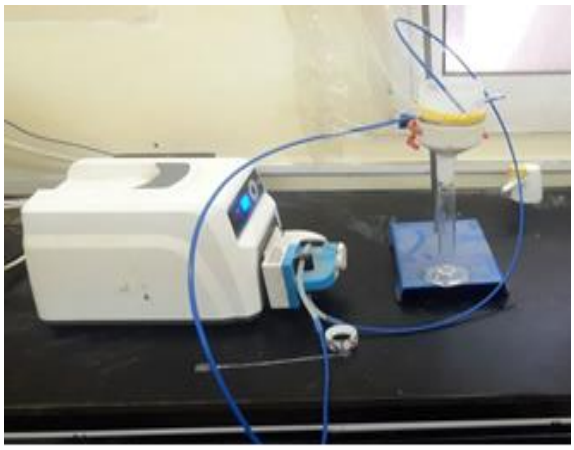

Fig.2: Schematic of utilized separation cell

2.5. Instruments used in this study

Electrospinning machine (SN-50, NaBond Technologies Co., Limited, China) used for nanofibers preparation. Viscometer (Brookfield DV-II+Pro, Brookfield Engineering Lab., INC., USA) is used to measure the viscosity of polymer solutions. The oil/water solution was pumped into the Separation Cell using a peristaltic pump [Cole-parmer@, Masterflex: Model 77800-60]. The morphology of synthesized membranes were examined by JEOL JSM-5900 scanning electron microscope (SEM, JEOL Ltd., Japan). Micrometer (Mitutoyo 293-821-30: Digital Micrometer 0-25mm, Anaum Trading Company L.L.C) is used to measure the thickness of the membrane.3. Results and discussion

Table 1 displays the viscosity of the solutions that have been prepared as well as the thickness of the membrane that has been fabricated. As can be seen in the table, the addition of GO causes the viscosity to rise from 80 to 48.5 cP, while it also increases from 80 to 56.6 cP with AC to PVDF-HFP. It is well known that an increase in the viscosity of the material results in a corresponding rise in the thickness of the produced NFs. The thickness of the fabricated membrane has increased from 160.1 to 288.6 m as a result of the addition of GO to PVDF-HFP. On the other hand, the membrane thickness has increased from 160.1 to 531.7 m as a result of the addition of AC to PVDF-HFP.

Table 1: Properties polymer solutions.

Polymer solution	Viscosity (cP)	Thickness (µm)
PVDF-HFP	80	160.1
GO@PVDF-HFP	48.5	288.6
AC@PVDF-HFP	56.6	531.7

The hydrophobicity of a nanofibers membrane may be improved by developing a rough surface on the membrane at the micro or nano scale. With this modification, the membrane's ability to absorb liquids will be enhanced. Coating PVDF nanofibers with precipitation allows for the incorporation of inorganic nanoparticles. A functional layer is formed on the surface of PVDF fibers, however it is easily damaged and lost due to the poor bonding strength between the particles and PVDF. Because of this, the separation membrane's durability and efficacy in application areas suffer greatly [28]. In this investigation,

the nanofiber membrane was produced by electrospinning a blending solution of GO or AC and PVDF-HFB. The nanoparticles were covered the surface of the PVDF-HFB. Furthermore, the NFs are continuous and beads-free. Figure 3 displays SEM images of the various types of nanofiber membranes that have been prepared together with the fiber diameter distributions that correlate to those images. As a result of the incorporation of AC or GO into PVDF-HFP, the morphology of the electrospun fibers has undergone a noticeable transformation, which is visible to the naked eye the formation of particles on the surface of PVDF-HFP NFs. It is clear from Figure 3 B and C that certain convex secondary structures appear on the surface of the fibers, which enhances the surface roughness of the fibers. This is shown by the fact that the surface of the fibers is improved. In addition, the incorporation of AC and GO causes the conformational changes on the surface of the fibers to grow denser, and also highlights the fibers' inherent roughness. It was noticed that the diameter of the NFs became larger when AC and GO were added to the mixture. This is due to increase in the viscosity of the spinning solution (**Table 1**). The average size of the NFs increased from 205 nm (in the PVDF-HFP) to 331 nm (in the GO@PVDF-HFP) and 357 nm (in the AC@PVDF-HFP). This is because of the agglomeration phenomena that occurs between the AC and GO when the viscosity is increased, which results in an increase in the fibers' diameter. As a result, the intermolecular force of the polymer is higher than the force exerted by the electric field.

Oil/Water separation

The pure PVDF-HFP membrane, the GO@PVDF-HFP membrane, and the AC@PVDF-HFP membrane were all used in the CF and DCM-water separation procedure. The output flow rate of CF or DCM was measured and compared to that of potassium permanganate aqueous solution (as colored water) in two separate 50-ml amounts. Each membrane was put through two tests, and the average flow rate was then determined. The results of the flow measurements are shown in Figs. 4 and 5. The results showed that in both the CF and DCM cases, GO had the highest flux relative to the pristine PVDF-HFP, AC@PVDF-HFP; the flux rose by a factor of 1.5 relative to the pristine PVDF-HFP membrane. The computed CF flow rates for pure PVDF-HFP, GO@PVDF-HFP, and AC@PVDF-HFP electrospun membranes are 2278.5, 3038, and 2531.7 L m^{-2} h^{-1}, respectively. On the other hand, the DCM flux across pure PVDF-HFP, GO@PVDF-HFP, and AC@PVDF-HFP electrospun membranes was 2025.3, 2658.3, and 2278.5 L m^{-2} h^{-1}. The separation efficiency of CF using GO@PVDF-HFP has reached 96%, which is much higher than the 72% achieved using pristine PVDF-HFP and the 80% attained using AC@PVDF-HFP. While the separation of DCM using GO@PVDF-HFP has reached 84%, this is in contrast to the 60% that was achieved using pristine PVDF-HFP and the 72% that was achieved using AC@PVDF-HFP. In conclusion, this demonstrates the superior performance of GO@PVDF-HFP compared to that of other membranes in the separation of CF and DCM. It also demonstrates the quick separation of CF in compassion to DCM. In the instance of the GO@PVDF-HFP membrane, the discernible increase in the flow may be ascribed to the dispersed GO that is present on the surface of the nanofibers. Therefore, one may argue that the GO make a smooth blanket, which leads to the

CF and DCM moving over the surface of the blanket more quickly.

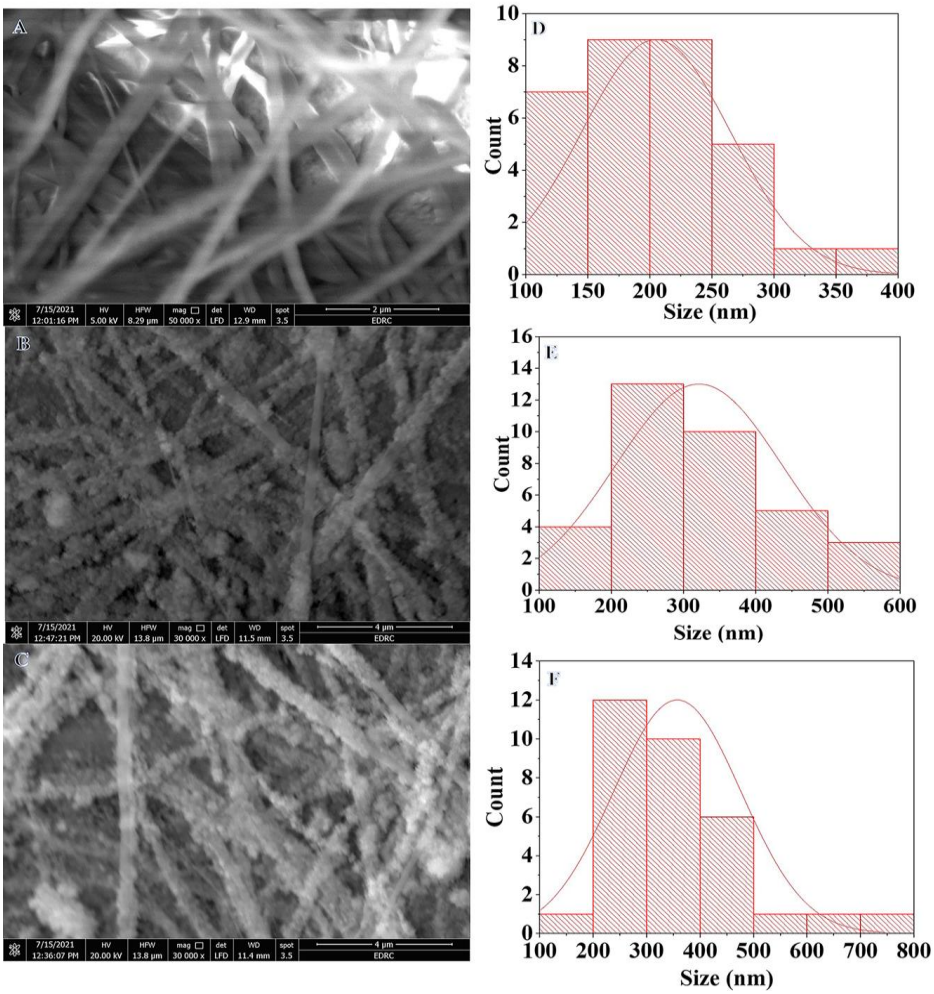

Fig.3: SEM images of PVDF-HFP (A), GO@PVDF-HFP (B), and AC@PVDF-HFP (C) and size distribution of PVDF-HFP (A), GO@PVDF-HFP (B), and AC@PVDF-HFP (C) membrane NFs.

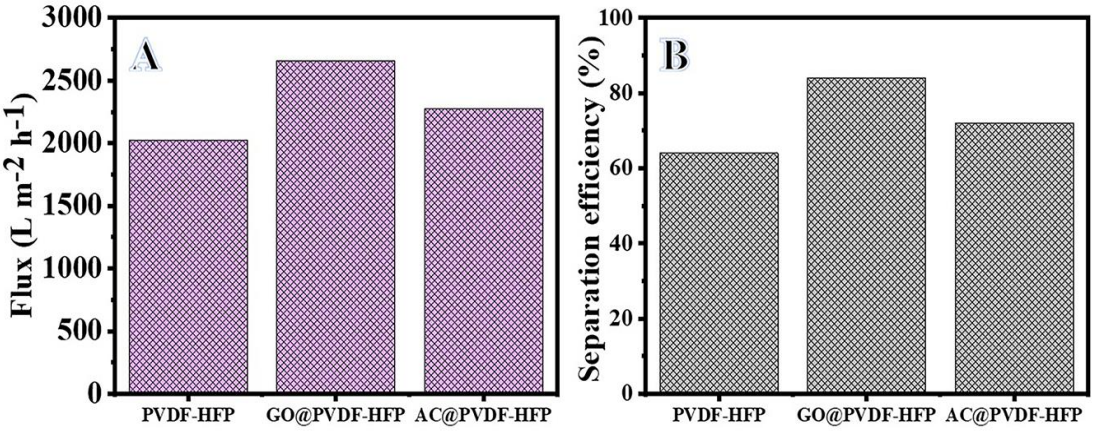

Fig.٤: (A) Oil flux and (B) oil separation efficiency of DCM using the PVDF-HFP, GO@PVDF-HFP, and AC@PVDF-HFP membranes.

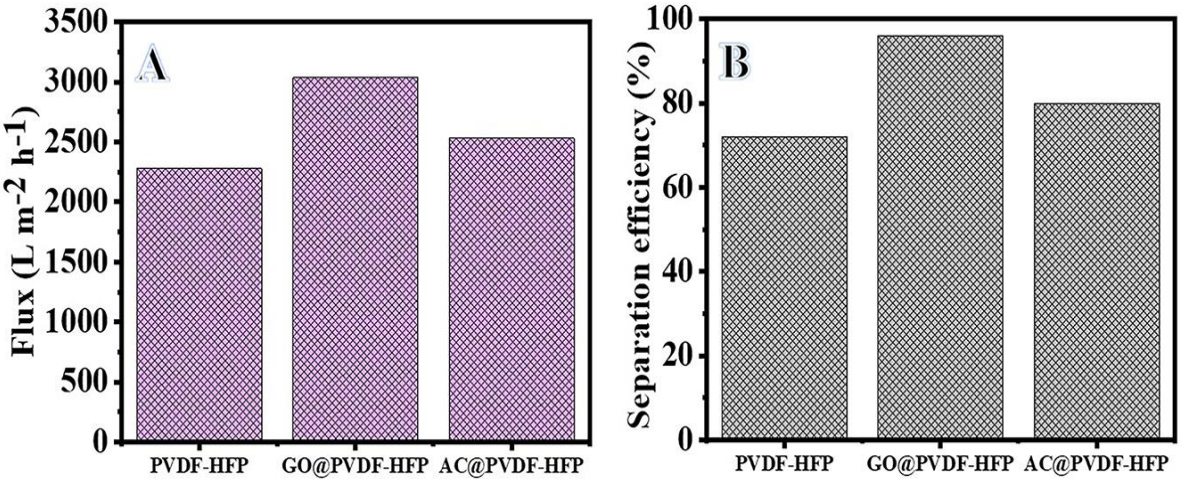

Fig.٥: (A) oil flux and (B) separation efficiency of CF utilized the PVDF-HFP, GO@PVDF-HFP, and AC@PVDF-HFP membranes

Conclusion

In conclusion, a pristine PVDF-HFP NFs membrane, a GO@PVDF-HFP NFs membrane, and an AC@PVDF-HFP NFs membrane with a roughness structure were all prepared by one-pot electrospinning process for the purpose of oil–water separation. The findings of the oil–water separation demonstrate that the nanofibers membrane is capable of efficiently separating the oil–water combination when subjected to the force of gravity. It is possible for the separation flux of CF to reach up to 3038 L m^{-2} h^{-1}, and the separation efficiency may reach as high as 96% when GO@PVDF-HFP NFs are utilized. While The DCM separation flux has the potential to reach up to 2658.3 L m^{-2} h^{-1}, and the separation efficiency may reach as high as 84% when GO@PVDF-HFP NFs are used. In light of this, the GO@PVDF-HFP NFs nanofibers membrane that has been developed has high separation performance, strong chemical stability, and is an appropriate material for applications involving oil–water separation.

References

[1] C.H. Peterson, S.D. Rice, J.W. Short, D. Esler, J.L. Bodkin, B.E. Ballachey, D.B. Irons, Long-term ecosystem response to the Exxon Valdez oil spill, Science, 302 (2003) 2082-2086.

[2] S. Jiang, X. Meng, B. Chen, N. Wang, G. Chen, Electrospinning superhydrophobic–superoleophilic PVDF-SiO2 nanofibers membrane for oil–water separation, Journal of Applied Polymer Science, 137 (2020) 49546.

[3] D. Mysore, T. Viraraghavan, Y.C. Jin, Oil/water separation technology-A review, Journal of Residuals Science & Technology, 3 (2006) 5-14.

[4] D. Yang, L. Li, B. Chen, S. Shi, J. Nie, G. Ma, Functionalized chitosan electrospun nanofiber membranes for heavy-metal removal, Polymer, 163 (2019) 74-85.

[5] G.M. Geise, H.S. Lee, D.J. Miller, B.D. Freeman, J.E. McGrath, D.R. Paul, Water purification by membranes: the role of polymer science, Journal of Polymer Science Part B: Polymer Physics, 48 (2010) 1685-1718.

[6] B.S. Lalia, V. Kochkodan, R. Hashaikeh, N. Hilal, A review on membrane fabrication: Structure, properties and performance relationship, Desalination, 326 (2013) 77-95.
[7] R.W. Baker, Membrane technology and applications, John Wiley & Sons2012.
[8] B. Van der Bruggen, Membrane technology, Kirk-Othmer Encyclopedia of Chemical Technology, (2000) 1-47.
[9] S. Sundarrajan, R. Balamurugan, S. Kaur, S. Ramakrishna, Potential of engineered electrospun nanofiber membranes for nanofiltration applications, Drying Technology, 31 (2013) 163-169.
[10] T. Fujioka, S.J. Khan, J.A. McDonald, A. Roux, Y. Poussade, J.E. Drewes, L.D. Nghiem, N-nitrosamine rejection by nanofiltration and reverse osmosis membranes: The importance of membrane characteristics, Desalination, 316 (2013) 67-75.
[11] L.A. Hoover, J.D. Schiffman, M. Elimelech, Nanofibers in thin-film composite membrane support layers: Enabling expanded application of forward and pressure retarded osmosis, Desalination, 308 (2013) 73-81.
[12] Y.H. Teow, A.L. Ahmad, J.K. Lim, B.S. Ooi, Preparation and characterization of PVDF/TiO2 mixed matrix membrane via in situ colloidal precipitation method, Desalination, 295 (2012) 61-69.
[13] L.M. Jin, S.L. Yu, W.X. Shi, X.S. Yi, N. Sun, Y.L. Ge, C. Ma, Synthesis of a novel composite nanofiltration membrane incorporated SiO2 nanoparticles for oily wastewater desalination, Polymer, 53 (2012) 5295-5303.
[14] M. Obaid, N.A.M. Barakat, O.A. Fadali, M. Motlak, A.A. Almajid, K.A. Khalil, Effective and reusable oil/water separation membranes based on modified polysulfone electrospun nanofiber mats, Chemical engineering journal, 259 (2015) 449-456.
[15] F. Liu, B.-R. Ma, D. Zhou, Y.-h. Xiang, L.-x. Xue, Breaking through tradeoff of Polysulfone ultrafiltration membranes by zeolite 4A, Microporous and mesoporous materials, 186 (2014) 113-120.
[16] Y. Medina-Gonzalez, J.-C. Remigy, Sonication-assisted preparation of pristine MWCNT–polysulfone conductive microporous membranes, Materials letters, 65 (2011) 229-232.
[17] Y. Zhang, L. Wang, Y. Xu, ZrO2 solid superacid porous shell/void/TiO2 core particles (ZVT)/polyvinylidene fluoride (PVDF) composite membranes with anti-fouling performance for sewage treatment, Chemical Engineering Journal, 260 (2015) 258-268.
[18] X. Zhang, Y. Wang, Y. Liu, J. Xu, Y. Han, X. Xu, Preparation, performances of PVDF/ZnO hybrid membranes and their applications in the removal of copper ions, Applied Surface Science, 316 (2014) 333-340.
[19] P. Gunawan, C. Guan, X. Song, Q. Zhang, S.S.J. Leong, C. Tang, Y. Chen, M.B. Chan-Park, M.W. Chang, K. Wang, Hollow fiber membrane decorated with Ag/MWNTs: toward effective water disinfection and biofouling control, Acs Nano, 5 (2011) 10033-10040.
[20] M. Khayet, J.P.G. Villaluenga, J.L. Valentin, M.A. López-Manchado, J.I. Mengual, B. Seoane, Filled poly (2, 6-dimethyl-1, 4-phenylene oxide) dense membranes by silica and silane modified silica nanoparticles: characterization and application in pervaporation, Polymer, 46 (2005) 9881-9891.
[21] Z. Kaijun, L. Qingshan, W. Jing, H. Wei, Preparation of PVDF-HFP@ FAS electrospun fibrous film with special wettability and the research of its oil-water separation performance, Integrated Ferroelectrics, 182 (2017) 218-227.

[22] A.M. Al-Enizi, M.M. El-Halwany, S.F. Shaikh, B. Pandit, A. Yousef, Electrospun nickel nanoparticles@ poly (vinylidene fluoride-hexafluoropropylene) nanofibers as effective and reusable catalyst for H2 generation from sodium borohydride, Arabian Journal of Chemistry, 15 (2022) 104207.
[23] S.A.A.N. Nasreen, S. Sundarrajan, S.A.S. Nizar, R. Balamurugan, S. Ramakrishna, Advancement in electrospun nanofibrous membranes modification and their application in water treatment, Membranes, 3 (2013) 266-284.
[24] A.M. Bazargan, M. Keyanpour-Rad, F.A. Hesari, M.E. Ganji, A study on the microfiltration behavior of self-supporting electrospun nanofibrous membrane in water using an optical particle counter, Desalination, 265 (2011) 148-152.
[25] R. Shukla, M. Cheryan, Performance of ultrafiltration membranes in ethanol–water solutions: effect of membrane conditioning, Journal of membrane science, 198 (2002) 75-85.
[26] A. Jamsaz, E.K. Goharshadi, Flame retardant, superhydrophobic, and superoleophilic reduced graphene oxide/orthoaminophenol polyurethane sponge for efficient oil/water separation, Journal of Molecular Liquids, 307 (2020) 112979.
[27] M.S. Islam, K.N. McPhedran, S.A. Messele, Y. Liu, M.G. El-Din, Isotherm and kinetic studies on adsorption of oil sands process-affected water organic compounds using granular activated carbon, Chemosphere, 202 (2018) 716-725.
[28] Y. Xu, H. Bai, G. Lu, C. Li, G. Shi, Flexible graphene films via the filtration of water-soluble noncovalent functionalized graphene sheets, Journal of the American Chemical Society, 130 (2008) 5856-5857.
[29] M. Motlak, N.A.M. Barakat, M.S. Akhtar, A.M. Hamza, A. Yousef, H. Fouad, O.B. Yang, Influence of GO incorporation in TiO2 nanofibers on the electrode efficiency in dye-sensitized solar cells, Ceramics International, 41 (2015) 1205-1212.

تكوين خليط من بولي (فلوريد فينيلدين - سداسي فلورو بروبيلين مشترك) مع كربون منشط وأكسيد الجرافين لتحسين فصل الزيت / الماء

أيمن أحمد يوسف حسن

قسم الهندسة الكيميائية-كلية الهندسة – جامعة جازان - المملكة العربية السعودية

الملخص

نظرًا للمخاطر التي تشكلها المياه الملوثة على كل من البشر والبيئة ، كان فصل الزيت عن الماء موضوعًا مهمًا للدراسة في السنوات الأخيرة. يعتبر أداء فصل الزيت عن الماء للاغشية المصنوع من الألياف النانوية المغزولة كهربائياً مرتفع للغاية. تم استخدام الغزل الكهربائي لتحضير أغشية الألياف النانوية بسطح خشن باستخدام مزيج من المحاليل تتكون من بولي (فينيلدين فلوريد - سداسي فلورو بروبيلين) - الكربون المنشط و بولي (فينيلدين فلوريد - سداسي فلورو بروبيلين)- أكسيدالجرافين كمادة خام. وفقًا للنتائج ، فإن بولي (فينيلدين فلوريد - سداسي فلورو بروبيلين)- أكسيدالجرافين يعمل بشكل أفضل بكثير من كل من بولي (فينيلدين فلوريد - سداسي فلورو بروبيلين) و بولي (فينيلدين فلوريد - سداسي فلورو بروبيلين) - الكربون المنشط عندما يتعلق الأمر بفصل الكلوروفورم وثاني كلورو ميثان عن الماء باستخدام قوة الجاذبية. عندما يتم استخدام بولي (فينيلدين فلوريد - سداسي فلورو بروبيلين)- أكسيدالجرافين في فصل الكلوروفورم عن الماء ، تم العثور على تدفق وكفاءة الفصل لتصل إلى ٣٠٣٨ لتر م$^{-٢}$ساعة$^{-١}$ و ٩٦٪ ، على التوالي. عندما تم استخدام بولي (فينيلدين فلوريد - سداسي فلورو بروبيلين)- أكسيدالجرافين في فصل ثاني كلورو ميثان عن الماء ، أمكن زيادة تدفق وكفاءة الفصل إلى ٢٦٥٨,٣ لتر م$^{-٢}$ساعة$^{-١}$ و ٨٤٪ ، على التوالي. والأهم من ذلك ، أن أغشية بولي (فينيلدين فلوريد - سداسي فلورو بروبيلين)- أكسيدالجرافين التي تم الحصول عليها أظهرت أداء فصل رائعًا للكلوروفورم وثاني كلورو ميثان ـ مقارنةً بـ استخدام بولي (فينيلدين فلوريد - سداسي فلورو بروبيلين) الأصلي و بولي (فينيلدين فلوريد - سداسي فلورو بروبيلين) - الكربون المنشط، مما سيوفر لهم فوائد كبيرة للتطبيق العملي لفصل الزيت عن الماء.

الكلمات المفتاحية: بولي (فينيلدين فلوريد - سداسي فلورو بروبيلين)؛ أكسيد الجرافين

Systematic Review of Contemporary Literature on Safety Methods of Internet Enabled Smart Vehicles

Mohammed Hameed Alhameed

College of Computer Science and Information Technology, Jazan University, Jazan, Saudi Arabia

Abstract

The Internet of Things (IoT) enables the use of intelligent application areas and smart devices in numerous facets of today's metropolis. Machine Learning (ML) strategies are used to augment computer-aided intelligence and functionality by increasing the amount of data available. Intelligent transportation has garnered considerable interest as a result of its application of ML and IoT methodologies. In this review, automated driving is defined as the process of optimizing travel paths, parking, and detecting and alerting about past and potential accidents. The purpose of this manuscript is to provide a comprehensive overview of techniques such as ML, blockchain, and black-box techniques that are used in Smart Vehicle (SV) transportation systems to handle accidents and identify coverage gaps.

Keywords: *Internet of Things, Machine Learning, Internet of Vehicles (IoV), PRISMA, Detection System, Neural Network, Intelligent Transportation.*

1. Introduction

With the increasing prevalence of smart gadgets in daily activities, such as smart automobiles fitted with communication network devices on the road [1], [2], large and diverse communications systems are being imagined. Interoperability across disparate networks necessitates the creation of novel intelligent design methodologies [3]. The IoT as well as its intelligent interfaces constitute a novel paradigm for the Internet of Vehicles as a result of pervasive sensing (IoV). The aim of the IoV is to enhance traffic effectiveness and security [4]. In such networks, vehicle nodes communicate in a semi-organized fashion, depending on the route structure, impediments, and traffic conditions [5]. Connecting data between vehicles is a challenging process and a challenging project due to a missing standards, extensibility, sporadic services, high computational overhead, collaborative dependencies, spectrum bandwidth limits, and network communication impact [6].

The incompatibility of this technology with other heterogeneous networks, namely cloud computing and the IoTs, renders it uncommercial. A high number of Base Stations (BSs) or access points can be installed in a given area with infrastructure-based communication. Due to a lack of cloud support along with integrated information services, smart gadgets are inefficient for vehicle nodes. In order to ensure that internet services are constantly available, new wireless technologies are being developed to expand the linked world via car nodes [7]. Cloud-based services will be integrated into the netwok, as will low cost solutions and improved cooperative dependency in VANETs thanks to the IoT. Even while IoV networks provide many advantages, they’ve run into a number of problems, including node incompatibility, slow internet connections, coping with large amounts of data and, most significantly, security [8]. The IoV should have sufficient connectivity and dependable communication services as shown in figure 1. A highly operationalized, controllable, and

manageable open integrated network is required. The IoV enables complex and dynamic data exchange on a big scale. Additionally, these networks are unpredictable and complex as a result of dense and sparse traffic conditions [9]. Numerous techniques for optimizing routing, path finding, obstacle handling, and routing efficiency have been developed [10–12]. This work intends to answer 'FOUR' research questions, which are enumerated below.

1. How can a vehicular IoT system guarantee the safety of drivers?
2. What are the unique research challenges in accident detection in Internet Enabled Smart Vehicles?
3. How the neural network and ML techniques aid to stop road accidents in smart vehicles?
4. What are propitious solutions to ameliorate safety measures in a smart vehicle?

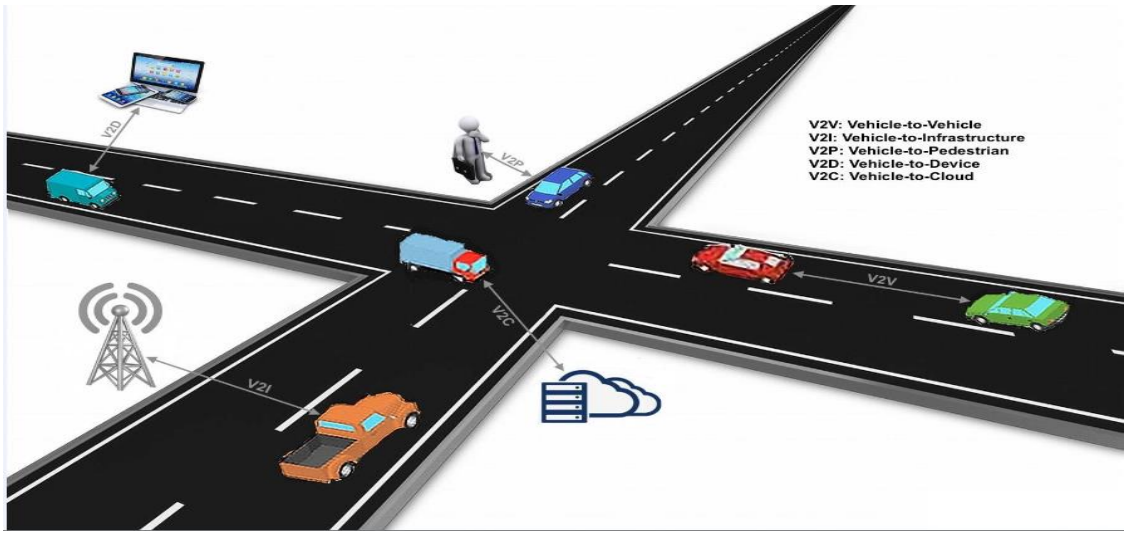

Figure 1. Communication Types in Internet of Vehicles

2. Architecture of IoV

The IoV is changing the transportation sector into a worldwide network. In general, the Internet of Vehicles is an amalgamation of three categories of networks as shown in table 1: an inter-vehicle network ITS applications, like vehicle communications, can widen the horizons of drivers and on-board sensors mostly beneficial on the road traffic safety and efficiency, an intra-vehicle network communication data is exchanged between the vehicle's ECUs, and the vehicular mobile Internet [49], [50].

Table 1: General Architecture of IoV

Communication Type	Objective	Information	Advantages
V2V	A key goal of V2V communications is vehicle-to-vehicle communication and collaboration	Vehicle mobility, vehicle status, road and weather	Accidents are avoided, driving is safer and more comfortable, and real-time alerts are available.
V2I	The concept is based on the connection between onboard services and infrastructure on the roadside	Traffic congestion is reduced, accidents are avoided, dangerous routes are identified, and overall safety is improved	It is designed to make driving easier
V2C	Over the top-cloud services	Traffic update, routing and media streaming	Supported by UE
V2P	The number of pedestrian and bicycle fatalities	Pedestrians, cyclists, people using wheelchairs	Environmental information to store and share using new technologies
V2D	Vehicles and any electronic devices connected to them exchange information	Surrounding vehicles and infrastructures	Improve driving safety

3. Internet of Vehicles Applications

With the emergence of new communication and connectivity technologies in the field of wireless and mobile communication, IoV applications are categorized intelligent transportation and smart cities as shown in Table 2. Intelligent transportation focuses on categories of driver safety, traffic efficiency, convenience and entertainment. It mainly serves the requirements for individual vehicle objects as well as IoV network connects to collision avoidance strategy [1]. Smart cities services are considered as data sensing and collection, environment monitoring, structural and road monitoring, and security surveillance essentially as cost-effective [2].

Table 2: Internet of Vehicle Applications

Intelligent Transportation			
Safety	Efficiency	Convenience	Information/ Entertainment
• Collision avoidance system • Collision warning • Roadside signal (Left –Right turn) • Lane change indication • Stop signal warning • Defect/ Fault/Repair vehicle warning	• Traffic signal • Route escalation • Cooperative driving	• Smart parking • Valet parking	• Quality of service (Weather, Navigation, Live news) • Video streaming

Smart Cities			
Data Collection	Environment Monitoring	Structural and Road Monitoring	Security / Surveillance
• Taxi cabs • Mobile vehicles	GPS monitoring	Electronic gadgets	Camera

Advanced technologies are incorporated to enhance vehicle and passengers safety on the roads by warning signals and messages. A cooperative collision avoidance system uses sensors to accurately detect a potential collision by and display a warning to the driver [26]. Most challenging tasks is to monitor collision warning, road side traffic can detect vehicle distance and warn the driver to avoid rear-end and intersection collisions [27]. Curve speed warning, traffic congestion, cooperative forward collision warning, emergency brake light warning, left turn assistant, traffic signal violation, navigation, lane change warning, and stop sign movement assistant are some of the safety-related applications identified by the Vehicle Safety Consortium (VSC)[26]. Our way of life is impacted by IoV technology in a number of areas, including urban congestion management, transportation and logistics, urban traffic, vehicle tracking, and many more. The equipped automobiles broadcast real-time data about a collision, as well as the vehicle's location, to emergency responders. This has the potential to save lives by speeding up the emergency response [27].

4. Methodology

4.1. Search Strategy

In order to perform a systematic review of the contemporary literature of "Vehicle Accident Detection" and "Accident Risk

Detection" using IoT the articles have been collected using search query ("internet of vehicles" AND "accident detection") that queried on the google scholar search engine. Among the 322 articles those listed as search results, 57 articles have been selected based on their relevancy to the adopted topic. Further filtered these articles; by type of the articles, publishing houses, keywords, year of publication. Finally, the resultant numbers of articles are 35. The detailed statistics are explored in the following subsequent section.

4.2. Search Statistics

Following the Preferred Reporting Items for Systematic Reviews and Meta-Analyses (PRISMA) criteria [13], all retrieved studies were systematically identified, reviewed, and extracted for pertinent information. Figure 2 shows the document search and selection approach (used in accordance with PRISMA principles) for the proposed systematic review.

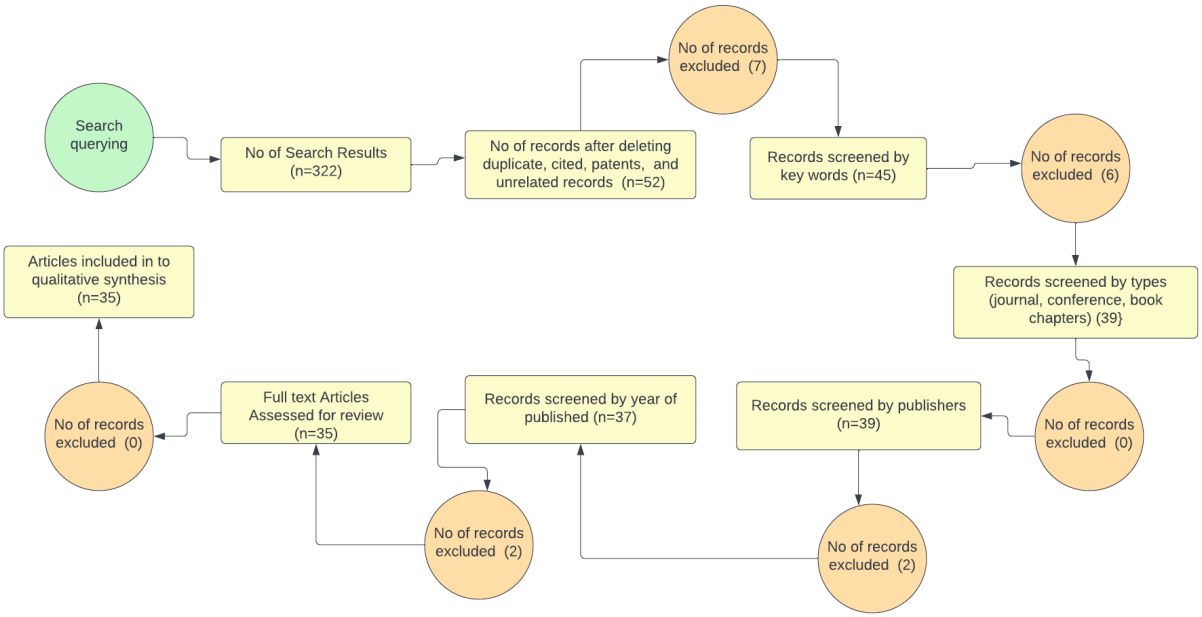

Figure 2: PRISMA Process and the Filtered Articles Count at Each Stage

The filtering process of the search results under PRISMA and resultant statistics explored following.

The total numbers of articles selected from initial search results are 332. The total numbers of articles filtered (after deleting duplicates, cited articles, and patents, unrelated articles) were 52.

Among these 45 articles were selected based on credible keywords. The statistics of the keywords and respective count of articles selected were listed in Table 3. Figure 3 exploring the ratio of articles for each keyword.

Table 3: The Keywords (25) and the Count of Related Articles Fetched (Total Number of Unique Articles 45)

S.No	Keywords	Number of Articles
1	Internet Of Things	9
2	Accident Detection	7
3	Traffic Safety	5
4	Smart Cities	4
5	Traffic Accidents	4
6	Autonomous Vehicles	4
7	Road Accident	4
8	Deep Learning	3
9	Real Time	3
10	Road Traffic	3
11	Autonomous Driving	3
12	Delivery Ratio	3
13	Data Set	3
14	Road Accidents	3
15	Internet Of Vehicles	3
16	Neural Network	2
17	Machine Learning	2
18	Smart City	2
19	Road Safety	2
20	Urban Areas	2

21	Detection System	2
22	Control Unit	2
23	Intelligent Transportation	2
24	Low Cost	2
25	Autonomous Vehicle	2

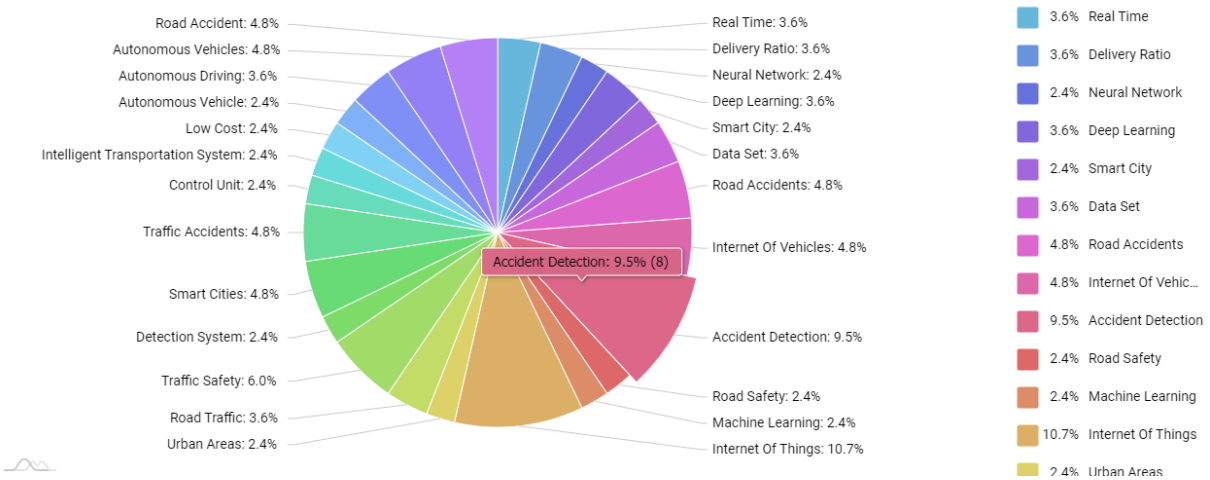

Figure 3: Ratio of Articles by Keywords

Further, articles were filtered by article publication type (journal, conference, book chapter and other contents), where 6 article were discarded. The statistics of the articles selected by their type were explored in table 4 and figure 4.

Table 4: The Publication Type and Number of Articles Selected

Type	**Number of Articles**
Journal Articles	39
Conferences	0
Book chapters	0
Other contents	0

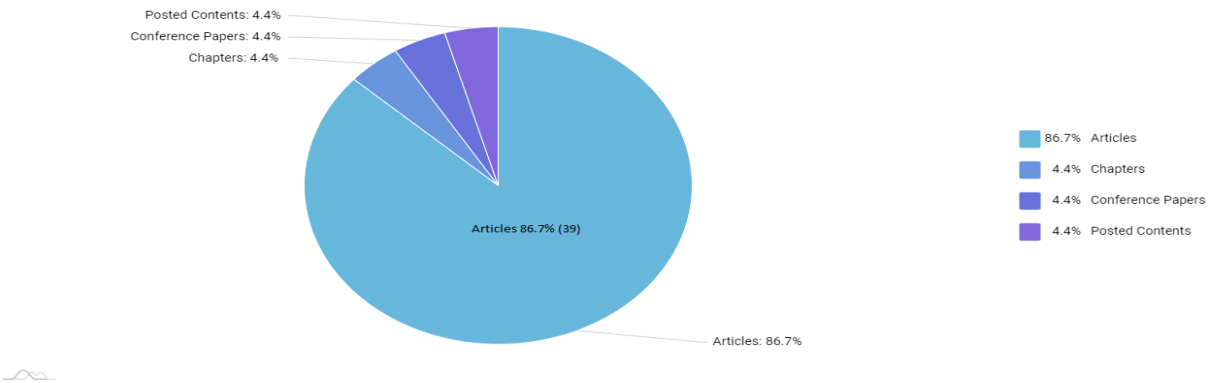

Figure 4: Ratio of Articles by Type

The resultant 39 articles were further processed to filter by publisher, where zero articles were discarded. The detailed statistics of the articles by publisher explored in Table 5 and depicted in Figure 5.

Table 5: Articles Filtered by Publisher

SR. No	Publisher	Number of articles
1	Fakultas Teknik Elektronika Dan Komputer Universitas Kristen Satya Wacana	1
2	American Scientific Publishers	1
3	MDPI AG	14
4	Blue Eyes Intelligence Engineering And Sciences Engineering And Sciences Publication - BEIESP	6
5	Inventive Research Organization	1
6	Trans Tech Publications, Ltd.	1
7	Institute Of Electrical And Electronics Engineers (IEEE)	1
8	ADD Technologies	1
9	Queensland University Of Technology	2
10	Walter De Gruyter Gmbh	1
11	Institute Of Advanced Engineering And Science	1
12	Science Publishing Corporation	1

13	Auricle Technologies, Pvt., Ltd.	1
14	IOS Press	1
15	Medip Academy	1
16	International Information And Engineering Technology Association	1
17	Publishing House Zaslavsky	1
18	Hindawi Limited	3
	Total number of Articles	**39**

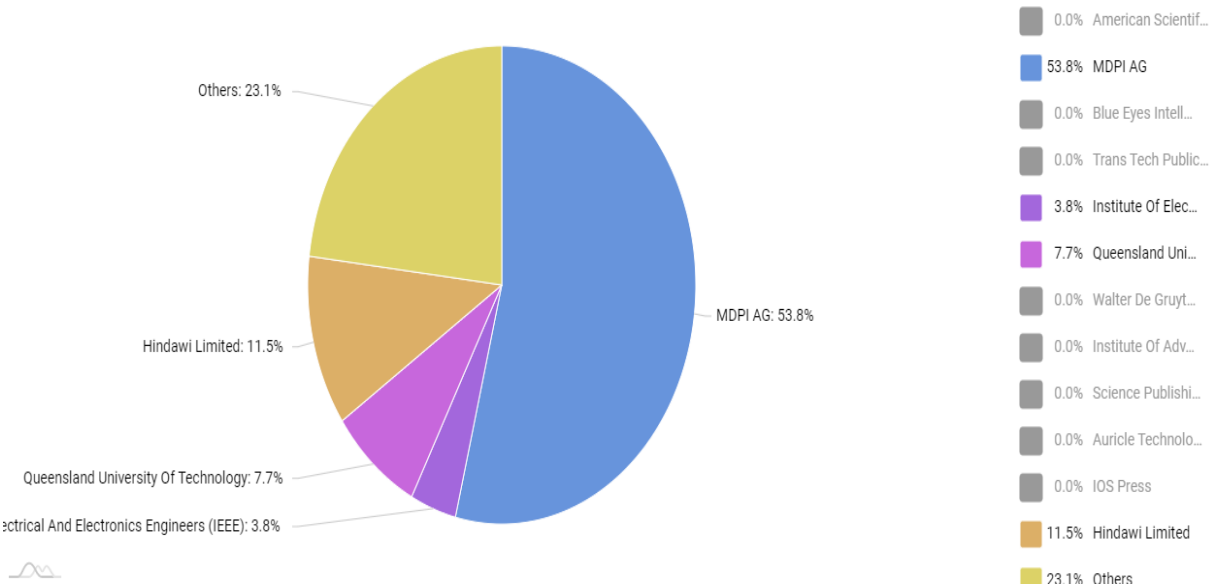

Figure 5: Ratio of Articles by Publisher

Finally articles were filtered by their year of publication. In this process, two articles were discarded. The resultant 37 articles were further filtered and discarded two more articles under qualitative synthesis factors. The statistics of the articles by year of publication were explored in Table 6 and figure 6.

Table 6: Articles Filtered by Year of Publication

SR. NO	Year	Count of Articles
1	2016	1
2	2017	2
3	2018	5
4	2019	11
5	2020	2
6	2021	16
	Total Number of Articles	**37**

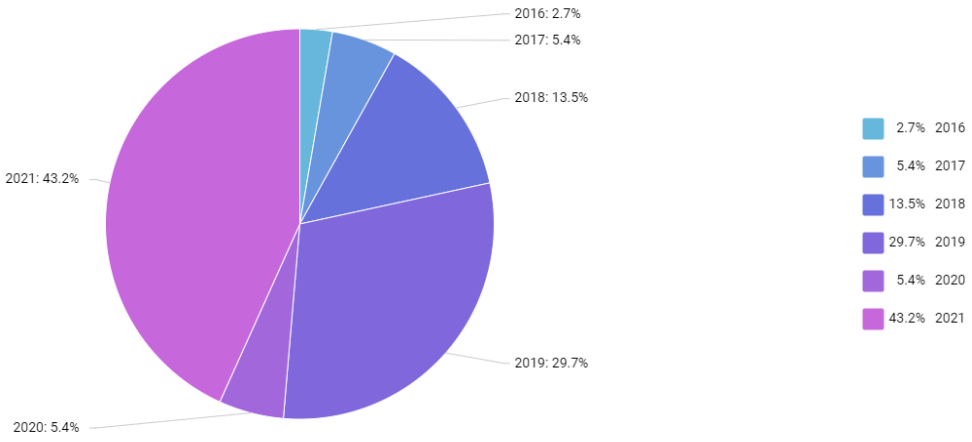

Figure 6: Ratio of Articles by Year of Publication

4.3. Review Strategy

The resultant articles were grouped into multiple topics, where topics were denoted by human annotation. The topics annotated and the lists of articles that fall in each topic have been listed in Table 7.

Table 7: The List of Articles Falls in Each Topic

Topic/ Category based on IoV applications	Reference ID
Accident Detection and Accident Alerts by data analysis	[14-35]
Route Monitoring and Congestion Avoidance	[36-39]
Driving Behavior Analysis to predict accident	[40], [41], [31]
Inter Vehicle Communication for safe driving	[42], [23], [43], [44]
Accident detection and Alerts in Autonomous Vehicles	[16], [36], [42], [33]
Vehicle safety analysis using Blockchain	[45]
Accident alerts and analysis by Black box	[18], [20]
Congestion alerts and control	[47], [48]
Data Analysis by Artificial Intelligence	[37], [40], [29], [44], [46], [31], [33-35]

Table 8. Abbreviations Used in this Manuscript

PRISMA	Preferred Reporting Items for Systematic Reviews and Meta-Analyses
GIDS	GAN Based Intrusion Detection System
RNN	Recurrent Neural Networks
IVI	In-Vehicle Infotainment
In-VGM	In-Vehicle Gateway Module
MOST	Media Oriented Systems Transport
CART	Classification and Regression Trees
DT	Decision Tree
NB	Naive-Bayes Tree
GMM	Gaussian Mixture Model
ITS	Intelligent Transport System
PDR	Packet Delivery Ratio
LTE	Long-Term Evolution
DSRC	Dedicated Short-Range Communication
CAN	Controller Area Network
SECCU	Security Control Unit
SIMATT	Simplified Attention
LSTM	Long Short-Term Memory
GRU	Gated Recurrent Unit
UE	User Equipment

5. Review of Literature

The main topic of the research articles is handling accidents in vehicles through technology, in particular, using Internet of Things. Table 7 detailed review of the contemporary literature follows.

Bhatti, F., et al. [14] created smart city accident detection along with reporting system centered on the IoTs. A cost effective smart transportation system can be implemented in existing autos using sophisticated smart phone characteristics. An Android app collects data on (i) speed, (ii) gravity, (iii) pressure, (iv) sound, along with (v) location in this case. Speed is

utilized to aid in the detection of accidents. It arises as a result of environmental differences (e.g., deceleration rate, and noise) between low-speed and high-speed collisions. After that, the data is analyzed to find traffic accidents. In addition, a navigation system is meant to alert the nearest hospital. Simulators and real data from the Road Safety Open Repository have been used to test the proposed approach, and the results are good.

Mai, Y. T., et al. [15] created an Intelligent Vehicular Warning System (IVWS) that sends out a warning in the event of a collision. Other cars or vehicles may have enough time after receiving the urgent warning signals to avoid a collision and make appropriate decisions such as slowing down, halting, or diverting. The local CMS (Changeable Message Sign) can display nearby automotive accident details after getting the warning message. The IVWS propose uses robot vehicles to simulate road traffic. Automobiles can also communicate via the ZigBee wireless interface. The authors stated that the system can show messages and keep cars safe by driving them in a safe way if found an accident.

Chan, T. K., et al. [16] defined enabling technology as driving from parking area, driving on the road, and parking at the required destination. The information gathered will be utilized to develop self-driving automobiles. While the driverless automobile is parking on the road, an unexpected obstruction is mentioned. Several social issues, such as the liability of an autonomous car accident, are discussed. The use of a smart device to look for unsafe driving is briefly discussed.

An IoV-ATCA-AO ‘2’-lane cellular automata model was proposed by Bao, J., et al. [17]. The two models are used to evaluate 2 types of traffic incidents involving abandoned objects: rear-end and vehicle-related. (1) Accidents happen when road density is low, but not when road density is large, according to the simulation findings. The results differ from the rate of single-lane rear-end collisions. In comparison to V-ATCA-visual-based AO's avoidance pattern, IoV-ATCA-AO might advise the vehicle to change lanes and decelerate early. There is a direct link between where and when a traffic bottleneck forms in front of an abandoned object and the number of accidents that happen.

J. Chen, et al. [18] described a multi-level car accident detection and alert system based on the Internet of Things. For accurate accident detection, the vehicles feature a "Black Box" board unit, a GPS accident location identification module, and mechanical sensors (accelerometer and gyroscope). The PDR of the proposed system was compared to relay nodes in this study. The evolution of the mobile/sensor node was studied using simulation results. The number of relay nodes also has an effect on the packet delivery rate.

Khaliq, K. A., et al. [19] presented a lower-cost accident detection and warning system centered on V2X communication along with Edge/Cloud computing. Automobiles with an Onboard Unit (OBU), gyroscope and accelerometer sensors, and a GPS module are used in this investigation to detect correct accident locations. The car also has a camera module attached to it to capture the moment of a collision. For inter-vehicle communication, each vehicle's OBU has a wireless networking interface as Inter-Vehicle Communications (IVC). It also serves as a link between the vehicle's sensors and the cloud server, preprocessing data. Road accident data can be used to come up with positive action plans that will help cut down on the number of people who die.

Usha Nandini, D., et al. [20] recommended employing a "Smart Black Box" that analyzes and collects data from adjacent autos to acquire accident safety information. The car that is at fault is first identified. Grayscale is used to depict the color image of the automobile. The image is then filtered on both sides. Canny edge detection is the algorithm used to detect the edges of the license plate. It is extracted and supplied to the server, which builds the video sequence for the application. GSM requests are received and responded to using the IoT.

To reduce fatalities, Jeyashree, et al. [21] designed an accident rescue system. Vehicles are tracked using Global System for Mobile communication (GSM), and accident sites are sent to an Accident Monitoring and Rescue Services Centre (AMRSC). The vehicle system's accelerometer gives real-time vehicle position data. The accelerometer delivers a signal to the controller when an accident happens. Accidents are detected by the Node MCU controller, which alerts the user and AMRSC. The system will now send the accident location and vehicle information to AMRSC via GSM. When the infected user's car system sends out an alert message, the rescue squad will be on its way to the accident site as soon as they can.

It was postulated by Tejashwini R et al. [22] that an affordable vehicle security system could be installed into a wide range of vehicles, and that the manufacturers could do the same. In a short time, a stolen car can be detected and tracked, and a notice can be sent to the owner. It's simple for the owner to turn the vehicle on and off, get the vehicle's location, and send a thief-photo link signal to the local police station in order to avoid vehicle theft and limit the number of accidents. In order to keep track of the vehicle's location, this software would take data from the vehicle's GPS tracking device and store it securely. Using this application, the user's current location can be retrieved. The thief’s photos have been sent. Also, Google Maps will show the vehicle's location in real time.

According to Wu, Q., et al. [23], vehicles traveling at varying speeds will have varying resident times within the road's coverage, successfully communicating varying amounts of data to the system. In regard to this, the cloud will provide various vehicles with varying amounts of critical data. As a result, faster vehicles are more likely than slower vehicles to be involved in a traffic accident. By adapting the minimal contention window for each vehicle to its velocity, the proposed fair-access technique ensures that cars traveling at varying speeds reliably communicate the same amount of data. Additionally, the proposed scheme's normalized throughput is calculated. Simulation is used to validate the fair-access strategy.

R. Nouh et al. proposed SafeDrive, a dynamic driver profile [24] (DDP). DDP is a collection of modules that examines a driver's behavior in light of prior violations and accidents. Primarily the authors created three synthetic data sets for 1,500 drivers based on their (a) profile, (b) risk factors, along with (c) risk probability. To forecast the driver's current and future risk ratings, they analyzed prior violation/accident data sets. In their study, they evaluated the effectiveness of proposed hybrid recommendation systems for reliably detecting driving data using multiple error calculation approaches. The findings are used to improve driving behavior and to alert other vehicles operating in the IoV environment, resulting in an overall increase in road safety. By monitoring vehicle movements, driver behavior, and road conditions on a regular basis, the proposed model also assists in anticipating vehicle, pedestrian, and road object safety.

Additionally, it reduces the complexity of on-road vehicles and fog/cloud computing server latency.

Meena, K., et al. [25] developed an Internet of Things-based approach to avoid and detect accidents. The safety of the vehicle's performance was regularly assessed. Maintaining speed balance and driver safety is a pain with this method. As a result, a novel method for averting accidents and saving victims is presented. When the distance between two vehicles is too close, sensors sound an alarm. If the camera is turned on by accident, it will snap photos at 180 degrees. Through a GSM modem, this information is sent to the nearest police station, ambulance service, and family. Major components include the (a) Arduino, (b) motion sensor, (c) touch sensor, relay, along with (d) GSM modem.

Satyamarda, F. W., et al., [26] aimed to improve Android Auto and CarPlay, particularly in the areas of vision and security. The most important factor to consider is that the motorist not be distracted. An Android phone and a Raspberry Pi are used in this car smartphone docking solution. Several test drives provided perfect results. According to an experiment, this strategy can cut down on the number of parts needed in a smart car.

According to Pathak, A., et al., [27], an IoT-based smart crossing system with object tracking is essential. A low-cost solution was offered based on the Arduino UNO R3 micro controller. The device is self-contained and can quickly compute the planned parameters of an IoT-based smart crossing platform for pedestrians. Ultrasonic and infrared sensors were used to assess the device's properties. Furthermore, this program is critical in Bangladesh. Road accidents are reduced by using this smart crossing technology.

According to Kavitha, K. V. N., et al. [28], the Internet of Things (IoT) can be employed in automotive systems to provide low-cost, continuous healthcare monitoring. Its purpose is to identify changes in the driver's health and prevent accidents on the road. Slowing down the car till it comes to a complete halt is one of these acts. Simultaneously, a warning or siren is transmitted to nearby motorists, alerting them to an impending emergency. The concerned medical personnel and the driver's emergency contacts receive an emergency message.

Chang, W. J., et al., [29] presented a Deep Crash-based Internet of Vehicles (IoV) system that includes an IVI telematics platform, a vehicle self-collision detection sensor, together with a front camera. An emergency notification is sent once accident detection information for self-collision vehicle recognition is sent to a cloud-based database server. According to the findings of the experiments, traffic collision detection accuracy can reach 96 percent, and emergency notification reaction time is roughly 7 seconds.

Yang Yong- Zheng, et al. [30] looked into the factors that impact underwater tunnel traffic accidents as well as built a model to forecast them. People who were involved in traffic accidents in the Jiaozhou Bay undersea tunnel were interviewed in person or over the phone, while those who traveled through were polled online. Based on traffic accidents, drivers with underwater tunnel experience were divided into accident and control groups. According to the data, drinking, bad driving behavior, traffic accident experience, speeding, and the other 13 variables all have a substantial impact on the occurrence of traffic accidents in the undersea tube. Using multivariate analysis of thirteen key parameters, a model for estimating the probability of accidents in underwater

tunnels was built. Tunnel length and traffic flow are linked to accidents in underwater tunnels. According to one of the studies, there are 1.96 daily traffic accidents in a 7-kilometer long underwater tunnel with a daily traffic flow of 50,000 cars. Undersea tunnel traffic accidents are primarily caused by driver violations and negligence.

According to Esteban Alejandro, et al. [31], demand for motorbikes is growing, necessitating the development of a strategy to reduce based on the analysis of dynamic driving behavior, the probability of road accidents. A 3-axis accelerometer sensor collected dynamic data regarding motorcycle riders' acceleration and behavior, which was then processed and analyzed for acceleration irregularities using three ML models: (a) Decision Trees, (b) K-Nearest Neighbors, and (c) Random Forests. The performance of every model was assessed to superior classify the degree of accident risk centered on definite acceleration levels. The random forest model outperformed the other two models with 97.24 percent accuracy, recall, precision, and an F1 score.

For accident prediction and perception in an IoV context, Huang, M., et al. [32] investigated VR technology with road network traffic updates. Real-time location and data transmission functions of the IoT can be used for virtual reality (VR) automotive management by using the IoV technology. When the time level is 2, the braking response sensitivity is 88.9 percent, which is a high percentage. To put it another way, 97.5 percent of the time, the distance level is 1. Thus, the IoV accident prediction effect is enhanced when time level 2 Virtual Reality technologies with traffic network information environment are used. At distance level 1, the VR-based and IoV-enabled road network traffic status information and accident perception work well. Real-time forecasting along with the perception of road network traffic status information can help prevent accidents.

Y. Jeong et al. [33] proposed a deep learning model that uses data from the vehicle's onboard internet-connected sensors to diagnose the vehicle and its components in order to achieve an Integrated Self System (ISS) for vehicle condition diagnosis in an IoT-based Autonomous Vehicle. The International Space Station is divided into three modules. To begin, the In-VGM collects data from in-vehicle sensors such as a black box, radar, and control messages and transmits it to the onboard diagnosis or actuators via the MOST, FlexRay, and CAN protocols. Data from in-vehicle sensors is collected using the CAN or FlexRay protocols, whereas data from media is collected using the MOST protocol. Messages are converted to the protocol message types used by the destination. The other module populates the training dataset with data from the vehicle's onboard sensors and calculates the probability of vehicle components and consumables failing and causing damage to other components. The third module of the model evaluates the vehicle's total risk. Edge Computing helps accelerate self-diagnosis and reduces system overhead. A Vehicle-to-Vehicle (V2X)-based Accident-Notification-Service (VANS) notifies neighboring vehicles and infrastructure of the OBD's self-diagnosis results.

Balfaqih, Mohammed, et al. [34] employed the IoT to detect and classify incidents. Car accidents are identified and classified by the technology, which then alerts emergency services. To identify vehicle motion parameters, the system employs a microcontroller, GPS, and sensors. The created approach was also put to the test with a variety of ML classifiers to determine which one was the most accurate. GMM, NB, DT, and CRT are the classifiers (CART). The CART as well as GMM

models have improved precision and sensitivity, according to the system. Accident severity is also affected by g-force and fire.

Mohanta, Bhabendu Kumar, et al. [35] discovered elements that influence the severity of car accidents. To forecast accident severity, this study used classification approaches such as Logistic Regression, Random Forests, Decision Trees, and Artificial Neural Networks. According to the testing data, these classification models are highly accurate. For ITS components to securely share information, the article also proposed a secure communication architectural paradigm.

Panadero, et al. [36] described route design as a team orienteering challenge. An 'agile'' optimization strategy for drones and other autonomous vehicles suggested which relied on a quick biased-randomized heuristic and parallel computation. The article centered on the web-based alert system for people who use smart IoT devices to get messages from their phones or other smart devices.

Aboulola, O., et al. [37] developed the multimodal driver analysis (MODAL) technique for the internet of connected vehicles (IoCV) using deep learning. This technique is divided into three steps. The hidden Markov models (HMM) are intended to forecast movement of the vehicle and changing of lanes in the first phase. In the second step, Squeeze Net would extract features from these classes. The final step introduces a tri-agent (TA)-based soft-actor critic (SAC) for route suggestion and planning. Finally, in terms of accuracy, latency, false alarm rate, and vehicle movement prediction error, Authors stated that the suggested MODAL-IoCV method has outperformed existing methods in experimental study.

To alleviate traffic congestion, Raiyn, J. et al. [38] presented a strategy for regulating traffic in smart cities. Searching, updating, and allocating are all part of the system (SUA). The SUA technique shortens the time it takes to forecast the conditions of all road segments in real time. It uses historical data to find the shortest route, and then uses real-time vehicle position to calculate journey time forecasts. A vehicle is assigned to the appropriate sector based on its current information, such as journey duration and accident forecasts. The SUA program is unique in that it refreshes vehicles in order to reduce traffic congestion. This strategy also encourages autonomy and self-regulation, making it a good fit for smart cities that use IoT technologies.

Paul, A., et al. [39] devised three approaches for reducing traffic congestion. The first two approaches use the number and direction of cars crossing intersections to control traffic congestion. An agent must detect the surroundings in order to control the succession of green signals along different pathways. In terms of storage, communication, and computing overhead, the three ITS techniques are compared. They are assessed at both a conceptual and statistical level. The quantitative performance of the three schemes is compared to that of five others. Because there is less time for vehicles to wait, the proposed solutions are shown to help with congestion better than existing schemes.

The relationships between IOT data and inadvertent driving behavior were examined by Chaikheatisak, A., et al. [40], who created machine learning models to categorize unintended driver behavior in natural gas vehicles. The information was obtained from Thailand's natural gas transportation system, which provided the data. The model was built using the Analytics Platform. The study discovered a

link between the latitude and longitude coordinates and the driver's inadvertent conduct. The maximum accuracy (73%) is achieved by a neural network with two hidden layers and five neurons in the hidden layer, followed by a support vector machine with S3.9 percent. A Neural Network [40] can be used to build a prediction model.

He, S., et al. [41] introduced a multi membership function, an entropy weight (EW) method, an analytic-hierarchy process (AHP), and a fuzzy evaluation algorithm. The first step is to develop a technique for evaluating the risk of commercial vehicles to increase the safety of those vehicles. Second, instead of using the usual AHP technique to determine each evaluation index's weight vector, EW-AHP is used. The matrix is then utilized to assess driving behavior safety using the multi membership function and fuzzy mathematics theory. Finally, trials are used to confirm real-world driving data and behavior. The model can accurately and fairly judge how safe it is to drive, which is very important for improving road safety.

Raghavendra, K., et al. [42] presented a comprehensive view of vehicular communication, including the antennas required for the most recent 5G communication, as well as the impact of fractal geometry-based antennas on vehicular communication and 5G for linked autonomous vehicles.

N. Azzaoui et al. [43] investigated the distribution of emergency messages in a dynamic network of Internet-enabled smart vehicles, referred to as IoV (Internet of Vehicles). By combining DSRC and cellular LTE wireless communication, they proposed a new method of emergency package distribution. This method employs dynamic clustering and a novel mechanism for selecting cluster heads to deal with broadcast storms. According to the authors, the proposed strategy also avoids packet collisions by assigning cluster heads to the most stable vehicles. A data dissemination scheme was compared to a simulation of the approach in an urban environment. This technique is said to reduce collisions and broadcast storms while increasing packet delivery ratios, throughput, and latency as compared to existing schemes.

J. Xiao and colleagues [44] examined a generic threat scenario in which attackers may acquire access to the CAN bus via standard access gateway points such as but not limited to WiFi, Bluetooth, and cellular communication. A machine learning-based mechanism for detecting in-vehicle network anomalies is proposed. SECCU and SIMATT are two models that achieve anomaly detection performance. To establish a lightweight method to anomaly detection, the authors aimed to minimize the computing costs associated with both the training as well as detection phases. The computational costs of the SIMATT concept have been reduced, and the SECCU system now consists of a single layer of 500 computing cells. When it comes to accuracy and recall rate, the SIMATT-SECCU architecture is almost as good as certain other algorithms, such as LSTM, GRU, GIDS, and RNN, or their derivatives.

To improve law violation detection, Davydov, V., et al. [45] presented blockchain-based accident detection systems. The authors propose an innovative technology known as "offline detection," which identifies accidents without the use of communication or the Internet. Blockchain technology has the potential to improve roadside honesty, transparency, and veracity. The reason that blockchain contents remain permanent and cannot be altered, it can be used to rebuild the whole road system, including cars and other infrastructure.

The use of city bridges as interception places was examined by Park, S., et al. [46]. Due to the high cost of installing car weighing devices on the road surface, IoT, sensors, including gyroscope and acceleration sensors, are used on bridges. Initially, they examined how the detected values differ between overloaded and non-overloaded cars. The authors then proposed a new strategy for identifying high-traffic zones based on the hypothesis. There are two steps to the proposed approach. A new classification model that uses bidirectional long-short-term memory (Bi–LSTM) was developed for bridge-traffic. Because of its symmetric neural network construction, which facilitates forward and backward processing of input data, the Bi–LSTM model outperforms other neural network models. Second, a new way of automatically determining high-traffic top-k time zones using the k-Nearest Neighbor (KNN) technique, identifies the closest sensing value to the actual sensing value of the overloaded vehicle. The difference in sensor values between overloaded and non-overloaded cars is statistically significant. The suggested method has a first-step accuracy of 75% and automatically identifies time zones with overloaded vehicles.

Shridevi Jeevan et al. [47] study emphasizes the use of Machine Learning to identify traffic congestion based on variety of criteria such as hard delay constraints, the speed available via GSP vehicle trajectory. The authors used the Gaussian process in Machine Learning to forecast traffic speed using three datasets i.e. training, prediction, and road sector data frame. In this study, the authors calculated the average speed of cars on the road sector during three separate time slots in order to predict vehicle traffic congestion.

Sun, et.al.[48] predicted the intensity of traffic congestion using processed GPS trajectory data. The GPS trajectory data is matched to the road network using a hidden Markov model, and the average speed of road sections computed using nearby GPS trajectory data. Congestion level prediction is performed using four deep learning models: convolution neural networks, recurrent neural networks, long short-term memory, and gated recurrent unit, as well as three traditional machine learning models: autoregressive integrated moving average model, support vector regression, and ridge regression. The results of the experiments, deep learning models forecast traffic congestion more accurately than traditional machine learning models in real-time, traffic forecasting, and short-term traffic forecasting.

6. Observations

IoV systems are fundamentally designed to provide real-time data links between vehicle nodes, IoT devices, and cloud services. Guaranteeing safety as well as faster travel, reduced energy consumption and better vehicle maintenance is the purpose of the IoV technology. A significant advantage of IoV is the ability to assess road conditions much more quickly and accurately. Controllable and maintainable IoV systems necessitate the development of novel intelligent models and solutions. However, open and heterogeneous systems complicate and confine these networks. The new solutions should enhance interoperability amongst IoV systems. Some of the abbreviations used in this article along with the meaning are given in Table 8. The IoV of big data can increase network pressure. Globally feasible and sustainable, the new system should be. Numerous users, several networks, security, large data analysis, scalability, and multimode communications all provide new challenges. The IoV

network model's resource usage, stability, scalability, and robustness must all be maximized. In some instances, technologies for big data and cognitive computing are merged. The issue of space-time distribution and service requirements, on the other hand, persists.

Due to the fact that IoV networks have multiple levels of connection, communication capability and joint optimization remain a challenge. Frequent movement of vehicle nodes, changing topologies, and unpredictable networks are only a few of the network issues. Another issue for IoV networks is the massive virtual platform for drivers within cooperative vehicles. The majority of drivers disregard the system and attempt to evade its restrictions. Due to the similarity in kind and degree of IoV services, network models confront a similar difficulty. In addition, network partitions, failures, disconnections, obstacles, low data rates, weak signals, delay, as well as overhead must be taken into account.

In the future, IoV systems will contribute to societal and economic progress by improving the safety, robustness, and scalability of transportation. Another future option for reducing fuel consumption is to implement more ecologically friendly modes of traffic control. Reduced traffic means that the new intelligent systems will consume less gasoline. This expands the market opportunities for businesses to promote their products. The following are the most vital benefits of the IoV.

Increased safety of transportation: Autonomous vehicles that work in an appropriate infrastructure considerably augment the safety of transportation. Sensors and software track (i) the speed of cars, (ii) the temperature of the road, and (iii) the number of cars at intersections. Besides eliminating human error, these schemes can as well monitor the diverse mechanical part's condition of the smart car, alert drivers, can detect potential problems prior to occurrence of accident. Moreover, the number of accidents is lessened by the IoV, yet it as well lessens the accident's consequences if the collision can't be evaded.

Faster travel and convenience: With vehicles connected to the internet, transit becomes more efficient and the user experience is enhanced significantly. A smart transportation infrastructure majorly assists in accomplishing the following:

- **Decreased congestion on the roads**: In order to avoid traffic jams, real-time traffic monitoring and autonomous technology combined together can optimize routes and speeds.
- **Optimized routes**: Mobile apps that obtain real-time data as of every user's location could recommend the optimal routes to reduce travel time.
- **Better parking**: IoV enables better parking; the most preferred features of the infrastructure is smart parking. Beacons placed in parking spaces could guide drivers to empty spots, whilst fully autonomous vehicles could park effectively devoid of any human interference.
- **Remote car management**: Smart cars that are noticeable on the network permit drivers to discover their vehicles rapidly in an (i) crowded parking lot, (ii) lock doors remotely, (iii) obtain information regarding the car's condition rapidly, along with (iv) track the car if somebody steals it.

Decreased energy consumption and costs: Internet-enabled vehicles can as well optimize the usage of (a) fuel, (b) electricity, along with (c) human resources. Smart lights, on the other hand, adapt to the traffic situation on the road and consume less electricity than traditional traffic lights that operate on timers. The decrease in operating expenses is guaranteed by the superior performance as well as resource allocation of IoV technology.

Environmental benefits: There are a number of incredible environmental benefits associated with IoV technology. In order to reduce CO2 emissions and promote a sustainable energy future, cities have the greatest impact.

By operating more effectively, connected vehicles will reduce greenhouse gas emissions. Furthermore, once car sharing along with the usage of public transport turns out to be comfortable and rapid as utilizing a private car, they are likely to augment. In addition to decreasing the number of vehicles on the roads, this will also lessen the detrimental effects on the environment. Furthermore, autonomous vehicles are chiefly electric cities can considerably decrease their fuel along with electricity consumption and recharging stations can be equipped with solar panels.

Future networks would be more sophisticated, necessitating a higher level of security. Additional intelligent models and architecture are required. Another upcoming advancement is data processing with improved operating support systems. Another avenue for communication providers to pursue is the reduction of IoV smart devices and other gear. Another issue is the accuracy of location data. GPS systems give accurate information, but they get worse when there are issues with nodes moving and signal availability, like tunnels, under bridges, as well as densely populated areas.

7. Discussion and Conclusion

Regarding vehicle safety, the outcomes of this literature review have evinced that Internet-enabled SVs have diverse benefits. Furthermore, they play a vital function in the technology era. (i) Ameliorated safety, (ii) efficacy, (iii) mobility, (iv) accessibility, and (v) intermodal connections are the benefits proffered by Internet-enabled SVs. Numerous areas take advantage by means of the SV system. (a) Freeway, (b) freight, (c) transit, (d) incident, (e) emergency, (f) data collection, (g) environmental issues, (h) traveller information, along with (i) accident control are the beneficiaries' areas. The performance investigation of the Internet-enabled SVs as well as the effective comparison regarding accuracy is exhibited in this section.

Table 9: Performance Analysis of the Existing Methodologies in Terms of Accuracy

References	Accuracy rate (%)
R[29]	96
R[31]	97.24
R[46]	75
R[40]	87.3

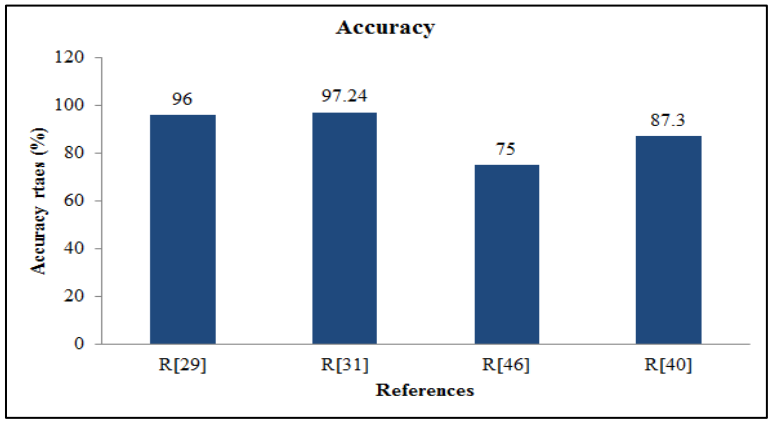

Figure 7: Methodologies Compared with Respect to the Accuracy Rates

Table 9 and Figure 7 evince the performance along with the comparative investigation of the diverse safety techniques of Internet-enabled SVs methodologies. Centered on the accuracy rates, this investigation is done. It is recognized from the investigation that R[31] achieved the utmost accuracy rates of 97.24% as analogized to the other prevailing algorithms, whereas other methods, namely R[29] accomplish 96%, R[46] accomplish 75%, along with R[40] achieves 87.3%.R[46] acquired an extremely lower rate of accuracy of 75% amongst them. So, it is inferred that the majority of the prevailing algorithms work well and withstand superior accuracy rates.

The "Internet of Vehicles (IoV)," also known as "Internet-enabled SVs," is a futuristic technology in which vehicles are linked via various short- and long-distance communication networks. IoV's major goal is to create secure and safe networks wherein consumers can access a variety of services. To produce intelligent processes, this sophisticated technology involves the analysis of data and cloud-enabled services. Different procedures have been handled by modern civilizations to enable smart automobiles to tackle critical difficulties like vehicle accidents. These recent contributions to research would be advantageous to IoV technology. ML, blockchain, and a "black box" have all been mentioned in recent literature as smart strategies. They can assist smart cars in remaining safe, but they can also cause accidents and increase the likelihood of them occurring. The fact that a wide range of ML algorithms has been developed and assessed for SV applications was emphasized in this study, evincing that the nature and scale of data accumulated in these applications are perfect for ML exploitation. However, a key constraint to the present contributions noted in this comprehensive analysis is the lack of feature engineering to address data unbalancing and high dimensionality. In addition, the majority of current models are focused on detecting accidents and alerting risk teams. Another major flaw with these new concepts is that they lack innovative ways to protect autos from human mistakes and traffic accidents. Most of the traditional methodologies are failed to maintain better reliability whenever a piece of hardware malfunctions or becomes unresponsive, the reliability is severely affected. There is still numerous works to be done in the future to develop new feature engineering techniques and ML-based smart strategies that can

forecast vehicle accident-prone events such as unusual vehicle movement and path anomalies to prevent needless deaths and infrastructure from being harmed. Moreover, the utilization of the prevailing techniques can't offer connectivity without errors. In SVs as the technologies involved are modelled exclusively for a restricted number of devices as well as bolstered for a specific range of communication. Thus, more focus should be given to facilitate unimpaired connectivity in SVs in the future.

References

1.Yaqoob, I., Hashem, I. A. T., Mehmood, Y., Gani, A., Mokhtar, S., & Guizani, S. (2017). Enabling communication technologies for smart cities. IEEE Communications Magazine, 55(1), 112-120.

2.Singh, P. K., Nandi, S. K., & Nandi, S. (2019). A tutorial survey on vehicular communication state of the art, and future research directions. Vehicular Communications, 18, 100164.

3.Qureshi, K. N., & Abdullah, A. H. (2013). A survey on intelligent transportation systems. Middle-East Journal of Scientific Research, 15(5), 629-642.

4.Iqbal, S., Qureshi, K. N., Kanwal, N., & Jeon, G. (2022). Collaborative energy efficient zone-based routing protocol for multihop Internet of Things. Transactions on Emerging Telecommunications Technologies, 33(2), e3885.

5.Cooper, C., Franklin, D., Ros, M., Safaei, F., & Abolhasan, M. (2016). A comparative survey of VANET clustering techniques. IEEE Communications Surveys & Tutorials, 19(1), 657-681.

6.Qureshi, K. N., Abdullah, A. H., Lloret, J., & Altameem, A. (2016). Road-aware routing strategies for vehicular ad hoc networks: Characteristics and comparisons. International Journal of Distributed Sensor Networks, 12(3), 1605734.

7.Qureshi, K. N., Din, S., Jeon, G., & Piccialli, F. (2020). Link quality and energy utilization based preferable next hop selection routing for wireless body area networks. Computer Communications, 149, 382-392.

8.Qureshi, K. N., Ahmad, A., Piccialli, F., Casolla, G., & Jeon, G. (2021). Nature-inspired algorithm-based secure data dissemination framework for smart city networks. Neural Computing and Applications, 33(17), 10637-10656.

9.Maglaras, L. A., Al-Bayatti, A. H., He, Y., Wagner, I., & Janicke, H. (2016). Social internet of vehicles for smart cities. Journal of Sensor and Actuator Networks, 5(1), 3.

10.Ning, Z., Zhang, K., Wang, X., Obaidat, M. S., Guo, L., Hu, X., ... & Kwok, R. Y. (2020). Joint computing and caching in 5G-envisioned Internet of vehicles: A deep reinforcement learning-based traffic control system. IEEE Transactions on Intelligent Transportation Systems, 22(8), 5201-5212.

11.Tuyisenge, L., Ayaida, M., Tohme, S., & Afilal, L. E. (2020). Handover mechanisms in Internet of vehicles (IoV): Survey, trends, challenges, and issues. In Global Advancements in Connected and Intelligent Mobility: Emerging Research and Opportunities (pp. 1-64). IGI Global.

12.Qureshi, K. N., Idrees, M. M., Lloret, J., & Bosch, I. (2020). Self-assessment based clustering data dissemination for sparse and dense traffic conditions for internet of vehicles. IEEE Access, 8, 10363-10372.

13.Moher, D., Liberati, A., Tetzlaff, J., Altman, D. G., & PRISMA Group*. (2009). Preferred reporting items for systematic reviews and meta-analyses: the PRISMA statement. Annals of internal medicine, 151(4), 264-269.

14.Bhatti, F., Shah, M. A., Maple, C., & Islam, S. U. (2019). A novel internet of things-enabled accident detection and reporting system for smart city environments. Sensors, 19(9), 2071.

15.Mai, Y. T., Chen, J. Y., Liu, Y. K., Lee, W. Y., Wu, G. T., & Li, M. Y. (2012). Intelligent vehicular warning system for VANET. In Applied Mechanics and Materials (Vol. 145, pp. 164-168). Trans Tech Publications Ltd.

16.Chan, T. K., & Chin, C. S. (2021). Review of autonomous intelligent vehicles for urban driving and parking. Electronics, 10(9), 1021.

17.Bao, J., Chen, W., Xiang, Z., Chen, Y., & Shui, Y. (2018). Effect analysis of early warning for abandoned object on highway based on Internet-of-Vehicles CA model. Discrete Dynamics in Nature and Society, 2018.

18.J. Chen, S. Smys (2021). Construction of Black Box to Detect the Location of Road Mishap in Remote Area in the IoT Domain. Semantic Scholar, 2021

19.Khaliq, K. A., Chughtai, O., Shahwani, A., Qayyum, A., & Pannek, J. (2019). Road accidents detection, data collection and data analysis using V2X communication and edge/cloud computing. Electronics, 8(8), 896.

20.Usha Nandini, D., Sathyabama Krishna, R., Nithya, M., & Pavithra, R. (2019). A resourceful information collecting system using smart black box. Journal of Computational and Theoretical Nanoscience, 16(8), 3346-3350.

21.Jeyashree Arthanareeswaran et al., (2021). Automatic Vehicle Accident Indication and Reporting System for Road Ways Using Internet of Things. International Journal of Safety and Security Engineering Vol. 11, No. 3, June, 2021, pp. 269-277.

22.Tejashwini R et al., (2021). Design and Development of Vehicle Theft Detection, Tracking and Accident Identifier System using IoT. Journal of University of Shanghai for Science and Technology, Volume 23, Issue 7, July - 2021

23.Wu, Q., Xia, S., Fan, P., Fan, Q., & Li, Z. (2018). Velocity-adaptive V2I fair-access scheme based on IEEE 802.11 DCF for platooning vehicles. Sensors, 18(12), 4198.

24.Nouh, R., Singh, M., & Singh, D. (2021). SafeDrive: Hybrid recommendation system architecture for early safety predication using Internet of Vehicles. Sensors, 21(11), 3893.

25.Meena, K., Amuthadevi, C., & Kumar, G. S. (2018). Internet of Things based accident prevention

and detection system. International Journal of Engineering & Technology,[S. 1.], 7(2.4), 85-87.

26.Satyamarda, F. W., Nugroho, N. P. W., & Yohanes, B. W. (2021). Multimedia Vehicular Smartphone Docking with GPS Tracking. Techné: Jurnal Ilmiah Elektroteknika, 20(1), 27-36.

27.Pathak, A., Adil, M., Hossain, M. J., Rafa, T. S., & Pushpa, U. S. (2020). Pedestrian-safer IoT-based Smart Crossing System with Object Tracking. Int. J. Recent Technol. Eng, 9(1), 1948-1953.

28.Kavitha, K. V. N., Kesarwani, K., Pranav, S. M., & Noah, T. (2018). Real-Time Monitoring of Driver's Biometrics to Prevent Multi-Vehicle Chain Collisions Caused by Impending Medical Emergencies. International Journal of Engineering & Technology, 7(3.6), 51-54.

29.Chang, W. J., Chen, L. B., & Su, K. Y. (2019). DeepCrash: a deep learning-based Internet of vehicles system for head-on and single-vehicle accident detection with emergency notification. IEEE Access, 7, 148163-148175.

30.Yang Yong- Zheng et al., (2020). Analysis of Influencing Factors of Traffic Accidents in Undersea Tunnel. Journal of Engineering Research and Reports. 2020, Volume 15, Issue 3, Page 37-49.

31.Esteban Alejandro Cárdenas-Lancheros et al., (2021). Incident forecasting model for motorcycle driving based on IoT and artificial intelligence. Indonesian Journal of Electrical Engineering and Computer Science, Vol 24(1), pp. 444.

32.Huang, M., Li, G., Bai, Z., & Shao, Q. (2020). VR Technology and the Theoretical Model and Method of Road Network Traffic State Information Accident Prediction and Perception under the Environment of Internet of Vehicles. IEEE Access. pp.1-1,

33.Jeong, Y., Son, S., Jeong, E., & Lee, B. (2018). An integrated self-diagnosis system for an autonomous vehicle based on an IoT gateway and deep learning. Applied Sciences, 8(7), 1164.

34.Balfaqih, Mohammed, et al.(2021) "An Accident Detection and Classification System Using Internet of Things and Machine Learning towards Smart City." Sustainability 14.1 : 210. Using Deep Learning. Applied Sciences, 11(21), 10462.

35.Mohanta, Bhabendu Kumar, et al. "Machine learning based accident prediction in secure iot enable transportation system." Journal of Intelligent & Fuzzy Systems 42.2 (2022): 713-725.

36.Panadero, J., Ammouriova, M., Juan, A. A., Agustin, A., Nogal, M., & Serrat, C. (2021). Combining parallel computing and biased randomization for solving the team orienteering problem in real-time. Applied Sciences, 11(24), 12092.

37.Aboulola, O., Khayyat, M., Al-Harbi, B., Muthanna, M. S. A., Muthanna, A., Fasihuddin, H., & Alsulami, M. H. (2021). Multimodal Feature-Assisted Continuous Driver Behavior Analysis and Solving for Edge-Enabled Internet of Connected Vehicles Using Deep Learning. Applied Sciences, 11(21), 10462.

sheltering in-vehicle network through lightweight machine learning. Symmetry, 11(11), 1388.

45.Davydov, V., & Bezzateev, S. (2020, January). Accident detection in internet of vehicles using blockchain technology. In 2020 international conference on information networking (ICOIN) (pp. 766-771). IEEE.

46.Park, S., On, B. W., Lee, R., Park, M. W., & Lee, S. H. (2019). A Bi–LSTM and k-NN Based Method for Detecting Major Time Zones of Overloaded Vehicles. Symmetry, 11(9), 1160.

47.Shridevi Jeevan Kamble, Manjunath R Kounte (2020), Machine Learning Approach on Traffic Congestion Monitoring System in Internet of Vehicles,Procedia Computer Science,Volume 171,Pages 2235-2241

48.Sun, Shuming, Juan Chen, and Jian Sun.(2019) "Traffic congestion prediction based on GPS trajectory data." International Journal of Distributed Sensor Networks.

49.Wang J, Shao Y, Ge Y, Yu R (2019) A survey of vehicle to everything (v2x) testing. Sensors 19:334–334. https://doi.org/10.3390/s19020334.

50.Kumar R, Dave M (2012) A review of various vanet data dissemination protocols. Int J u-and e-service. Sci Technol 5:27–44

38.Raiyn, J. (2017). Road traffic congestion management based on a search-allocation approach. Transport and Telecommunication Journal, 18(1), 25-33.

39.Paul, A., Ghosh, K., & Mitra, S. (2021). Three Fog Computing Based Variants of Congestion Control in ITS.International Journal of Recent Technology and Engineering (IJRTE) ISSN: 2277-3878, Volume-10 Issue-1, May 2021

40.Chaikheatisak, A., & Chaiwuttisak, P. (2021, April). Analysis of Driver's Attention through the Internet of Things (IOTs) for Preventing Road Accident of Natural Gas Vehicles. In 2021 7th International Conference on Engineering, Applied Sciences and Technology (ICEAST) (pp. 168-172). IEEE.

41.He, S., Wang, Y., Chen, Y., Xiao, F., Deng, J., & Xu, E. (2021). Research on Safety Evaluation of Commercial Vehicle Driving Behavior Based on Data Mining Technology. Journal of Sensors, 2021.

42.Raghavendra, K., & Kakkar, D. (2021). A Review on Fractal Geometry Enhanced Vehicular Communication under 5G Environment. AIJR Proceedings, 280-288.

43.Azzaoui, N., Korichi, A., Brik, B., & Fekair, M. E. A. (2021). Towards optimal dissemination of emergency messages in Internet of vehicles: a dynamic clustering-based approach. Electronics, 10(8), 979.

44.Xiao, J., Wu, H., & Li, X. (2019). Internet of things meets vehicles:

مراجعة منهجية لطرق الأمان للمركبات الذكية المزودة بالإنترنت

محمد حميد محمد الحميد

كلية علوم الحاسب وتقنية المعلومات، جامعة جازان ، المملكة العربية السعودية

الملخص

مكن إنترنت الأشياء (IoT)من استخدام مناطق التطبيقات الذكية والأجهزة الذكية في العديد من جوانب المدن الكبرى اليوم. تُستخدم استراتيجيات تعلم الآلة (ML) لزيادة الذكاء والوظائف بمساعدة الكمبيوتر عن طريق زيادة كمية البيانات المتاحة. اكتسب النقل الذكي اهتمامًا كبيرًا نتيجة لتطبيقه لمنهجيات تعلم الآلة وإنترنت الأشياء. في هذه المراجعة، تُعرَّف القيادة الآلية بأنها عملية تحسين مسارات السفر ووقوف السيارات واكتشاف الحوادث السابقة والمحتملة والتنبيه إليها. الغرض من هذا البحث هو تقديم نظرة شاملة على تقنيات مثل تعلم الآلة وسلسلة الكتل والصندوق الأسود المستخدمة في أنظمة النقل بالمركبات الذكية للتعامل مع الحوادث وكيفية تغطية الفجوات. وبالتالي، سيكون هذا البحث مفيدًا وسيمكن الباحثين من استخدام تقنيات إنترنت المركبات IoV وتعلم الآلة لحل مشاكل النقل والأتمتة المعقدة.

الكلمات المفتاحية: إنترنت الأشياء، تعلم الآلة، إنترنت المركبات (IoV)، PRISMA، نظام الكشف، الشبكة العصبية، النقل الذكي.

Optimal Locations of Capacitors in a Radial Distribution System via Slime Mould Algorithm

E. S. Ali[1], S. M. Abd Elazim[2]

[1]Electric Department, Faculty of Engineering, Jazan University, Jazan, KSA

[2]Computer Science Department, Faculty of Computer Science and Information Technology, Jazan University, KSA.

Abstract

A new and powerful approach called Slime Mould Algorithm (SMA) is suggested in this paper, for optimal siting and sizing of capacitors for an IEEE distribution network. First, the most nominee buses for installing capacitors are developed using various indices. Loss Sensitivity Factors (LSF), Voltage Stability Index (VSI), and Power Loss Index (PLI) are employed to determine the elected buses. Then the proposed SMA is used to deduce the size of capacitors and their positions from the picked buses. The objective function is introduced to minimize the net cost and then, increase the total saving per year. The developed approach is tested on the IEEE distribution network. The obtained results are compared with others to highlight the advantages of the developed approach. Also, the results are presented to confirm its influence in minifying the losses, and net cost and to improve the voltage profile and total saving for a radial distribution network.

Key-Words: Slime Mould Algorithm; Loss Sensitivity Factors**;** Voltage Stability Index; Power Loss Index; Optimal Capacitor Locations; Distribution System.

1. Introduction

Transmission and distribution system losses are considered the main consumption in any power network. Due to the growth in the load, and environmental limits, the transmission, and distribution networks are being worked under overloaded situations, and losses in the distribution systems have become the main concern. To attain economic advantages, the fundamental conditions to get agreeable power quality and enhanced efficiency have formed a very auspicious environment for the matter of loss minimization approaches and using recent operational practices. Power loss reduction is the only alternative to enhance the efficacy of the distribution network. Therefore, it is noted that in the last few decades many researchers have concentrated on distribution network loss reduction and voltage stability. There are many helpful techniques in the literature for distribution network loss reduction [1]. However, the most often used mechanisms like (a) capacitor siting, (b) network restructure [2] (c) DG siting [3], (d) DSTATCOM siting and its mixed versions to realize upper potential interests are (e) simultaneous restructure and capacitor siting, (f) simultaneous restructure and DG siting, (g) simultaneous DG and DSTATCOM siting, and (h) simultaneous restructure, capacitor, and DG siting are presented in [1]. Conventionally, loss reduction has focused mainly on network restructure optimizing or capacitor siting for reactive power policy. Since installing capacitors are the simplest and most famous solution, they are getting steadily to be important components of the distribution network [1].

Pending last years, diverse algorithms are presented to find the proper locations and optimal sizes of shunt capacitors. Simulated Annealing (SA) [4], Tabu Search (TS) [5], Genetic Algorithm (GA) [6], Mixed Integer Nonlinear Programming Approach (MINPA) [7]**,** Direct Search Algorithm (DSA) [8], Teaching Learning Based Optimization (TLBO) [9], Plant Growth Simulation Algorithm (PGSA) [10], Heuristic Algorithm [11], Cuckoo Search Algorithm (CSA) [12], Particle Swarm Optimization (PSO) [13], Fuzzy Genetic Algorithm (FGA) [14], Differential Evolution (DE) [15], Flower Pollination Algorithm (FPA) [16-17], Improved Harmony Search (IHS) [18], Mine Blast Algorithm (MBA) [19], and Moth Swarm Algorithm (MSA) [20] are developed to deal with the capacitor placement task. However, these techniques may drop to compass the optimum cost. To conquer these abuses, the SMA is chosen in this article to treat the process of optimum capacitor placement.

SMA is a vigorous population-based optimizer based on the oscillation mode of slime mould in nature [21-23]. It proves its effectiveness in many applications [24-25]. It is suggested here as a modern optimization approach to minify the net active power losses, the net cost and to promote the voltage profiles for an IEEE distribution network [26-27]. The stations of the shunt capacitors procedure are acquired firstly by inspecting the points according to many indices. Then SMA is submitted to deduct the optimum siting and sizing of capacitors from specific nodes. The validation of the suggested algorithm in progressing the voltage profile and lowering resistive losses is given for an IEEE distribution system. The results of the SMA are compared with several algorithms to assert its superiority.

The rest of the paper is constituted as follows: Section 2 shows the different indices for capacitor installing techniques. Section 3 presents the cost function and limits. Section 4 introduces Slime Mould Algorithm. Section 5 examines the results on voltage profiles and power loss. Section 6 gives the conclusion and future works to treat the distribution network optimization process.

2. Various Indices

In this section, three different indices with their equations are introduced.

2.1 Power Loss Index

In this article, PLI is utilized to specify the nominee points for capacitors. The region of inspection is diminished greatly and then wasted time in the optimization procedure. The demerit of this index is the pivotal computations. It is desired to execute load flow and define the attenuation in power losses by intromission reactive power at every bus except the slack one [28-29]. The PLI is given as the following equation.

$$\text{PLI(i)} = \frac{lr(i)-lr_l}{lr_u-lr_l} \quad (1)$$

Where

lr_u : The upper attenuation in actual power losses.

lr_l : The lower attenuation in actual power losses.

$lr(i)$: The attenuation in actual power losses at the bus i.

The buses of greater PLI will have the primacy to be the nominee bus to constitute compensator apparatus.

2.2 Loss Sensitivity Factors

LSFs are appointed to specify the nominee buses to install capacitors [30]. Figure 1, shows a transmission line 'l' linked between 'i' and 'k' buses.

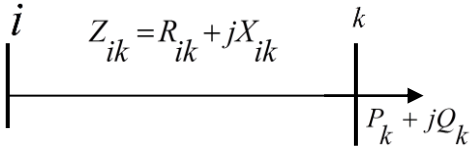

Fig. 1. Radial distribution network equivalent circuit.

The actual power loss is obtained by $I_l^2 R_{ik}$ in this line that can be computed by

$$P_{ik-loss}=\frac{(P_k^2+Q_k^2)R_{ik}}{(V_k)^2} \quad (2)$$

The LSFs can be given from the following equation:

$$\frac{\partial P_{ik-loss}}{\partial Q_k}=\frac{2Q_k * R_{ik}}{(V_k)^2} \quad (3)$$

The typical voltages are specified by dividing the base voltages by 0.95. If these voltages are lower than 1.01 they can be suggested as nominee nodes for capacitor installation. It is account note that the LSFs judge the series in which nodes are to be prepared to install capacitors.

2.3 Voltage Stability Index

VSI amount is close to 1 so the least VSI amounts, the mightily sensitive points to voltage collapse. Thus, VSI is utilized to elect the lowest points that have more probability of voltage collapse along all points. VSI amount is designated as the following equation [31-33]:

$$VSI(k)=|V_i|^4-4\left(P_k\cdot X_{ik}-Q_k\cdot R_{ik}\right)^2 -4\left(P_k\cdot R_{ik}+Q_k\cdot X_{ik}\right)\cdot|V_i|^2 \quad (4)$$

where

V_i : The magnitude of the voltage at the bus i.

3. Cost Function

The developed cost function of the optimum capacitor position task is to lessen the net cost which is planned as the following equation:

$$Cost=K_P * P_{Loss} * T + D\left(K_I * CB + K_C * \sum_i^{CB} Q_{Ci}\right) + K_o CB \quad (5)$$

Where the parameters are given as [17].

K_P : The price per KW-Hours equalizes to 0.06 \$/KW-Hours,

P_{Loss}: The net losses after compensation,

T : The time in Hours equalizes to 8760,

D : The depreciation agent equalizes to 0.2,

CB: The number of compensated points,

K_C: The price per Kvar equalizes to 25 \$/Kvar,

K_I : The price per inauguration equalizes to 1600\$,

Q_{Ci}: The value of inaugurated reactive power in Kvar,

K_o : The working price equalizes to 300 \$/year/position.

The overhead equation is constricted whereas accepting the following equality and inequality limits.

3.1 Equality Limit

- **Load flow limit**

Conventional methods cannot be utilized in distribution networks due to ill conditions. The forward sweep method has been presented in [31] to treat the load flow process of distribution networks. The equality limit is shown by the following equation:

$$P_{Slack} = \sum_{i=1}^{L} P_{Lineloss}(i) + \sum_{q=1}^{N} Pd(q) \quad (6)$$

$$Q_{Slack} + \sum_{b=1}^{CB} Q_C(b) = \sum_{i=1}^{L} Q_{Lineloss}(i) + \sum_{q=1}^{N} Qd(q) \quad (7)$$

where

P_{Slack}: The active power of the slack node,

Q_{Slack}: The reactive power of slack node,

L : The size of the transmission line in a distribution network,

$Pd(q)$: The request for active power at bus q,

$Qd(q)$: The request for reactive power at bus q,

N : The size of total nodes.

3.2 Inequality Limits

- **Voltage Limit**

The magnitude of the voltage at every node must be constrained by the following limit:

$$0.90 \le V \le 1.05 \quad (8)$$

- **Compensation Limit**

The injected reactive power at every nominee node should be lower than its efficient reactive power.

- **Power Factor Constraint**

Power Factor (PF) should override the lower amount and less than the upper amount as given by the following limit.

$$PF_{\min} \le PF \le PF_{\max} \quad (9)$$

- **Total Reactive Power Limit**

Remarkably, the net injected reactive power is lower than 0.7 of the net reactive power request to extend the operating of the power system with lagging PF and prohibition the leading one.

$$\sum_{b=1}^{CB} Q_C(b) \le 0.7 \sum_{q}^{N} Qd(q) \quad (10)$$

4. Conventional SMA

Physarum polycephalum has been named slime mould because it is considered a fungus [21].

4.1 Approach food

SMA is illustrated by the mathematical equations of [21,22]. The equations represent the contraction mechanism as follows:

$$\vec{X}(t+1) = \begin{cases} \vec{X}_b(t) + \vec{vb}\left(\vec{W}.\vec{X}_A(t) - \vec{X}_B(t)\right) & if\ r < p \\ \vec{vc}.\vec{X}(t) & if\ r \ge p \end{cases} \quad (11)$$

Where, $\vec{vb}$ is a value $[-a, a]$,

$\vec{vc}$ is reduced linearly from 1 to 0,

t is the t_{th} iteration,

$\vec{X}_b$ is the individual location with the most concentrated scent,

$\vec{X}$ is the location of slime mould (solution),

$\vec{X}_A$ and $\vec{X}_B$ are the random selection of two individuals from the population,

$\vec{W}$ is the weight solution,

p is computed as:

$$p=\tanh\left|S(i)-DF\right| \quad (12)$$

$i\in 1,2,3,\cdots,n, S(i)$ is to the competence of $\vec{X}$, DF is the most competence calculated over all iterations.

$\vec{vb}$ is computed as follows:

$$\vec{vb}=[-a,a] \quad (13)$$

$$a=\text{arctanh}\left(-\left(\frac{t}{\max t}\right)+1\right) \quad (14)$$

$\vec{W}$ is computed as follows:

$$\vec{W}(SmellInd(i))=\begin{cases}1+t.\log\left(\frac{bF-S(i)}{bF-wF}+1\right) & condition\\ 1-t.\log\left(\frac{bF-S(i)}{bF-wF}+1\right) & others\end{cases} \quad (15)$$

$$smellInd=sort(S) \quad (16)$$

Where

$S(i)$ ranks the first half of the given solutions,

r a random number $[0,1]$,

bF is the optimal competence exist in the current iteration,

wF is the worst competence exist in the current iteration,

$smellInd$ is the sequence of the sorted competence values.

Fig. 2 shows the impacts of (11).

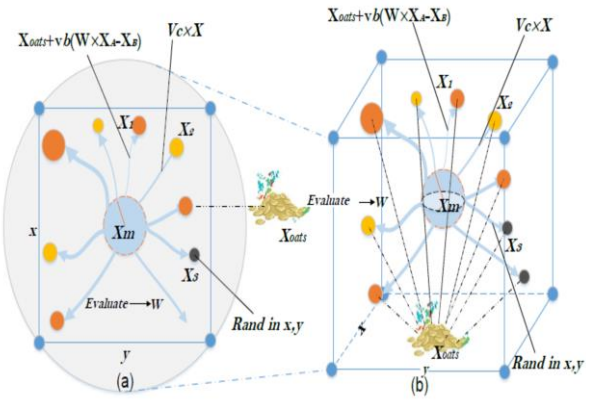

Figure 2. Potential location in 2_dimensional and 3_dimensional

4.2 Wrap food

When the search area extends to an area with a rather low concentration of food, its importance will decrease and the food group will go to explore other areas. Fig. 3 shows the competence evaluation functions for slime mould [23-24].

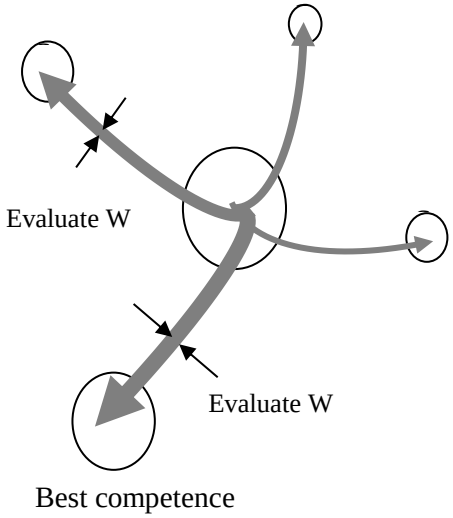

Figure 3. Evaluation of the competence function

The solution location is updated according to the following equation:

$$\vec{X}^*=\begin{cases}rand(UB-LB)+LB & rand<z\\ \vec{X}_b(t)+\vec{vb}\left(\vec{W}.\vec{X}_A(t)-\vec{X}_B(t)\right) & if\ r<p\\ \vec{vc}.\vec{X}(t) & if\ r\geq p\end{cases} \quad (17)$$

Where, LB is the lower limit of the search space,

UE is the upper limit of the search space,

r is a random value $[0,1]$.

4.3 Grabble food

$\vec{vb}$ is a random vector between $[-a,a]$ and regularly accessed zero as the repetitions advance.

The $\vec{vc}$ values lay between $[-1,1]$ and are driven to zero in the end. Synergistic cooperation between $\vec{vb}$ and $\vec{vc}$ imitate the specific manner of slime mould. Although sticky mould is a better source of

nutrition, it is preferable to distribute the organic matter to explore other areas to find the best food source rather than pouring it all into one source to find a more reliable source of food. The Pseudo-code of the SMA algorithm is shown below [25-26].

Pseudo-code of SMA

Initialize $population\_size$, $\dim$, LB, UE, z, Max_iter;

Initialize a set of Slime Mould random locations $X_i (i = 1, 2, \cdots, n)$;

While ($t \le Max\_iter$)

Compute and sort the competence of all Slime Mould;

Update the best and the worst competence

Calculate the weight of Slime Mould ($\vec{W}$);

Update the best competence, the best location $\vec{X}_b$

For each search agent

Update p, $\vec{vb}$, $\vec{vc}$

Update the position of search agent

End For

$t = t + 1$

End While

Return the best competence, best location $\vec{X}_b$

5. Results and Discussion

The prevalence of the suggested SMA is applied to an IEEE distribution systems. The results of 15 radial distribution systems are offered below in detail. The suggested algorithm has been completed via Matlab [34]. Simulations were performed under the Matlab environmental (release 2013 a) and done on a Lenovo laptop with Intel core i7 CPU 2.90 GHz processor with 4 GB RAM and a 64-bit operating system.

15 Bus Test System

The tested case is 15 bus system as given in Figure (4). The system data are displayed in [31]. The total load for this system is 1752 KVA with PF=0.7. The losses without compensation are 60.5844 KW. Figure (5) gives the nominee buses according to their PLI. The ordered of these buses are 15, 11, 4, 7, 6, 12, 14, 3, 8, 13, .. 2. The nominee buses are obtained in Figure (6) according to LSF. The ordered of buses are 6, 3, 11, 4, 12,…Figure (7) shows the nominee buses according to VSI values. The improvements in system voltages due to install one and two capacitors are shown in Figures (8, 9) respectively. A comparison between various indices is performed and shown in Table (1, 2) for installing one and two capacitors respectively. It is clear that, PLI gives better results than VSI and LSF for this system. Based on these results, SMA is proposed with PLI to give the better response in terms of cost and losses. The notability of the suggested SMA is demonstrated compared with other algorithms in [13, 14, 15, 35, and 36]. The value of installed capacity of reactive power is 850 KVAR. The minimum voltage is increased from 0.9424 to 0.9679 p.u. The losses with compensation are decreased to 32.2499 KW due to capacitors installation as given in Table (3). The percentage reduction in losses is increased to be 46.768%. Moreover, the value of total cost due to the proposed objective algorithm is 23060.54 $ which is the smallest one. Also, the net saving with the proposed SMA is improved to 29.183 % which is the maximum one compared with other algorithms.

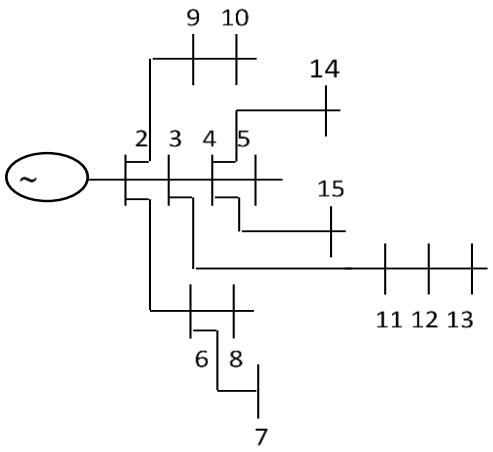

Fig. 4. The connection diagram of the 15-point system.

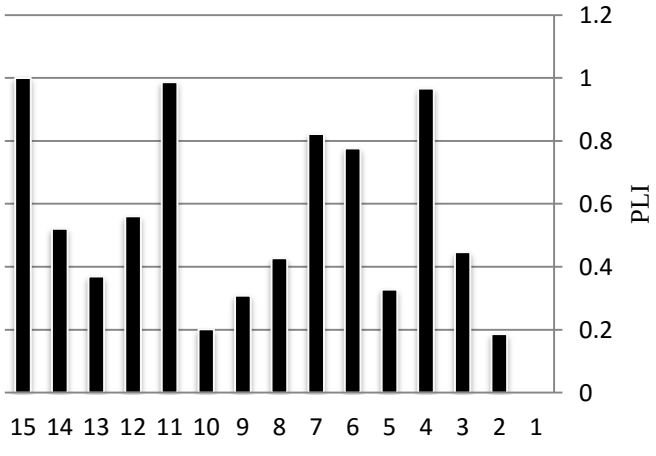

Fig. 5. PLI for the 15 system.

Table (1) Comparison of various indices for injection of one capacitor.

Items	Un-compensated	Compensated		
		PLI	LSF	VSI
Total losses (Kw)	60.5844	40.2634	43.8035	47.365
Loss reduction (%)	-	33.54	27.698	21.819
Minimum voltage	0.9459	0.9619	0.9550	0.9601
Optimal location and size in Kvar	-	700@ Bus15	750@ Bus 6	400@ Bus 13
Total Kvar	-	700	750	400
Annual cost($/year)	32563.4	25282.44	27393.12	27515.04
Net saving ($/year)	-	7280.96	5170.28	5048.36
% saving	-	22.36	15.877	15.5

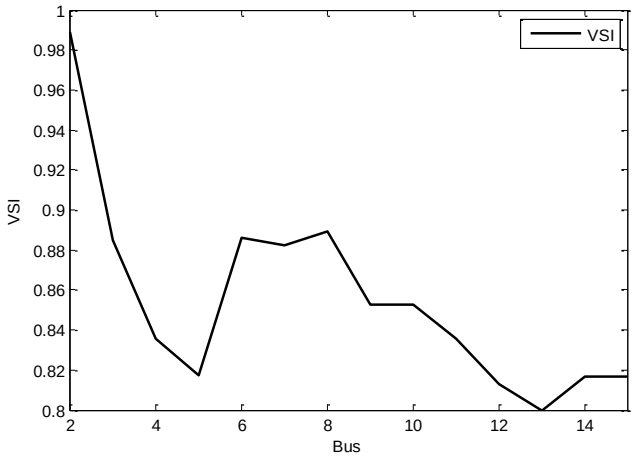

Fig. 7. VSI for the 15 system.

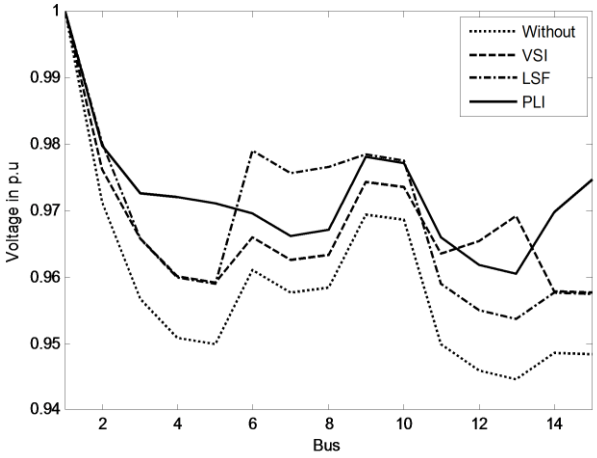

Figure. 8. Effect of installing one capacitor on system voltage.

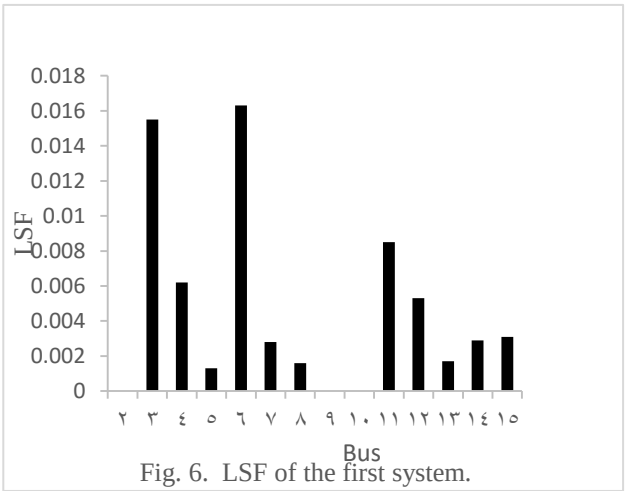

Fig. 6. LSF of the first system.

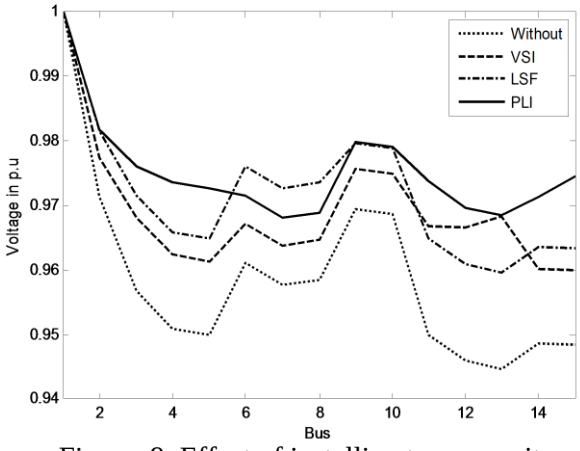

Figure. 9. Effect of installing two capacitors on system voltage.

Table (2) Comparison of various indices for injection of two capacitors

Items	Un-compensated	Compensated		
		PLI	LSF	VSI
Total losses (Kw)	60.5844	34.9447	35.1231	42.5608
Loss reduction (%)	-	42.32	42.026	29.75
Minimum voltage	0.9459	0.9697	0.9615	0.9623
Optimal location and size in Kvar	-	450@ Bus15 400@ Bus11	450@ Bus 3 400@ Bus 6	250@ Bus 13 250@ Bus 11
Total Kvar	-	850	850	500
Annual cost($/year)	32563.4	23856.93	23950.7	26109.96
Net saving ($/year)	-	8706.47	8612.7	6453.44
% saving	-	26.74	26.45	19.82

Table (3) Comparison between various algorithms.

Items	Un-compensated	Compensated											
		FGA[14]		[35]		PSO[13]		DE [15]		[36]		**Proposed**	
Total losses (KW)	61.9547	30.4411		32.6		32.7		32.3		33.2		**32.2499**	
Loss reduction (%)	-	50.86		47.38		47.22		47.86		46.41		**46.768**	
Lower voltage	0.9424	0.9677		-		-		-		-		**0.9679**	
Optimum siting and size in KVAR	-	4	200	3	805	6	871	3	454	3	150	**6**	**250**
		6	100	6	388	11	321	6	500	4	300	**11**	**300**
		7	300					11	178	6	300	**15**	**300**
		11	300							11	150		
		15	200										
Total KVAR	-	1100		1193		1192		1132		900		**850**	
Annual cost($/year)	32563.4	24599.8		24339.6		24387.1		24496.8		24429.9		**23060.54**	
Net saving ($/year)	-	7963.6		8223.8		8176.3		8066.4		8133.5		**9502.86**	
% saving	-	24.46		25.26		25.11		24.77		24.98		**29.183**	

6. Conclusion

In this paper, SMA has been applied successfully to solve the tasks of optimum positions and sizing of capacitors in distribution system that have been established as an objective optimization task with competing power losses, cost of installation, operation and injected vars. The superiority of the suggested approach is clarified by using IEEE test system. Also, the results have been compared with those obtained using recent optimization techniques. Moreover, it provides a promising and preferable performance over other approaches in terms of voltage profiles, active power losses, net cost, and total saving. Implementation of the network reconfiguration and distributed generation with the most novel optimization algorithm to enhance the voltage profile and to reduce the active losses is the future scope of this work.

7. References

[1] K. S. Sambaiah, and T. Jayabarathi, "Loss Minimization Techniques for Optimal Operation and Planning of Distribution Systems: A Review of Different Methodologies", *Int. Transactions on Electrical Energy Systems*, Vol. 30, No. 2, February 2020, e12230.

[2] S. M. Abd-Elazim, and E. S. Ali, "Optimal Network Restructure via Improved Whale Optimization Approach", *Int. Journal of Communication Systems*, Vol. 34, No. 1, e4617, January 2021.

[3] A. Awad, H. Abdel-Mawgoud, S. Kamel, A. A. Ibrahim, and F. Jurado, "Developing a Hybrid Optimization Algorithm for Optimal Allocation of Renewable DGs in Distribution Network", *Clean Technol*. 2021, 3, pp. 409-423.

[4] H. Chiang, J. Wang, O. Cockings, and H. Shin, "Optimal Capacitor Placements in Distribution Systems: Part 1: A New Formulation and the Overall Problem", *IEEE Trans. Power Del*., Vol. 5, pp. 634-642, 1990.

[5] R. Gallego, A. Monticelli, and R. Romero, "Optimal Capacitor Placement In Radial Distribution Networks using Tabu Search", *IEEE Trans. Power Syst.,* Vol. 16, 2001, pp. 630-637.

[6] M. Sydulu, and V. Reddy, "Index and GA based Optimal Location and Sizing of Distribution System Capacitors", *IEEE Power Engineering Society General Meeting*, pp. 1-4, Tampa, FL, 24–28 June 2007.

[7] S. Nojavan, M. Jalali, and K. Zare, "Optimal Allocation of Capacitors in Radial/Mesh Distribution Systems Using Mixed Integer Nonlinear Programming Approach", *Electr. Power Syst. Res.*, Vol. 107, 2014, pp. 119-124.

[8] M. Raju, K. Murthy, and K. Avindra, "Direct Search Algorithm for Capacitive Compensation in Radial Distribution Systems", *Int. J. Electr. Power Energy Syst*., Vol. 42, 2012, pp. 24-30

[9] S. Sultana, and P. Roy, "Optimal Capacitor Placement in Radial Distribution Systems Using Teaching Learning based Optimization*", Int. J. Electr. Power Energy Syst.*, Vol. 54, 2014, pp. 387-398.

[10] A. Sarma, "Optimal Selection of Capacitors for Radial Distribution Systems Using Plant Growth Simulation Algorithm", *Int. J. Adv. Sci. Technol.*, Vol. 30, 2011, pp. 43-54.

[11] A. Hamouda, and S. Sayah, "Optimal Capacitors Sizing in Distribution Feeders Using Heuristic Search based Node Stability Indices", *Int. J. Electr. Power Energy Syst*., Vol. 46, 2013, pp. 56-64.

[12] P. Das, and S. Banerjee, "Placement of Capacitor in A Radial Distribution System Using Loss Sensitivity Factor and Cuckoo Search Algorithm", *Int. J. Sci. Res. Manag*., Vol. 2, 2013, pp. 751-757.

[13] K. Prakash, and M. Sydulu, "Particle Swarm Optimization based Capacitor Placement on Radial Distribution Systems", *IEEE Power Engineering Society General Meeting*, 2007; 24-28 June 2007. pp. 1-5.

[14] P. V. Prasad, S. Sivanagaraju, and N. Sreenivasulu, "A Fuzzy Genetic Algorithm for Optimal Capacitor Placement in Radial Distribution Systems", *ARPN J Eng Appl Sci* 2007, Vol. 2, No. 3, pp.28-32.

[15] K. Prakash, and M. Sydulu, "Optimal Capacitor Placement in Radial Distribution Systems Using Differential Evolution", *J. Electr Eng* 2012; Vol. 12, No. 2, pp. 144-149.

[16] A. Y. Abd-Elaziz, E. S. Ali and S. M. Abd-Elazim, "Flower Pollination Algorithm for Optimal Capacitor Placement and Sizing in Distribution Systems", *Electric Power Components and System*, Vol. 44, Issue 5, 2016, pp. 544-555.

[17] A. Abd-Elaziz, E. S. Ali and S. M. Abd-Elazim, "Flower Pollination Algorithm and Loss Sensitivity Factors for Optimal Sizing and Placement of Capacitors in Radial Distribution Systems*", Int. J. of Electrical Power and Energy Systems*, Vol. 78 C, June 2016, pp. 207-214.

[18] E. S. Ali, S. M. Abd-Elazim and A. Abd-Elaziz, "Improved Harmony Algorithm and

Power Loss Index for Optimal Locations and Sizing of Capacitors in Radial Distribution Systems", *Int. J. of Electrical Power and Energy Systems*, Vol. 80 C, September 2016, pp. 252-263.

[19] E. S. Ali, and S. M. Abd-Elazim, "Optimal Locations and Sizing of Capacitors in Radial Distribution Systems Using Mine Blast Algorithm", *Electrical Engineering*, Springer, Vol. 100, No.1, 2018, pp. 1-9.

[20] T. L. Duong, T. T. Nguyen, and V. D. Phan, Thang Trung Nguyen, "Determining Optimal Location and Size of Capacitors in Radial Distribution Networks Using Moth Swarm Algorithm", *Int. J. of Electrical and Computer Engineering (IJECE)*, Vol. 10, No. 5, October 2020, pp. 4514-4521.

[21] S. Li, H. Chen, M. Wang, A. A. Heidari, and S. Mirjalili, "Slime Mould Algorithm: A New Method for Stochastic Optimization", *Future Generation Computer Systems*, 2020, Vol. 111, pp. 300- 323.

[22] R. E. Precup, R. C. David, R. C. Roman, E. M. Petriu, and A. I. S. Stinean, "Slime Mould Algorithm Based Tuning of Cost-Effective Fuzzy Controllers for Servo Systems", *Int. Journal of Computational Intelligence Systems*, Vol. 14, No. 1, 2021, pp. 1042-1052.

[23] Z. M. Gao, J. Zhao, Y. Yang, and X. J. Tian, "The Hybrid Grey Wolf Optimization Slime Mould Algorithm", *2nd International Conference on Electronic Engineering and Informatics*, 1617, 2020, 012034.

[24] K. Yu, L. Liu and Z. Chen, "An Improved Slime Mould Algorithm for Demand Estimation of Urban Water Resources", *Mathematics*, 2021, 9, 1316.

[25] A. M. A. El Hameda, M. Ebeedb, A. Refaib, M. A. El Sattarc, A. A. Elbasetd, and T. A. Ahmed, "Application of Slime Mould Algorithm for Optimal Allocation of DSATACOM and PV System in Real Egyptian Radial Network", *Sohag Engineering Journal (SEJ)*, Vol. 1, No. 1, March 2021, pp. 16-24.

[26] L. C. Kien, T. T. Nguyen, T. D. Pham, and T. T. Nguyen, "Cost Reduction for Energy Loss and Capacitor Investment in Radial Distribution Networks Applying Novel Algorithms", *Neural Computing and Applications* 2021, Vol. 33, pp.15495-15522.

[27] F. F. Amigue, S. N. Essiane, S. P. Ngoffé, G. A. Ondoa, G. M. Mengounou, and T. P. Nna, "Slime Mould Optimization Algorithms for Optimal Distributed Generation Integration in Distribution Electrical Network", *World Academy of Science, Engineering and Technology Int. Journal of Electrical and Computer Engineering*, Vol.15, No.8, 2021, pp. 325-334.

[28] S. M. Kannan, P. Renuga and A. R. G. Monica, "Optimal Capacitor Placement and Sizing Using Combined Fuzzy-HPSO Method", *Int. J. of Engineering, Science and Technology*, Vol. 2, No. 6, 2010, pp. 75-84.

[29] V. U. Reddy and A. Manoj, "Optimal Capacitor Placement for Loss Reduction in Distribution Systems Using Bat Algorithm", *IOSR J. of Engineering*, Vol. 2, No. 10, October 2012, pp. 23-27.

[30] S. Jalilzadeh, M. Sabouri and E. Sharifi, "Optimal Capacitor Placement in a Radial Distribution System Using Shuffled Frog Leaping and Particle Swarm Optimization Algorithms", *Int. J. on Network Security*, Vol. 3, April 2012. pp. 16-20.

[31] D. Das, D. P. Kothari and A. Kalam, "Simple and Efficient Method for Load Flow Solution of Radial Distribution Networks", *Int. J. of Electrical Power and Energy Systems*, Vol. 17, 1995, pp. 335-346.

[32] M. Chakravorty and D. Das, "Voltage Stability Analysis of Radial Distribution Networks", *Int. J. of Electrical Power and Energy Systems*, Vol. 23, 2001, pp. 129-135.

[33] J. Garg and P. Swami, "Calculating Voltage Instability Using Index Analysis In Radial Distribution System", *Int. J. of Modern Engineering Research*, Vol. 4, 2014, pp. 15-26.

[34] MathWorks, available at: http:// www.mathworks.com.

[35] M. H. Haque, "Capacitor Placement in Radial Distribution Systems for Loss Reduction", *IEE Proceed Gener, Trans Distrib* 1999, Vol.146, No. 5, pp.501-505.

[36] H. M. Khodr, A. Zita, and C. Vale Ramos, "Optimal Cost Benefit for the Location of Capacitors in Radial Distribution Systems", *IEEE Trans Power Deliv*, 2009; Vol. 24, No. 2, pp.787-796.

المواقع المثلى للمكثفات في نظام التوزيع الشعاعي عبر خوارزمية قوالب الوحل

ايهاب سالم علي

قسم الهندسة - الكهربائية كلية الهندسة - جامعة جازان- المملكة العربية السعودية

سحر محمد عبد العظيم

قسم علوم الحاسب- كلية الحاسب الالي و تقنية المعلومات- جامعة جازان -المملكة العربية السعودية

الملخص

تم اقتراح طريقة جديدة وقوية تسمى خوارزمية قوالب الوحل (SMA) في هذا البحث ، لتحديد موقع المكثفات وحجمها الأمثل لشبكة توزيع IEEE. أولاً ، تم تطوير النقاط الأكثر ترشيحًا لتركيب المكثفات باستخدام مؤشرات مختلفة. يتم استخدام عوامل حساسية الخسارة (LSF) ، ومؤشر استقرار الجهد (VSI) ، ومؤشر فقدان الطاقة (PLI) لتحديد النقاط المنتخبة. ثم يتم استخدام SMA المقترح لاستنتاج حجم المكثفات ومواقعها من النقاط المختارة. يتم تقديم وظيفة الهدف لتقليل صافي التكلفة ومن ثم زيادة إجمالي التوفير سنويًا. تم اختبار النهج المقترح على شبكة توزيع IEEE. يتم مقارنة النتائج التي تم الحصول عليها من خلال النهج المقترح مع الأساليب الأخرى لتسليط الضوء على مزايا النهج المقترح. كما تم عرض النتائج لتأكيد تأثير النهج المقترح لتقليل الخسائر وصافي التكلفة وتحسين قيم الجهد والادخار الكلي لشبكة التوزيع الشعاعي

الكلمات المفتاحية: خوارزمية قوالب الوحل ؛ عوامل حساسية الخسارة ؛ مؤشر استقرار الجهد ؛ مؤشر فقدان الطاقة ؛ مواقع المكثفات المثلى ؛ نظام التوزيع

Synthesis and Characterization of Iron Oxide Nanoparticles for Sensing Application

Mehraj-ud-din Naik[1,*], Mohd. Imran[1], Musab Alghamdi[1], Yehya Hakami[1], Mohammed Arishi[1], Waleed Abdullah[1]

[1]Department of Chemical Engineering, College of Engineering, Jazan University, Saudi Arabia

ABSTRACT

This work aims to develop a nano-material-based sensor for harmful organic compounds at relatively low temperatures and concentrations. The harmful organic compounds come from various reasons. This research aims to synthesize the appropriate nano-material that has good chemical potential with these harmful organic compounds concerning two factors that are considered the main factors affecting the sensing duties (selectivity and sensitivity). The nano-materials were prepared by co-precipitation method which produced different particle shapes and sizes. It was observed that particle shapes are regular and smaller resulting in better characteristics. We used the bottom-up approach particularly chemical co-precipitation instead of the top-down approach because it gives a more regular shape and smaller particles. After preparation we characterized the materials using several characterization techniques like X-ray diffraction to confirm the cubic structure of iron oxide and crystallite size of particle was found to be approximately 10 nm. Scanning electron microscopy explains the nanoparticle nature of Iron oxide, and other techniques such as Fourier Transform Infrared Spectroscopy, Ultraviolet-Visible Spectroscopy, and Cyclic Voltammetry were used to confirm it. The carbon-coated samples tend to reduce the sensitivity of metal oxides. However, It was observed that different concentrations of glucose solutions affect the sensitivity of iron oxide. We also observed that iron oxide sensing properties increased due to the increase in glucose concentration. The results obtained by this technique are satisfactory.

Keywords: Nanomaterials, Sensors, Iron oxide, Glucose, Cyclovoltametry

INTRODUCTION:

In the field of nanotechnology, simple metal and their oxide nanoparticles (NPs) have been gaining a good position due to their exceptional properties and prospective applications. The materials which are in the range of size in Nanos will control several parameters etc. There are several applications of nanoscale materials used as supporting material for a catalyst [1], in the biomedical field to separate the magnetic particles from the solution [2], in the field of data storage, using as electrode material in the cell, use to protect the material from corrosion [3, 4], energy storage, bio-sensing, and in medicine, etc. [5, 6, 7, 8]. In the medical field, nano-materials are also used in many observations like biomedical therapeutics, biosensing, implant devices, monitoring and control the diseases by nanomaterials, bioimaging, and also diagnostics [9]. Different metal oxides such as ZnO, NiO, TiO_2, Fe_2O_3, and CuO are used for different purposes. Fe_2O_3, and CuO were used for the detection of glucose, H_2O_2 and hydrocarbon gases [10-11]. On the other hand, Fe_2O_3 NPs also have magnetic properties and considered applicable in different fields of biology [12-13].

In addition to having outstanding nanoscale properties, Fe_2O_3 magnetic NPs display potential applications in some magnetic

systems due to its most stable and nontoxic nature within a band gap of 2.1 eV [14]. Iron oxide has two types of phases that can be transit from one phase to another at calcination: the γ-phase with a cubic structure and α-phase which has a rhombohedral structure [15]. It has been observed that gas detection plays a key role in almost every industrial process due to its influence on the environment (like chlorofluorocarbon gases) and living creatures (like carbon monoxide, hydrogen sulfide, and hydrocarbon gases). And due to the industrial expansion and industrial movement nowadays, the need and the investment grows day by day. On the other hand, nano-technology has developed greatly in the last few years and we know the effect of reaching nanosizes on the materials, and how almost all the characteristics of the material improve including sensitivity [16].

To make a highly sensitive material and by merging the two fields, such as gas detection and nanotechnology, we get a new field that is gas detection using nanomaterials or nano-based gas sensors [17]. This field is very wide due to many factors including nanomaterials preparation methods, materials sensitivity, materials selectivity, doping, and others [18]. This work aim to provide a nano-metal oxide based hydrocarbon gas sensor, which can be used to detect hydrocarbon gases at relatively low temperature and concentration [16-17]. Different routes have been employed to prepare iron oxide nanoparticles to prepare homogenous nano-particles like the hydrothermal process [19] which required special apparatus and high temperature, sol-gel process was difficult to remove impurities, and is time-consuming [20]. On the other hand, the co-precipitation method is good as compared to other methods due to the formation of well-ordered size NPs [21]. Nevertheless, the synthesis route plays a crucial role in determining magnetite nanoparticles' physical and chemical properties; however to do it simplistically and efficiently ruins a task. Several parameters strongly depend upon the activity of substances such as using a solvent in the production of material, the reactants which are in solid or gas form, the pH of the solutions, and the action of reducing agent in the reaction. The goal of this research is to prepare the NPs which will have excellent gas sensing properties and good selectivity for any sample, more catalytic activity in a reaction, and in a short interval of time will have good response and stability. For this purpose, it has been considered that metal oxide is a good material for the sensing purpose but composite materials also show good sensing properties. The sensitivity of the substance can be increased by employing a more effective catalyst, by improving the morphology of materials, moistness also affects the sensitivity of NMs, as well as temperature, which will play an important role in the chemical reaction [22].

In this paper, nanoparticles of ferric oxide were prepared by co-precipitation method using an iron chloride forerunner. The prepared material is characterized by different techniques such as XRD, SEM, FTIR, UV-Vis, and electrochemical detection by CV. In this research, we are looking for a sensor of hydrocarbon gases using nanomaterials oxides at relatively low temperatures and concentrations. Therefore, we prepared nanomaterials oxides and tested their ability to detect gases at lowest concentration, and then analyzed via cyclovoltametry for its gas sensing applications. As some studies showed that nanomaterials oxides have higher sensing properties compared to the other compounds.

MATERIALS:

For the preparation of Fe_3O_4 by using the coprecipitation method, we use the following materials as precursors: Ferric chloride ($FeCl_3$) 99.9%, 8NaOH 99.8%, Ferris sulfate heptahydrate ($FeSO_4$.$7H_2O$) (99.9%), and sodium hydroxide (NaCl) (95.9%) and D-fructose for coating of carbon as shown in figure 1 (a-d). On the other hand, the effect of carbon coating (C) on Fe_2O_3 sensitivity was also measured in this study.

MATERIALS PREPARATION:

We followed a bottom-up approach instead of a top-down to prepare our nanomaterials oxides [1]. Solution 1, ferric chloride ($FeCl_3$): 15.57 g of pure ferric chloride was dissolved in 100 ml of distilled water. Solution 2, ferrous sulfate (Fe $(SO_4)_2.7H_2O$): 13.34 g of pure ferrous sulfate was dissolved in 100 ml of distilled water. Solution 3, sodium hydroxide (NaOH): 9 g of pure sodium hydroxide was dissolved in 100ml of distilled water. In this step, ferric chloride solution and ferrous sulfate solution were mixed together (just rapid and direct mixing), taking in mind that there is no chemical potential between ferric chloride and ferrous sulfate solution, so this mixing forms $FeCl_3$+ $Fe(SO_4)_2.7H_2O$. In the next step, the chemical co-precipitation method started by mixing NaOH solution with ferric chloride and ferrous sulfate solution, and we did that in two different ways: first, direct co-precipitation: just mixed the two solutions directly with some stirring and in the second controlled co- precipitation method, we controlled the mixing rate by dropper. NaOH solution on the stirrer in continuous stirring motion and the ferric chloride and ferrous sulfate solution in the dropper, and the dropping takes approximately 45 minutes. We did both direct and indirect (controlled) methods to study the difference between these two ways in terms of particle size and shape. After we finish the dropping we maintain the pH to 12 and then we left the solutions (direct and indirect) on the stirrer for 24 hours to make sure all reactants are converted and the reaction is done. After maintaining the pH and the reaction, there will be some contaminants with product (Fe_3O_4) so we separated these contaminants in two step process (washing and drying). First, we remove as much as possible water carefully by syringe then put methanol and water instead of water (the ratio of methanol to water is 1). After the addition of water/alcohol, the samples were left for 24 hours to settle down then repeated the same step. We repeated the washing thrice with water/alcohol and another three times with pure water, six washes in total. The purpose of washing is to remove the salts, after that the samples were dried completely. After we remove all the contaminants, sample Fe_3O_4 is ready for characterization. On the other hand, to enhance the characteristics of the material, carbon as a coating agent was used. We prepared 1M of fructose solution ($C_6H_{12}O_6$) by adding 18 g fructose to 100 ml of distilled water (four solutions for four samples), then added some samples to these solutions, and the decomposition reaction takes place in auto-cleave at 40 psi and 140^oC for 5 hours. The coating was the last step in the synthesis of iron oxide nano-particle. The reaction between the materials is given below in eq. I.

$$2FeCl_3 + FeSO_4.7H_2O + 8NaOH \rightleftharpoons Fe_3O_4 + 6NaCl + Na_2SO_4 + 11H_2O \text{ ----------(I)}$$

Fig. 1: Raw material used for the preparation of Fe_3O_4, **(a)** Ferric chloride ($FeCl_3$), **(b)** Ferris sulfate heptahydrate ($FeSO_4.7H_2O$) **(c)** Sodium Hydroxide (NaCl) **(d)** D-fructose

CHARACTERIZATION OF PREPARED MATERIAL:

In this study prepared material were characterized by different techniques like crystalline phase identified by X-Ray diffraction (Ultima IV, Rigaku, Tokyo, Japan), the morphology of the prepared material observed by scanning electron microscopy, the absorbance of visible light or ultraviolet measured with the help of UV-visible spectrometers (JASCO spectrophotometer model V-670) [23]. FT-IR model ‘‘Nicolet IS 10” (Thermo Fisher Scientific, MA USA) was used for the information regarding functional group present [24], and electrochemical performance of the material were performed by cyclic voltammetry (Autolab – High Performance Modular Potentiostat) [25].

RESULTS AND DISCUSSION:

The crystallites were identified in phases and their sizes were estimated using X-ray diffraction (XRD) at 40 kV. Fig. 2 shows the pattern of x-ray diffraction, where it is clearly observed that the peaks appear at 2θ = 30.6, 36.24, 43.99, 54.73, and 57.93 with planes 220, 311, 400, 422, and 511 respectively. There is a difference in lattice spacing found for the nano-particles of 0.26 nm and 0.34 nm, which corresponds to the (311) plane assigned for the Fe_3O_4 cubic crystal plane [26]. From the XRD pattern, to find the value of FWHM (full width at half maximum) and apply the Debye-Sherrer formula to find the crystallite size of iron oxide appeared within the range of 10 nm and the lattice parameter was a = 5.03 angstrom and c = 13.75 angstrom [27]. It has been noted that there will be a phase change in the nanoparticles of iron oxide but the XRD peak with hkl value (311) relates to the cubic structure.

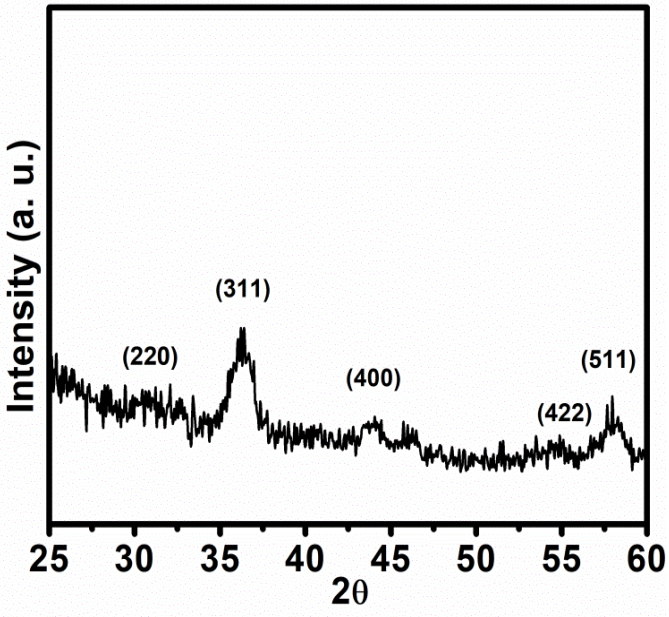

Fig. 2: XRD pattern of Fe_3O_4 nanoparticles

We analyzed the surface morphology of calcined and as-synthesized samples using scanning electron microscopy, which provides evidence of iron oxide's nano-particle nature. Nanoparticles of Fe_3O_4 are prepared by the co-precipitation method as shown in figure 3. It was revealed that the Fe_3O_4 nanocrystals formed on the surface of the sample become more sphere-like as the temperature is increased, may change the phase, and become less or more agglomerate. High crystallinity is detected on the surface of the samples [27].

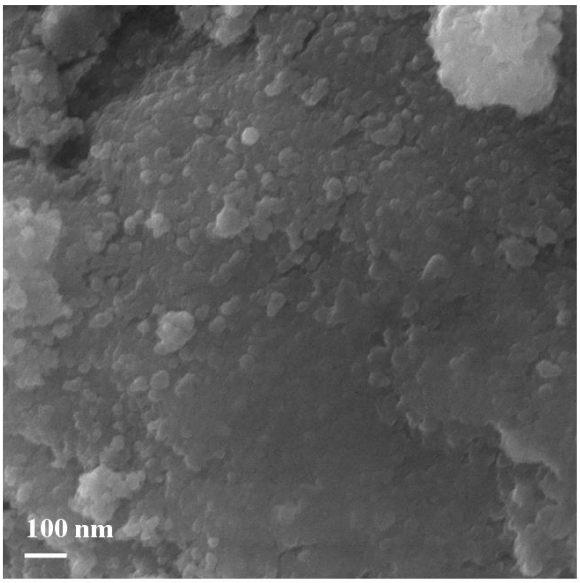

Fig. 3: SEM image of the iron oxide nanoparticles

Fig. 4 shows the FTIR spectra of α-Fe_2O_3 (a), α-Fe_2O_3@CC (CC = Carbon Coating) (b), Fe_3O_4@CC (c), Fe_3O_4 (d), and γ-Fe_2O_3 (e) prepared samples. The FTIR spectra of all samples showed an IR band in the range of 540 to 580 cm^{-1} can be assigned to (Fe-O) stretching vibrations. Peaks in the range of 1535 to 1635 cm^{-1} can be assigned to (the COO group). At the peaks between the range from 2800 to 2900 cm^{-1} can be assigned (CH groups).

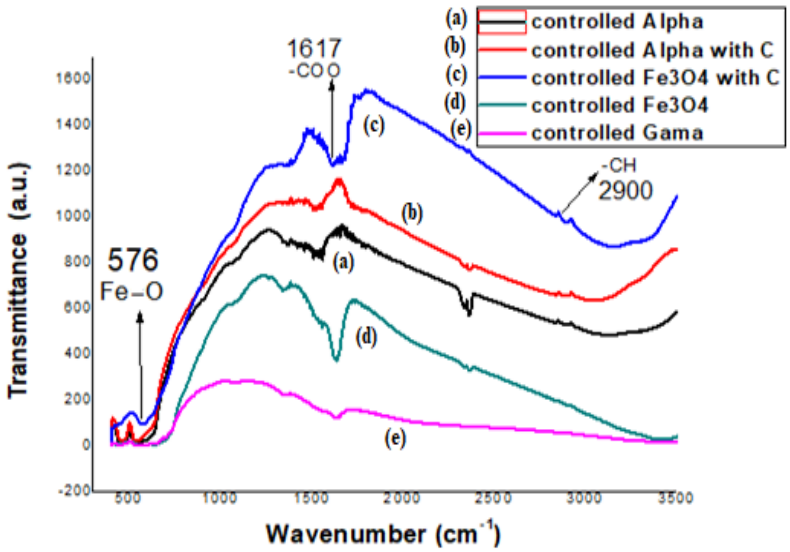

Fig. 4: FTIR of different iron oxide samples

Fig. 5 shows UV-Visible absorption spectra of Fe_3O_4 and Fe_3O_4@CC nanoparticles as a function of wavelength. Figure 5(a) shows the spectra of as-prepared iron oxide NPs, indicated the absorption peak at 290 nm. In figure 5(b) spectra of carbon-coated iron oxide NPs indicated the absorption peak at 286 nm which showed that the carbon coating on the surface of iron oxide does not have more effects on the absorption but decreased in small quantity.

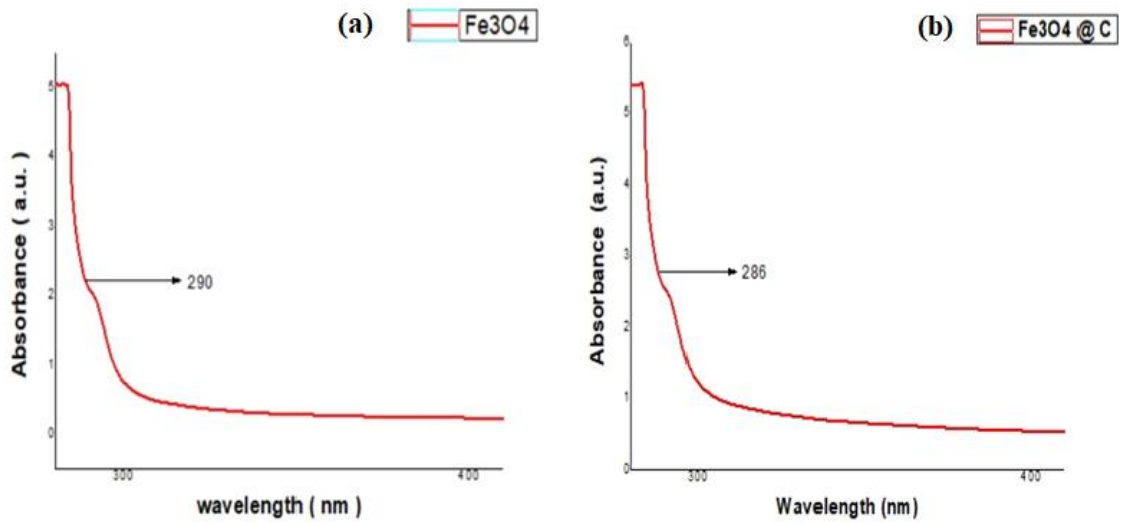

Fig.5: UV spectrum of Iron oxide, (a) Fe_3O_4 and (b) Fe_3O_4@C

At a scan rate of 10 m V/s, the current density of various electrodes in glucose solution is shown in Figure 6 as a function of electrode potential. In figure 6(a), the bare FTO (Fluorine-doped Tin Oxide) gives small current reduction and oxidation peaks illustrated in the range between -0.2 V to 1 V. Pure Fe_3O_4 via controlled method at 1 mM of glucose solution shows the redox peaks of current in the range -0.1 V to 1 V (which oxidizes at 0.5 V and reduces at 0.1 V). The 5 mM solution shows a small current and small peak oxidization at 0.1 V and reduces at 0.3 V, whereas at 10 mM the electrochemical (EC) response is different. It has been concluded that the increase in current intensity is due to the metallic particles and their Redox peaks observed at 0.6 V (oxidation) and 0.1 V (reduction). This performance proposes that the iron oxide NPs increase the electroactive surface area which depends upon the concentration of the glucose and also facilitates the transfer of an electron between electroactive species [28]. At the same scan rate and concertation of glucose employed for iron oxide carbon coating material, the observed reduction and oxidation peaks are shown in Figure 6(b). For pure Fe_3O_4 the redox peaks of current in the range -0.1 V to 1 V (which oxidizes at 0.5 V and reduces at 0.4 V) with 5 mM solution redox peaks observed at 0.1 V and 0.7 V, whereas at 10 mM the EC are also observed at 0.7 V (oxidation) and 0.1 V (reduction). It observed that with carbon coating the performance of iron oxide for oxidation and reduction is increased which indicates that iron oxide with carbon coating is good for sensing applications [28].

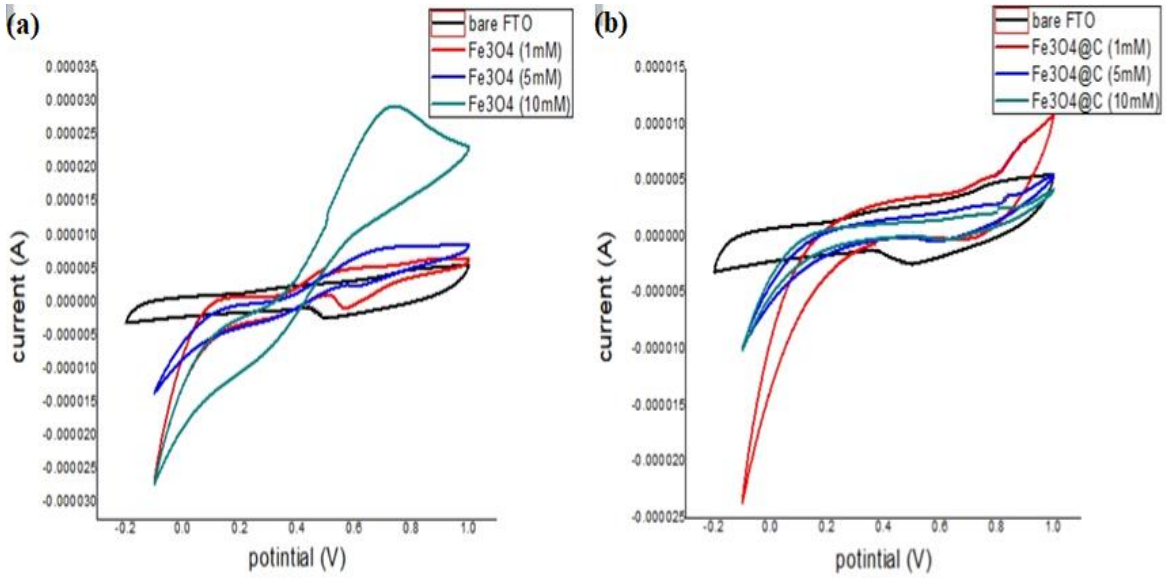

Fig. 6: Cyclic voltammetry curve of iron oxide, (a) Fe_3O_4 and (b) Fe_3O_4@C

Figure 7 shows the cyclic voltammetry studies of bare Fe_3O_4 and carbon coated Fe_3O_4 samples. The bare sample gives very small current reduction and oxidation peaks distinguished in the range of -0.2 to 1 V. In Figure 7(a), Fe_3O_4 in buffer solution shows a very small current reduction at 0.7 V and oxidation peak at 0.4 V respectively. In Figure 7(b), Fe_3O_4 @CC in buffer solution shows a very small current reduction at 0.4 V and an oxidation peak at 0.6 V. Finally the obtained results were analyzed to find out the major changes on the electro chemical of Fe_3O_4 samples, which concluded the responses with carbon coating is different as compared to that of raw sample. The obtained results need more investigations to find out the carbon coating with different concentrations on the metal oxides sensing properties.

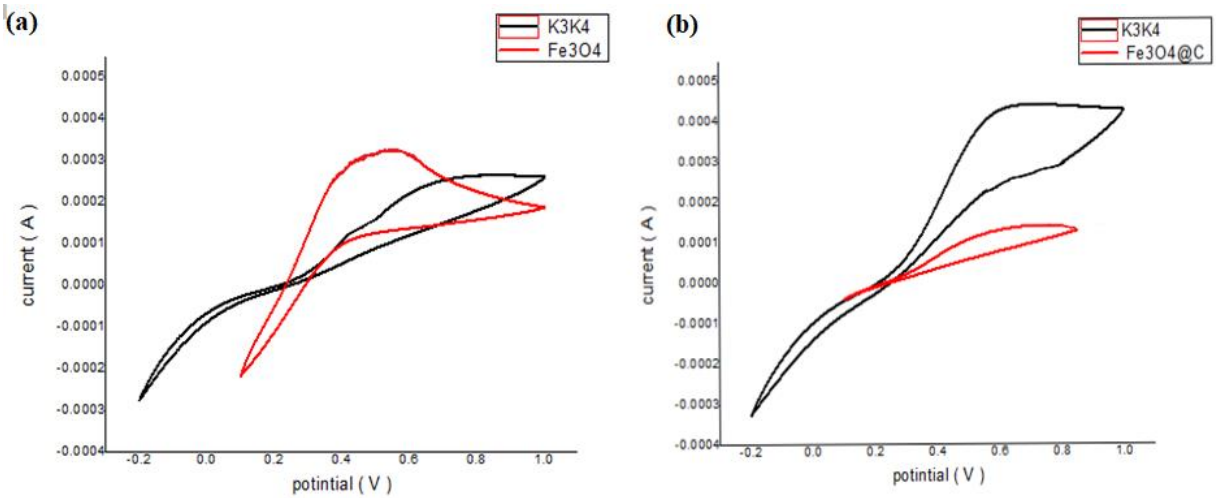

Fig. 7: Cyclic voltammetry with K_3K_4 solution of (a) Fe_3O_4, and (b) Fe_3O_4 @C

CONCLUSION:

Detection of chemicals is important for a variety of reasons, including waste gases that are exited from industries and are harmful to mankind. The hydrocarbon gases are very harmful to the people when exposed during the leaking of such gases. Sometime the presence of such gases is not felt due to their odorless nature. The sensors must be placed to such places for the detection of these gases at the lowest concentration possible. To increase the sensitivity of the sensors by using nanomaterial oxides, it is necessary to use doping materials for their better surface morphology, which increases the sensing property of the metal. Iron oxide NPs were prepared by the co-precipitation method, and their characterization was done by using several techniques like CV, UV-Vis, and FTIR spectroscopy. During the investigation of iron oxide in cyclic voltammetry analysis, we found that the carbon-coated samples tend to reduce the sensitivity of metal oxides. The different concentrations of glucose solutions affect iron oxide sensitivity. We observed that the sensitivity of iron oxide was increased by the increased concentration of glucose. These findings are helpful in the further study of the role of metal oxides as the potential materials for their use in sensor applications.

ACKNOWLEDGMENTS

The authors are grateful for the financial support of Jazan University under the 6th Future Scientist Program (Project No. FR6-146).

REFERENCES:

[1] Farahmandjou, M., & Soflaee, F. "Synthesis and characterization of α-Fe_2O_3 nanoparticles by simple co-precipitation method". *Physical Chemistry Research*, *3*(3), 191-196 (2015).

[2] Yoon, T. J., Lee, W., Oh, Y. S., & Lee, J. K. "Magnetic nanoparticles as a catalyst vehicle for simple and easy recycling". *New Journal of Chemistry*, *27*(2), 227-229 (2003).

[3] Bell, A. T. "The impact of nanoscience on heterogeneous catalysis". *Science*, *299*(5613), 1688-1691 (2003).

[4] Jing, Z. H., & Wu, S. H. "Preparation and magnetic properties of spherical α-Fe_2O_3 nanoparticles via a non-aqueous medium". *Materials Chemistry and Physics*, *92*(2-3), 600-603 (2005).

[5] Hubbell JA, Chilkoti A. "Nanomaterials for drug delivery". *Science* 337(80):303–305 (2012).

[6] Alves AK, Berutti FA, Sánchez FAL. "Nanomaterials and catalysis. In: Nanostructured materials for engineering applications". *Springer, Berlin*, pp 93–117 (2011).

[7] Rahman MM, Ahammad AJS, Jin J-H et al. "A comprehensive review of glucose biosensors based on nanostructured metal oxides". *Sensors* 10:4855–4886 (2010).

[8] Morais, P. C., Garg, V. K., Oliveira, A. C., Silveira, L. B., Santos, J. G., Rodrigues, M. M. A., & Tedesco, A. C. "Nanoscaled biocompatible magnetic drug-delivery system: preparation and characterization". In *ISIAME 2008* (pp. 269-275). Springer, Berlin, Heidelberg. (2009)

[9] Duan L, Li M, Liu H. "Biosynthesised palladium nanoparticles using Eucommia ulmoides bark aqueous extract and their catalytic activity". *IET Nanobiotechnol* 9:349–354 (2015).

[10] Chen X, Wu G, Cai Z, Oyama M, Chen X. "Advances in enzyme-free electrochemical sensors for hydrogen peroxide, glucose, and uric acid". *Microchim Acta* 181:689–705 (2014).

[11] Batchelor-McAuley C, Wildgoose GG, Compton RG, Shao L, Green MLH. "Copper oxide nanoparticle impurities are responsible for the electroanalytical detection of glucose seen using multiwalled carbon nanotubes". *Sensors Actuators B Chem* 132:356–360 (2008).

[12] Rastogi L, Beedu SR, Kora AJ. "Facile synthesis of palladium nanocatalyst using gum kondagogu (Cochlospermum Gossypium): a natural biopolymer". *IET Nanobiotechnol 9:362–367 (2015).*

[13] Sharmila G, Haries S, Farzana Fathima M, Geetha S, Manoj Kumar N, Muthukumaran C.

"Enhanced catalytic and antibacterial activities of photosynthesized palladium nanoparticles using Santalum album leaf extract". *Powder Technol 320:22–26 (2017).*

[14] Cao, D., He, P., & Hu, N. "Electrochemical biosensors utilizing electron transfer in heme proteins immobilized on Fe 3 O 4 nanoparticles". *Analyst*, *128*(10), 1268-1274 (2003).

[15] Wang, B., Wei, Q., & Qu, S. "Synthesis and characterization of uniform and crystalline magnetite nanoparticles via oxidation-precipitation and modified co-precipitation methods". *Int. J. Electrochem. Sci*, *8*(3), 3786-3793 (2013).

[16] Aroutiounian, V. M. "Metal oxide gas sensors decorated with carbon nanotubes". *Lithuanian Journal of Physics*, *55*(4) (2015).

[17] Katz E, Willner I, Wang J "Electroanalytical and electroanalytical systems based on metal and semiconductor nanoparticles". *Electroanalysis* 16:19–44 (2004).

[18] Pumera M. "Graphene-based nanomaterials for energy storage". *Energy Environ Sci* 4:668–674 (2011).

[20] Hossain, M. F., Biswas, S., Zhang, Z. H., & Takahashi, T. "Bubble-like CdSe nanoclusters sensitized TiO_2 nanotube arrays for improvement in the solar cell". *Journal of Photochemistry and Photobiology A: Chemistry*, *217*(1), 68-75 (2011).

[19] Chaianansutcharit, S., Mekasuwandumrong, O., & Praserthdam, P. "Synthesis of Fe_2O_3 nanoparticles in different reaction media". *Ceramics International*, *33*(4), 697-699 (2007).

[21] Rockenberger, J. "A new non-hydraulic single-precursor approach to surfactant-capped nanocrystals of transition metal oxides" (1999)

[22] Chauhan P, Sharma S, "Nanomaterials for Sensing Applications". *J Nanomed Res* 3(5): 00067 (2016).

[23] JoVE Science Education Database. Analytical Chemistry. Ultraviolet-Visible (UV-Vis) Spectroscopy. JoVE, Cambridge, MA, (2019).

[24] Berna F. Fourier Transform Infrared Spectroscopy (FTIR). In: Gilbert A.S. (eds) Encyclopedia of Geoarchaeology. Encyclopedia of Earth Sciences Series. Springer, Dordrecht. (2017)

[25] Quiroga, Amanda. "Cyclic Voltammetry-Chemistry LibreTexts." The LibreTexts libraries, UCD (2017).

[26]. Hussain, Shahir, Md Mottahir Alam, Mohd Imran, Nasser Zouli, Abdul Aziz, Kashif Irshad, Mohammad Haider, and Afzal Khan. "Fe_3O_4 nanoparticles decorated multi-walled carbon nanotubes based magnetic nanofluid for heat transfer application." *Materials Letters* 274 (2020): 128043.

[27] Farahmandjou, Majid, and Farzane Soflaee. "Synthesis and characterization of α-Fe2O3 nanoparticles by simple co-precipitation method." *Physical Chemistry Research* 3, no. 3 (2015): 191-196.

[28] Lei Geng, Zenglai Gao, and Qibo Deng. "Electrochemical Performance of Iron Oxide Nanoflakes on Carbon Cloth under an External Magnetic Field" *Metals*, 939 8(11) 2018.

تخليق وتوصيف جسيمات أكسيد الحديد النانوية لتطبيقات الاستشعار

ميهراج الدين نايك [١،*]، محمد عمران [١]، مصعب الغامدي[١]، يحيى حكمي[١]، محمد العريشي [١]،وليد عبد الله

[1] قسم الهندسة الكيميائية - كلية الهندسة - جامعة جازان - المملكة العربية السعودية

ملخص

يهدف هذا العمل إلى تطوير مستشعر قائم على مادة النانو للمركبات العضوية الضارة عند درجات حرارة وتركيزات منخفضة نسبيًا. تأتي المركبات العضوية الضارة من أسباب مختلفة. يهدف هذا البحث إلى تخليق مادة النانو المناسبة ذات الإمكانات الكيميائية الجيدة مع هذه المركبات العضوية الضارة فيما يتعلق بعاملين يعتبران من العوامل الرئيسية التي تؤثر على واجبات الاستشعار (الانتقائية والحساسية). تم تحضير المواد النانوية بطريقة الترسيب المشترك والتي أنتجت أشكال وأحجام مختلفة من الجسيمات. لوحظ أن أشكال الجسيمات منتظمة وأصغر مما يؤدي إلى خصائص أفضل. استخدمنا النهج التصاعدي خاصة الترسيب الكيميائي المشترك بدلاً من النهج التنازلي لأنه يعطي شكلاً أكثر انتظامًا وجزيئات أصغر. بعد التحضير ، قمنا بتمييز المواد باستخدام عدة تقنيات توصيف مثل حيود الأشعة السينية لتأكيد التركيب المكعب لأكسيد الحديد ووجد أن حجم البلورات للجسيم يبلغ حوالي ١٠ نانومتر. يشرح الفحص المجهري الإلكتروني طبيعة الجسيمات النانوية لأكسيد الحديد ، وقد تم استخدام تقنيات أخرى مثل مطيافية فوريه لتحويل الأشعة تحت الحمراء ، والتحليل الطيفي للأشعة فوق البنفسجية المرئية ، وقياس الجهد الدوري لتأكيد ذلك. تميل العينات المغلفة بالكربون إلى تقليل حساسية أكاسيد المعادن. ومع ذلك ، لوحظ أن تراكيز مختلفة من محاليل الجلوكوز تؤثر على حساسية أكسيد الحديد. لاحظنا أيضًا أن خصائص استشعار أكسيد الحديد زادت بسبب زيادة تركيز الجلوكوز النتائج التي تم الحصول عليها بهذه التقنية مرضية.

الكلمات المفتاحية: المواد النانوية ، أجهزة الاستشعار ، أكسيد الحديد ، الجلوكوز ، قياس السيكلوفولتاميتر.

Restraint and Immobilisation on Pediatric Patients during Radiographic Procedures: Knowledge and practice among Radiographers in Saudi Arabia

Nada A. Alomairy
Diagnostic Radiograph Technology (DRT) Department Faculty of Applied Medical Sciences Jazan University Saudi Arabia

Abstract

Introduction: Paediatric patients are often active and frequently pose a significant challenge to radiographers during radiographic examinations when they are uncooperative and in distress. Paediatric patients must be restrained and immobilised to complete examinations and obtain high-quality radiographs with minimal patient distress and time.

Purpose: To assess radiographers' knowledge and experience with restraint and immobilisation techniques (RIT) during paediatric patient examinations.

Materials and Methods: A survey study was conducted using a self-administered and structured questionnaire. Data were collected and analysed for descriptive statistics.

Results: A total of 90 radiographers participated in the study. Most participants (94%) agreed on the need for training courses on the guidelines for a more effective practice. The result of this study revealed that only 62% (n = 56) of the participants used RIT. The most influential factors that impacted the use of RIT was patient age (69.6%) with aged 1 to 3 years were considered to be in particular need of RIT. For radiographers (n = 34, 37.8%) who did not use RIT, 35.3% (n = 12) of them stated that they are "always" used distraction methods as an alternative technique, and the major reported reason was unavailability of these techniques (73.5%, n = 25). Repeated and prolonged examination time were reported by both the radiographers who used and those who did not use RIT in their clinical practice.

Conclusion: The radiographers' practices in using RIT in the radiology departments in Saudi Arabia were inadequate. Applying RIT for paediatric patients whenever necessary should be encouraged.

Keywords: radiography, radiographers, restraint, immobilisation, pediatric.

INTRODUCTION

Radiographic techniques for the paediatric patient requires special attention of radiology departments personnel (1). Paediatric imaging requires extensive knowledge of imaging protocols and radiation dose as well as different communication and emotional needs compared with adults (2,3). Radiographers are frequently placed in situations where a child's demands must be understood quickly in order for the examination to be completed smoothly (4). In the paediatric population, anxiety, fear, and discomfort are common reactions to imaging procedures (5). The children undergoing radiographic examination at the radiology department is exposed to unfamiliar people, technical equipment, noises, and sometimes darkened rooms. They may be separated from their parent or a loved object, such as a favourite blanket or toy (6). Attempts to restrain them to prevent movement during the x-ray can be frightening and uncomfortable. These stressors can elicit common paediatric emotions and expressions such as fear,

anxiety, pain, and protest (7). This behaviour in children might manifest as crying and refusing to remain still for the scan, which is exacerbated by pain and discomfort caused by trauma or illness. As a result, undiagnostic images with severe motion artifacts are frequently produced as a result of the child's movement, causing repeat imaging. However, the greatest concern with repeat imaging is the biological effects of ionising radiation on the child (8, 9).

Radiographers are required to be knowledgeable about pathology, radiation protection, radiographic techniques, and paediatric anatomy. Also, they must understand psychosocial development to gain confidence in dealing with children and to perform successful diagnostic examinations (10). When children become uncomfortable during the radiographic imaging process, they are more likely to be uncooperative, thus increasing the need for restraint and immobilisation. Graham and Hardy describe immobilisation as a technique used to hold a person still and incapable of moving, whereas restraint is defined as the forcible restriction, limitation, or confinement of a person (11). According to Demir, restraint is the most commonly used technique for children during different clinical and medical procedures, as it helps ensure that the medical process is performed safely, even when the patient resists it (12).

Radiographers often argue that restraint provides the most appropriate way of managing children during examinations. Kangasniemi et al believe that restraint is acceptable and inevitable when dealing with children (13). In most cases, restraint provides the best method of handling children who are uncooperative to radiographers. However, controversy surrounds the use of restraint on children, with Demir reporting that in some countries, parent consent is mandatory before medical practitioners can use the technique on paediatric patients (12). Despite this, coercive medical procedures for children are not regarded as an issue under international clinical guidelines. Therefore, an ethical challenge arises from the absence of clear guiding rules on when and how to utilise restraint.

Ng and Doyle postulate that immobilisation and restraint are critical techniques in diagnostic imaging (8). These techniques help to guarantee image quality and reduce the radiation dose from repeated examinations. For the safety of paediatric patients, the duty of care calls on radiographers to minimise radiation exposure doses (1). Thus, practitioners restraining children against their will is a common practice.

However, care must be taken to ensure that children do not incur injuries, which are often observed after they undergo examinations in the imaging department. Most often, these injuries are overlooked, while sedatives pose a challenge to minor patients because of their harmful side effects (1). Consequently, Brenner highlighted the effects of restraint on both parents and their children psychosocially and emotionally, such as distress and severe anxiety. This means that radiographers must be calculative about its use (14). Therefore, they must circumvent the negative effects of immobilisation and restraint on paediatric patients. In particular, they should find a balance between protecting children from radiation and avoiding emotional and physical injuries (4, 14). However, when radiation protection becomes the primary target, avoiding emotional and physical injuries becomes a secondary priority (15).

With the exception of children's hospitals, the majority of radiology department staff members are not specialists in paediatric nursing or imaging. There is a need for education and practical training for

staff who work in paediatric radiography (16). Evaluation of the existing knowledge and practices regarding restraint and immobilisation is critical. Limited number of studies have addressed restraint and immobilisation on paediatric patients during radiographic procedures. The need for such studies is necessary to enrich the literature to cover facets of restraint and immobilisation during radiography. Therefore, the objective of this study was to determine radiographers' use of restraint and immobilisation procedures on paediatric patients in major hospitals.

MATERIALS AND METHODS

This survey study was conducted in Saudi Arabia and comprised radiographers working in major hospitals. Radiologic internship students were excluded due to the different perspective on experience, training and attitudes. Due to the lack of accessibility of all radiographers' contact information and the difficulty of finding data on the population size, A non-probability sampling was used in this study. Convenience samples of 90 radiographers were collected for this study using personal contacts. The questionnaire was distributed online for the purposes of cost, time and geographical coverage (17), using Google Forms (Google, Mountain View, US). Radiographers were invited to participate via email. This study was approved by the ethical committee at Jazan University before data collection. Participant confidentiality was protected by de-identifying all responses.

Data were collected using a self-administered and structured questionnaire to elicit responses from radiographers. The questionnaire applied the technicality recommended in a previously published work related to the aim of the present study (11) to ensure its effectiveness. The questionnaire consisted of three parts. The first section includes the demographic items (gender, age, years of experience), awareness of local guidelines in the department regarding the restraint of children and use of immobilization techniques, and the need for a proper training course regarding the use of restraint or immobilization devices for paediatric patients during radiography. The second section include an item with "Yes" or "No" answers about if normally use any kind of restraint or immobilization techniques on paediatric patients during radiography. The third section was based on the participant's previous answer in the second section as shown in Table 1.

The survey's cover page included an introduction information sheet that contains the definition of restraint and immobilisation terminologies (to provide the respondents with a better understanding of the scope of the questions), the study's objective, duration, and the option to withdraw at any time, privacy and confidentiality statements. The survey's first page included the consent form, where participants should approve their participation in order to access to the survey. A pilot study was conducted to test the feasibility and applicability of the questionnaire. Ten participants were surveyed and took about 10 min to complete the questionnaire. Amendments in the questionnaire were not needed. The pilot study responses were excluded from analysis of the main data.

The Statistical Package for Social Sciences (SPSS), (Version 27, IBM Corp., Armonk, N.Y., USA). Descriptive statistics were calculated and presented as frequency and percentage. Chi-square test for independence was conducted to evaluate the relationship between variables. A p-value of <0.05 was used to determine that the findings of the inferential statistics were statistically significant.

RESULTS

A total of 90 respondents composed of radiographers from different hospitals participated in the study, of whom 50 were men and 40 were women. 57 (63.3%) respondents had ≤5 years, 17 (18.9%) had

6–10 years, and 16 (17.8%) had ≥ 11 years of experience in examining paediatric patients (Table 2). Of the respondents, 72% (n = 65) were aware of the local guidelines in the department regarding the use of restraint and immobilisation techniques on children. Most participants (94%) agreed on the need for training courses on the guidelines for a more effective practice. Regarding the use of any kind of restraint or immobilization techniques on paediatric patients during radiography, 56 (62.2%) of radiographers answered yes and 34 (37.8%) answered no. There were no significant statistical differences between radiographers' demographic characteristics, awareness of local guidelines in the department, and the need for a proper training course with using of restraint or immobilization techniques.

Radiographers who do not use restraint or immobilisation techniques.

The participants who did not use restraint or immobilisation techniques on paediatric patients during radiography were 37.8% (n = 34). The reasons for not using restraint and immobilisation techniques reported by those radiographers were the technique was unavailable (73.5%, n = 25), carelessness (14.7%, n = 5) and the least number of participants were aware of the techniques but did not know how to use them (11.8%, n = 3). The participants who did not use restraint or immobilisation techniques were asked whether they used distraction methods during radiographic examinations. Approximately 35.3% (n = 12) always used distraction methods for paediatric patients as an alternative to restraint or immobilisation during examinations. On the other hand, 23.5% (n = 8), 14.7% (n = 5), and 26.5% (n = 9) often, sometimes, and rarely used distraction methods, respectively. Also, the result indicated that most radiographers (91.2%, n=31) had to repeat the examination because of unwanted movements of the child or infant being examined, and 97.1% (n=33) believe that this unwanted movements contribute to the increased time of examination.

Radiographers who use restraint or immobilisation techniques.

The participants who used child restraint in their clinical practice (n = 56). Figure 1 shows the percentage frequency distribution of the influential factors that influenced radiographers' use of restraining or immobilisation techniques. Patient age was the most crucial factor that impacted the use of physical, chemical, and physiological methods of immobilisation and restraint, accounting for 69.6% (n = 39) of the responses. Mental or physical disorders (53.6%) and the necessity of the examination (53.6%) also influence radiographers to use immobilisation devices or restraint on children during radiographic examinations.

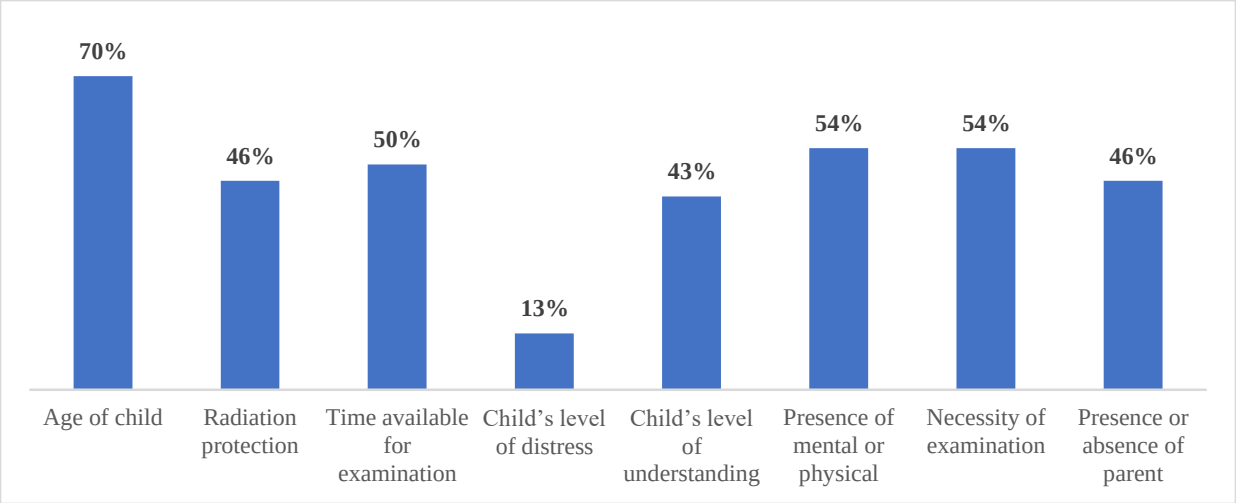

Figure 1. Percentage frequency distribution of factors that influenced the radiographers to use an immobilisation device or restraint on children during radiographic examination (n = 56).

In response to the questions regarding the common method(s) of restraint or equipment used for paediatric patients during radiography, the physical method (holding by parent) was the immobilisation method most frequently used, followed by mechanical techniques (tape/bandages, immobilisation devices and sandbags). The least likely option was holding by staff members (Figure 2).

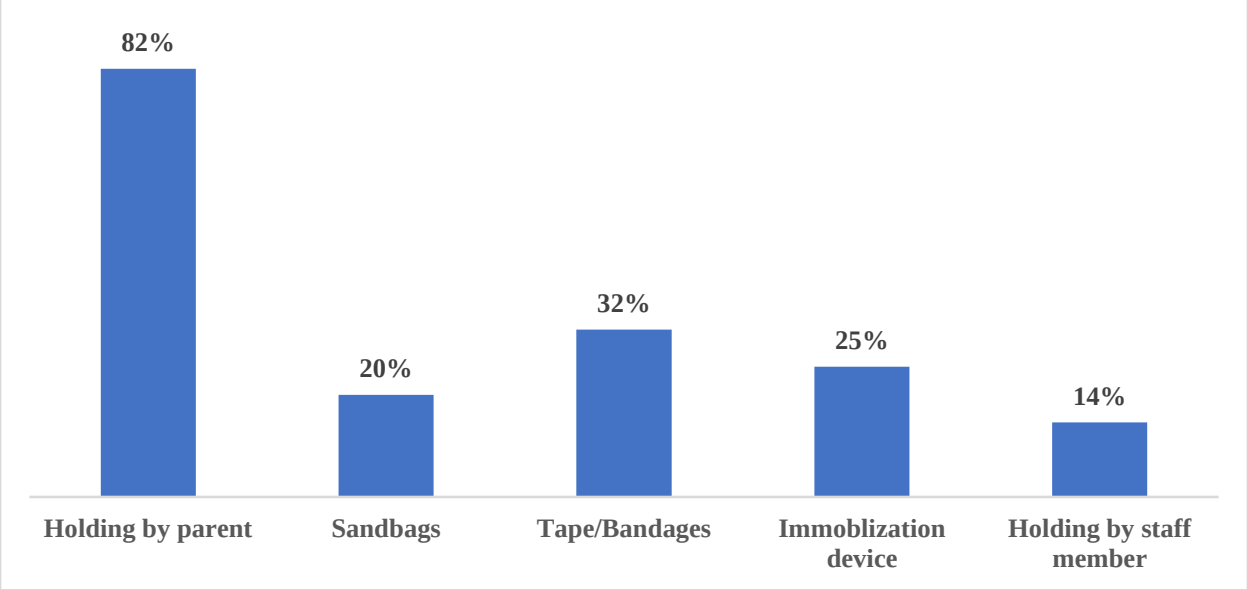

Figure 2. Percentage frequency distribution of methods of restraint/equipment use (n = 56).

Figure 3 shows the specific age groups that usually radiographers use the restraining technique during radiography. The result revealed that patients aged 1 to 3 years (71%) were considered to be in particular need of immobilisation because they were more prone to distress and less likely to understand the need to keep motionless, putting them in a position to be uncooperative.

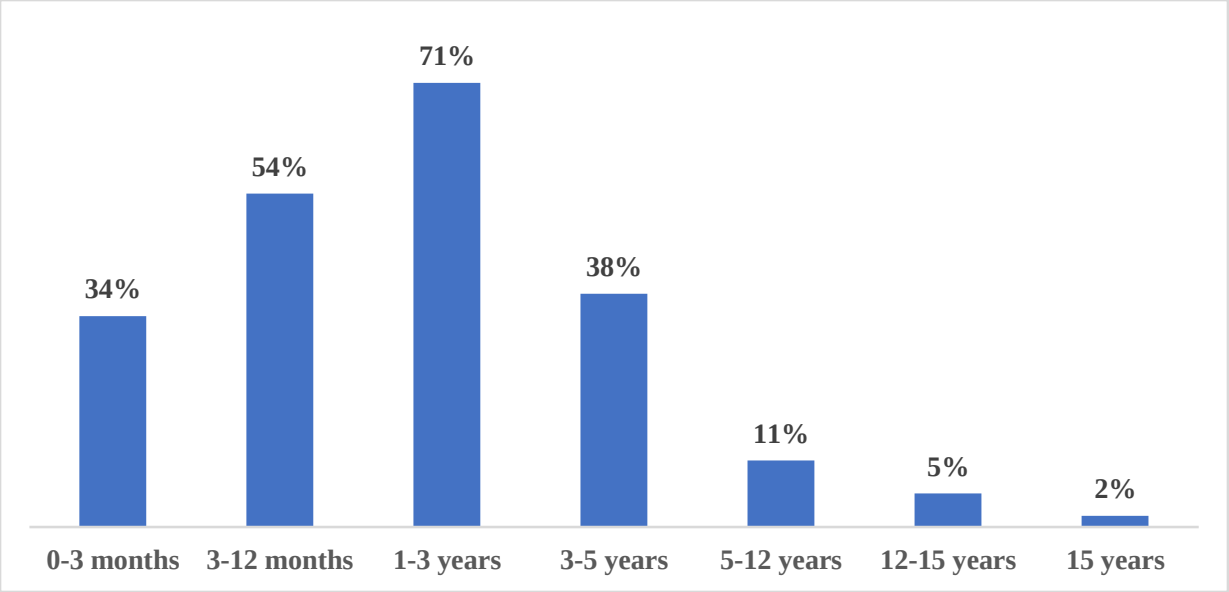

Figure 3: Percentage frequency distribution of perceived need for restrain according to age of child (n = 56).

Of the participants who used child restraint in their clinical practice, 60% had to repeat the examination because of the movements of the child or infant being examined and 58.9% believe that this unwanted movements contribute to the increased time of examination.

DISCUSSION

Immobilisation and restraint during paediatric radiography warrant high image quality and reduce the radiation dose from repeated examinations (6). The current study seeks to provide a better understanding of the vital role of child restraint and immobilisation techniques to radiographers in different major hospitals in Saudi Arabia.

In this study, 72% (n = 65) of the radiographers were aware of the guidelines on the use of immobilisation techniques in their departments. This proportion is significantly higher than the 54% (n = 42) reported by Dashti et al. in Kuwait (18). Moreover, 62% (n = 56) of the participants in this study reported the use of restraints and immobilisation techniques for paediatric patients, which is similar to the result of the study conducted in Kuwait in which 69% (n = 54) of participants reported the use of restraint equipment. The fact that 38% (n = 34) of the participants did not restrain or immobilise infants or children during examinations is a concerning finding that shows that patient care in hospitals is undervalued and below the standard of care. Also, about 74% (n = 25) of the respondents (who did not use restraints and immobilisation techniques) in this study reported the unavailability of restraint devices in their departments. This result is comparable with a previous study from the United Kingdom, where 78% of respondents indicated having no access restraining devices in their department (11).

Several methods were used to prevent child movement during radiographic procedures. In the present study, the radiographers (82%, n = 46) indicated that asking parents to hold their children was the most commonly used method by radiographers, which is in line with previous studies (18). However, this finding indicates the lack of distraction equipment in the radiology department in the region. Also, radiographers encounter a variety of communication and interaction challenges with paediatric patient custodians, which hindered service delivery. The reaction of

the paediatric patient in the imaging room may have an additional impact on the interaction between the radiographer and the custodian (19).

Regarding the factors that influenced the decision to restrain a child, the most important situational influence identified in this study was the age of the child (69%, n = 39), which is consistent with the findings in previous research on immobilisation practice (15, 18, 20, 22). On the other hand, Graham et al. reported that child safety (97%, n = 126/130) is the most influential factor (11). Another significant finding in this study was that children aged 1 to 3 years were the most active and distressed. This finding is in contrast to the result of the study by Dashti et al., where 3–12 months was the age group that had the most influence on the decision to restrain or immobilise (18).

Previous studies have shown that restraint and immobilisation are the most suitable methods of managing children during examinations. They reduce the time of examination by controlling the movements of the child or infant being examined, thus easing the medical practitioners' work. They are inexpensive, are simple to operate, and provide comfort to patients through human contact (15, 20-22). The findings of this study showed that prolonged examination time due to child or infant movements is the biggest challenge faced by both the participants who used and those who did not use child restraint in their clinical practice. Likewise, repeated examinations due to child or infant movements are also an issue for both groups. Poor radiographic images are more likely to be obtained when children prove uncooperative to radiographers. Immobilisation and restraint warrant high image quality and reduce the radiation dose from repeated examinations (2, 10, 23). However, in this study, a lower percentage of repeated examinations and prolonged examination time were reported by radiographers who use restraint and immobilisation techniques compared with who do not use these techniques. This is clearly indicating the importance of using restraint and immobilisation techniques. The topic of restraint and immobilization techniques in pediatric radiography is essential since repeat or retakes rates, accurate diagnostic, patient dose, and many other factors are controlled by it (24).

The proper implementation of restraint and immobilisation techniques in hospitals is a topic of great necessity. Applying restraint and immobilisation for paediatric patients whenever necessary should be encouraged, and radiographers should be trained on how to use various restraint and distraction methods techniques efficiently to improve their ability to perform examinations with minimal patient distress in various situations. Moreover, the immobilisation techniques used by radiographers in clinical settings should be examined to identify the preferred methods and the indications for using them. Also, experimental investigations could be undertaken to determine which paediatric immobilisation methods are most beneficial. Moreover, future studies should include a qualitative research approach that could highlight more profound perceptions toward the use of immobilisation and restraint techniques in paediatric radiography.

To the best of our knowledge, this is the first study to examine the use of immobilisation and restraint techniques in paediatric radiography in Saudi Arabia. However, some limitations need to be acknowledged, including the small sample size and that the study population was obtained through a convenience sampling method, which the findings might not statistically generalizable beyond the sample. Larger sample size would serve to confirm aspects of the current study. Also,

the use of personal contacts for participant recruitment might introduce bias to the study. However, this approach was in line with the recruitment approach of convenience sampling.

CONCLUSION

In conclusion, the current practices in using immobilisation protocols in the radiography departments of hospitals in Saudi Arabia were comparable with practices in several countries. However, further development and employment of standardised policies that support evidence-based practice will guide radiographers in applying paediatric immobilisation. This will enable more standardised practices at the national level. To increase radiographers' comprehension and ability to critically select various constraint and immobilisation procedures, more training and guidance are required.

Acknowledgements: The authors would like to thank radiology departments' supervisors who facilitated communication with radiologic technologists and the survey distribution.

Conflict of interest: The Authors declare that there is no conflict of interest.

Funding: This research received no specific grant from any funding agency in the public, commercial, or not-for-profit sectors.

References

1. Linder JMB. Safety Considerations in Immobilizing Pediatric Clients for Radiographic Procedures. Journal of Radiology Nursing. 2017;36(1):55-58.

2. Thukral BB. Problems and preferences in pediatric imaging. The Indian journal of radiology & imaging. 2015;25(4):359-364.

3. Harding J, Davis M. An observational study based on the interaction between the paediatric patient and radiographer. Radiography. 2015;21(3):258-263.

4. Goske MJ, Charkot E, Herrmann T, John SD, Mills TT, Morrison G, et al. Image Gently: challenges for radiologic technologists when performing digital radiography in children. Pediatric radiology. 2011;41(5):611-619.

5. Björkman B, Golsäter M, Enskär K. Children's Anxiety, Pain, and Distress Related to the Perception of Care While Undergoing an Acute Radiographic Examination. Journal of Radiology Nursing. 2014;33(2):69-78.

6. Mathers SA, Anderson H, McDonald S. A survey of imaging services for children in England, Wales and Scotland. Radiography. 2011;17(1):20-27.

7. Iobst CA, Stillwagon M, Ryan D, Shirley E, Frick SL. Assessing Quality and Safety in Pediatric Supracondylar Humerus Fracture Care. Journal of pediatric orthopedics. 2017;37(5):303-207.

8. Ng JHS, Doyle E. Keeping Children Still in Medical Imaging Examinations-Immobilisation or Restraint: A Literature Review. Journal of medical imaging and radiation sciences. 2019;50(1):179-187.

9. Cho H-H, Lee SM, You SK. Effect of using immobilization device in fluoroscopic study in pediatric patient: Focused on radiation dose reduction in voiding cystourethrogram. PLOS ONE. 2019;14

10. Allison A, McHugh K. Immobilisation and restraining of paediatric patients in the Radiology Department: A perspective and review of legislation

relevant to UK radiographic professions. Radiography. 2008;14(1):57-62.

11. Graham P, Hardy M. The immobilisation and restraint of paediatric patients during plain film radiographic examinations. Radiography. 2004;10(1):23-31.

12. Demir A. The use of physical restraints on children: practices and attitudes of paediatric nurses in Turkey. 2007;54(4):367-374.

13. Kangasniemi M, Papinaho O, Korhonen A. Nurses' perceptions of the use of restraint in pediatric somatic care. Nursing Ethics. 2014;21(5):608-620.

14. Brenner M. Child Restraint in the Acute Setting of Pediatric Nursing: An Extraordinarily Stressful Event. Issues in Comprehensive Pediatric Nursing. 2007;30(1-2):29-37.

15. Christie S, Ng CKC, C SDR. Australasian radiographers' choices of immobilisation strategies for paediatric radiological examinations. Radiography (London, England : 1995). 2020;26(1):27-34.

16. Morrison G, John SD, Goske MJ, Charkot E, Herrmann T, Smith SN, et al. Pediatric digital radiography education for radiologic technologists: current state. Pediatric radiology. 2011;41(5):602-610.

17. Dykema J, Jones NR, Piché T, Stevenson J. Surveying Clinicians by Web: Current Issues in Design and Administration. Evaluation & the Health Professions. 2013;36(3):352-381.

18. Dashti M, Al-Abbad M, Faleh A, Al-Ostath S. Current immobilization implementation of pediatric patients in five major public hospitals in Kuwait: a prospective study into policies and guidelines for radiology departments. Indian Journal of Innovations Developments. 2012;1(8):647-652.

19. Ketema SF, Kekana RM, Essop H, Msonza HW. Diagnostic radiographers' experiences when interacting with the custodians of paediatric patients presenting for general radiographic imaging. Radiography. 2021;27(4):1021-1026.

20. Bray L, Carter B, Ford K, Dickinson A, Water T, Blake L. Holding children for procedures: An international survey of health professionals. Journal of Child Health Care. 2018;22(2):205-215.

21. Bray L, Ford K, Dickinson A, Water T, Snodin J, Carter B. A qualitative study of health professionals' views on the holding of children for clinical procedures: Constructing a balanced approach. Journal of Child Health Care. 2018;23(1):160-171.

22. Brenner M, Treacy MP, Drennan J, Fealy G. Nurses' Perceptions of the Practice of Restricting a Child for a Clinical Procedure. Qualitative Health Research. 2014;24(8):1080-1089.

23. Quan X, Joseph A, Nanda U, Moyano-Smith O, Kanakri S, Ancheta C, et al. Improving Pediatric Radiography Patient Stress, Mood, and Parental Satisfaction Through Positive Environmental Distractions: A Randomized Control Trial. Journal of Pediatric Nursing. 2016;31(1):11-22.

24. Kohda E, Tsutsumi Y, Nagamoto M, Gomi T, Terada H, Kawawa Y, et al. Revisit image control for pediatric chest radiography. Radiation medicine. 2007;25(2):60-64.

Table 1: The series of questions based on the participant's answer.

Do you normally use any kind of restraint or immobilization techniques on paediatric patients during radiography?	
Yes	**No**
1. Which influential factors affecting you to use one or more form of restraining or immobilization techniques? 2. What is the most common method(s) of restraint or equipment used for paediatric patients during radiography? 3. From the following specific age groups, in which group do you usually use the restraining technique during radiography? 4. Have you ever repeated an examination because of the movement of child or infant? 5. Does usually the movement of the child or the infant increase the time of examination?	1. What is the reason in not using this technique? 2. Do you use distraction methods for children as an alternative to restraint or immobilize paediatric patients during examination? 3. Have you ever repeated an examination because of the movement of child or infant? 4. Does usually the movement of the child or the infant increase the time of examination?

Table ٢: Summary of demographic characteristics and general items and associations with usability of restraint or immobilization techniques.

	Count (N=90)	**P-value**
Gender		
Female	40 (44.4%)	0.409
Male	50 (55.6%)	
Years of experience		
≤ 5 years	57 (63.3%)	0.189
6-10 years	17 (18.9%)	
≥ 11 years	16 (17.8%)	
Awareness of local guidelines in the department		
No	25 (27.8%)	0.095
Yes	65 (72.2%)	
Need for a proper training course		
No	5 (5.6%)	0.292
Yes	85 (94.4%)	
Using any kind of restraint or immobilization techniques		
No	34 (37.8%)	
Yes	56 (62.2%)	

تقنية التقييد والتثبيت (عدم الحركة) لمرضى الأطفال خلال الاجراءات الاشعاعيه: المعرفة والممارسة بين مصوري الأشعة في المملكة العربية السعودية

ندى عبدالله العميري[1*]

قسم تقنية الأشعة التشخيصية ،كلية العلوم الطبية التطبيقية، جامعه جازان ،المملكة العربية السعودية

الملخص

المقدمة: غالبًا ما يكون مرضى الأطفال نشيطين وغالبًا ما يشكلون تحديًا كبيرًا لمصوري الأشعة أثناء فحوصات التصوير الإشعاعي عندما يكونون غير متعاونين. ولابد من تقييد مرضى الأطفال وتثبيتهم لإستكمال الفحوصات والحصول على صور إشعاعية عالية الجودة مع الحد الأدنى من الوقت المستغرق للعملية الإشعاعيه.

الغرض: تقييم معرفة المصورين الإشعاعيين وخبراتهم في تقنيات ضبط النفس وتثبيت الحركة أثناء فحوصات المرضى من الأطفال.

المواد والطريقة: أجريت دراسة استقصائية بإستخدام استبيان. تم جمع البيانات وتحليلها من أجل الإحصاء الوصفي.

النتائج: شارك في تعبئة الإستبيان ٩٠ أخصائي تصويرإشعاعي. اتفق معظم المشاركين (٩٤٪) على الحاجة إلى دورات تدريبية حول المبادئ التوجيهية لممارسة أكثر فعالية. وكشفت نتائج هذه الدراسة أن ٦٢ ٪ فقط (العدد = ٥٦) من المشاركين يستخدمون تقنية التقييد والتثبيت وان العامل الأكثر تأثيرًا على استخدام تقنية التقييد والتثبيت هي عمر المريض (٦٩,٦٪) الذين تتراوح أعمارهم من ١ إلى ٣ سنوات. وأوضحت الدراسات ايضاً أن حوالي (العدد = ٣٤ ، ٣٧,٨٪) لا يستخدمون تقنية التقييد والتثبيت بينما يستخدمون دائماً طرق التشتيت كأسلوب بديل بسبب عدم توفر هذه التقنيات في المستشفيات التي يعملون بها.

الخلاصة: ممارسات التصوير بالأشعة في استخدام تقنية التقييد والتثبيت في أقسام الأشعة في المملكة العربية السعودية كانت غير كافية. ويجب تشجيع تطبيق هذه التقنية على مرضى الأطفال عند الضرورة.

الكلمات المفتاحية: التصوير الإشعاعي ، أخصائي الأشعة ، ضبط النفس ، التثبيت ، طب الأطفال.

Radon Gas Emission from Different Homes in Jazan Region

Entesar. H. EL-Araby and A. Azazi

Physics Department, Faculty of Science, Jazan University, Saudi Arabia

ABSTRACT

Ventilation and central air conditioning systems contribute to a significant increase in indoor radon levels. Therefore, it is necessary to study and analyze the parameters that affect the rates of radon emission and the increase of the radiation dose in homes. This current work is concerned with measuring the rates of radon gas emissions by nuclear track detector "CR-39" in homes with different ventilation and air conditioning systems in Jazan region. The results showed that the average concentration of radon in homes with different ventilation systems ranged between 453.79 ± 12.79 to 63.22 ± 9.43 Bq/m^3. The radiation dose that people living in these homes were exposed to showed that it is affected by air conditioning and ventilation systems inside homes. The radiation dose results showed that 20% of the annual effective dose values were very close to the upper limit of internationally permissible values in homes with central air conditioning and 10% of the results in homes with non-central air conditioning systems were very close to the upper limit values. The dose values measured in the old, self-ventilated homes were within the limits recommended by the International Commission on Radiological Protection (ICRP). The results showed that all values of lung cancer cases per year per million people (CPPP) were within the recommended limit.

Keywords: Radon gas, Ventilation, radioactive dose, Concentration of radon, CR39 detector, CPPP.

1- INTRODUCTION

Jazan region (also called Jizan) has an area estimated to be 40,457 km² in addition to around 80 islands on the Red Sea, of which the famous is Farasan, covering around 752 km² (Emirate of Jazan Province) with a population of 1,٦٠٣,٦٥٩,(20٢0 census) and it is known for its great number of flowing rivers, due it became important and highly known for its agricultural products. However, it's important to highlight the fact that there could be various issues harming these agricultural products, natural radiation is one of them and the focus of much research [1-4].

Natural radiation is a part of the environment, it comes from nature, in addition to manmade sources, among these natural sources, we can cite cosmic radiation from space, radioactive rocks, and radioactive soil. Since the beginning of humanity, humans have always been exposed to natural radioactivity. An element is radioactive when the atoms transform from the unstable form to the stable form and release energy (radiation). But most elements are stable, which means they don't release energy, so they are not considered radioactive. [5,6].

One of the most important problems facing the world is materials of radioactive origin because of their harmful effects on humans and the environment. Therefore, controlling the environmental risks of radioactive materials is of great importance [7,8]. Radon is a radioactive gas produced by the decay of radium and produces the nucleus of the helium atom, a low-penetrating alpha particle. Other types of radiation are gamma radiation, with very high penetrating, and beta particles, which are high-velocity electrons or positrons [8,9].

Radon gas has three isotopes ($^{222}_{86}Rn$) resulting from the decay of ($^{238}_{92}U$), ($^{220}_{86}Rn$) resulting from the decay of ($^{232}_{90}Th$) and ($^{219}_{86}Rn$) a decay produced from the chain originating with ($^{235}_{92}U$) [10]. The half-life of all isotopes is very short. 3.82 days is the half-life of the isotope ($^{222}_{86}Rn$), while 55 seconds are the half-life of, ($^{220}_{86}Rn$), and the half-life of ($^{219}_{86}Rn$) is about 3.9 seconds [11]. The isotopes of Radon are present in all types of soil, rock, and water. Radon is heavier than air eight times [1,4].

Only a small amount of created Radon can emerge from the mineral grains and into the void space which is filled with gas. Then, Radon spreads out further by diffusion in carrier gases, and in a slow process, it exhales into the air [2]. Radon's presence in the air in sufficient quantities makes it a health hazard because when Radon is inhaled it possibly leads to lung cancer [8,2].

Various studies have shown that there is a correlation between the values of radon pollution and increased rates of lung cancer. The increase in radon gas inside homes depends on building materials and sources from which they were manufactured [12, 13]. Ventilation of homes and the method of covering floors affect the increase of indoor radon gas in homes, which negatively affects public health. Therefore, it is necessary to focus on increasing the ventilation of homes and inventing ways to insulate floors to reduce the values of radon gas and preserve the general health of the public [14,15].

Case studies of miners in Europe revealed that indoor exposure to radon contributes significantly to the risk of lung cancer in the general population [16]. Although the effect of 222Rn on

lung cancer is not high, conducting studies indoors is of great importance because humans currently spend about 80% of their time in closed rooms [17,18]. The Jazan region in Saudi Arabia is considered a hot place, so most residents tend to not ventilate their homes, and rely on air conditioners. A study conducted in some public places in Saudi Arabia showed that the radon concentration was highly dependent on ventilation [19]. Expanding studies on the values of radon gas in homes will contribute to determining the correct way to ventilate homes and maintain public health.

The research is interested in studying the presence of radon gas in different types of houses in jazan region (the area contains old-style non-air-conditioned buildings, air-conditioned building styles، and others with central air-conditioning).

The area contains old-style non-air-conditioned buildings, air-conditioned building styles، and others with central air-conditioning. Therefore, the study focused on calculating radioactive contamination in patterns of different buildings because of its negative impact on the health of the public. The increase in radioactive pollution causes great danger to public health and is one of the causes of lung cancer resulting from inhaling radon gas generated from building materials and soil containing radioactive nuclei. The study aims to calculate the levels of radon gas in different buildings in Jazan region using CR-39 because of its high sensitivity and stability against weather factors. Develop recommendations to reduce the concentration of radioactive materials in homes if there is a high concentration.

2- METHODS

Table 1: Type of houses in different places**.**

Type of houses	Code	place	Type of houses	Code	place
First Modern Houses	S1	Fayfa	Second Modern Houses	L1	Almusarhah
	S2			L2	
	S3			L3	Abu Arish
	S4	Abysh		L4	
	S5			L5	
	S6			L6	
	S7	Jizan		L7	Jizan
	S8			L8	
	S9			L9	
	S10			L10	
	S11		The Old Houses	D1	Al-Karbus
	S12			D2	
	S13			D3	Damad
	S14			D4	
	S15	Sabya		D5	Almabuj
	S16			D6	
	S17			D7	Al-Shuqayri
	S18	Samtah		D8	
	S19			D9	Al-Shawajrah
	S20			D10	

2.1 Sampling

Three different types of houses were tested in Jazan region to study the differences in radon radiation rates between them. The first type is modern homes, which depend on the central air conditioning system and the ventilation system that relies only on hoods. It has a very limited number of ventilation holes. The second type is modern homes that rely on regular air conditioning systems. The ventilation system is high and has many ventilation holes. The third type is the old houses that do not have an air conditioning system and are built with mud and a high ventilation system (considered like greenhouses). Table 1 shows the types of houses, the places where samples are distributed, and the code for each type.

Samples were distributed in different places in Jazan region, as shown in Map 1, to expand the study area and the quality of the results.

Figure 1: Type of houses under study in jazan Region

٢.٢- The sample analysis.

The detector SSNTD CR-39, after being cut (1.5 cm x 1.5 cm), was placed in a container with dimensions 8 diameters by 10 in height, and then it was placed in the selected places in the houses. A paper filter is placed to cover the can which allows radon to enter. Five cans were placed in each house. The CR-39 detector has high sensitivity and accuracy in measuring radioactive materials, which makes it a good choice for determining the concentration of radiation in the place of study. Many studies depend on the detector because of its high radiation retention properties for long periods, and environmental factors do not affect the measured values [1-4,19]. The reagent was placed in study areas for 60 days to reach the radioactive balance between radon and its progeny [1]. The exposed detectors are collected to measure the radiation tracks recorded inside the detector. These paths can only be seen by a chemical etching technique. To see the tracks, a chemical etching should be done using a sodium hydroxide solution at a temperature of 70°C for 6 hours. Etched detectors were washed with rinse water for 20 min. Track density (track/cm) was calculated using optical microscopy.

2.3 Theoretical aspects

To calculate the effective exposure time in hours "t_e" we use the following equation [1,19] :

$$t_e = t - \frac{1-e^{-\lambda t}}{\lambda} \qquad (1)$$

Where $\lambda =$ 7.55 x 10^{-3} h^{-1} represents the decay constant of radon and t represents the exposure time. Based on the track density and using the relation (2) we can find the equilibrium concentration of radon C_{eq} (Bq/m^3) using the equation:

$$C_{eq} = \frac{\rho}{kt_{ef}} \qquad (2)$$

Where K (K = 0.045987 tracks cm^{-2} d^{-1}/Bqm^{-3} [16,17, 4]) is the calibration factor of the SSNTDs detector. Based on the result of the equilibrium concentration of radon "C_{eq}" and using equation (3) [16-18] we determine the surface exhalation rate (E_a) ($Bqm^{-2}{\cdot}h^{-1}$) for the radon

$$E_a = C_{eq}\, V\lambda / A \qquad (3)$$

Where A (m^2) and V (m^3) represent the cross-section area and the effective volume of the can respectively.

The annual effective dose (mSv/yr) was calculated using the equation (4) [19] :

$$H = C \times D \times F \times T = 25.2C\ (\frac{mSv}{y}) \qquad (4)$$

where C, D, F, and T represent respectively; the measured mean radon activity concentration in air in B /qm^3, the dose conversion factor (D=9 nSv/h per Bq/m^3), the indoor equilibrium factor between radon and its progeny (F=0.4), and the time (T=8760 hy^{-1}) [7, 8].

Lung cancer cases per year per million people (CPPP), were obtained using the equation :[19-26]

$$(CPPP) = H \times (18 \times 10^{-6}\ mSv^{-1}.y) \qquad (5)$$

3- RESULTS

The average radon concentration was calculated in different types of buildings in Jazan region (old and modern buildings with central and modern air conditioning). **Figure 2** shows the relation between the average concentration of radon gas in different buildings. The results showed that the highest percentage of radon concentration was in the first type of modern buildings (which depend on central air conditioning as the main ventilation pattern for the house) at 49%. The lowest concentration of radon was recorded in old buildings (which depend on natural ventilation) at 12%. Natural ventilation allows gases from buildings to leave the building without affecting the health of the building's occupants [19]. Therefore, they are considered healthy green buildings that take care of the health of their residents

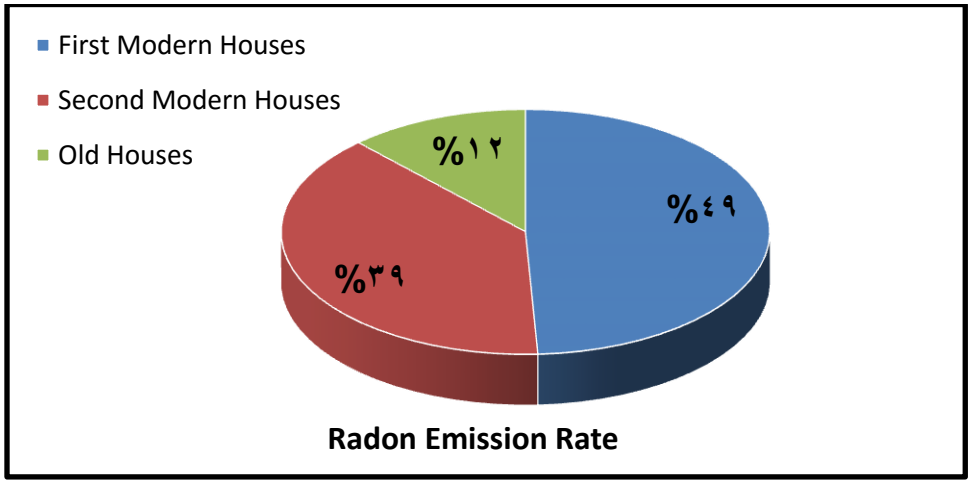

Figure 2: The radon gas emissions rate in different types of houses.

Figure 3 shows the concentration of radon in different types of houses. The highest value of radon gas concentration in the first type was recorded in sample S1 with a value of 453.79 ± 12.79 Bq/m^3 and the lowest concentration in S18 with a value of 218.11 ± 86.20 Bq/m^3 with an average of 346.99 ± 62.09 Bq/m^3. While the second type had the highest value of radon concentration in sample L9 with a value of 443.97 ± 25.73 Bq/m^3 and the lowest value was 160.28 ± 51.19 Bq/m^3 in sample L3 with an average of 273.76 ± 37.51 Bq/m^3

The old houses recorded the lowest values of radon gas,
where the highest value was in sample D10 with a value of 103.45 ± 3.29 Bq/$m^3$and the lowest value was 63.22 ± 9.43 Bq/m^3 in the sample D1 with an average of 84.64 ± 10.36 Bq/m^3.

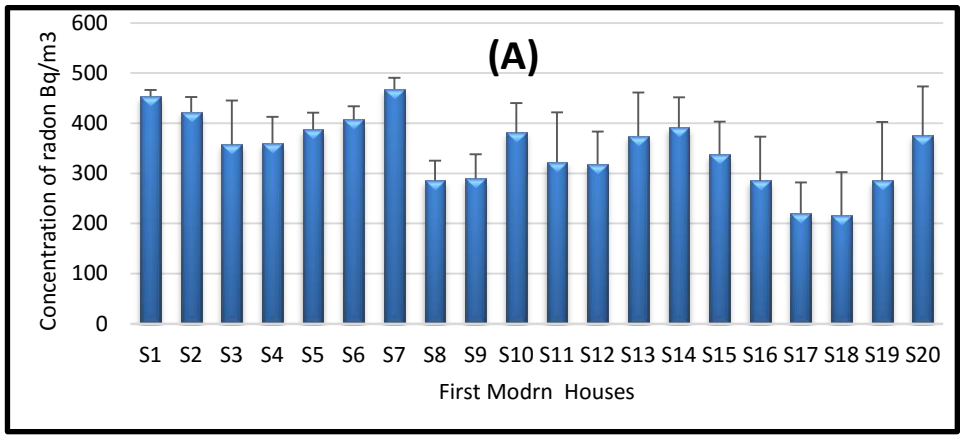

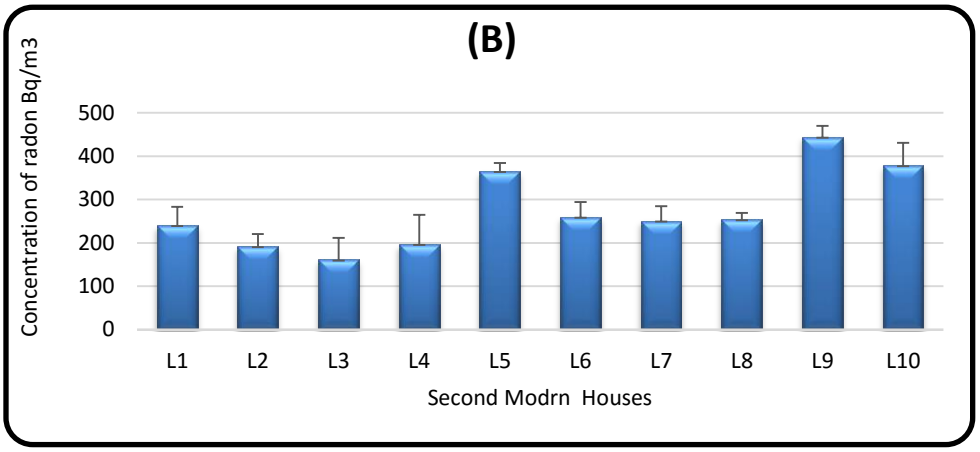

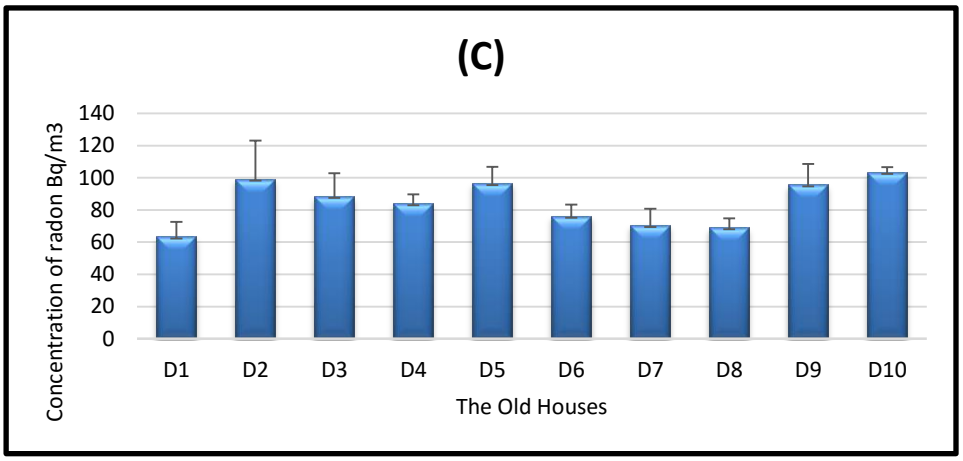

Figure 3: The concentration of radon in different types of houses.

The results of the first type of building showed that 20% of the concentration of radon gas was higher than the internationally permissible values and that 10% of the results concentration of radon gas for the second type are higher than the internationally permissible, while the results of the gas concentration of the third type

were within the internationally permissible limits according to the results International Commission on Radiological Protection ICRP [7,9] which has the limit values of radon from 200 to 400 Bq/m^3. It is clear from the results that ventilation has a large factor in the effect of radon gas, so it is necessary to ensure high ventilation of the houses and follow-up to verify the gas values through the continuous study of the houses, to maintain the general health of the public.

The annual effective dose values measured in different houses in Jazan region are shown in **Figure 4**. Where it indicates that the average dose values were 7.09 ± 1.28, 5.59 ± 0.77, and 2.13 ± 0.26 mSv/year in the first type of houses, the second type of houses, and the old houses, respectively. The results showed that 20% of the annual effective dose values for the first type were close to the upper limit of the recommended ICRP limits, which limited the radon dose values to (3:10 mSv/yr). Also, 10% of annual effective dose values for the second type approach the upper limit of permissible limits, while all values for old homes were within the internationally permissible limit.

The results of the exhalation rate of radon and lung cancer cases per year per million people (CPPP) in different types of homes in Jazan region are illustrated in **Table 2**. The average exhalation rate was 628.74 ± 112.50 $Bqm^{-2}{\cdot}h^{-1}$ in the first type of houses, 469.05 ± 67.97 $Bqm^{-2}{\cdot}h^{-1}$in the second type, while it was 189.25 ± 22.98 $Bqm^{-2}{\cdot}h^{-1}$ in houses Old. There is a clear difference between the values due to the different building materials and ventilation method at different types of houses which is an important role in increasing radon levels in the studied places. Lung cancer cases per year per million people (CPPP) in different houses ranged from 166.80±4.74 to 79.43±31.93 with an average value of 100.63±13.90 per million people in type I and ranged from 139.03±19.39 to 58.92±18.96 with an average value 100.63±13.90 per million people in the second type while in the old home type, the value of CPPP ranged from 46.92±1.49 to 28.68±4.28 with an average value of 38.39±4.70 per million people. All results for the different households were within the internationally recommended limit recommended by the International Commission on Radiological Protection, which set values for the permissible limit from 230 to 170 per million people [1].

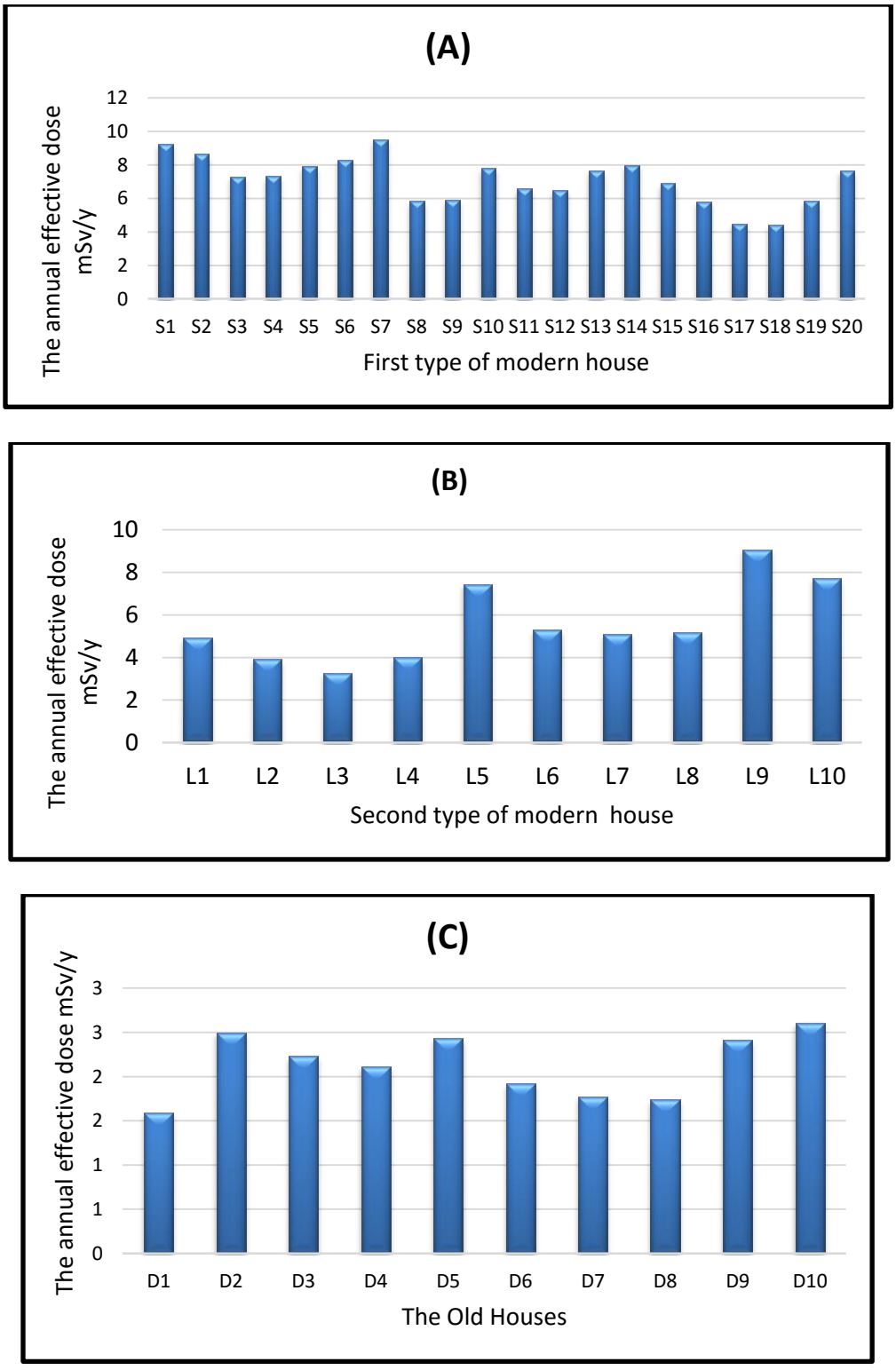

Figure 4: The annual effective dose in different types of houses.

Table 2: The relation between the average value for area exhalation rate E_A ($Bqm^{-2}\cdot h^{-1}$), and the lung cancer cases per year per million people (CPPP) for different types of houses.

	No. of sample	EA ($Bqm^{-2}\cdot h^{-1}$)	CPPP $\times 10^6$		No. of sample	EA ($Bqm^{-2}\cdot h^{-1}$)	CPPP $\times 10^6$
First Modern Houses	S1	822.26±23.17	166.80±4.74	Second Modern Houses	L1	435.22±77.80	88.29±15.91
	S2	766.02±53.26	155.39±10.89		L2	346.98±52.09	70.39±10.65
	S3	647.65±159.94	131.38±32.70		L3	290.43±92.76	58.92±18.96
	S4	651.59±96.20	132.18±19.67		L4	355.55±124.59	72.12±25.47
	S5	701.88±61.27	142.38±12.52		L5	660.54±35.57	133.99±7.27
	S6	738.26±47.49	149.76±9.71		L6	469.49±63.60	95.24±13.00
	S7	847.02±42.20	171.82±8.63		L7	453.21±62.74	91.94±12.83
	S8	517.57±71.98	104.99±14.72		L8	459.21±29.13	93.15±5.95
	S9	524.83±87.84	106.46±17.96		L9	804.48±46.62	163.19±9.53
	S10	690.84±107.35	140.14±21.95		L10	685.39±94.84	139.03±19.39
	S11	585.04±178.98	118.68±36.59		Average	496.05±67.97	100.63±13.90
	S12	577.19±117.49	117.09±24.02	The Old Houses	D1	141.36±20.93	28.68±4.28
	S13	679.14±156.63	137.77±32.02		D2	221.90±53.25	45.01±10.89
	S14	708.61±109.54	143.75±22.39		D3	197.91±32.09	40.15±6.56
	S15	612.49±118.71	124.25±24.27		D4	187.63±12.83	38.06±2.62
	S16	516.89±159.66	104.85±32.64		D5	215.90±23.02	43.80±4.71
	S17	398.24±112.54	80.78±23.01		D6	170.49±15.81	34.58±3.23
	S18	391.58±156.19	79.43±31.93		D7	157.64±22.97	31.98±4.70
	S19	517.95±211.95	105.07±43.33		D8	154.21±13.07	31.28±2.67
	S20	679.82±177.59	137.91±36.30		D9	214.18±28.49	43.45±5.83
	Average	628.74±112.50	127.54±23.00		D10	231.32±7.31	46.92±1.49
					Average	189.25±22.98	38.39±4.70

Figure 5 shows the correlation between the exhalation rate of radon and the radon concentration, where the relationship was linear with a correlation coefficient equal to one. This indicates a strong correlation between the radon concentration values and the exhaled rate. The mathematical relationship between each of the exhalation rates and the radon gas concentration indicates that all values cut the axes at points very close to the origin.

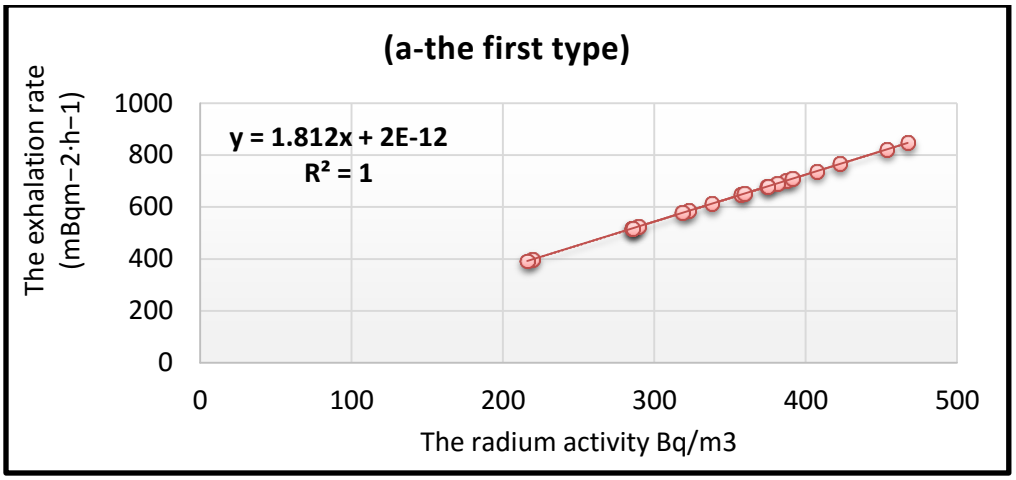

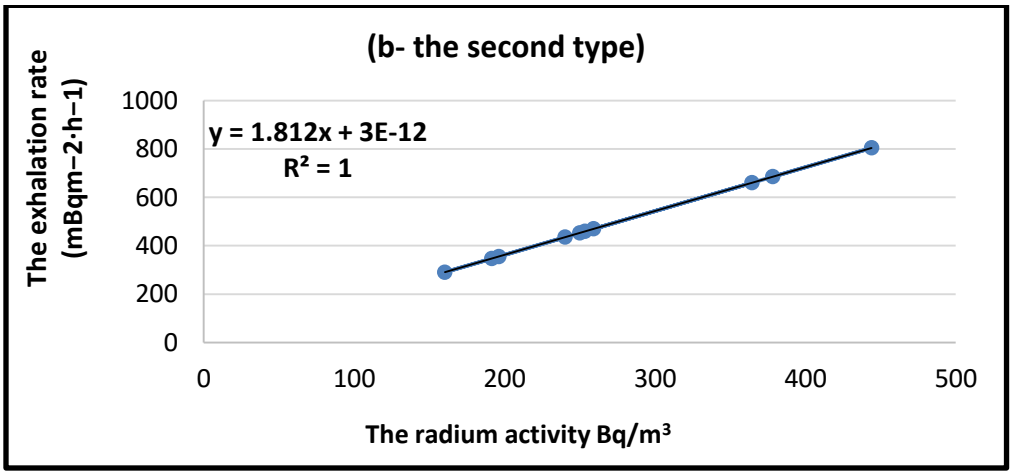

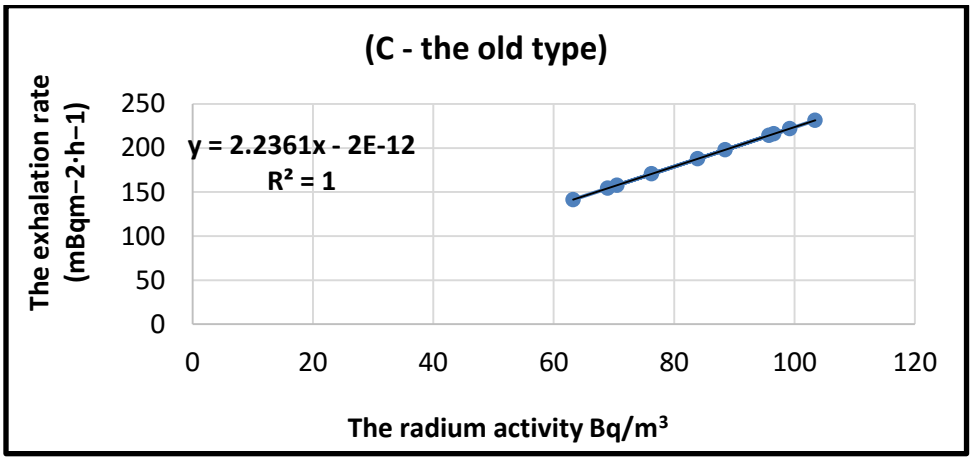

Figure 5a,b,c: The Correlation between Area Exhalation Rate and Radon Concentration of indoor air for different houses.

The functions (y = 1.812x + 2E-12, y = 1.812x + 3E-12, y = 2.2361x - 2E-12) are neutral functions, that is, each value of the exhalation rate has a single value of the concentration values of radon gas, and one of its characteristics is that it is linear, and the correlation between the values of x and y is very strong, and this was confirmed by the value of the correlation coefficient R^2. The mathematical equation confirms the strong correlation between the exhalation rates and the concentration of radon gas.

4- CONCLUSION

The method of ventilation of buildings and air conditioning systems contributes to controlling indoor radon levels. From the results, the emission of radon gas increases with the increase in air conditioning systems and the lack of ventilation, and it decreases significantly with the absence of air conditioning and the increase in ventilation systems inside homes. The secondary effective dose is affected by indoor ventilation. The results showed that the lowest value of exhalation rate was in the old houses, which have high ventilation and lack of air conditioning. Lung cancer cases per year per million people (CPPP) values were within the recommended limits for ICRP. The exhalation rates show an agreement with the radon gas concentration values, with a correlation coefficient equal to the unit. From the results, ventilation has a close relationship with the values of radiation doses of radon gas inside homes. Therefore, attention must be paid to the importance of ventilation with accommodation to reduce the potential radiation doses from the accommodation.

According to the previous conclusion, it is recommended to increase ventilation inside the house and not to rely on air conditioners only, and buildings should be designed with sufficient openings for ventilation.

References

1) Entesar H. E., Doaa S. H. and Zainab Y., (2021) “Evaluation of radioactive exposure in soil”, International Journal of Radiation Research, 19**,** 719-727.
2) Entesar H. E., (2013) “Environmental Air Dosimetry in Some locations of Gazan Using Passive Track Detectors”, Journal of life sciences and Technologies, 1, 75-78.
3) Zarrag AF., Entesar H. E., and Hanan E. (2012) “Monitoring of Radon Concentrations in Jazan beach soil”, Journal of Applied Sciences Research, 8, 823-827.
4) Entesar H. E., (2018)" Direct measurement of the radioactive radon gas activity in water in Saudi Arabia" AIP Conference Proceedings 1976 (1), 020019.
5) Teng T., Sun L.F., (1986) “Research on ground water radon as aid phase precursor to earthquake”, Journal of Geophysics, Research, 91, 305-311.
6) King, C. Y., (1978) “Radon emanation on san Adreas Fault”, Nature, 271, 516-519.
7) UNSCEAR, (2008) United nations scientific committee on the effects of atomic radiation volume (I): "effects of ionizing radiation", In: UNSCEAR 2006 Report to the General Assembly, with scientific Annexes.
8) ICRP (2007) International Commission on Radiation units, Publication 103 Recommendations of the International Commission on Radiological Protection Annals of the ICRP 37/2-4.
9) Ibrahim H. S., Ibrahim M. A. and Samhan F. A., (2009) “Distribution and bacterial bioavailability of selected metals in sediments of Ismailia Canal, Egypt”, Journal Hazard Material, 168, 1012-1016.

10) Karim, M.S., Abdullah, M.H. and Abass, W.H. (2012) "Measurement of Radon Gas Concentration in Cement Samples by Using Nuclear Track Detector (CR-39)", Diyala Journal for Pure Sciences, 8, 2222-8373.
11) Singh, A.K., Ashavani, K. and Rajendra, P., (2006) "Distribution of Radon Levels in Udaipur", Asian Journal of Chemistry, **18**, 3408-3411.
12) Nuccetelli C., Leonardi F., Trevisi R. (2020) "Building material radon emanation and exhalation rate: Need of a shared measurement protocol from the european database analysis", Journal of Environmental Radioactivity, 225, 106438.
13) Ahmad C. S., Seongjin P., Muttaqin M. N., Sang H. L., (2020) "Indoor radon and thoron from building materials: Analysis of humidity, air exchange rate, and dose assessment", Nuclear Engineering and Technology, 52, 2370- 2378
14) Andreea C. T., Aurora S., and Dorin T., (2022) "Determination of the radon concentration in homes depending on the insulation used for the floor", MATEC Web of Conferences, 354, 00074.
15) María L., Francisco H., Juan P. D., Pedro A. S., (2022)"Determination of the indoor radon concentration in schools of Tenerife (Canary Islands): a comparative study, Air Quality", Atmosphere & Health, 15,825-835.
16) H.E. Wichmann, J. Heinrich, M. Gerken, M. Kreuzer, J. Wellmann, G. Keller,L. Kreienbrock, (2002) "Domestic radon and lung cancerdcurrent status including new evidence from Germany", Int. Congr. Ser. 1225, 247e252,
17) Ahmad Ciptadi Syuryavin, Seongjin Park, Muttaqin Margo Nirwono, b,Sang Hoon Lee, (2020) "Indoor radon and thoron from building materials: Analysis of humidity, air exchange rate, and dose assessment", Nuclear Engineering and Technology, 52 2370- 2378
18) Andreea Cristina Tataru, Aurora Stanci, and Dorin Tataru (2022)" Determination of the radon concentration in homes depending on the insulation used for the floor", MATEC Web of Conferences, 354, 00074.
19) Entesar H. E., Doaa H. Shabaan, (2022) "Investigation of the radioactive rates of radon gas and its progeny in new buildings", Journal of Radioanalytical and Nuclear Chemistry, 331, 2779–2784.
20) Lee E M, Menezes G and Finch EC (2004) "Assessment of Natural Radioactivity in Irish Building Materials", International Congress of IRPA, **23,** 28.05.
21) Entesar H. E., Soliman H. A. and Abo-Elmagda M. (2019) "Measurement of radon levels in water and the associated health hazards in Jazan", Saudi Arabia, Journal of radiation research and applied sciences, **12,** 31-36.
22) Tayseer I. Al-Nagaar and Doaa H. S., (2021) "Study the Optical Characteristics of CR-39 Nuclear Track Detector Using Ultraviolet Irradiation", Arab Journal of Nuclear Science and Application, 54, 85-88.

23) Abdalsattar K. H., Laith A. N., (2015) "Radium and Uranium Concentrations Measurements in Vegetables Samples of Iraq", Detection, 3, 21-28.

24) ICRP (2009) "International Commission on Radiological Protection Statement on Radon", ICRP, Ref, 00/902/09.

25) Ismail A.H., Jaafar M.S., (2010) "Indoor Radon concentration and its Health Risks in Selected Locations in Iraqi Kurdistan using CR-39 NTDs Bioinformatics and Biomedical Engineering (iCBBE) ", ldo 4th international Conference in Cheng du, 18-20.

26) H.E. Wichmann, J. Heinrich, M. Gerken, M. Kreuzer, J. Wellmann, G. Keller,L. Kreienbrock, (2002) "Domestic radon and lung cancerdcurrent status including new evidence from Germany", Int. Congr. Ser. 1225, 247e252,

انبعاثات غاز الرادون من منازل مختلفة بمنطقة جازان

انتصار حنفي العربي و امال عزازي
قسم الفيزياء - كلية العلوم - جامعة جازان - المملكة العربية السعودية

الملخص

تساهم أنظمة التهوية والتكييف المركزي في زيادة كبيرة في مستويات غاز الرادون الداخلي. لذلك من الضروري دراسة وتحليل المعلمات التي تؤثر على معدلات انبعاث غاز الرادون وزيادة جرعة الإشعاع داخل المنازل. يهتم العمل الحالي بقياس معدلات انبعاث غاز الرادون بواسطة كاشف المسار النووي CR-39 في المنازل ذات أنظمة التهوية والتكييف المختلفة في منطقة جازان. أظهرت النتائج أن متوسط تركيز غاز الرادون في المنازل ذات أنظمة التهوية المختلفة تراوح بين 346.98 ± 62.09 to 84.63 ± 10.35 Bq/m^3. أظهرت جرعة الإشعاع التي يتعرض لها الأشخاص الذين يعيشون في المنازل تأثرها بأنظمة التكييف والتهوية داخل المنازل. كانت قيم الجرعة الفعالة السنوية أعلى بنسبة ٢٠٪ من المسموح بها دوليًا في المنازل المزودة بتكييف هواء مركزي وأعلى بنسبة ١٠٪ من المسموح به دوليًا في المنازل ذات أنظمة تكييف الهواء غير المركزية. في حين كانت قيم الجرعات التي تم قياسها في المنازل القديمة ذات التهوية الذاتية ضمن الحدود التي أوصت بها اللجنة الدولية للحماية من الإشعاع (ICRP).كما أظهرت النتائج أن جميع قيم حالات سرطان الرئة لكل مليون شخص (CPPP) كانت ضمن الحد الموصى به.

الكلمات المفتاحية: غاز الرادون ، التهوية ،تركيز غاز الرادون، الجرعة الفعالة السنوية ، معدلات الزفير ، CPPP.

Perspectives on the seroprevalence of Arbovirus infections in Saudi Arabia

Ahmed A. Abdulhaq[1]*, Majid Ahmed Darraj[2], Almonther Abdullah Hershan[3], Rym Hassani[4]

[1]Unit of medical Microbiology, College of Applied Medical Sciences, JazanUniversity, Jazan, Saudi Arabia

[2]Department of Medicine, Faculty of Medicine, Jazan University, Jazan, SaudiArabia.

[3]The University of Jeddah, College of Medicine, Department of MedicalMicrobiology and Parasitology, Jeddah, Saudi Arabia.

[4]University College of Sabya, Jazan University, Jazan, Saudi Arabia

Abstract

Worldwide, mosquitoes are the most significant arthropods vectors that causes disease. Arbovirus outbreaks are happening in various locations in KSA. The present review was done to understand pervasiveness of Arbovirus-associated risk factors and preventive measures implemented to overcome the prevalence. The PubMed/MEDLINE, Science direct, Scopus, Embase, and Google Scholar databases were searched to locate publications between 1985 and 2022 that met the criteria. Dengue fever is one of the arbovirus infections that has been identified in Saudi Arabia for more than two decades, and endemic transmission of the illness takes place during the rainy season. It is especially widespread in the western region, and Jeddah and Makkah are the most notable cities. Understanding the seasonal effect of new interventions enables decision-makers to adequately prepare for and react to future shifts in dengue risk by providing them with more information. The review concentrated on the epidemiological perspectives and possible prophylaxis. It is critical to comprehend these factors so as to educate the public. The outcome of this review article will benefit the medical community and the public by providing them with more knowledge and understanding about this disease.

Keywords: Saudi Arabia; Arboviruses; Dengue viruses; Chikungunya virus; Zika virus fever; Alkhurma haemorrhagic fever virus; Ritz valley fever virus.

Introduction

Arboviruses are RNA viruses that originate in arthropods such as mosquitos and ticks but do not appear to harm them. Arboviruses infect vertebrate hosts, causing illnesses like dengue, yellow fever, Mayaro virus, flavivirus, Chikungunya virus (CHIKV), Zika virus (ZIKV), Japanese encephalitis virus, West Nile virus (WNV), and St. Louis encephalitis (Fang et al., 2021). Globally, the frequency and magnitude of arthropod-borne virus (arbovirus) outbreaks, particularly those transmitted by Aedes mosquitoes, have increased owing to a combination of ecological, economic, and social factors. Rapid urbanization, migration, climate change, pesticide resistance, poverty, and limited access to water and sanitation are some of the factors that contribute to this problem (WHO, 2021). As a direct consequence of this, the World Health Organization (WHO) decided in October 2021 to forma committee of knowledgeable individuals who would be known as the Technical Advisory Group on Arbovirus (TAG-Arbovirus). The TAG-Arbovirus is expected to meet regularly to discuss and analyze the global impact of arboviruses and provide technical, scientific, and strategic considerations on arboviruses and the Global Arbovirus Initiative.

Arboviruses which comprise the families Flaviviridae and Togaviridae, are responsible for haemorrhagic fever, sometimes known as "bone-breaker fever" (Hakami et al., 2021; Pfeffer et al., 2006). Dengue fever cases were mostly recorded in Makkah and Jeddah in Saudi Arabia between 2013 and 2015, with relatively few cases reported in Jazan and Asir (Al Nazawi et al., 2017). Figure 1 depicts the prevalence of Arbo virus infection in Saudi Arabia. Four different types of arboviruses have been reported in Saudi Arabia (Al-Saeed et al., 2017). These four arboviruses are dengue virus (DENV), the alkhurma fever virus, the rift Valley fever virus, and the crimean-congo haemorrhagic fever virus. These four types of arboviruses possess potential for triggering serious illness and mortality.

Currently, DENV is the most common virus in Saudi Arabia, even though studies have suggested that the country was historically a DENV-free zone (Alhaeli et al., 2016). The recent DENV outbreaks in Jeddah, Makkah (Mecca) and Madinah in the western region, as well as in Jazan in the southwestern region, indicate that the virus is widely circulated and transmitted throughout the country, according to the earlier reports (Organji et al., 2017; Mohammed et al., 2018; Alhaeli et al., 2016; Hashem et al., 2018). In Saudi Arabia, Jazan Region is located inside the tropical zone and is characterized by a hot and humid environment. Mosquitoes which transmit haemorrhagic viruses such as the virus that causes dengue fever, are the predominant pests in this area. Another type of arbovirus that first appeared in the Jazan Region in the year 2000 and has since spread throughout the world, is known as the Rift Valley fever (RVF) virus.

As a result of the major climatic and geographical differences between the regions of Asir and Jazan, there are differences in the variety of mosquitoes and the number of mosquitoes that may be found in each site (Khater et al., 2013; Abdoon et al., 2003). In recent years, the highlands of the Asir region have not shown any signs of being inhabited by Aedes species. In spite of this, the endemicity of the dengue virus has only been confirmed in the Tihamah part of the Asir region (Tihmat Asir) which has climatic conditions that are analogous to those of the Jazan region (Zakham et al., 2017; Al-Azraqi et al., 2013), suggesting that Aedes species are prevalent in this region. The mosquitoes Aedes aegypti and Aedes albopictus are the primary vectors for the transmission of the most serious human viral illnesses, including dengue, chikungunya, and zika. To limit arbovirus transmission, it is necessary to manage the Aedes species using insecticides, and to provide risk maps with information on vector population to the public. The present review highlights current knowledge on the factors and underlying mechanisms that

drive arbovirus infection and transmission, as well as crucial components and pathways that have the potential of becoming targets for intervention and therapies.

METHODS

Search strategy and selection criteria

The current systematic review made use of electronic search techniques to locate articles that were published in a range of online journals. The databases of Scopus, Nature Research, Medline (PubMed), Science Direct, Ovid, Google Scholar, and POPLINE were searched for papers that were published up to 2022, for the purpose of this systematic review. The primary search terms that were utilized were Arbovirus incidence, prevalence, number of cases reported, mortality, and illness burden in Saudi Arabia. The current study used previously published research from Saudi Arabia spanning more than two decades to make an estimate of the burden of diseases caused by arboviruses. The systemic search covered publication dates from 1985 through 2022. The comprehensive literature review of articles selected is depicted in the flow chart in Figure 2.

Results and Discussion

Several hypotheses have been put up to explain the categories of arbovirus infections that have been prevalent in Saudi Arabia, and the factors involved in their prevalence. The prevalence of arbovirus is discussed below.

Dengue

Mosquitoes are the most important vectors responsible for worldwide transmission of various dreadful human diseases e.g., dengue, thereby causing morbidity and mortality in millions of people every year (WHO, 2013). In the past two decades, dengue epidemics have become increasingly prevalent and extensive. The first instance of dengue fever disease in Saudi Arabia was confirmed in 1994 when dengue serotype-2 virus (DEN-2V) was identified in virology laboratory of Dr. Soliman Fakeeh Hospital in Jeddah. This was the country's first case of dengue fever illness (Fakeeh and Zaki, 2001). Since 1994, virologically confirmed cases of dengue fever have been found in Jeddah, Saudi Arabia; these are responsible for annual outbreaks of the disease. According to extant research, dengue viruses which are considered endemic to this region, were found to be relatively common among Jeddah locals. Infection was mostly asymptomatic or only related to minor illnesses for which individuals did not seek medical attention (Jamjoom et al., 2016). Researchers from all around the world have focused their attention on mapping out the mosquito population in Saudi Arabia (Akbar et al., 2020; Ahmed et al., 2011; Al Ghamdi et al., 2008; Al Kuriji et al. 2007; Abdoon and Alshahrani 2003). The Dengue virus, also known as DENV, is now considered to be one of the most important arthropod-borne viral infections that can impact people. The causative agent is a virus with a single strand of positive-sense RNA. It is a member of the family Flaviviridae. There are four serotypes of this virus which are related to one another antigenically (Murrell et al., 2011; Lindenbach and Rice, 2003).

The DENV is structurally defined by three proteins: the core protein (C), a membrane-associated protein (M), and the envelope protein (E). The seven non-structural proteins encoded by the DENV genome are NS1, NS2a, NS2b, NS3, NS4a, NS4b, and NS5 (Idrees et al., 2012). It is possible to diagnose dengue fever based on either the primary or secondary infection in the earliest stages using the glycoprotein NS1 which is found in all dengue serotypes and in all dengue virus strains. Individuals infected with DENV present a range of symptoms ranging from light feverish condition to fatal haemorrhagic pyrexia and DENV shock. After an incubation period of five to eight days, patients usually present with typical dengue fever symptoms such as dermatitis, migraine, nausea, vomiting, cold, and swollen lymph nodes. The condition known as dengue haemorrhagic fever is characterized by

an increased permeability of blood vessels. In initial infections, circulating IgM antibodies to viral coat proteins can be identified five to six days after the onset of symptoms. When an illness has been present for one to two months, the levels of these antibodies begin to progressively decrease. In primary infections, IgG antibodies to the dengue virus can be detected approximately 14 days after the beginning of the infection. However, in secondary infections, these antibodies may be found as early as on day 2. Although IgM may slowly decrease, IgG remains and can be found in high titres in secondary infections if the initial illness is severe enough. IgM antibody may reappear but gradually decreases. In this way, the patterns of dengue antibody production can be distinguished between primary and subsequentinfections by serological testing. A characteristic of acute primary DENV is that affected individuals present a larger ratio of IgM: IgG, relative to those with 2o DENV. Increased level of immunoglobulin and elevated IgM are used for distinguishing acquired or recent DENV (Changal et al., 2016).

Following the findings of a previous study, the threat of the dengue virus (DENV) and related antibodies being transferred through blood transfusions have recently emerged throughout the world. Dengue fever is a condition that is thought to be prevalent in KSA, especially in the country's western section. Thus, according to the findings of the study, thereis need for blood testing facilities especially in blood banks, to minimise the risk of spread of DENV in KSA. This can be done to enhance safety of transfused blood while minimising the spread of the disease (Ashshi et al., 2017). An earlier finding published in 2019 revealed dominance of anti-DENV IgG in some major cities of KSA, as well as identification of the pre-disposing conditions related to hospitals, populations and the environment. Subjects from 4 major cities were chosen for the study through a multi-stage stratified cluster sampling procedure. Blood samples were obtained from each participant in order to screen for anti- DENV IgG. According to the study, 26.7 % of the population was infected with dengue, with Jizan and Madinah having the highest and least percentage infections, respectively (Al- Raddadi et al., 2019).

The number of dengue fever illnesses reported to the World Health Organization has increased by more than eight folds in the last two decades, with over 4032 morbidities, mostly in the younger population, especially in 2015. However, in the last 2 years, the numbers of reported DENV patients and associated mortalities appear to have reduced,although the outbreak of COVID-19 might have negatively affected data collection in several countries (WHO, 2022). The World Health Organization previously estimated that nearly 3 billion individuals were at risk of DENV illness each year (Tang and Ooi, 2012). Dengue (DENV) is primarily transmitted to humans by infected Aedes aegypti, the most common epidemic vector. However, dengue outbreaks have also been produced by Aedes albopictus and Aedes polynesiensis (Lambrects et al., 2010; Xu et al., 2004; Gubler, 1998). It is commonly believed that the Aedes aegypti mosquito is the primary vector that used to breed in natural containers such as tree holes and bromeliads. However, today's dengue virus has become well-conditioned to citified environments: currently, it multiplies mostly in artificial devices such as pails, household vessels, trash cans, disused tires, stormwater drainage, and other structures like these, all of which make dengue a particularly insidious disease in densely-populated areas. It eats in daytime and its top bite periods are at dawn and at dusk, just prior to sunset (WHO, 2022).

Dengue virus has four different serotypes: DEN-1, DEN-2, DEN-3, and DEN-4. Moreover, DENV fever is caused by contacting any of these virus strains through a bite from a female Aedes aegypti mosquito. It is most widespread in tropical and subtropical areas, especially in impoverished urban, suburban, and rural settings. According to a retrospective serological investigation, the first reported

DENV infection in Africa and the world happened in Durban, SA in 1927. In the following years, DENV cases were diagnosed in Nigeria

(DENV-1 and 2), Mozambique (DENV3), the Sudan (DENV-2 and 3), and Senegal (DENV- 4) (Konongoi, et al., 2016). Dengue virus serotype 2, also known as DENV-2, originated from KSA in the year 1994. Indeed, DENV-2 was the cause of a large epidemic in Jeddah, Kingdom of Saudi Arabia, where 289 confirmed cases were reported. Since that time, instances of dengue have been reported in a variety of locations around the Kingdom of Saudi Arabia (Sami et al., 2021; Fakeeh and Zaki, 2001).

According to the results of past studies, four cities located in western area of KSA, and the Southern city of Jazan in Saudi Arabia, are all considered to be endemic for dengue fever. The western region of Saudi Arabia has tested positive for all 4 types of DENV. According to a theory that has been put forward, pilgrims may have performed a crucial and possibly peculiar function in the introduction of the 2 serotypes of DENV into Saudi Arabia during Hajj and Umrah seasons. Both of these events take place in Saudi Arabia. However, there is scarcity of DENV-3 data in Saudi Arabia (Hashem et al., 2018). The situation in Jeddah appears to be complicated, with various reasons contributing to the high incidence of dengue fever in the city. These include warm climatic conditions, fast urbanization, presence of many non-Saudi residents, and migration. As a consequence of these factors, aspects of theurban ecology such as high housing densities, particularly in less affluent areas, have exacerbated the already existing inequities amongst neighbourhoods in terms of exposure to risk factors and the consequences of dengue outbreaks (Alkhaldy and Barnett, 2021). Dengue seroprevalence was 26.7 %, with Jizan and Madinah having the highest and the least values, respectively. Dengue virus seropositivity was found in one out of every four people in Western Saudi Arabia. As a result, it is critical that key Government organizations in Saudi Arabia and Jeddah consider the importance of local neighbourhood variables while developing and implementing dengue control plans. Recently, the Dengue virus, also known as DENV, and its antibodies, which can be passed on through blood transfusions, have

emerged as a global health concern. These findings highlight the need for implementing mandatory testing for DENV at various departments involved in blood banking throughout Saudi Arabia so as to improve the safety of recipients of transfused blood and restrict the spread of DENV (Ashshi et al., 2017). The most effective strategy for preventing the disease is to avoid being bitten by infected mosquitoes. This is important, especially for people who live in, or plan to visit a tropical area. The FDA has approved a dengue immunisation drug Dengvaxia for prevention of the disease in individuals within the age range of 9 - 16 years who had a history of dengue fever attack (CDC, 2021).

In an earlier study, researchers attempted to estimate areas of high dengue risk using a mixture of characteristics bordering on the surroundings and economic status (Khormi et al., 2012). These variables included populations of clinically confirmed patients, population of mosquitoes, the demographics of districts, availability of water, the standard of the neighborhood, and the spatiotemporal risk of dengue fever on the basis of number of cases of dengue fever per week. The risk of dengue fever was significantly affected by rising average population density which was a key contributor (Alkhaldy and Barnett, 2021).

According to an earlier study, there was a higher chance of dengue in KSA men than in non-Saudi males in 2018. Interestingly, there was a higher risk of contracting dengue fever in 2019 amongst non-KSA men than amongst Saudi males. In three years of investigation, there was much higher chance of infection amongst KSA females than amongst non-KSA females (Melebari et al., 2021). The study

reported that people in the age range of 25 to 44 years were the most likely persons to be affected by dengue. This age group was responsible for almost half of all dengue cases reported each year. Men had higher chance of developing dengue fever than women.

According to the findings of another study carried out in 2013, there was a rise in the prevalence of dengue fever during the first half of that year. Males between the ages of 15

and 29 years were shown to have a significantly increased risk of infection. Two additional studies, one carried out in 2006 and the other in 2008, came to the same conclusion and identified the same two factors. The areas with the highest infection rates were the central- north and southern regions (Alzahrani et al., 2013; Khan et al., 2008; Ayyub et al., 2006). A study on hospitalised dengue fever patients in Makkah was published by Khan et al. (2008). In this study, a seroprevalence of 56.25 percent was found amongst the 160 patients who were suspected of having dengue fever. Malaise, musculoskeletal pain, and stomach pain were the most prevalent symptoms presented by those who had dengue fever. In the study that was carried out between 2006 and 2010, rashes, haemorrhagic symptoms, and tests that came back positive for tourniquet use were quite uncommon. In each of the three investigations, the most notable haematological abnormalities were decreased thrombocytopenia and leukopenia. On the other hand, a previous study demonstrated higher levels of serum alanine aminotransferase (ALT) and aspartate aminotransferase (AST) in most patients (Ahmed, 2010; Khan et al., 2008; Ayyub et al., 2006). Finally, owing of the rising circulation of several dengue virus serotypes and a high prevalence of dengue fever with a higher risk of severity in Saudi Arabia, it is vital to conduct effective mosquito monitoring in Saudi Arabia to identify danger zones and prevent the spread of dengue infection by promoting appropriate individual behaviours and environmental management techniques for limiting the development of dengue infection. To aid in the prevention of dengue fever, it is recommended that comprehensive and effective health education campaigns concerning dengue fever risk factors be adopted. On the other hand, the paucity of large epidemiological studies makes it difficult to generalize the conclusions from such studies. The spread of dengue fever to new cities within Saudi Arabia should be the primary focus of any future research in this country. There is a requirement for more investigations on the epidemiology of dengue fever based using bigger sample size to obtain an accurateestimate of the exact population of patients with dengue fever in KSA.

Chikungunya

The Kingdom of Saudi Arabia (KSA) is home to a significant number of the mosquitoes that spread parasitic and arboviral diseases around the world. However, little research has been conducted on their regional range and larval habitat characteristics. There is a significant difference in mosquito variety and abundance between the Asir and Jazan regions because of the significant climatic and geographical differences between the two locations (Khater et al., 2013). The Chikungunya virus (CHIKV), an RNA virus, is a member of the genus alphavirus, and family Togaviridae. The CHIKV is transmitted by the Aedes aegypti and Aedes albopictus mosquitoes which are the primary vectors of the virus. Fever and joint discomfort are the most prevalent signs, but patients also have muscular pain, joint oedema, headache, dermatitis and tiredness (WHO, 2020). Since there are no existing immunization drugs for dengue, the therapy is focused on relieving the disease symptoms naturally. The CHIKV is believed to have started in Africa and spread to Asian countries via trade through shipping. It was formerly connected with periodic epidemics, primarily in Africa and Asia, until 2004. However, the virus resurfaced in 2004 and spread over the world, impacting millions of people (Ignacio et al., 2022). The CHIKV virus was shown to beendemic in several nations

in Africa, as well as in South-East Asia. More specifically, the virus has been found to be endemic in Indonesia, Thailand, Vietnam, Myanmar, Cameroon, the Philippines, and Malaysia (Paquet et al., 2006). An earlier study found that the endemic state of dengue fever in Jeddah, as well as the underlying fluctuating degrees of influenza, make it difficult to obtain an accurate diagnosis of CHIKV, more so in endemic cases. Due to

the autochthonous presence of dengue fever in Jeddah, it is difficult to make an accurate clinical diagnosis of CHIKV infection. Furthermore, a CHIKV outbreak has been reported in nearby Yemen, with 1,000 patients and 75 mortalities as at December, 2010. Due to assumed concomitant presence of DENV serotypes, the monitoring of viral prevalence in Jeddah should be a focus of concern: there is need to carry out heightened monitoring and thorough epidemiological and laboratory surveillance (Hussain et al., 2013).

According to recent reports, even though CHIKV was for long thought to be a disease confined to Asia and Africa, it has lately been identified throughout the entire Western Hemisphere, including a significant portion of South and Central America as well as the Caribbean. The epidemiology of CHIKV in the Middle East and North Africa (MENA) is still not well understood, despite recent reports of outbreaks and new transmission in the Arabian Peninsula (Humphrey et al., 2017). According to Hakami et al. (2021), CHIKV is a viral infection that is frequently ignored in Saudi Arabia. Therefore, the focus of study in the future should be on conducting an exhaustive investigation of this viral infection and the vectors that spread it. In an earlier study, Hakami et al. (2021) reported that forty specimens were obtained from two hospitals in south of Saudi Arabia between the months of December 2019 and February 2020. They were examined for the presence of chikungunya virus IgG antibodies as well as viral RNA. The findings showed absence of DENV RNA in all the specimens, implying that the virus was removed quickly in patients. According to a recent report, chikungunya vaccine candidates are being developed at the study level using various technologies (Lutmer, 2022). The monovalent, single-dose, attenuated live chikungunya vaccine candidate VLA1553 from Valneva SE is the only chikungunya vaccine candidate now in clinical studies (Carlson and Lutmer, 2002). According to a recent study (Hakami et al., 2021), the southern region of Saudi Arabia is home to an underdiagnosed case of chikungunya, which is a viral infection. As a consequence of this, future work has to center

on determining the endemicity of arboviruses within the vector by doing fieldwork collection of Aedes species within specific regions.

Zika virus fever

The Zika virus (ZIKV) sickness is caused by a teratogenic flavivirus that is mostly transmitted by Aedes mosquitos which bite daily. The most common symptoms are malaise or headache, along with fever, rash, conjunctivitis, and soreness in the muscles and joints. An infection with the Zika virus that occurs during pregnancy can lead to microcephaly and other congenital defects in the developing fetus as well as in the infant. Infection with Zika virus during pregnancy can lead pregnancy complications such as preterm birth, stillbirth, and fetal loss (WHO, 2018).

These mosquitos often deposit their eggs in or near stagnant water containers such as buckets, bowls, animal dishes, flowerpots, and vases. They enjoy biting people, and they dwell near people both indoors and outdoors. The ZIKV spread by mosquitoes was initially identified in 1947 in monkeys in Uganda. In 1952, it was identified for the first time in human patients in Uganda and Tanzania, both of which are still home to the virus today. There have been reports of ZIKV illness epidemics in several parts of the world, including Africa, the Americas, Asia, and the Pacific. In the decades spanning from the 1960s to the 1980s, occasional cases of human infections were found across the

continents of Africa and Asia. Majority of these cases were accompanied with moderate symptoms (WHO, 2018). Most infections are asymptomatic, or cause minor sicknesses such as low fever, rash on the skin, conjunctivitis, muscle and joint discomfort, malaise, or headache. Infection with the ZIKV during pregnancy may result in microcephaly and other congenital deformities in

babies; these are referred to as congenital Zika syndromes. A pregnant mother who is infected with ZIKV can pass it on to her foetus during the pregnancy or shortly after birth. Indeed, breast milk from infected mothers has been shown to contain ZIKV, and breast-fed babies have been found to have possible ZIKV infections. However, ZIKV transmission through breast milk has not yet been established. In addition, not much is known about the long-term effects of ZIKV infection after delivery on young children who are infected with the virus. Current evidence suggests that the benefits of breastfeeding outweigh the risk of ZIKV transmission through breast milk. Consequently, the CDC continues to encourage mothers to breastfeed, even if they have been infected with Zika or have lived in, or travelled to a Zika-affected area. This is the case even though the risk of ZIKV transmission through breast milk has been shown to outweigh the benefits of breastfeeding (CDC, 2019). Following the announcement that Brazil was experiencing an outbreak of ZIKV in May of 2015, ZIKV was declared a global health emergency. Recently, the pathogen has been responsible for devastating epidemics worldwide. The Saudi health authority has attempted to avert any outbreaks (Alshammari et al., 2018). In Saudi Arabia, there have been no recorded instances, most likely because there was no active surveillance for ZIKV at any time. The presence of the vector throughout the country, primarily in the western and southern regions, poses a risk. Residents of the Najran region are at danger of contracting ZIKV because oftheir frequent travel to Mecca for the Hajj and Umrah, and to other countries where they may meet pilgrims from ZIKV-endemic areas (Alayed et al., 2018). According to a recent survey, most participants wanted to learn more about ZIKV, emerging diseases, and travel epidemiology. Finally, a survey has revealed that medical students exhibited minimal awareness of ZIKV but a positive attitude toward learning more about it (Ibrahim et al., 2018). Thus, it is necessary to conduct ZIKV teaching initiatives and mount courses on epidemiology of emerging diseases. In a previous study, the seroprevalence of the zika virus

in asymptomatic pregnant mothers and their newborns infants in the Najran region was investigated. Furthermore, due to the presence of the vector organism in the country, the presence of presumptive positive serology, and the continued danger of ZIKV entrance via a frequent influx of travellers from endemic areas, it seems likely that the country is already infected with the virus (Alayed et al., 2018).

According to a recent study, because of the annual Hajj pilgrimage, the city of Makkah in the Kingdom of Saudi Arabia is home to a significant number of the world's mosquito vectors of parasitic and arboviral disease. As a direct consequence of this, there is a possibility that vector-borne viruses such as the re-emerging ZIKV will be exported and spread around the world (Yezli et al., 2021). The goal of the research by Yezli et al. (2021) was to determine whether or not flaviviruses (like ZIKV) were present in mosquitoes in Makkah before, during, and after Hajj in 2016. During and after the Hajj in 2016, mosquitoes (both adults and larvae) were collected from 15 different places across the city of Makkah, and morphological keys were utilized to determine the species of each mosquito. Yezli et al., (2021) reported that not a single mosquito tested positive for a pathogenic flavivirus such as ZIKV. Rather, all the mosquitoes were infected with a novel flavivirus that is found only in insects. The findings of the study revealed that there were no dangerous flaviviruses circulating in Makkah city prior to, or after the Hajj in 2016, and there was also no

indication that ZIKV was transmitted via the pilgrimage. The authors, based on their findings, suggested that increased surveillance of vector-carrying infections is crucial in the Kingdom of Saudi Arabia (KSA), particularly during the annual Hajj, to avoid viral infections that have the potential to cause epidemics and pandemics.

Alkhurma haemorrhagic fever

The Alkhurma haemorrhagic pyrexia virus (AHFV) causes Alkhurma haemorrhagic fever (AHF) which is transmitted to humans via a bite from an infected tick. Flaviviruses are members of the family Flaviviridae (CDC, 2014). Instances of AHFV, a tick-borne zoonotic disease outbreak, have been documented, with sporadic incidence and prevalence among shepherds, livestock owners, butchers, and even occasionally pilgrims who slaughter sacrificial animals. This disease is transmitted by ticks. It is possible to contract the disease by coming into touch with infected animals or tissues such as those of sheep, goats, and camels (Memish et al., 2014). In the year 1994, the AHF virus was found for the first time in the body of an individual who had succumbed to haemorrhagic fever following the slaughter of an infected sheep (Alzahrani et al., 2010). Additional cases of AHF have been found since then, with death rates reaching as high as 25 percent. Between 2006 and 2009, a disease screening amongst Najran households in KSA indicated the presence of AHF (Alzahrani et al., 2010). Infections with AHFV were found in two Italian tourists after they visited Egypt, as reported in an earlier study, which suggested that the virus may have a larger geographic distribution (Carletti et al., 2010). Although researchers were working to characterize the complete geographic spread and severity of AHFV infection, the data from the earlier study imply a greater range of endemicity than was previously documented. By way of illustration, most seropositive individuals originated from Tabouk and Eastern directorates (Carletti et al., 2010).

Epidemiological studies have shown that AHFV infections can be traced back to either direct or indirect contact with infected blood and/or organs of slaughtered animals, as well as the ingestion of raw milk that was contaminated with the virus. Another factor thathas been connected to the spread of the AHFV is the consumption of milk that has not been pasteurized. Hypotheses on the transmission of infection through the bites from arthropods such as those transmitted by Hyalomma spp. ticks and migrating birds, as well as through the faeces of tiny and/or bigger mammals, are currently being researched on (Tambo et al., 2018; Madani, 2005). According to the statistical yearbook (1437 H) published by the Saudi Ministry of Health in 2016, there were a total of 38 newly discovered infections in Makkah and Najran (Saudi Ministry of Health, 1437). Since then, occasional incidents were seen elsewhere, e.g., in new southern districts as well as in other parts of Saudi Arabia (Madani and Abuelzein, 2021; Memish et al., 2014). According to Madani and Abuelzein (2021), for preventive measures to be effective, an interdisciplinary approach is required. This approach should include representatives from the human and veterinary health sectors, the municipality responsible for slaughterhouses, the ministry of agriculture responsible for farms and farm- related measures, the vector control sector, as well as representatives from academic and research institutions who conduct research related to viruses. Researchers should focus on determining the involvement of arthropods as virus carriers, involvement of animals as virus vectors, identification of natural virus reservoirs, and determination of seroprevalence of AHFV immunoglobulins in man and foreign livestock, as well as the development of a safe and effective vaccine against AHFV.

Ritz valley fever

Rift Valley fever (RVF) is a viral zoonosis that primarily affects animals, but it also infects humans. Rift Valley fever can be transmitted from animals to humans. Insects thatfeed on blood, such as

mosquitoes, are responsible for its spread. Previous research had shown that a low level of circulating virus would indicate a modest new RVF outbreak. In addition, the study suggests that over long inter-epidemic periods, maintenance of the virus occurs in vectors and most probably in buffaloes within a cryptic cycle. This is the stage at which random, minor, and local epidemics may occur (Mroz et al., 2017). An earlier study found evidence that RVFV is circulating in Cameroon's livestock population, with prevalence rates that vary greatly across the country. Even in areas with low IgM seroprevalence rates, it is possible for RVF outbreaks to take place without anyone noticing (Sado et al., 2020). According to a cross-sectional study conducted in Tanzania, RVFV is likely spreading endemically throughout the area. The presence of livestock, lush vegetation, and temperate weather favor mosquito reproduction in the vector and appear to play significant roles in the spread and circulation of viruses. The environmental risk-factors that were discovered may help to pinpoint more precisely the regions at risk for RVFV endemicity (Heinrich et al., 2012).

In humans, the disease can manifest as anything from a minor flu-like illness to a life- threatening haemorrhagic fever. On September 10, 2000, cases of human haemorrhagic fever and the accompanying mortality of animals were brought to the attention of MOH of the KSA from the southern border of Saudi Arabia and Yemen. These cases were subsequently reported to the Ministry of Health of Yemen. On September 15, 2000, the Centres for Disease Control and Prevention announced that the diagnosis of RVF had been established in each of the four serum samples that had been sent in from Saudi Arabia. Polymerase chain reaction, ELISA, virus isolation, and immunohistochemistry were some of the tests that were carried out. ELISA was used to identify antigens and determine IgM levels. This report provides a summary of the preliminary findings of a collaborative epidemiologic investigation into the first confirmed occurrence of RVF outside of Africa. The investigation was carried out in conjunction with the Centres for Disease Control and Prevention.

Clinical identification of suspicious herds and determination of RVF viral immunoglobulin M (IgM) antibodies were the two methods that were used in the investigation of RVF in sheep and goats in Jazan, Saudi Arabia. In order to quantify the level of herd immunity, antibodies against immunoglobulin G (IgG) were analyzed. Rift Valley fever was discovered in six out of the eight areas that were investigated during this survey. The research came to the conclusion that RVF management programs need to be maintained in order to stop the recurrence of outbreaks in the area and the likely spread of infection elsewhere in KSA (Elfadil et al., 2006). The serological predominance of IgG against the RVF virus was examined in 22 main areas across 5 Saudi Arabian provinces where RVFV immunization was not implemented, according to a report (Al-Afaleq et al., 2012). The research did not include the southwestern region which witnessed severe outbreak of RVF in 2000, and ruminant immunization was done annually. An earlier study compared the seroprevalence of RVF among infants born after the Saudi Arabian outbreak of 2000-2001 with that of teenagers born before the outbreak. According to the study, despite the recent reports of low virus activity in animals, no clinically obvious RVF infections or outbreaks in humans have been confirmed, demonstrating that the management methods of Ministry of Agriculture and Ministry of Health were effective (Al Azraqi et al., 2013).

Conclusion

The findings of this extensive study indicate that there is a significant level DENV in Saudi Arabia, as well as enhanced chance of severe illness due to increasing circulation of a wide variety of dengue virus serotypes. In addition, the risk of severe disease has increased because of the increased circulation of dengue virus serotypes. This analysis has led to the

conclusion that there is relatively high level of dengue fever in KSA. It is crucial to conduct comprehensive mosquito surveillance to locate dengue infection hotspots and restrict their spread. This can be achieved by promoting individual behaviors and environmental management methods that limit the spread of the dengue virus. It is strongly suggested that comprehensive and successful health education campaigns regarding risk factors for dengue fever be implemented to aid in the prevention of dengue fever. On the other hand, the insufficiency of large epidemiological investigations makes it challenging to generalize the findings of this type of study. The further spread of dengue fever to cities inside the bordersof KSA should be primary focus of any future research conducted in that country. To provide

an accurate assessment of the level of dengue fever in KSA, more extensive epidemiological studies are required. In Saudi Arabia, chikungunya is an under-appreciated viral disease. The focus of future research should be on a thorough examination of this viral illness and its vectors. In Saudi Arabia, a new zoonotic Alkhurma haemorrhagic fever has been reported. In a large population, researchers should determine the involvement of arthropod virus carriers, the involvement of animals as virus vectors, and natural virus reservoirs. Ritz valley fever outbreaks in Saudi Arabia were well-controlled.

Conflict of Interest: The author declares that there is no conflict of interest either financially or non-financially.

Acknowledgement: The author express sincere thanks to…..

References

Ahmed, M.M., 2010. Clinical profile of dengue fever infection in King Abdul Aziz University Hospital Saudi Arabia. J. Infect. Dev. Countries, 4, 503-510

Alkhaldy, I., Barnett, R., 2021. Explaining neighbourhood variations in the incidence of dengue fever in Jeddah City, Saudi Arabia. Int J Environ Res Public Health., 18(24), 13220. https://doi.org/0.3390/ijerph182413220

Alzahrani, A.G., Al Mazroa, M.A., Alrabeah, A.M., Ibrahim, A.M., Mokdad, A.H., Memish, Z.A., 2013. Geographical distribution and spatio-temporal patterns of dengue cases in Jeddah Governorate from 2006–2008. Trans. R. Soc. Trop. Med. Hyg., 107,23-29. https://doi.org/10.1093/trstmh/trs011

Ayyub, M., Khazindar, A.M., Lubbad, E.H., Barlas, S., AlfiA, Y., Al-Ukayli, S., 2006. Characteristics of dengue fever in a large public hospital, Jeddah, Saudi Arabia. J. Ayub Med.Coll. Abbottabad, 18, 9-13.

Abdoon, A.M.M.O., Alsharani A.M, 2003. Prevalence and distribution of anopheline mosquitoes in malaria endemic areas of Asir region, Saudi Arabia. East Mediterr Health J., 9(3), 240-247.

Akbar, N.A., Assiri, A.M., Shabouni, O.I., Alwafi, O.M., Al-Raddadi, R., H., Alzahrani, M., Azhar, E.I., Amir, A., Aljiffri, A.M., Althaqafi, A.O. T., 2020. The economic burden of dengue fever in the Kingdom of Saudi Arabia. PLoS Negl. Trop.Dis.,14(11),e0008847. https://doi.org/10.1371/journal.pntd.0008847

Al Azraqi, T.A., El Mekki, A.A., Mahfouz, A.A., 2013. Rift Valley fever among children andadolescents in southwestern Saudi Arabia. J. Infect. Public Health, 6(3), 230-235. https://doi.org/10.1016/j.jiph.2012.11.011

Al Nazawi, A.M., Aqili, J., Alzahrani, M., McCall, P.J., Weetman, D., 2017. Combined target site (kdr) mutations play a primary role in highly pyrethroid resistant phenotypes of Aedes aegypti from Saudi Arabia. Parasites Vectors 10, 161. https://doi.org/10.1186/s13071- 017-2096-6

Al-Afaleq, A.I., Hussein, M.F., Al-Naeem, A.A., Housawi, F., Kabati, A.G., 2012. Seroepidemiological study of Rift Valley fever (RVF) in animals in Saudi Arabia. Trop. Anim Health Prod., 44(7), 1535-1539. https://doi.org/10.1007/s11250-012-0100-x

Alahmad, A., Sallam, M.F., Khuriji, M.A., Kheir, S.M., Azari-Hamidian, S., 2011. Checklist and Pictorial Key to Fourth-Instar Larvae of Mosquitoes (Diptera: Culicidae) of Saudi Arabia. J. Med. Entomol., 48 (4), 717-737. https://doi.org/10.1603/me10146

Alayed, M.S., Qureshi, M.A., Ahmed, S., Alqahtani, A.S., Al-qahtani, A.M., Alshaybari, K., Alshahrani, M., Ahmed, M. A., 2018. Seroprevalence and molecular study of Zika virus among asymptomatic pregnant mothers and their newborns in the Najran region of southwest Saudi Arabia. Ann Saudi Med., 38(6): 408-412. https://doi.org/10.5144/0256-4947.2018.408

Al-Azraqi, T.A., El Mekki, A.A., Mahfouz, A.A., 2012. Rift Valley Fever in Southwestern Saudi Arabia: a sero-epidemiological study seven years after the outbreak of 2000–2001. Acta Trop., 123, 111–116. https://doi.org/10.1016/j.actatropica.2012.04.007

Al-Azraqi, T.A., El Mekki, A.A., Mahfouz, A.A., 2013. Seroprevalence of dengue virus infection in Aseer and Jizan regions, Southwestern Saudi Arabia. Trans. R. Soc. Trop. Med. Hyg. 107, 368–371. https://doi.org/10.1093/trstmh/trt022

Al-Ghamdi, K., Alikhan, M., Mahayoub, J., Afifi, Z.I., 2008. Studies on identification and population dynamics of Anopheline mosquito from Jeddah, Saudi Arabia. Biosci. Biotech. Res. Commun 1, 19-24. https://doi.org/10.1016/j.jiph.2015.05.006

Alhaeli A., Bahkali S., Ali A., Househ M. S., El-Metwally A. A., 2016. The epidemiology of dengue fever in Saudi Arabia: A systematic review. J. Infect. Public Health, 9, 117–124. https://doi.org/10.1016/j.jiph.2015.05.006

Alikhan M., Al Ghamdi K., Mahyoub J. A., 2014. Aedes mosquito species in western SaudiArabia. J. Insect Sci. 14, 69. https://doi.org/10.1093/jis/14.1.69

Alkhaldy,I., Barnett, R., 2021. Explaining Neighbourhood Variations in the Incidence of Dengue Fever in Jeddah City, Saudi Arabia. Int. J. Environ. Res. Public Health 18, 13220. https://doi.org/10.3390/ijerph182413220

Al-Raddadi, R., Alwafi, O., Shabouni, O., Akbar, N., Alkhalawi, M., Ibrahim, A., Hussain, R., Alzahrani, M., Al Helal, M., Assiri, A., 2019. Seroprevalence of dengue fever and the associated sociodemographic, clinical, and environmental factors in Makkah, Madinah, Jeddah, and Jizan, Kingdom of Saudi Arabia. Acta Trop., 189,54-64. https://doi.org/10.1016/j.actatropica.2018.09.009

Al-Saeed M. S., El-Kafrawy S. A., Farraj S. A., Al-Subhi T. L., Othman N. A., Alsultan A.,Ben Helaby, H.G., Alshawdari, M.M., Hassan, A.M., Charrel, R.N., Azhar, E.I., Hashem,

A.M., 2017. Phylogenetic characterization of circulating Dengue and Alkhumra Hemorrhagic Fever viruses in western Saudi Arabia and lack of evidence of Zika virus in the region: a retrospective study 2010–2015. J. Med. Virol. 89, 1339–1346. https://doi.org/10.1002/jmv.24785

Alshabi, A., Marwan, A., Fatima, N., Madkhali, A.M., Alnagai, F., Alhazmi, A., Al- Mekhlafi, H.M., Abdulhaq, A.A., Ghailan, K.Y., Sali, A., Refaei, T., 2022. Epidemiological screening and serotyping analysis of dengue fever in the Southwestern region of Saudi Arabia. Saudi J Biol Sci., 29(1):204-210. https://doi.org/10.1016/j.sjbs.2021.08.070

Alshammari, S.A., Alamri, Y.S., Rabhan, F.S., Alabdullah, A.A., Noura, A. A., Fatma, A. A.,Amal N. A., 2018. Overview of dengue and Zika virus similarity, what can we learn from the Saudi experience with dengue fever?. Int. J. Health Sci., (Qassim), 12(1), 77-82.

Alzahrani, A.G., Al Shaiban, H.M., Al Mazroa, M.A., Al-Hayani, O., Macneil, A., Rollin, P.E., Ashshi, A.M., Alghamdi, S., El-Shemi, A.G., Almdani, S., Refaat, B., Mohamed, A.M., Ghazi, H.O., Azhar, E.I., Al-Allaf, F.A., 2017. Seroprevalence of asymptomatic dengue virus infection and its antibodies among healthy/eligible Saudi blood donors: Findings from Holy Makkah City. Virology (Auckl) 8, 1-5. https://doi.org/10.1177/1178122X17691261

Ashshi, A. M., Alghamdi, S., El-Shemi, A. G., Almdani, S., Refaat, B., Mohamed, A. M., Ghazi, H. O., Azhar, E. I., & Al-Allaf, F. A., 2017. Seroprevalence of asymptomatic dengue virus infection and its antibodies among healthy/eligible Saudi blood donors: Findings from Holy Makkah City. Virology: research and treatment, 8, 1–5. https://doi.org/10.1177/1178122X17691261

Blacksell, S.D., Jarman, R.G., Bailey, M.S., Tanganuchitcharnchai, A., Jenjaroen, K., Gibbons, R.V., Paris, D.H., Premaratna, R., de Silva, H.J., Lalloo, D.G., Day, N.P., 2011. Evaluation of six commercial point-of-care tests for diagnosis of acute dengue infections: the need for combining NS1 antigen and IgM/IgG antibody detection to achieve acceptable levels of accuracy. Clin. Vaccine Immunol. 18(12), 2095–2101. https://doi.org/10.1128/CVI.05285-11

CDC, 2014. https://www.cdc.gov/vhf/alkhurma/index.html

CDC, 2019. https://www.cdc.gov/zika/prevention/transmission-methods

Carletti, F., Castilletti, C., DiCaro, A., Capobianchi, M.R., Nisii, C., Suter, F., Marco, R., Alessandra, T., Antonio, G., Cristiana, P.T., Giuseppe, I., 2010. Alkhurma hemorrhagic fever in travelers returning from Egypt. Emerg Infect Dis., 16, 1979-1982.

Centres for Disease Control and Prevention (CDC), 2000. Outbreak of Rift Valley fever--Saudi Arabia, August-October, 2000. MMWR Morb Mortal Wkly Rep., 49(41), 940.

Changal, K. H., Raina, A. H., Raina, A., Raina, M., Bashir, R., Latief, M., Mir, T., & Changal, Q. H., 2016. Differentiating secondary from primary dengue using IgG to IgM ratio in early dengue: an observational hospital based clinico-serological study from North India. BMC infectious diseases, 16(1), 715. https://doi.org/10.1186/s12879-016-2053-6

Chikungunya outbreak in Reunion: epidemiology and surveillance, 2005 to early January 2006. Euro Surveillance 2006, 11, E060202.

Dafalla, O., Alsheikh, A., Mohammed, W., Shrwani, K., Alsheikh, F., Hobani, Y., Noureldin, E., 2019. Knockdown resistance mutations contributing to pyrethroid resistance in Aedes aegypti population, Saudi Arabia. East Mediterr Health J., 25(12), 905-913. https://doi.org/10.26719/emhj.19.081

Dafalla, O., Hakami, A., Noureldin, E., Siddig, A., Yehya, H., Tareq, K., Jaber, G.,Omar, M.,Khalid, S., Tariq, H., Abdullatif, M., Abdullah, A., Zaki, E., 2021. Distribution of Dengue Virus Serotypes in Jazan Region, Southwest Saudi Arabia. Ann Public Health Reports 5(2), 207-215. https://doi.org/10.36959/856/520

De Paula, S.O., Fonseca, B.A., 2004. Dengue: a review of the laboratory tests a clinician must know to achieve a correct diagnosis. Braz. J. Infect. Dis., 8(6): 390–398.https://doi.org/10.1590/s1413-86702004000600002

Elfadil, A.A., Hasab-Allah, K.A., Dafa-Allah, O.M., Elmanea, A.A., 2006. The persistence ofrift valley fever in the Jazan region of Saudi Arabia. Rev. Sci. Tech., 25(3),1131-1136.

Fakeeh, M., Zaki, A.M., 2001. Virologic and serologic surveillance for dengue fever in Jeddah, Saudi Arabia, 1994-1999. Am. J. Trop. Med. Hyg., 65, 764–767. https://doi.org/10.4269/ajtmh.2001.65.764

Fang, Y., Tambo, E., Jing-Bo, X., Zhang, Y., Xiao-Nong, Z., Khater Emad, I.M., 2021. Detection of DENV-2 and insect-specific flaviviruses in mosquitoes collected from Jeddah, Saudi Arabia. Front. Cell. Infect. Microbiol., 11. https://doi.org/10.3389/fcimb.2021.626368

Gubler DJ., 1998. Dengue and dengue hemorrhagic fever. Clin. Microbiol. Rev., 11(3), 480 –486. https://doi.org/10.1128/cmr.11.3.480

Hakami, A. R., Alshamrani, A. A., Alqahtani, M., Alraey, Y., Alhefzi, R. A., Alasmari, S., Makkawi, M., Dobie, G., Mir, M., Alshahrani, M., Dera, A., Alfaifi, M., Al Shahrani, M., Matari, A., Asiry, A. E., 2021. Detection of chikungunya virus in the Southern region, Saudi Arabia. Virology journal, 18(1), 190. https://doi.org/10.1186/s12985-021-01660-7

Hashem, A.M., Sohrab, S.S., El-Kafrawy, S.A., El-Ela, S.A., Abd-Alla, A.M.M., Farraj, S.A., Othman, N.A., Hassan, A.M., El-Daly, M.M., Charrel, .RN., Madani, T.A., Azhar, E.I., 2018. First complete genome sequence of circulating dengue virus serotype 3 in Jeddah, Saudi Arabia. New Microbes New Infect. 21, 9–11. https://doi.org/10.1016/j.nmni.2017.09.005

Hashem, A.M., Sohrab, S.S., El-Kafrawy, S.A., Abd-Alla, A.M.M., El-Ela, S.A., Abujamel, T.S., Hassan, A.M., Farraj, S.A., Othman, N.A., Charrel, R.N., Azhar, E.I., 2018. Diversity ofdengue virus-3 genotype III in Jeddah, Saudi Arabia. Acta Trop., 183, 114-118. https://doi.org/10.1016/j.actatropica.2018.04.002

Hegazi, M.A., Bakarman, M.A., Alahmadi, T.S., Butt, N.S., Alqahtani, A.M., Aljedaani, B.S., Almajnuni, A.H., 2020. Risk factors and predictors of severe dengue in Saudi population in Jeddah, Western Saudi Arabia: a retrospective study. J. Trop. Med. Hyg.,102(3), 613–621. https://doi.org/10.4269/ajtmh.19-0650

Heilman, J. M., De Wolff, J., Beards, G. M., Basden, B. J., 2014. Dengue fever: a Wikipedia clinical review. Open Med. 8, e105–e115.

Heinrich, N., Saathoff, E., Weller, N., Clowes, P., Kroidl, I., Ntinginya, E., Harun, M., Leonard, M., Thomas, L., Gerhard, D., Michael, H., 2012. High Seroprevalence of Rift Valley Fever and Evidence for Endemic Circulation in Mbeya Region, Tanzania, in a Cross- Sectional Study. PLoS Negl Trop.Dis.6(3), e1557. https://doi.org/10.1371/journal.pntd.0001557

Hussain, R., Alomar I, Memish, Z.A., 2013. Chikungunya virus: emergence of an arthritic arbovirus in Jeddah, Saudi Arabia. Eastern Mediterranean Health Journal, 19 (5), 506-508. https://www.cdc.gov/dengue/vaccine/hcp/index.html, 2021.

Holly Lutmer, 2022. Chikungunya Vaccines. https://www.vaxbeforetravel.com/chikungunya-vaccines-2022

Humphrey, J.M., Cleton, N.B., Reusken, C.B.E.M., Glesby, M.J., Koopmans, M.P.G., Abu- Raddad, L.J., 2017. Urban Chikungunya in the Middle East and North Africa: A systematic review. PLoSNegl. Trop. Dis., 11(6), e0005707. https://doi.org/10.1371/journal.pntd.0005707

Hunsperger, E.A., Yoksan, S., Buchy, P., Nguyen, V.C., Shamala, D.S., Delia, A.E., Jose, L.P., Susana, V., Harvey, A., Michael, D., Duane, J.G., Scott, B.H., María, G.G., Harold, S.M., Nathanson, C.M., Nidia, R.R.L., Kovi, E.B., Srisakul, K., Rosanna, W.P., 2009. Evaluation of commercially available anti-dengue virus immunoglobulin M tests. Emerging Infect. Dis. 15(3), 436–440.

https://www.who.int/news-room/fact-sheets/detail/dengue-and-severe-dengue (2022).

Ibrahim, A., Ross, B., 2021 Explaining Neighbourhood Variations in the Incidence of Dengue Fever in Jeddah City, Saudi Arabia. Int. J. Environ. Res. Public Health, 18, 13220. https://doi.org/10.3390/ijerph182413220

Ibrahim, N.K., Moshref, R.H., Moshref, L.H., Walid, J.B., Alsati, H.S., 2018. Knowledge and attitudes towards Zika virus among medical students in King Abdulaziz University, Jeddah, Saudi Arabia. J. Infect Public Health, 11(1), 18-23. https://doi.org/10.1016/j.jiph.2017.02.015

Idrees, S., Ashfaq, U.A., 2012. A brief review on dengue molecular virology, diagnosis, treatment and prevalence in Pakistan. Genet Vaccines Ther., 10(1), 6. https://doi.org/10.1186/1479-0556-10-6

Innis, B.L., Nisalak, A., Nimmannitya, S., Kusalerdchariya, S., Chongswasdi, V., Suntayakorn, S., Puttisri, P., Hoke, C.H., 1989. An enzyme-linked immunosorbent assay to characterize dengue infections where dengue and Japanese encephalitis co-circulate. Am. J. Trop. Med. Hyg., 40(4), 418-427. https://doi.org/10.4269/ajtmh.1989.40.418

Jamjoom, G.A., Azhar, E.I., Kao, M.A., Radadi, R.M., 2016. Seroepidemiology of asymptomatic dengue virus infection in Jeddah, Saudi Arabia. Virology (Auckl)., 7, 1-7. https://doi.org/10.4137/VRT.S34187

Juan, I.C., Juan, M.F., María, G. N., 2022. Chapter 8 - Chikungunya & Heart, Editor(s): Clara Saldarriaga, Adrian Baranchuk, neglected tropical diseases and other infectious diseases affecting the heart, Academic Press, 2022, 83-93. https://doi.org/10.4137/VRT.S34187

Khormi, H.M., Kumar, L., 2012. Assessing the risk for dengue fever based on socioeconomicand environmental variables in a geographical information system environment. Geospatial Health, 6, 171-176. https://doi.org/10.4081/gh.2012.135

Khater, E.I., Sowilem, M.M., Sallam, M.F., Alahmed, A.M., 2013. Ecology and habitat characterization of mosquitoes in Saudi Arabia. Trop. Biomed. 30:409–427.

Khawsak, P., Phantana, S., Chansiri, K., 2003. Determination of dengue virus serotypes in Thailand using PCR based method. Southeast Asian J. Trop. Med. Public Health., 34(4), 781 – 785.

Khan, N.A., Azhar, E.I., El-Fiky, S., Madani, H.H., Abuljadial, M.A., Ashshi, A.M., Turkistani, A.M., Hamouh, E.A., 2008. Clinical profile and outcome of hospitalized patients during first outbreak of dengue in Makkah, Saudi Arabia. Acta Trop., 105, 39-44. https://doi.org/10.1016/j.actatropica.2007.09.005

Konongoi, L., Ofula, V., Nyunja, A. et al., 2016. Detection of dengue virus serotypes 1, 2 and3 in selected regions of Kenya: 2011–2014. Virol. J., 13, 182. https://doi.org/10.1186/s12985-016-0641-0

Lambrechts, L., Scott, T.W., Gubler, D.J., 2010. Consequences of the expanding global distribution of Aedes albopictus for dengue virus transmission. PloS Negl. Trop. Dis., 4(5), e646. https://doi.org/10.1371/journal.pntd.0000646

Limon-Flores, A.Y., Perez-Tapia, M., Estrada-Garcia, I., Vaughan, G., Escobar-Gutierrez, A., Calderon-Amador, J., Herrera-Rodriguez, S.E., Brizuela-Garcia, A., Heras-Chavarria, M., Flores-Langarica, A., Cedillo-Barron, L., Flores-Romo, L., 2005. Dengue virus inoculation to human skin explants: an effective approach to assess in situ the early infection and the effects on cutaneous dendritic cells. Int. J. Exp. Pathol.,86(5), 323-334.https://doi.org/10.1111/j.09599673.2005.00445.x

Lindenbach, B.D., Rice, C.M., 2003. Molecular Biology of Flaviviruses. Adv. Virus Res., 59,23 - 61.

Madani, T.A., 2005. Alkhumra virus infection, a new viral haemorrhagic fever in SaudiArabia. J Infect 51: 91–97. https://doi.org/10.1371/journal.pntd.0001604

Madani, T.A., Abuelzein, ET.M.E., 2021. Alkhumra haemorrhagic fever virus infection.Arch. Virol., 166, 2357–2367.

Memish, Z.A., Fagbo, S.F., Ali, A.O., Al Hakeem, R., Elnagi, F.M., Bamgboye, E.A., 2014. Is the epidemiology of Alkhurma hemorrhagic fever changing?: A three-year overview in Saudi Arabia. PLoS ONE., 9(2), e85564. https://doi.org/10.1371/journal.pone.0085564

Memish, Z.A., 2010. Alkhurma hemorrhagic fever in humans, Najran, Saudi Arabia. Emerg.Infect. Dis., 16(12), 1882-1888. https://doi.org/10.3201/eid1612.100417

Mohammed, M.S., Abakar, A.D., Nour B. Y., Dafalla O.M., 2018. Molecular surveillance of dengue infections in Sabya governate of Jazan region, Southwestern Saudi Arabia. Int. J. Mosq. Res., 5, 125–132.

Mroz, C., Gwida, M., El-Ashker, M., El-Diasty, M., El-Beskawy, M., Ute, Z., Martin, E., Martin, H.G., 2017. Seroprevalence of Rift Valley fever virus in livestock during inter- epidemic period in Egypt, 2014/15. BMC Vet. Res., 13, 87. https://doi.org/10.1186/s12917- 017-0993-8

Murrell, S., Wu, S.C., Butler M., 2011. Review of dengue virus and the development of avaccine. Biotechnology advances., 29, 239-247. https://doi.org/10.1016/j.biotechadv.2010.11.008

Ommer, D., Abdualziz, H., Mohammed Jubran, Ahmed Alzhrani, Muhannad Mujally, Othman Shajari, Ali Khardali,and Zaki Eisa, 2021. Culex (Diptera: Culicidae) mosquitoes in Jazan region, Saudi Arabia, and their molecular identification. International Journal of Zoology, 5563916. https://doi.org/10.1155/2021/5563916

Organji, S.R., Abulreesh, H.H., Osman, G.E., 2017. Circulation of dengue virus serotypes in the City of Makkah, Saudi Arabia, as determined by reverse transcription polymerase chain reaction. Can. J. Infect. Dis. Med. Microbiol. 2017, 1646701. https://doi.org/10.1155/2021/5563916

Osama, B. A., Amani, O.A., Abeer, A., Alanood, D., Kawakeb, D., Marwah, H., Hanan, S., Shareefa, S., Marwah, G., Rana, H., Mohammed, S. M., 2021. Knowledge, attitude, and practice regarding dengue infection among Jazan inhabitants, Saudi Arabia 2019. Medical Science 25(108), 337-346.

Pfeffer, M., Dobler, G., Löscher, T., Hassler D., 2006. Bone-breaker fever" in paradise. Chikungunya fever raged on dreamy tropical islands before it did on the east coast of Africa. Dtsch Med. Wochenschr., 131, 601–602.

Prince, H.E., Matud, J.L., 2011. Estimation of dengue virus IgM persistence using regression analysis. Clin. Vaccine Immunol., 18(12), 2183–2185. https://doi.org/10.1186/s12879-018- 3058-0

Robert Carlson and Holly Lutmer, 2002. Valneva Chikungunya Vaccine (VLA1553). https://www.precisionvaccinations.com/vaccines/valneva-chikungunya-vaccine-vla1553

Sami, M., Rowaida, B., Abdul, H., Fadel, Q., Asim, K., Ismail, A., Sultan, A., Yehya, A., Rasha, B., Razaz, G., Ashwaq, H., Ahmed, A., Mohamed, B., Thanaa, M., 2021. The epidemiology and incidence of dengue in Makkah, Saudi Arabia, during 2017-2019. SaudiMed. J., 42 (11) 1173-1179. https://doi.org/10.15537/smj.2021.42.11.20210124

Sami, M., Rowaida, B., Abdul, H., Fadel, Q., Asim, K., Ismail, A., Sultan, A., Yehya, A., Rasha, B., Razaz, G., Ashwaq, H., Ahmed, A., Mohamed, B., Thanaa, M., 2021. The epidemiology and incidence of dengue in Makkah, Saudi Arabia, during 2017-2019. Saudi Med. J., 42 (11) 1173-1179. https://doi.org/10.15537/smj.2021.42.11.20210124

Saudi Ministry of Health (MOH), Statistical Yearbook, 1437, 142-148.

Sado, F.Y., Tchetgna, H.S., Kamgang, B., Djonabaye, D., Nakouné, E., McCall, P.J., Roland,
N. N., Charles, S. W., 2022. Seroprevalence of Rift Valley fever virus in domestic ruminants of various origins in two markets of Yaoundé, Cameroon. PLoS Negl. Trop. Dis., 16(8), e0010683. https://doi.org/10.1371/journal.pntd.0010683

Siregar, A.R., Wibbawa, T., Wijayanti, N., 2011. Early detection and sero typing of dengue viruses by using reverse transcription polymerase chain reaction (RT – PCR) 2 Primers. Indones. J. Biotechnol., 16(2), 71-75.

Tambo, E., El-Dessouky, A.G., 2018. Defeating re-emerging Alkhurma haemorrhagic fever virus outbreak in Saudi Arabia and worldwide. PLoS Negl. Trop. Dis., 12(9), e0006707. https://doi.org/10.1371/journal.pntd.0006707

Tang KF and Ooi EE., 2012. Diagnosis of dengue: an update. Expert Rev. Anti infect. Ther., 10(8), 895-907. https://doi.org/10.1586/eri.12.76

Vorndam, V., Kuno, G., 1997. Laboratory diagnosis of dengue virus infections. In: Gubler, D.J., Kuno, G., (eds), Dengue and Dengue hemorrhagic fever. New York, CAB International,313 – 333.

WHO, 2013. Dengue guidelines for diagnosis, treatment, prevention and control. New Edition. Geneva. World Health Organization.

WHO, 2018. Zikavirus. https://www.who.int/news-room/fact-sheets/detail/zika-virus

WHO, 2020. https://www.who.int/news-room/fact-sheets/detail/chikungunya

Xu, G., Dong, H., Shi, N., Liu, S., Zhou, A., Cheng, Z., Chen, G., Liu, J., Fang, T., Zhang, H., Gu, C., Tan, X., Ye, J., Xie, S., Cao, G., 2007. An outbreak of dengue virus serotype 1 infection in Cixi, Ningbo, People's Republic of China, 2004, associated with traveller from Thailand and high density of Aedes albopictus. Am.J. Trop. Med. Hyg., 76(6), 1182 – 1188.

Yezli, S., Yasir, M., Yassin, Y., Almazrua, A., Al-Subhi, T., Othman, N., Omar, A., Abdoon, A., Elamin, Y., Abuzaid, A., Bafaraj, T., Alzahrani, H., Almahmoodi, S., Alzahrani, H., Bieh,K., Alotaibi, B., Khan, A., Alzahrani, M., Azhar, E.I., 2021. Lack of Zika virus and other recognized flaviviruses among the mosquito vectors during and post the Hajj Mass gathering.Int. J. Environ. Res. Public Health.,10, 18(12), 6275.
https://doi.org/10.3390/ijerph18126275

Zakham, F., Al-habal, M., Taher, R., Alaoui, A., El Mzibri, M., 2017. Viral hemorrhagic fevers in the Tihamah region of the western Arabian Peninsula. PLoS Negl Trop Dis.,11(4):e0005322.

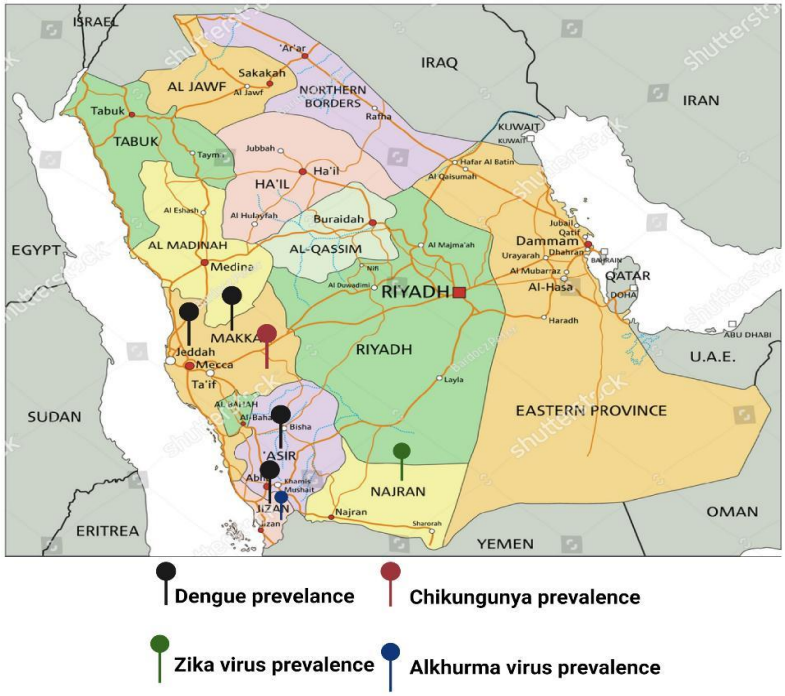

Figure 1. Prevalence of Arbo virus infection in Saudi Arabia

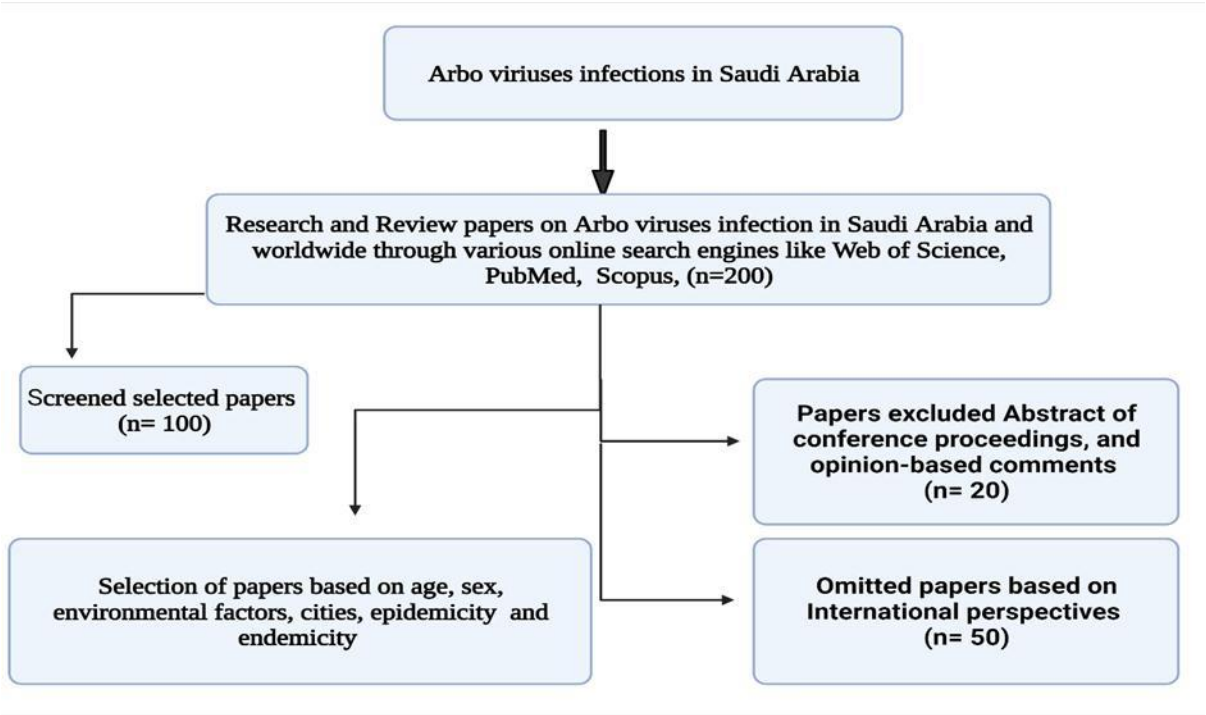

Figure 2. The flowchart illustrating the criterion and selection criteria for the literature includedin this systematic review.

Table 1: List of recent studies on dengue prevalence in Saudi Arabia

S.no	Title of the work	Focal theme	Outcome of the study	References
1	Epidemiological screening and serotyping analysis of dengue fever in the Southwestern region of Saudi Arabia	The study governs the epidemiology and molecular analysis of dengue in the Southwestern region of Saudi Arabia	The recent study found a dramatic increase in DENV prevalence from 2012 to 2020. Pre-pandemic cases were high. The DENV screening was done using RT-PCR, and the NSI antigen should be used to cross-check the results.	Alkhansa Alshabi et al., 2022
2	Distribution of Dengue Virus Serotypes in Jazan Region, Southwest Saudi Arabia	The study emphasizes the need of tracking and monitoring dengue virus serotypes.	This investigation revealed that the dengue virus types DENV-1, DENV-2, and DENV-3 circulated in the Jazan region, with DENV-2 dominating.	Ommer Dafalla et al., 2021
3	The epidemiology and incidence of dengue in Makkah, Saudi Arabia, during 2017-2019	The study determines the epidemiology of dengue fever and how it spreads in Makkah, Kingdom of Saudi Arabia between 2017 and 2019.	The prevalence of dengue fever in Makkah, Saudi Arabia, increased in 2019 as compared to the previous two years, owing to high rainfall in 2019. Post-rainfall vector management operations in Makkah, Saudi Arabia, may aid in the restraint of the disease.	Sami Melebari et al., 2021
4	Culex (Diptera: Culicidae) Mosquitoes in Jazan Region, Saudi Arabia, and Their Molecular Identification	The goal of this study was to identify adult Culex mosquitoes (Diptera: Culicidae) and their distribution in the Jazan region using morphological and genomic (molecular) identification.	The research of combining morphological and molecular identification to refine the list of Culex mosquito species in the Jazan region and precisely describe their geographical distribution. This integration has the potential to encourage and improve vector surveillance and control programs, as well as define the region's genetic diversity.	Elsiddig Noureldin et al., 2021
5	Knowledge, attitude and practice regarding dengue infection among Jazan inhabitants, Saudi Arabia 2019	The purpose of this study was to analyze dengue infection knowledge, attitude, and practice among Saudi Jazan residents.	Knowledge of dengue disease transmission, symptoms, and severity was adequate. But preventing mosquito bites was rarely done. Policymakers can develop strategies to improve knowledge and practice.	Osama B Albasheer et al., 2021
6	Explaining Neighborhood Variations in the Incidence of Dengue Fever in Jeddah City, Saudi Arabia	This study investigated dengue fever (DF) and its distribution over 56 neighborhoods in Jeddah City, Saudi Arabia, where the prevalence of dengue fever remains high despite recent improvements.	The report recommended that Saudi Arabian government entities consider local neighborhood considerations while developing and implementing dengue control measures. Future study should focus on the routes that relate local social status to dengue and wider health effects.	Ibrahim Alkhaldy and Ross Barnett, 2021
7	Risk Factors and Predictors of Severe Dengue in Saudi Population in Jeddah, Western Saudi Arabia: A Retrospective	This study sought to identify severe dengue fever risk variables and predictors in the Saudi population of Jeddah, Western Saudi Arabia.	A multicenter study evaluating severe dengue fever in the Saudi population and considering the WHO 2009 dengue classification revealed that adults and males were the most infected with dengue, that there were	Hegazi et al., 2020

	Study		few severe dengue fever cases with low mortality, andthat predictors of severe dengue fever in adults were different from those in children. It is possible that considering warning indications of severe dengue would result in hospitalization, which will result in closer monitoring, early and appropriate interventions,and a reduction in mortality in severe dengue fever cases.	
8	The economic burden of denguefever in the Kingdom of Saudi Arabia	The study evaluated the cost of illness of DENV infection in Saudi Arabia from 2013–2017 using national data from referral centers inthe country's endemic western area.	The study estimated that dengue causes a significant local economic burden that costs US$110.2 million per year, underscoring the urgent need for an effectivenational prevention approach that can save significantamounts of money while also reducing morbidity and mortality.	Akbar et al., 2020
9	Knockdown resistance mutationscontributing to pyrethroid resistance in Aedes aegyptipopulation, Saudi Arabia	The present study was conducted inJazan, to investigate *Ae. aegypti* pyrethroid resistance and theunderlying mechanisms.	Environmentally, pyrethroids are frequently utilizedto control the vector Aedes aegypti in Jeddah, Makkah, Asir and Jazan. Most of these places haveAe. aegypti pyrethroid pesticide resistance.	Dafalla et al., 2019

نظرة عامة على انتشار العدوى بالفيروسات المنقولة بالحيوانات المفصلية في المملكة العربية السعودية

احمد عبدالحق، ماجد احمد دراج، المنذر عبدالله هرشان، ريم حساني

١ قسم تقنية المختبرات الطبية، كلية العلوم الطبية التطبيقية، جامعة جازان ، جازان المملكة العربية السعودية

٢ قسم الباطنة، كلية الطب، جامعة جازان ، جازان المملكة العربية السعودية

٣ قسم الاحياء الدقيقة والطفيليات، كلية الطب، جامعة جدة ، جدة، المملكة العربية السعودية

٤ كلية التمريض، جامعة جازان ، جازان المملكة العربية السعودية

الملخص

تنتشر العدوى بالفيروسات المنقولة بالحيوانات المفصلية (الأربوفيروسات) في العديد من مناطق المملكة العربية السعودية. وتقدم هذه الورقة المرجعية توضيحاً لانتشار الأربوفيروسات وعوامل الخطورة المتصلة بها والإجراءآت الوقائية اللآزمة للتغلب على انتشار هذه الفيروسات. وقد تم في هذا الصدد مراجعة محرك البحث PubMed وقاعدة بيانات MEDLINE التابعة له، وقواعد بيانات النشر العلمي Science Direct و Scopus و Google Scholar، وكذلك قاعدة بيانات الطب الحيوي Embase في الفترة ١٩٨٥ إلى ٢٠٢٢ وتحديد الأوراق العلمية المهتمة بموضوع العدوى بالفيروسات المنقولة بالحيوانات المفصلية (الأربوفيروسات).

وتركز هذه الورقة البحثية المرجعية على الصفات الوبائية لهذه الأمراض وطرق الوقاية منها حيث من الأهمية كشف هذه الحقائق والوقوف على عوامل الخطورة لأجل تهرف العامة بها في إطار التوعية المجتمعية. وسوف تعود هذه الورقة المرجعية بالفائدة على المجتمع الطبي والعامة بتوفير المعرفة بهذه الأمراض وطرق الوقاية منها.

نسيج طارد للبعوض معالج بكبسولات دقيقة من مستخلص قشر الرمان

نبراس إبراهيم عيسى و سلوى محمد طاشكندي

قسم الأزياء والنسيج جامعة الملك عبد العزيز

وفاء أبو بكر باوزير

قسم الكيمياء عضوية جامعة الملك عبد العزيز

حنان سلمان اليحيى

قسم علم الحشرات جامعة الملك عبد العزيز

الملخص

يشكل البعوض تهديداً كبيراً على صحة الإنسان، فهو ينقل العديد من الأمراض إليه، وبالتالي هناك حاجة ماسة إلى منتجات متخصصة لمكافحته والوقاية منه. وقد تكون المنسوجات المعالجة بمواد نباتية طبيعية أفضل فاعلية وطاردة للبعوض للمحافظة على سلامة الإنسان والبيئة. وتوجد العديد من النباتات التي تحتوي على مركبات كيميائية فعالة في طرد البعوض وغير سامة وتتحلل بيولوجياً، ومستخلصة ومحضرة بطريقة صديقة للبيئة. ومن عيوب استخدام المواد الطبيعية النباتية في معالجة النسيج هو ضعف الرابط بين المادة والنسيج، وتعد الكبسلة الدقيقة من أفضل الحلول للتغلب على ذلك .

وأظهرت الدراسة الحالية أثر وفاعلية الكبسلة الدقيقة لمستخلص قشر الرمان في طرد البعوض الزاعجة المصرية *Aedes aegypti*.

اتبع البحث المنهج التجريبي من خلال ابتكار طريقة صديقة للبيئة تتلخص في تحضير كبسولات دقيقة تحتوي على مستخلص قشر الرمان ومعالجة النسيج بها، واختبار فاعليتها في طرد البعوض وأثر تلك المعالجة على النسيج، وذلك باستخدام مستخلص قشر الرمان كمادة أساسية والصمغ العربي كغلاف. كما تم استخدام محلول ألجينات الصوديوم لعملية الكبسلة الدقيقة.

و أظهرت النتائج أن النسيج القطني المعالج بالكبسولات الدقيقة لمستخلص قشر الرمان طارداً للبعوض بمتوسط نسبة ٦٣,٥٣%، في حين حقق النسيج القطني المعالج بمستخلص قشر الرمان فاعلية في طرد البعوض بمتوسط نسبة ٥٧,٣٩%. وجاء معامل الجودة الكلية لاختبارات نسيج القطن المعالج وغير المعالج بمستخلص قشر الرمان والمعالج بكبسولات مستخلص قشر الرمان لصالح العينة المعالجة بالكبسلة الدقيقة لمستخلص قشر الرمان.

وتوصي الدراسة بإعداد عدة تراكيز مختلفة لمستخلص قشر الرمان للوصول إلى نسبة التركيز الأفضل لطرد البعوض، وكذلك غسل النسيج لمعرفة مدى بقاء أثر المعالجة على النسيج.

الكلمات المفتاحية : الكبسلة الدقيقة، طارد البعوض، مواد طبيعية، معالجة النسيج، قشر الرمان.

المقدمة:

نتج عن انتشار الحشرات في جميع البيئات وجود علاقة نافعة أو ضارة بينها وبين الإنسان، وقد يكون ضررها هو الأكثر شيوعا وانتشارا، فتوجد بعض الأمراض التي لا تنتقل إلا عن طريق النشاط الحشري (المحمادي، ٢٠٠٩م)، ومنها الملاريا التي ينقلها أنثى بعوض الأنوفيليس *Anopheles*، وحمى الضنك و الشيكونغونيا التي ينقلها أنثى بعوض الزاعجة المصرية *Aedes aegypti*، وفيروس التهاب الدماغ الياباني وطفيلي الفيلاريات التي ينقلها أنثى بعوض الكيولكس *Culex* (Raja et al., 2015). ويثير البعوض بذلك قلقا كبيرا على الصحة العامة بنقله للأمراض المميتة، التي تعد معظمها بدون لقاح. والطريقة الوحيدة للوقاية من هذه الأمراض هي مكافحتها وتجنب لدغة البعوض (Mullah et al., 2019)، ويمكن تجنب لدغ البعوض باستخدام طارد الحشرات أو وضع ما يجذب البعوض في مكان بعيد عن الشخص نفسه.

ومع التقدم الصناعي والتكنولوجي في صناعة النسيج ظهرت المنسوجات الواقية، وما يندرج تحتها من المنسوجات الطاردة للبعوض، وهي أحدث الإبتكارات في مجال النسيج التي توفر المميزات التي تشتد الحاجة إليها لطرد البعوض وإبعاده عن جلد الإنسان ومنعها من لدغه (Krishnaveni, 2009)، ويمكن إضافة خاصية الطرد النسيجي عن طريق المعالجة النهائية للنسيج بمادة طاردة للبعوض.

وتنقسم المواد الطاردة للبعوض إلى مواد صناعية ومواد طبيعية، وغالبا ما يتم استخدام المواد الصناعية، ومع ذلك فهي ليست صديقة للبيئة وبعضها يرتبط بالتهاب وحساسية الجلد.

ويعتبر ثنائي أثيل تولواميد (Diethyltoluamide) ما يعرف بـ (DEET) طارد صناعي للبعوض وهو أحد المنتجات القليلة الفعّالة ضد البعوض التي تم توثيق فاعليتها للحماية من البعوض. وعلى الرغم من ذلك هناك مخاوف مرتبطة باستعمال المواد الصناعية لطرد البعوض (Phasomkusolsil & Soonwera, 2010). وقد أدى استخدام المواد الصناعية الطاردة للبعوض بكميات كبيره وبشكل مستمر غلى العديد من المشكلات في البيئة، فهي غير قابلة للتحلل الحيوي وتؤثر على صحة الإنسان (Ghosh et al., 2012). فقد تم الإبلاغ عن حدوث تسمم للإنسان عند استخدام الطارد الصناعي DEET مع تفاوت في الأعراض من أعراض خفيفة إلى شديدة. لذلك أصبح هناك حاجة لإيجاد بدائل أكثر أماناً من المواد الصناعية، وإجراء أبحاث بشأن المواد الطبيعية الطاردة للحشرات من مستخلصات نباتية (Phasomkusolsil & Soonwera, 2010).

يختلف تأثير المستخلصات النباتية وفقاً لعدة أسباب منها نوع النبات وموقعه الجغرافي والجزء المستخدم ومنهجية الاستخلاص (Ghosh et al., 2012).ويرجع الاختلاف حسب الدراسات عند تطبيقه على المنسوجات لتصبح طاردة للحشرات إلى عوامل مختلفة منها نوع النسيج المستخدم ونوع التقنية المستخدمة لنقل المادة الطاردة إلى النسيج.

ومن المأمول الوصول إلى طارد بعوض جيد يطبق على نسيج مناسب له، مع تنفيذ طريقة اختبار ملائمة لاختبار نسبة فاعلية الطرد (Anuar & Yusof, 2016).

وتعد المواد الطبيعية النباتية صديقة للبيئة قابلة للتحلل البيولوجي وأقل سميه وأكثر أماناً للاستخدام البشري (Karthigeyan & Premalatha, 2019).

وتُنتج النباتات العديد من المواد الكيميائية، والكثير منها له خصائص طبية وطارد للحشرات (Ghosh et al., 2012)، مثل نبات العشار والعرعر والنيم والأقحوان الذهبي (الحكيم، ٢٠١٥م). ويتم استخراج المواد الكيمائية النباتية إما من أجزاء النبتة كاملة أو من أجزاء مختلفة كالثمار أو الأوراق أو السيقان أو اللحاء أو البذور وغيرها (Ghosh et al., 2012). وقد ثبت أن النسيج المعالج بقشر البرتقال له فعالية ممتازة في طرد البعوض (Gupta & Singh, 2017). وأظهرت دراسة (اليحيى، ٢٠١١م) أن مركبات ومستخلصات بذور النيم لديها فاعليه على البعوض في أطواره المختلفة، وإمكانية استخدام بذور النيم في برامج المكافحة الحيوية للبعوض.

من ناحية أخرى، أثبتت دراسة (Singh, 2017) أن عينات النسيج المصبوغة بمستخلص قشر الرمان لها فعالة بنسبة ٨٠% لطرد البعوض.

وتعرف الكبسلة الدقيقة بأنها عملية يتم فيها تحضير كبسولات دقيقة تحتوي على جزيئات أو قطرات صغيرة، بمادة غلاف تحتوي على العديد من الخصائص المرغوبة. وتسمى المادة الموجودة داخل الغلاف بالمادة الأساسية أو اللب، بينما يطلق على الغلاف الخارجي الجدار أو الغشاء أو القشرة. ويتراوح قطر الكبسولة من بضعة مايكرو متر إلى بضعة مليمترات (Samanta et al., 2020). وفي الدراسة الحالية يعد مستخلص قشر الرمان هو المادة الأساسية بينما الصمغ العربي والجينات الصوديوم هي الجدار أو الغشاء الخارجي.

وقد أثبتت الكبسلة فاعليتها من حيث ثباتها على النسيج، للتغلب بذلك على بعض التحديات التي أشارت اليها العديد من الدراسات السابقة التي تناولت معالجة النسيج باستخدام المواد الطبيعية النباتية، مثل ثبات المادة على النسيج عند الغسيل، حيث وجدت الدراسات أن معظم المواد المعالجة تزول أثناء عملية الغسيل فهي لا تمتلك ترابطاً جيداً مع سطح النسيج (Raja et al., 2015).

وتعد عملية الكبسلة الدقيقة للمواد الطبيعية هي أفضل طريقة لمعالجة النسيج فهي توفر امكانية بقاء المادة على سطح النسيج وعدم تأثره بفعل عملية الغسيل (Subrata, 2021). وقد أظهر المستخلص النباتي لعشبة (*Andrographis paniculata*) بعد كبسلته فاعليته بما لا يزيد عن ١٠ غسلات (Ramya & Maheshwari, 2014)، واظهر المستخلص النباتي (*Moringa oleifera* gum) حماية أطول ومتانة حتى ٣٠ غسلة، فالكبسلة الدقيقة تتحكم في إطلاق المادة الفعالة الموجودة داخلها(Ghayempour & Montazer, 2016).

يساهم البحث في توفير آلية للحفاظ على بقاء المادة الطبيعية المستخدمة على النسيج لأطول فترة ممكنة، وبالتالي تحمي الإنسان من الأمراض المنقولة إليه فتحافظ على صحته وتحقق بيئة آمنه مستدامة باستخدام المواد الطبيعية القابلة للتحلل بيولوجياً دون أثر يذكر، بما يتوافق مع رؤية المملكة العربية السعودية ٢٠٣٠.

الهدف من الدراسة:

تهدف الدراسة الحالية أولاً: إلى إنتاج كبسولات دقيقة تحتوي على مستخلص قشر الرمان ومعرفة أثر الكبسلة الدقيقة على عملية طرد البعوض.

ثانياً: التعرف على أثر المعالجة بمستخلص قشر الرمان والكبسولات الدقيقة للمستخلص على النسيج.

منهج البحث:

اتبع البحث المنهج التجريبي، ويعّرف المنهج التجريبي بأنه المنهج الذي يستطيع الباحث من خلاله أن يعرف أثر السبب على النتيجة (العساف، ١٤٣١هـ). ويعّرف أيضا بأنه التحكم في جميع المتغيرات والعوامل الأساسية باستثناء متغير واحد بحيث يقوم الباحث بتغيره أو تطويعه بهدف قياس وتحديد تأثيره في العملية (الصديق، ١٤٢٥هـ). وقد تم تطبيق المنهج التجريبي للكشف عن تأثير الأقمشة المعالجة بمستخلص قشر الرمان والمعالجة بالكبسلة الدقيقة للمستخلص على طرد البعوض.

المواد وطريقة العمل:

أدوات البحث:

١- بعوض من نوع الزاعجة المصرية (*Aedes aegypti*).

٢- قشر الرمان.

٣- نسيج قطني ١٠٠% بتركيب نسجي سادة ١/١.

٤- انبوب اختبار الحساسية للمبيدات الحشرية التابع لمنظمة الصحة العالمية (WHO).

إجراءات البحث:

اولا: تطبيق المادة الطاردة على النسيج

أ. مستخلص قشر الرمان بدون كبسلة:

تم تحضير المستخلص بنسبة (١:٥)؛ ٥٠٠ ملليتر (مل) من الميثانول و ١٠٠ غم من مسحوق قشر الرمان، باستخدام آلة التحريك المغناطيسي " Stirrer machine"، حيث تم التحريك لمدة ساعتين بسرعة ١٢٨٠ دورة في الدقيقة، ثم ترك المستخلص مغطى بإحكام لمدة ٢٤ ساعة ثم رشح باستخدام ورق الترشيح، واستخدم جهاز المبخر الدوار "Rotary evaporator" لتبخير الميثانول. وبعد استخلاص قشر الرمان تم معالجة النسيج بغمره في محلول يحتوي على ١٠مل من المستخلص مقابل ١٦٥مل ماء مقطر ثم تجفيف النسيج في الهواء الطلق (صورة ١) نسيجP1.

ب. مستخلص قشر الرمان بالكبسلة:

تم إجراء الكبسلة الدقيقة باستخدام مستخلص قشر الرمان كمادة أساسية والصمغ العربي كغلاف، ثم السماح لعشرة غرامات من الصمغ العربي بالتضخم لمدة نصف ساعة عن طريق خلط ١٠٠ مل من الماء الساخن مع ١٠غم صمغ عربي باستخدام جهاز "Stirrer machine"، ثم أضيف ٥٠ مل من الماء الساخن إلى الخليط، والتحريك لمدة ١٥د مع الحفاظ على درجة الحرارة بين ٤٠ و٥٠ درجة مئوية، ثم أضيف ١٠ مل من المادة الأساسية مع التحريك بسرعة ٣٠٠-٥٠٠ دورة في الدقيقة لمدة ١٥د أخرى، تليها إضافة نسبة ٢٠ ٪ من محلول ألجينات الصوديوم (١٠ مل) لمدة ٥ - ١٠د، وخفيض سرعة التحريك ثم تمت إضافة ٥ مل من الفورمالدهايد بنسبة ١٧%، ثم جففت المادة الناتجة بالتجفيد باستخدام جهاز"Freeze-drying". وبعد عملية الكبسلة لمستخلص قشر الرمان تم معالجة النسيج بغمره في محلول يحتوي على كبسولات دقيقة بنسبة

١٠%، ثم تجفيف النسيج في الهواء الطلق (صورة١) نسيج P2.

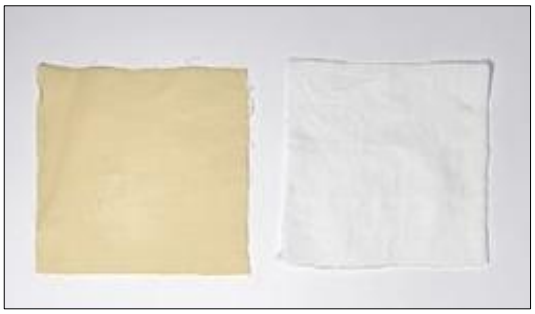

نسيج معالج P1 بمستخلص قشر الرمان بدون كبسلة دقيقة

نسيجمعالج P2 بمستخلص قشر الرمان بالكبسلة

صورة (١): النسيج قبل وبعد المعالجة بمستخلص قشر الرمان

ثانيا: اختبار طرد النسيج للبعوض:

اختيار نوع البعوض:

تمت تربية بعوض الزاعجة المصرية *Aedes aegypti* في وحدة أبحاث حمى الضنك ومكافحة النواقل التابع لجامعة الملك عبد العزيز بجدة، وتم تغذية البعوض بمحلول السكروز طوال ٤ ساعات قبل عمل التجارب المعملية (صورة ٢) وذلك لإلغاء أثر التجويع.

صورة (٢): حاوية تربية البعوض البالغ من نوع "Aedes aegypti "

يعد اختبار الحساسية للمبيدات الحشرية التابع لمنظمة الصحة العالمية (WHO) (أنبوب اختبار منظمة الصحة العالمية) طريقة معيارية يتم تنفيذها لتقييم المقاومة في عدد من البعوض البالغ. قامت الدراسة بتعديل بعض خطوات الاختبار، ومنها استخدام النسيج المعالج بدلا من الورق المشبع بالمواد المعالجة، وحساب نسبة الطرد كل ١٠دقائق إلى ساعة، بينما يقوم الاختبار الأساسي على حساب نسبة الوفيات خلال ٢٤ساعة بعد تعريض البعوض للمادة لمدة ساعة لحساب نسبة الطرد للنسيج المعالج بمستخلص قشر الرمان و بكبسولات مستخلص قشر الرمان، بابتعاد البعوض عن النسيج المعالج وهروبه إلى النسيج الغير معالج. خلال هذا الاختبار تم تبطين الأنبوب الأول بنسيج غير معالج (نسيج تحكمO)

والأخر مبطن بنسيج معالج. تم تثبيت النسيج في مكانه بمشابك زنبركيه (صورة ٣ (C)، تم فصل كلا الأنبوبين بواسطة وحدة إنزلاقيه (صورة ٣ (E) وشريحة منزلقة "مزلاق" (صورة ٣ (F)، بينما تم تغطية نهايات الأنابيب بشاشة شبكية (صورة ٣ (B) وغطاء لولبي (صورة ٣ (A) (Tomlinson et al., 2019). تم إدخال البعوض إلى الأنبوب الأول "أنبوب التحكم" وإيصال الأنبوب الأخر به، وفتح الممر بين الأنبوبين بتحريك المزلاق، ودفع البعوض من خلال نفخ القليل من الهواء للسماح للبعوض بالانتقال بين الأنبوبين. ولأن البعوض يستقر في المكان الملائم له أولا وقد لا يتحرك، وبعد ١٠ دقائق تم إغلاق الممر بين الأنبوبين بالمزلاق، وحساب عدد البعوض في كل أنبوب وتسجيله. بعدها تم تحريك المزلاق ودفع البعوض بنفخ القليل من الهواء والانتظار ١٠ دقائق أخرى، وتكرار العملية السابقة إلى أن أصبح الوقت الإجمالي للاختبار ٦٠ دقيقة (صورة ٤).

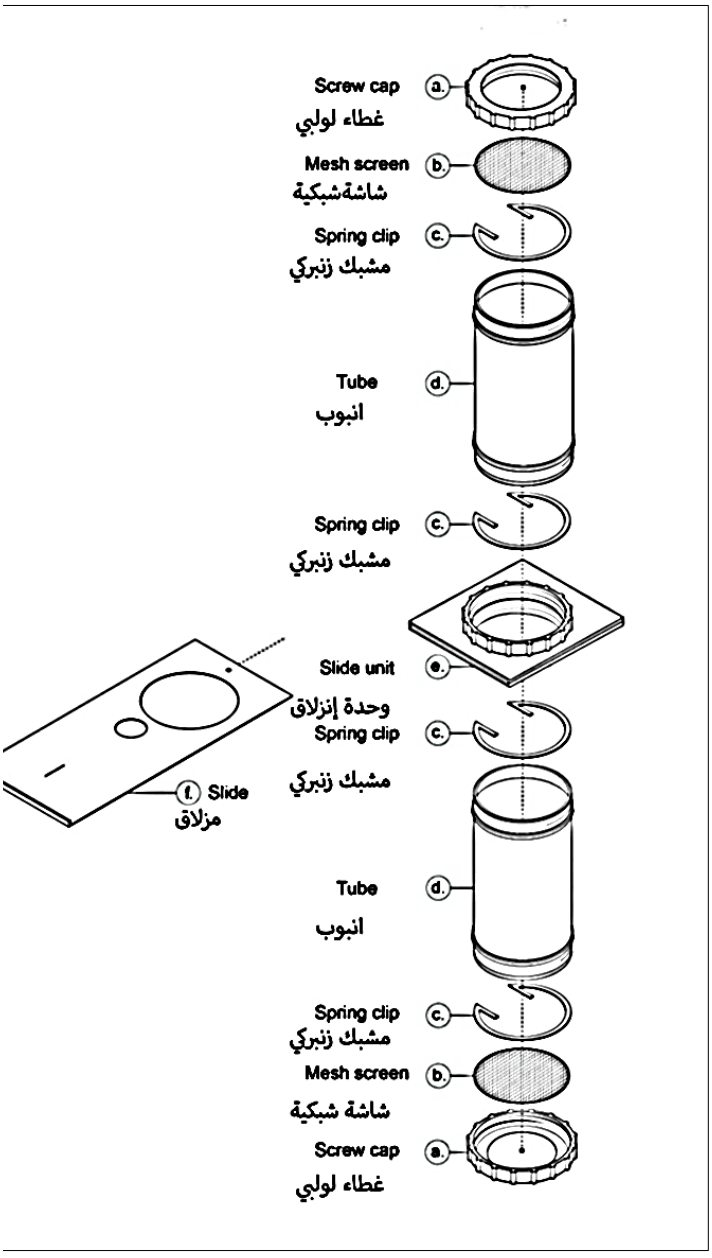

صورة (٣): أجزاء أنبوب اختبار منظمة الصحة العالمية للبعوض " **WHO Tomlinson et al., 2019 "Tube Test**

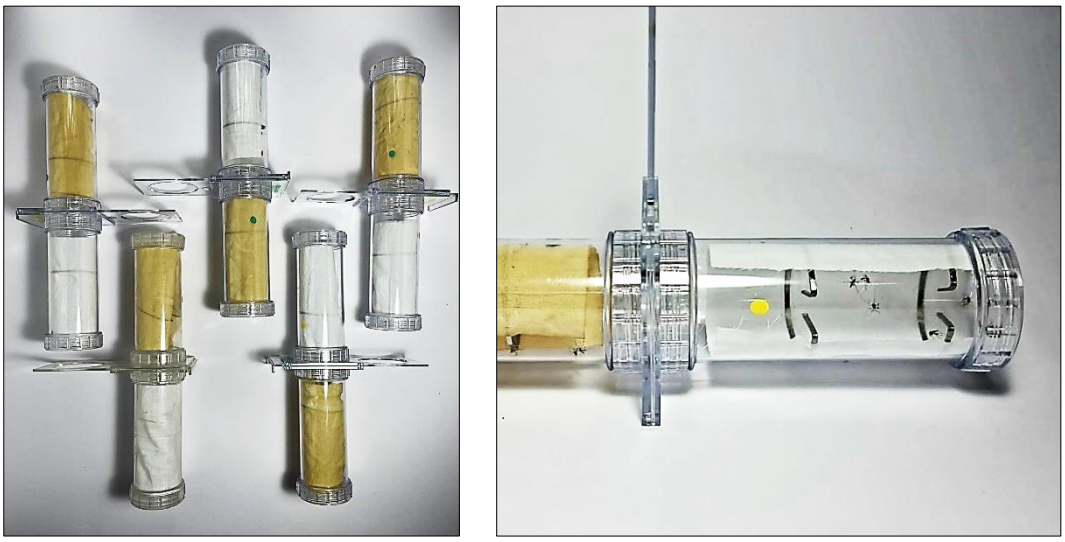

صورة (٤): اختبار البعوض باستخدام أنبوب اختبار منظمة الصحة العالمية للبعوض

تم تكرار الاختبار ٥ مرات وتلا ذلك حساب النسبة المئوية لطرد البعوض باستخدام الصيغة التالية: (Kantheti et al., 2020) لكل أنبوب وكل ١٠دقائق:

$$\%\text{Mosquito protection} = \frac{\text{No of specimen escaped + No of specimen dead}}{\text{No of specimen exposed}} \mathbf{X}\ 100$$

ثالثا: اختبارات النسيج:

تم اختيار نسيج قطني ١٠٠% بتركيب نسجي سادة ١/١. تم غسل النسيج عند درجة حرارة ١٠٠ مئوية لمدة ٦٠ دقيقة (د)، باستخدام محلول يحتوي على Na_2CO_3 "كربونات الصوديوم" (٢ غرام (غم) / لتر، عامل ترطيب، ١ ٪) للتأكد من تنقيته وخلوه من الشوائب والمواد الكيمائية، ثم غسله جيدًا بالماء وتجفيفه في الظروف الطبيعية المحيطة ورمز له بالرمز (O) النسيج الغير معالج أو ما يسمى بعينة التحكم أو العينة الضابطة. وتشير العينة (P1) إلى النسيج المعالج بمستخلص قشر الرمان، وتشير العينة (P2) إلى النسيج المعالج بالكبسولات الدقيقة لمستخلص قشر الرمان، وتم عمل الاختبارات التالية:

١) تحليل سطح النسيج:

تم إجراء تحليل سطح النسيج باستخدام جهاز المجهر الإلكتروني الماسح Scanning Electron Microscope واختصاره (SEM)، وهو نوع من المجاهر الإلكترونية التي تنتج صوراً بمسح السطح بشعاع مركز من الإلكترونات، وتتفاعل الإلكترونات مع الذرة في العينة، وتنتج إشارات مختلفة تحتوي على معلومات عن طبوغرافيا السطح وتكوين العينة.

٢) التركيب النسجي:

تم إجراء هذا الاختبار عن طريق الفحص البصري والعدسة المكبرة. والتركيب النسجي هو وصف لطريقة تعاشق خيوط طولية تسمى خيوط السداء مع خيوط عرضية تسمى خيوط اللحمة لتشكل نسيجاً.

٣) سمك النسيج:

تم قياس سماكة النسيج وفقاً للمواصفات القياسية الأمريكية (ASTM D1777-96). تم وضع عينة على قاعدة مقياس سمك وتم إنزال قدم الضغط على العينة، وتم قياس الإزاحة بين النعل والدواسة والنتيجة المعطاة تسمى بسماكة العينة.

٤) وزن المتر المربع للنسيج:

تم قياس وزن المتر المربع وفقاً للمواصفات القياسية الأمريكية (ASTM D3776) حيث تقاس كتلة النسيج لكل وحدة مساحة (وزن) ويوفر الاختبار طرق صالحة لمعظم الأقمشة. يقدم المعيار أربع طرق اختبار. تم اختيار طريقة "Small Swatch of Fabric" أي عينة نسيج صغيرة وتم التعبير عن كتلة النسيج لكل وحدة مساحة بغرام لكل متر مربع.

٥) نفاذية الهواء:

تم قياس نفاذية الهواء وفقا للمواصفات القياسية (ASTM D737). وتعبر نفاذية الهواء عن معدل تدفق الهواء عمودياً من خلال منطقة معينة معروفة للحصول على فرق ضغط هواء محدد مسبقًا بين سطحين من القماش. ويتم تحديد نفاذية الهواء للنسيج من معدل تدفق الهواء..

وقد تم أخذ المتوسط لقراءات الاختبارات (اختبار سمك النسيج ويقاس بالمليمتر، اختبار وزن المتر المربع للنسيج ويقاس بالغرام لكل متر مربع (غم/م^{٢})، ونفاذية الهواء للنسيج وتقاس بالسنتيمتر مكعب لكل ثانية عبر١٠٠سنتيمتر مربع (سم^{٣}/ث/سم^{٢})).

النتائج ومناقشتها:

أولاً: أثر المنسوجات المعالجة بالكبسولات الدقيقة لمستخلص قشر الرمان على البعوض:

يشير الجدول (١) إلى نتائج اختبار نسبة طرد عينات نسيج معالج بمستخلص قشر الرمان (P1) للبعوض في ٥ أنابيب مختلفة من أنابيب الاختبار كل ١٠دقائق ومتوسط نسبة الطرد لجميع الأنابيب لكل ١٠دقائق.

جدول (١) نتائج اختبار البعوض للعينة (P1)

رقم الأنبوب	١	٢	٣	٤	٥	متوسط نسبة الطرد
المدة الزمنية بالدقيقة	عدد البعوض ١٥	عدد البعوض ١٥	عدد البعوض ١١	عدد البعوض ١٣	عدد البعوض ١٢	
١٠	٥٣,٣	٦٦,٦	٥٤,٥	٤٦,١	٦٦,٦	٥٧,٤
٢٠	٦٠	٥٣,٣	٤٥,٤	٣٨,٤	٥٨,٣	٥٧
٣٠	٦٠	٨٠	٧٢,٧	٤٦,١	٨٣,٣	٦٨,٤
٤٠	١٣,٣	٧٣,٣	٥٤,٥	٤٦,١	٧٥	٥٢,٤
٥٠	٤٠	٦٦,٦	٦٣,٦	٣٠,٧	٧٥	٥٥,١
٦٠	٧٣,٣	٥٣,٣	٦٣,٦	٢٣	٨٣,٣	٥٧,٣

ويتضح من الجدول أن أعلى متوسط نسبة طرد كان ٦٨,٤% بعد ٣٠ دقيقة وكان مدى متوسط نسبة الطرد بين ٥٢% و ٦٨%، واعلى نسبة طرد ٨٣,٣% في العينة رقم ٥ في الدقيقة ٣٠ والدقيقة ٦٠.

كما يشير الجدول (٢) إلى نتائج اختبار نسبة طرد عينات نسيج معالج بالكبسولات الدقيقة لمستخلص قشر الرمان (P2) للبعوض في ٥ أنابيب مختلفة من أنابيب الاختبار كل ١٠دقائق ومتوسط نسبة الطرد لجميع الأنابيب لكل ١٠دقائق.

جدول (٢) نتائج اختبار البعوض للعينة (P2)

رقم الأنبوب	١	٢	٣	٤	٥	متوسط نسبة الطرد
المدة الزمنية بالدقيقة	عدد البعوض ١١	عدد البعوض ١٠	عدد البعوض ١٠	عدد البعوض ٩	عدد البعوض ١٠	
١٠	٦٣,٦	٣٠	٤٠	١٠٠	١٠٠	٦٦,٧٢
٢٠	٧٢,٧	٦٠	٣٠	٧٧,٧	١٠٠	٦٨,٠٨
٣٠	٧٢,٧	٦٠	٥٠	٨٨,٨	٨٠	٧٠,٣
٤٠	٧٢,٧	٦٠	٤٠	٣٣,٣	٩٠	٥٩,٢
٥٠	٨١,٨	٦٠	٤٠	٤٤,٤	٥٠	٥٥,٢٤
٦٠	٧٢,٧	٦٠	٥٠	٥٥,٥	٧٠	٦١,٦٤

ويتضح من الجدول أن أعلى متوسط نسبة طرد كان ٧٠,٣% بعد ٣٠ دقيقة، وكان مدى متوسط نسبة الطرد بين ٥٥% و ٧٠%، وأعلى نسبة طرد ١٠٠% في العينة رقم ٥ في العشرون دقيقة الأولى والعينة رقم ٤ في العشر دقائق الأولى.

ويمكن تمثيل متوسط نسبة طرد البعوض للعينتين (P1) و(P2) لكل ١٠دقائق بيانيا بالشكل (١)

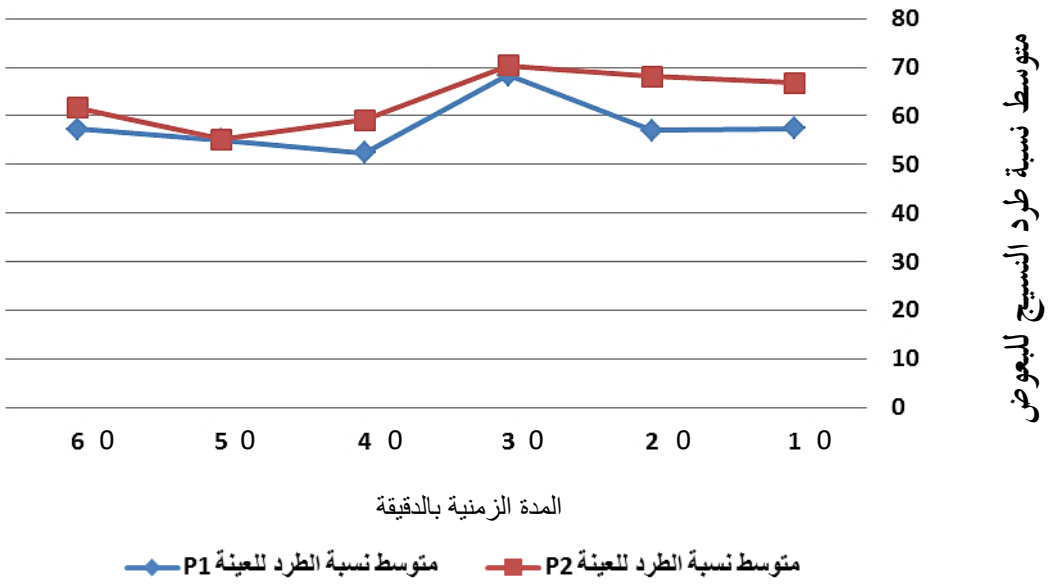

شكل (١) متوسط نسبة الطرد للعينات P1، P2

يتضح من الجدول (١) و (٢) والشكل (١) أن نسب الطرد لم تكن متفاوتة حيث لوحظ ذلك بشكل واضح في الدقيقة ٣٠ والدقيقة ٥٠.

جدول (٣): تحليل التباين الأحادي في اتجاه (One – Way ANOVA) لنسبة الطرد للبعوض

مصدر التباين	مجموع المربعات	درجات الحرية	متوسط المربعات	قيمة "ف"	مستوى المعنوية
بين المجموعات	93.968	1	93.968	2.960	.116
داخل المجموعات	317.510	10	31.751		
الكلي	411.478	11			

ويتضح من نتائج جدول (٤) عدم وجود فرق دال إحصائياً عند مستوى (٠,٠١) بين متوسط نسب الطرد بين العينة (P1) والعينة (P2).

جدول (٤): المتوسطات والانحرافات المعيارية لنسبة الطرد للبعوض

العينة	المتوسط	الانحراف المعياري	الترتيب
عينة P1	57.93	5.47	2
عينة P2	63.53	5.79	1

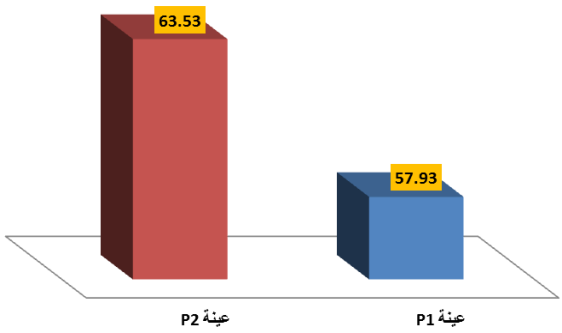

شكل (٢) المتوسطات لنسبة الطرد للبعوض

نستخلص من الجدول (٤) والشكل (٢) أن متوسط نسب طرد العينة (P2) للبعوض أفضل من نسب طرد العينة (P1).

كان الهدف من هذه الدراسة معرفة اثر الكبسلة لمستخلص قشر الرمان على طرد البعوض اثناء استخدامة في معالجة النسيج. وقد اثبتت الدراسة الحالية ان نسبة الطرد للنسيج المعالج بكبسولات مستخلص قشر الرمان وصلت إلى ٧٠% تقريباً، بينما النسيج المعالج بالمستخلص لم تتجاوز نسبة الطرد ٦٨%. على الرغم من إختلاف طريقة تطبيق المستخلص على النسيج إلى أنها أظهرت نشاطاً متقارباً لنسبة الطرد وبأفضلية بسيطة للمعالجة بالكبسولات، يرجع ذلك إلى معدل نسبة إطلاق الماده الفعالة وتبخرها. ففي دراسة (Raja & Priyadarshinirajkumar, 2015) أثبتت العينة المعالجة بالمستخلص العشبي بالطريقة التقليدية أعلى معدل اطلاق، وكذلك في دراسة (Turek & Stintzing, 2013) أثبتت ان اطلاق المادة الفعالة لم يكن مستديماً، بينما اظهرت دراسة (Specos et al., 2010) أن النسيج المعالج بكبسولات السيترونيلا اعطى حماية أفضل من البعوض مقارنة بالنسيج المعالج بدون الكبسلة.

وقد يرجع تقارب نسبة الطرد في النسيج المعالج بمستخلص قشر الرمان والمعالج بكبسولات مستخلص قشر الرمان إلى المواد المستخدمة اثناء الكبسلة ففي دراسة (Geethadevi & Maheshwari, 2015) تم استخدام ثلاث انواع مختلفة من مواد الغلاف ألجينات الصوديوم (Sodium alginate) والسنط العربي (*Acacia arabica*) صمغ البان الزيتوني (*Moringa oleifera*) كغلاف لخليط من زيت الزعتر و زيت

السرو وزيت بذور العنب. كانت أعلى نسبة للطرد لصالح صمغ البان الزيتوني بنسبة ٨٤% ووصلت إلى ٦٠% بعد ٣٠ غسلة، بينما أقل نسبة كانت٦٠% لصالح ألجينات الصوديوم ووصلت إلى ٤٤% بعد ٣٠غسلة.

وعند مقارنة الدراسة الحالية بدراسة (Singh, 2017) اظهر النسيج المعالج بمستخلص قشر الرمان نسبة طرد تصل إلى ٨٠% بينما الدراسة الحالية لم تتجاوز ٦٨% عند تطبيق المستخلص بدون كبسلة، وقد اتفقت الدراستان على استخدام نسيج القطن، بينما تظهر دراسة (Sumithra & Raja, 2012) أن إختلاف الياف النسيج تؤثر في نسبة الطرد فقد تم اختبار أربع عينات مختلفة عينة (A) ٦٨% قطن و ٣٢% بوليستر(Polyester) و عينة (B) ٦٨% قطن و٣٢% بولي ليكرا (Poly Lycra) وعينة (C) ٦٨% قطن و ٣٢% ليكرا (Core Spun lycra) وعينة (D) ١٠٠% قطن، فكانت نسبة الطرد ١٠٠% في النسيج القطني واعلى كفاءه للمعالجات.

كما اتفقت الدراسة الحالية مع الدراسات السابقة في استخدام مذيب الميثانول في إعداد مستخلص قشر الرمان، فقد أثبتت الدراسات ان إختلاف المذيب يؤدي إلى نتائج مختلفة. ففي دراسة (Ben Hamouda et al., 2014) اظهر المستخلص الإيثانولي لقشر الرمان نشاطاً أفضل في الطرد من المستخلص المائي والميثانولي لأحد أنواع الحشرات، ويظهر إختلاف التركيز للمستخلص بين الدراستين سبباً لاختلاف النتائج كذلك على الرغم من تشابة وقت المعالجة حيث تمت المعالجة خلال ٩٠دقيقه. ففي الدراسة الحالية تم وضع ٢٠غم من قشر الرمان في ١٠٠مل ميثانول وبعد الاستخلاص تم اخذ ١٠مل وتخفيفه في ١٦٥مل ماء مقطر، بينما في دراسة (Singh, 2017) تم وضع ١٥جرام من قشر الرمان في ١٠٠ مل ميثانول وبعد الاستخلاص تم تخفيفه بنسبة ٥٠%. وقد اكدت نتائج دراسة (Gupta & Singh, 2017) أن اختلاف تركيز قشر البرتقال في المستخلص الميثانولي وإختلاف نسبة تركيزه عند المعالجة ووقت المعالجة أدى إلى اختلاف في نسبة الطرد للبعوض، فقد أظهرت النتائج ان نسبة الطرد ازدادت عند المعالجة لمدة ١٢٠دقيقة وبتركيز ٦٠% من المستخلص طرداً للبعوض بنسبة ٨٠%.

وقد يرجع السبب أيضا، إلى إختلاف نوع البعوض فقد استخدمت الدراسة الحالية بعوض من النوع (Aedes aegypti) بينما لم يذكر في دراسة (Singh, 2017) نوع البعوض، وتؤكد ذلك دراسة (Phasomkusolsil & Soonwera, 2010) فقد تم دراسة عدة نباتات منها الزيت الأساسي لعشبة السترونيلا ضد ثلاث انواع من البعوض، بعوضة الأنوفليس (*Anopheles*) والزاعجة المصرية (*Aedes aegypti*) وبعوضة الكيولكس (*Culex quinquefasciatus*)، فكان معدل وقت الحماية ونسبة اللدغ مختلفة. ففي بعوضة الأنوفليس كان ١٣٠د وبنسبة ٠,٩%، وفي بعوضة الكيولكس كان ١٤٠د وبنسبة ٠,٨%، وفي بعوضة الزاعجة المصرية كان ١١٥د وبنسبة ٠,٨%.

ومن الممكن أن يرجع الإختلاف أيضا إلى طريقة تقييم النسيج المعالج لطرد البعوض وزمن الإختبار وعدد التكرارات، فهناك عدة طرق لتقييم النسيج المعالج لطرد البعوض وأكثرها إستخداما اختبار القفص (Cage test) واختبار المخروط (Cone test) وغرفة الإثارة (Excito chamber test)(Anuar & Yusof, 2016) . فقد تم في الدراسة الحالية استخدام أنبوب منظمة الصحة العالمية لإختبارالنسيج المعالج لمدة تصل ل٦٠د وحساب نسبة الطرد كل ١٠ دقائق وتكرار الاختبار ٥ مرات. بينما في دراسة (Singh, 2017) تم استخدام القفص المعدل بحيث لا يوجد تدخل بشري، فتم وضع صندوق زجاجي بقياس ٣٠×٣٠×٣٠سم ووضع النسيج المعالج بداخله ووضع ٢٠ بعوضة في الصندوق وتركها لمدة دقيقتين وحساب عدد البعوض الذي سيستقر على العينة المعالجة خلال دقيقتين وتكرار الاختبار أربع مرات ثم حساب نسبة الطرد، (Anuar & Yusof, 2016). ويتم اختيار الاختبار وتعديله وفقا للهدف من المادة أو النسيج. فعلى سبيل المثال، يعد إختبار المخروط أكثر ملاءمة للتحقق من سمية السطح المشبعة المختلفة، وغرفة الإثارة تفيد في مراقبة سلوك البعوض تجاه المنسوجات المعالجة وغير المعالجة والمقارنة بينهما، بينما يحاكي اختبار القفص، الذي يشمل الإنسان كمتطوع، الوضع الحقيقي للدغ البعوض وقد يعطي نتائج دقيقة.

ثانياً: تأثير الكبسلة الدقيقة على النسيج المعالج :

١) تحليل سطح النسيج:

تم طلاء النسيج بطبقة رقيقة للغاية من مادة موصلة للكهرباء، وأخذ صور مكبره لسطحه، وتحليل ركائز النسيج قبل معالجته بمستخلص قشر الرمان (صورة ٥أ، ٥ب) وبعد معالجته بمستخلص قشر الرمان (صورة ٥ج، ٥د) وكذلك بعد معالجته بكبسولات مستخلص قشر الرمان (صورة ٥هـ، ٥و). من الملاحظ تفاوت مساحة الفجوات بين خيوط السداء واللحمة بعد المعالجة فقد زادت المساحة في العينة (P1) (صورة ٥ج) و(P2) (صورة ٥هـ) مقارنة بعينة (O) (صورة ٥أ). ويمكن كذلك ملاحظه أن سطح ألياف القطن لعينة (O) (صورة ٥أ) كانت نظيفة وناعمة وغير مرتبطة بجسيمات، في حين أن ألياف القطن للعينة (P1) (صورة ٥د) تثبت وجود

مواد مختلفة الحجم والشكل على سطحه، بينما العينة (P2) (صورة ٥و) توضح وجود مادة على ألياف القطن قد تكون ناجمة عن تفاعل معين بين ألياف النسيج ومحلول الكبسولات لمستخلص قشر الرمان حيث جعلت بعض الكبسولات الدقيقة تغير من مورفولوجيتها وترتبط بالسطح على شكل قشور.

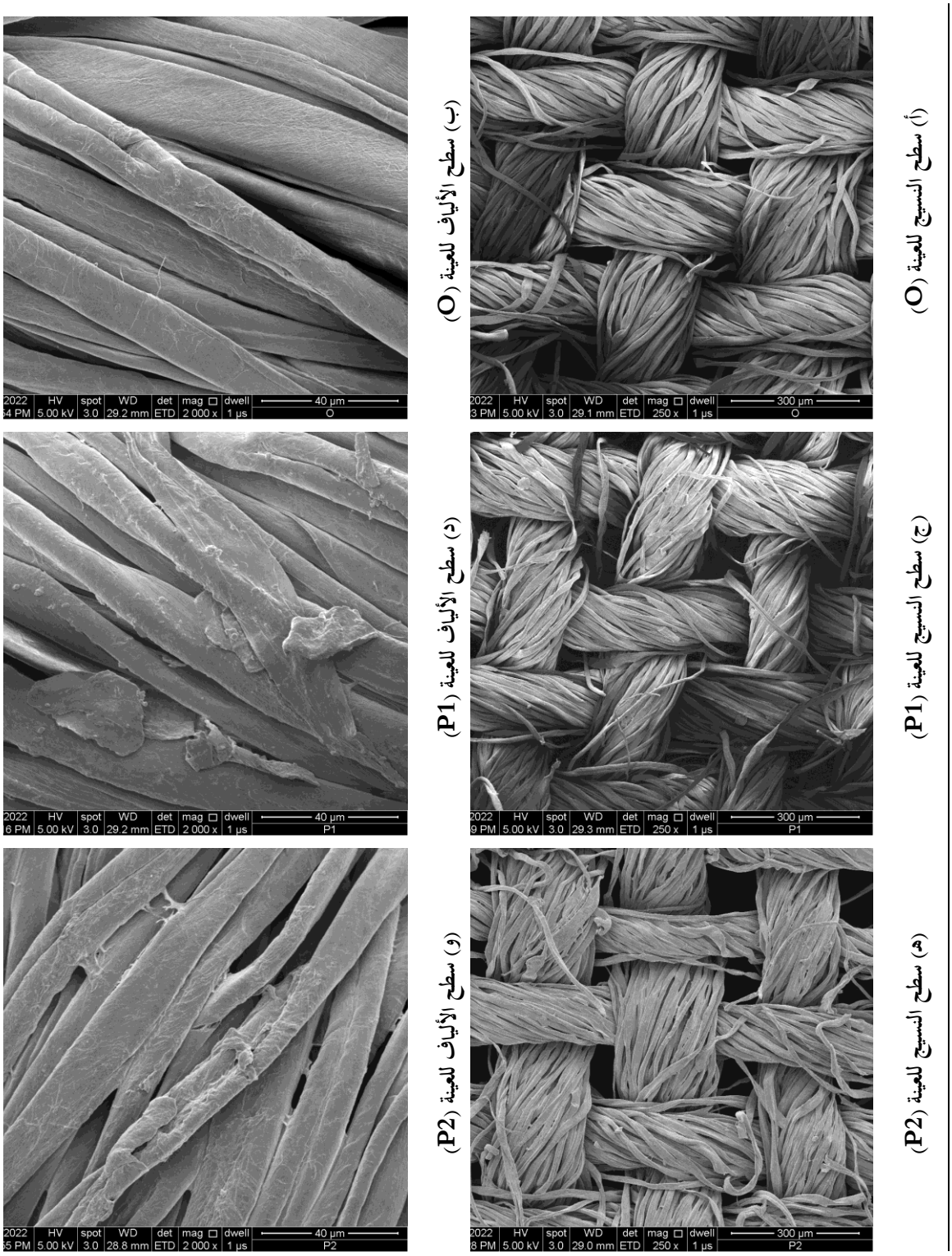

صورة (٥) صور لسطح النسيج بالمجهرالالكتروني الماسح (SEM)

٢) التركيب النسجي:

عند الفحص البصري والاستعانة بالعدسة المكبرة يتضح التركيب النسجي للنسيج سادة ١/١، وهو أبسط تركيب نسجي، ومظهره السطحي للوجه يشبه مظهره السطحي للظهر، ويتميز عن التراكيب الأخرى بالمتانة ومرونة أقل، و إذا قورن مع أقمشة ذات تراكيب مختلفة وبخيوط من النمرة والنوع نفسه، تكون نسبة التشريب فيه كبيرة، و لا تنزلق خيوط السداء واللحمة فيها خارج الحياكة نتيجة الترابط القوي بينها.

٣) سمك النسيج:

يوضح الشكل (٣) ترتيب العينات حسب متوسط سمك النسيج. فقد أظهرت النتائج ان العينة (P2) أعلى سماكة، بينما العينة (O) أقل سماكة، مما يدل على أن النسيج مشبع بالمعالج.

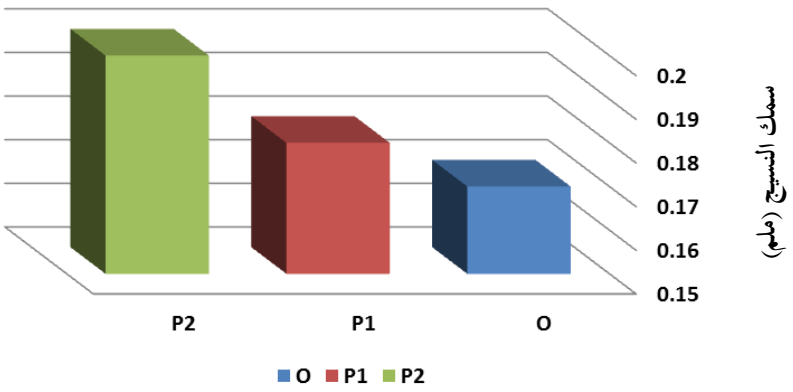

شكل (٣) متوسط سمك النسيج لعينات الدراسة

٤) وزن المتر المربع للنسيج:

يوضح الشكل (٤) ترتيب العينات حسب وزن المتر المربع للنسيج للعينة (P2)، و العينة (O)، والعينة (P1). أظهرت النتائج أن العينة (P2) أعلى وزن، بينما العينة (P1) اقل وزن مما يدل على أن المعالجة بمستخلص قشر الرمان أدت الى زيادة وزن النسيج وتشبع النسيج بالمستخلص.

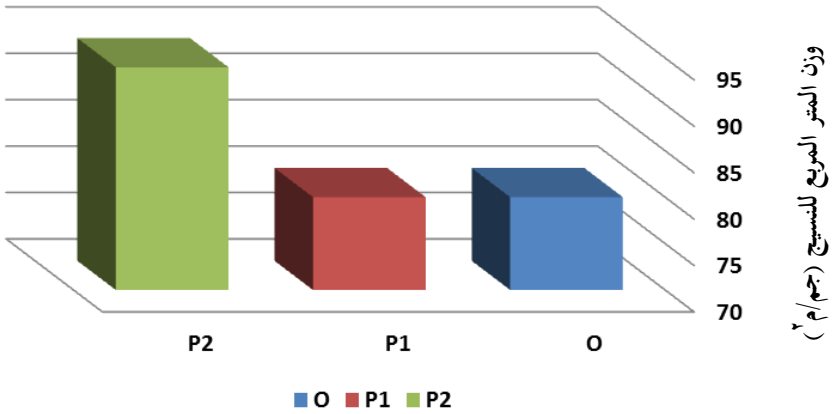

شكل (٤) متوسط وزن المتر المربع لعينات الدراسة

٥) نفاذية الهواء:

يتضح من الشكل (٥) ترتيب العينات حسب نفاذية الهواء في النسيج. فقد أظهرت النتائج أن العينة (P1) أعلى نفاذية للهواء، بينما العينة (O) أقل نفاذية، مما يدل على أن المعالجة بمستخلص قشر الرمان زادت من مساحة الفجوات بين خيوط النسيج.

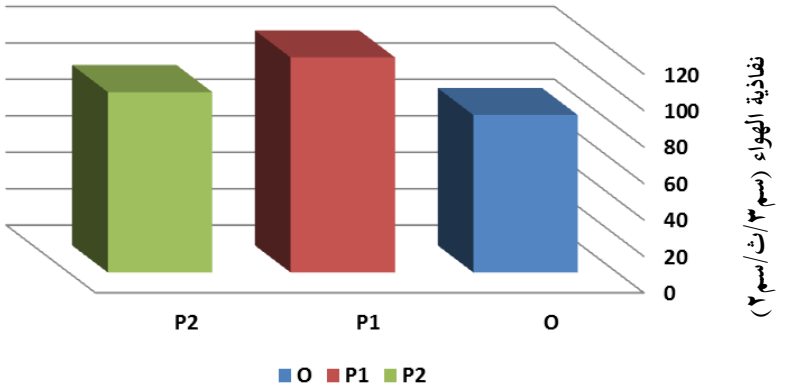

شكل (٥) متوسط نفاذية الهواء لعينات الدراسة

٦) تقييم الجودة الكلية:

تم عمل تقييم لجودة الأقمشة المنتجة تحت البحث لملائمتها للغرض الوظيفي، وذلك باستخدام أشكال الرادار Radar Chart متعدد المحاور ليعبر عن تقييم الجودة الكلية للمنسوجات تحت الدراسة من خلال استخدام الخواص التالية: السمك، وزن المتر المربع، نفاذية الهواء، وذلك بتحويل نتائج قياسات هذه الخواص إلى قيم مقارنة، حيث أن القيمة المقارنة الأكبر تكون الأفضل مع السمك، ووزن المتر المربع، ونفاذية الهواء جدول (٥).

جدول (٥) يوضح معامل الجودة الكلية لاختبارات عينات نسيج الدراسة

العينة	السمك	وزن المتر المربع	نفاذية الهواء	المساحة المثالية	معامل الجودة
O	85.00	85.11	73.22	243.33	81.11
P1	90.00	85.11	100	275.11	91.70
P2	100.00	100	83.90	283.90	94.63

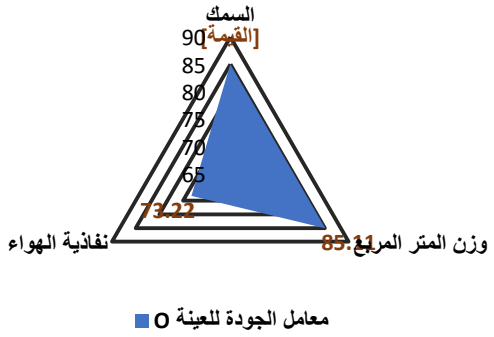

شكل (٦) معامل الجودة **الكلية للعينة** (O) **بمساحة** مثالية (٢٤٣,٣٣) ومعامل الجودة (٨١,١١) **بترتيب** (الثالث).

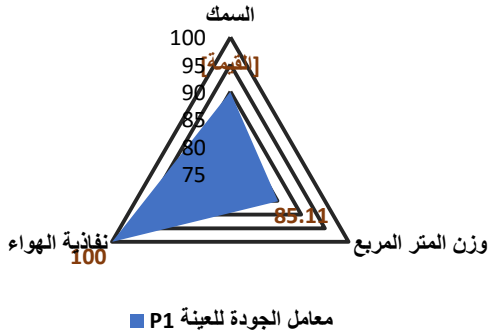

شكل (٧) معامل الجودة **الكلية للعينة** (P1) **بمساحة** مثالية (٢٧٥,١١) ومعامل الجودة (٩١,٧٠) بترتيب (الثاني).

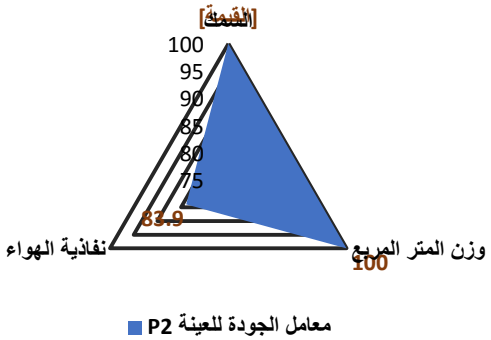

شكل (٨) معامل الجودة **الكلية للعينة** (P2) **بمساحة** مثالية (٢٨٣,٩٠) ومعامل الجودة (٩٤,٦٣) بترتيب (الأول).

وكان الهدف الآخر من هذه الدراسة معرفة أثر المعالجة بمستخلص قشر الرمان والكبسلة الدقيقة للمستخلص على النسيج بعد معالجته، ويوضح جدول (٥) أن العينة (P2) حققت أعلى سمك للنسيج مقداره ٠,٢٠ملم بينما كانت نتيجة العينة (O) هي الأقل وقد يرجع ذلك إلى أن خيوط النسيج في العينة (P2) أصبحت أكثر سمكاً بعد معالجته بكبسولات مستخلص قشر الرمان من العينة (O) الغير معالجة، لوجود علاقة طردية بين قطر خيط السداء وبين سمك العينة المنسوجة (عثمان، ٢٠٢٢م).

ويتضح كذلك من جدول (٥) أن العينة (P2) حققت أعلى وزن للنسيج في المتر المربع مقداره ٩٤غم^{٢} بينما كانت نتيجة العينة (O) والعينة (P1) متساويتين بمقدار ٨٠غم^{٢} وقد يرجع ذلك إلى أن خيوط النسيج في العينة (P2) أصبحت أكثر سمكاً بعد معالجته بكبسولات مستخلص قشر الرمان من العينة (O) الغير معالجة والعينة (P1) المعالجة بمستخلص قشر الرمان، لوجود علاقة طردية بين قطر خيط اللحمة ووزن المتر المربع مع خاصية السمك في العينة المنسوجة (عثمان، ٢٠٢٢م).

ويظهر التحليل السطحي للنسيج بجهاز (SEM) في (صورة ٥ج) وجود فراغات بين خيوط السداء واللحمة للتركيب النسجي للعينة (P1) بمقارنتها بعينة التحكم (O) في (صورة ٥أ) ويؤكد ذلك جدول (٥) أن العينة (P1) حققت أعلى نسبة نفاذية للهواء بمقدار ١١٨سم^{٣}/ث/سم^{٢} ويعود السبب إلى أنها أقل العينات كثافة لخيوط السداء واللحمة، بينما كانت نتيجة العينة (O) ٨٦,٤ سم^{٣}/ث/سم^{٢} بسبب كثافة خيوط السداء واللحمة، حيث تزداد نفاذية الهواء طردياً بزيادة حجم وعدد الفراغات المتكونة بالنسيج والتي تتحكم فيها بدرجة كبيرة قيمة معامل التغطية للمنسوجات، وينخفض معدل نفاذية الهواء بزيادة قيمة معامل تغطية السداء أو اللحمة أو بزيادة أحدهما (عثمان، ٢٠٢٢م)، وبالتالي لم تختلف العينة (P1)عن العينة (O) على الرغم من وجود مستخلص قشر الرمان، وقد يرجع السبب في ذلك إلى انخفاض معامل التغطية فأصبح النسيج أخف وزناً وحل محله وزن المادة المعالجة.

ويوضح التحليل الإحصائي أن العينة (P2) المعالجة بكبسولات مستخلص قشر الرمان جاءت الأولى في تقييم معامل الجودة مما يعني أنها تتمتع بأفضل النتائج بدرجة عالية مثل السمك والوزن ونفاذية الهواء وقد يرجع ذلك إلى الكبسولة الدقيقة المعالجة للنسيج، بينما العينة (O) الغير معالجة كانت الأقل في تقييم معامل الجودة. وقد ذكر (عمر، ١٤٣٢هـ) أن نفاذية الهواء تعتمد على وزن القماش وتركيبة (السماكة والمسامية) وعلى الفراغات بين الخيوط، حيث أن الأقمشة المنسوجة تنتج من تشابك خيوط السداء واللحمة، ووجود فراغ بين خيوط السداء واللحمة في النسيج، وحجم الفراغ الموجود يلعب دوراً كبيراً في نفاذية الهواء، فعدد خيوط السداء واللحمة في السنتيمتر ونمرة ونوعية وبنية الخيط ومقدار برمه، والتركيب النسجي جميعها عوامل تؤثر في نفاذية الهواء.

الاستنتاج:

نستنتج من الدراسة الحالية والدراسات السابقة أن جميع العناصر (كالنبات، ونوع البعوض وطريقة استخلاص المادة الفعالة من النبات وتركيزها والنسيج وتركيبه النسجي وما يحتويه من ألياف وما يميزه من خصائص فيزيائية وغيرها وطريقة معالجة النسيج وطريقة تقييم الفاعلية ومناسبتها للخواص الوظيفية) جميعها تتفاعل معاً للوصول إلى نسيج طارد للبعوض ذو كفاءة عالية.

التوصيات:

١) معالجة النسيج بعدة تراكيز مختلفة من الكبسولات الدقيقة لمستخلص قشر الرمان للوصول لأفضل تركيز ممكن لعملية طرد البعوض.

٢) العمل على غسل النسيج بعد معالجته عدة مرات لمعرفة مدى بقاء الكبسولات الدقيقة في النسيج.
٣) اختبار النسيج المعالج ضد البكتيريا والفطريات لما يحتويه قشر الرمان من مركبات كيميائية تعمل كمضادات للأكسدة والالتهابات.

المراجع:

المراجع العربية:

الحكيم، عبير حمدي (٢٠١٥م)، استخدام النباتات السامة كمواد طاردة وقاتلة للحشرات ، *العلوم والتقنية*،٣٢-٣٣-٣٤-٣٥.

الصديق، مختار عثمان (١٤٢٥هـ)، مناهج البحث العلمي ، (أم درمان: دار جامعة القرآن الكريم للطباعة).

العساف، صالح حمد (١٤٣١هـ)، المدخل إلى البحث في العلوم السلوكية ، (الرياض: دار الزهراء).

المحمادي ، رقية محمد (٢٠٠٩م)، علم الحشرات العام ، (جدة: مركز النشر العلمي جامعة الملك عبد العزيز).

اليحيى، حنان سلمان (٢٠١١م)، تقييم فاعلية نبات النيم والدفلة على البعوض ، رسالة ماجستير، جامعة الملك عبد العزيز ، جدة.

عثمان، شيرين سيد (٢٠٢٢م)، تأثير بعض عوامل التركيب البنائي النسجي على خواص الأداء الوظيفي لأقمشة بلوزات السيدات الصيفية ، *مجلة العمارة والفنون*.

عمر، ربيع أحمد (١٤٣٢هـ)، دراسة تأثير نوعية الخيط والنسيج على نفوذية الأقمشة للهواء ، رسالة ماجستير، جامعة حلب ، حلب.

المراجع الأجنبية

Anuar, A. A., & Yusof, N. (2016). Methods of imparting mosquito repellent agents and the assessing mosquito repellency on textile. *Fashion and Textiles*, *3*(1). https://doi.org/10.1186/s40691-016-0064-y

Ben Hamouda, A., Mechi, A., Chaieb, I., & Laarif, A. (2014). Insecticidal Activities of Fruit Peel Extracts of Pomegranate (Punica granatum) against the red flour beetle Tribolium castaneum. *Tunisian Journal of Plant Protection*, *91*.

Geethadevi, R., & Maheshwari, V. (2015). Long-lasting UV protection and mosquito repellent finish on bamboo/tencel blended fabric with microencapsulated essential oil. *IJFTR Vol.40(2) [June 2015]*. http://nopr.niscpr.res.in/handle/123456789/31624

Ghayempour, S., & Montazer, M. (2016). Micro/nanoencapsulation of essential oils and fragrances: Focus on perfumed, antimicrobial, mosquito-repellent and medical textiles. *Journal of Microencapsulation*, *33*(6), 497–510. https://doi.org/10.1080/02652048.2016.1216187

Ghosh, A., Chowdhury, N., & Chandra, G. (2012). Plant extracts as potential mosquito larvicides. *The Indian Journal of Medical Research*, *135*(5), 581–598.

Gupta, A., & Singh, D. A. (2017). Efficacy of orange peel as a mosquito repellent. *International Journal of Home Science*, *3*(2), 143–146.

Kantheti, D. P., Rajitha, D. I., & Padma, D. A. (2020). Development of Eco-friendly mosquito repellent printed textiles with synthesized Ocimum basilicum leaf dye extract. *International Journal of Mosquito Research*, *7*(4), 31–38.

Karthigeyan, V., & Premalatha, C. (2019). Mosquito Repellent Finish on Cotton Fabric using Justicia Adhatoda Vasica Extract by Micro Encapsulation. *International Journal of Research in Engineering, Science and Management*.

Krishnaveni, V. (2009). Mosquito Repellent Finish, Textiles, Mosquito Repellent Textile, Cotton Fabrics, Padding Method, Mosquito Repellents, *Fibre2fashion*.

Repellents on Cotton Fabric through Dyeing. *International Journal for Innovative Research in Multidisciplinary Field*. 3. 63-65

Specos, M. M. M., García, J. J., Tornesello, J., Marino, P., Vecchia, M. D., Tesoriero, M. V. D., & Hermida, L. G. (2010). Microencapsulated citronella oil for mosquito repellent finishing of cotton textiles. *Transactions of the Royal Society of Tropical Medicine and Hygiene*, *104*(10), 653–658. https://doi.org/10.1016/j.trstmh.2010.06.004

Subrata, D. (2021, January 23). Insect Repellent Textile Finishing using Natural Bio-molecules. *Textile School*. https://www.textileschool.com/6795/insect-repellent-textile-finishing-using-natural-bio-molecules/

Sumithra, M., & Raja, N. V. (2012). Mosquito repellency finishes in blended denim fabrics. *Life Sci.*, *3*(4), 3.

Tomlinson, S., Yates, H. C., Oruni, A., Njoroge, H., Weetman, D., Donnelly, M. J., & Hof, A. E. V. (2019). Open source 3D printable replacement parts for the WHO insecticide susceptibility bioassay system (p. 762849). bioRxiv. https://doi.org/10.1101/762849

Turek, C., & Stintzing, F. C. (2013). Stability of Essential Oils: A Review. *Comprehensive Reviews in Food Science and Food Safety*, *12*(1), 40–53. https://doi.org/10.1111/1541-4337.12006

http://www.fibre2fashion.com/industry-article/4457/mosquito-repellent-finish-on-textiles

Mullah, A., Shinde, I., Shivankar, V., & Raichurkar, P. (2019). *Eco-friendly mosquito repellent textiles*. *Technical Textiles–Technische Textilien*, *62*.

Phasomkusolsil, S., & Soonwera, M. (2010). Insect repellent activity of medicinal plant oils against Aedes aegypti (Linn.), Anopheles minimus (Theobald) and Culex quinquefasciatus Say based on protection time and biting rate. *The Southeast Asian Journal of Tropical Medicine and Public Health*, *41*(4), 831–840.

Raja, A., Kawlekar, S., Saxena, S., Arputharaj, A., & Patil, P. G. (2015). Mosquito protective textiles-A review. *International Journal of Mosquito Research*, *2*(4), 49-53.

Raja, N. V., & Priyadarshinirajkumar, A. (2015). *).* Innovative herbal nanofinishing on cotton fabric. *Int. J. Fiber Text. Res*, *5*, *44*.

Ramya, K., & Maheshwari, V. (2014). Development of eco friendly mosquito repellent fabric finished with andrographis paniculata plant extracts. *International Journal of Pharmacy and Pharmaceutical Sciences*, *6*, 115–117.

Samanta, A. K., Awwad, N. S., & Algarni, H. M. (2020). *Chemistry and Technology of Natural and Synthetic Dyes and Pigments*. https://doi.org/10.5772/intechopen.83199

Singh, A. (2017). Protection and Application of Mosquito

Mosquito repellent fabric treated with microcapsules of pomegranate peel extract

Nibras Ibrahim Issa

Fashion and Textile Department King Abdulaziz University

Salwa Muhammad Tashkandi

Department of Fashion and Textiles, King Abdulaziz University

Wafaa Abu Bakr Bawazeer

Department of Organic Chemistry, King Abdulaziz University

Hanan Salman Al Yahya

Department of Entomology, King Abdulaziz University

Abstract

Mosquitoes pose a great threat to human health, as they transmit many diseases to them, and therefore they urgently need specialized products to combat and prevent them. Textiles treated with natural plant materials may be more effective and mosquito repellent to maintain human and environmental safety. There are many plants that contain effective chemical compounds in repelling mosquitoes, non-toxic and biodegradable, extracted and prepared in an environmentally friendly manner. One of the disadvantages of using natural plant materials in textile processing is the weak bond between the material and the fabric, and microencapsulation is one of the best ways to overcome this.

The current study showed the effect of microencapsulation of pomegranate peel extract on its effectiveness in repelling mosquitoes *Aedes aegypti* and on the fabric. The research followed the experimental method as an environmentally friendly method to prepare microcapsules containing pomegranate peel extract and treat the fabric with it, and test its effectiveness in repelling mosquitoes and the effect of that treatment on the fabric. Using pomegranate peel extract as a base material and Arabic Gum as a coating, and sodium alginate solution was used for the microencapsulation process.

The results showed that the cotton fabric treated with microcapsules of pomegranate peel extract repellent to mosquitoes with an average rate of 63.53%, while treated with pomegranate peel extract was mosquito repellent with an average of 57.39%, and the total quality coefficient of tests of cotton fabric treated and untreated with pomegranate peel extract and treated with pomegranate peel extract capsules was in favor of the treated sample. By capsule of pomegranate peel extract.
The study recommends preparing several different concentrations of pomegranate peel extract to reach the best concentration in the rate of mosquito repellent, as well as washing the fabric to see how long the effect of the treatment remains on the fabric.

keywords: Microencapsulation, Mosquito Repellent, Natural Materials, Textile Processing, Pomegranate Peel.

مجلة جامعة جازان

للعلوم التطبيقية

دورية علمية محكمة

المراسلات

توجه جميع المراسلات إلى:

رئيس هيئة التحرير مجلة جامعة جازان للعلوم التطبيقية جازان –المدينة الجامعية –البرج الإداري – ص ب ١١٤. –الرمز البريدي ٤٥١٤

المملكة العربية السعودية أو على البريد الإلكتروني jas@jazanu.edu.sa

المملكة العربية السعودية

وزارة التعليم

جامعة جازان

مجلة جامعة جازان

للعلوم التطبيقية

دورية علمية محكمة

المجلد ١١ العدد ١ (ذو القعدة ١٤٤٤هـ - يونيو ٢٠٢٣م)

ردمد : ١٦٥٨-٦٩١٣

قواعد النشر في المجلة

مجلة جامعة جازان للعلوم التطبيقية دورية علمية محكمة تنشرها الجامعة، وهي تهدف إلى إتاحة الفرصة للباحثين لنشر إنتاجهم العلمي وتقوم المجلة بنشر المواد الآتية :

١ـ البحث : ويندرج تحت تخصص الباحث ويجب أن يحتوي على إضافة للمعرفة في مجاله .

٢ـ المقالة الاستعراضية التي تتضمن عرضًا نقدياً لبحوث سبق إجراؤها في مجال معين أو أجريت في خلال فترة زمنية محددة.

٣ـ البحث المختصر.

٤ـ نقد الكتب .

٥ـ الخطابات الموجهة إلى المحرر ، والملاحظات والردود ، والنتائج الأولية .

تقوم هيئة التحرير، بالنظر في نشر المواد المعرفية ذات الصلة بذلك الفرع، وتقدم البحوث الأصلية، التي لم يسبق نشرها، وفي حال قبول البحث للنشر تؤول كل حقوق النشر للمجلة و لا يجوز نشره في أي منفذ نشر آخر ورقيا أو إلكترونياً، دون إذن كتابي من رئيس هيئة التحرير .

تعليمات النشر في المجلة

١ـ تقديم المواد : يقدم أصل البحث مخرجا في صورته النهائية متضمنا الإشارة إلى أماكن الجداول والأشكال داخل المتن و مطبوع على هيئة صفحات مرقمة ترقيما متسلسلا، مع ضرورة إرفاق قرص ممغنط مطبوع عليه البحث على برنامج Ms Word باستخدام النظام المتوافق مع IBM ، وسيعتذر عن قبول أي بحث لا يلتزم مؤلفه بهذه التعليمات.

٢ـ الملخصات: يرفق ملخصان بالعربية والإنجليزية للبحوث و المقالات الاستعراضية والبحوث المختصرة على ألا يزيد عدد كلمات كل منهما على ٢٠٠ كلمة، وعلى عمود واحد بعرض كتابة ١٣ سم.

٣ـ لا بد من احتواء كل بحث على كلمات مفتاحية (Key Words) توضع أسفل الملخصين العربي والانجليزي على ألا تزيد عن عشر كلمات.

٤ـ الجداول والمواد التوضيحية: يجب أن تكون الجداول والرسومات واللوحات مناسبة لمساحة الصف في صفحة المجلة ١٦ ٢٤ سم بالحواشي، ويتم إعداد الأشكال الخطية على برامج الحاسب الآلي، ولا تقبل إلا أصول الأشكال. كما يجب أن تكون الخطوط واضحة ومحددة ومنتظمة من حيث كثافة الحبر وتناسب سمكها مع حجم الرسم، ويراعى أن تكون الصور الفوتوغرافية (الضوئية) الملونة وغير الملونة مطبوعة على ورق لماع، أو محملة على برنامج (Adobe Photoshop) مع كتابة عنوان لكل جدول، وتعليق لكل شكل وصورة، والإشارة إلى مصدر المادة إن كانت مقتبسة.

٥ـ الاختصارات: يجب استخدام الاختصارات المقننة دولية مثل : سم، مم، م، كم، سم، مل، مجم، كجم...إلخ.

٦ـ المراجع :يشار إلى المراجع داخل المتن بنظام الاسم والتاريخ، وتوضع المراجع جميعها في قائمة المراجع بنهاية المادة مرقمة ومتبعة نظام ترتيب البيانات الببليوجرافية التالي :

أـ يشار إلى الدوريات في المتن بنظام الاسم والتاريخ بين قوسين على مستوى السطر، أما في قائمة المراجع فيبدأ المرجع بذكر الاسم الأخير للمؤلف، ثم الاسم الأول، ثم الأسماء الأخرى أو اختصاراتها بالخط الأسود، ثم سنة النشر بين قوسين، فعنوان البحث كاملا بين علامتي تنصيص" " ، فاسم الدورية، فرقم المجلد، ثم رقم العدد : ثم أرقام الصفحات تفصل بشرطة .

مثال : هادي، أحمد بن جابر. (٢٠١١م)،" استخدام تقنية النانو لتعريف الشفرات الوراثية "مجلة جامعة جازان، ١، ١ : ٢٠٠ـ٢٢٠.

بـ يشار إلى الكتب في المتن داخل قوسين بالاسم والتاريخ . أما في قائمة المراجع، فيكتب الاسم الأخير للمؤلف، ثم الاسم الأول، ثم الأسماء الأخرى أو اختصارا تها، ثم سنة النشر بين قوسين، فعنوان الكتاب بين علامتي تنصيص، ثم بيان الطبعة، فالناشر، فمدينة النشر :ثم صفحات الكتاب إن وجدت.

مثال :

عبدالهادي، محمد علي، (١٤٣٣هـ)،" مقدمة في التقنية الحيوية"، جامعة جازان، جازان.

ويجب عدم استخدام الاختصارات المرجعية مثل :المرجع نفسه . المرجع السابق...إلخ.

٧ـ أـ الحواشي: تستخدم لتزويد القارئ بمعلومات توضيحية، ويشار إليها في المتن بأرقام مرتفعة عن السطر .وترقيم التعليقات متسلسلة داخل المتن. وفي حال الضرورة؛ يمكن الإشارة إلى مرجع داخل الحاشية عن طريق استخدام كتابة الاسم والتاريخ بين قوسين وبنفس طريقة استخدامها في المتن، وتوضع الحواشي أسفل الصفحة التي تخصها والتي ذكرت بها و تفصل بخط عن المتن وبخط أصغر.

بـ يستخدم في تخريج الأحاديث والآثار الطريقة المنهجية المعتمدة في هذا الفن وهي كالآتي : اسم المؤلف ـ اسم الكتاب ـ رقم الجزء والصفحة والحديث.

٨ـ المواد المنشورة في المجلة تعبر عن وجهة نظر صاحبها، ولا تعبر بالضرورة، عن رأي مجلة جامعة جازان.

٩ـ يتأكد الباحث من صحة اللفظ وسلامة لغة البحث، وخلوه من الأخطاء اللغوية والنحوية.

١٠ـللمجلة الحق في تحديد أولويات نشر البحوث.

١١ـالمجلة غير ملزمة بإعادة البحوث التي تصل إليها سواء أجيزت للنشر أم لم تجز.

١٢ـيتم إخضاع جميع البحوث المستلمة لفحص مبدئي، من قبل هيئة التحرير، لتقرير أهليتها للتحكيم، ويحق لها أن تعتذر عن قبول البحث دون إبداء الأسباب.

١٣ـتصدر المجلة مرتين في العام.

المملكة العربية السعودية
وزارة التعليم
جامعة جازان

مجلة جامعة جازان

للعلوم التطبيقية

دورية علمية محكمة

المجلد ١١ العدد ١ (ذو القعدة ١٤٤٤هـ - يونيو ٢٠٢٣م)

ردمد: ١٦٥٨-٦٩١٣